

**Towards novel BH3-mimetics –  
structure-guided development of  
small molecule inhibitors targeting  
prosurvival BCL-2 family proteins**

**Michael James Roy**

Submitted in total fulfillment of the requirements  
of the degree of Doctor of Philosophy

October 2016

**Walter & Eliza Hall Institute of Medical Research  
Faculty of Medicine, Dentistry and Health Sciences  
The University of Melbourne**

## Abstract

Defects in apoptosis (programmed cell death) due to overexpression of prosurvival members of the BCL-2 family (eg. BCL-2, MCL-1 and BCL-X<sub>L</sub>) are a genetic feature of many cancers and a common reason for the development of resistance to conventional anti-cancer chemotherapies. A program was initiated at WEHI to find novel small molecule inhibitors of prosurvival BCL-2 family proteins, as potential targeted anti-cancer therapies or novel tool molecules. This identified a series of molecules possessing a benzoylurea core that showed promising inhibition of prosurvival BCL-X<sub>L</sub>, including compound **1.1**, which had an IC<sub>50</sub> for BCL-X<sub>L</sub> in the low-sub micromolar range. This Thesis describes structure-guided medicinal chemistry efforts to progress this benzoylurea series towards more potent and selective BCL-X<sub>L</sub> inhibitors.

A crystal structure solved of the BCL-X<sub>L</sub>:**1.1** complex revealed that compound **1.1** bound along a hydrophobic groove present on the surface of BCL-X<sub>L</sub>, interacting directly with two hydrophobic pockets (p4 and p5) and proximal to a third pocket (p2). Based on modeling, two new extended benzoylurea scaffolds were synthesised that incorporated groups designed to interact with the p2 pocket, as well as analogues incorporating a sulfonyl 'linker' group designed to form an additional hydrogen bond interaction with the backbone –NH of Gly138 of BCL-X<sub>L</sub>. Building on this work, this Thesis firstly describes atomic structures solved of two such extended scaffold benzoylurea compounds in complex with BCL-X<sub>L</sub>, to validate their binding mode. Next, two approaches are described that explored the synthesis of simple analogues of **1.1** with the aim of forming an additional pi-stacking interaction in the p4/p5 pockets with Tyr195 of BCL-X<sub>L</sub> (Chapter 3).

To investigate whether the p5 pocket could be specifically targeted, this work next describes the synthesis, characterisation and binding studies of a series of 16 analogues of compound **1.1** incorporating a sulfonyl linker, which explore structure-activity-relationship (SAR) in this pocket (Chapter 4). Extending from

this, a strategy utilising an amide moiety as a possible isostere for the sulfonyl linker was also explored. After validating this approach with an initial trial series, it was adapted to a parallel format to generate two sets of amide-linked analogues (amide series A and B, total 16 analogues) to further explore SAR in the p5 pocket (Chapter 5). Combined, the binding and structural data described in these two Chapters represent the first reported detailed study of the p5 pocket for drug-discovery efforts; revealing it to be structurally rigid and to favour hydrophobic substituents with a level of 3-dimensional character. This led to the discovery of novel analogues with >5-fold improved binding to BCL-X<sub>L</sub> (IC<sub>50</sub>(BCL-X<sub>L</sub>) ~ 100 nM) relative to compound **1.1**.

Finally, compounds **6.1-6.3** were synthesised, which combined some of the modified substituents targeting the p5 pocket with one of the extended scaffolds targeting the p2 pocket (based on a tetrahydroisoquinoline (THIQ) core). These analogues showed a >10-fold improvement in binding to BCL-X<sub>L</sub> (IC<sub>50</sub>(BCL-X<sub>L</sub>) ~ 40 nM) relative to compound **1.1**. Selectivity studies conducted using an orthogonal surface plasmon resonance (SPR) competition assay confirmed the nanomolar binding to BCL-X<sub>L</sub> and revealed significant selectivity relative to other prosurvival proteins tested to date (BCL-W, MCL-1, or A1). Preliminary mechanism-of-action and cellular studies have been undertaken using **6.1** and **6.2** and suggest weak on-target activity (Chapter 6). Finally, a high-resolution structure has been characterised of the most potent analogue in the series, compound **6.1**, in complex with BCL-X<sub>L</sub>. These studies provide proof-of-principle studies to validate the benzoylurea series and suggest new avenues to improve affinity for BCL-X<sub>L</sub> in future.

## **Declaration**

This is to certify that

- i) this Thesis comprises only my original work towards the degree of Doctor of Philosophy except where indicated in the Preface;
- ii) due acknowledgement has been made in the text to all other material used;
- iii) this Thesis is fewer than 100,000 words in length, exclusive of tables, maps, bibliographies and appendices.

Michael James Roy

## Preface

In accordance with the regulations of the University of Melbourne, I acknowledge that some of the work in this Thesis was carried out in collaboration with colleagues at the Walter & Eliza Hall Institute (WEHI).

Specifically:

- All AlphaScreen Assay data described throughout this Thesis was provided by the Screening Group at WEHI. Various members of the Screening Group conducted these experiments.
- All HRMS data described throughout this Thesis was provided by Jason Dang at the Monash University Mass Spectrometry Facility.
- **Chapter 1** describes background unpublished work performed by others and myself, not intended to form part of my PhD work. In particular:
  - The synthesis of compounds **1.1**, **1.2**, **1.3**, **1.5**, **1.9**, **1.10** was performed by Guillaume Lessene.
  - Structural studies of compounds **1.1** and **1.10** in complex with BCL-X<sub>L</sub> were performed by Peter Czabotar.
  - The synthesis of compounds **1.4**, **1.6 – 1.8** and structural studies of compound **1.8** in complex with BCL-X<sub>L</sub> were performed by me as part of an Honours project.

- All chemical synthesis/characterisation, protein expression/purification, structural studies, SPR binding studies, mechanism-of-action studies and cellular viability assays described in **Chapters 2-7** were conducted by me, with the exception of the following (as also noted in the relevant section(s) of the text):
  - The synthesis of compounds **3.1** and **3.2c** described in **Chapter 3** was performed by Amelia Vom.
  - A repeat synthesis of compound **6.2** was performed by Amelia Vom as described in **Chapter 6** (for further characterisation studies).
  - Purified protein stocks of recombinant BCL-W and A1 used for SPR binding studies described in **Chapter 6** were provided by the Czabotar/Colman labs.
  - The generation of *BAX*<sup>-/-</sup>/*BAK*<sup>-/-</sup> chimeric mice and isolation of wild-type (WT) and *BAX*<sup>-/-</sup>/*BAK*<sup>-/-</sup> platelets for use in viability studies was performed by Stephane Chappaz

## Acknowledgments

I would like to acknowledge the expertise, enthusiasm, guidance and tremendous support of my supervisors: Guillaume Lessene, Peter Czabotar and Peter Colman. It has been wonderful to be a part of such an insightful, inspiring and cohesive team.

I thank my partner Anna for many laughs, much patience and her incredible support. My mum Janet, dad Graeme and my sister Megan have been an unshakeable source of inspiration, giving me the drive and determination to never give up. I thank Peter and Lotta Thang for welcoming me with a home away from home and my close friends family.

I would also to particularly thank Amelia Vom for her friendship, advice and collaboration on many aspects of our related projects over the past few years.

I thank all of the Chemical Biology Division, in particular the Medicinal Chemistry group (Bundoora and Parkville, both past and present): Brad Sleebs, Wilco Kersten, Romina Lessene, Ryan Brady, Jean-Marc Garnier, Michelle Gazdik, Duong Nhu, Nicole McKenzie, Christoph Grohmann, Pat Sharp, Catia Pierotti, Kimberley Kallaghan, Chris Traill, Rachel Chambers, Yelena Khakham, George Nikolakopoulos, Danny Ganame, Georgina Holloway, Jeff Mitchell, Will Nguyen, Dana Buczek, Bill Hawkins, Nick Kirk, Ping Lan, Louisa Phillipson, Jelena Medan, Thao Nguyen, Chinh Bui, Chris Burns, Ethan Goddard-Borger. I have tremendously valued the discussions I've had with each and every one of you. I additionally thank Dana Buczek and Wilco Kersten for their assistance in running numerous LCMS and mass-directed preparative HPLC samples. Thanks also to Michelle Lam, Christine DeNardo, Kylee Aumann, Mark van Delft and all members of the Kile lab, in particular Ben Kile and Stephane Chappaz for discussions and assistance with running platelet assays.

I have been fortunate to have a second home in the Structural Biology Division. I thank all of the members of the Czabotar and Colman labs (past and present):

in particular Adeline Robin, Ahmad Wardak, Rich Birkinshaw, Jason Brouwer, Angus Cowan and Geoff Thompson and Yan Hong Tan. I also thank all of the Structural Biology Division, in particular Amanda Voudouris, Matt and Melissa Call, Loges Krshnan, and lunchtime quiz host extraordinaire Cyrus Tan.

I thank David Huang and David Segal for their incredible generosity of spirit, advice and reagents and Chris Riffkin for assistance with cell culture work. I also thank the members of the WEHI Screening Group (past and present) who have been closely involved in this project over the years, in particular Kate Jarman and Helene Jousset, Hong Yang, Pat Novello and Kurt Lackovic.

I have been kept on track by a truly excellent PhD committee: Grant Dewson, Paul Stupple, Nadia Kershaw. Thank you for your enthusiasm and useful suggestions from start to finish. I also thank Keely Bumsted-O'Brien, Sue Hardy for their advice and support particularly during the challenging times that life occasionally throws your way. I thank the amazing WEHI IT gurus, in particular Rod van Cooten and Chris Fitzgerald, for keeping me plugged-in, on-line, functioning and sane.

I would like to thank our collaborators, including Doug Fairlie, Erinna Lee, Marco Evangelista at the Olivia Newton-John Cancer Research Institute; and Brian Smith at La Trobe University. Jason Dang at the Jason Dang at the Monash University Mass Spectrometry Facility has provided expert assistance with running high-resolution mass-spectrometry (HRMS) samples. I thank the CSIRO C3 Facility, in particular Janet Newman and Shane Seabrook for assistance with crystallisation screening. This use of the Australian Synchrotron has been essential for much of this work and I thank the expert beam line staff for their hard work and assistance.

I acknowledge the Walter & Eliza Hall Institute (WEHI) and Director Doug Hilton for providing such a wonderful place to have undertaken my PhD. I also acknowledge the support of the Australian Government for providing me with an Australian Postgraduate Award.



# Table of Contents

<b>Abstract.....</b>	<b>i</b>
<b>Declaration .....</b>	<b>iii</b>
<b>Preface.....</b>	<b>iv</b>
<b>Acknowledgments.....</b>	<b>vi</b>
<b>Table of Contents .....</b>	<b>viii</b>
<b>List of Figures.....</b>	<b>xiii</b>
<b>List of Tables .....</b>	<b>xvi</b>
<b>List of Schemes .....</b>	<b>xviii</b>
<b>Abbreviations used .....</b>	<b>xx</b>
<b>1 Chapter one – Introduction .....</b>	<b>1</b>
<b>1.1 Introduction.....</b>	<b>2</b>
<b>1.2 Structure-based drug design (SBDD) .....</b>	<b>4</b>
1.2.1 Notable examples of SBDD .....	4
1.2.2 Use of structure-based approaches in drug development.....	5
<b>1.3 An Overview of Apoptosis and Cancer .....</b>	<b>9</b>
<b>1.4 Interactions between members of the BCL-2 Protein Family .....</b>	<b>10</b>
<b>1.5 The BH3 domain and ‘BH3-mimetics’ .....</b>	<b>13</b>
1.5.1 BH3-mimetic molecules for anti-cancer therapy.....	13
1.5.2 Targeting Protein-Protein Interactions (PPIs) using small molecules.....	15
1.5.3 Markers of a selective BH3-mimetic .....	19
<b>1.6 Small molecule BH3-mimetics reported in the literature.....</b>	<b>22</b>
1.6.1 First generation BH3-mimetics: Acylsulfonamides .....	22
1.6.2 Second generation BH3-mimetics.....	24
<b>1.7 Therapeutic rationale for targeting BCL-X<sub>L</sub> .....</b>	<b>31</b>
<b>1.8 Origins of the benzoylurea series.....</b>	<b>33</b>
<b>1.9 Structure-guided optimisation of the benzoylurea series.....</b>	<b>37</b>
1.9.1 Negative structure-activity-relationship (SAR) studies .....	37
1.9.2 Incorporation of hydrogen bond acceptors in linker.....	38
1.9.3 Development of extended scaffolds targeting p2 pocket.....	39

1.10 Thesis Outline/Aims .....	42
1.11 References .....	43
<b>2 Chapter two – Experimental Section .....</b>	<b>57</b>
2.1 Introduction to techniques .....	58
2.1.1 X-ray Crystallography .....	58
2.1.2 Measuring binding affinity and selectivity .....	58
2.1.3 Measuring mechanism-based activity <i>in vitro</i> .....	59
2.2 General Chemistry Methods .....	61
2.2.1 General Chemistry Methods .....	61
2.2.2 General Procedure A: Carbamoyl chloride formation .....	62
2.2.3 General Procedure B: <i>In-situ</i> protection of amino acid and benzoylurea formation .....	63
2.2.4 General Procedure C: Cysteine S-alkylation and Boc-protection .....	64
2.2.5 General Procedure D: Thioether oxidation .....	64
2.2.6 General Procedure E: Boc-deprotection with HCl .....	65
2.2.7 General Procedure F: Parallel amide-coupling to benzoylurea .....	66
2.2.8 General Procedure G: TFA-deprotection .....	66
2.3 Recombinant proteins and synthetic peptides .....	67
2.3.1 Protein expression and purification .....	68
2.4 Measuring binding affinity and selectivity .....	72
2.4.1 AlphaScreen competition assay .....	72
2.4.2 SPR competition assay (Biacore 3000) .....	75
2.5 Measuring mechanism-based activity <i>in vitro</i> .....	76
2.5.1 <i>In vitro</i> cytochrome c release assay .....	76
2.5.2 Platelet-killing assay .....	78
2.5.3 MEF-viability assay .....	80
2.6 Crystallisation, X-ray data acquisition, structure determination and refinement .....	82
2.6.1 Crystallisation .....	82
2.6.2 Crystallography data collection, processing and structure refinement .....	83
2.7 References .....	85
<b>3 Chapter three – Initial studies .....</b>	<b>88</b>
3.1 Introduction .....	89
3.1.1 Interactions in the p2 pocket .....	89
3.1.2 Pi-stacking interactions in the p4 pocket .....	92

<b>3.2</b>	<b>Structure determination of extended scaffold lead molecules .....</b>	<b>97</b>
3.2.1	Structure determination of lead compounds <b>1.9</b> and <b>3.1</b> .....	97
<b>3.3</b>	<b>Pi-stacking interactions in the p4 pocket.....</b>	<b>103</b>
3.3.1	Study of benzoylurea arylsulfonamide compounds.....	103
3.3.2	Synthesis and evaluation of benzoylurea compounds <b>3.7a – 3.16</b> .....	113
3.3.3	Evaluation of BCL-X <sub>L</sub> and MCL-1 binding using AlphaScreen competition assay.....	114
3.3.4	Structure determination of the BCL-X <sub>L</sub> : <b>3.10c</b> complex .....	116
<b>3.4</b>	<b>Discussion / Conclusion.....</b>	<b>120</b>
<b>3.5</b>	<b>Experimental.....</b>	<b>122</b>
3.5.1	Chemical synthesis.....	122
3.5.2	Crystallisation and X-ray structure determination.....	126
<b>3.6</b>	<b>References.....</b>	<b>130</b>
<b>4</b>	<b>Chapter four – Sulfonyl series exploring structure-activity-relationship (SAR) of p5 pocket of BCL-X<sub>L</sub>.....</b>	<b>132</b>
<b>4.1</b>	<b>Introduction.....</b>	<b>133</b>
4.1.1	Description of the p5 pocket.....	134
4.1.2	Analogues probing the p5 pocket.....	135
<b>4.2</b>	<b>Synthesis of p5 benzoylurea sulfonyl analogues on simple biphenyl scaffold .....</b>	<b>138</b>
4.2.1	General synthesis of p5 sulfonyl analogues .....	139
4.2.2	Evaluation of BCL-X <sub>L</sub> and MCL-1 binding using AlphaScreen competition assay.....	140
4.2.3	Conclusions – initial p5 analogues.....	145
<b>4.3</b>	<b>Synthesis of p5 adamantyl analogues .....</b>	<b>146</b>
4.3.1	Introduction: the adamantyl group in drug design.....	146
4.3.2	Overcoming synthetic challenges to access adamantyl precursor .....	148
4.3.3	Synthesis of adamantyl benzoylurea analogues .....	155
4.3.4	Evaluation of BCL-X <sub>L</sub> and MCL-1 binding using AlphaScreen competition assay.....	155

<b>4.4 Structural evaluation of p5 analogues using X-ray crystallography .....</b>	<b>158</b>
4.4.1 Structure determination of the BCL-X <sub>L</sub> : <b>4.6l</b> and BCL-X <sub>L</sub> : <b>4.25</b> complexes .....	158
<b>4.5 Discussion / Conclusion.....</b>	<b>162</b>
<b>4.6 Experimental.....</b>	<b>164</b>
4.6.1 Chemical synthesis.....	164
4.6.2 Crystallisation and X-ray structure determination.....	183
<b>4.7 References.....</b>	<b>185</b>
 <b>5 Chapter five – Structure-guided linker rescaffolding to generate novel benzoylurea amides and parallel synthesis of a library of benzoylurea amides to further explore SAR of the p5 pocket of BCL-X<sub>L</sub>.....</b>	 <b>188</b>
<b>5.1 Introduction.....</b>	<b>189</b>
5.1.1 Rationale and design of an ‘amide’ linker .....	190
<b>5.2 Synthesis of a trial set of amide-linked analogues .....</b>	<b>193</b>
5.2.1 Synthesis of trial amide-linked analogues.....	194
5.2.2 Trial amide series – evaluation of BCL-X <sub>L</sub> and MCL-1 binding using AlphaScreen competition assay .....	194
5.2.3 Conclusions of trial amide-linked analogues.....	196
<b>5.3 Parallel synthesis of amide-linked analogues varying p5 substituent.....</b>	<b>197</b>
5.3.1 Synthetic approach for parallel chemistry .....	198
5.3.2 Synthesis of amide series A and series B.....	198
<b>5.4 Evaluation of BCL-X<sub>L</sub>/MCL-1 binding and binding mode .....</b>	<b>200</b>
5.4.1 Amide series A - evaluation of BCL-X <sub>L</sub> and MCL-1 binding using AlphaScreen competition assay .....	204
5.4.2 Amide series A - Structural analysis of binding interactions .....	206
5.4.3 Amide series B - evaluation of BCL-X <sub>L</sub> and MCL-1 binding using AlphaScreen competition assay .....	215
5.4.4 Amide series B - Structural analysis of binding interactions.....	216
<b>5.5 Discussion/Conclusion.....</b>	<b>220</b>
<b>5.6 Experimental.....</b>	<b>221</b>
5.6.1 Synthesis of trial amide series .....	221
5.6.2 Parallel Synthesis of amide series A and B .....	227
5.6.3 Crystallisation and X-ray structure determination.....	235
<b>5.7 References.....</b>	<b>239</b>

<b>6 Chapter six – Generation of p2 extended compounds and structural/biochemical evaluation .....</b>	<b>240</b>
<b>6.1 Introduction.....</b>	<b>241</b>
<b>6.2 Synthesis of cyclohexyl- and adamantyl- analogues using extended THIQ scaffold targeting the p2 pocket.....</b>	<b>245</b>
6.2.1 General synthetic approach to compound <b>6.1</b> .....	245
6.2.2 Synthetic challenges encountered during synthesis of compound <b>6.2</b> .....	246
6.2.3 Modified approaches to access compound <b>6.2</b> .....	251
<b>6.3 Evaluation of binding of compounds 6.1 – 6.3.....</b>	<b>257</b>
6.3.1 Extended scaffold compounds <b>6.1 – 6.3</b> - evaluation of BCL-X <sub>L</sub> and MCL-1 binding using AlphaScreen competition assay.....	257
6.3.2 Crystallisation and X-ray structure determination.....	259
6.3.3 Evaluation of selectivity – SPR competition assay (Biacore 3000).....	263
<b>6.4 Further biochemical validation – preliminary selectivity/mechanism of action and cell-viability studies .....</b>	<b>267</b>
6.4.1 Evaluation of compounds <b>6.1</b> and <b>6.2</b> in the <i>in-vitro</i> cytochrome <i>c</i> release assay.....	267
6.4.2 Platelet-killing assay .....	270
6.4.3 MEF viability assay .....	273
<b>6.5 Discussion/Conclusion.....</b>	<b>277</b>
<b>6.6 Experimental.....</b>	<b>279</b>
6.6.1 Chemical synthesis.....	279
6.6.2 Crystallisation and X-ray structure determination.....	288
<b>6.7 References.....</b>	<b>289</b>
<b>7 Chapter seven – Conclusions.....</b>	<b>291</b>
<b>7.1 Conclusions and future directions .....</b>	<b>292</b>
<b>7.2 References.....</b>	<b>305</b>
<b>8 Appendices.....</b>	<b>307</b>

## List of Figures

### Chapter 1

Figure 1.1: Overview of the BCL-2 protein family and interactions.	11
Figure 1.2: Selectivity of BH3 peptide and small molecule antagonists of prosurvival BCL-2 family proteins.	21
Figure 1.3: Targeting structural/sequence differences between BCL-2 and BCL-X <sub>L</sub> .	27
Figure 1.4: Structure-guided <i>de novo</i> design of benzoylurea series.	34
Figure 1.5: Initial studies on AlphaScreen hit compound <b>1.1</b>	36
Figure 1.6: Design of scaffolds with p2 extension to make use of interactions in p2 pocket.	40

### Chapter 3

Figure 3.1: Series progression to compounds <b>1.9</b> and <b>3.1</b> .	91
Figure 3.2: Analogues exploring pi-stacking interaction in p4 pocket.	95
Figure 3.3: X-ray crystal structures of the BCL-X <sub>L</sub> : <b>1.9</b> and BCL-X <sub>L</sub> : <b>3.1</b> complexes	100
Figure 3.4: Analysis of the self-rotation function and unit cell of the BCL-X <sub>L</sub> : <b>3.2c</b> complex.	106
Figure 3.5: Compound <b>3.2c</b> modeled into the groove of a representative BCL-X <sub>L</sub> monomer in the BCL-X <sub>L</sub> : <b>3.2c</b> structure.	110
Figure 3.6: X-ray crystal structure of BCL-X <sub>L</sub> : <b>3.10c</b> complex	118

### Chapter 4

Figure 4.1: Structural engagement of ligands in the p5 pocket of BCL-X <sub>L</sub> .	136
Figure 4.2: Plot of AlphaScreen data for p5 sulfonyl analogues.	143
Figure 4.3: Use of the adamantyl group as an isostere of an aromatic pi-stacking interaction in the p4 and p5 pockets of BCL-X <sub>L</sub> .	147
Figure 4.4: Relative reactivity of various alkyl halides to nucleophilic substitution.	150
Figure 4.5: X-ray crystal structures of BCL-X <sub>L</sub> : <b>4.6l</b> and BCL-X <sub>L</sub> : <b>4.25</b> complexes.	160

## Chapter 5

Figure 5.1: Origins of the amide-linked series.	192
Figure 5.2: Initial amide-linked analogues organised according to the overall linker length.	196
Figure 5.3: Crystal structures of BCL-X <sub>L</sub> : <b>5.19g</b> and BCL-X <sub>L</sub> : <b>5.10b</b> complexes from amide series A.	208
Figure 5.4: Crystal structure of the BCL-X <sub>L</sub> : <b>5.19e</b> complex from amide series A.	212
Figure 5.5: Crystal structures of the BCL-X <sub>L</sub> : <b>5.19d</b> complex (as a mixture of stereoisomers) from amide series A.	213
Figure 5.6: Crystal structures of BCL-X <sub>L</sub> : <b>5.15a</b> and BCL-X <sub>L</sub> : <b>5.23e</b> complexes from amide series B.	218

## Chapter 6

Figure 6.1: Summary of benzoylurea series described in this Thesis.	243
Figure 6.2: X-ray crystal structure of the BCL-X <sub>L</sub> : <b>6.1</b> complex.	261
Figure 6.3: Plot of selectivity data (from <b>Table 6.4</b> ) for selected lead compounds tested against BCL-X <sub>L</sub> , BCL-W, MCL-1 and A1, determined by SPR competition assay (Biacore 3000).	266
Figure 6.4: Preliminary results suggesting compounds <b>6.1</b> and <b>6.2</b> are able to induce a partial release of cytochrome c from isolated mitochondria from <i>MCL-1</i> <sup>-/-</sup> MEFs (which contain only BCL-X <sub>L</sub> to restrain BAK/BAX).	269
Figure 6.5: Results from platelet killing assay using washed wild-type (WT) and BAX/BAK-deficient ( <i>BAX</i> <sup>-/-</sup> / <i>BAK</i> <sup>-/-</sup> ) platelets.	272
Figure 6.6: Results from cell viability assay using cultured <i>MCL-1</i> <sup>-/-</sup> and wild-type (WT) MEFs.	275

## Chapter 7

Figure 7.1: Summary of benzoylurea series progression described in this Thesis.

303

## Appendix

Figure A1:  $^1\text{H}$  NMR and LCMS data for compound **6.15**. A1

Figure A2:  $^1\text{H}$  NMR and LCMS data for compound **6.18**. A2

Figure A3: LCMS Analysis of direct benzoylurea reaction to form compound **6.2** (at 5 minutes), showing formation of species A-E and the assigned chemical structures of these species (black box). A3

Figure A4: (A) LCMS of reaction mixture (at 1 h) for conversion of compound **6.18** to **6.21**. (B) LCMS of reaction mixture (at 1 h) for conversion of compound **6.15** to **6.22**. A4

Figure A5: (A) LCMS Analysis of reaction mixture (at 16 h) for conversion of compound **6.21** to **1.10**, showing peak for product formation. (B)  $^1\text{H}$  NMR spectrum (MeOD) of purified compound **1.10**. A5

Figure A6: LCMS Analysis of compound **6.2** synthesised using the direct route (A, B) or alternative route *via* reductive amination (C). A6

Figure A7:  $^1\text{H}$  NMR spectra of compound **6.2** synthesised using the direct route (A, B) and alternative route *via* reductive amination (C). A7

Figure A8:  $^1\text{H}$  NMR spectra of compound **6.8** isolated from the same reaction as the free tertiary amine (A) and as the corresponding HCl salt (B), showing changes in chemical shift of the four methylene protons adjacent to the THIQ tertiary amine in response to the protonation state of the tertiary amine. A8

Figure A9:  $^1\text{H}$  NMR spectra of compound **6.7** synthesised using two different methods, either (A) *via* N-alkylation with compound **6.6**, or (B) *via* reductive amination with compound **6.4**. A9



## List of Tables

### Chapter 1

Table 1.1: IC <sub>50</sub> values of benzoylurea compounds for BCL-X <sub>L</sub> and MCL-1 (determined by AlphaScreen competition assay (A.S.))	41
---	----

### Chapter 2

Table 2.1: Purified recombinant protein stocks	67
Table 2.2: Expression constructs	68

### Chapter 3

Table 3.1: IC <sub>50</sub> values of benzoylurea compounds for BCL-X <sub>L</sub> and MCL-1 (determined by AlphaScreen competition assay, pre-2015 data)	90
Table 3.2: Crystallographic statistics for the BCL-X <sub>L</sub> : <b>1.9</b> and BCL-X <sub>L</sub> : <b>3.1</b> complexes	102
Table 3.3: Refinement statistics for the BCL-X <sub>L</sub> : <b>3.2c</b> complex, with the ligand (4 copies) modeled in either the 'closed' or 'open' benzoylurea conformations	109
Table 3.4: Crystallographic statistics for the BCL-X <sub>L</sub> : <b>3.2c</b> complex	111
Table 3.5: IC <sub>50</sub> values for compounds <b>3.7a-b</b> , <b>3.10a-c</b> , <b>3.13</b> and <b>3.16</b> for BCL-X <sub>L</sub> and MCL-1 (determined by AlphaScreen Assay, pre-2015 data)	114
Table 3.6: Crystallographic statistics for the BCL-X <sub>L</sub> : <b>3.10c</b> complex	119

### Chapter 4

Table 4.1: IC <sub>50</sub> values of benzoylurea p5 sulfonyl compounds for BCL-X <sub>L</sub> and MCL-1 (determined by AlphaScreen competition assay, pre-2015 data)	141
Table 4.2: IC <sub>50</sub> values of benzoylurea compounds <b>4.23</b> and <b>4.25</b> for BCL-X <sub>L</sub> and MCL-1 (determined by AlphaScreen competition assay, post-2015 data)	157
Table 4.3: Crystallographic statistics for the BCL-X <sub>L</sub> : <b>4.6l</b> and BCL-X <sub>L</sub> : <b>4.25</b> complexes	161

## Chapter 5

Table 5.1: IC <sub>50</sub> values of initial amide-linked benzoylurea compounds for BCL-X <sub>L</sub> and MCL-1 (determined by AlphaScreen competition assay, pre-2015 data)	195
Table 5.2: IC <sub>50</sub> values of amide series A benzoylurea compounds for BCL-X <sub>L</sub> and MCL-1 (determined by AlphaScreen competition assay, pre-2015 data)	201
Table 5.3: IC <sub>50</sub> values of amide series B benzoylurea compounds for BCL-X <sub>L</sub> and MCL-1 (determined by AlphaScreen competition assay, pre-2015 data)	202
Table 5.4: IC <sub>50</sub> values of selected amide series A compounds for BCL-X <sub>L</sub> and MCL-1 (determined by AlphaScreen competition assay, post-2015 data)	203
Table 5.5: Crystallographic statistics for the BCL-X <sub>L</sub> : <b>5.19g</b> and BCL-X <sub>L</sub> : <b>5.10b</b> complexes	209
Table 5.6: Four diastereomers modeled into BCL-X <sub>L</sub> : <b>5.19d</b> structure and final refinement statistics for each.	211
Table 5.7: Crystallographic statistics for the BCL-X <sub>L</sub> : <b>5.19e</b> and BCL-X <sub>L</sub> : <b>5.19d(SRR)</b> complexes	214
Table 5.8: Crystallographic statistics for the BCL-X <sub>L</sub> : <b>5.15a</b> and BCL-X <sub>L</sub> : <b>5.23e</b> complexes	219

## Chapter 6

Table 6.1: Affinity of simple biphenyl and extended scaffold compounds for BCL-X <sub>L</sub> and MCL-1 (determined by AlphaScreen Assay, post-2015 data)	244
Table 6.2: Affinity of extended scaffold compounds <b>6.1-6.3</b> for BCL-X <sub>L</sub> and MCL-1 (determined by AlphaScreen Assay, post-2015 data)	258
Table 6.3: Crystallographic statistics for the BCL-X <sub>L</sub> : <b>6.1</b> complex	262
Table 6.4: Selectivity data for selected lead compounds tested against BCL-X <sub>L</sub> , BCL-2, MCL-1 and A1, determined by SPR competition assay (Biacore 3000)	265

## List of Schemes

### Chapter 2

Scheme 2.1: General Procedures A and B.	62
Scheme 2.2: General Procedures C – E.	64
Scheme 2.3: General Procedures F – G.	65

### Chapter 3

Scheme 3.1: Synthetic approach to form compounds <b>3.2a-b</b> .	112
Scheme 3.2: Synthesis of analogues <b>3.7a-b</b> , <b>3.10a-c</b> , <b>3.13</b> and <b>3.16</b> , to explore pi-stacking interactions in the p4 pocket of BCL-X <sub>L</sub> .	113

### Chapter 4

Scheme 4.1: Synthesis of sulfonyl series of p5 analogues.	138
Scheme 4.2: Proposed synthetic routes to adamantyl-substituted L-cysteine derivatives.	148
Scheme 4.3: Successful synthetic route to adamantyl-substituted L-cysteine derivatives <b>4.19</b> and <b>4.21</b> and benzoylurea analogues <b>4.23</b> and <b>4.25</b> .	154

### Chapter 5

Scheme 5.1: Synthesis of trial set of amide-linked analogues.	193
Scheme 5.2: General strategy for parallel synthesis of amide series A and B.	197
Scheme 5.3: Parallel synthesis of amide series A and series B.	199

## Chapter 6

Scheme 6.1: Synthesis of cyclohexyl sulfonyl analogue <b>6.1</b> on extended tetrahydroisoquinoline (THIQ) scaffold, designed to interact with p2 pocket and have modified substituent in p5 pocket.	246
Scheme 6.2: Unanticipated loss of p2 chlorobiphenyl fragment during synthesis of compounds <b>6.2</b> and <b>1.10</b> , to instead form debenzylated derivatives <b>6.15</b> and <b>6.18</b> .	248
Scheme 6.3: Possible mechanism of debenzylation side-reaction.	250
Scheme 6.4. Reinstallation of p2 fragment via decarbonylation followed by reductive amination.	254
Scheme 6.5. Synthesis of compound <b>6.3</b> using the alternative synthetic route.	256

## Abbreviations used

(NH <sub>4</sub> ) <sub>2</sub> SO <sub>4</sub>	Ammonium sulfate
Å	Ångström (1Å = 10 <sup>-10</sup> m)
ADME	Absorption, distribution, metabolism and excretion
ADMET	Absorption, distribution, metabolism, excretion and toxicity
AJ	Aster Jandl anticoagulant
ALL	Acute lymphoblastic leukemia
AlphaScreen™	<u>A</u> mplified <u>l</u> uminescent <u>p</u> roximity <u>h</u> omogeneous <u>a</u> ssay (Perkin-Elmer Lifesciences)
A.S.	AlphaScreen
A.S.U.	Asymmetric unit
a.u.	Absorbance units
BEI	Binding efficiency index
BH domain	<u>B</u> CL-2 <u>h</u> omology domain
BTMSA	<i>N,O</i> -bis(trimethylsilyl)acetamide
BSA	Bovine serum albumin
CLL	Chronic lymphocytic leukaemia
ClogP	Calculated log P (base 10 logarithm of the calculated octanol/water partition coefficient)
DIEA	Diisopropylethylamine
DME	Dulbecco's modified Eagle's medium
DMF	Dimethylformamide
DMSO	Dimethyl sulfoxide
DNA	Deoxyribonucleic acid
DTT	Dithiothreitol
ECL	Enhanced chemiluminescence
EC <sub>50</sub>	Half-maximal effective concentration
EDCI	1-Ethyl-3-(3-dimethylaminopropyl)carbodiimide
EDTA	Ethylenediaminetetraacetic acid
EGTA	Ethylene glycol tetraacetic acid

ER	Endoplasmic reticulum
Et <sub>2</sub> O	Diethyl ether
EtOAc	Ethyl acetate
FACS	Fluorescence-assisted cell sorting
FBDD	Fragment-based drug discovery
FCS	Foetal calf serum
FDA	US Food and Drug Administration
GPCR	G-protein coupled receptor
GST	Glutathione S-transferase
HBTU	<i>O</i> -(Benzotriazol-1-yl)- <i>N,N,N',N'</i> -tetramethyluronium hexafluorophosphate
HDAC	Histone deacetylase
HEPES	4-(2-hydroxyethyl)-1-piperazineethanesulfonic acid
HOBt	1-Hydroxybenzotriazole
HPLC	High-performance liquid chromatography
HRP	Horseradish peroxidase
HSA	Human serum albumin
HSQC	Heteronuclear single-quantum correlation
HTPBS	Human tonicity phosphate buffered saline
IC <sub>50</sub>	Half-maximal inhibitory concentration
IPTG	Isopropyl β-D-1-thiogalactopyranoside
IR	Infra-red
K <sub>D</sub>	Equilibrium dissociation constant
K <sub>i</sub>	Inhibition constant
LCMS	Liquid chromatography / mass spectrometry
LE	Ligand efficiency
LLE	Lipophilic ligand efficiency
MeCN	Acetonitrile
MEF	Mouse embryonic fibroblast
MES	2-( <i>N</i> -morpholino)ethanesulfonic acid
MgOAc	Magnesium acetate
MOMP	<u>M</u> itochondrial <u>o</u> uter- <u>m</u> embrane <u>p</u> ermeabilisation

MTPBS	Mouse tonicity phosphate buffered saline
MW	Molecular weight
MWCO	Molecular weight cut-off
NaOAc	Sodium acetate
NCI	US National Cancer Institute
NCS	Non-crystallographic symmetry
ND	Not determined
NHS	N-hydroxysuccinimide
NiCl <sub>2</sub>	Nickel chloride
NMR	Nuclear magnetic sesonance
NSCLC	Non-small cell lung cancer
OD	Optical density
PARP	Poly (ADP-ribose) polymerase
PDB	Protein Data Bank
PEG	Polyethylene glycol
PI	Propidium iodide
PI3K	Phosphatidylinositol-3-kinase
PMSF	Phenylmethylsulfonyl fluoride
PPI	Protein-protein interaction
PS	Phosphatidylserine
R.U.	Response units
RFU	Relative fluorescence units
rmsd	Root-mean-square deviation
RO5	'Rule-of-5' (Lipinski and others)
SAR	Structure-activity relationship
SBDD	Structure-based drug design
SCLC	Small cell lung cancer
SCX	<u>S</u> trong <u>c</u> ation <u>e</u> xchange
S.D.	Standard deviation
SDS-PAGE	<u>S</u> odium <u>d</u> odecyl <u>s</u> ulfate <u>p</u> oly <u>a</u> crylamide <u>g</u> el <u>e</u> lectrophoresis
S.E.M.	Standard error-of-mean
S <sub>N</sub> 1	<u>U</u> nimolecular <u>n</u> ucleophilic <u>s</u> ubstitution

S <sub>N</sub> 2	<u>B</u> imolecular <u>n</u> ucleophilic <u>s</u> ubstitution
SPR	Surface plasmon resonance
STD	Saturation transfer difference
SV40	Simian vacuolating virus 40
TBS	Tris buffered saline
TFA	Trifluoroacetic acid
THIQ	Tetrahydroisoquinoline
TLS	Translation, libration and screw-rotation
TM	Transmembrane
TMSOTf	Trimethylsilyl trifluoromethanesulfonate
Tris	Tris(hydroxymethyl)aminomethane
U.	Units
VDAC	Voltage-dependant anion channel
WEHI	Walter & Eliza Hall Institute
WT	Wild-type



# **1 Chapter one – Introduction**

## 1.1 Introduction

Apoptosis (a key form of programmed cell death) is a cellular mechanism with important roles in normal tissue development, homeostasis and the immune response<sup>(1)</sup>. Proteins of the BCL-2 family are key regulators of the intrinsic (or mitochondrial) pathway to apoptosis. This family contains both prosurvival and proapoptotic members, whose complex competing interactions control the life/death fate of the cell. Importantly, deregulated apoptosis is observed in most types of cancer - often *via* overexpression of prosurvival BCL-2 family proteins, such as BCL-X<sub>L</sub>. Overexpression of BCL-X<sub>L</sub> in certain cancer types appears to contribute to both malignant progression as well as to acquired resistance to traditional anti-cancer chemotherapeutics<sup>(2)</sup>, many of which rely on inducing tumour cell apoptosis.

The idea that cancer cells may depend on heightened expression of prosurvival BCL-2 family proteins in order to escape apoptosis has led to the search for novel targeted anti-cancer therapeutics to inhibit these proteins. This includes so-called 'BH3 mimetic' compounds, which aim to inhibit prosurvival proteins by mimicking the key functional domain that mediates BCL-2 family interactions, the 'BH3' domain. Information on the key molecular interactions from structural studies of BH3 domains from various BCL-2 family proteins in complex with prosurvival counterparts has informed the development of a number of small molecule BH3-mimetics<sup>(3-7)</sup>. One such BH3 mimetic is **ABT-737**, which potently inhibits a subset of prosurvival BCL-2 family proteins, including BCL-X<sub>L</sub>, BCL-2 and BCL-W<sup>(8)</sup>. Design of small molecule inhibitors able to selectively target one or more prosurvival BCL-2 family proteins is an area of significant current research interest<sup>(9)</sup>.

A rational design program in the Chemical Biology (Medicinal Chemistry) division at WEHI led to the discovery of compound **1.1** (see **Section 1.7, Figure 1.5**), a lead small molecule exhibiting promising ( $\mu$ M) binding and selectivity for BCL-X<sub>L</sub>. An X-ray crystal structure solved of this compound in complex with BCL-X<sub>L</sub> provided the opportunity for structure-based design of new analogues. Drawing on

comparisons with successful published BH3-mimetics (in particular the published X-ray crystal structure of **ABT-737** in complex with BCL-X<sub>L</sub><sup>(10)</sup>), this thesis will address the structure-based rational design, synthesis and characterisation of novel analogues of compound **1.1**, seeking inhibitors with improved affinity and selectivity towards BCL-X<sub>L</sub>. For new analogues binding affinity data for BCL-X<sub>L</sub>, crystal structural analysis of the binding mode with BCL-X<sub>L</sub>, relevant BCL-2 family selectivity data and preliminary mechanistic studies will be presented.

## **1.2 Structure-based drug design (SBDD)**

Over the last 25-30 years, owing in particular to close collaborations between medicinal chemists and structural biologists, structure-guided approaches have played instrumental roles in the development of many novel therapeutics <sup>(11-17)</sup>. Knowledge of the 3-dimensional structure of a biological target - based on data from complementary approaches including X-ray crystallography, nuclear magnetic resonance (NMR) spectroscopy or molecular modelling - has become a powerful aid to the process of designing, selecting and optimising of small molecule inhibitors against known biological targets. Coupled with sensitive biophysical approaches and screening technologies (including fragment-based, high-throughput and virtual screening), some form of SBDD is nowadays a near-essential component of most drug development pipelines within both industry and academia.

### **1.2.1 Notable examples of SBDD**

The potential value of X-ray or NMR-derived structural information for the development of novel therapeutics was already anticipated over 30 years ago, but at that time reportedly structure-based approaches were still prohibitively expensive and time-consuming for routine use<sup>(11)</sup>. Since then however, improvements in protein production methodologies, instrumentation, automation, computing power and software, have gradually increased the availability of SBDD as a tool in the complex process of pharmaceutical development, in particular to accelerate early-stage drug discovery<sup>(18)</sup>.

It is important to note that the majority of drugs marketed to date have not been developed directly or solely using SBDD - many were approved before its routine use and equally for many targets detailed structures are simply not yet routinely possible. It is estimated for example that 60-70% of drugs on the market target integral membrane proteins<sup>(15)</sup>, which still represent challenging targets for both structural biology and drug design (notwithstanding the significant advances that

have been achieved in the study of certain target classes, for example GPCRs and ion channels)<sup>(19-21)</sup>.

In spite of this, over the last 30 years there have certainly been some profound examples of SBDD enabling drug discovery efforts; in particular, the successful development during the 1980s and 1990s of novel anti-viral drugs designed to target the known structures of the HIV-1 protease and the influenza virus neuraminidase<sup>(17, 22-28)</sup>. A 2003 study by Hardy and Malikayil reported over 40 compounds stemming from structure-based drug design efforts which, at that time, had reached clinical trials. Of those, 7 had successfully been approved and marketed<sup>(14)</sup>. In the cancer therapeutics field alone, SBDD has contributed to inhibitor development for targets including protein kinases, lipid phosphatidylinositol-3-kinases (PI3Ks), Histone deacetylases (HDACs), Poly (ADP-ribose) polymerase (PARP), heat shock protein 90 (Hsp90) as well as recent inhibitors of protein-protein interactions (PPIs), eg. bromodomain-containing proteins and BCL-2 family proteins<sup>(15, 29)</sup>.

### **1.2.2 Use of structure-based approaches in drug development**

Structure-based approaches have proven to be useful at a number of stages of the drug-discovery process: from understanding the target as a structural class, generating novel hits, optimising affinity and selectivity during the hit-to-lead stage, even to understanding resistance and metabolism - this section will provide a short summary and relevant examples of each.

#### ***1.2.2.1 Defining the target and hit-generation***

As high-resolution structural information becomes more available, knowledge from structural biology is now being used at an earlier stage than ever to guide the drug development process.

In the initial stages, structural information can assist in the identification and selection of a target, including assessment of the “druggability” of a particular interface<sup>(30)</sup>. This is particularly important as we expand our outlook to consider more challenging target classes, such as protein-protein interactions (PPIs), in which structural information in combination with techniques such as alanine-scanning mutagenesis can be useful to identify targetable “hotspot” residues<sup>(11, 29)</sup>.

Structural studies can guide our knowledge about a particular protein class – such as kinases, for which comparison of multiple bound and unbound structures has built up over time an understanding of the architectural features of the protein family and the different conformational states which might be targeted by inhibitors<sup>(15)</sup>.

Improvements in computation, automation and fragment-based techniques are also assisting in hit generation. The structural genomics era has yielded new crystallisable constructs, protocols for expression and purification, as well as methods for automation<sup>(15)</sup>. In recent years fragment-based drug discovery (FBDD) methods have increased in popularity as a starting-point for hit generation, as an alternative to traditional high-throughput screening of large chemical libraries<sup>(31)</sup>. In general, FBDD utilises much smaller libraries of low molecular weight chemical ‘fragments’, coupled with very sensitive screening techniques such as NMR-based saturation transfer difference (STD) experiments<sup>(32)</sup>, or other biophysical methods such as surface plasmon resonance (SPR), as a starting point to leads with hopefully higher ligand efficiency. Improved automation is also enabling fragment screening by X-ray crystallography (by soaking individual fragments or pools of fragments into a protein crystal), which can additionally yield information on the site and mode of fragment binding<sup>(11, 31)</sup>.

In addition, while still incredibly challenging, X-ray crystal structures can guide virtual screening of molecules to generate novel hits or to assist in the ranking of possible synthesisable compounds, in certain cases for *de novo* design or structure-

guided chemistry, or simply as a guide for developing combinatorial libraries for use in more conventional screening<sup>(11)</sup>.

Finally, two-dimensional NMR experiments (such as <sup>15</sup>N-/<sup>1</sup>H-heteronuclear single-quantum correlation (HSQC) experiments) are another important method for ligand screening, that can also provide valuable binding site information where resonance assignments have been mapped (which is particularly amenable for smaller protein targets eg. 30-40 kDa) <sup>(32)</sup>. This approach has also been successfully extended to the lead optimisation stage, such as the ‘SAR by NMR’ method pioneered by the Fesik lab at Abbott Laboratories<sup>(33)</sup>.

#### *1.2.2.2 Hit-to-lead drug development – driving affinity, selectivity*

Chemical space is vast - it is estimated for example that there exist over 10<sup>40</sup> possible compounds with a molecular weight < 750Da<sup>(34, 35)</sup>. In light of these many combinatorial possibilities, structure-guided design can be an incredibly useful guide to accelerate the iterative design/synthesis/evaluation process of optimising of a lead molecule for a target<sup>(15)</sup>. Although ultimate progress toward clinical application of a small molecule drug candidate also requires favourable ADMET properties (absorption, distribution, metabolism, excretion, toxicity) such as oral bioavailability, initial development will generally focus on developing high target binding affinity and selectivity<sup>(30, 36)</sup>. Both high affinity and selectivity are important to minimise the required dose and the likelihood of off-target toxicities, or to ensure the biological utility of a tool compound.

High binding affinity for a protein target requires complementarity of ligand size, shape and electronic configuration for the binding site in question<sup>(37, 38)</sup>. A high-resolution protein structure obtained *via* X-ray crystallography or solution NMR spectroscopy can thus quickly enable the visualisation and quantification of potential targetable contacts - such as hydrogen bonds, electrostatic interactions or nearby hydrophobic pockets<sup>(37)</sup>. In this way, rational changes can be made to the molecule in an attempt to “design in” affinity for the target of interest. Conversely, useful structural comparisons might be made to related proteins in

order to “design out” certain interactions and improve selectivity. Successful examples include: using structures of BCL-2 family inhibitors bound to human serum albumin (HSA) to guide modifications designed to decrease off-target HSA binding and thereby improve potency <sup>(8)</sup>; as well as the structure-guided changes important for development of the BCL-2 selective inhibitor **ABT-199** (described below, **Section 1.4.3**).

If the structure of the direct target is not known, but the structure of a related protein has been solved, homology modelling can also provide a useful guide for drug design. In general a good homology model can be generated if the related protein shares > 30% sequence identity<sup>(11)</sup>. Numerous drug design efforts against protein kinases have utilised this approach - experimentally determined structures are only available for approximately 50% of the > 500 kinases described in the human genome<sup>(15)</sup>.

#### *1.2.2.3 Understanding resistance, metabolism*

Even in cases where no structural information was available prior to the development of first-generation inhibitors, retrospective structural analysis can also prove useful for the development of second- or third- generation inhibitors, or to understand drug metabolism. For example, crystallographic analysis of the ABL tyrosine kinase bound to imatinib has assisted with understanding how structural mutations in ABL confer resistance to the drug<sup>(11, 39)</sup>. Structures of human cytochrome P450 enzymes and co-crystal structures in complex with bound compounds have also contributed to our understanding of drug metabolism<sup>(11)</sup>.



### 1.3 An Overview of Apoptosis and Cancer

Apoptosis is a carefully regulated biological process of programmed cell death, which plays a crucial role in multicellular organisms for ensuring correct tissue development, homeostasis and for removing damaged and infected cells<sup>(1, 40, 41)</sup>. Many disease states are associated with dysregulation of the apoptotic process, most notably degenerative diseases (unwanted cell death) and cancer (unwanted cell survival).

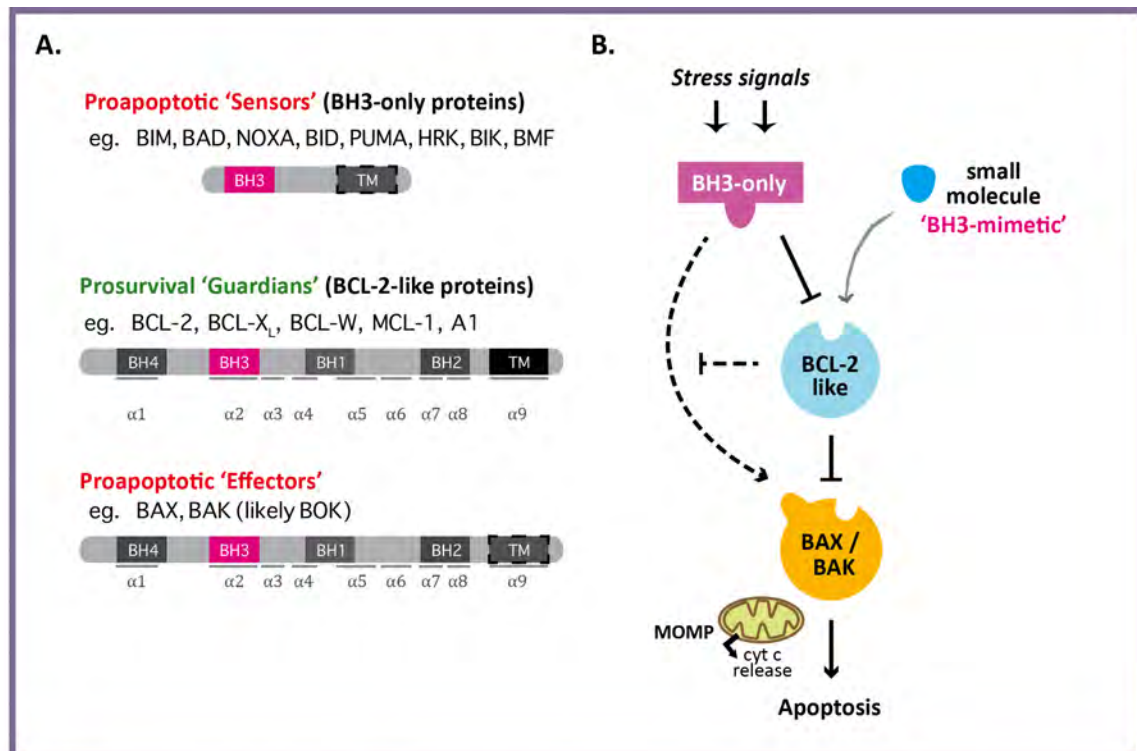
In normal cells, a variety of cellular stress signals (e.g. hypoxia, DNA damage, or nutrient withdrawal) can act upstream to trigger apoptosis by way of the ‘intrinsic’ (or mitochondrial) pathway. The ultimate downstream effect is an irreversible permeabilisation of the mitochondrial outer membrane (MOMP), which commits the cell to death. MOMP causes release of cytochrome *c* (and other factors) into the cytosol, where it combines with APAF1 to form the apoptosome<sup>(42-45)</sup>. This triggers activation of the initiator caspases-9 and downstream effector caspases that then demolish vital functional and structural cellular components, until the dying cell is ultimately engulfed by macrophages<sup>(45, 46)</sup>. At the mitochondrial outer membrane, the key effectors of MOMP are the proteins BAK and BAX, part of an extended ‘BCL-2 family’ of pro- and anti-apoptotic proteins whose interactions together form a ‘molecular switch’ regulating intrinsic apoptotic cell death<sup>(9)</sup>.

Interruption of normal apoptosis has been recognised as a hallmark of the development and continued proliferation of cancer cells<sup>(47)</sup>. For example, as cancer cells commonly experience stress conditions such as hypoxia in the tumour microenvironment, there tends to be a positive selection pressure for cells that have acquired adaptations that interrupt the stress-induced BCL-2-regulated apoptosis pathway. Similarly, most anti-cancer therapies rely at least in part on triggering tumour cell death via the intrinsic apoptotic pathway. Deregulation of BCL-2 family-mediated apoptosis is thus also associated both with poor initial response to chemotherapy, as well as the subsequent emergence of acquired resistance to chemotherapy.

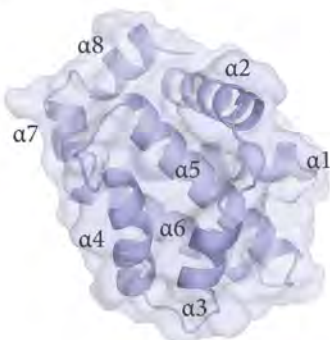
## 1.4 Interactions between members of the BCL-2 Protein Family

In mammals, five prosurvival BCL-2 family proteins (BCL-X<sub>L</sub>, BCL-W, MCL-1, and A1) hold apoptosis at bay, by binding to and sequestering BAK and BAX<sup>(46, 48, 49)</sup>. Despite their opposing functions, the prosurvival proteins as well as BAK and BAX share remarkable sequence and structural homology: each have four conserved so-called 'BCL-2 homology' (BH) domains (BH1 - BH4), a C-terminal membrane anchoring sequence, and similar overall fold (**Figure 1.1A**)<sup>(1, 3, 46, 50, 51)</sup>.

Cellular stress signals lead to upregulation or activation of a third more distantly related group, the proapoptotic 'BH3-only' proteins (e.g. BIM, BAD, PUMA, NOXA)<sup>(52)</sup> which are able to unleash BAK/BAX from an inactive state, allowing them to oligomerise and trigger MOMP<sup>(53, 54)</sup>. Ongoing studies into this mechanism point to both the disruption of complexes formed with prosurvival proteins by 'sensitizer' BH3-only proteins, as well as the existence of 'activator' BH3-only proteins that can additionally directly activate BAK and BAX (**Figure 1.1B**, solid and dashed lines, respectively)<sup>(55, 56)</sup>. BH3-only proteins share only their namesake, the BH3 domain, with their BCL-2 family relatives. This region is crucial for their killing activity; mutational, biochemical and structural studies have shown it to be a key mediator of hetero-typic interactions between BCL-2 family members<sup>(4, 5, 55, 57, 58)</sup>.



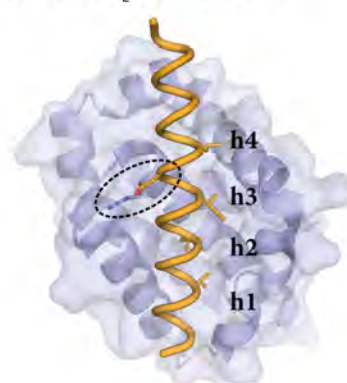
**C.** BCL-X<sub>L</sub>



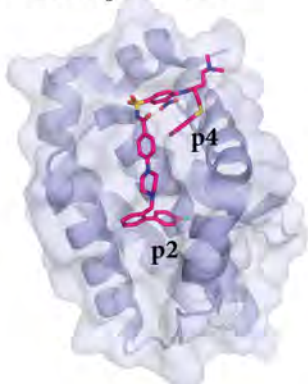
**D.** BCL-X<sub>L</sub>: BIM BH3



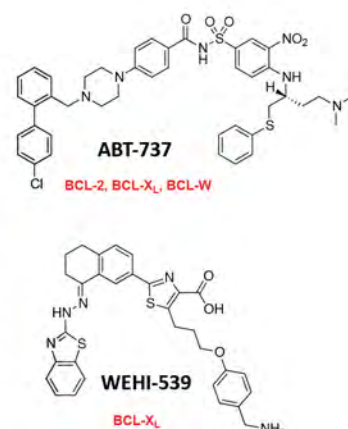
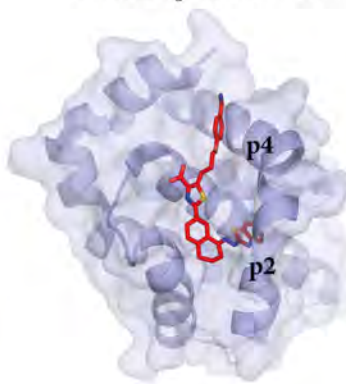
**E.** BCL-X<sub>L</sub>: BAX BH3



**F.** BCL-X<sub>L</sub>: ABT-737



**G.** BCL-X<sub>L</sub>: WEHI-539



## Figure 1.1: Overview of the BCL-2 protein family and interactions.

(previous page)

(A) The BCL-2 family of proteins and their domain architecture. Both the prosurvival ‘Guardians’ (including BCL-2, BCL-X<sub>L</sub>) and the proapoptotic ‘Effectors’ (including BAK, BAX) share regions of sequence homology, so-called BCL-2 Homology (BH) Domains (BH1-4) and a similar overall fold, consisting of a characteristic 8  $\alpha$ -helical bundle and a C-terminal membrane-anchoring (TM) sequence. The ‘Sensor’ BH3-only proteins share only the BH3 domain and are otherwise structurally more diverse. Notably, not all BH3-only proteins possess a C-terminal membrane-anchoring (TM) sequence, and the C-terminal TM domain of BOK differs in that it targets BOK for specific localisation to the Golgi apparatus and endoplasmic reticulum (ER)<sup>(59)</sup>. **(B) Interactions of BCL-2 family proteins in the intrinsic apoptotic pathway.** Small molecules designed to mimic the BH3 domain of BCL-2 family proteins (‘BH3-mimetics’) are able to bind prosurvival BCL-2 family proteins such as BCL-X<sub>L</sub>. Inhibition of the requisite complement of prosurvival proteins in a particular cell type can relieve the inhibition on BAK and BAX, triggering mitochondrial outer membrane permeabilisation (MOMP) and subsequent cytochrome *c* release, allowing apoptosis to occur. **(C-E) X-ray crystal structures of *apo* BCL-X<sub>L</sub> and BCL-X<sub>L</sub> in complex with BH3 peptides or small molecule BH3-mimetics (PDB entries: 1MAZ<sup>(3)</sup>, 1PQ1<sup>(6)</sup>, 3PL7<sup>(60)</sup>, 2YXJ<sup>(10)</sup>, 3ZLR<sup>(61)</sup>.** In all cases BCL-X<sub>L</sub> molecules are depicted in analogous orientations. The four key hydrophobic residues (h1-h4) of the BH3 peptides (and corresponding hydrophobic pockets p2, p4) are indicated, as well as the salt bridge formed between the conserved Asp of the BH3 peptides and Arg139 of BCL-X<sub>L</sub> (circled).

## 1.5 The BH3 domain and ‘BH3-mimetics’

The crystal structure solved in 1996 of human prosurvival BCL-X<sub>L</sub> revealed an elongated hydrophobic cleft present on the surface of the protein formed by the helices  $\alpha$ 2-5 of BCL-X<sub>L</sub> (**Figure 1.1C**)<sup>(3)</sup>. A subsequent NMR solution structure of BCL-X<sub>L</sub> in complex with a peptide comprising the BAK BH3 domain<sup>(5)</sup> confirmed this hydrophobic cleft as the location at which the amphipathic alpha-helical BH3 domain of a BH3-only protein can bind, and neatly demonstrated *via* alanine scanning mutagenesis the key hydrophobic and electrostatic interactions required for BH3 binding. Later structures of other BH3 domain peptides in complex with prosurvival proteins have confirmed these interactions (**Figure 1.1D-E**)<sup>(4, 6, 60, 62, 63)</sup>, as illustrated in the crystal structure of mouse BCL-X<sub>L</sub> bound to the BIM BH3 domain (**Figure 1.1D**)<sup>(6)</sup>. Four key conserved hydrophobic residues on the amphipathic BIM BH3 alpha-helix (‘h1 - h4’), interact with corresponding hydrophobic pockets on BCL-X<sub>L</sub> (p1 - p4) and a salt bridge forms between D99 of the BIM BH3 peptide and a conserved arginine, R139 in the  $\alpha$ 5 helix of BCL-X<sub>L</sub>.

Knowledge of the key molecular determinants of this interaction gave rise to the idea that it might be possible to develop small molecules able to functionally mimic BH3 ligands (‘BH3-mimetics’), which would hold promise for targeted anti-cancer therapy.

### 1.5.1 BH3-mimetic molecules for anti-cancer therapy

As described earlier, the ability to evade normal cell death *via* apoptosis is now well-regarded as a hallmark of cancer<sup>(47)</sup>. The strong association of BCL-2 with cancer was clear right from its discovery as the gene involved in the (14;18) chromosomal translocation that is a common feature of follicular lymphoma<sup>(64-68)</sup>. Subsequent studies confirmed BCL-2 to be an oncogene that promoted cell survival<sup>(69)</sup> (rather than proliferation) and that BCL-2 transformation led to the abnormal survival of many cell types<sup>(70-74)</sup>. As identity and function of different BCL-2 family proteins have gradually been elucidated over time, it has become clear that in addition to inactivating mutations of the tumour suppressor p53<sup>(75)</sup>,

genetic changes involving the BCL-2 family are another important mechanism by which cancer cells can become resistant to apoptosis<sup>(76)</sup>. Many cancers acquire constitutively elevated levels of prosurvival BCL-2 family proteins (such *via* translocations, overexpression or copy number alterations)<sup>(40)</sup>, on which they subsequently rely for their continued survival, which may render them “primed for death”<sup>(77)</sup>.

The development of small molecules able to mimic the function of BH3 ligands (‘BH3 mimetics’) by antagonising prosurvival BCL-2 family protein function to trigger apoptosis (downstream of p53) is thus an attractive prospect for targeted anti-cancer therapy. It was imagined that suitable BH3-mimetics might either have therapeutic usage as single-agents in certain cases, or alternatively to prime cancer cells for apoptosis when used in combination with traditional chemotherapies<sup>(76)</sup>.

As it became clear that different BH3 domains exhibit differential binding selectivity for prosurvival proteins<sup>(78)</sup> (**Figure 1.2A**), this suggested that that generation of selective BH3-mimetic small molecules might also be possible. This principle was reinforced by discovery of the potent BCL-X<sub>L</sub>, BCL-W and BCL-2 inhibitors **ABT-737**, **ABT-263** and related molecules, leading to eventual development of the BCL-2 selective inhibitor **ABT-199** (described in detail in **Section 1.5** below). The subsequent success of the BH3-mimetic small molecules **ABT-263** and **ABT-199** in the clinic (the first of this novel class) has confirmed the clinical applicability of inhibiting prosurvival BCL-2 family proteins as a useful approach for targeted anti-cancer therapy.

However, development of inhibitors targeting a protein-protein interaction (PPI) of this kind has not been without its significant challenges, some of which are outlined in the next section.

### 1.5.2 Targeting Protein-Protein Interactions (PPIs) using small molecules

Traditionally, targeting the interfaces between proteins with small ‘drug-like’ molecules has been incredibly challenging, due particularly to the nature of the interfaces involved.

In the context of PPIs accessible from outside the cell, antibodies and other protein-based therapies have led to a number of important therapeutics<sup>(79)</sup>. Many compelling PPI targets do not fall into this category, however, and in most cases small ‘drug-like’ molecules are preferable as they have the advantage of being cheaper and often capable of oral administration<sup>(13, 79)</sup>.

In recent years a number of notable successes have challenged the conventional wisdom that PPIs are inherently ‘undruggable’; Arkin and Wells have recently reported that > 40 different PPIs have now been successfully targeted with inhibitors, several of which in the last 10 years have reached clinical trials (encompassing 6 different targets)<sup>(29, 80-82)</sup>. In particular, it is encouraging to note the recent FDA approval of the selective BCL-2 inhibitor **Venetoclax (ABT-199)** (Described below, **Section 1.5**).

#### *1.5.2.1 PPIs typically represent large, shallow and hydrophobic interfaces*

The majority of drugs on the market today inhibit proteins that have naturally evolved to bind small bioactive molecules (such as enzymes, and G-protein coupled receptors (GPCRs)). These proteins in general harbour relatively deep, defined cavities (with contact surface areas in the range of  $\sim 300\text{--}500 \text{ \AA}^2$ ), which are more easily targeted with a small molecule<sup>(29)</sup>. By comparison, the interface of most PPIs is typically much larger (each side of the interface typically has a buried surface area in the range of  $\sim 750\text{--}1500 \text{ \AA}^2$ )<sup>(12, 83, 84)</sup>, often characterised by large, shallow interaction surfaces, a predominance of hydrophobic interactions, and in many cases binding epitopes comprised of secondary or tertiary structure based on amino acid residues non-contiguous in the peptide sequence<sup>(12)</sup>. Perhaps not surprisingly, the difficulty of successfully targeting a PPI with a small molecule

generally increases with the size of the interface and the nature of the epitope (primary < secondary < tertiary structure)<sup>(12, 29)</sup>. Thus, the most successful PPI inhibitors generated to date target either pockets that bind short epitopes of 1-4 amino acids (for example, inhibitors of bromodomains<sup>(85-90)</sup> and Inhibitor of Apoptosis Proteins<sup>(91, 92)</sup>) or helix/groove interactions (such as 'nutlin' inhibitors of the P53/MDM2 interaction<sup>(93-95)</sup> and inhibitors of the BH3 domain/BCL-2 family interaction<sup>(29)</sup>). The BAK/BCL-X<sub>L</sub> interaction has thus been noted to be somewhat exceptional as a PPI, in that the interface involves only approximately 500 Å<sup>2</sup> of the protein surface and the helix/groove interaction harbours some relatively deep pockets<sup>(96)</sup>.

The silver lining to the challenge of large interfaces is that many PPIs appear to display binding 'hotspots'. Mutagenesis studies (eg. alanine scanning) of many PPIs have shown that not all of an interface need necessarily be targeted by a small molecule - certain 'hotspot' regions may contribute most of the binding energy of a particular interaction<sup>(29)</sup>. 'Hotspots' tend to be clustered near the centre of an interface, are often hydrophobic in character and can be conformationally flexible<sup>(29)</sup>. In the case of proteins exhibiting significant structural plasticity, such as is the case for BCL-X<sub>L</sub><sup>(10)</sup>, knowledge of ligand conformation and considerations of 'induced fit' also become important.

#### *1.5.2.2 Optimising drug-like compounds*

As Arkin and Wells have noted, it is also important to be mindful of the distinction between ligandability ("druggability") of a PPI versus the ability to make orally bioavailable drugs<sup>(29)</sup>. Large and hydrophobic interfaces such as PPIs present a particular challenge for medicinal chemistry, as it can often be a difficult balance to strike between developing the affinity and selectivity of the molecule and maintaining the necessary overall chemical properties required of a typical 'drug-like' or orally bioavailable molecule<sup>(97)</sup>, in particular relating to absorption, distribution, metabolism, excretion and toxicology (ADMET).



One yardstick for predicting the likelihood of solubility and permeability of a small molecule, as required for oral dosing, is the so-called 'rule of 5' (RO5) reported by Lipinski and others<sup>(36)</sup>. RO5 predicts that poor absorption or permeability is more likely where the molecule possesses more than 5 H-bond donors, 10 H-bond acceptors, has a molecular weight greater than 500 Da and a calculated Log P (ClogP) greater than 5.<sup>(36)</sup> ClogP refers to the base 10 logarithm of the calculated octanol/water partition coefficient, a measure of compound lipophilicity.

In addition to their lower aqueous solubility, highly lipophilic compounds tend to be problematic for clinical development due to an increased risk of promiscuity and nonspecific toxicity <sup>(98-100)</sup>. As a general rule, increased molecular weight and complexity tend to correlate with increases in potency<sup>(101)</sup>. Simply chasing potency by adding mass can lead to an increase in non-specific and non-directional interactions (capable of promiscuous binding), primarily driven by entropic rather than enthalpic contributions (such as the 'hydrophobic effect')<sup>(99)</sup>. This is a particular challenge in the PPI field, in which targets typically represent large, predominantly hydrophobic interaction surfaces. Various efficiency indices have been developed relating molecular weight (MW) to potency (particularly in the fragment-based drug design field) as a way to monitor and address this trend, including 'ligand efficiency' (LE), 'lipophilic ligand efficiency' (LLE) and 'binding efficiency index' (BEI).

**LE** relates potency normalized by dividing by the number of heavy (non-H) atoms [inhibitors should ideally fall in the range  $LE = 0.3 - 0.4$ ]<sup>(102)</sup>.

$$LE = \Delta G / \# \text{heavy-atoms}$$

$$\text{Where } \Delta G \text{ in kcal/mol} = -1.37 \log K_D$$

**LLE** relates potency normalized by lipophilicity (to ensure specific rather than nonspecific effects) [nanomolar inhibitors should ideally fall in the range 5-7]<sup>(98)</sup>.

$$\text{LLE} = \text{pIC}_{50} - \text{ClogP}$$

Where  $\text{pIC}_{50}$  is defined as the negative base-10 logarithm of the  $\text{IC}_{50}$  value expressed in molar units

**BEI** relates potency normalized for molecular weight

[ideal enzyme inhibitors typically fall in the range 20-30, whilst inhibitors of more challenging targets such as large PPIs are more likely to have a BEI of  $\sim 12$ ]<sup>(103, 104)</sup>.

$$\text{BEI} = (-\text{pK}_i \text{ or } -\text{pK}_D) / \text{MW}$$

Where  $\text{pK}_D$  is defined as the negative base-10 logarithm of the  $K_D$  value expressed in molar units (or  $\text{pK}_i$  for an inhibitor), and MW is in kDa.

Just as these metrics have been developed to assist in balancing chemical and physiochemical properties of an inhibitor to improve its chances of falling within typical drug-like space, depending on the target class other additional criteria will also be important to demonstrate the correct mechanism of action.

In the BCL-2 context, whilst myriad mechanisms of cellular toxicity may precipitate cell death *via* apoptosis, the next section outlines specific criteria that have been proposed to validate that a putative BH3-mimetic is acting on pathway.

### 1.5.3 Markers of a selective BH3-mimetic

As described above, inhibitors that have poor affinity, selectivity or physiochemical properties have in general an increased likelihood of non-specific cellular toxicity. Thus, where the ultimate aim is to trigger (tumour) cell death *via* apoptosis, it is important to have stringent criteria to assess that a putative inhibitor is acting on-target, in this case, *via* the BCL-2 mediated pathway. Four criteria have been proposed to evaluate a 'true' BH3-mimetic:<sup>(105)</sup>

#### 1. Tight binding to one or more prosurvival BCL-2 family proteins.

Important interactions between prosurvival BCL-2 family proteins and their BH3 partner molecules (eg. BH3-only proteins or BAX/BAX) are typically of high affinity (nM to sub-nM range)<sup>(4, 78)</sup>. To displace these interactions effectively, an inhibitor of a prosurvival BCL-2 family protein must also ideally achieve affinity in this range, reproducibly over multiple biochemical assays using independent technologies.

#### 2. BAX/BAK-dependent biological activity ('mechanism-based activity').

The BCL-2 regulated intrinsic pathway to apoptosis converges at a 'point of no return' whereby activated BAX/BAX molecules disrupt the outer mitochondrial membrane, releasing apoptogenic factors including cytochrome *c*, which precipitate the downstream apoptotic cascade leading to cell death. Cells lacking both BAK and BAX are thoroughly resistant to apoptotic stimuli<sup>(106)</sup>. A true BH3-mimetic should thus demonstrate BAX/BAK-dependant apoptotic activity, or relevant cellular correlates of this activity, such as triggering release of cytochrome *c* from mitochondria only where BAX or BAK are present in the cell.

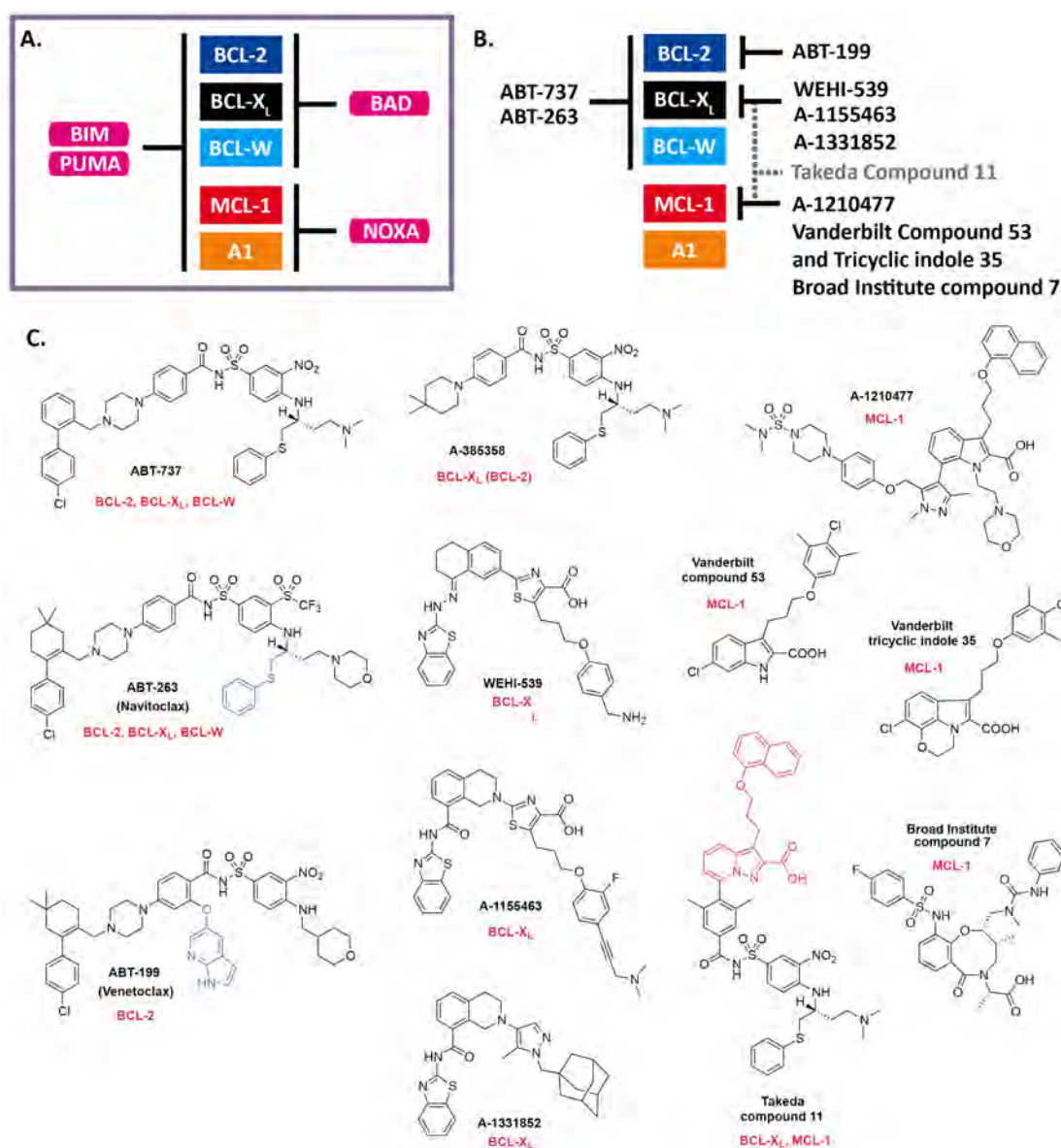
### 3. Cytotoxicity correlated with expression levels of targeted prosurvival proteins and the compound selectivity profile.

Multiple prosurvival BCL-2 family proteins have the ability to restrain intrinsic apoptosis. Thus for a selective BH3 mimetic that binds to only a subset of prosurvival proteins, cellular toxicity should broadly reflect this binding profile. That is, cellular toxicity should be high in cells that express only the targeted prosurvival BCL-2 family proteins; conversely cells in which a non-targeted prosurvival BCL-2 family protein is highly expressed should be more resistant to apoptosis on inhibitor treatment.

### 4. *In vivo* observation of biomarkers indicative of *on-target* side-effects.

Certain cell types have been shown to be particularly reliant on individual prosurvival BCL-2 family proteins for survival. A prominent example is the important role of BCL-X<sub>L</sub> in maintaining platelet survival<sup>(107, 108)</sup>. Loss of function mutations of BCL-X<sub>L</sub> in mice have been shown to trigger dose-dependent, cell-intrinsic reductions in platelet lifespan<sup>(108, 109)</sup>. Similarly, *in vivo* studies in animal models and humans using BH3-mimetics that potently inhibit BCL-X<sub>L</sub>, including **ABT-737** and **ABT-263** (described below), have consistently reported an acute thrombocytopenia (low platelet count) as an *on-target* side effect of BCL-X<sub>L</sub> inhibition<sup>(107, 108, 110-112)</sup>. For BH3-mimetic molecules that reach this stage of *in vivo* evaluation, relevant *on-target* side-effects such as this provide an important biomarker of activity.

Of the many putative BH3-mimetics reported in the literature, surprisingly few satisfy two or more of these criteria. The next section will provide a brief overview of BH3 mimetic small molecules that have been well validated. The focus will be on non-peptide inhibitors, although it must be noted that peptide-based strategies (including using  $\alpha/\beta$  foldamers or stapled peptides) have also yielded potent and selective BCL-2 family inhibitors, primarily as tool molecules to date, although in future some of these may also progress into clinical trials<sup>(113-116)</sup>.



**Figure 1.2: Selectivity of BH3 peptide and small molecule antagonists of prosurvival BCL-2 family proteins.** (A) Selectivity of different BH3 peptides for prosurvival BCL-2 family proteins. Image adapted from Chen *et al.* 2005 and Van Delft *et al.* 2006<sup>(78, 117)</sup>. (B) Selectivity of first generation (left) and second-generation (right) BH3-mimetic small molecules for prosurvival BCL-2 family proteins. (C) Chemical structures of a subset of published selective BH3-mimetic small molecules. Highlighted in blue are the S-phenyl and azaindole moieties of **ABT-263** and **ABT-199** respectively, important for the development of the BCL-2 selective compound **ABT-199** (described in detail in the main text). Highlighted in red on Takeda Compound **11** is a fragment derived from an MCL-1 inhibitor disclosed in a patent by Abbott Laboratories<sup>(118)</sup>, whilst the remainder of the molecule is derived from the **ABT-737** acylsulfonamide series<sup>(119)</sup>.

## 1.6 Small molecule BH3-mimetics reported in the literature

### 1.6.1 First generation BH3-mimetics: Acylsulfonamides

At the forefront of drug development efforts targeting BH3-mimetics has been pioneering work by the team at AbbVie (formerly Abbott) utilising a 'SAR-by-NMR' fragment-screening/linking approach<sup>(33)</sup>. This led to the discovery of the potent BCL-X<sub>L</sub>, BCL-W and BCL-2 inhibitor **ABT-737** ( $K_i < 1\text{nM}$  for BCL-X<sub>L</sub>, BCL-2 and BCL-W).<sup>(8)</sup> **ABT-737** has been shown to trigger apoptosis *in vitro* and *in vivo* in cells expressing low levels of MCL-1. It was also shown *in vivo* to sensitise BCL-2 expressing breast tumours to treatment with docetaxel. In the 10 years since its disclosure, **ABT-737** has been extensively studied and utilised as a chemical probe and its mechanism-of-action well validated. Similar to the BH3 only protein BAD (**Figure 1.2A,B**), **ABT-737** sensitises cells to BAX/BAK-dependent cell death by binding to and neutralising its prosurvival binding partners (BCL-2/BCL-X<sub>L</sub>/BCL-W)<sup>(8, 110, 117, 120, 121)</sup>.

The crystal structure of **ABT-737** in complex with BCL-X<sub>L</sub> solved in 2007 represented the first published crystal structure of a small molecule in complex with a prosurvival protein and yielded significant information on the highly plastic binding groove of BCL-X<sub>L</sub> (**Figure 1.1F, Figure 1.3**)<sup>(10)</sup>. In particular it showed that **ABT-737**, whilst a functional mimetic of BAD, was not a strict structural mimetic of this BH3 peptide. In particular, rather than binding along the full length of the groove, **ABT-737** engaged primarily the p2 and p4 pockets<sup>(10)</sup>. In the p2 pocket, the chlorobiphenyl moiety of **ABT-737** bound more deeply than the typical h2 residue of BH3 peptide ligands (due to surprising protein flexibility *via* movement of the  $\alpha$ -3 and  $\alpha$ -4 helices of BCL-X<sub>L</sub>, enabling a cryptic pocket to be revealed)<sup>(10, 122)</sup>. At the other end of the groove, in the p4 pocket, hydrophobic collapse of the S-phenyl and nitro-aryl rings of **ABT-737** formed an intramolecular pi-stacking arrangement, facilitating an extended pi-stacking network with Phe97 and Tyr195 of BCL-X<sub>L</sub> (**Figure 1.1F, Figure 1.3**)<sup>(10, 123)</sup>. Lastly, the acylsulfonamide of **ABT-737** did not mimic the conserved aspartyl residue present on all BH3 domains, in that it did not engage Arg139, but rather formed a hydrogen bond with the backbone -NH of Gly138 of BCL-X<sub>L</sub> (**Figure 1.1F, Figure 1.3**)<sup>(10)</sup>.

Subsequent work to improve the pharmacological properties of **ABT-737** led to the development of an orally bioavailable derivative, **ABT-263 (Navitoclax)**, with the same binding profile as its parent (**Figure 1.2B,C**)<sup>(110)</sup>. This was certainly an impressive feat of medicinal chemistry to demonstrate that a oral bioavailability could be achieved for such a large (MW >800 Da) and hydrophobic molecule, falling way outside of traditional orally bioavailable RO5 'drug-like' space<sup>(97)</sup>. Clinical trials conducted using **ABT-263** represented the first example of a BCL-2 inhibitor reaching the clinic <sup>(112, 124, 125)</sup>. In a Phase I study **ABT-263** showed very promising single-agent activity in patients with relapsed or refractory chronic lymphocytic leukaemia (CLL)<sup>(112)</sup>. **ABT-263** has also been evaluated in clinical trials for treating small cell lung cancer (SCLC), however in this context appears to be more likely to be used as part of a combination therapy<sup>(125)</sup>. Throughout these trials, the primary dose-limiting toxicity of **ABT-263** was found to be an anticipated thrombocytopenia (low platelet count) due to *on-target* inhibition of BCL-X<sub>L</sub> (discussed below). Based on this, it was anticipated that the promising activity of **ABT-263** against CLL might be further improved by optimising this compound into a BCL-2 selective drug, such that higher clinical dosing could be achieved <sup>(112)</sup>.

**ABT-737** and **ABT-263** thus represent the first true 'BH3-mimetic' small-molecules with a well-validated mechanism of action; and the first demonstration that structure-based drug design approaches could render such traditionally challenging PPIs as tractable targets for medicinal chemistry. This pioneering work has since inspired the discovery of other potent molecules with related structures (and similar binding profiles) to **ABT-737**, many attempting to improve solubility or address potential metabolic liabilities of this compound<sup>(126-134)</sup>, as well as paved the way for subsequent generations of BH3-mimetics with even greater selectivity.

### 1.6.2 Second generation BH3-mimetics

More recently, some examples of small molecule BH3-mimetics have been published which exhibit remarkable potency and selectivity for individual BCL-2 family members – greater selectivity in fact than the native BH3 peptides - as well as rationally designed combinations thereof (**Figure 1.2B**).

#### 1.6.2.1 Selective targeting of individual prosurvival BCL-2 family proteins

Different prosurvival BCL-2 family proteins naturally have a selective binding repertoire for certain BH3-only partners (**Figure 1.2A**). This selectivity depends both on variation in primary structure of the BH3-only proteins, as well as subtle differences in the topography of pockets along the prosurvival binding groove. The restricted binding repertoire of BAD (BCL-2/BCL-XL/BCL-W) versus NOXA (MCL-1/A1) for example, delineates two ‘subgroups’ of prosurvival proteins that might share certain targetable differences. Yet, it appears no native BH3-only protein selectively binds a single prosurvival partner<sup>(135)</sup>, although peptides that do have been generated<sup>(63, 136, 137)</sup>. To achieve such selectivity using a small molecule (with far fewer potential contact sites than a peptide, and utilising relatively non-specific hydrophobic interactions) might thus be anticipated to be an incredibly challenging task. However, this has been facilitated in part by the unexpected flexibility of the canonical binding groove, as well as particular sites of sequence difference neighbouring the groove (**Figure 1.3**).

#### 1.6.2.2 BCL-2 selective compounds

Clinical data for **ABT-263** suggested that a BCL-2 selective inhibitor might have improved single-agent efficacy and avoid the *on-target* thrombocytopenia due to BCL-X<sub>L</sub> inhibition<sup>(112)</sup>. Based on this, AbbVie/Genentech/WEHI in collaboration subsequently developed a BCL-2 selective molecule **ABT-199 (Venetoclax)**<sup>(138)</sup>. **ABT-199** has shown very promising single agent activity in clinical trials for treating relapsed chronic lymphocytic leukaemia (CLL)<sup>(139)</sup> and has recently obtained FDA approval for use in 17p-deleted CLL that has failed at least one prior treatment<sup>(140)</sup>.



The development of **ABT-199** was directly enabled by structure-guided methods; in particular, a fortuitous observation in the crystal structure of an intermediate compound in the series bound to BCL-2. This compound is structurally related to **ABT-263** but without the S-phenyl group that binds in the p4 pocket (see **Figure 1.2C**, **ABT-263**, highlighted in blue). The structure revealed that a tryptophan side-chain from a neighbouring protein monomer intercalated into the free space in the p4 pocket, forming a pi-stacking interaction with the nitro-aryl group of the compound as well as an additional hydrogen bond with Asp103 of BCL-2. Asp103 corresponds to Glu96 in BCL-X<sub>L</sub> and is one of the few amino acid differences within the BH3-binding domains of the two proteins (**Figure 1.3**). Based on this, an azaindole moiety was incorporated at this position, which was shown to be able to interact with the neighbouring Asp103 residue of BCL-2, but not with the corresponding Glu96 residue of BCL-X<sub>L</sub> (**Figure 1.2C**, **ABT-199**, highlighted in blue). This was a key modification that led ultimately to the BCL-2 selective compound **ABT-199**<sup>(138)</sup>.

#### 1.6.2.3 BCL-X<sub>L</sub> selective compounds

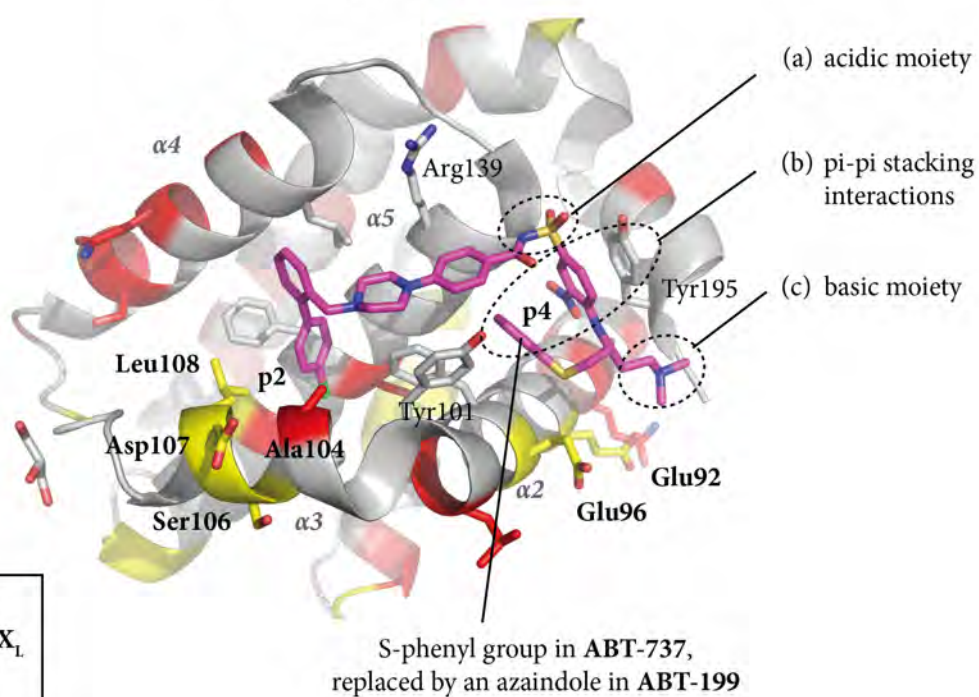
BCL-2 and BCL-X<sub>L</sub> share a remarkably similar structure and bind a similar subset of BH3-only proteins. Whilst according to primary structure BCL-X<sub>L</sub> and BCL-2 share only approximately 50% sequence identity, the majority of this difference lies away from the canonical hydrophobic groove, in particular in the large unstructured loop between  $\alpha 1$  and  $\alpha 2$ . In terms of overall fold, omitting the  $\alpha 1$ -2 loop, both proteins overlay closely - the global root-mean-square deviation (rmsd) of the backbones of these two proteins is only  $\sim 1.85$  Å<sup>(122)</sup>.

In the course of developing **ABT-737**, AbbVie also reported potent inhibitors of BCL-X<sub>L</sub>, including **A-385358**, which showed relative selectivity for BCL-X<sub>L</sub> versus BCL-2 (K<sub>i</sub>'s of 0.80 and 67 nM for BCL-X<sub>L</sub> and BCL-2 respectively)<sup>(96, 123, 141)</sup>. **A-385358** showed only modest single-agent activity against most tumour cell lines, but was able to enhance the cytotoxic activity of other chemotherapeutics (eg. Paclitaxel, etoposide, cisplatin, doxorubicin) in many tumour cell lines<sup>(141)</sup>. **A-385358** makes use of similar interactions to **ABT-737** within the p4 pocket to

drive affinity to BCL-X<sub>L</sub>, although the basis for its selectivity is less clear (Compare **Figure 1.3 (a)-(c)**).

A HTS screen also provided the starting point for another series of inhibitors of BCL-X<sub>L</sub><sup>(142)</sup>, leading to the discovery of **WEHI-539**, a remarkably potent and selective inhibitor of BCL-X<sub>L</sub> ( $K_D$ (BCL-X<sub>L</sub>) = 0.4 nM). **WEHI-539** showed mechanism-based killing of mouse embryonic fibroblast cells (MEFs) engineered to be dependent on BCL-X<sub>L</sub> via loss of MCL-1 (*MCL-1*<sup>-/-</sup>)<sup>(61)</sup>. Optimisation of the molecule (to remove the potentially labile hydrazone moiety and improve pharmacokinetic properties)<sup>(143)</sup> led to **A-1155463**<sup>(144)</sup>, with improved potency and *in vivo* activity. In mice this molecule showed an *on-target* effect on platelets (as a biomarker of BCL-X<sub>L</sub> inhibition) but had modest single-agent activity in a xenograft model with BCL-X<sub>L</sub>-dependent H146 tumour cells. Further optimisation of this series using structure-based design led to **A-1331852**, a potent BCL-X<sub>L</sub>-selective molecule that also demonstrated oral bioavailability<sup>(145)</sup>. In cell-viability assays using BCL-X<sub>L</sub> dependent Molt-4 cells (a human acute lymphoblastic leukemia (ALL) cell line) **A-1331852** had a measured EC<sub>50</sub> of 6 nM (more than 10-fold more active than **A-1155463** in the same assay) and also showed single-agent efficacy *in vivo* in a murine Molt-4 xenograft model<sup>(145)</sup>. The **WEHI-539/A-1155463/A-1331852** series represent the most potent and selective series of BCL-X<sub>L</sub> inhibitors reported to date and derive their affinity from unique interactions within the p2 and p4 pockets of BCL-X<sub>L</sub> (refer **Figure 1.3**).

### A. BCL-X<sub>L</sub>:ABT-737

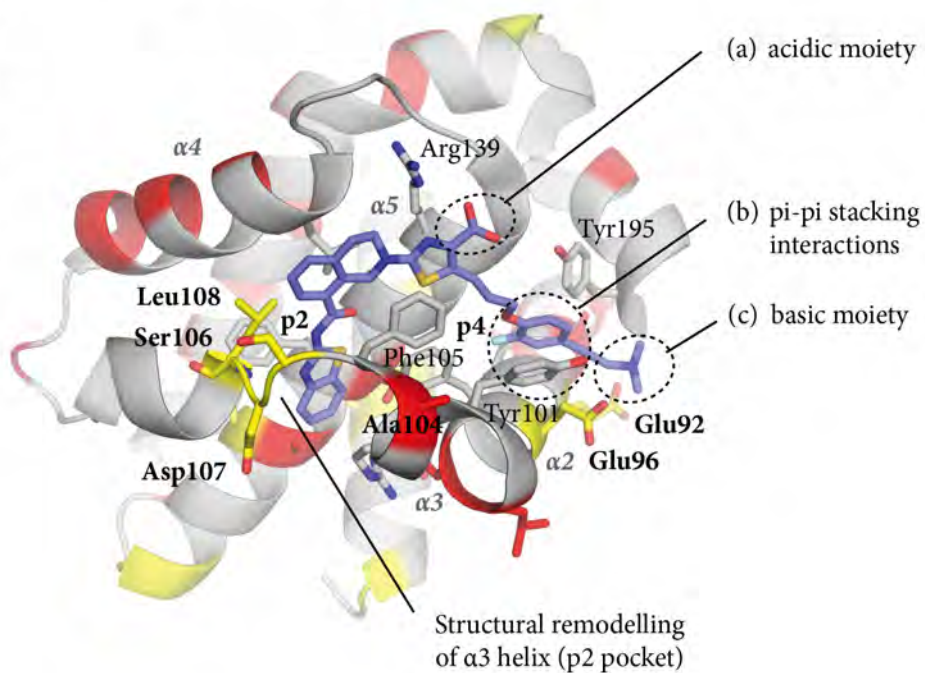


Non-identical  
residues in BCL-X<sub>L</sub>  
versus BCL-2  
(yellow/red)

Corresponding  
residues

BCL-X <sub>L</sub>	BCL-2
Glu92	Gln99
Glu96	Asp103
Ala104	Asp111
Ser106	Ala113
Asp107	Glu114
Leu108	Met115

### B. BCL-X<sub>L</sub>:A-1155463



**Figure 1.3: Targeting structural/sequence differences between BCL-2 and BCL-X<sub>L</sub>.** Structural comparison of the binding modes of (A) **ABT-737** (BCL-X<sub>L</sub>/BCL-2/BCL-W inhibitor) and (B) **A-1155463** (selective BCL-X<sub>L</sub> inhibitor) in complex with BCL-X<sub>L</sub>; highlighting the relatively few positions of difference in primary structure between BCL-X<sub>L</sub> and BCL-2 (yellow = similar non-identical residue; red = different residue). Whilst the particular binding mode of each compound differs significantly, both utilise some common features: including deep engagement the p2 pocket (with varying degrees of structural remodelling of the protein); an acidic moiety (a) (in **A-1155463** this group is involved in direct interactions with Arg139 of BCL-X<sub>L</sub>, whilst in **ABT-737** the precise role of this moiety is less clear); groups able to engage in aromatic pi-stacking interactions with neighbouring protein Phe/Tyr residues within the p4 pocket (b); and a basic moiety projecting into solvent space in proximity to the acidic patch of Glu92/Glu96 of BCL-X<sub>L</sub> (c). The remarkable affinity for BCL-X<sub>L</sub> of the series of compounds exemplified by **A-1155463** likely derives from their high level of shape complementarity for the BCL-X<sub>L</sub> groove. The series has a unique binding mode within the p2 pocket, involving significant structural remodelling to the  $\alpha$ 3 helix of BCL-X<sub>L</sub> and flip of Phe105 from the floor to the side of the hydrophobic groove to pack against the compound. Interestingly, this region of the  $\alpha$ 3 helix is also one of the few positions along the binding groove in which there is sequence difference between BCL-2 and BCL-X<sub>L</sub>. In this binding mode, the compound packs closely near Leu108 in of BCL-X<sub>L</sub> in the p2 pocket. In BCL-2 this residue corresponds to a larger methionine residue (Met115), which may occlude the close packing and partially explain the selectivity for BCL-X<sub>L</sub> over BCL-2. In comparison, the BCL-2 selective inhibitor **ABT-199** utilises an amino-acid sequence difference near the p4 pocket - in **ABT-199** the azaindole group (which replaces the S-phenyl group of **ABT-737** in the p4 pocket) is able to facilitate a selective hydrogen-bonding interaction with Asp103 of BCL-2, which is not possible with the corresponding Glu96 of BCL-X<sub>L</sub><sup>(138)</sup>.

#### 1.6.2.4 MCL-1 selective compounds

Recently, lead molecules have also been reported based on an indole-2-carboxylic acid core which potently and selectively inhibit MCL-1. These leads include compound **53** (**Figure 1.2C**)<sup>(146)</sup> and a series of tricyclic indoles including compound **35** ( $K_i$  (MCL-1) = 9 nM)(**Figure 1.2C**)<sup>(147)</sup>, which were disclosed by researchers at Vanderbilt University. More recently AbbVie have also described more potent analogues based on a similar core, including **A-1210477** (**Figure 1.2C**), which has sub-nanomolar affinity for MCL-1<sup>(148, 149)</sup>. The selectivity of these molecules towards MCL-1 has been ascribed to their ability to engage binding conformations within the p2 pocket of the protein not observed with native BH3 peptides<sup>(148)</sup>, due to structural rearrangement of the  $\alpha 4$  helix. However, despite this high affinity and selectivity for MCL-1, **A-1210477** has only shown moderate activity in *in vitro* cell viability assays using MCL-1 dependent non-small cell lung cancer (NSCLC) cell lines (HC23 and H2110,  $EC_{50} \sim 5 - 7 \mu M$ )<sup>(149)</sup>.

The Broad Institute have also recently disclosed a lead molecule that selectively binds to MCL-1, compound **7** (**Figure 1.2C**), which uses a different scaffold based on a single diastereomer of a macrolactam core<sup>(150)</sup>. Compound **7** has a measured  $IC_{50}$  for MCL-1 of  $4.5 \mu M$  (using a fluorescence polarisation-based competition assay) and reveals a novel mode of binding from previously described MCL-1 inhibitors<sup>(150)</sup>.

At the time of submitting this Thesis, another series of highly potent and selective MCL-1 inhibitors developed by Servier and Vernalis was reported<sup>(151)</sup>; this study provides important preclinical data towards validating the therapeutic utility of small molecules that selectively target MCL-1.

#### 1.6.2.5 Dual BCL-X<sub>L</sub>/MCL-1 selective compounds

In an interesting example of structure-guided design, based on some of the published selective inhibitors of each of MCL-1 and BCL-X<sub>L</sub>, a group from Takeda recently managed to rationally fuse parts of these inhibitors to generate a novel BCL-X<sub>L</sub>/MCL-1 dual inhibitor with nanomolar binding to each of these two proteins (**Figure 1.2C**)<sup>(119)</sup>.

These examples demonstrate the remarkable success that has been achieved in generating highly selective and well-validated BH3-mimetics against prosurvival BCL-2 family proteins (either as small subgroups or as individual proteins) - yet for each target these distil into only a few different structural classes. Novel structural classes of selective, validated BH3-mimetic are still needed.

## 1.7 Therapeutic rationale for targeting BCL-X<sub>L</sub>

Despite a known *on-target* side-effect of BCL-X<sub>L</sub> inhibition on platelet lifespan, BCL-X<sub>L</sub> remains a compelling oncology target - as a single-agent or perhaps more likely, as part of a combination therapy. Potent and selective targeting of BCL-X<sub>L</sub> may provide novel anti-cancer therapeutic options, whilst mitigating potential toxicity to healthy tissues caused by unnecessary pan inhibition of other prosurvival proteins.

Inhibitors of BCL-X<sub>L</sub> developed to date have been invaluable biochemical tools for probing the normal physiological role of BCL-X<sub>L</sub>. In particular, through the use of such tools in combination with genetic studies, BCL-X<sub>L</sub> has been demonstrated to be the primary prosurvival protein responsible for determining platelet lifespan. Genetic ablation, hypomorphic mutation or the use of pharmacological inhibitors of BCL-X<sub>L</sub> have all been shown *in vivo* to result in a reduction in platelet half-life and a dose-dependent thrombocytopenia<sup>(107, 108, 152)</sup>. In validating potential BH3-mimetic molecules, this effect on platelet lifespan provides an important cellular marker for demonstrating on-target BCL-X<sub>L</sub> inhibition, but it does provide an important challenge to be addressed for potential future clinical use of BCL-X<sub>L</sub>-targeting inhibitors. So far in clinical studies using the BCL-2/BCL-W/BCL-X<sub>L</sub> inhibitor **ABT-263**, *on-target* thrombocytopenia due to BCL-X<sub>L</sub> inhibition has been the major dose-limiting toxicity<sup>(111, 112, 139, 145)</sup>; although it may be possible to ameliorate this effect somewhat using modified dosing strategies (such as a lower lead-in dose, to allow platelet levels to recover, followed by dose-escalation)<sup>(112)</sup>.

BCL-X<sub>L</sub> has been shown to be overexpressed in many tumour types, and its expression correlated with both malignant transformation and disease progression of both solid-tumour and haematological malignancies<sup>(153-157)</sup>. BCL-X<sub>L</sub> is also implicated as a survival factor important for chemoresistance to conventional anti-cancer therapy<sup>(2, 158)</sup> – for example, in a number of cancer cell lines from the US National Cancer Institute (NCI) a strong correlation was observed between BCL-X<sub>L</sub> overexpression and resistance to most standard chemotherapy agents<sup>(2)</sup>. The FDA approval of Venetoclax marks the beginning of

BH3-mimetics entering regular clinical use. Whilst data is not yet available, it is anticipated that a potential mechanism of resistance BH3-mimetics used in the clinic might be the upregulation of other non-targeted prosurvival members. In this context, second- and third-generation selective inhibitors of BCL-X<sub>L</sub> or MCL-1 may find future use.

Agents targeting BCL-X<sub>L</sub> may also see eventual clinical utility in combination therapy. In the context of solid tumours, data from clinical trials utilising **ABT-263 (Navitoclax)** in combination with conventional chemotherapies, suggest that the observed synergy is primarily due to BCL-X<sub>L</sub> (rather than BCL-2) inhibition<sup>(111, 112)</sup>. In tumours dependent on BCL-X<sub>L</sub>, use of a selective BCL-X<sub>L</sub> inhibitor may also avoid some of the immune-suppressive effects associate with dual inhibition of BCL-2/BCL-X<sub>L</sub><sup>(145)</sup>. As well as the role of BCL-2 in survival of B and T lymphocytes<sup>(159)</sup>, clinical trials using **ABT-263/ABT-199** have reported significant neutropenia, possibly as a class-effect of *on-target* BCL-2 inhibition<sup>(111,-112, 139, 145)</sup>.

Recently, preliminary work has also suggested a potential use for BCL-X<sub>L</sub> inhibitors as part of a host-directed therapeutic strategy in combatting infectious disease due to intracellular pathogens<sup>(160)</sup>. In Legionnaires' disease, invaded alveolar macrophages become a reservoir for the intracellular replication of pathogenic *Legionella* bacteria. These macrophages thus become reliant on BCL-X<sub>L</sub> for survival, as pathogen-mediated inhibition of host protein-synthesis downregulates production of the short-lived MCL-1, which quickly degrades and is not replaced. In a mouse model of Legionella infection, a single dose of a BCL-X<sub>L</sub>-targeted BH3-mimetic therapy, or myeloid cell-restricted deletion of BCL-X<sub>L</sub>, was found to trigger apoptosis of infected macrophages, limiting pathogen replication and thus preventing lethal lung infections<sup>(160)</sup>.

The development of novel potent and selective BCL-X<sub>L</sub> inhibitors is thus of significant therapeutic interest in a number of disease contexts.

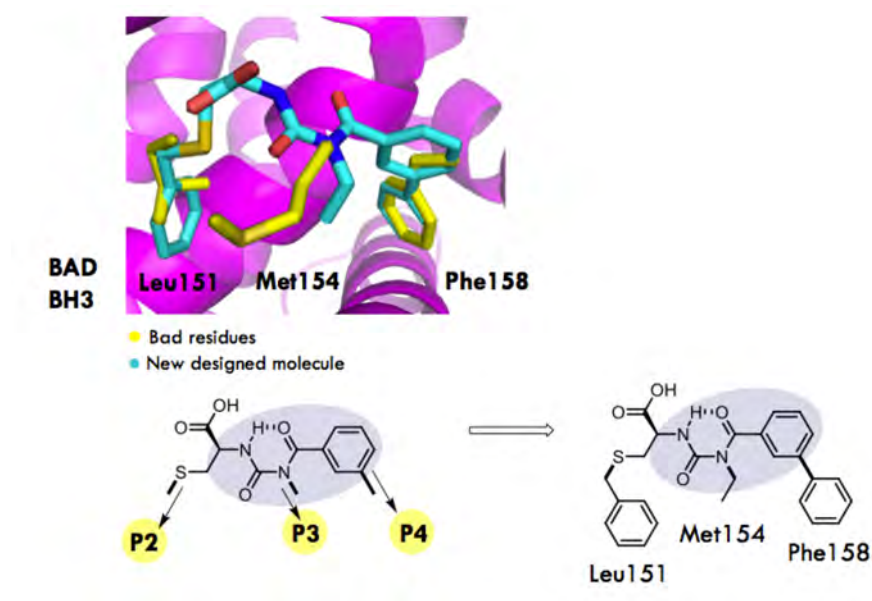


## 1.8 Origins of the benzoylurea series

A SBDD program was embarked upon at WEHI seeking novel small molecule BH3-mimetics targeting BCL-X<sub>L</sub>. A small library of approximately 130 molecules were synthesised based on a benzoylurea scaffold. This scaffold had been utilised previously by the group for the modular synthesis of compounds as potential  $\alpha$ -helix topographical mimetics targeting the BCL-2 family (**Figure 1.4**)<sup>(161-163)</sup>. This library of benzoylurea was screened against BCL-X<sub>L</sub> and MCL-1 in an AlphaScreen assay based on competitive displacement of the BIM peptide from either of these proteins. This led to the discovery of compound **1.1** (**Figure 1.5A**), which showed promising BCL-X<sub>L</sub> binding and selectivity ( $IC_{50}(BCL-X_L) = 4.6 \mu M$  as initially determined)(**Table 1.1 – ‘pre-2015 data’**).

Following the relocation of our Screening Group, a consistent shift in the  $IC_{50}$  values determined using the AlphaScreen competition assay was observed. The signifiers ‘**pre-2015 data**’ and ‘**post-2015 data**’ indicate respectively data acquired prior and subsequent to this relocation. [For further information refer to note in **Chapter 2, Section 2.4.1.3.**]

Subsequent retesting of compound **1.1** confirmed the BCL-X<sub>L</sub> binding and selectivity relative to MCL-1 ( $IC_{50}(BCL-X_L) = 0.51 \mu M$ ) (**Table 1.1 – ‘post-2015 data’**). For clarity,  $IC_{50}$  values referred to for the remainder this Chapter will describe only ‘**post-2015 data**’, however both sets of data reflected similar trends and are presented for comparison in **Table 1.1**.



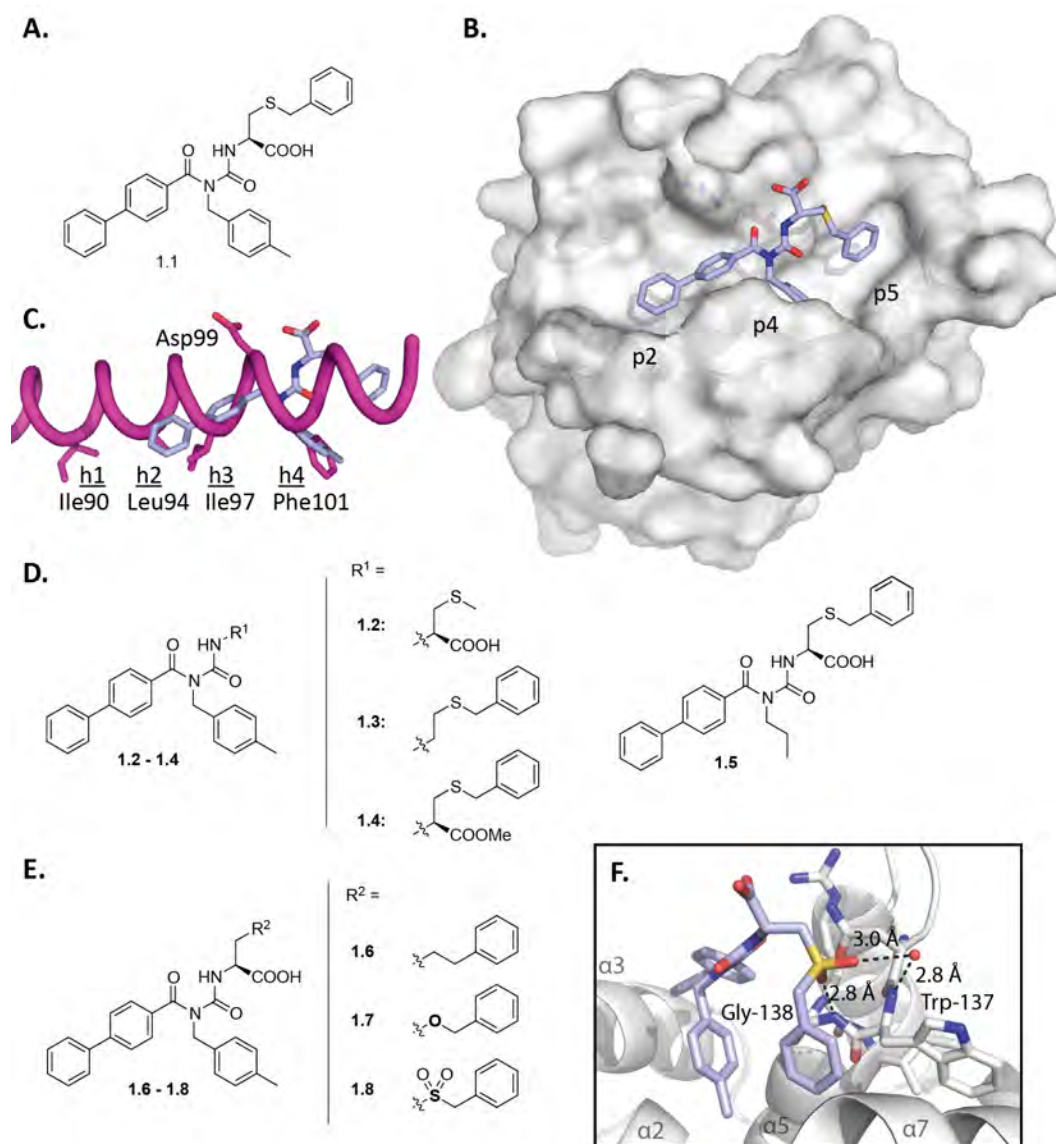
**Figure 1.4: Structure-guided *de novo* design of benzoylurea series.**

Using the published structure of the BH3 domain of BAD bound to BCL-X<sub>L</sub>, computer modeling was undertaken to search for novel scaffolds as potential  $\alpha$ -helical topographical mimetics<sup>(161)</sup>. A benzoylurea scaffold was selected due to its amphiphilic character, versatile synthesis and ability to conformationally pre-organise *via* a pseudo 6-membered ring when suitably substituted<sup>(161, 163)</sup>, enabling functionalised groups to be incorporated in a modular fashion with the aim of engaging the p2, p3 and p4 pockets of BCL-X<sub>L</sub>.

To determine the binding mode, an X-ray crystal structure was solved of compound **1.1** in complex with BCL-X<sub>L</sub> (**Figure 1.5B**), which revealed that the compound bound along the canonical hydrophobic groove of BCL-X<sub>L</sub> overlapping a number of key interactions sites of the published structure of the BIM BH3 bound to mouse BCL-X<sub>L</sub> (**Figure 1.5C**). In particular, the biphenyl moiety of compound **1.1** projects along the groove towards the p2/p3 hydrophobic pockets; the tolyl group interacts deeply into the p4 pocket in a manner reminiscent of Phe101 of BIM and the carboxylic acid moiety of **1.1** projects out of the groove into solvent in a position generally similar to Asp99 of BIM. Interestingly, unlike Asp99 of BIM, the carboxylic acid moiety of **1.1** was not observed to directly interact with Arg139 of BCL-X<sub>L</sub> in the bound state (see further below). At the top end of the groove, the S-benzyl moiety of **1.1** was shown to sit into an extended space neighbouring the p4 pocket, which we have termed 'p5', formed by a movement of Tyr195 of BCL-X<sub>L</sub> (**Figure 1.5B**).

Notably, the binding mode differed from the original design (**Figure 1.4**) in two respects. Firstly, the compound bound in the reverse orientation within the hydrophobic groove to the original benzoylurea design. Despite this, the compound still maintained remarkably similar hydrophobic/aromatic interactions in the p2/p3 and p4 pockets. Secondly, the reversed binding mode resulted in the carboxylic acid moiety of **1.1** being located in a position in effect one helix-turn further along the modeled BH3 peptide than the conserved aspartate residue (eg. Asp99 of BIM, **Figure 1.5C**, compare **Figure 1.4**). Interestingly this position, near the N-terminus of the BCL-X<sub>L</sub> α5 helix, actually corresponds closely to the location of the acidic acylsulfonamide moiety of **ABT-737** when bound to BCL-X<sub>L</sub> (**Figure 1.3A**).

The structure of the BCL-X<sub>L</sub>:**1.1** complex formed the basis for rational optimisation of compound **1.1** to target BCL-X<sub>L</sub>.



**Figure 1.5: Initial studies on AlphaScreen hit compound 1.1.**

(A) Structure of compound **1.1** (B) X-ray crystal structure of the BCL-XL:**1.1** complex, showing binding along the canonical groove of BCL-XL and interactions in the p2, p4 and p5 pockets (C) Overlay of compound **1.1** with BIM (from the mouse BCL-XL:BIM BH3 complex, PDB entry 1PQ1<sup>(6)</sup>) indicating conserved hydrophobic residues h1-h4 and conserved Asp99. (D) Negative structure-activity-relationship (SAR) studies based on compound **1.1**. (E) Compounds exploring replacement of thioether linker of compound **1.1** with methylene or various hydrogen bond acceptors (F) X-ray crystal structure of the BCL-XL:**1.8** complex, indicating hydrogen bond formed between sulfonyl oxygen and backbone -NH of Gly138 of BCL-XL, as well as a coordinated water molecule.

## 1.9 Structure-guided optimisation of the benzoylurea series

This Section outlines some initial studies performed around the initial hit, compound **1.1**, based on the crystal structure of **1.1** in complex with BCL-X<sub>L</sub>.

It comprises background unpublished work performed by others and myself, not intended to form part of my PhD work. In particular:

- The synthesis of compounds **1.1**, **1.2**, **1.3**, **1.5**, **1.9**, **1.10** was performed by Guillaume Lessene and structural studies of compounds **1.1** and **1.10** in complex with BCL-X<sub>L</sub> were performed by Peter Czabotar.
- The synthesis of compounds **1.4**, **1.6** – **1.8** and structural studies of compound **1.8** in complex with BCL-X<sub>L</sub> were performed by me as part of an Honours project.

### 1.9.1 Negative structure-activity-relationship (SAR) studies

An initial set of negative structure-activity-relationship (SAR) analogues were synthesised and assayed to explore and validate the binding mode of **1.1** to BCL-X<sub>L</sub> as suggested by the BCL-X<sub>L</sub>:**1.1** crystal structure (compounds **1.2-1.5**, **Figure 1D**, **Table 1.1** – ‘**post-2015 data**’). This set highlighted the relative importance of the tolyl, S-benzyl and carboxylic acid moieties of **1.1**.

Similar to Phe101 of BIM, the tolyl group of **1.1** engages in pi-stacking interactions with Phe97 in the p4 pocket of BCL-X<sub>L</sub>. This residue of BIM is important for BCL-X<sub>L</sub> binding (mutation of this residue in human BIM to alanine has been shown to diminish affinity for BCL-X<sub>L</sub> 90-fold<sup>(137)</sup> but is less important for MCL-1 binding) – similarly for **1.1**, replacement of this group with an n-propyl (compound **1.5**) results in a 60-fold loss in BCL-X<sub>L</sub> binding (but < 4-fold loss in binding to MCL-1). By comparison, removal of the aromatic ring of **1.1** from the BCL-X<sub>L</sub> p5 pocket (compound **1.2**, S-benzyl replaced by S-methyl moiety) results in a 25-fold loss in BCL-X<sub>L</sub> binding (and only 5-fold loss in binding to MCL-1) (**Table 1.1** – ‘**post-2015 data**’). In view of this, we considered that whilst the S-benzyl group does contribute to binding, there might be scope to further optimise this interaction.

The carboxylic acid moiety of **1.1** was also found to be crucial, as removal (compound **1.3**) or methylation (compound **1.4**) resulted in no measurable binding to either BCL-X<sub>L</sub> or MCL-1 (**Table 1.1 – ‘post-2015 data’**). This mirrors other published BCL-X<sub>L</sub> inhibitors, in which the acidity of groups in this position has been shown to be important for BCL-X<sub>L</sub> binding affinity (**Figure 1.3**)<sup>(132)</sup>, presumably to mimic in some way the conserved aspartate residue of BH3 domains. Interestingly, as described earlier the carboxylic acid of **1.1** is not observed to interact with Arg139 of BCL-X<sub>L</sub> in the bound crystal structure – presumably it is still important for a transient ionic interaction with Arg139 (possibly as part of an initial interaction between **1.1** and the protein resembling an ‘encounter complex’<sup>(164)</sup>).

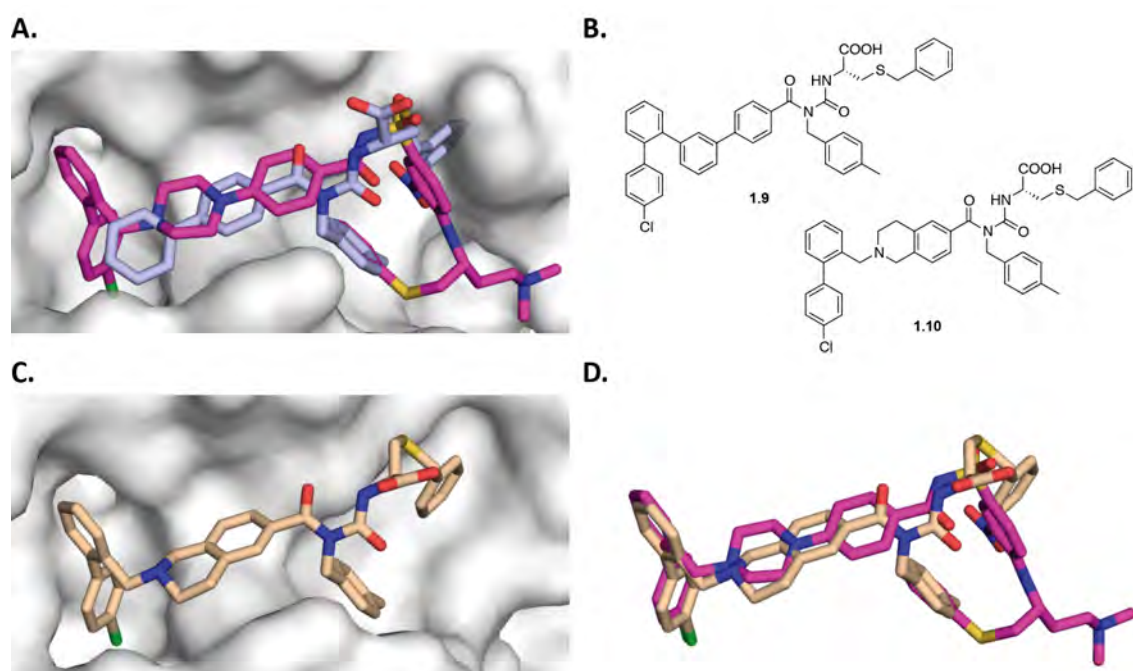
Based on these results, with a view to further improving the affinity of this series for BCL-X<sub>L</sub>, we next focused our attention on attempting to build additional interactions around the p2 and p5 pockets of BCL-X<sub>L</sub>.

### 1.9.2 Incorporation of hydrogen bond acceptors in linker

A series of compounds (**1.6-1.8**, **Figure 1.5E**) were synthesised exploring replacement of the thioether moiety ‘linker’ adjacent to the p5 pocket with a methylene, or with groups able to act as hydrogen-bond acceptors (in order to potentially mediate an additional interaction with the nearby –NH of Gly138 of BCL-X<sub>L</sub>). These changes had little overall effect on BCL-X<sub>L</sub> binding (compound **1.6-1.8**, **Table 1.1 – ‘post-2015 data’**), although a crystal structure of the sulfonyl compound **1.8** with BCL-X<sub>L</sub> revealed that the desired hydrogen bond interaction had in fact been achieved (**Figure 1.5F**). Presumably the entropic penalty of desolvating the –NH and one of the sulfonyl oxygen atoms almost entirely off-set the enthalpic gain of due to the additional bond formed.

### 1.9.3 Development of extended scaffolds targeting p2 pocket

On superimposing the BCL-X<sub>L</sub>:**1.1** complex with the published structure of the BCL-X<sub>L</sub>:**ABT-737** complex (**Figure 1.6A**)<sup>(10)</sup>, noting the close overlap of the two structures, we drew inspiration from the deep binding of the chlorobiphenyl group of **ABT-737** into the p2 pocket of BCL-X<sub>L</sub>. Two novel extended scaffolds were designed, compounds **1.9** and **1.10**, which we proposed might make use of this additional interaction in the p2 pocket and thereby potentially improve the affinity for BCL-X<sub>L</sub> (**Figure 2B**). Of the two designed scaffolds, compound **1.9** represented a synthetically simpler, but more lipophilic and structurally rigid alternative, whereas the tetrahydroisoquinoline (THIQ) scaffold compound **1.10** would be more flexible and potentially more drug-like. Indeed, when these two compounds were synthesized and an X-ray crystal structure was determined for compound **1.10** in complex with BCL-X<sub>L</sub>, compound **1.10** was found to bind exactly as designed, overlaying remarkably closely with **ABT-737** in the region of the p2 pocket (**Figure 1.6C,D**). In spite of this, for both scaffolds with the p2 extension only very moderate gains in binding to BCL-X<sub>L</sub> were observed (2-3-fold for compounds **1.9** and **1.10**, relative to **1.1**; (**Table 1.1** – ‘post-2015 data’).



**Figure 1.6: Design of scaffolds with p2 extension to make use of interactions in p2 pocket.**

(A) Overlay of X-ray crystal structures of the BCL-X<sub>L</sub>:**1.1** complex and the BCL-X<sub>L</sub>:**ABT-737** complex (PDB entry 2YXJ)<sup>(10)</sup>, indicating potential to grow the molecule into the p2 pocket. (B) Two different scaffolds designed to extend into p2 pocket - compound **1.9** (rigid biphenyl p2 scaffold) and compound **1.10** (flexible tetrahydroisoquinoline (THIQ) scaffold). (C) X-ray crystal structure of BCL-X<sub>L</sub>:compound **1.10** complex (D) Overlay of compound **1.10** (from BCL-X<sub>L</sub>:**1.10** complex) with **ABT-737** (from BCL-X<sub>L</sub>:**ABT-737** complex).



**Table 1.1: IC<sub>50</sub> values of benzoylurea compounds for BCL-X<sub>L</sub> and MCL-1 (determined by AlphaScreen competition assay (A.S.))**

Compound	IC <sub>50</sub> A.S. <sup>[a]</sup> (pre-2015 data) <sup>[b]</sup>			IC <sub>50</sub> A.S. <sup>[a]</sup> (post-2015 data) <sup>[b]</sup>		
	BCL-X <sub>L</sub>	MCL-1	N=	BCL-X <sub>L</sub>	MCL-1	N=
<b>1.1</b>	4.6 ±1.0	74 ±20	3	0.51 ±0.07	7.7 ±1.6	3
<b>1.2</b>	38 ±11	73 ±12	6	13.0 ±0.4	44 ±8	3
<b>1.3</b>	>100 -	>100 -	3	>100 -	>100 -	3
<b>1.4</b>	ND -	ND -	-	>100 -	>100 -	3
<b>1.5</b>	>100 -	83 ±34	4	31 ±9	28 ±5	3
<b>1.6</b>	23 ±7	70 ±20	3	1.1 ±0.05	8 ±2	3
<b>1.7</b>	2.1 ±0.4	43 ±6	5	0.38 ±0.07	11.8 ±0.8	3
<b>1.8</b>	1.5 ±0.3	68 ±11	5	0.59 ±0.11	11.6 ±1.0	3
<b>1.9</b>	1.7 ±0.6	23 ±7	4	0.24 ±0.04	1.5 ±0.05	3
<b>1.10</b>	1.8 ±0.4	28 ±5	4	0.21 ±0.09	2.0 ±0.1	3
<b>ABT-737</b>	<0.001 -	>100 -	5	0.004 ±0.004	44 ±59	2

<sup>[a]</sup> IC<sub>50</sub> values are reported in  $\mu\text{M} \pm \text{S.D.}$

<sup>[b]</sup> Following the relocation of our Screening Group, a consistent shift in the IC<sub>50</sub> values determined using the AlphaScreen competition assay was observed. The signifiers '**pre-2015 data**' and '**post-2015 data**' indicate respectively data acquired prior and subsequent to this relocation. For further information refer to note in **Chapter 2, Section 2.4.1.3.**

## 1.10 Thesis Outline/Aims

Although a challenging target for medicinal chemistry, the development of selective inhibitors of prosurvival BCL-2 family proteins (including BCL-X<sub>L</sub>) is of therapeutic interest in a number of disease contexts, in particular oncology.

My PhD aimed to build on this initial benzoylurea series (based on lead **1.1**) and utilise structure-based methods to guide the development of novel inhibitors with improved potency and selectivity towards BCL-X<sub>L</sub>.

### Aims:

The particular aims of my PhD were to:

- Use available structural data to guide the design and synthesis of novel benzoylurea analogues of compound **1.1** with a view to improving the affinity and selectivity for BCL-X<sub>L</sub>.
  - Initially to prepare analogues based on the synthetically simpler 'biphenyl' scaffold of compound **1.1** to test simple hypotheses.
  - Subsequently, translate promising modifications to the synthetically more complex 'extended' scaffolds represented by compounds **1.9/1.10**.
- Prepare, crystallise and determine X-ray crystal structures for particular analogues of interest within the series in complex with BCL-X<sub>L</sub>, in order to validate and structurally characterise their mode of interaction.
- Biochemically characterise analogues within the series, in terms of:
  - Binding affinity for BCL-X<sub>L</sub>
  - Selectivity within the BCL-2 family
  - Mechanism-of-action studies

## 1.11 References

1. Strasser A, Cory S, & Adams JM (2011) Deciphering the rules of programmed cell death to improve therapy of cancer and other diseases. *The EMBO Journal* 30(18):3667-3683.
2. Amundson SA, *et al.* (2000) An informatics approach identifying markers of chemosensitivity in human cancer cell lines. *Cancer Research* 60:6101-6110.
3. Muchmore SW, *et al.* (1996) X-ray and NMR structure of human Bcl-xL, an inhibitor of programmed cell death. *Nature* 381(6580):335-341.
4. Petros AM, *et al.* (2000) Rationale for Bcl-xL/Bad peptide complex formation from structure, mutagenesis, and biophysical studies. *Protein Science* 9(12):2528-2534.
5. Sattler M (1997) Structure of Bcl-xL-Bak peptide complex: recognition between regulators of apoptosis. *Science* 275(5302):983-986.
6. Liu X, Dai S, Zhu Y, Marrack P, & Kappler JW (2003) The structure of a Bcl-xL/Bim fragment complex: implications for Bim function. *Immunity* 19(3):341-352.
7. Oberstein A, Jeffrey PD, & Shi Y (2007) Crystal structure of the Bcl-XL-Beclin 1 peptide complex: Beclin 1 is a novel BH3-only protein. *Journal of Biological Chemistry* 282(17):13123-13132.
8. Oltersdorf T, *et al.* (2005) An inhibitor of Bcl-2 family proteins induces regression of solid tumours. *Nature* 435(7042):677-681.
9. Adams JM & Cory S (2007) The Bcl-2 apoptotic switch in cancer development and therapy. *Oncogene* 26(9):1324-1337.
10. Lee EF, *et al.* (2007) Crystal structure of ABT-737 complexed with Bcl-xL: implications for selectivity of antagonists of the Bcl-2 family. *Cell Death and Differentiation* 14(9):1711-1713.
11. Congreve M, Murray CW, & Blundell TL (2005) Keynote review: Structural biology and drug discovery. *Drug Discovery Today* 10(13):895-907.
12. Arkin MR & Wells JA (2004) Small-molecule inhibitors of protein-protein interactions: progressing towards the dream. *Nature Reviews. Drug Discovery* 3(4):301-317.

13. Wells JA & McClendon CL (2007) Reaching for high-hanging fruit in drug discovery at protein-protein interfaces. *Nature* 450(7172):1001-1009.
14. Hardy LW & Malikayil A (2003) The impact of structure-guided drug design on clinical agents. *Current Drug Discovery* 3:15-20.
15. van Montfort RLM & Workman P (2009) Structure-based design of molecular cancer therapeutics. *Trends in biotechnology* 27(5):315-328.
16. Colman PM (1994) Structure-based drug design. *Current Opinion in Structural Biology* 4(6):868-874.
17. von Itzstein M, *et al.* (1993) Rational design of potent sialidase-based inhibitors of influenza virus replication. *Nature* 363(6428):418-423.
18. Stevens RC (2003) The cost and value of three-dimensional protein structure. *Drug Discovery World*.
19. Jacobson KA (2015) New paradigms in GPCR drug discovery. *Biochemical pharmacology* 98(4):541-555.
20. Piscitelli CL, Kean J, de Graaf C, & Deupi X (2015) A molecular pharmacologist's guide to G protein-coupled receptor crystallography. *Molecular Pharmacology* 88(3):536-551.
21. Shi Y (2014) A glimpse of structural biology through X-ray crystallography. *Cell* 159(5):995-1014.
22. Varghese JN, Laver WG, & Colman PM (1983) Structure of the influenza virus glycoprotein antigen neuraminidase at 2.9 Å resolution. *Nature* 303(5912):35-40.
23. Colman PM, Varghese JN, & Laver WG (1983) Structure of the catalytic and antigenic sites in influenza virus neuraminidase. *Nature* 303(5912):41-44.
24. Colman PM, *et al.* (1987) Three-dimensional structure of a complex of antibody with influenza virus neuraminidase. *Nature* 326(6111):358-363.
25. Colman PM (2005) Zanamivir: an influenza virus neuraminidase inhibitor. *Expert Review of Anti-Infective Therapy* 3(2):191-199.
26. Lapatto R, *et al.* (1989) X-ray analysis of HIV-1 proteinase at 2.7 Å resolution confirms structural homology among retroviral enzymes. *Nature* 342(6247):299-302.

27. Miller M, *et al.* (1989) Structure of complex of synthetic HIV-1 protease with a substrate-based inhibitor at 2.3 Å resolution. *Science* 246(4934):1149-1152.
28. Gait MJ & Karn J (1995) Progress in anti-HIV structure-based drug design. *Trends in Biotechnology* 13(10):430-438.
29. Arkin MR, Tang Y, & Wells JA (2014) Small-molecule inhibitors of protein-protein interactions: progressing toward the reality. *Chemistry & Biology* 21:1102-1114.
30. Hopkins AL & Groom CR (2002) The druggable genome. *Nature Reviews. Drug Discovery* 1(9):727-730.
31. Congreve M, Chessari G, Tisi D, & Woodhead AJ (2008) Recent developments in fragment-based drug discovery. *Journal of Medicinal Chemistry* 51(13):3661-3680.
32. Pellecchia M, *et al.* (2008) Perspectives on NMR in drug discovery: a technique comes of age. *Nature Reviews. Drug discovery* 7(9):738-745.
33. Shuker SB, Hajduk PJ, Meadows RP, & Fesik SW (1996) Discovering high-affinity ligands for proteins: SAR by NMR. *Science* 274(5292):1531-1534.
34. Berg JM (2007) *Biochemistry* (W. H. Freeman, New York) 6th ed.
35. Lipinski C & Hopkins A (2004) Navigating chemical space for biology and medicine. *Nature* 432(7019):855-861.
36. Lipinski CA, Lombardo F, Dominy BW, & Feeney PJ (2001) Experimental and computational approaches to estimate solubility and permeability in drug discovery and development settings. *Advanced Drug Delivery Reviews* 46(1-3):3-26.
37. Andricopulo A, Salum L, & Abraham D (2009) Structure-based drug design strategies in medicinal chemistry. *Current Topics in Medicinal Chemistry* 9(9):771-790.
38. Kuntz ID (1992) Structure-based strategies for drug design and discovery. *Science* 257(5073):1078-1082.
39. Wong S & Witte ON (2004) The BCR-ABL story: bench to bedside and back. *Annual Review of Immunology* 22:247-306.

40. Delbridge ARD, Grabow S, Strasser A, & Vaux DL (2016) Thirty years of BCL-2: translating cell death discoveries into novel cancer therapies. *Nature Reviews. Cancer* 16(2):99-109.
41. Lindsten T, *et al.* (2000) The combined functions of proapoptotic Bcl-2 family members bak and bax are essential for normal development of multiple tissues. *Molecular Cell* 6(6):1389-1399.
42. Liu X, Kim CN, Yang J, Jemmerson R, & Wang X (1996) Induction of apoptotic program in cell-free extracts: requirement for dATP and cytochrome c. *Cell* 86(1):147-157.
43. Yang J, *et al.* (1997) Prevention of apoptosis by Bcl-2: release of cytochrome c from mitochondria blocked. *Science* 275(5303):1129-1132.
44. Kluck RM, Bossy-Wetzel E, Green DR, & Newmeyer DD (1997) The release of cytochrome c from mitochondria: a primary site for Bcl-2 regulation of apoptosis. *Science* 275(5303):1132-1136.
45. Bratton SB & Salvesen GS (2010) Regulation of the Apaf-1-caspase-9 apoptosome. *Journal of Cell Science* 123(Pt 19):3209-3214.
46. Youle RJ & Strasser A (2008) The BCL-2 protein family : opposing activities that mediate cell death. *Nature Reviews. Molecular Cell Biology* 9(1):47-59.
47. Hanahan D & Weinberg RA (2000) The Hallmarks of Cancer. *Cell* 100(1):57-70.
48. Fletcher JL, *et al.* (2008) Apoptosis is triggered when prosurvival Bcl-2 proteins cannot restrain Bax. *Proceedings of the National Academy of Sciences of the United States of America* 105(47):18081-18087.
49. Willis SN, *et al.* (2005) Proapoptotic Bak is sequestered by Mcl-1 and Bcl-xL, but not Bcl-2, until displaced by BH3-only proteins. *Genes & Development* 19(11):1294-1305.
50. Moldoveanu T, *et al.* (2006) The X-ray structure of a BAK homodimer reveals an inhibitory zinc binding site. *Molecular Cell* 24(5):677-688.
51. Suzuki M, Youle RJ, & Tjandra N (2000) Structure of Bax: coregulation of dimer formation and intracellular localization. *Cell* 103(4):645-654.
52. Huang DC & Strasser A (2000) BH3-Only proteins-essential initiators of apoptotic cell death. *Cell* 103(6):839-842.

53. Czabotar PE, *et al.* (2013) Bax crystal structures reveal how BH3 domains activate Bax and nucleate its oligomerization to induce apoptosis. *Cell* 152(3):519-531.
54. Brouwer JM, *et al.* (2014) Bak core and latch domains separate during activation, and freed core domains form symmetric homodimers. *Molecular Cell* 55(6):938-946.
55. Letai A, *et al.* (2002) Distinct BH3 domains either sensitize or activate mitochondrial apoptosis, serving as prototype cancer therapeutics. *Cancer Cell* 2(3):183-192.
56. Llambi F, *et al.* (2011) A unified model of mammalian BCL-2 protein family interactions at the mitochondria. *Molecular Cell* 44(4):517-531.
57. Simonen M, Keller H, & Heim J (1997) The BH3 domain of Bax is sufficient for interaction of Bax with itself and with other family members and it is required for induction of apoptosis. *European Journal of Biochemistry* 249(1):85-91.
58. Wang K, Gross a, Waksman G, & Korsmeyer SJ (1998) Mutagenesis of the BH3 domain of BAX identifies residues critical for dimerization and killing. *Molecular and Cellular Biology* 18(10):6083-6089.
59. Echeverry N, *et al.* (2013) Intracellular localization of the BCL-2 family member BOK and functional implications. *Cell Death and Differentiation* 20(6):785-799.
60. Czabotar PE, *et al.* (2011) Mutation to Bax beyond the BH3 domain disrupts interactions with pro-survival proteins and promotes apoptosis. *Journal of Biological Chemistry* 286(9):7123-7131.
61. Lessene G, *et al.* (2013) Structure-guided design of a selective BCL-XL inhibitor. *Nature Chemical Biology* 9(6):390-397.
62. Czabotar PE, *et al.* (2007) Structural insights into the degradation of Mcl-1 induced by BH3 domains. *Proceedings of the National Academy of Sciences of the United States of America* 104(15):6217-6222.
63. Lee EF, *et al.* (2008) A novel BH3 ligand that selectively targets Mcl-1 reveals that apoptosis can proceed without Mcl-1 degradation. *Journal of Cell Biology* 180(2):341-355.

64. Tsujimoto Y, Finger L, Yunis J, Nowell P, & Croce C (1984) Cloning of the chromosome breakpoint of neoplastic B cells with the t(14;18) chromosome translocation. *Science* 226(4678):1097-1099.
65. Tsujimoto Y & Croce CM (1986) Analysis of the structure, transcripts, and protein products of bcl-2, the gene involved in human follicular lymphoma. *Proceedings of the National Academy of Sciences of the United States of America* 83(14):5214-5218.
66. Bakhshi A, *et al.* (1985) Cloning the chromosomal breakpoint of t(14;18) human lymphomas: clustering around JH on chromosome 14 and near a transcriptional unit on 18. *Cell* 41(3):899-906.
67. Cleary ML & Sklar J (1985) Nucleotide sequence of a t(14;18) chromosomal breakpoint in follicular lymphoma and demonstration of a breakpoint-cluster region near a transcriptionally active locus on chromosome 18. *Proceedings of the National Academy of Sciences of the United States of America* 82(21):7439-7443.
68. Cleary ML, Smith SD, & Sklar J (1986) Cloning and structural analysis of cDNAs for bcl-2 and a hybrid bcl-2/immunoglobulin transcript resulting from the t(14;18) translocation. *Cell* 47(1):19-28.
69. Vaux DL, Cory S, & Adams JM (1988) Bcl-2 gene promotes haemopoietic cell survival and cooperates with c-myc to immortalize pre-B cells. *Nature* 335(6189):440-442.
70. McDonnell TJ, *et al.* (1989) bcl-2-immunoglobulin transgenic mice demonstrate extended B cell survival and follicular lymphoproliferation. *Cell* 57(1):79-88.
71. Nunez G, *et al.* (1989) Growth- and tumor-promoting effects of deregulated BCL2 in human B-lymphoblastoid cells. *Proceedings of the National Academy of Sciences of the United States of America* 86(12):4589-4593.
72. Nunez G, *et al.* (1990) Deregulated Bcl-2 gene expression selectively prolongs survival of growth factor-deprived hemopoietic cell lines. *Journal of Immunology* 144(9):3602-3610.
73. Tsujimoto Y (1989) Stress-resistance conferred by high level of bcl-2 alpha protein in human B lymphoblastoid cell. *Oncogene* 4(11):1331-1336.



74. Hockenbery D, Nuñez G, Milliman C, Schreiber RD, & Korsmeyer SJ (1990) Bcl-2 is an inner mitochondrial membrane protein that blocks programmed cell death. *Nature* 348(6299):334-336.
75. Vazquez A, Bond EE, Levine AJ, & Bond GL (2008) The genetics of the p53 pathway, apoptosis and cancer therapy. *Nature Reviews. Drug Discovery* 7(12):979-987.
76. Khaw SL, Huang DCS, & Roberts AW (2009) BH3-mimetics--the solution to chemoresistance? *Leukemia & Lymphoma* 50(7):1069-1072.
77. Certo M, *et al.* (2006) Mitochondria primed by death signals determine cellular addiction to antiapoptotic BCL-2 family members. *Cancer Cell* 9(5):351-365.
78. Chen L, *et al.* (2005) Differential targeting of prosurvival Bcl-2 proteins by their BH3-only ligands allows complementary apoptotic function. *Molecular Cell* 17(3):393-403.
79. Whitty A & Kumaravel G (2006) Between a rock and a hard place? *Nature Chemical Biology* 2(3):112-118.
80. Basse MJ, *et al.* (2013) 2P2Idb: a structural database dedicated to orthosteric modulation of protein-protein interactions. *Nucleic Acids Research* 41(D1):D824-827.
81. Higuieruelo AP, *et al.* (2009) Atomic interactions and profile of small molecules disrupting protein-protein interfaces: the TIMBAL database. *Chemical Biology & Drug Design* 74(5):457-467.
82. Labbe CM, Laconde G, Kuenemann MA, Villoutreix BO, & Sperandio O (2013) iPPI-DB: a manually curated and interactive database of small non-peptide inhibitors of protein-protein interactions. *Drug Discovery Today* 18(19-20):958-968.
83. Jones S & Thornton JM (1996) Principles of protein-protein interactions. *Proceedings of the National Academy of Sciences of the United States of America* 93(1):13-20.
84. Lo Conte L, Chothia C, & Janin J (1999) The atomic structure of protein-protein recognition sites. *Journal of Molecular Biology* 285(5):2177-2198.
85. Filippakopoulos P, *et al.* (2010) Selective inhibition of BET bromodomains. *Nature* 468(7327):1067-1073.

86. Picaud S, *et al.* (2013) RVX-208, an inhibitor of BET transcriptional regulators with selectivity for the second bromodomain. *Proceedings of the National Academy of Sciences of the United States of America* 110(49):19754-19759.
87. Filippakopoulos P & Knapp S (2014) Targeting bromodomains: epigenetic readers of lysine acetylation. *Nature Reviews. Drug Discovery* 13(5):337-356.
88. Rooney TPC, *et al.* (2014) A Series of Potent CREBBP Bromodomain Ligands Reveals an Induced-Fit Pocket Stabilized by a Cation- $\pi$  Interaction. *Angewandte Chemie International Edition*.
89. Garnier J-M, Sharp PP, & Burns CJ (2014) BET bromodomain inhibitors: a patent review. *Expert Opinion on Therapeutic Patents* 24(2):185-199.
90. Ferguson FM, *et al.* (2013) Targeting low-druggability bromodomains: fragment based screening and inhibitor design against the BAZ2B bromodomain. *Journal of Medicinal Chemistry* 56(24):10183-10187.
91. Zobel K, *et al.* (2006) Design, synthesis, and biological activity of a potent Smac mimetic that sensitizes cancer cells to apoptosis by antagonizing IAPs. *ACS Chemical Biology* 1(8):525-533.
92. Bai L, Smith DC, & Wang S (2014) Small-molecule SMAC mimetics as new cancer therapeutics. *Pharmacology & Therapeutics* 144(1):82-95.
93. Vassilev LT, *et al.* (2004) In vivo activation of the p53 pathway by small-molecule antagonists of MDM2. *Science* 303(5659):844-848.
94. Shangary S & Wang S (2009) Small-molecule inhibitors of the MDM2-p53 protein-protein interaction to reactivate p53 function: a novel approach for cancer therapy. *Annual Review of Pharmacology and Toxicology* 49:223-241.
95. Rew Y, *et al.* (2012) Structure-Based Design of Novel Inhibitors of the MDM2-p53 Interaction. *Journal of Medicinal Chemistry* 55(11):4936-4954.
96. Petros AM, *et al.* (2006) Discovery of a potent inhibitor of the antiapoptotic protein Bcl-xL from NMR and parallel synthesis. *Journal of Medicinal Chemistry* 49(2):656-663.
97. Lipinski CA (2016) Rule of five in 2015 and beyond: Target and ligand structural limitations, ligand chemistry structure and drug discovery project decisions. *Advanced Drug Delivery Reviews* 101:34-41.

98. Leeson PD & Springthorpe B (2007) The influence of drug-like concepts on decision-making in medicinal chemistry. *Nature Reviews. Drug Discovery* 6(11):881-890.
99. Hann MM (2011) Molecular obesity, potency and other addictions in drug discovery. *Medicinal Chemistry Communications* 2(5):349.
100. Waring MJ (2010) Lipophilicity in drug discovery. *Expert Opinion on Drug Discovery* 5(3):235-248.
101. Selzer P, Roth HJ, Ertl P, & Schuffenhauer A (2005) Complex molecules: do they add value? *Current Opinion in Chemical Biology* 9(3):310-316.
102. Hopkins AL, Groom CR, & Alex A (2004) Ligand efficiency: a useful metric for lead selection. *Drug Discovery Today* 9(10):430-431.
103. Hajduk PJ (2006) Fragment-based drug design: how big is too big? *Journal of Medicinal Chemistry* 49(24):6972-6976.
104. Wendt MD (2008) Discovery of ABT-263, a Bcl-family protein inhibitor: observations on targeting a large protein-protein interaction. *Expert Opinion on Drug Discovery* 3(9):1123-1143.
105. Lessene G, Czabotar PE, & Colman PM (2008) BCL-2 family antagonists for cancer therapy. *Nature Reviews. Drug Discovery* 7(12):989-1000.
106. Wei MC, *et al.* (2001) Proapoptotic BAX and BAK: a requisite gateway to mitochondrial dysfunction and death. *Science* 292(5517):727-730.
107. Zhang H, *et al.* (2007) Bcl-2 family proteins are essential for platelet survival. *Cell Death and Differentiation* 14(5):943-951.
108. Mason KD, *et al.* (2007) Programmed anuclear cell death delimits platelet life span. *Cell* 128(6):1173-1186.
109. Josefsson EC, *et al.* (2011) Megakaryocytes possess a functional intrinsic apoptosis pathway that must be restrained to survive and produce platelets. *The Journal of Experimental Medicine* 208(10):2017-2031.
110. Tse C, *et al.* (2008) ABT-263: a potent and orally bioavailable Bcl-2 family inhibitor. *Cancer Research* 68(9):3421-3428.
111. Wilson WH, *et al.* (2010) Navitoclax, a targeted high-affinity inhibitor of BCL-2, in lymphoid malignancies: a phase 1 dose-escalation study of safety, pharmacokinetics, pharmacodynamics, and antitumour activity. *The Lancet Oncology* 11(12):1149-1159.

112. Roberts AW, *et al.* (2012) Substantial susceptibility of chronic lymphocytic leukemia to BCL2 inhibition: results of a phase I study of navitoclax in patients with relapsed or refractory disease. *Journal of Clinical Oncology* 30(5):488-496.
113. Sadowsky JD, *et al.* (2005) Chimeric (alpha/beta + alpha)-peptide ligands for the BH3-recognition cleft of Bcl-XL: critical role of the molecular scaffold in protein surface recognition. *Journal of the American Chemical Society* 127(34):11966-11968.
114. Sadowsky JD, *et al.* (2007) (alpha/beta+alpha)-peptide antagonists of BH3 domain/Bcl-x(L) recognition: toward general strategies for foldamer-based inhibition of protein-protein interactions. *Journal of the American Chemical Society* 129(1):139-154.
115. Lee EF, *et al.* (2009) High-resolution structural characterization of a helical alpha/beta-peptide foldamer bound to the anti-apoptotic protein Bcl-xL. *Angewandte Chemie International Edition* 48(24):4318-4322.
116. Stewart ML, Fire E, Keating AE, & Walensky LD (2010) The MCL-1 BH3 helix is an exclusive MCL-1 inhibitor and apoptosis sensitizer. *Nature Chemical Biology* 6(8):595-601.
117. Delft MFV, *et al.* (2006) The BH3 mimetic ABT-737 targets selective Bcl-2 proteins and efficiently induces apoptosis via Bak/Bax if Mcl-1 is neutralized. *Cancer Cell* 10(5):389-399.
118. Elmore SW, *et al.* (2008) WO2008131000A2.
119. Tanaka Y, *et al.* (2013) Discovery of potent Mcl-1/Bcl-xL dual inhibitors by using a hybridization strategy based on structural analysis of target proteins. *Journal of Medicinal Chemistry* 56(23):9635-9645.
120. Konopleva M, *et al.* (2006) Mechanisms of apoptosis sensitivity and resistance to the BH3 mimetic ABT-737 in acute myeloid leukemia. *Cancer Cell* 10(5):375-388.
121. Del Gaizo Moore V, *et al.* (2007) Chronic lymphocytic leukemia requires BCL2 to sequester prodeath BIM, explaining sensitivity to BCL2 antagonist ABT-737. *Journal of Clinical Investigation* 117(1):112-121.
122. Bruncko M, *et al.* (2007) Studies leading to potent, dual inhibitors of Bcl-2 and Bcl-xL. *Journal of Medicinal Chemistry* 50(4):641-662.

123. Wendt MD, *et al.* (2006) Discovery and structure-activity relationship of antagonists of B-cell lymphoma 2 family proteins with chemopotential activity in vitro and in vivo. *Structure* 1:1165-1181.
124. Gandhi L, *et al.* (2011) Phase I study of Navitoclax (ABT-263), a novel Bcl-2 family inhibitor, in patients with small-cell lung cancer and other solid tumors. *Journal of Clinical Oncology* 29(7):909-916.
125. Rudin CM, *et al.* (2012) Phase 2 study of single agent navitoclax (ABT-263) and biomarker correlates in patients with relapsed small cell lung cancer. *Clinical Cancer Research* 18(11):3163-9.
126. Chen J, *et al.* (2012) Structure-based discovery of BM-957 as a potent small-molecule inhibitor of Bcl-2 and Bcl-xL capable of achieving complete tumor regression. *Journal of Medicinal Chemistry* 55(19):8502-8514.
127. Schroeder GM, *et al.* (2012) Pyrazole and pyrimidine phenylacylsulfonamides as dual Bcl-2/Bcl-xL antagonists. *Bioorganic & Medicinal Chemistry Letters* 22(12):3951-3956.
128. Perez HL, *et al.* (2012) Identification of a phenylacylsulfonamide series of dual Bcl-2/Bcl-xL antagonists. *Bioorganic & Medicinal Chemistry Letters* 22(12):3946-3950.
129. Zhou H, *et al.* (2012) Design of Bcl-2 and Bcl-xL Inhibitors with subnanomolar binding affinities based upon a new scaffold. *Journal of Medicinal Chemistry* 55(10):4664-4682.
130. Aguilar A, *et al.* (2013) A potent and highly efficacious Bcl-2/Bcl-xL inhibitor. *Journal of Medicinal Chemistry* 56(7):3048-3067.
131. Sleebs BE, *et al.* (2011) Quinazoline sulfonamides as dual binders of the proteins B-cell lymphoma 2 and B-cell lymphoma extra long with potent proapoptotic cell-based activity. *Journal of Medicinal Chemistry* 54(6):1914-1926.
132. Touré BB, *et al.* (2013) The role of the acidity of N-heteroaryl sulfonamides as inhibitors of Bcl-2 family protein–protein interactions. *ACS Medicinal Chemistry Letters* 4(2):186-190.
133. Yusuff N, *et al.* (2012) Lipophilic isosteres of a  $\pi$ – $\pi$  stacking interaction: new inhibitors of the Bcl-2-Bak protein–protein Interaction. *ACS Medicinal Chemistry Letters* 3:579-583.

134. Bai L, *et al.* (2014) BM-1197: a novel and specific Bcl-2/Bcl-xL inhibitor inducing complete and long-lasting tumor regression in vivo. *PLoS ONE* 9(6):e99404.
135. Rautureau GJP, *et al.* (2012) The restricted binding repertoire of Bcl-B leaves Bim as the universal BH3-only prosurvival Bcl-2 protein antagonist. *Cell Death & Disease* 3(12):e443.
136. Dutta S, *et al.* (2010) Determinants of BH3 binding specificity for Mcl-1 versus Bcl-x L. *Journal of Molecular Biology* 398(5):747-762.
137. Boersma MD, Sadowsky JD, Tomita YA, & Gellman SH (2008) Hydrophile scanning as a complement to alanine scanning for exploring and manipulating protein-protein recognition: application to the Bim BH3 domain. *Protein Science* 17(7):1232-1240.
138. Souers AJ, *et al.* (2013) ABT-199, a potent and selective BCL-2 inhibitor, achieves antitumor activity while sparing platelets. *Nature Medicine* 19:202-208.
139. Roberts AW, *et al.* (2016) Targeting BCL2 with venetoclax in relapsed chronic lymphocytic leukemia. *New England Journal of Medicine* 374(4):311-322.
140. Green DR (2016) A BH3 mimetic for killing cancer cells. *Cell* 165(7):1560.
141. Shoemaker AR, *et al.* (2006) A small-molecule inhibitor of Bcl-XL potentiates the activity of cytotoxic drugs in vitro and in vivo. *Cancer Research* 66(17):8731-8739.
142. Sleebs BE, *et al.* (2013) Discovery of potent and selective benzothiazole hydrazone inhibitors of Bcl-XL. *Journal of Medicinal Chemistry* 56(13):5514-5540.
143. Koehler MFT, *et al.* (2014) Structure-guided rescaffolding of selective antagonists of BCL-XL. *ACS Medicinal Chemistry Letters* 5(6):662-667.
144. Tao Z-F, *et al.* (2014) Discovery of a potent and selective BCL-XL inhibitor with in vivo activity. *ACS Medicinal Chemistry Letters* 5(10):1088-1093.
145. Levenson JD, *et al.* (2015) Exploiting selective BCL-2 family inhibitors to dissect cell survival dependencies and define improved strategies for cancer therapy. *Science Translational Medicine* 7(279):279ra240.

146. Friberg A, *et al.* (2013) Discovery of potent myeloid cell leukemia 1 (Mcl-1) inhibitors using fragment-based methods and structure-based design. *Journal of Medicinal Chemistry* 56(1):15-30.
147. Burke JP, *et al.* (2015) Discovery of tricyclic indoles that potently inhibit Mcl-1 using fragment-based methods and structure-based design. *Journal of Medicinal Chemistry* 58(9):3794-3805.
148. Bruncko M, *et al.* (2015) Structure-guided design of a series of MCL-1 inhibitors with high affinity and selectivity. *Journal of Medicinal Chemistry* 58(5):2180-2194.
149. Levenson JD, *et al.* (2015) Potent and selective small-molecule MCL-1 inhibitors demonstrate on-target cancer cell killing activity as single agents and in combination with ABT-263 (navitoclax). *Cell Death & Disease* 6:e1590.
150. Fang C, *et al.* (2014) Single diastereomer of a macrolactam core binds specifically to myeloid cell leukemia 1 (MCL1). *ACS Medicinal Chemistry Letters* 5(12):1308-1312.
151. Kotschy A, *et al.* (2016) The MCL1 inhibitor S63845 is tolerable and effective in diverse cancer models. *Nature* 538(7626):477-482.
152. Schoenwaelder SM, *et al.* (2011) Bcl-xL-inhibitory BH3 mimetics can induce a transient thrombocytopenia that undermines the hemostatic function of platelets. *Blood* 118(6):1663-1674.
153. Kelly PN, Grabow S, Delbridge ARD, Strasser A, & Adams JM (2011) Endogenous Bcl-xL is essential for Myc-driven lymphomagenesis in mice. *Blood* 118(24):6380-6386.
154. Espana L, *et al.* (2004) Overexpression of Bcl-xL in human breast cancer cells enhances organ-selective lymph node metastasis. *Breast Cancer Research and Treatment* 87(1):33-44.
155. Olopade OI, *et al.* (1997) Overexpression of Bcl-x protein in primary breast cancer is associated with high tumor grade and nodal metastases. *The Cancer Journal from Scientific American* 3(4):230-237.
156. Boise LH, *et al.* (1993) bcl-x, a bcl-2-related gene that functions as a dominant regulator of apoptotic cell death. *Cell* 74(4):597-608.

157. Fennell DA, Corbo MV, Dean NM, Monia BP, & Cotter FE (2001) In vivo suppression of Bcl-XL expression facilitates chemotherapy-induced leukaemia cell death in a SCID/NOD-Hu model. *British Journal of Haematology* 112(3):706-713.
158. Simonian PL, Grillot Da, & Nuñez G (1997) Bcl-2 and Bcl-XL can differentially block chemotherapy-induced cell death. *Blood* 90(3):1208-1216.
159. Veis DJ, Sorenson CM, Shutter JR, & Korsmeyer SJ (1993) Bcl-2-deficient mice demonstrate fulminant lymphoid apoptosis, polycystic kidneys, and hypopigmented hair. *Cell* 75(2):229-240.
160. Speir M, *et al.* (2016) Eliminating Legionella by inhibiting BCL-XL to induce macrophage apoptosis. *Nature Microbiology* 1:15034.
161. Brady RM, *et al.* (2014) De-novo designed library of benzoylureas as inhibitors of BCL-XL: synthesis, structural and biochemical characterization. *Journal of Medicinal Chemistry* 57(4):1323-1343.
162. Brady RM, *et al.* (2012) Synthesis of conformationally constrained benzoylureas as BH3-mimetics. *Organic & Biomolecular Chemistry* 10(27):5230-5237.
163. Lessene G, Smith BJ, Gable RW, & Baell JB (2009) Characterization of the two fundamental conformations of benzoylureas and elucidation of the factors that facilitate their conformational interchange. *Journal of Organic Chemistry* 74(17):6511-6525.
164. Ubbink M (2009) The courtship of proteins: Understanding the encounter complex. *FEBS Letters* 583(7):1060-1066.



## **2 Chapter two – Experimental Section**

## 2.1 Introduction to techniques

This Section provides a brief background to the main experimental techniques described in this Thesis; detailed experimental procedures are provided in **Sections 2.3 - 2.6**.

### 2.1.1 X-ray Crystallography

An excellent background on the principles and practice of protein X-ray Crystallography is presented in the textbook 'Biomolecular Crystallography' by Bernhard Rupp<sup>(1)</sup>.

### 2.1.2 Measuring binding affinity and selectivity

#### 2.1.2.1 AlphaScreen™ solution competition assay

A solution competition-based assay was developed at WEHI utilising the AlphaScreen™ technology ('amplified luminescent proximity homogeneous assay', Perkin-Elmer Lifesciences) to determine the binding of different compounds to BCL-X<sub>L</sub> or MCL-1. Initially developed for high-throughput screening (HTS), this assay measures the ability of each compound at a given concentration to out-compete a BH3 peptide (BIM-BH3 or BAK-BH3 respectively) for binding to the prosurvival protein.

This system utilises donor beads (Streptavidin-coated) and acceptor beads (Glutathione-coated) bound respectively to biotinylated BH3 peptide or GST-tagged prosurvival protein. Illumination at 680nm causes the donor beads to excite ambient oxygen to a short-lived excited singlet state. This in turn excites acceptor beads in close proximity resulting in a fluorescent emission at 520-620nm<sup>(2)</sup> As the short-lived oxygen species can only diffuse approximately 200nm in solution before returning to the ground state,<sup>(2)</sup> compounds which disrupt the BH3 peptide/prosurvival protein interaction will interrupt the close donor-acceptor proximity, resulting in a measurable drop in measured emission fluorescence intensity.

A dose-response curve is then generated from the measured emission intensity relative to no-protein (minimum intensity) and DMSO-only (maximum intensity) controls, from which relative binding affinity as a half maximal inhibitory concentration ( $IC_{50}$ ) is then calculated.

#### 2.1.2.2 Surface plasmon resonance (SPR) competition assay (Biacore 3000)

Instruments utilizing surface plasmon resonance (SPR)-based biosensors such as the Biacore Instruments (GE Healthcare) provide a very sensitive and reproducible method for analyzing protein-protein or protein-small molecule interactions. SPR instruments detect small changes in the refractive index of the buffer flowing over the biosensor chip; as occurs when a target molecule interacts with a protein which has been immobilised to the chip surface<sup>(3, 4)</sup>.

As a measure of compound selectivity,  $IC_{50}$  values for all analogues towards each of the prosurvival proteins (BCL-2, BCL- $X_L$ , BCL-W, MCL-1, A1) were determined using a solution competition assay on a Biacore 3000 SPR instrument using an immobilized BIM peptide (as described below).

#### 2.1.3 Measuring mechanism-based activity *in vitro*

##### 2.1.3.1 Cytochrome *c* release assay

Binding studies have demonstrated that in mouse embryonic fibroblast cells (MEFs), restraint of the proapoptotic activity of BAK is essentially provided by MCL-1 and BCL- $X_L$  and no other prosurvival proteins<sup>(5)</sup>. BAK-mediated apoptosis *via* the mitochondrial pathway will thus be induced in wild-type MEFs if both MCL-1 and BCL- $X_L$  are first neutralized. Hence, an *in vitro* cell-derived method to evaluate whether compounds will inhibit BCL- $X_L$  prosurvival activity, is to test whether the compounds are able to cause release of cytochrome *c* from the intact mitochondria of lysed MCL-1 deficient (*MCL-1*<sup>-/-</sup>) MEFs.

Mitochondria from wild-type (WT) and *BAX*<sup>-/-</sup>/*BAK*<sup>-/-</sup> MEFs are utilised as controls to ensure, respectively, that cytochrome *c* release is due to the effect of the compound on BCL-X<sub>L</sub> alone, and that any cytochrome *c* release from the mitochondria occurs *via* a BAX/BAK-dependent mechanism rather than by disrupting the integrity of the mitochondrial membrane in some other fashion.

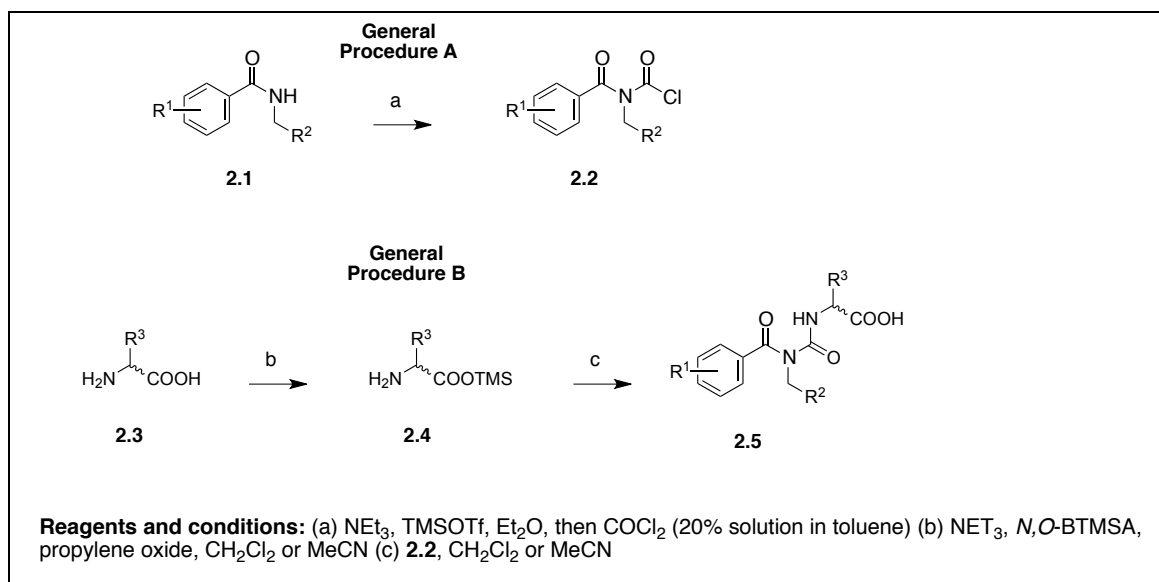
## 2.2 General Chemistry Methods

In this Chapter general synthetic methods are described; detailed synthetic methods are provided in the 'Experimental' sub-section of each Chapter.

### 2.2.1 General Chemistry Methods

All non-aqueous reactions were performed in oven-dried glassware under inert atmosphere, unless otherwise specified. Tetrahydrofuran, dichloromethane, diethyl ether and ethanol were obtained from a solvent drying apparatus (MBraun). Anhydrous dimethylformamide (DMF), dioxane and acetonitrile were obtained from Aldrich and used without further purification. All other solvents were reagent grade. Petroleum ether describes a mixture of hexanes in the bp range 40-60 °C. Analytical thin-layer chromatography was performed on Merck silica gel 60F<sub>254</sub> aluminum-backed plates and were visualized by fluorescence quenching under UV light. Flash chromatography was performed with silica gel 60 (particle size 0.040-0.063 mm) either manually or using a Combiflash platform. Some of the final compounds described herein were purified using a mass-directed preparative HPLC using a mixture of 0.1% formic acid in water and acetonitrile (exact gradient included for corresponding compounds). NMR spectra were recorded on a Bruker Avance DRX 300 (<sup>1</sup>H NMR at 300 MHz, <sup>13</sup>C NMR at 75 MHz), Varian 600 (<sup>1</sup>H NMR at 600 MHz) or a Bruker AVIII 600MHz (<sup>1</sup>H NMR at 600 MHz, <sup>13</sup>C NMR at 151 MHz) using the solvents indicated. Chemical shifts are reported in ppm on the  $\delta$  scale and referenced to the appropriate solvent peak. HRMS analyses were carried out at the Monash University Mass Spectrometry Facility on an Agilent 6224 TOF LC/MS mass spectrometer coupled to an Agilent 1290 Infinity (Agilent, Palo Alto, CA). All data were acquired and reference mass corrected via a dual-spray electrospray ionisation (ESI) source. Acquisition was performed using the Agilent Mass Hunter Data Acquisition software version B.06.01 Build 6.01.6157 and analysis was performed using Mass Hunter Qualitative Analysis version B.07.00 Build Service Pack 1. LCMS were recorded on a Waters ZQ 3100 using a 2996 diode array detector. LCMS conditions used to assess purity of compounds were as follows, column: XBridge TM C18 5  $\mu$ m 4.6 x 100 mm, injection

volume 10  $\mu\text{L}$ , gradient: 10-100% B over 10 min (solvent A: water 0.1% formic acid; solvent B: AcCN 0.1% formic acid), flow rate: 1.5 mL/min, detection: 100-600 nm. All final compounds were analyzed using ultrahigh performance liquid chromatography/ultraviolet/evaporative light scattering detection coupled to mass spectrometry.



**Scheme 2.1: General Procedures A and B**

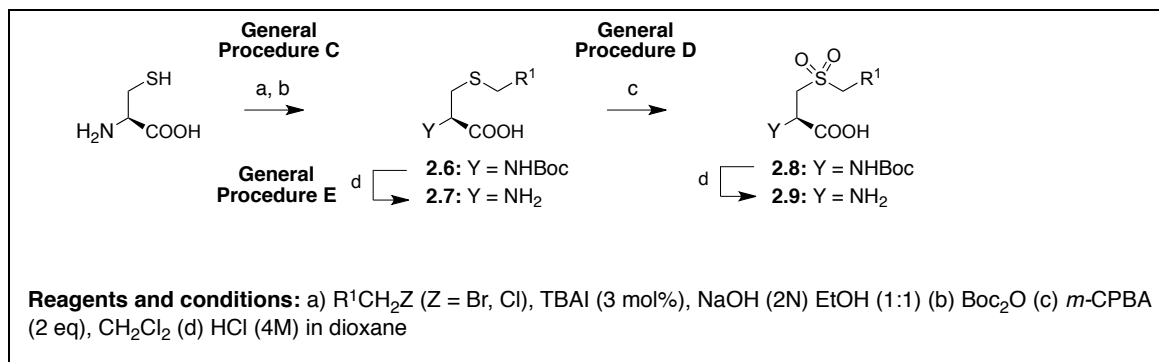
### 2.2.2 General Procedure A: Carbamoyl chloride formation [described in Chapters 3-6]

To a stirred solution of the amide (of generalised structure **2.1**) (1 eq.) in anhydrous diethyl ether (2 mL per mmol of amide starting material) in an oven-dried Schlenk tube under  $\text{N}_2$  was added triethylamine (1.1 eq.), followed by TMSOTf (1.1 eq.) and the reaction was stirred under  $\text{N}_2$  at room temperature for 30 minutes. After this time, phosgene (2 mL per mmol of amide starting material, 20% w/v in toluene, **CAUTION!**) was added to the solution at  $0^\circ\text{C}$ , which was then allowed to warm to room temperature and stirred under  $\text{N}_2$  for 1.5 h. After this time, the reaction was concentrated *in vacuo* (using an in-line solvent trap) over a room temperature water bath to afford the carbamoyl chloride residue **2.2**. This compound was used in the subsequent benzoylurea formation step without further purification.

### 2.2.3 General Procedure B: *In-situ* protection of amino acid and benzoylurea formation [described in Chapters 3-6]

The requisite amino acid (of generalised structure **2.3**) (1.5 eq. relative to the starting amide for carbamoyl chloride formation) was suspended in anhydrous dichloromethane (or acetonitrile where indicated) (4 mL per mmol of amino acid) and stirred under N<sub>2</sub> at room temperature. For amino acid HCl salts, triethylamine (1.1 eq. relative to the amino acid HCl salt) was initially added to neutralise the HCl salt. Propylene oxide (2 mL per mmol of amino acid) and *N,O*-bistrimethylsilylacetamide (BTMSA) (0.24 mL per mmol of amino acid) were then added and the reaction was stirred at room temperature for 30 minutes. The *in-situ* protected amino acid (of general structure **2.4**) was used directly in the next step without further purification.

Under a N<sub>2</sub> atmosphere, the carbamoyl chloride **2.2** from **General Procedure A** was redissolved in anhydrous dichloromethane (or acetonitrile where indicated) (1 mL per mmol of starting amide) and then transferred to the stirred suspension of the *in situ* protected amino acid **2.4** at 0°C. The reaction was allowed to warm to room temperature and stirred at room temperature for 1.5 h. After this time, the reaction was diluted with EtOAc and poured onto aqueous 1M HCl. The reaction mixture was extracted three times with EtOAc. The combined organic layers were washed with water, then brine, dried over MgSO<sub>4</sub> and concentrated. Purification *via* flash chromatography, eluting with a gradient of methanol/dichloromethane (0:100 to 5:95) afforded the desired benzoylurea product **2.5**.



**Scheme 2.2: General Procedures C - E**

#### 2.2.4 General Procedure C: Cysteine S-alkylation and Boc-protection [described in Chapter 4]

Alkylated cysteine derivatives were generally prepared according to a procedure described in the literature<sup>(6)</sup>. Briefly, to a stirred solution of L-cysteine (200 mg, 1.65 mmol) in a 1:1 solution of NaOH (2 N) and EtOH (total 2.0 mL/mmol of amino acid) was added the alkyl halide (1.1 eq.) followed by tetrabutylammonium iodide (TBAI) (3 mol%). The reaction was allowed to proceed for 3 days at room temperature, then di-*tert*-butyl dicarbonate (1.1 eq.) was added and the reaction was stirred for a further 24 h at room temperature. Ethanol was removed under reduced pressure, the residue was taken up in EtOAc (20 mL) and then 10% aq. citric acid solution (20 mL) was added. The two phases were separated, the aqueous phase was further extracted with EtOAc (2 x 10 mL), and the combined organic phases washed with brine, dried over anhydrous  $MgSO_4$ , filtered and concentrated under reduced pressure to yield the crude thioether product of general structure **2.6**.

#### 2.2.5 General Procedure D: Thioether oxidation [described in Chapter 4]

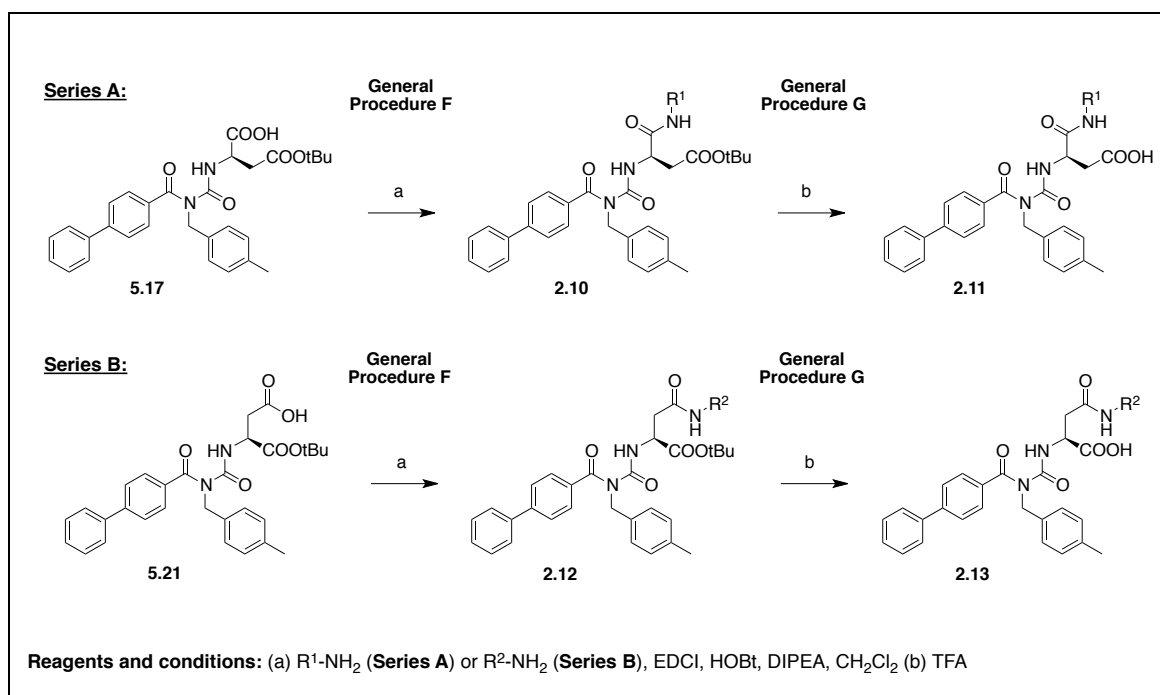
To a stirred solution of the thioether **2.6** (1 eq.) in dichloromethane (10 mL/mmol) at 0°C was added *m*-CPBA (max 77%, 2 eq.) and the reaction was allowed to warm to room temperature and proceed for 3 h. After this time, the reaction was diluted with  $CH_2Cl_2$  (20 mL) then washed with 10% aq. sodium metabisulfite, 10% aq.  $NaHCO_3$ , and brine, dried over anhydrous  $MgSO_4$  and concentrated under



reduced pressure. Purification *via* flash chromatography, eluting with a gradient of methanol/dichloromethane (0:100 to 5:95 to 10:90) afforded the desired purified sulfone product of general structure **2.8**.

### 2.2.6 General Procedure E: Boc-deprotection with HCl [described in Chapter 4]

The Boc-protected amino acid (of generalised structure **2.6** or **2.8**) (1.0 eq.) was treated with HCl (4M) in 1,4-dioxane (1.5 mL per mmol of protected amino acid) under N<sub>2</sub> with stirring for 3 h at room temperature. Where a precipitate formed, this was filtered, washed with a small volume of diethyl ether and dried *in vacuo*. Alternatively, the reaction mixture was concentrated to dryness, residues were triturated with diethyl ether and again concentrated to dryness. The resulting HCl salt (of general structure **2.7** or **2.9**) was used directly in the next step without further purification.



**Scheme 2.3: General Procedures F – G.**

### 2.2.7 General Procedure F: Parallel amide-coupling to benzoylurea [described in Chapter 5]

The general procedure described below was scaled to conduct multiple reactions in parallel using different primary/secondary amines; typically ~5-10 reactions were conducted in parallel.

To a stirred solution of the *tert*-butyl-protected benzoylurea (compound **5.17** (*Series A*) or compound **5.21** (*Series B*)) (1 eq.) in anhydrous dichloromethane (1 mL) was added EDCI (1.2 eq.) and HOBt (1.2 eq.) followed by DIEA (2.5 eq.) and allowed to stir at room temperature for 30 minutes. After this time, 1 mL (1 eq.) of the reaction mixture was transferred to a stirred sample of amine **B** (1.1 eq.) followed by an additional portion of dichloromethane (1 mL) used to rinse the reaction vessel.

The reaction was allowed to proceed at room temperature until TLC indicated the reaction was complete (generally ~6 h). The reaction mixture was then purified by passing through a short plug of silica (~3 cm in glass pipette) into a glass vial, using a low back-pressure of nitrogen gas. Product remaining on the silica was eluted with dichloromethane (up to three 1 mL fractions) followed by methanol (up to two 1 mL fractions); fractions were analysed by TLC and fractions containing pure product were pooled then concentrated (under a steady flow of nitrogen gas over a 30°C heat block) to yield crude the *tert*-butyl-protected benzoylurea amide intermediate.

### 2.2.8 General Procedure G: TFA-deprotection [described in Chapter 5]

The *tert*-butyl protecting group was removed by dissolving the crude *tert*-butyl-protected benzoylurea amide intermediate in TFA (~0.500 mL) then allowing the reaction to proceed for 1 h at room temperature. After this time, TFA was carefully removed (under a steady flow of nitrogen gas over a 40°C heat block) (caution!) to yield the crude final benzoylurea amide product, which was further purified by mass-directed preparative HPLC to yield the pure product.

## 2.3 Recombinant proteins and synthetic peptides

The recombinant proteins listed in **Table 2.1** were provided by the Czabotar and Colman labs as purified protein stocks stored at -20°C. The expression constructs listed in **Table 2.2** were provided by the Czabotar and Colman labs as cell stocks stored at -80°C. Peptides were purchased from Mimotopes.

**Table 2.1: Purified recombinant protein stocks**

Construct		Source	Ref
<i><b>AlphaScreen competition assay</b></i>			
GST-BCL-X <sub>L</sub>	human BCL-X <sub>L</sub> (ΔC24), N-terminal GST fusion	Czabotar/ Colman labs	(7, 8)
GST-MCL-1	human/mouse chimeric MCL-1 (ΔN170, ΔC23), N-terminal GST fusion	Czabotar/ Colman labs	(8, 9)
Biotin-GST	biotinylated GST (for counter screen)	Perkin-Elmer	
<i><b>SPR competition assay</b></i>			
BCL-W	human BCL-W (ΔC29, C29S/A128E), N-terminal 6-His fusion	Czabotar/ Colman labs	(7, 10)
A1	mouse A1 (ΔC20, P104K)	Czabotar/ Colman labs	(11)

**Table 2.2: Expression constructs**

	<b>Construct</b>	<b>Vector</b>	<b>Cell type</b>	<b>Ref</b>
<b><i>SPR competition assay</i></b>				
BCL-X <sub>L</sub>	human BCL-X <sub>L</sub> ( $\Delta$ C24)	pGEX-6P-3 (Amersham Biosciences)	BL21(DE3)	(7)
MCL-1	human/mouse chimeric MCL-1 ( $\Delta$ N170, $\Delta$ C23)	pGEX-6P-3 (Amersham Biosciences)	C41(DE3)	(9)
BCL-2	“Loop-deleted” BCL-2 N-terminal 6-His fusion	human ( $\Delta$ C22), (Qiagen)	pQE-9 BL21(DE3)	(7, 10)
<b><i>Structural studies</i></b>				
‘BCL-X <sub>L</sub> ’	“Loop-deleted” BCL-X <sub>L</sub> ( $\Delta$ 27-82, $\Delta$ C24)	human (Amersham Biosciences)	pGEX-6P-3 BL21(DE3)	(12)

### 2.3.1 Protein expression and purification

#### 2.3.1.1 BCL-X<sub>L</sub> for SPR competition assay

A C-terminally truncated form of human BCL-X<sub>L</sub> ( $\Delta$ C24) was expressed as a GST fusion protein and cleaved from glutathione-sepharose columns with PreScission protease.

A starter culture containing Luria-broth medium with ampicillin (100  $\mu$ g/mL, Sigma) was inoculated from the glycerol stock provided, then incubated overnight in a shaking incubator at 37°C (200 rpm). Cultures were grown in Super-broth medium with ampicillin (100  $\mu$ g/mL) inoculated with starter culture (8 mL per 1 L flask of medium) in a shaking incubator (200 rpm) at 37°C to OD<sub>600nm</sub> ~ 0.7 a.u. Protein expression was induced with IPTG (1 mM, BioVectra) and cultures were grown for 3 h at 37°C (200 rpm), then cell pellets harvested by ultracentrifugation (5000 rpm, 20 minutes) and frozen at -80°C.

Cell pellets (2 L expression) were resuspended in GST buffer (50 mL), consisting of 50 mM Tris (pH 8.0), 150 mM NaCl, 1 mM EDTA (Ajax Finechem). DNase I (250 U, Roche) was added and cells were lysed using either a high-pressure homogeniser (EmulsiFlex-C5, Avestin Inc) or *via* sonication (18 x 10 s pulses at 74 W, Sonicator 3000, Misonix) on ice in the presence of lysozyme (~ 0.5 mg/mL, Sigma). Cellular debris was removed by centrifugation (20,000 rpm, 15 minutes, 4°C) and filtration (0.4 µm syringe filter). The clarified supernatant was passed twice over a 4B glutathione sepharose column (1 mL bed volume, GE Healthcare), which had been pre-equilibrated in GST buffer. The column was washed twice with GST buffer (2 x 20 mL), then on-column cleavage of the GST affinity tag was performed by passing over a solution of 60 µL PreScission Protease (provided by the Call lab) in GST buffer (10 mL) until 1 mL remained, then storing the sealed column at 4°C for 18 h. The GST-cleaved protein was eluted from the column, then purified on a Superdex 75 16/60 column in TBS buffer. Fractions were analysed by SDS-PAGE, then pooled and concentrated to ~1.6 mg/mL (10 kDa MWCO Amicon Ultra-4 and Ultra-0.5, Millipore), snap-frozen in liquid nitrogen (50 µL aliquots) and stored at -80°C, for use in SPR experiments. Protein concentrations were calculated from the measured  $A_{280\text{nm}}$  absorbance using a NanoDrop 3000 (Thermo Scientific).

#### 2.3.1.2 MCL-1 for SPR competition assay

Human/mouse chimeric MCL-1 ( $\Delta\text{N170}$ ,  $\Delta\text{C23}$ ) was expressed as a GST fusion protein and cleaved from glutathione-sepharose columns with PreScission protease and purified as described previously<sup>(9)</sup>.

Cultures were expressed and purified as for human BCL-X<sub>L</sub> ( $\Delta\text{C24}$ ) (above), with the modification that they were grown to  $\text{OD}_{600\text{nm}} \sim 1.0$  a.u. prior to induction with IPTG (1 mM, BioVectra).

### 2.3.1.3 BCL-2 for SPR competition assay

Recombinant human BCL-2 ( $\Delta$ C22) was expressed as N-terminal 6-His fusion protein in *E. coli* and purified as described previously<sup>(10)</sup>.

Briefly, a starter culture containing Luria-broth medium with ampicillin (100  $\mu$ g/mL, Sigma) was inoculated from the glycerol stock provided, then incubated overnight in a shaking incubator at 37°C (200 rpm). Cultures were grown in Super-broth medium with ampicillin (100  $\mu$ g/mL) inoculated with starter culture (30 mL per 0.66 L flask of medium) in a shaking incubator (200 rpm) at 37°C to OD<sub>600nm</sub> ~ 0.7 a.u. Protein expression was induced with IPTG (0.5 mM, BioVectra) and cultures were grown for 2 h at 37°C (200 rpm), then cell pellets harvested by ultracentrifugation (14,000 rpm, 2 minutes) and frozen at -80°C.

Cell pellets (1 L expression) were resuspended in a 50 mL Falcon Tube in lysis buffer (60 mL), consisting of 50 mM Tris-HCl pH 8.0, 100 mM NaCl, supplemented with 2-mercaptoethanol (0.5 mol%). PMSF (160  $\mu$ L, 50 mM stock) and lysozyme (160  $\mu$ L, 100 mg/mL stock) were added, the tube shaken vigorously and mixed for 20 minutes on a room temperature roller bed. Deoxycholic acid (80 mg) was then added, the mixture shaken vigorously and incubated for 10 minutes in a 37°C water bath. DNase I (250 U, Roche) was then added and the lysate mixed for a further 20 minutes on a room temperature roller bed until no longer viscous. Cellular debris was removed by centrifugation (20,000 rpm, 20 minutes, 4°C) and filtration (0.4  $\mu$ m syringe filter). The clarified supernatant was passed twice over a HiTrap Chelating HP column (1 mL bed volume, GE Healthcare), which had been charged with NiSO<sub>4</sub> and pre-equilibrated in lysis buffer (5 mL) immediately before use. The column was washed with 50 mM imidazole (10 mL) and the protein eluted in 625 mM imidazole (5 mL), which was then purified directly on a Superdex 75 16/60 column in TBS buffer, supplemented with 2-mercaptoethanol (0.5 mol%). Fractions were analysed by SDS-PAGE and stored at 4°C for immediate use in SPR experiments.

#### 2.3.1.4 Loop-deleted BCL-X<sub>L</sub> for Structural Studies

The “loop-deleted” form of human BCL-X<sub>L</sub> ( $\Delta 27-82$ ,  $\Delta C24$ )<sup>(12)</sup> used for structural studies was expressed in *E. coli* as an N-terminal GST fusion and purified as described previously<sup>(8, 11, 13)</sup>.

Briefly, cultures were expressed and purified as for human BCL-X<sub>L</sub> ( $\Delta C24$ ) (above), with the modification that following induction with IPTG (1 mM, BioVectra) the cultures were grown for 16 h overnight at 17°C (180 rpm) before cell pellets were harvested and frozen at -80°C. Following GST-purification/cleavage and purification by size exclusion chromatography, the eluted purified protein fractions were analysed by SDS-PAGE, pooled and concentrated to 10 mg/mL (10 kDa MWCO Amicon Ultra-4 and Ultra-0.5, Millipore), snap-frozen in liquid nitrogen (25  $\mu$ L aliquots) and stored at -80°C, for use in crystallization trials.

## 2.4 Measuring binding affinity and selectivity

### 2.4.1 AlphaScreen competition assay

Relative binding affinities of compounds for GST-BCL-X<sub>L</sub> and GST-MCL-1 were determined using a solution competition assay based upon an AlphaScreen™ GST donor/acceptor bead detection system (Perkin-Elmer Lifesciences) as described in detail elsewhere<sup>(8, 11, 14)</sup>. These assays were performed by members of the Screening Group at WEHI. Briefly, AlphaScreen donor beads (Streptavidin-coated) were used to bind a biotinylated BH3 peptide (BIM or BAK) and acceptor beads (Glutathione coated) to bind GST tagged prosurvival protein (GST-BCL-X<sub>L</sub> or GST-MCL-1 respectively). As these beads are light-sensitive, all solutions were prepared or incubated in a darkened room or under green light.

The assay buffer was prepared on the day of testing and consisted of 25 mM HEPES pH 7.4 (Sigma) 25 mM Tris-HCl (pH 7.4), 5 mM DTT (BioVectra), 50 mM NaCl, 0.03% Tween-20 (Sigma) and 0.1 mg/mL Casein (Sigma), prepared in MilliQ water. Stocks of GST-BCL-X<sub>L</sub> (23.5  $\mu$ M), GST-MCL-1 (114  $\mu$ M) and biotinylated-GST (77  $\mu$ M), along with biotinylated-BAK (500  $\mu$ M, Auspep) and biotinylated-BIM (500  $\mu$ M, Auspep) were provided as frozen stocks at -80°C and thawed on ice prior to use. GST-mhMCL-1 is a GST-tagged chimera consisting of residues 152-189 from mouse MCL-1 and 209-327 from human MCL-1. Biotinylated-BAK and biotinylated-BIM peptides and GST-mhMCL-1 were initially diluted 1:10 in assay buffer.

#### 2.4.1.1 Compound plate preparation

One compound plate was prepared for each independent set of stock solutions. Into columns 1 and 12 of a new row on a 384-well low volume conical polypropylene microplate (Corning Life Sciences) was added each compound at a concentration of 3.3 mM (for 100  $\mu$ M resulting concentration in assay), by adding 6.2  $\mu$ L of compound stock solution (10 mM) to 11.8  $\mu$ L 100% DMSO (AnalaR). Into all empty rows and columns 22 and 24 was added 15  $\mu$ L 100% DMSO.



Compound plates were sealed with foil and centrifuged (2000 rpm, 1 min) then serially titrated over 11 points (2.5-fold dilution) over columns 1-11 and 12-22 using the MiniTrak™ robot (PerkinElmer Lifesciences) then re-sealed with foil to prevent evaporation.

#### *2.4.1.2 Assay plate preparation*

MCL-1, BCL-X<sub>L</sub> and GST-counter acceptor bead solutions were prepared by adding 12.5 µg/mL AlphaScreen™ acceptor beads (50 µL of 5 mg/mL stock, Perkin-Elmer Lifesciences) to a solution in assay buffer (20 mL) of either 2 nM GST-mhMCL-1 (3.5 µL of 11.4 µM solution), 1.2 nM GST-BCL-X<sub>L</sub> (1.0 µL of 23.5 mM stock), or 4 nM biotinylated-GST (1.0 µL of 77 µM stock). MCL-1, BCL-X<sub>L</sub> and GST-counter donor bead solutions (20 mL each) were prepared similarly in assay buffer, containing respectively 12.5 µg/mL AlphaScreen™ Donor beads (50 µg of 5 mg/mL stock) and 10 nM biotinylated-BAK (4 µL of 50 µM solution), 12.5 µg/mL AlphaScreen™ Donor beads and 4 nM biotinylated-BIM (1.60 µL of 50 µM solution), or 12.5 µg/mL AlphaScreen™ Donor beads only. A 'no-protein acceptor' solution containing 12.5 µg/mL AlphaScreen™ acceptor beads (10 µL of 5 mg/mL stock) in 4 mL assay buffer was prepared as a negative control.

Assay plates (384-well low volume white round-bottom polystyrene microplate, Corning Life Sciences) were prepared in duplicate for each of MCL-1, BCL-X<sub>L</sub> and GST-counter, by adding 5 µL of the relevant acceptor solution to columns 1-23 (Multi-drop Combi bulk reagent dispenser, Thermo Scientific) followed by 5 µL of donor solution to columns 1-24 (Multi-drop Combi). 5 µL of 'no protein acceptor' solution was added to column 24. One set of duplicate assay plates was prepared for each compound plate. Assay plates were covered and incubated at room temperature for 10 minutes. The Microlab STAR robot (Hamilton Robotics) was used to transfer 0.3 µL of sample from well on each compound plate to the corresponding well on each duplicate assay plate. Assay plates were sealed (MicroAmp Optical adhesive film, Invitrogen), incubated in a darkened room for 4 h then read on the Envision Multilabel Reader (Perkin-Elmer Lifesciences).

Briefly, compounds (prepared from 10 mM stocks in DMSO) were titrated into 384-well assay plates (low volume conical polypropylene microplate, Corning Life Sciences) (1% (v/v) DMSO final concentration) and following a 4 h incubation, their relative ability to bind to prosurvival protein (attached to acceptor beads) and thereby displace the binding of BH3 peptide (attached to donor beads) led to a corresponding decrease in donor-acceptor proximity. The resulting drop in measured emission fluorescence intensity was detected using an Envision Multilabel Reader (Perkin Elmer Lifesciences).

Dose-response curves are then generated with ActivityBase software (IDBS) using the measured emission intensity relative to no-protein (minimum intensity) and DMSO-only (minimum intensity) controls.

Data was loaded into the ActivityBase database (IDBS) and percent inhibition was calculated using the following equation:

$$\%Inhibition = 100 * \left( 1 - \frac{(x - \mu_{c-})}{(\mu_{c+} - \mu_{c-})} \right)$$

where

x = RFU obtained after compound treatment

$\mu_{c-}$  = RFU obtained for the negative controls (no protein controls, column 24)

$\mu_{c+}$  = RFU obtained for the positive controls (DMSO vehicle controls, column 23)

IC<sub>50</sub> values were obtained by non-linear least squares fitting of the above data to XLfit3 equation 205:  $y=A+((B-A)/(1+[(C/x)^D]))$  (Microsoft Excel).

#### *2.4.1.3 Note on variation between AlphaScreen assay dates (pre-2015/post-2015 data)*

The AlphaScreen competition assay, to determine binding to BCL-X<sub>L</sub> and MCL-1, was performed by the WEHI Screening group. In mid-2015, the group relocated buildings within the Institute. Since the time of the move, we have observed a potency shift in the AlphaScreen IC<sub>50</sub> values for all of the different compound series that are measured using this assay. Whilst in general the trends and relative

values within a series have been maintained, the absolute IC<sub>50</sub> values determined since the date of the move appear in the range 6-10-fold higher affinity. The basis for the difference has not been determined. For clarity, within this Thesis all AlphaScreen-derived IC<sub>50</sub> values determined before or since this time are indicated as 'pre-2015' and 'post-2015' respectively.

#### **2.4.2 SPR competition assay (Biacore 3000)**

Expression and purification of loop-deleted human BCL-2  $\Delta$ C22, human BCL-X<sub>L</sub>  $\Delta$ C24 and human/mouse chimeric MCL-1 ( $\Delta$ N170, $\Delta$ C23) were performed as described above<sup>(7, 9, 15)</sup>. Purified frozen protein stocks of human BCL-W  $\Delta$ C29 (C29S/A128E) and mouse A1-(P104K) were provided by the Czabotar/Colman labs. Synthetic peptides were synthesized by Mimotopes and purified by reverse-phase HPLC to >90% purity.

##### *2.4.2.1 Binding Affinity Measurements – SPR competition assay*

Solution competition assays were performed using a Biacore 3000 instrument as described previously<sup>(8, 11, 16)</sup>.

Briefly, prosurvival proteins (10 nM) were incubated with varying concentrations of compounds (12.5  $\mu$ M – 0.0001  $\mu$ M) for 2 h in running buffer [10 mM HEPES, 150 mM NaCl, 3.4 mM EDTA, and 0.005% (v/v) Tween 20, pH 7.4] prior to injection onto a CM5 sensor chip onto which either a wild-type mBIMBH3 (DLRPEIRIAQELRRIGDEFNETYTRR) peptide or an inert mBIMBH3 (DLRPEIREAQE**ER**REGDE**EN**ETYTRR) mutant peptide (mutations in bold) were immobilized (via N-hydroxysuccinimide coupling) to a density of approximately 100 RU. Specific binding of the prosurvival protein to the surface in the presence and absence of compounds was quantified by subtracting the signal from the BIM mutant channel from that obtained on the wild-type BIM channel, following 'global analysis' baseline correction for each using the BIAevaluation software (version 4.1, Biacore). IC<sub>50</sub> values were calculated by nonlinear curve fitting of the data with Prism software (version 6.0h for Macintosh OS X, GraphPad Software).

## 2.5 Measuring mechanism-based activity *in vitro*

### 2.5.1 *In vitro* cytochrome c release assay

#### 2.5.1.1 Tissue culture

Cells were maintained at 37°C in a humidified 10% CO<sub>2</sub> incubator, in FMA medium - a high glucose DME medium supplemented with 10% (v/v) foetal calf serum (FCS) (Bovogen), 250 mM L-asparagine and 50 mM 2-mercaptoethanol.

#### 2.5.1.2 *In vitro* cytochrome c release assay

The following buffers were used:

- Permeabilisation buffer, consisting of 0.025% digitonin (10% (v/v) stock, Calbiochem) in 100 mM KCl, 5 mM MgCl<sub>2</sub>, 1 mM EDTA, 1 mM EGTA, 250 mM sucrose. Digitonin was added immediately prior to use.
- Onyx buffer, consisting of 20 mM Tris-HCl (pH 7.4), 135 mM NaCl, 1.5 mM MgCl<sub>2</sub>, 1.0 mM EDTA, 10% glycerol, 1% Triton X-100.
- 2x SDS buffer (without 2-mercaptoethanol).

Primary antibodies were provided by the Huang Lab. Cultured wild-type (WT), *MCL-1*<sup>-/-</sup> and *BAX*<sup>-/-</sup>/*BAK*<sup>-/-</sup> MEFs were provided by the Huang lab and grown to confluence in T150 flasks. After washing twice with 10 mL MT-PBS, cells were detached by adding 3 mL Trypsin (5 minutes at room temperature), resuspended in a further 7 mL FMA medium, then each cell suspension pooled and placed on ice. After cell counting, the required number of cells (15 x 10<sup>5</sup> cells per 50 µL final sample volume) were aliquotted, pelleted by centrifugation (1500 rpm, 5 minutes, 4°C) then lysed by resuspending in 50 µL permeabilisation buffer supplemented with Complete Protease Inhibitor (Roche) and incubating at 5 minutes in ice.

Cell permeabilisation was confirmed by trypan blue and 50 µL crude lysates (containing mitochondria) were incubated with 10 µM test compound (final DMSO

concentration 3%) for 1 h at 30°C. After this time, lysates were centrifuged (13,000 rpm, 5 minutes, 4°C), supernatant collected and added to 2x SDS loading buffer, boiled at 95°C for 5 minutes then frozen at -80°C (soluble fraction). Each pellet (intact mitochondria fraction) was resuspended in 50  $\mu$ L Onyx buffer supplemented with Complete Protease Inhibitor (Roche), then incubated for 15 minutes on ice. Pellet fractions were centrifuged (13,000 rpm, 5 minutes, 4°C), supernatant collected, added to 2x SDS loading buffer, boiled at 95°C for 5 minutes, then frozen at -80°C (pellet fraction).

Thawed 'supernatant' and 'pellet' fractions (40  $\mu$ L samples; 8  $\mu$ L SeeBlue Plus2 molecular weight marker, Invitrogen) were resolved by SDS-PAGE (NuPAGE 10% Bis-Tris 1.5 mm 10-well pre-cast gels, Invitrogen) then transferred to a nitrocellulose membrane for western blot analysis using the iBlot Gel Transfer System (Invitrogen). Membranes were cut into two bands by molecular weight (actin ~ 40 kDa, cytochrome *c* ~13 kDa) and blocked for 15 minutes at room temperature with PBST buffer (MT-PBS/0.01% Tween) with 5% Skim milk.

Primary antibody, either mouse anti-actin (1:2000, clone AC-40, Sigma) or mouse anti-cytochrome *c* (1:1000, BE2, BD Pharmingen) was added and membranes incubated overnight at 4°C. Membranes were washed three times with PBST buffer (10 minutes room temperature incubations), incubated for 1 h at room temperature with anti-mouse-HRP (1:2000, Goat Anti-mouse Ig(H+L)-HRP, human adsorbed, Southern Biotech) in PBST buffer with 5% Skim milk, washed again three times with PBST buffer, then developed with ECL western blotting detection reagents (Amersham Biosciences) using a ChemiDoc MP Imager (Bio-Rad).

## 2.5.2 Platelet-killing assay

Generation of *BAX*<sup>-/-</sup>/*BAK*<sup>-/-</sup> chimeric mice and isolation of platelets was performed by Stephane Chappaz.

### 2.5.2.1 *BAX*<sup>-/-</sup>/*BAK*<sup>-/-</sup> Chimeric Mice

Chimeric mice were generated by reconstituting lethally irradiated wild type Ly5.1 recipients (2 x 550 Rad) with CD45.2+ *BAX*<sup>-/-</sup>/*BAK*<sup>-/-</sup> foetal livers isolated from 14.5 days post coitus embryos. 6 weeks post transplant, chimerism was assessed by flow cytometry to confirm that haematopoietic cells were derived exclusively from donor origin.

### 2.5.2.2 Platelet preparation

Blood was collected from either wild-type or *BAX*<sup>-/-</sup>/*BAK*<sup>-/-</sup> chimeric mice (C57 Bl/6) by cardiac puncture into 0.1 volume of Aster Jandl anticoagulant (AJ) (85 mM sodium citrate dihydrate, 69 mM citric acid, 20 mg/mL glucose, pH 4.6). Mouse platelet rich plasma was obtained by centrifugation at 125 x g for 8 minutes. Platelets were washed by two sequential centrifugations at 860 x g for 5 minutes in wash buffer (140 mM NaCl, 5 mM KCl, 12 mM sodium citrate, 10 mM glucose, 12.5 mM sucrose, pH 6.0) and resuspended in a small volume of re-suspension buffer (RB) (140 mM NaCl, 3 mM KCl, 0.5 mM MgCl<sub>2</sub>, 0.5 mM NaHCO<sub>3</sub>, 10 mM HEPES, 10 mM glucose, pH 7.4). The platelet concentration was determined using Sphero blank calibration particles (3.5-4.0  $\mu$ m, Spherotech Inc., Libertyville, IL) on a FACSCalibur flow cytometer (BD). For a typical experiment, platelets were diluted RB to a final concentration of 10 x 10<sup>6</sup> cells/mL.

### 2.5.2.3 Compound titration, platelet incubation and CD41/Annexin-V staining

Compounds (including DMSO-only negative control) were prepared in 96-well round-bottom plates in a 65  $\mu$ L volume as an 11-point, 1.5-fold serial titration series starting from 0.25  $\mu$ M (**ABT-737**) or 25  $\mu$ M (test compounds) in 1%DMSO/RB. A buffer-only control was included in the final row. To each well was added 65  $\mu$ L of the platelet suspension ( $10 \times 10^6$  cells/mL) and the 96-well plates incubated at 37°C in a humidified incubator (5% CO<sub>2</sub>) for 1.5 h. The resulting final highest compound concentrations were thus 0.125  $\mu$ M (**ABT-737**) or 12.5  $\mu$ M (test compounds). After 37°C incubation, platelets were stained by transferring 30  $\mu$ L of the compound-treated platelet mixture to 20  $\mu$ L of a stain solution, containing FITC-conjugated Annexin-V (Life Technologies), allophycocyanin (APC)-conjugated rat anti-mouse CD41 (WEHI) and 2.5 mM CaCl<sub>2</sub> (final concentration) in RB. Plates were incubated in the dark for 20 minutes at room temperature then samples were transferred to fluorescence-assisted cell sorting (FACS) tubes for analysis.

#### 2.5.2.4 Flow cytometry

Platelets were then assessed for Annexin-V binding on a FACSCalibur cytometer. Platelets were identified by forward and side scatter and positivity for CD41-APC. Thereafter the percentage of platelets positive for Annexin-V-FITC was determined. 3000 events were acquired (Cell Quest), and data analysed with FlowJo software (Treestar). Forward/side scatter was used as an indicator of whether platelets had become activated due to compound treatment. The percentage of Annexin-V positive platelets as a function of compound concentration was plotted using Prism (GraphPad) and EC<sub>50</sub> values were determined by curve-fitting using non-linear regression.

### 2.5.3 MEF-viability assay

#### 2.5.3.1 Tissue culture

Cells were maintained at 37°C in a humidified 10% CO<sub>2</sub> incubator, in FMA medium - a high glucose DME medium supplemented with 10% (v/v) foetal calf serum (FCS) (Bovogen), 250 mM L-asparagine (Sigma) and 50 mM 2-mercaptoethanol (Sigma).

Cultured wild-type (WT), *MCL-1*<sup>-/-</sup> and *BAX*<sup>-/-</sup>/*BAK*<sup>-/-</sup> MEFs were provided by the Huang lab. Cells were seeded in 24-well plates at a concentration of 1 x 10<sup>4</sup> cells/well in 500 µL of FMA medium. After 24 h, media was aspirated and cells washed with FMA medium supplemented with either 1% or 10% FCS. Test compounds were prepared as a titration series by diluting compound stocks (0.5 mM for **ABT-737** and 25 mM for all other compounds in neat DMSO) in FMA medium supplemented with either 1% or 10% FCS. For **ABT-737** a 5-point 8-fold serial dilution was used (1.0 – 0.00024 µM) and for all other compounds a 5-point 2.5-fold serial dilution was used (50 – 1.3 µM), resulting in a final DMSO concentration of 0.4%. A negative DMSO-only control was also included. Diluted test compounds were then added to the cells (500 µL per well, in duplicate) and test plates incubated for 24 h.

After this time, the media from each well (containing dead cells) was aspirated and transferred to corresponding labelled FACS tubes (on ice). Trypsin (200 µL per well, 0.5% trypsin) was added to each well and once cells had detached (~5-10 minutes), FMA medium was added (200 µL per well) and cells resuspended and transferred to the corresponding FACS tubes. FACS buffer (5 mL) was added to all tubes and tubes were centrifuged (1500 rpm, 5 minutes, 4°C). The FACS buffer consisted of KDS BSS (150 mM NaCl, 3.7 mM KCl, 2.5 mM CaCl<sub>2</sub>, 1.2 mM MgSO<sub>4</sub>, 7.4 mM HEPES.NaOH, 1.2 mM KH<sub>2</sub>PO<sub>4</sub>, and 0.8 mM K<sub>2</sub>HPO<sub>4</sub>) supplemented with 2% FCS. After centrifugation the supernatant was decanted and propidium iodide (PI) was added (100 µL per tube, 0.1% (v/v) diluted in FACS buffer) and cells were resuspended ready for FACS analysis.



#### *2.5.3.2 Flow cytometry*

Cells were identified by forward and side scatter and assessed for PI positivity (FL3 channel) using a FACSCalibur cytometer. 1000 events were acquired (Cell Quest) and data was analysed with FlowJo software (Treestar). The percentage of live cells (PI negative) was determined, normalised to 100% based on the relevant DMSO-only control for each compound titration series, and plotted as a function of compound concentration using Prism (GraphPad). EC<sub>50</sub> values were determined by curve-fitting using non-linear regression.

## 2.6 Crystallisation, X-ray data acquisition, structure determination and refinement

### 2.6.1 Crystallisation

Co-crystallisation of compound complexes with BCL-X<sub>L</sub> was performed as described previously <sup>(11, 13, 14, 17)</sup>.

Briefly, BCL-X<sub>L</sub>, a C-terminally truncated, “loop-deleted” form of human BCL-X<sub>L</sub> ( $\Delta$ 27-82  $\Delta$ C24)<sup>(12)</sup> was combined with a 1.5 molar excess the relevant compound in 20 mM Tris-HCl, pH 8.0, 150 mM NaCl, supplemented with 2% DMSO. The complex was then concentrated to 10 mg/mL (10 kDa MWCO Amicon Ultra-0.5 Concentrator).

Crystals were grown at room temperature in hanging drops, by mixing 1  $\mu$ L of concentrated protein/ligand complex with 1  $\mu$ L of reservoir solution. Where indicated, streak-seeding was also utilised to improve nucleation and single crystal formation; either from crystals in neighbouring drops or from other crystal forms utilising the same protein that were known to diffract well.

Prior to flash-freezing in liquid N<sub>2</sub>, crystals were equilibrated into cryoprotectant consisting of reservoir solution and increasing concentrations of ethylene glycol to a final concentration of 25% (v/v) for ammonium sulfate conditions.

## 2.6.2 Crystallography data collection, processing and structure refinement

Further data for each complex, including crystallisation conditions and processing/refinement statistics, are provided in the relevant Chapter.

### 2.6.2.1 Data collection

X-ray data were collected at the Australian Synchrotron (MX1 or MX2 beamlines) and acquired using Blu-Ice software<sup>(18)</sup>.

### 2.6.2.2 Data processing

X-ray diffraction data for all complexes were integrated, merged and scaled with XDS<sup>(19)</sup>. Using the indexed unit cell parameters, the Matthews' Probability Calculator MATTPROB (<http://www.ruppweb.org/Mattprob/>)<sup>(20-22)</sup> was used to estimate the number of protein molecules per asymmetric unit based on estimated solvent content. This was important as a number of different crystal forms have been observed to form for different complexes with BCL-X<sub>L</sub>.

Each structure was solved by molecular replacement with PHASER<sup>(23, 24)</sup> using the search model described in the relevant Chapter (most commonly the model used consisted of the BCL-X<sub>L</sub> coordinates from the BCL-X<sub>L</sub>:1.1 complex, in each case with the ligand removed).

### 2.6.2.3 Refinement

Several iterative rounds of model building and real-space refinement in COOT<sup>(25)</sup> followed by reciprocal space refinement in with PHENIX<sup>(26)</sup> were utilised, incorporating in all cases an initial round of simulated annealing in the refinement protocol to minimise model bias. Statistics for the final models described are given in the relevant Chapter (see note in Section 2.6.2.3).

The “loop deleted” BCL-X<sub>L</sub> construct (with the large, flexible and disordered  $\alpha$ 1-2 loop removed) crystallises in the form of a domain-swapped dimer, involving a reciprocal exchange of the  $\alpha$ 1-helix of one monomer of BCL-X<sub>L</sub> into the neighbouring monomer (on the opposite face of the protein from the canonical hydrophobic groove to which small molecules are targeted)<sup>(12, 13, 27)</sup>. The increased symmetry and stability of these dimers appear to facilitate rapid crystallisation and so this construct has been incredibly useful drug discovery efforts<sup>(13)</sup>.

#### *2.6.2.4 Generation of ligand restraints and ligand searching*

Ligand geometry restraint (cif) files for each compound were generated from SMILES strings using ELBOW<sup>(28)</sup> in general using automatic geometry optimisation, or where otherwise indicated in the text, using geometry optimisation derived from the Cambridge Structural Database using MOGUL<sup>(29)</sup>.

#### *2.6.2.5 Tables of crystallographic statistics*

Tables of crystallographic statistics described in this Thesis were generated using PHENIX.TABLE\_ONE using data from XDS<sup>(19)</sup>, PHENIX<sup>(26)</sup> and MOLPROBITY<sup>(30)</sup>. Values in parentheses are for highest-resolution shell. Ligand/ions represents all nonprotein and nonwater atoms, including, for example, synthetic compounds, sulfate ions and ethylene glycol. Crystallographic data were collected in all cases from a single crystal of each complex.

## 2.7 References

1. Rupp B (2010) *Biomolecular crystallography : principles, practice, and application to structural biology* (Garland Science, New York).
2. Eglen RM, *et al.* (2008) The use of AlphaScreen technology in HTS: current status. *Current chemical genomics* 1:2-10.
3. Myszka DG (2004) Analysis of small-molecule interactions using Biacore S51 technology. *Analytical Biochemistry* 329(2):316-323.
4. Day YSN, Baird CL, Rich RL, & Myszka DG (2002) Direct comparison of binding equilibrium, thermodynamic, and rate constants determined by surface- and solution-based biophysical methods. *Protein Science* 11(5):1017-1025.
5. Willis SN, *et al.* (2005) Proapoptotic Bak is sequestered by Mcl-1 and Bcl-xL, but not Bcl-2, until displaced by BH3-only proteins. *Genes & Development* 19(11):1294-1305.
6. Seko T, *et al.* (2003) Structure–activity study of l-amino acid-based N-type calcium channel blockers. *Bioorganic & Medicinal Chemistry* 11(8):1901-1913.
7. Chen L, *et al.* (2005) Differential targeting of prosurvival Bcl-2 proteins by their BH3-only ligands allows complementary apoptotic function. *Molecular Cell* 17(3):393-403.
8. Sleebs BE, *et al.* (2011) Quinazoline sulfonamides as dual binders of the proteins B-cell lymphoma 2 and B-cell lymphoma extra long with potent proapoptotic cell-based activity. *Journal of Medicinal Chemistry* 54(6):1914-1926.
9. Czabotar PE, *et al.* (2007) Structural insights into the degradation of Mcl-1 induced by BH3 domains. *Proceedings of the National Academy of Sciences of the United States of America* 104(15):6217-6222.
10. Wilson-annan J, *et al.* (2002) Proapoptotic BH3-only proteins trigger membrane integration of prosurvival Bcl-w and neutralize its activity. *Cell*:877-887.

11. Brady RM, *et al.* (2014) De-novo designed library of benzoylureas as inhibitors of BCL-XL: synthesis, structural and biochemical characterization. *Journal of Medicinal Chemistry* 57(4):1323-1343.
12. Kvansakul M, *et al.* (2008) Vaccinia virus anti-apoptotic F1L is a novel Bcl-2-like domain-swapped dimer that binds a highly selective subset of BH3-containing death ligands. *Cell Death and Differentiation* 15(10):1564-1571.
13. Kvansakul M & Czabotar PE (2016) Preparing samples for crystallization of Bcl-2 family complexes. In Puthalakath H & Hawkins J (eds.), *Programmed Cell Death: Methods and Protocols, Methods in Molecular Biology*, vol. 1419:pp 213-229.
14. Lessene G, *et al.* (2013) Structure-guided design of a selective BCL-XL inhibitor. *Nature Chemical Biology* 9(6):390-397.
15. Lee EF, *et al.* (2008) A novel BH3 ligand that selectively targets Mcl-1 reveals that apoptosis can proceed without Mcl-1 degradation. *Journal of Cell Biology* 180(2):341-355.
16. Lee EF, *et al.* (2009) Novel Bcl-2 homology-3 domain-like sequences identified from screening randomized peptide libraries for inhibitors of the pro-survival Bcl-2 proteins. *Journal of Biological Chemistry* 284(45):31315-31326.
17. Lee EF, *et al.* (2007) Crystal structure of ABT-737 complexed with Bcl-xL: implications for selectivity of antagonists of the Bcl-2 family. *Cell Death and Differentiation* 14(9):1711-1713.
18. McPhillips TM, *et al.* (2002) Blu-Ice and the distributed control system: software for data acquisition and instrument control at macromolecular crystallography beamlines. *Journal of Synchrotron Radiation* 9(6):401-406.
19. Kabsch W (2010) Xds. *Acta Crystallographica Section D Biological Crystallography* 66(Pt 2):125-132.
20. Matthews BW (1968) Solvent content of protein crystals. *Journal of Molecular Biology* 33(2):491-497.
21. Kantardjieff KA & Rupp B (2003) Matthews coefficient probabilities: Improved estimates for unit cell contents of proteins, DNA, and protein-nucleic acid complex crystals. *Protein Science* 12(9):1865-1871.

22. Weichenberger CX & Rupp B (2014) Ten years of probabilistic estimates of biocrystal solvent content: new insights via nonparametric kernel density estimate. *Acta Crystallographica Section D Biological Crystallography* 70(Pt 6):1579-1588.
23. McCoy AJ, *et al.* (2007) Phaser crystallographic software. *Journal of Applied Crystallography* 40(Pt 4):658-674.
24. McCoy AJ (2007) Solving structures of protein complexes by molecular replacement with Phaser. *Acta Crystallographica Section D Biological Crystallography* 63(Pt 1):32-41.
25. Emsley P & Cowtan K (2004) Coot: model-building tools for molecular graphics. *Acta Crystallographica Section D Biological Crystallography* 60(Pt 12 Pt 1):2126-2132.
26. Adams PD, *et al.* (2010) PHENIX: a comprehensive Python-based system for macromolecular structure solution. *Acta Crystallographica Section D Biological Crystallography* 66(Pt 2):213-221.
27. Oberstein A, Jeffrey PD, & Shi Y (2007) Crystal structure of the Bcl-XL-Bcl-2 peptide complex: Bcl-2 is a novel BH3-only protein. *Journal of Biological Chemistry* 282(17):13123-13132.
28. Moriarty NW, Grosse-Kunstleve RW, & Adams PD (2009) electronic Ligand Builder and Optimization Workbench (eLBOW): a tool for ligand coordinate and restraint generation. *Acta Crystallographica Section D Biological Crystallography* 65(Pt 10):1074-1080.
29. Bruno IJ, *et al.* (2004) Retrieval of crystallographically-derived molecular geometry information. *Journal of Chemical Information and Computer Sciences* 44(6):2133-2144.
30. Chen VB, *et al.* (2009) MolProbity: all-atom structure validation for macromolecular crystallography. *Acta Crystallographica Section D Biological Crystallography* 66(1):12-21.

### **3 Chapter three – Initial studies**



## 3.1 Introduction

**Chapter 1** introduced the benzoylurea series of BCL-X<sub>L</sub> inhibitors stemming from compound **1.1**, which was shown to bind BCL-X<sub>L</sub> with a low micromolar IC<sub>50</sub> and bind along the canonical groove of this protein. Important points of interaction of compound **1.1** with BCL-X<sub>L</sub> included a tolyl moiety that engaged the p4 hydrophobic pocket of BCL-X<sub>L</sub> and an S-benzyl moiety that engaged a neighbouring hydrophobic pocket, which we have termed p5 (**Chapter 1, Figure 1.5**). Among the initial SAR studies described in **Chapter 1** were analogues in which the thioether linkage of compound **1.1** was replaced with an ether (compound **1.7**), or sulfonyl linkage (compound **1.8**), which bound BCL-X<sub>L</sub> with similar affinity to compound **1.1**. Structural overlay of the BCL-X<sub>L</sub>:**1.1** complex with the published BCL-X<sub>L</sub>:**ABT-737** complex<sup>(1)</sup> formed the basis for the rational design of analogues to target some of the interactions utilised by **ABT-737** with the protein within the p2 and p4 pockets of BCL-X<sub>L</sub> (**Figure 3.1**).

This Chapter outlines, firstly, initial structural studies on two important lead molecules in the benzoylurea series that were designed to target the p2 pocket of BCL-X<sub>L</sub> (compounds **1.9** and **3.1**, described in detail below). Secondly, two alternative synthetic strategies are outlined to incorporate substituents aiming to generate additional interactions in the p4 pocket of BCL-X<sub>L</sub>. The synthesis of analogues using each strategy is described, as well as binding and structural analysis for selected analogues.

### 3.1.1 Interactions in the p2 pocket

To target the p2 pocket of BCL-X<sub>L</sub>, two new scaffolds were designed, one more rigid and the second more flexible (represented by compounds **1.9** and **1.10** respectively, **Figure 3.1C**), each incorporating a 4-chlorobiphenyl moiety designed to interact with the p2 pocket of BCL-X<sub>L</sub> in a manner similar to **ABT-737** (**Chapter 1, Figure 1.6**). A crystal structure of **1.10** bound to BCL-X<sub>L</sub> revealed that the compound bound as designed (**Chapter 1, Figure 1.6, Figure 3.1C**), however compounds **1.9** and **1.10** each showed only modest gains in binding to BCL-X<sub>L</sub>.

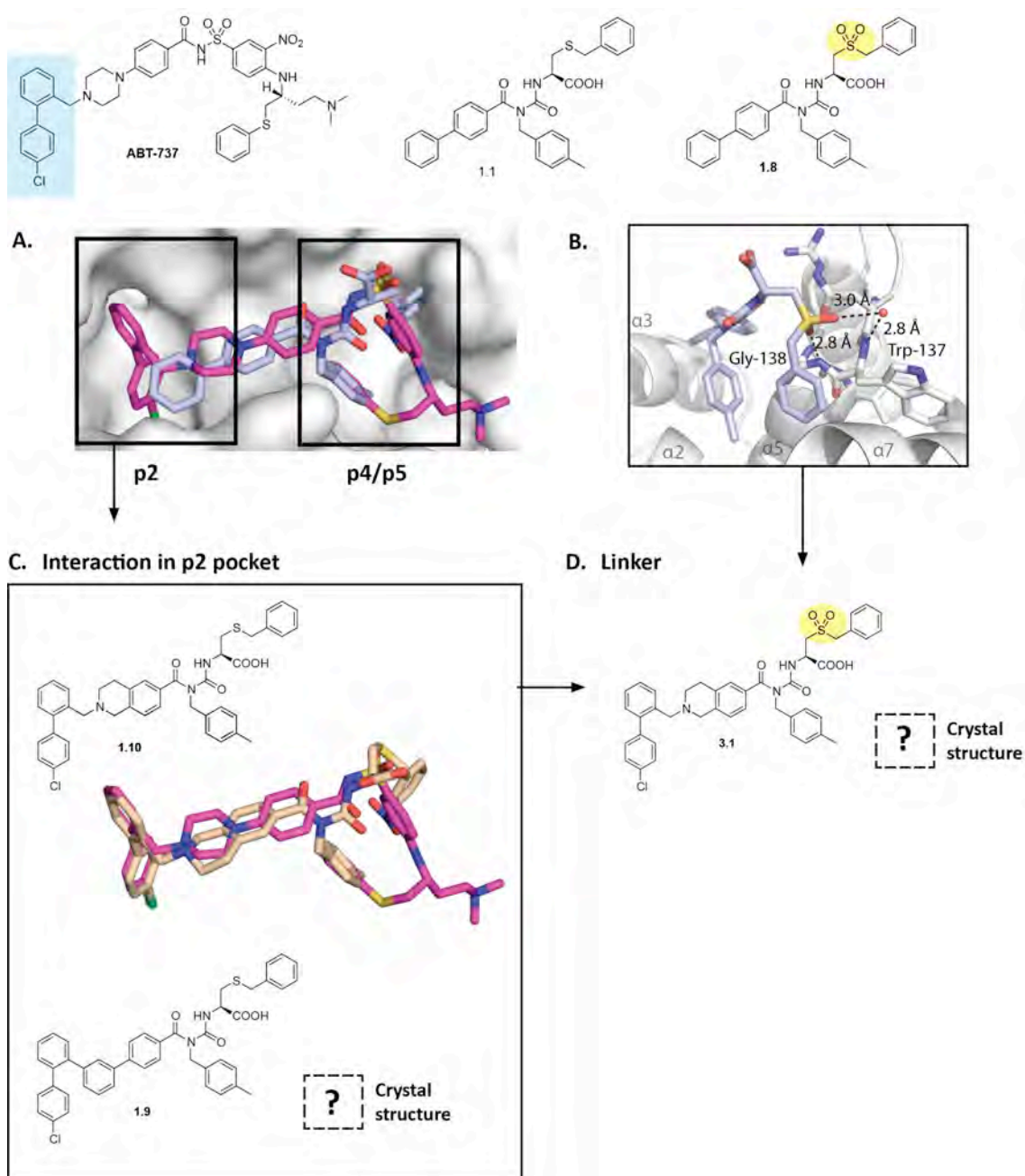
(2-3-fold for compounds **1.9** and **1.10**, relative to **1.1**; **Chapter 1, Table 1.1**). No crystal structure had been solved at that time of the BCL-X<sub>L</sub>:**1.9** complex to confirm its binding mode. Compound **3.1**, an analogue of compound **1.10** incorporating a sulfonyl linker similar to **1.8**, had also been synthesised by Amelia Vom at WEHI and appeared to be the most potent analogue in the series to date (compound **3.1** IC<sub>50</sub>(BCL-X<sub>L</sub>) = 0.9  $\mu$ M, **Table 3.1**). X-ray crystal structures of each of compounds **1.9** and **3.1** in complex with BCL-X<sub>L</sub> were thus desirable to confirm the binding modes of each (**Figure 3.1C,D**).

**Table 3.1: IC<sub>50</sub> values of benzoylurea compounds for BCL-X<sub>L</sub> and MCL-1 (determined by AlphaScreen competition assay, pre-2015 data)<sup>[a]</sup>**

Compound	IC <sub>50</sub> A.S. <sup>[b]</sup>				Fold Selectivity
	BCL-X <sub>L</sub>	MCL-1	N =	(BCL-X <sub>L</sub> /MCL-1)	
<b>1.1</b>	4.6 ± 1.0	74 ± 20	3	16	
<b>1.7</b>	2.1 ± 0.4	43 ± 6	5	20	
<b>1.8</b>	1.5 ± 0.6	68 ± 25	5	44	
<b>1.9</b>	1.7 ± 0.6	23 ± 7	4	14	
<b>1.10</b>	1.8 ± 0.4	28 ± 5	4	16	
<b>3.1</b>	0.9 ± 0.3	29 ± 6	4	32	
<b>ABT-737</b>	< 0.001 -	> 1 -	5	> 1000	

<sup>[a]</sup> Following the relocation of our Screening Group, a consistent shift in the IC<sub>50</sub> values determined using the AlphaScreen competition assay was observed. The signifiers ‘pre-2015 data’ and ‘post-2015 data’ indicate respectively data acquired prior and subsequent to this relocation. For further information refer to note in **Chapter 2, Section 2.4.1.3**.

<sup>[b]</sup> IC<sub>50</sub> values are reported in  $\mu$ M ± S.D.



**Figure 3.1: Series progression to compounds 1.9 and 3.1.**

(A) Overlay of BCL-XL:1.1 (light blue) and BCL-XL:ABT-737 (magenta, PDB entry: 2YZJ<sup>(1)</sup>) complexes. The chlorobiphenyl moiety of ABT-737 is highlighted in blue. (B) BCL-XL:1.8 complex, showing hydrogen bond formed between one oxygen atom of the sulfonyl moiety of compound 1.8 (highlighted in yellow) and the backbone -NH of residue Gly138 of BCL-XL (C) Extended scaffold compounds 1.9 and 1.10 (each incorporating chlorobiphenyl group to interact in p2 pocket) and overlay of ligands from BCL-XL:1.10 complex (straw colour) and BCL-XL:ABT-737 complex (magenta). (D) Compound 3.1 is derived from compound 1.9 but incorporates an additional sulfonyl linker moiety (analogous to compound 1.8).

### 3.1.2 Pi-stacking interactions in the p4 pocket

As described in **Chapter 1**, **ABT-737** binds to BCL-X<sub>L</sub> with high affinity in part due to an extended pi-stacking interaction formed in the p4 pocket of BCL-X<sub>L</sub>, involving both the nitroaryl and S-phenyl rings of **ABT-737** and Phe97 and Tyr195 of the protein (**Figure 3.2A(i)**). In particular, pi-pi interactions of this type may involve either face-to-face, face-to-edge, or partially off-set arrangements of aromatic rings and can be enhanced by the incorporation of electron-withdrawing substituents onto one aromatic ring (such as the nitro- group of **ABT-737**) to render it electron-deficient and stabilise pi-pi electronic interactions with neighbouring rings that are electron-rich<sup>(2)</sup>.

In comparison, the crystal structure of benzoylurea lead **1.1** in complex with BCL-X<sub>L</sub> showed that whilst the tolyl moiety engaged the p4 pocket, packing closely against Phe97 of BCL-X<sub>L</sub>, the S-benzyl moiety did not engage in pi-stacking interaction with Tyr195. Rather, the side-chain of Tyr195 was 'flipped' outwards opening up the p5 pocket into which the S-benzyl moiety was observed to bind (**Figure 3.2A(ii)**).

In the development of the acylsulfonamide series (exemplified by **ABT-737**) the formation of this 'bent-back' conformation, driven by the intramolecular hydrophobic collapse of the two aromatic rings, had marked a significant improvement in activity against BCL-2 and BCL-X<sub>L</sub><sup>(3, 4)</sup>. We rationalised that if the S-benzyl cysteine portion of compound **1.1** could be successfully replaced or modified such that it could engage in pi-stacking within the p4 pocket of BCL-X<sub>L</sub>, this might similarly improve the activity of this series.

### 3.1.2.1 Benzoylurea arylsulfonamides

The first strategy proposed was to explore a series of benzoylurea arylsulfonamide compounds. Overlay of the BCL-X<sub>L</sub>:**1.1** or BCL-X<sub>L</sub>:**1.9** structures with the BCL-X<sub>L</sub>:**ABT-737** complex (**Figure 3.1B-C**) revealed that the amino acid -NH of compounds **1.1** and **1.9** co-localised with the sulfonamide -NH of **ABT-737**. Based on this, we anticipated that formation of a direct benzoylurea/aryl sulfonamide linkage (such as shown in compounds **3.2a** – **3.2b**, **Figure 3.2B**) might allow installation of an aryl/nitro-aryl ring in a similar position to the nitroaryl group in **ABT-737**, in a suitable position to engage in a pi-stacking interaction both with Tyr195 of BCL-X<sub>L</sub> and the tolyl group on the same molecule. Additionally, an oxygen atom of the sulfonyl linkage might act as a hydrogen bond acceptor for the backbone -NH of Gly138.

Acylsulfonamides are known to be acidic ( $pK_a$  in the range 4-5, similar to carboxylic acids) and are hence utilised as carboxylic acid isosteres<sup>(5)</sup>. Certainly, the acidity of this group has been shown to be important for the activity of **ABT-737**<sup>(4, 6)</sup>. This raised the strong possibility therefore that a benzoylurea arylsulfonamide such as those depicted in **Figure 3.2B**, if stable, at physiological pH might favour the 'open' conformation (**Figure 3.2B**) due to the deprotonation of the sulfonamide -NH, rather than the 'closed' conformation in which the -NH is engaged in a hydrogen bond to form the benzoylurea pseudo 6-membered ring (as initially modeled). This had the potential to challenge our design strategy.

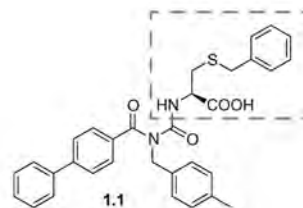
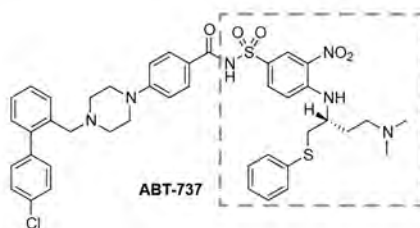
To explore this possibility, I aimed to determine the X-ray crystal structure in complex with BCL-X<sub>L</sub> (**Figure 3.2B**) of a related compound, **3.2c**, which had also been synthesised Amelia Vom at WEHI. Compound **3.2c** incorporates the right-hand nitroaryl sulfonamide fragment of **ABT-737** (**Figure 3.2A(i)**, dotted line) (necessary for pi-stacking within the p4 pocket) fused with the biphenyl benzoylurea core of compound **1.1** (omitting the tolyl group that would engage the p4 pocket) and was found to bind to BCL-X<sub>L</sub> with a  $IC_{50}$  of  $\sim 0.2 \mu M$  (AlphaScreen). Interestingly this measured  $IC_{50}$  for BCL-X<sub>L</sub> was comparatively weaker than the reported  $K_i$  of a similar compound described in the literature,

compound **1** (Wendt *et al.*) (Figure 3.2D) without the urea linking moiety that had a reported  $K_i$  for BCL-X<sub>L</sub> of 0.036  $\mu$ M<sup>(7)</sup>. We postulated that understanding the ‘open’ vs. ‘closed’ conformational preference of this compound *via* determination of a sufficiently high-resolution crystal structure in complex with BCL-X<sub>L</sub> might help to explain this difference and assist in the design of more potent analogues.

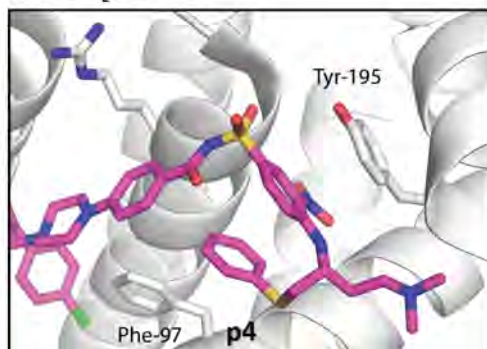
#### 3.1.2.2 Benzoylurea compounds **3.7a** – **3.16**

The second approach was based on the hypothesis that the stereochemical preferences and linker length of the S-benzyl-L-cysteine moiety of compound **1.1** might preclude the terminal aryl group from accessing a conformation suitable for pi-stacking with Tyr195 of BCL-X<sub>L</sub>. Thus, a small set of benzoylurea analogues (compounds **3.7a** – **3.16**) were designed based on commercially available amino acids to explore the effect of shortening the linker (to 1-2 atoms), altering the stereochemistry at the chiral centre and incorporating different aromatic groups. Compounds **3.13** and **3.16** (synthesised as a racemic mixture) additionally explored homologation of the carboxylic acid moiety.

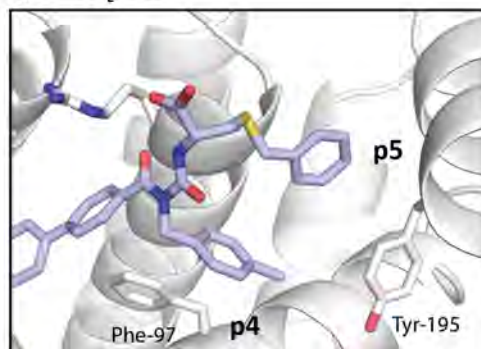
A.



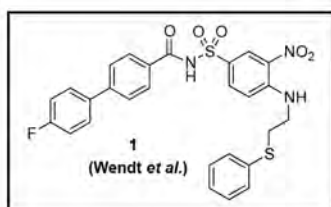
i) BCL-X<sub>L</sub>:ABT-737



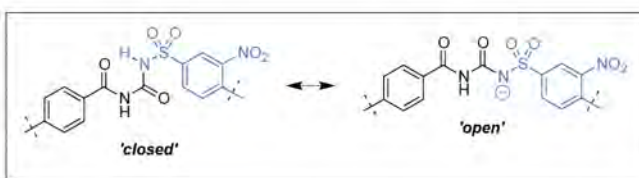
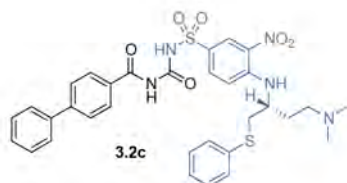
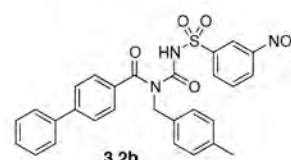
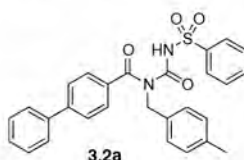
ii) BCL-X<sub>L</sub>:1.1



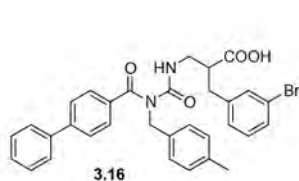
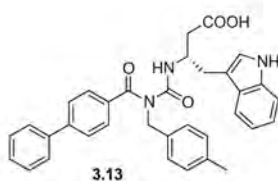
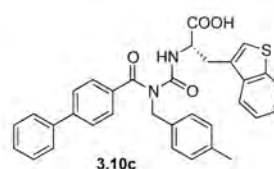
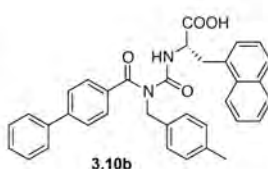
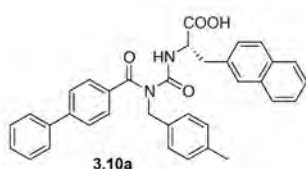
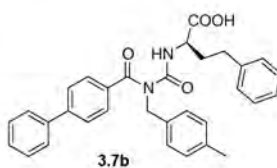
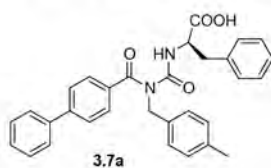
B.



C. Benzoylurea arylsulfonamides (3.2a - c)



D. Benzoylurea (3.7a - 3.16)



**Figure 3.2 (previous page): Analogues exploring pi-stacking interaction in p4 pocket.**

(A)(i) BCL-X<sub>L</sub>:**ABT-737** complex (PDB entry: 2YXZ<sup>(1)</sup>) showing pi-stacking interactions within p4 pocket driven by intramolecular hydrophobic collapse of the nitroaryl and S-phenyl rings of **ABT-737** (highlighted with dashed box, left) which pack closely against Phe97 and Tyr195 of the protein. In comparison, in the BCL-X<sub>L</sub>:**1.1** complex, whilst the tolyl moiety packs against Phe97 in the p4 pocket, the S-benzyl (highlighted with dashed box, right) is observed to occupy a pocket we have termed p5, created by an outward rotation of the side-chain of Tyr195.

(B) A series of benzoylurea arylsulfonamides (compounds **3.2a-b**) were designed to introduce an arylsulfonyl group to mimic the nitroarylsulfonyl moiety of **ABT-737**. Compound **3.2c** is a related compound that incorporates the nitroarylsulfonyl fragment of **ABT-737** (compound **3.2c**, highlighted in blue). Structural studies sought to ascertain the conformational preferences ('open'/'closed') of compound **3.2c** bound to BCL-X<sub>L</sub> at physiological pH to aid in the design of other benzoylurea arylsulfonamide compounds.

(C) A series of benzoylurea designed to introduce simple aryl-containing amino acids that might potentially engage in pi-stacking interactions in the p4/p5 pockets of BCL-X<sub>L</sub>.

(D) Chemical structure of compound **1** (**Wendt *et al.***)<sup>(7)</sup> referred to in the main text.



## 3.2 Structure determination of extended scaffold lead molecules

In order to validate their binding mode with BCL-X<sub>L</sub>, crystal structures of compounds **1.9** and **3.1** were determined, to a resolution of 2.9 Å and 1.6 Å respectively, and are depicted in **Figure 3.3**. Statistics for the two structures are provided in **Table 3.2**.

### 3.2.1 Structure determination of lead compounds **1.9** and **3.1**

#### 3.2.1.1 Structure determination of the BCL-X<sub>L</sub>:**1.9** complex

Relevance:

- Confirm binding mode of important 'rigid' lead scaffold

Following extensive screening of crystallization conditions for compound **1.9** in complex with BCL-X<sub>L</sub> small crystals were obtained which diffracted to ~2.6 Å resolution, from which a structure of the BCL-X<sub>L</sub>:**1.9** complex was solved by molecular replacement. The asymmetric unit contained 3 copies of the BCL-X<sub>L</sub> monomer (one domain-swapped dimer in the asymmetric unit and a further domain-swapped dimer between the third copy of BCL-X<sub>L</sub> and its symmetry mate), each with clear positive difference density corresponding to a single copy of compound **1.9** bound in the groove (100% occupancy of ligand). Only limited rebuilding and refinement was performed (due to poor data quality and relatively high R<sub>merge</sub> of 0.2938) as the observed ligand density was sufficient to confirm the predicted binding orientation of **1.9**; despite the more rigid scaffold, the chlorobiphenyl moiety as designed did indeed project deeply into the p2 binding pocket on BCL-X<sub>L</sub> as for the complex of BCL-X<sub>L</sub>:**1.10** (**Figure 3.3A**).

Whilst minimal refinement was performed, in general, poor electron density was observed in particular for the α-3 helix of BCL-X<sub>L</sub> - perhaps due to a structural rearrangement necessary to accommodate the more rigid scaffold. Such structural remodeling of the BCL-X<sub>L</sub> α-3 helix upon ligand binding has been reported for other series previously (see eg. **Chapter 1, Figure 1.3**)<sup>(8, 9)</sup>. In the benzoylurea

series, direct binding studies by surface plasmon resonance (SPR) (Biacore 4000), performed by Hong Yang at the Institute, had previously revealed relatively slow association/dissociation kinetics for compound **1.9** binding to immobilized BCL-X<sub>L</sub>, in comparison to much faster association/dissociation kinetics for **1.10** (data not shown). Such an observation would be consistent with a structural rearrangement of the protein upon binding.

Interestingly, the structure of the BCL-X<sub>L</sub>:**1.9** complex also showed a very close overlay with the crystal structure of another compound described in the literature, compound **19** (**Figure 3.3B**, PDB entry: 3SP7<sup>(10)</sup>, orange), including breakdown of the helicity of the  $\alpha$ -3 helix. It was reported for analogues related to **19**, that incorporation of bulky substituents at the position marked (red arrow, **Figure 3.3B**) was found to improve selectivity toward BCL-X<sub>L</sub> (eg. compound **21**<sup>(10)</sup>, **Figure 3.3B**). Changes of this nature might provide a possible avenue to further optimise selectivity towards BCL-X<sub>L</sub> in future for compounds based on the scaffold of **1.9**.

### 3.2.1.2 Structure determination of the BCL-X<sub>L</sub>:**3.1** complex

Relevance:

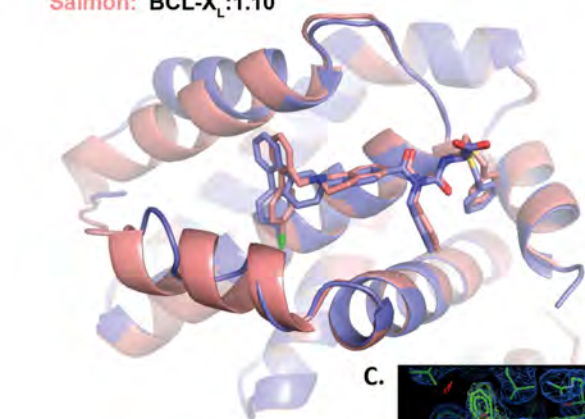
- Most potent analogue in series to date
- Confirm sulfonyl hydrogen-bonding interaction with Gly138 of BCL-X<sub>L</sub>

Small-scale in-house crystallization trials for compound **3.1** in complex with BCL-X<sub>L</sub> successfully yielded crystals which diffracted to ~1.6 Å resolution. The resulting X-ray crystal structure determined for the complex showed four BCL-X<sub>L</sub> monomers (as two domain-swapped dimers) per asymmetric unit, bound to BCL-X<sub>L</sub> with 100% occupancy but in two different conformations (**Figure 3.3B**).

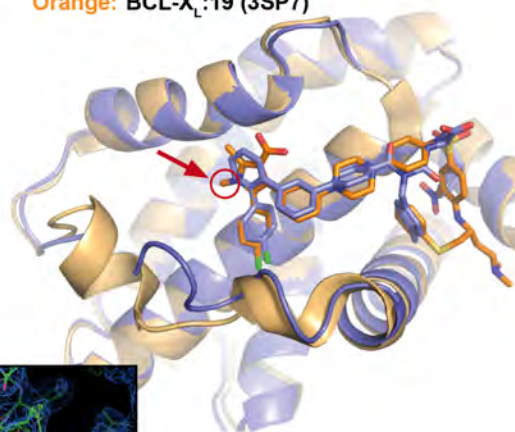
The predominant confirmation observed (3/4 monomers, **Figure 3.3B**, green) confirmed the expected binding mode of compound **3.1** along the hydrophobic groove of BCL-X<sub>L</sub>; showing the chlorobiphenyl moiety projecting into the p2 pocket and indicating that the designed hydrogen bonding interaction between the

backbone –NH of Gly138 of BCL-X<sub>L</sub> and sulfonyl moiety of compound **3.1** had been achieved (as for compound **1.8**, **Figure 3.1B**). An alternate confirmation (1/4 monomers, **Figure 3.3B**, orange) was observed in which compound **3.1** was in the reverse orientation in the binding groove with the chlorobiphenyl moiety instead projecting into the p4 pocket and the terminal sulfonyl-benzyl moieties projecting outward to pack into an interface with a neighbouring BCL-X<sub>L</sub> monomer; indicating that this conformation is likely due to crystal packing and unlikely to represent the bound conformation in solution.

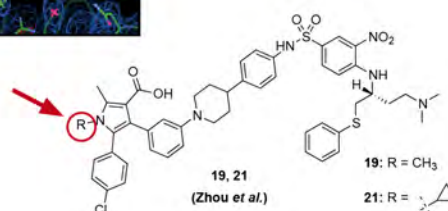
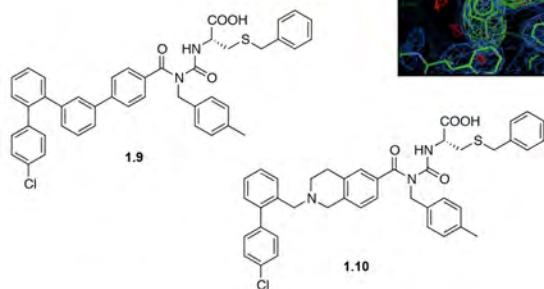
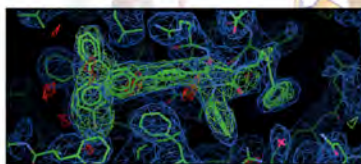
A. Blue: BCL-X<sub>L</sub>:1.9  
Salmon: BCL-X<sub>L</sub>:1.10



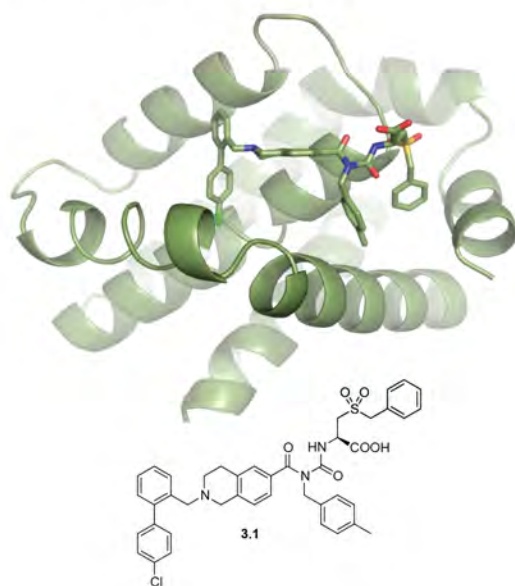
B. Blue: BCL-X<sub>L</sub>:1.9  
Orange: BCL-X<sub>L</sub>:19 (3SP7)



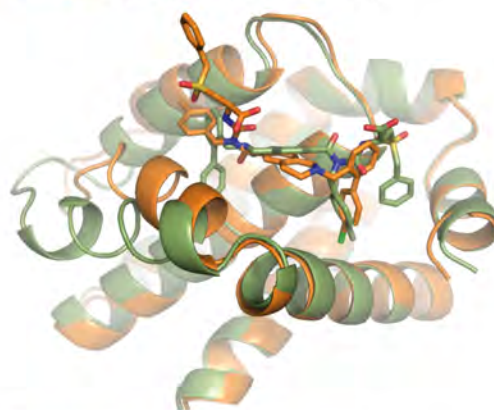
C.



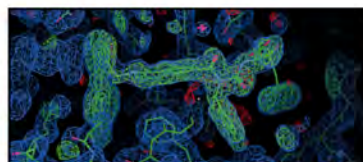
D. Green: BCL-X<sub>L</sub>:3.1 (primary, 3/4)



E. Green: BCL-X<sub>L</sub>:3.1 (primary, 3/4)  
Orange: BCL-X<sub>L</sub>:3.1 (alternate, 1/4)



F.



**Figure 3.3: X-ray crystal structures of the BCL-X<sub>L</sub>:1.9 and BCL-X<sub>L</sub>:3.1 complexes (previous page).**

(A) X-ray structure of BCL-X<sub>L</sub>:1.9 complex solved to 2.6 Å resolution (blue) overlaid upon the previously solved structure of the similar BCL-X<sub>L</sub>:1.10 complex (salmon). (B) X-ray structure of BCL-X<sub>L</sub>:1.9 complex (blue) overlaid upon the structure of the BCL-X<sub>L</sub>:19 complex (PDB entry: 3SP7<sup>(10)</sup>, orange). A site for possible modification to further improve selectivity for BCL-X<sub>L</sub> is indicated (red arrow). (C) Simulated annealing omit map of BCL-X<sub>L</sub>:1.9 complex, showing 2Fo-Fc and difference density, Fo-Fc. (D) X-ray Structure of BCL-X<sub>L</sub>:3.1 complex solved to 1.6 Å resolution showing primary conformation (green) and (E) overlay with alternative conformation (orange). (F) Simulated annealing omit map of BCL-X<sub>L</sub>:3.1 complex (primary conformation). For all omit maps, 2Fo-Fc is contoured at 1σ (blue), and Fo-Fc is contoured at ± 3σ (green/red).

**Table 3.2: Crystallographic statistics for BCL-X<sub>L</sub>:1.9 and BCL-X<sub>L</sub>:3.1 complexes.**

<b>Structure <sup>Ψ</sup></b>	<b>BCL-X<sub>L</sub>:1.9 <sup>Φ</sup></b>	<b>BCL-X<sub>L</sub>:3.1</b>
Wavelength (Å)	0.9537	0.9537
Resolution range (Å)	53.58 - 2.874 (2.977 - 2.874)	38.39 - 1.599 (1.656 - 1.599)
Space group	<i>P</i> 4 <sub>3</sub> 2 <sub>1</sub> 2	<i>C</i> 2
Unit cell		
<i>a</i> , <i>b</i> , <i>c</i> (Å)	148.57, 148.57, 57.44	150.36, 66.53, 77.64
α, β, γ (°)	90, 90, 90	90, 98.48, 90
Total reflections	209613 (15720)	361495 (35115)
Unique reflections	14964 (1261)	98759 (9718)
Multiplicity	14.0 (12.5)	3.7 (3.6)
Completeness (%)	0.98 (0.85)	0.99 (0.97)
Mean <i>I</i> / σ <i>I</i>	12.83 (1.65)	14.76 (1.69)
Wilson <i>B</i> factor (Å <sup>2</sup> )	59.18	21.99
<i>R</i> <sub>merge</sub>	0.2938 (1.867)	0.05543 (0.9416)
<i>R</i> <sub>meas</sub>	0.3048 (1.943)	0.06526 (1.106)
CC <sub>1/2</sub>	0.996 (0.525)	0.999 (0.592)
CC*	0.999 (0.83)	1 (0.862)
Reflections used in refinement	14956 (1261)	98738 (9717)
Reflections used for R-free	748 (63)	4937 (486)
<i>R</i> <sub>work</sub>	0.2458 (0.3665)	0.2057 (0.2753)
<i>R</i> <sub>free</sub>	0.3142 (0.4304)	0.2256 (0.2999)
CC <sub>work</sub>	0.925 (0.673)	0.944 (0.804)
CC <sub>free</sub>	0.860 (0.601)	0.933 (0.784)
Number of non-hydrogen atoms	3481	4933
macromolecules	3306	4501
ligands/ions	160	227
RMS(bond lengths) (Å)	0.009	0.007
RMS(bond angles) (°)	1.2	1
Ramachandran favored (%)	91	99
Ramachandran allowed (%)	6.9	1.1
Ramachandran outliers (%)	1.7	0
Rotamer outliers (%)	2.8	4.5
Clashscore	10.75	4.01
Average <i>B</i> factors (Å <sup>2</sup> )	45.72	25.8
Macromolecules	45.55	25.15
ligands	50.31	32.83
solvent	34.58	32.16

<sup>Ψ</sup> Statistics are outlined in Section 2.6.2.5. <sup>Φ</sup> This structure has poor merging statistics, likely due to underlying crystal pathology – attempts to reduce *R*<sub>merge</sub> were unsuccessful, however despite the poor *R*<sub>merge</sub>, the simulated annealing omit map showed well-resolved positive difference density corresponding to the structure of compound **1.9**, allowing the ligand to be accurately modeled.

### 3.3 Pi-stacking interactions in the p4 pocket

In order to understand the ‘open’ vs. ‘closed’ conformational preference of the benzoylurea arylsulfonamide compound **3.2c** upon binding to BCL-X<sub>L</sub> at near-physiological pH, a crystal structure of a BCL-X<sub>L</sub>:**3.2c** (at pH 7.0) was determined to 2.85 Å by X-ray crystallography. Statistics for this structure are provided in **Table 3.4**.

#### 3.3.1 Study of benzoylurea arylsulfonamide compounds

##### 3.3.1.1 Structure determination of the BCL-X<sub>L</sub>:**3.2c** complex

Relevance:

- Provide structural guidance on the binding mode and ‘open’ vs. ‘closed’ conformational preference of compound **3.2c** to guide synthesis of other analogues

##### Data collection and processing for BCL-X<sub>L</sub>:**3.2c** complex

A dataset for the BCL-X<sub>L</sub>:**3.2c** complex was collected to 2.85 Å resolution from a single crystal on the MX2 beamline at the Australian Synchrotron. Data were indexed and integrated using XDS<sup>(11)</sup> indicating space group P 3<sub>1</sub> or P 3<sub>2</sub> with  $a = 100.72$ ,  $b = 100.72$ ,  $c = 167.29$  Å,  $\alpha = \beta = 90^\circ$ ,  $\gamma = 120^\circ$ . Analysis (using PHENIX.XTRIAGE<sup>(12)</sup>) of intensity statistics using the L-test suggested that twinning was unlikely. Using the refined unit cell parameters, analysis of the Matthews’ coefficient and Solvent Content (using MATTPROB<sup>(13, 14)</sup>) suggested that the asymmetric unit (A.S.U.) contained either 5 or 6 BCL-X<sub>L</sub>  $\alpha$ -1 domain-swapped dimers ( $V_m = 2.72$  Å<sup>3</sup>/Da, 31.6% probability and  $V_m = 2.27$  Å<sup>3</sup>/Da, 46.4% probability respectively).

To further analyse the possibility of higher-order symmetry or pseudo-symmetry, the self-rotation function was calculated using the UCLA self-rotation function server (which incorporates the CCP4-supported program POLARRFN). Resulting plots of the  $\kappa = 120^\circ$  and  $\kappa = 180^\circ$  sections (used to indicate 3-fold and 2-fold

rotational axes respectively) are shown in **Figure 3.4A**. The peak at the origin in the plot of the  $\kappa = 120^\circ$  section represents the crystallographic 3-fold axis along  $c$  (**Figure 3.4A**). On the  $\kappa = 180^\circ$  section, noncrystallographic dyads are evident parallel to  $c$  ( $\omega = 0^\circ$ ) and additional dyads appear as marked (A, B, C; **Figure 3.4A**) in the  $a/b$  plane.

The structure was subsequently solved by Molecular Replacement with PHASER<sup>(15)</sup> using as a search model coordinates for the BCL-X<sub>L</sub> monomer taken from the BCL-X<sub>L</sub>:1.1 complex. A single solution was obtained, which contained 10 copies of the BCL-X<sub>L</sub> monomer (arranged as five  $\alpha$ -1 domain-swapped dimers) in the space group P 3<sub>2</sub>. Following a round of refinement in PHENIX<sup>(16)</sup> that incorporated a simulated annealing step, visual inspection of the maps using COOT<sup>(17)</sup> indicated further electron density consistent with the likely presence of one additional BCL-X<sub>L</sub> domain-swapped dimer. A further BCL-X<sub>L</sub> monomer was built using PHENIX.AUTOBUILD<sup>(18)</sup> then following refinement in PHENIX<sup>(16)</sup> a second BCL-X<sub>L</sub> monomer was able to be placed manually into the remaining observable electron density using COOT<sup>(17)</sup> to complete the final domain-swapped dimer. The model was subsequently refined with PHENIX<sup>(16)</sup> incorporating a simulated annealing step.

The final structure comprised 12 copies of BCL-X<sub>L</sub> in the A.S.U. arranged in a highly symmetrical manner as three sets of two domain-swapped dimers (pseudo 2 2 2 tetramers). The resulting unit cell is shown in **Figure 3.4B**, showing (i) the single asymmetric unit (a single BCL-X<sub>L</sub> monomer from a domain-swapped dimer is highlighted in blue) and (ii) the asymmetric unit and its two additional symmetry mates within the unit cell. Also shown are crystallographic trigonal symmetry operators (black) as well as the approximate positions of non-crystallographic pseudo dyad axes (red)). Significant non-crystallographic symmetry is obvious from this structure, reflecting the self-rotation function (in particular pseudo dyad peaks present in the  $\kappa = 180^\circ$  section). Within the structure, each BCL-X<sub>L</sub> domain-swapped dimer is arranged such that it has a local 2-fold axis approximately parallel to the unit cell  $c$  edge (corresponding to the  $\omega = 0^\circ$  peak in the  $\kappa = 180^\circ$  section of the self-rotation function). Pairs of dimers are stacked along



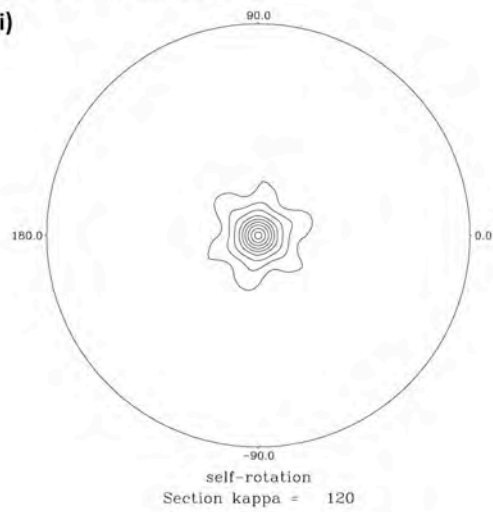
the *c* axis to form a tetramer; this stacking generates (per tetramer) two further local pseudo 2-fold axes in the *a/b* plane perpendicular to one another. As the relationship between the three sets of tetramers within the A.S.U. is not quite trigonal (they are also off-set with respect to one another along the *c* axis), these sets of local dyad axes in the *a/b* plane are also non-symmetrical with respect to one-another (**Figure 3.4B(i)**).

#### **Analysis of ligand binding in BCL-X<sub>L</sub>:3.2c complex**

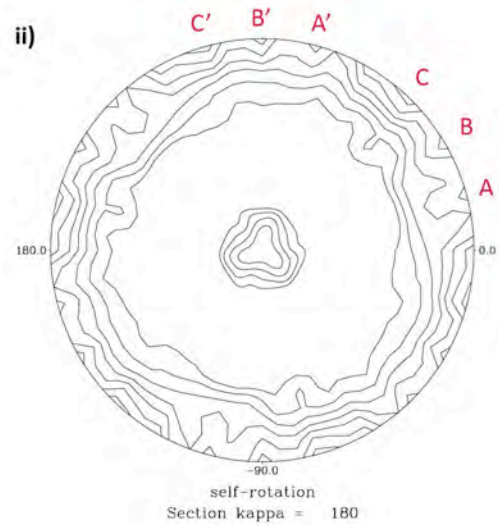
Clear electron density for the compound **3.2c** was observed in the groove in four of the BCL-X<sub>L</sub> molecules in the A.S.U. The compound was modeled into this density in either the 'open' or 'closed' benzoylurea conformations and each of these models was refined separately (**Figure 3.5**). Two further BCL-X<sub>L</sub> molecules had some poorly-defined electron density present in the groove likely corresponding to compound **3.2c** but which was not modeled. The remaining six BCL-X<sub>L</sub> molecules had no apparent electron density for the ligand in the groove.

# A. Self-rotation function

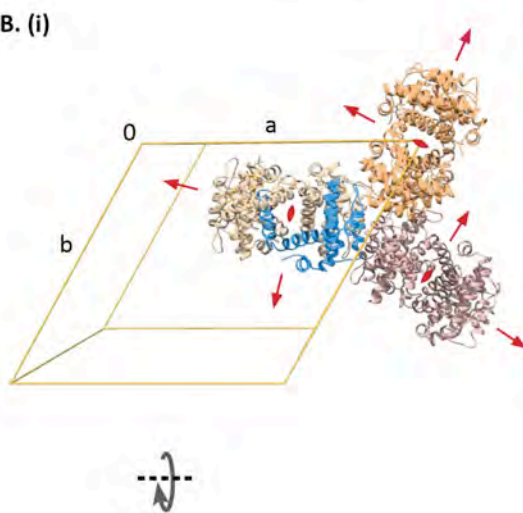
i)



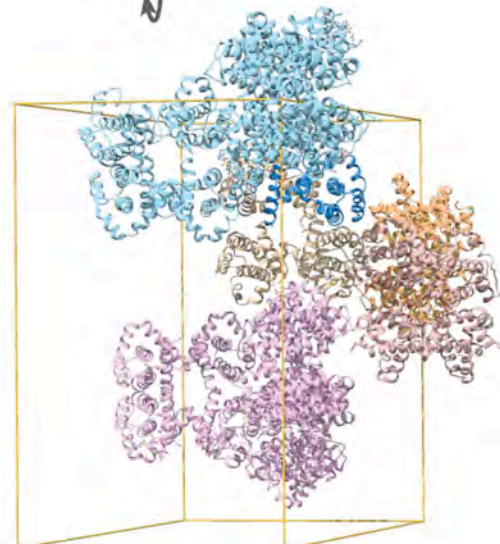
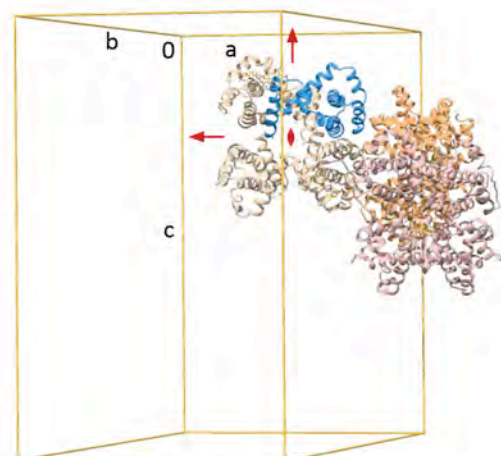
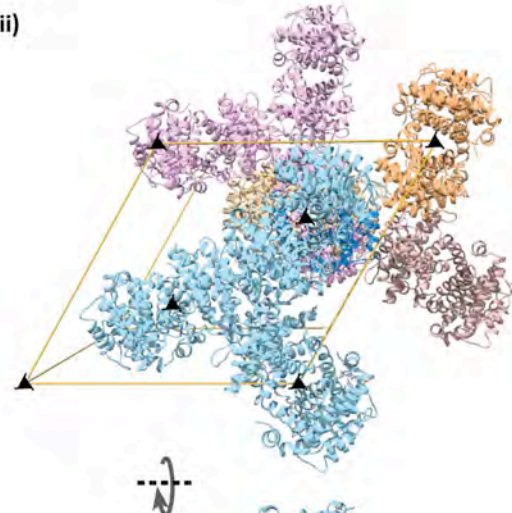
ii)



B. (i)



(ii)



**Figure 3.4: (previous page) Analysis of the self-rotation function and unit cell of the BCL-X<sub>L</sub>:3.2c complex.**

(A) Self-rotation function in space group  $P 3_1/P 3_2$  plotted for the (i)  $\kappa = 120^\circ$  and (ii)  $\kappa = 180^\circ$  sections. The self-rotation function was calculated using the UCLA self-rotation function server (incorporating the CCP4-supported program POLARRFN), using an integration radius of 25 Å and data between 9 Å and 4 Å resolution. The crystallographic 3-fold axis is at  $\kappa = 120^\circ$ ,  $\omega = 0^\circ$  and additional non-crystallographic two-fold axes are indicated along  $c$  and in the  $a/b$  plane (marked A-C). (B) The structure of the BCL-X<sub>L</sub>:3.2c complex solved assuming the space group  $P 3_2$ , showing (i) the single asymmetric unit (a single BCL-X<sub>L</sub> monomer from a domain-swapped dimer is highlighted in blue) and (ii) the asymmetric unit and its two additional symmetry mates within the unit cell; also shown are crystallographic trigonal symmetry operators (black) as well as the approximate positions of non-crystallographic pseudo dyad axes (red)). Image generated using UCSF Chimera package from the Computer Graphics Laboratory, University of California, San Francisco (supported by NIH P41 RR-01081)<sup>(19)</sup> utilising the Persistence of Vision Raytracer (Version 3.6) (Persistence of Vision Pty. Ltd., 2004).

The BCL-X<sub>L</sub>:**3.2c** structure revealed that the fragment derived from **ABT-737** forms the expected pi-stacking interactions within the p4 pocket as for **ABT-737** (**Figure 3.5**, compare **Figure 3.2A(i)**). As regards the ‘open’/‘closed’ conformational preference of the ligand, whilst some the electron density maps provide some subtle clues, the moderate resolution obtained for this structure (2.85 Å resolution) is ultimately insufficient to provide a definitive answer.

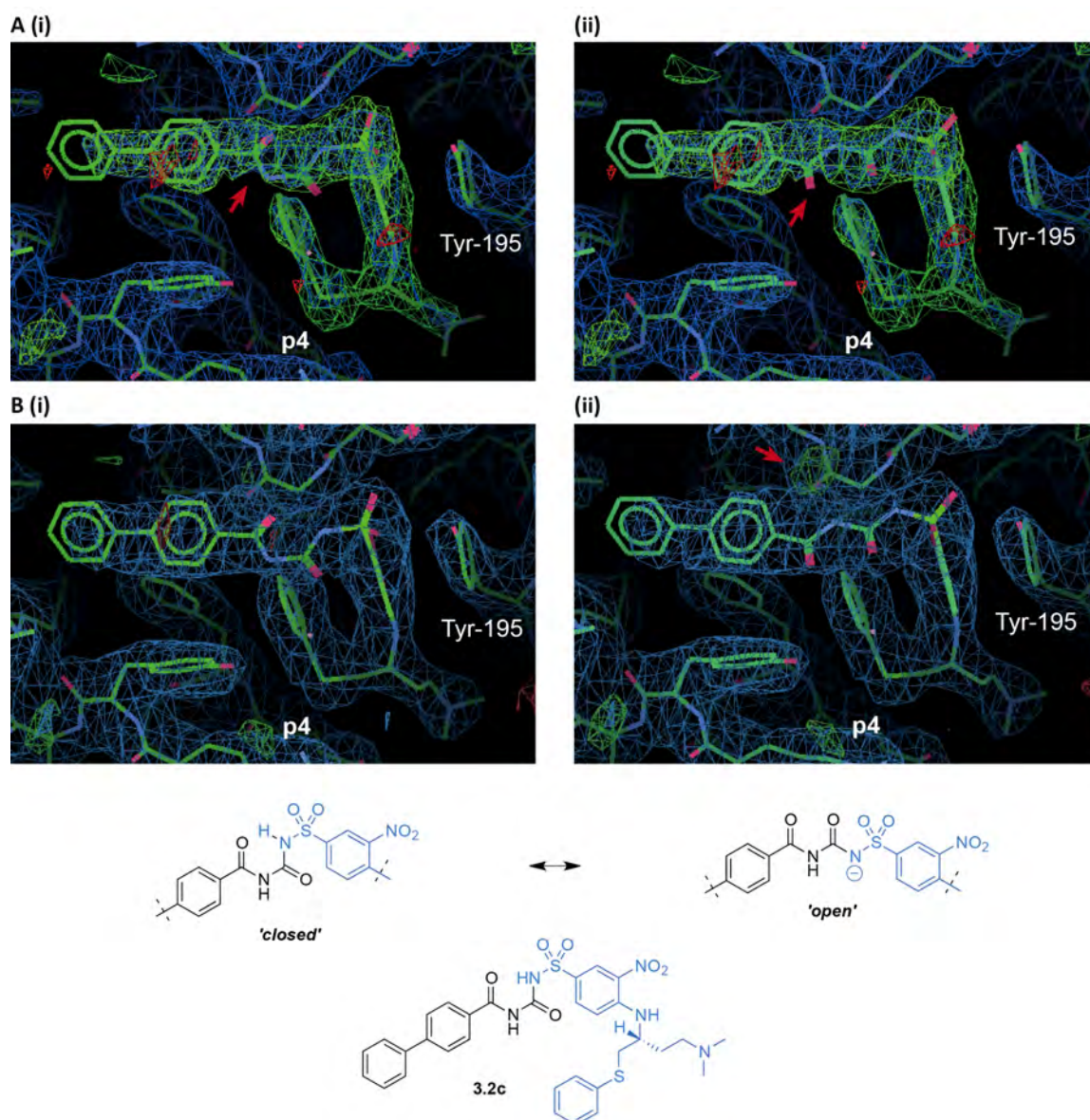
On analyzing the ligand electron density simulated annealing omit map (**Figure 3.5A**) with compound **3.2c** modeled in either the ‘closed’ or ‘open’ benzoylurea conformations, it appears that the ‘closed’ conformation better reflects the observed electron density (note in particular the carbonyl moiety indicated by the red arrows, which flips position in the two models and projects out of the Fo-Fc map in the ‘open’ conformation, **Figure 3.5A**). Similarly, following refinement with either of these models, although each provide a reasonable fit to the density in the 2Fo-Fc maps (**Figure 3.5B**), the ‘open’ benzoylurea model shows residual positive density in the Fo-Fc map in the region occupied by the flipped carbonyl moiety in the ‘closed’ conformation (red arrow, **Figure 3.5B(ii)**). Combined, these would tend to support the ‘closed’ conformation predominating over the open conformation.

In contrast, refinement statistics following a separate round of refinement of each model (‘open’/‘closed’) in PHENIX<sup>(16)</sup> tell a different story. Whilst the statistics were similar, of the two models, the model in which all four ligand copies were in the ‘open’ conformation provided a slightly lower final  $R_{\text{free}}$  value (**Table 3.3**). Thus it appears at this resolution it is difficult to distinguish which of these two conformations predominates. To solve this, better diffracting crystals *via* further crystal optimisation would likely be required.

**Table 3.3: Refinement statistics for the BCL-X<sub>L</sub>:3.2c complex, with the ligand (4 copies) modeled in either the ‘closed’ or ‘open’ benzoylurea conformations.**

<b>Model</b>	<b>Final <math>R_{\text{work}}</math></b>	<b>Final <math>R_{\text{free}}</math></b>
‘closed’	0.1847	0.2640
‘open’	0.1846	0.2627

In conclusion, although the structure of the BCL-X<sub>L</sub>:**3.2c** complex did not confirm the binding mode unambiguously, the data was certainly consistent with a ‘closed’ benzoylurea core and the structure did show that a nitroaryl sulfonyl moiety (**Figure 3.2B**, blue highlight) directly attached to a benzoylurea core (albeit devoid of a p4 substituent) could pi-pi stack in the desired manner with Tyr195. The real test of this approach would be in the synthesis of analogues **3.2a** and **3.2b**, incorporating the p4 tolyl moiety.



**Figure 3.5: Compound 3.2c modeled into the groove of a representative BCL-X<sub>L</sub> monomer in the BCL-X<sub>L</sub>:3.2c structure.**

(A) Simulated annealing omit map showing ligand binding site in BCL-X<sub>L</sub>:**3.2c** complex showing the modeled (i) 'closed' and (ii) 'open' benzoylurea conformations of compound **3.2c** and position of Tyr195. (B) Electron density map following refinement of compound **3.2c** in either the (i) 'closed' or (ii) 'open' benzoylurea conformations. In all cases the 2Fo-Fc maps are contoured at 1 $\sigma$  (blue), and the Fo-Fc maps are contoured at  $\pm 3\sigma$  (green/red). Image generated using COOT<sup>(17)</sup>. The overall pose of the molecule is similar to that of **ABT-737**, as shown in **Figure 3.3A**.



**Table 3.4: Crystallographic statistics for the BCL-X<sub>L</sub>:3.2c complex.**

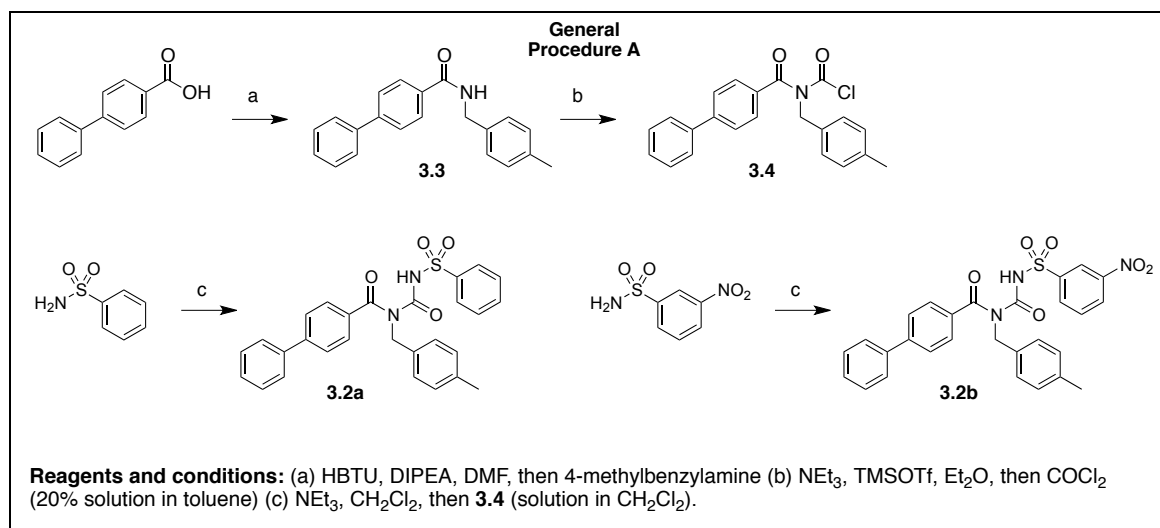
<b>Structure <sup>Ψ</sup></b>	<b>BCL-X<sub>L</sub>:3.2c <sup>Φ</sup></b>
Wavelength (Å)	0.9537
Resolution range (Å)	37.37 - 2.854 (2.956 - 2.854)
Space group	<i>P</i> 3 <sub>2</sub>
Unit cell	
<i>a</i> , <i>b</i> , <i>c</i> (Å)	100.72, 100.72, 167.29
α, β, γ (°)	90, 90, 120
Total reflections	250728 (24456)
Unique reflections	44040 (4380)
Multiplicity	5.7 (5.6)
Completeness (%)	1.00 (0.98)
Mean <i>I</i> / σ <i>I</i>	11.68 (2.13)
Wilson <i>B</i> factor (Å <sup>2</sup> )	61.19
<i>R</i> <sub>merge</sub>	0.1338 (0.9789)
<i>R</i> <sub>meas</sub>	0.1475 (1.079)
CC <sub>1/2</sub>	0.996 (0.664)
CC*	0.999 (0.893)
Reflections used in refinement	44026 (4380)
Reflections used for R-free	2201 (219)
<i>R</i> <sub>work</sub>	0.1847 (0.3251)
<i>R</i> <sub>free</sub>	0.2639 (0.4074)
CC <sub>work</sub>	0.966 (0.765)
CC <sub>free</sub>	0.938 (0.538)
Number of non-hydrogen atoms	13766
macromolecules	13554
ligands/ions	180
RMS(bond lengths) (Å)	0.011
RMS(bond angles) (°)	1.42
Ramachandran favored (%)	93
Ramachandran allowed (%)	5
Ramachandran outliers (%)	1.9
Rotamer outliers (%)	2.5
Clashscore	16.38
Average <i>B</i> factors (Å <sup>2</sup> )	76.23
Macromolecules	76.29
ligands	77
solvent	43.74

<sup>Ψ</sup> Statistics are outlined in Section 2.6.2.5.

<sup>Φ</sup> Statistics provided are for compound **3.2c** modeled in the ‘closed’ conformation. Only limited building and refinement has been performed on this structure, as it is unlikely to be published. For publication, some further model building would be necessary to improve the overall model validation statistics.

### 3.3.1.2 Synthesis of benzoylurea arylsulfonamides (compounds **3.2a-b**)

We anticipated that compounds **3.2a** and **3.2b** might be formed by utilising established conditions to form the carbamoyl chloride intermediate **3.4**, which can then be reacted with a primary arylsulfonamide, such as benzene sulfonamide or 3-nitrobenzene sulfonamide to form the desired products (**Scheme 3.1**).



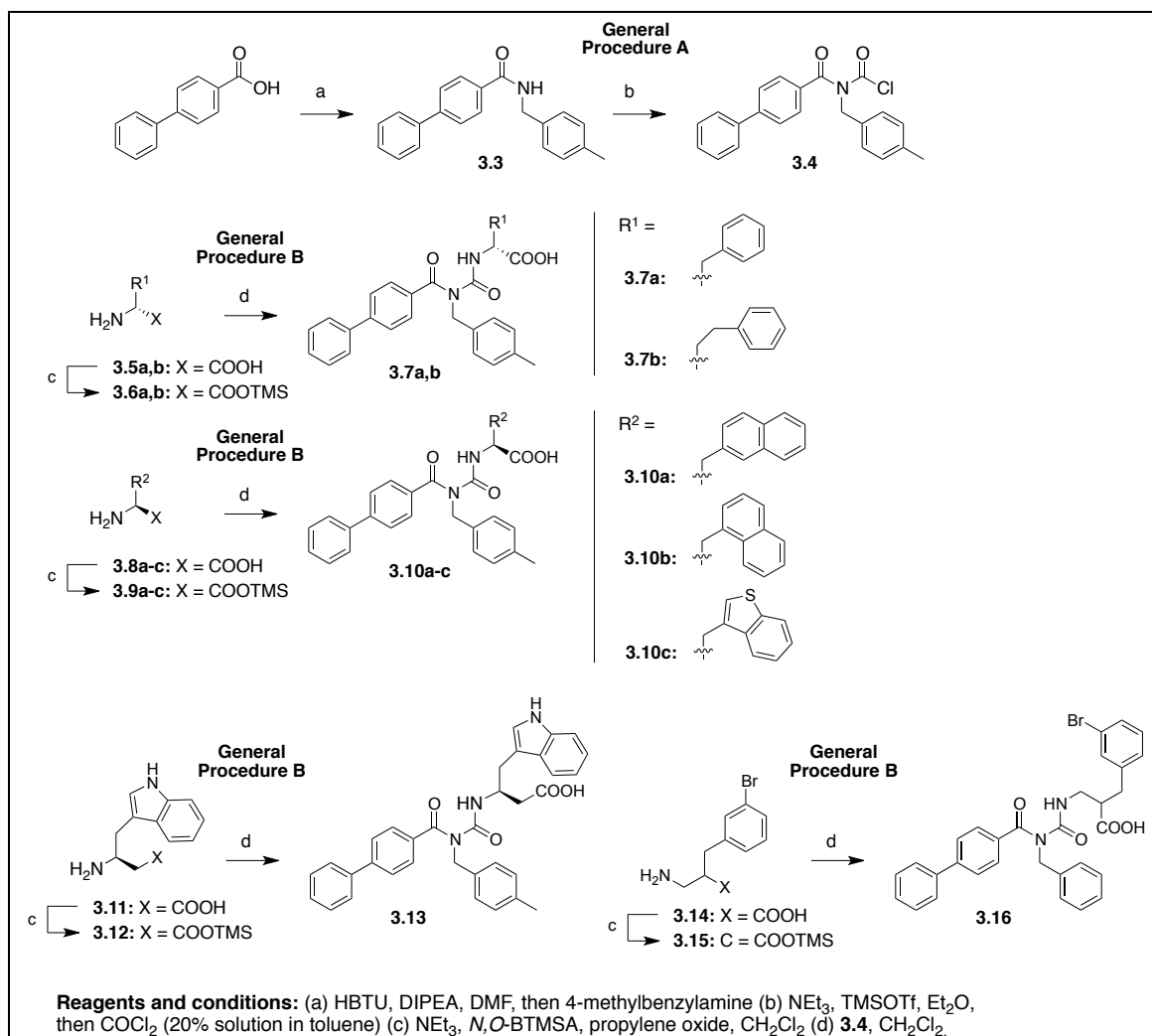
**Scheme 3.1: Synthetic approach to form compounds 3.2a-b.**

Multiple attempts to were made to synthesise compounds **3.2a** and **3.2b**; TLC and LCMS analysis appeared to indicate good conversion to a single product (with the correct  $m/z$  ratio of the desired product) and this was retained on workup. However neither **3.2a** nor **3.2b** was able to be successfully isolated on subsequent purification attempts *via* purification by either flash chromatography ( $\text{SiO}_2$ ) or by mass-directed preparative HPLC. In all cases it appeared that the product degraded during purification (to form a mixture of species, including the starting amide **3.3**) Based on these results we suspected that the core structure of these molecules might be acid labile, particularly when the central benzoylurea nitrogen was substituted (with the p4 tolyl group), leading to degradation on extended exposure to the mildly acidic silica or TFA in the HPLC eluent. This possibility was not explored further. As an inherently labile core would be undesirable for medicinal chemistry optimisation, we ultimately decided to abandon this approach and instead incorporate amino acid derivatives containing an aromatic ring separated by a shortened linker.



### 3.3.2 Synthesis and evaluation of benzoylurea compounds 3.7a – 3.16

Using commercially-available amino acids we next generated a small set of seven benzoylurea analogues, which we hoped might be able to achieve stabilising pi-stacking interactions in the p4 pocket of BCL-X<sub>L</sub> (**Scheme 3.1**). Analogues **3.7a-b**, **3.10a-c**, **3.13** and **3.16** were all furnished in good-excellent yields using the established benzoylurea chemistry and screened for binding to BCL-X<sub>L</sub> and MCL-1 using the AlphaScreen assay.



**Scheme 3.2: Synthesis of analogues 3.7a-b, 3.10a-c, 3.13 and 3.16, to explore pi-stacking interactions in the p4 pocket of BCL-X<sub>L</sub>.**

### 3.3.2.1 Evaluation of BCL-X<sub>L</sub> and MCL-1 binding using AlphaScreen competition assay

All 7 analogues were screened for their binding towards BCL-X<sub>L</sub> and MCL-1 using the AlphaScreen (A.S.) competition assay described in **Chapter 1**. The results are summarised in **Table 3.5**.

**Table 3.5: IC<sub>50</sub> values for compounds 3.7a-b, 3.10a-c, 3.13 and 3.16 for BCL-X<sub>L</sub> and MCL-1 (determined by AlphaScreen Assay, pre-2015 data) <sup>[a]</sup>**

Compound	IC <sub>50</sub> A.S. <sup>[b]</sup>				Fold Selectivity	BEI <sup>[c]</sup>
	BCL-X <sub>L</sub>	MCL-1	N =		(BCL-X <sub>L</sub> /MCL-1)	
<b>1.1</b>	4.6 ± 1.0	74 ± 20	3		16	9.9
<b>1.8</b>	1.5 ± 0.6	68 ± 25	5		44	10.2
<b>3.7a</b>	60 ± 13	46 ± 5	2		0.8	8.6
<b>3.7b</b>	36 ± 6.4	51 ± 8	2		1.4	8.8
<b>3.10a</b>	46 ± 12	95 ± 9	2		2.1	8.0
<b>3.10b</b>	48 ± 16	60 ± 17	2		1.3	8.0
<b>3.10c</b>	10 ± 5.8	69 ± 30	4		6.7	9.1
<b>3.13</b>	67 ± 20	73 ± 7	2		1.1	7.7
<b>3.16</b>	53 ± 12	99 ± 1	2		1.9	7.5

<sup>[a]</sup> Following the relocation of our Screening Group, a consistent shift in the IC<sub>50</sub> values determined using the AlphaScreen competition assay was observed. The signifiers '**pre-2015 data**' and '**post-2015 data**' indicate respectively data acquired prior and subsequent to this relocation. For further information refer to note in **Chapter 2, Section 2.4.1.3**.

<sup>[b]</sup> IC<sub>50</sub> values are reported in  $\mu\text{M} \pm \text{S.D.}$

<sup>[c]</sup> BEI (Binding efficiency index, refer Section 1.4.1.2) =  $\text{pIC}_{50}/\text{MW}$ , where  $\text{pIC}_{50}$  is the negative base 10 logarithm of the IC<sub>50</sub> (in molar units) and MW is the compound molecular weight (in kDa).

As shown in **Table 3.5**, all analogues with the possible exception of compound **3.10c** showed significantly reduced binding for BCL-X<sub>L</sub> relative to compound **1.1** and **1.8** (and a concomitant loss of selectivity for BCL-X<sub>L</sub> relative to MCL-1). This indicated that for these compounds the modifications had the effect of disrupting binding in the p4/p5 pockets of BCL-X<sub>L</sub> rather than generating additional fruitful interactions, and almost certainly the desired pi-stacking interaction was not achieved.

It was interesting to note that compound **3.10c** (incorporating a 3'-substituted benzothiophene moiety attached by a short single methylene linker) retained much of the binding of compound **1.1** (~2-fold weaker IC<sub>50</sub> relative to compound **1.1**, **Table 3.5**) despite this group being likely substantially more conformationally restricted than the S-benzyl moiety of **1.1**. In comparison, compounds **3.10b** and **3.13** that were structurally quite similar to compound **3.10c** (incorporating respectively a 1'-substituted naphthyl and 3'-substituted indole moiety on the same short linker) had notably weaker binding for BCL-X<sub>L</sub> (> 10-fold weaker IC<sub>50</sub> relative to compound **1.1**). Compound **3.13** also had a second point of difference, in that the carboxylic acid moiety was homologated by one carbon. As this binding data for these three compounds appeared to reveal a relatively defined structure-activity-relationship (SAR), we were interested to determine an X-ray crystal structure for compound **3.10c** bound to BCL-X<sub>L</sub> in order to further explore the binding mode.

### 3.3.3 Structure determination of the BCL-X<sub>L</sub>:**3.10c** complex

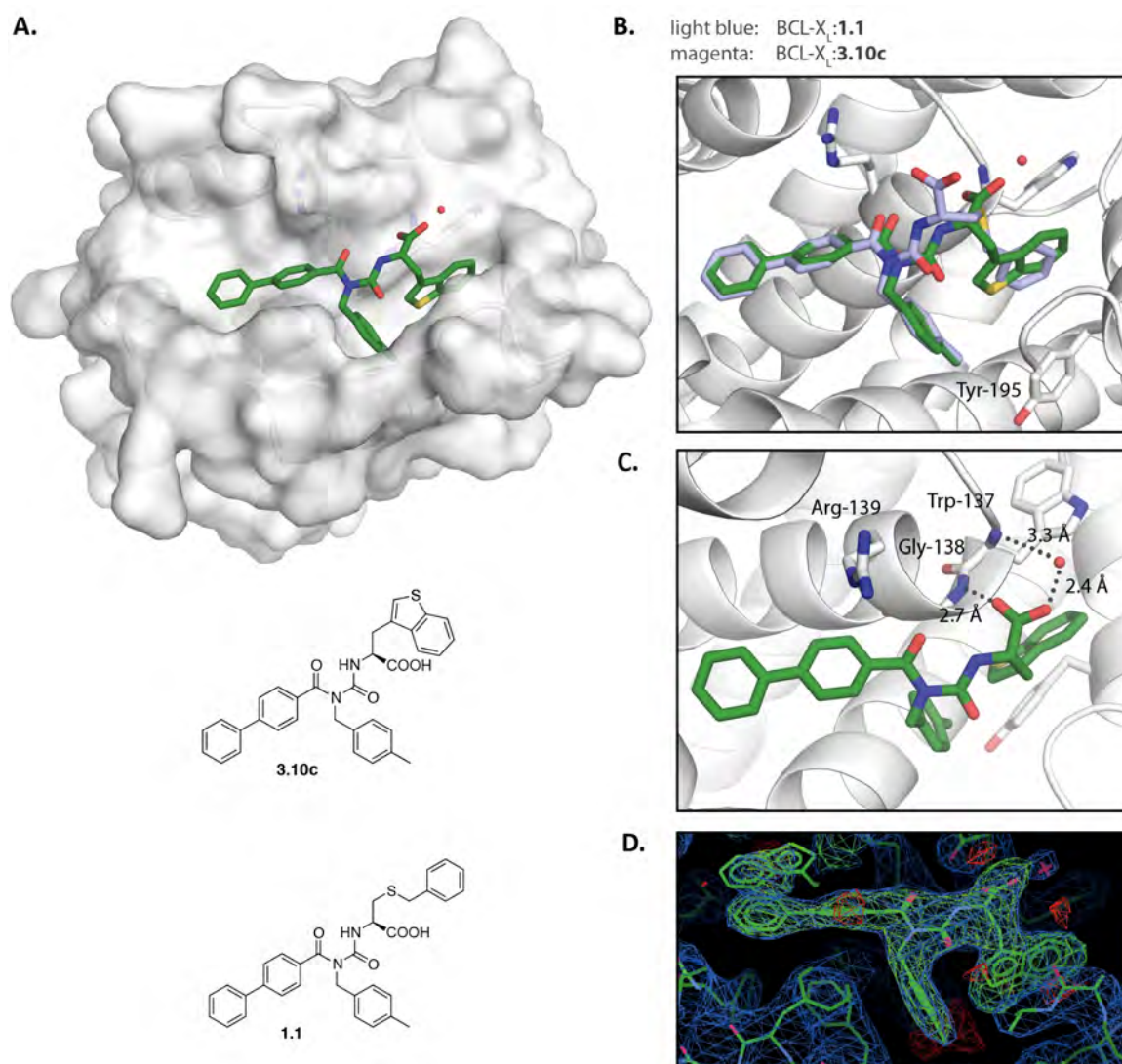
Relevance:

- Provide structural information on the binding mode of compound **3.10c** to BCL-X<sub>L</sub>
- Understand the basis for the difference in IC<sub>50</sub> values for BCL-X<sub>L</sub> between compound **3.10c** and the structurally similar compounds **3.10b** and **3.13**.

Small-scale in-house crystallization trials for the BCL-X<sub>L</sub>:**3.10c** complex successfully yielded crystals that diffracted to 2.5 Å resolution. The resulting X-ray crystal structure determined for the complex showed two BCL-X<sub>L</sub> monomers per asymmetric unit (as a single domain-swapped dimer). In one monomer a single molecule of compound **3.10c** was observed to occupy the hydrophobic groove in a binding mode similar to that of compound **1.1** (shown in **Figure 3.6**). A second molecule of compound **3.10c** was observed to bind to the other BCL-X<sub>L</sub> monomer, but in an alternative conformation that appeared to be simply a result of crystal packing and thus unlikely to represent the bound state in solution. In this second conformation, compound **3.10c** bound the groove in a reversed orientation, with the benzothiophene group bridging across the interface to another symmetry-related BCL-X<sub>L</sub> monomer (not shown). Statistics for the structure of the BCL-X<sub>L</sub>:**3.10c** complex are provided in **Table 3.6**.

Overlay of the BCL-X<sub>L</sub>:**3.10c** and BCL-X<sub>L</sub>:**1.1** complexes reveals that whilst the binding of the biphenyl and tolyl moieties is unchanged, the compound **3.10c** structure shows some important differences in the mode of interaction near the p5 pocket (**Figure 3.6B**). Whilst the desired pi-stacking interaction has again not been formed with Tyr195, most notably in the BCL-X<sub>L</sub>:**3.10c** complex, the carboxylic acid moiety of compound **3.10c** interacts directly with backbone –NH of Gly138 (similar to hydrogen bonding network of the sulfonyl moiety of compound **1.8**, **Figure 3.1B**) to accommodate the benzothiophene moiety in the p5 pocket. This appears to be mediated by the shortened and conformationally-restricted methylene linker to the benzothiophene in compound **3.10c**, relative to the longer and more flexible S-benzyl group of compound **1.1**.

The close intramolecular packing of the benzothiophene moiety of compound **3.10c** against the tolyl group reveals the basis for the loss in binding of both the naphthyl analogue compound **3.10b** and the  $\beta$ -homotryptophan analogue compound **3.13**. For compound **3.10b**, the larger 6-membered ring would lead to steric clash with both the tolyl moiety and likely the central carbonyl of the benzoylurea core. In comparison, the homologated acid of compound **3.13** would be unable to form the same direct hydrogen bonding interaction with Gly138, moreover to accommodate the tryptophan indole moiety in the same binding orientation as the benzothiophene would involve a significant entropic penalty on desolvation of the indole nitrogen to pack in the hydrophobic p4/p5 pocket. Ultimately, compound **3.10c** appeared to have slightly lower binding efficiency as compared to compounds **1.1** or **1.8** (calculated BEI, **Table 3.5**) and so subsequent derivatives have stemmed from compounds **1.1/1.8**. However, understanding the novel binding mode of compound **3.10c** to BCL-X<sub>L</sub> may guide future inhibitor design efforts targeting this region of the protein.



**Figure 3.6: (A) X-ray crystal structure of BCL-X<sub>L</sub>:3.10c complex (B) Overlay of the BCL-X<sub>L</sub>:1.1 complex with BCL-X<sub>L</sub>:3.10c complex. (C) Hydrogen bonding interaction of carboxylic acid moiety of compound 3.10c with backbone -NH of Gly138 of BCL-X<sub>L</sub>. (D) Simulated annealing omit map (2Fo-Fc and Fo-Fc contoured at 1σ and ±3σ respectively) showing the primary conformation of compound 3.10c in the BCL-X<sub>L</sub>:3.10c complex.**

**Table 3.6: Crystallographic statistics for the BCL-X<sub>L</sub>:3.10c complex.**

<b>Structure <sup>Ψ</sup></b>	<b>BCL-X<sub>L</sub>:3.10c</b>
Wavelength (Å)	0.9537
Resolution range (Å)	42.15 - 2.496 (2.585 - 2.496)
Space group	<i>P</i> 3 <sub>1</sub> 2 1
Unit cell	
<i>a</i> , <i>b</i> , <i>c</i> (Å)	97.35, 97.35, 73.61
α, β, γ (°)	90, 90, 120
Total reflections	155977 (14061)
Unique reflections	14313 (1365)
Multiplicity	10.9 (10.3)
Completeness (%)	1.00 (0.98)
Mean <i>I</i> / σ <i>I</i>	18.68 (1.56)
Wilson <i>B</i> factor (Å <sup>2</sup> )	55.78
<i>R</i> <sub>merge</sub>	0.1066 (1.585)
<i>R</i> <sub>meas</sub>	0.1119 (1.668)
CC <sub>1/2</sub>	0.999 (0.622)
CC*	1 (0.876)
Reflections used in refinement	14309 (1364)
Reflections used for R-free	716 (68)
<i>R</i> <sub>work</sub>	0.1938 (0.2739)
<i>R</i> <sub>free</sub>	0.2464 (0.3263)
CC <sub>work</sub>	0.963 (0.822)
CC <sub>free</sub>	0.952 (0.706)
Number of non-hydrogen atoms	2454
macromolecules	2317
ligands/ions	90
RMS(bond lengths) (Å)	0.008
RMS(bond angles) (°)	1.06
Ramachandran favored (%)	98
Ramachandran allowed (%)	2.1
Ramachandran outliers (%)	0
Rotamer outliers (%)	0.41
Clashscore	4.99
Average <i>B</i> factors (Å <sup>2</sup> )	54.1
Macromolecules	53.77
ligands	61.96
solvent	55.62

<sup>Ψ</sup> Statistics are outlined in Section 2.6.2.5.

### 3.4 Discussion / Conclusion

This Chapter has described initial structural studies on two important lead molecules in the benzoylurea series targeting BCL-X<sub>L</sub>, compounds **1.9** and **3.1**. X-ray crystal structures have been solved for each in complex with BCL-X<sub>L</sub> (to 2.9 Å and 1.6 Å resolution respectively) and confirmed the binding modes - in particular key interactions with the p2 pocket and, for the BCL-X<sub>L</sub>:**3.1** structure, a hydrogen bond from a sulfonyl oxygen of compound **3.1** to the backbone -NH Gly138 of BCL-X<sub>L</sub>.

Based on structural overlay of the BCL-X<sub>L</sub>:**1.1** and BCL-X<sub>L</sub>:**ABT-737** complexes, a related series of benzoylurea arylsulfonamides were proposed, which aimed to append a suitably-placed arylsulfonamide group to generate an additional pi-stacking interaction with Tyr195 of BCL-X<sub>L</sub>, towards improving the overall affinity. A crystal structure of a related molecule with a similar structure (compound **3.2c**) in complex with BCL-X<sub>L</sub> was solved to 2.85 Å resolution and the binding mode of the nitroarylsulfonamide group supported the general design strategy. This structure was unfortunately of insufficient resolution to give a definitive answer to an outstanding question regarding the 'open'/'closed' conformational preference of the benzoylurea core of this scaffold at near-physiological pH. Attempts were made to synthesise and isolate two trial benzoylurea arylsulfonamides, compounds **3.2a** and **3.2b**, but were hampered by low product stability to chromatographic purification and so this particular design strategy was not pursued further.

An alternative approach to targeting pi-stacking interactions was next trialed, utilising a small set of amino acid moieties to which various aryl groups were connected *via* a relatively short carbon linker, to generate benzoylurea compounds **3.7a-b**, **3.10a-c**, **3.13** and **3.16**. Assay for BCL-X<sub>L</sub> or MCL-1 binding revealed that only compound **3.10c** retained significant binding for BCL-X<sub>L</sub>, indicating that for the other compounds the desired pi-stacking interaction had not been formed. A crystal structure of compound **3.10c** in complex with BCL-X<sub>L</sub> solved to 2.5 Å resolution revealed that this compound also did not form the

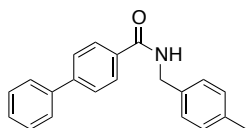


pi-stacking interaction but displayed a novel binding mode of the benzothiophene amino acid moiety in the p5 pocket. **Chapter 4** explores the synthesis of analogues of compounds **1.1** and **1.8** that further explore modifications targeted to the p5 pocket.

## 3.5 Experimental

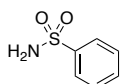
### 3.5.1 Chemical synthesis

For **General Procedures A and B**, refer to **Chapter 2, Section 2.2**.

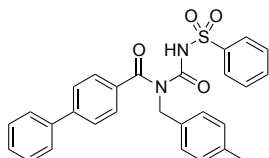


**N-[(4-methylphenyl)methyl]-4-phenylbenzamide (3.3):** To a stirred solution of biphenyl-4-carboxylic acid (1.0 g, 5.0 mmol) in 12.5 mL of anhydrous DMF was added HBTU (3.8 g, 10 mmol) and DIEA (1.74 mL, 10 mmol) and the reaction was stirred under N<sub>2</sub> at room temperature for 15 minutes. 4-Methylbenzylamine (1.30 mL, 10.1 mmol) was then added and the reaction was allowed to proceed at room temperature for 18 h. After this time, the reaction mixture was poured over an ice/water mixture and the off-white solid precipitate formed was collected by vacuum filtration, washed copiously with cold water and then dried in a 30°C oven *in vacuo*. The resulting solid was purified *via* flash chromatography eluting with EtOAc/hexane (25:75) to afford compound **3.3** as fine white needles (1.46 g, 97%). <sup>1</sup>H NMR (300 MHz, CDCl<sub>3</sub>)  $\delta$  7.86 (d, *J* = 8.67 Hz, 2H), 7.65 (d, *J* = 8.58 Hz, 2H), 7.61 (dd, *J* = 8.25, 1.32 Hz, 2H), 7.49–7.43 (m, 2H), 7.41–7.36 (m, 1H), 7.27 (d, *J* = 7.92 Hz, 2H), 7.18 (d, *J* = 7.92 Hz, 2H), 6.41 (br s, 1H), 4.63 (d, *J* = 5.52 Hz, 2H), 2.36 (s, 3H). <sup>13</sup>C NMR (75 MHz, CDCl<sub>3</sub>)  $\delta$  166.9, 144.4, 140.0, 137.4, 135.2, 133.1, 129.5, 128.9, 128.0, 127.5, 127.2, 127.2, 44.0, 21.1. MS (ES<sup>+</sup>), *m/z* 302.1, (M + H). HRMS (ES<sup>+</sup> TOF) calculated for C<sub>21</sub>H<sub>19</sub>NO (M + H): 302.1539; found 302.1532.

#### 3.5.1.1 Attempted synthesis of benzoylurea arylsulfonamide analogues

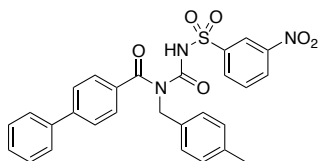


**Benzene sulfonamide** was prepared according to a procedure described in the literature<sup>(20)</sup>. To a stirred solution of 10% ammonia in water (40 mL) at -5°C in an ice/salt/water bath was slowly added benzene sulfonyl chloride (1.45 mL, 11.3 mmol). A white precipitate slowly formed. The mixture was allowed to warm to room temperature during 1 h and was then stirred at room temperature for a further 22 h. The fine white precipitate was filtered, washed with copious cold water and dried for 24 h in a 30°C vacuum oven to yield the title product directly as a fine white powder (1.0 g, 50%). MS (ES<sup>+</sup>), *m/z* 158.1, (M + H), 99% purity.



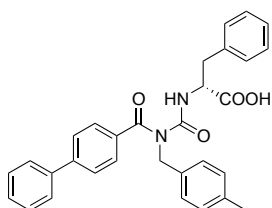
**N-(4-methylbenzyl)-N-((phenylsulfonyl)carbonyl)-[1,1'-biphenyl]-4-carboxamide (3.2a):** **General Procedure A** was followed using compound **3.3** (100 mg, 0.32 mmol) to form the carbamoyl chloride intermediate **3.4**. Under a N<sub>2</sub> atmosphere, **3.4** was redissolved in anhydrous dichloromethane (1 mL) and transferred dropwise to a stirred solution at 0°C of benzene sulfonamide (50 mg, 0.32 mmol) and triethylamine (48  $\mu$ L, 0.35 mmol) in anhydrous dichloromethane (1 mL). The reaction was allowed to warm to room temperature and stirred at room temperature for 2 h. After this time, the reaction was diluted with EtOAc and poured onto aqueous 1M HCl. The reaction mixture was extracted three times with EtOAc. The combined organic layers were washed with water, then brine, dried over MgSO<sub>4</sub> and concentrated to yield a crude white solid (116 mg). TLC and LCMS of this crude material appeared to indicate product formation, however attempted purification of the crude *via* flash chromatography, eluting with a

gradient of methanol/dichloromethane (0:100 to 3:97) led to apparent degradation on the column and product fractions isolated contained significant impurities. Subsequent re-purification by mass-directed preparative HPLC led to further degradation to a species with the same  $m/z$  as the starting amide. None of the desired product was successfully isolated.

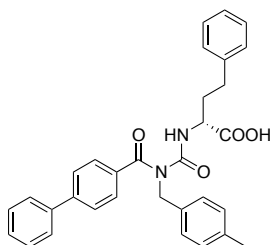


***N*-(4-methylbenzyl)-*N*-(((3-nitrophenyl)sulfonyl)carbamoyl)-[1,1'-biphenyl]-4-carboxamide (3.2b):** General Procedure A was followed using compound **3.3** (100 mg, 0.32 mmol) to form the carbamoyl chloride intermediate **3.4**. Under a  $N_2$  atmosphere, **3.4** was redissolved in anhydrous dichloromethane (1 mL) and transferred dropwise to a stirred solution at 0°C of 3-nitrobenzene sulfonamide (64 mg, 0.32 mmol) and triethylamine (48  $\mu$ L, 0.35 mmol) in anhydrous dichloromethane (1 mL). The reaction was allowed to warm to room temperature and stirred at room temperature for 2 h. Subsequent workup and attempted purification *via* flash chromatography and mass-directed preparative HPLC as for **3.2a** led to identical product degradation. None of the desired product was successfully isolated.

#### 3.5.1.1.1 Benzoylurea formation [Scheme 3.2 (b, c, d)]

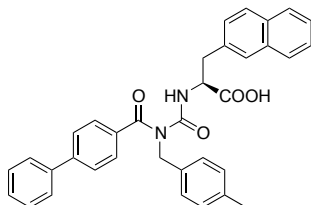


**(*R*)-2-(3-([1,1'-biphenyl]-4-carbonyl)-3-(4-methylbenzyl)ureido)-3-phenylpropanoic acid (3.7a):** General Procedures A and B were followed using compound **3.3** (50 mg, 0.16 mmol) and D-phenylalanine (29 mg, 0.17 mmol). Purification *via* flash chromatography, eluting with a gradient of methanol/dichloromethane (0:100 to 5:95) afforded the title compound as a colourless glass (72 mg, 84%).  $^1H$  NMR (600 MHz,  $CDCl_3$ )  $\delta$  9.42 (d,  $J$  = 6.1 Hz, 1H), 7.60–7.51 (m, 4H), 7.45 (tdd,  $J$  = 7.8, 1.4, 0.5 Hz, 2H), 7.41–7.35 (m, 3H), 7.35–7.30 (m, 2H), 7.28 (dd,  $J$  = 7.4, 1.8 Hz, 1H), 7.25–7.23 (m, 1H), 7.05 (d,  $J$  = 7.1 Hz, 2H), 6.85 (dd,  $J$  = 7.9, 1.3 Hz, 1H), 4.94 (s, 2H), 4.87–4.80 (m, 1H), 3.31 (ddd,  $J$  = 13.7, 5.0, 1.0 Hz, 1H), 3.15 (ddd,  $J$  = 13.6, 7.9, 1.2 Hz, 1H), 2.30 (s, 1H).  $^{13}C$  NMR (75 MHz,  $CDCl_3$ )  $\delta$  175.20, 174.54, 155.38, 143.83, 139.97, 137.08, 136.01, 134.61, 134.51, 129.50, 129.42, 129.10, 128.88, 128.24, 127.37, 127.31, 127.29, 127.24, 126.61, 55.26, 50.06, 37.61, 21.23. MS ( $ES^+$ ),  $m/z$  493.3, ( $M + H$ ), 99% purity. HRMS ( $ES^+$  TOF) calculated for  $C_{31}H_{28}N_2O_4$  ( $M + H$ ): 493.2122; found 493.2122.

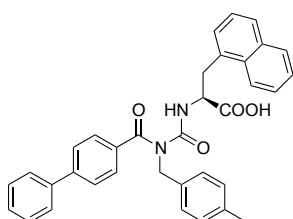


**(*R*)-2-(3-([1,1'-biphenyl]-4-carbonyl)-3-(4-methylbenzyl)ureido)-4-phenylbutanoic acid (3.7b):** General Procedures A and B were followed using compound **3.3** (50 mg, 0.16 mmol), D-homophenylalanine hydrochloride (37 mg, 0.18 mmol) and triethylamine (63  $\mu$ L, 0.26 mmol) to neutralise the amino acid HCl salt. Purification *via* flash chromatography, eluting with a gradient of methanol/dichloromethane (0:100 to 5:95) afforded the title compound as a colourless glass (59 mg, 70%).  $^1H$  NMR (600 MHz,  $CDCl_3$ )  $\delta$  9.52 (d,  $J$  = 6.4 Hz, 1H), 7.59 (t,  $J$  = 7.4 Hz, 4H), 7.50–7.42 (m, 4H), 7.39 (t,  $J$  = 7.4 Hz, 1H), 7.31–7.26 (m, 2H), 7.22–7.17 (m, 3H), 7.08 (d,  $J$  = 7.8 Hz, 2H), 6.95

(d,  $J$  = 7.8 Hz, 2H), 5.00 (s, 2H), 4.60 (dd,  $J$  = 12.5, 7.2 Hz, 1H), 2.77 (t,  $J$  = 7.9 Hz, 2H), 2.39–2.26 (m, 4H), 2.16 (td,  $J$  = 15.4, 7.7 Hz, 1H).  $^{13}\text{C}$  NMR (75 MHz,  $\text{CDCl}_3$ )  $\delta$  176.50, 175.36, 155.27, 143.85, 140.56, 139.94, 137.13, 134.70, 134.57, 129.43, 129.09, 128.65, 128.63, 128.23, 127.35, 127.31, 127.27, 126.67, 126.37, 53.64, 50.15, 33.46, 31.87, 21.21. MS ( $\text{ES}^+$ ),  $m/z$  507.3, ( $\text{M} + \text{H}$ ), 99% purity. HRMS ( $\text{ES}^+$  TOF) calculated for  $\text{C}_{32}\text{H}_{30}\text{N}_2\text{O}_4$  ( $\text{M} + \text{H}$ ): 507.2278; found 507.2280.



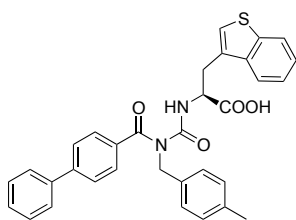
**(S)-2-(3-([1,1'-biphenyl]-4-carbonyl)-3-(4-methylbenzyl)ureido)-3-(naphthalen-2-yl)propanoic acid (3.10a):** General Procedures A and B were followed using compound 3.3 (33 mg, 0.10 mmol) and L-2-naphthylalanine (34 mg, 0.16 mmol). Purification *via* flash chromatography, eluting with a gradient of methanol/dichloromethane (0:100 to 5:95) afforded the title compound as a colourless glass (39 mg, 68%).  $^1\text{H}$  NMR (600 MHz,  $\text{CDCl}_3$ )  $\delta$  9.48 (d,  $J$  = 6.8 Hz, 1H), 7.86–7.76 (m, 3H), 7.72 (s, 1H), 7.57–7.54 (m, 2H), 7.53 (d,  $J$  = 8.0 Hz, 2H), 7.49–7.43 (m, 4H), 7.40–7.35 (m, 2H), 7.33 (d,  $J$  = 8.0 Hz, 2H), 6.93 (d,  $J$  = 7.9 Hz, 2H), 6.78 (d,  $J$  = 7.9 Hz, 2H), 4.96 (dt,  $J$  = 7.2, 4.9 Hz, 1H), 4.94 (d,  $J$  = 12.7 Hz, 1H), 4.88 (d,  $J$  = 16.2 Hz, 1H), 3.50 (dd,  $J$  = 14.1, 5.0 Hz, 1H), 3.28 (dd,  $J$  = 14.1, 8.4 Hz, 1H), 2.27 (s, 3H).  $^{13}\text{C}$  NMR (75 MHz,  $\text{CDCl}_3$ )  $\delta$  175.62, 175.15, 155.30, 143.74, 139.96, 136.97, 134.57, 134.50, 133.67, 133.66, 132.73, 129.36, 129.07, 128.57, 128.33, 128.20, 127.96, 127.85, 127.46, 127.29, 127.26, 127.17, 126.49, 126.28, 125.90, 55.24, 49.99, 37.97, 21.18. MS ( $\text{ES}^+$ ),  $m/z$  543.2, ( $\text{M} + \text{H}$ ), 99% purity. HRMS ( $\text{ES}^+$  TOF) calculated for  $\text{C}_{35}\text{H}_{30}\text{N}_2\text{O}_4$  ( $\text{M} + \text{H}$ ): 543.2278; found 543.2281.



**(S)-2-(3-([1,1'-biphenyl]-4-carbonyl)-3-(4-methylbenzyl)ureido)-3-(naphthalen-1-yl)propanoic acid (3.10b):** General Procedures A and B were followed using compound 3.3 (33 mg, 0.10 mmol) and L-1-naphthylalanine (34 mg, 0.16 mmol). Purification *via* flash chromatography, eluting with a gradient of methanol/dichloromethane (0:100 to 5:95) afforded the title compound as a colourless glass (45 mg, 78%).  $^1\text{H}$  NMR (300 MHz,  $\text{CDCl}_3$ )  $\delta$  9.53 (d,  $J$  = 6.7 Hz, 1H), 8.16 (dd,  $J$  = 8.3, 0.7 Hz, 1H), 7.89 (dd,  $J$  = 8.2, 1.2 Hz, 1H), 7.81 (dq,  $J$  = 6.5, 3.2 Hz, 1H), 7.64–7.28 (m, 13H), 7.02 (d,  $J$  = 7.9 Hz, 2H), 6.80 (d,  $J$  = 8.0 Hz, 2H), 4.98 (ddd,  $J$  = 9.1, 6.6, 5.1 Hz, 1H), 4.89 (s, 2H), 3.89 (dd,  $J$  = 14.4, 5.1 Hz, 1H), 3.49 (dd,  $J$  = 14.4, 9.2 Hz, 1H), 2.29 (s, 3H).<sup>[a]</sup>  $^{13}\text{C}$  NMR (75 MHz,  $\text{CDCl}_3$ )  $\delta$  176.00, 175.21, 155.27, 143.73, 139.97, 137.00, 134.59, 134.54, 134.12, 132.32, 132.06, 129.37, 129.08, 128.28, 128.21, 127.98, 127.30, 127.30, 127.20, 127.19, 126.63, 126.60, 125.96, 125.60, 123.54, 54.88, 49.95, 35.26, 21.21.<sup>[b]</sup> MS ( $\text{ES}^+$ ),  $m/z$  542.6, ( $\text{M} + \text{H}$ ), 97% purity. HRMS ( $\text{ES}^+$  TOF) calculated for  $\text{C}_{35}\text{H}_{30}\text{N}_2\text{O}_4$  ( $\text{M} + \text{H}$ ): 543.2278; found 543.2280.

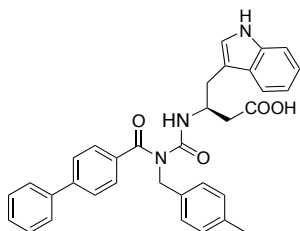
<sup>[a]</sup> The peaks at 2.11, 2.09, 1.26–1.09 ppm are due to impurities.

<sup>[b]</sup> One aromatic peak is not observed due to overlap.



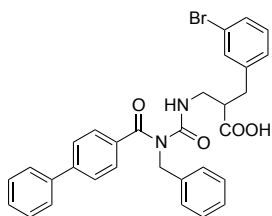
**(S)-2-(3-([1,1'-biphenyl]-4-carbonyl)-3-(4-methylbenzyl)ureido)-3-(benzo[b]thiophen-3-yl)propanoic acid (3.10c):** General Procedures A and B were followed using compound 3.3

(33 mg, 0.10 mmol) and L-3-benzothienylalanine (35 mg, 0.16 mmol). Purification *via* flash chromatography, eluting with a gradient of methanol/dichloromethane (0:100 to 5:95) afforded the title compound as a colourless glass (53 mg, 92%).  $^1\text{H}$  NMR (300 MHz,  $\text{CDCl}_3$ )  $\delta$  9.53 (d,  $J$  = 6.9 Hz, 1H), 7.92–7.78 (m, 2H), 7.63–7.30 (m, 11H), 7.26 (s, 1H), 7.04 (d,  $J$  = 7.8 Hz, 2H), 6.85 (d,  $J$  = 7.9 Hz, 2H), 5.12–4.87 (m, 3H), 3.58 (dd,  $J$  = 15.1, 4.6 Hz, 1H), 3.41 (dd,  $J$  = 14.8, 8.2 Hz, 1H), 2.30 (s, 3H).  $^{13}\text{C}$  NMR (75 MHz,  $\text{CDCl}_3$ )  $\delta$  175.34, 175.23, 155.29, 143.83, 140.58, 139.95, 138.79, 137.12, 134.57, 134.45, 130.60, 129.44, 129.09, 128.23, 127.30, 127.29, 127.23, 126.65, 124.59, 124.54, 124.34, 123.08, 121.68, 53.86, 50.07, 30.73, 21.23. MS ( $\text{ES}^+$ ),  $m/z$  549.6, ( $\text{M} + \text{H}$ ), 99% purity. HRMS ( $\text{ES}^+$  TOF) calculated for  $\text{C}_{33}\text{H}_{28}\text{N}_2\text{O}_4\text{S}$  ( $\text{M} + \text{H}$ ): 549.1843; found 549.1846.



**(S)-3-(3-((1,1'-biphenyl)-4-carbonyl)-3-(4-methylbenzyl)ureido)-4-(1H-indol-3-yl)butanoic acid (3.13):** General Procedures A and B were followed using compound 3.3 (33 mg, 0.10 mmol), L- $\beta$ -homotryptophan hydrochloride (40 mg, 0.16 mmol) and triethylamine (22  $\mu\text{L}$ , 0.16 mmol) to neutralise the amino acid HCl salt. Purification *via* flash chromatography, eluting with a gradient of methanol/dichloromethane (0:100 to 5:95) afforded the title compound as a colourless glass (26 mg, 45%).  $^1\text{H}$  NMR (300 MHz,  $\text{CDCl}_3$ )  $\delta$  9.26 (d,  $J$  = 8.0 Hz, 1H), 8.16 (d,  $J$  = 1.3 Hz, 1H), 7.68 (d,  $J$  = 7.6 Hz, 1H), 7.61–7.50 (m, 4H), 7.49–7.28 (m, 6H), 7.23–7.01 (m, 2H), 6.89 (d,  $J$  = 8.0 Hz, 2H), 4.96 (s, 2H), 4.76–4.52 (m, 1H), 3.20 (dd,  $J$  = 14.5, 6.4 Hz, 1H), 3.10 (dd,  $J$  = 14.5, 7.4 Hz, 1H), 2.69 (dd,  $J$  = 14.6, 3.8 Hz, 1H), 2.62 (dd,  $J$  = 14.6, 4.1 Hz, 1H), 2.29 (s, 3H).  $^{13}\text{C}$  NMR (75 MHz,  $\text{CDCl}_3$ )  $\delta$  175.97, 175.05, 154.78, 143.64, 139.99, 136.95, 136.40, 134.92, 134.86, 129.37, 129.07, 128.18, 127.78, 127.29, 127.21, 126.72, 123.32, 122.23, 119.75, 119.13, 111.57, 111.26, 49.93, 48.56, 37.91, 29.97, 21.22.<sup>[a]</sup> MS ( $\text{ES}^-$ ),  $m/z$  545.6, ( $\text{M} - \text{H}$ ), 98% purity. HRMS ( $\text{ES}^+$  TOF) calculated for  $\text{C}_{34}\text{H}_{31}\text{N}_3\text{O}_4$  ( $\text{M} + \text{H}$ ): 546.2387; found 546.2390.

<sup>[a]</sup> One aromatic peak is not observed due to overlap



**3-(3-((1,1'-biphenyl)-4-carbonyl)-3-(4-methylbenzyl)ureido)-2-(3-bromobenzyl)propanoic acid (3.16):** General Procedures A and B were followed using compound 3.3 (33 mg, 0.10 mmol), 3-amino-2-(3-bromobenzyl)propionic acid hydrochloride (46 mg, 0.16 mmol) and triethylamine (22  $\mu\text{L}$ , 0.16 mmol) to neutralise the amino acid HCl salt. Purification *via* flash chromatography, eluting with a gradient of methanol/dichloromethane (0:100 to 5:95) afforded the title compound as an enantiomeric mixture as a colourless glass (33 mg, 53%).  $^1\text{H}$  NMR (300 MHz,  $\text{CDCl}_3$ )  $\delta$  9.25 (t,  $J$  = 5.8 Hz, 1H), 7.61–7.50 (m, 4H), 7.50–7.30 (m, 7H), 7.17–7.10 (m, 2H), 7.06 (d,  $J$  = 7.8 Hz, 1H), 6.93 (d,  $J$  = 8.0 Hz, 2H), 5.05–4.86 (m, 2H), 3.63 (ddd,  $J$  = 13.5, 5.9, 5.0 Hz, 1H), 3.57–3.43 (m, 1H), 3.03 (ddd,  $J$  = 19.5, 14.7, 7.3 Hz, 2H), 2.81 (dd,  $J$  = 12.8, 5.8 Hz, 1H), 2.29 (s, 3H).  $^{13}\text{C}$  NMR (75 MHz,  $\text{CDCl}_3$ )  $\delta$  177.49, 175.25, 155.42, 143.77, 140.58, 139.94, 137.08, 134.83, 134.69, 132.11, 130.30, 130.02, 129.42, 129.09, 128.22, 127.75, 127.30, 127.29, 127.26, 126.68, 122.74, 50.12, 46.54, 41.54, 35.29, 21.21. MS ( $\text{ES}^+$ ),  $m/z$  585.5, ( $\text{M} + \text{H}$ ), 99% purity. HRMS ( $\text{ES}^+$  TOF) calculated for  $\text{C}_{32}\text{H}_{29}\text{BrN}_2\text{O}_4$  ( $\text{M} + \text{H}$ ): 585.1383; found 585.1386.

### 3.5.2 Crystallisation and X-ray structure determination

#### 3.5.2.1 Structure determination of the BCL-X<sub>L</sub>:**1.9** complex

The complex of BCL-X<sub>L</sub>:**1.9** (8.0 mg/mL) was prepared for crystallisation as described in **Chapter 2, Section 2.6** and subjected to extensive co-crystallisation trials at the CSIRO C3 facility in various conditions; yielding three promising conditions. Subsequent in-house fine-screening and optimization by streak-seeding yielded small yet diffraction-quality crystals in the following condition: 0.9M trisodium citrate, 0.1M MES pH 6.0, 5% (v/v) PEG400. Crystals were flash-cooled in cryoprotectant solution containing 0.9M trisodium citrate, 0.1M MES pH 6.0, 5% (v/v) PEG400, supplemented with ethylene glycol (20%). Data were collected on the MX2 beamline at the Australian Synchrotron, processed (to 2.9 Å resolution) with XDS<sup>(11)</sup> and the structure solved by molecular replacement as described in **Chapter 2, Section 2.6** (using the BCL-X<sub>L</sub> coordinates from the BCL-X<sub>L</sub>:**1.10** structure as a search model). Further rounds of building with COOT and refinement with PHENIX resulted in the final structure. The asymmetric unit contained 3 copies of the BCL-X<sub>L</sub> monomer (one domain-swapped dimer within in the asymmetric unit and a further domain-swapped dimer between the third copy of BCL-X<sub>L</sub> and its symmetry mate), each with a bound copy of compound **1.9** bound in the groove.

#### 3.5.2.2 BCL-X<sub>L</sub>:**3.1** complex

The complex of BCL-X<sub>L</sub>:**3.1** (8.7 mg/mL) was prepared for crystallisation as described in **Chapter 2, Section 2.6** and crystallised under the following condition: 1.1 M ammonium sulfate, 0.1 M HEPES pH 6.5. Crystals were flash-cooled in cryoprotectant solution containing 1.2 M ammonium sulfate, 0.1 M HEPES pH 6.5 supplemented with ethylene glycol (25%). Data were collected on the MX2 beamline at the Australian Synchrotron to approximately 1.6 Å and processed with XDS<sup>(11)</sup>. The structure was solved by molecular replacement with PHASER<sup>(15)</sup> using the BCL-X<sub>L</sub> monomer from the structure of the BCL-X<sub>L</sub>:**1.10** complex as a search model. Multiple rounds of building in COOT<sup>(17)</sup> and refinement

in PHENIX<sup>(16)</sup>, incorporating in the first round of refinement a simulated annealing step, resulted in the final structure.

The asymmetric unit contained four copies of the BCL-X<sub>L</sub> monomer, arranged as two domain-swapped dimers. In three of the four copies, the ligand was observed to occupy the groove in the expected conformation (as for compound **1.10**); in the final copy, the ligand was observed to occupy an alternative conformation, in which the ligand was reversed within the groove, with chlorobiphenyl moiety engaging the p4 pocket and tolyl moiety located in the vicinity of the p2 pocket and interacting with a neighbouring symmetry-related monomer. As this region of the molecule mediated a crystal contact, this conformation appears to be a result of crystal packing and is unlikely to represent the bound conformation in solution.

#### 3.5.2.3 BCL-X<sub>L</sub>:**3.2c** complex

The complex of BCL-X<sub>L</sub>:**3.2c** (10 mg/mL) was prepared for crystallisation as described in **Chapter 2, Section 2.6** and sent for crystallisation screening at the CSIRO C3 facility. Crystals were obtained using a Hampton additive screen based around an initial hit, under the following condition: 0.18 MgCl<sub>2</sub> 16% (w/v) PEG 6000, 0.09 M sodium MES pH 7.0, 0.025 w/v dichloromethane. Crystals were flash-cooled by adding directly to the drop a cryoprotectant solution containing 18% (w/v) PEG 6000, 0.2 M MgCl<sub>2</sub>, 0.1 M Tris pH 7.0, 20% ethylene glycol. Data were collected on the MX2 beamline at the Australian Synchrotron to approximately 2.85 Å and processed with XDS<sup>(11)</sup>. The structure was solved by molecular replacement with PHASER<sup>(15)</sup> using the BCL-X<sub>L</sub> monomer from the structure of the BCL-X<sub>L</sub>:**1.1** complex as a search model, to correctly place 10 BCL-X<sub>L</sub> molecules (as five domain-swapped dimers). Following a single round of refinement in PHENIX<sup>(16)</sup> incorporating a simulated annealing step, visual inspection of the electron density maps suggested the presence of an additional two BCL-X<sub>L</sub> molecules in the A.S.U. The first of these remaining BCL-X<sub>L</sub> monomers was built using PHENIX.AUTOBUILD. Following refinement in PHENIX<sup>(16)</sup>, the second BCL-X<sub>L</sub> monomer was able to be placed manually using COOT<sup>(17)</sup> (to complete the final domain-swapped dimer). Further rounds of building in COOT<sup>(17)</sup>

and refinement in PHENIX<sup>(16)</sup> (incorporating a simulated annealing step in the first round of refinement and TLS refinement utilising NCS torsion-angle restraints) resulted in the structure described in the text. Note that only limited building and refinement has been conducted so far on this model – further model optimisation would be necessary if this structure were to be published.

The asymmetric unit contained 12 copies of the BCL-X<sub>L</sub> monomer, arranged as six domain-swapped dimers (as described more fully in the main text). The ligand was observed to occupy the groove in four copies of the monomer and was modeled in either the ‘closed’ or ‘open’ benzoylurea conformations. Some additional (poorly resolved) electron density was observed in the groove in a further two copies of the BCL-X<sub>L</sub>, which likely corresponded to compound **3.2c**, but this was not modeled. The remaining six copies of BCL-X<sub>L</sub> in the A.S.U. appeared to have no compound bound.

#### 3.5.2.4 BCL-X<sub>L</sub>:**3.10c** complex

The complex of BCL-X<sub>L</sub>:**3.10c** (10 mg/mL) was prepared for crystallisation as described in **Chapter 2, Section 2.6** and crystallised under the following condition: 1.1 M ammonium sulfate, 0.1 M HEPES pH 6.5. Crystals were flash-cooled in cryoprotectant solution containing 1.2 M ammonium sulfate, 0.1 M HEPES pH 6.5 supplemented with ethylene glycol (25%). Data were collected on the MX2 beamline at the Australian Synchrotron to 2.5 Å resolution and processed with XDS<sup>(11)</sup>. The structure was solved by molecular replacement with PHASER using BCL-X<sub>L</sub> monomer from the structure of the BCL-X<sub>L</sub>:**1.1** complex as a search model. Multiple rounds of building in COOT<sup>(17)</sup> and refinement in PHENIX<sup>(16)</sup>, incorporating in the first round of refinement a simulated annealing step, resulted in the final structure.

The asymmetric unit contained two copies of the BCL-X<sub>L</sub> monomer, arranged as a domain-swapped dimer. In one monomer the ligand was observed to occupy the groove in a similar mode of binding to compound **1.10**, in the second copy the ligand was observed to occupy an alternative conformation in which the ligand



was reversed within the groove, with the benzoylurea moiety in an 'open' conformation and the benzothiazole moiety projecting outwards from the groove and interacting with a neighbouring symmetry-related monomer, mediating a crystal contact. This conformation appeared to be a result of crystal packing and unlikely to reflect the bound conformation in solution.

### 3.6 References

1. Lee EF, *et al.* (2007) Crystal structure of ABT-737 complexed with BCL-xL: implications for selectivity of antagonists of the Bcl-2 family. *Cell Death and Differentiation* 14(9):1711-1713.
2. Bissantz C, Kuhn B, & Stahl M (2010) A medicinal chemist's guide to molecular interactions. *Journal of Medicinal Chemistry* 53(14):5061-5084.
3. Oltersdorf T, *et al.* (2005) An inhibitor of Bcl-2 family proteins induces regression of solid tumours. *Nature* 435(7042):677-681.
4. Wendt MD (2008) Discovery of ABT-263, a Bcl-family protein inhibitor: observations on targeting a large protein-protein interaction. *Expert Opinion on Drug Discovery* 3(9):1123-1143.
5. Ballatore C, Huryn DM, & Smith AB (2013) Carboxylic acid (bio)isosteres in drug design. *ChemMedChem* 8(3):385-395.
6. Touré BB, *et al.* (2013) The role of the acidity of N-heteroaryl sulfonamides as inhibitors of Bcl-2 family protein–protein interactions. *ACS Medicinal Chemistry Letters* 4(2):186-190.
7. Wendt MD, *et al.* (2006) Discovery and structure-activity relationship of antagonists of B-cell lymphoma 2 family proteins with chemopotential activity in vitro and in vivo. *Structure* 1:1165-1181.
8. Lessene G, *et al.* (2013) Structure-guided design of a selective BCL-XL inhibitor. *Nature Chemical Biology* 9(6):390-397.
9. Tao Z-F, *et al.* (2014) Discovery of a potent and selective BCL-XL inhibitor with in vivo activity. *ACS Medicinal Chemistry Letters* 5(10):1088-1093.
10. Zhou H, *et al.* (2012) Design of Bcl-2 and Bcl-xL inhibitors with subnanomolar binding affinities based upon a new scaffold. *Journal of Medicinal Chemistry* 55(10):4664-4682.
11. Kabsch W (2010) Xds. *Acta Crystallographica Section D Biological Crystallography* 66(Pt 2):125-132.
12. Zwart PH, Grosse-Kunstleve RW, & Adams PD (2005) Xtriage and Fest: automatic assessment of X-ray data and substructure structure factor estimation. *CCP4 Newsletter Winter*(Contribution 7).

13. Matthews BW (1968) Solvent content of protein crystals. *Journal of Molecular Biology* 33(2):491-497.
14. Kantardjieff KA & Rupp B (2003) Matthews coefficient probabilities: Improved estimates for unit cell contents of proteins, DNA, and protein-nucleic acid complex crystals. *Protein Science* 12(9):1865-1871.
15. McCoy AJ, *et al.* (2007) Phaser crystallographic software. *Journal of Applied Crystallography* 40(Pt 4):658-674.
16. Adams PD, *et al.* (2010) PHENIX: a comprehensive Python-based system for macromolecular structure solution. *Acta Crystallographica Section D Biological Crystallography* 66(Pt 2):213-221.
17. Emsley P & Cowtan K (2004) Coot: model-building tools for molecular graphics. *Acta Crystallographica Section D Biological Crystallography* 60(Pt 12 Pt 1):2126-2132.
18. Terwilliger TC, *et al.* (2008) Iterative model building, structure refinement and density modification with the PHENIX AutoBuild wizard. *Acta crystallographica. Section D, Biological crystallography* 64(Pt 1):61-69.
19. Pettersen EF, *et al.* (2004) UCSF Chimera-a visualization system for exploratory research and analysis. *Journal of Computational Chemistry* 25(13):1605-1612.
20. Gaillard P, *et al.* (2007) WO2007023186A1.

**4 Chapter four – Sulfonyl series exploring  
structure-activity-relationship (SAR) of p5 pocket of  
BCL-X<sub>L</sub>**

## 4.1 Introduction

**Chapter 1** introduced the benzoylurea series of BCL-X<sub>L</sub> inhibitors stemming from compound **1.1**, which was shown to bind along the canonical groove of BCL-X<sub>L</sub> with a low micromolar IC<sub>50</sub>. Important points of interaction of compound **1.1** with BCL-X<sub>L</sub> included a tolyl moiety that engaged the p4 hydrophobic pocket of BCL-X<sub>L</sub> and a S-benzyl moiety that engaged a neighbouring hydrophobic pocket which we have termed p5 (**Figure 4.1C**). Among the initial SAR studies described in **Chapter 1** were analogues in which the thioether linkage of **1.1** was replaced with a methylene (compound **1.6**), ether (compound **1.7**), or sulfonyl linkage (compound **1.8**), which all bond to BCL-X<sub>L</sub> with similar IC<sub>50</sub> to **1.1**. An analogue in which the S-benzyl was replaced with an S-methyl (compound **1.2**) showed approximately 25-fold reduced binding to BCL-X<sub>L</sub>.

**Chapter 3** described the structural characterisation by X-ray crystallography of two analogues designed to interact in the p2 pocket of BCL-X<sub>L</sub> **1.9** and **3.1**, as well as attempts to improve affinity of the series by generating a pi-stacking interaction in the p4/p5 pockets.

Strikingly, overlay of the X-ray crystal structures of compound **1.1** with those of compounds **1.6**, **1.7**, **1.8**, **1.9** and **3.1** revealed a remarkably consistent binding position of the terminal aromatic ring in the p5 pocket. This was so despite some subtle differences in the position of the remainder of the molecule and linker region (**Figure 4.1E**), suggesting that this p5 interaction might be important for binding. In each case the benzyl aromatic ring occupied the same position, stacked in a perpendicular arrangement against the aromatic ring of the tolyl group of the same molecule. Moreover, in adopting this binding mode, it partially occluded the space typically occupied by Tyr195 of BCL-X<sub>L</sub> (such as in the *apo* BCL-X<sub>L</sub> structure<sup>(1)</sup>, or the BCL-X<sub>L</sub>:**ABT-737**<sup>(2)</sup> or BCL-X<sub>L</sub>:**WEHI-539**<sup>(3)</sup> complexes).

#### 4.1.1 Description of the p5 pocket

The p5 pocket is created by a rotation of the sidechain Tyr195 of BCL-X<sub>L</sub> in order to accommodate S-benzyl moiety of compound **1.1** (**Figure 4.1A,C**). Whilst this p5 pocket is not present in the X-ray crystal structures of *apo* BCL-X<sub>L</sub> (**Figure 4.1A,B**, PDB entry: 1MAZ<sup>(1)</sup>), nor in the published structures of BCL-X<sub>L</sub> in complex with **ABT-737** (**Figure 4.1D**, PDB entry: 2YXJ<sup>(2)</sup>) or **WEHI-539** (not depicted, PDB entry: 3ZLR<sup>(3)</sup>), it is observed in some other structures including the BCL-X<sub>L</sub>/BAD BH3 complex (not depicted, PDB entry: 2BZW<sup>(4)</sup>).

It is perhaps not surprising that Tyr195 exhibits some flexibility, occurring in a solvent-exposed area on the protein periphery, close to the C-terminus in constructs in which the  $\alpha$ 9 (TM domain) has been removed. B-factor analysis of the *apo* BCL-X<sub>L</sub> structure (PDB entry: 1MAZ<sup>(1)</sup>) suggests the C-terminal end of the  $\alpha$ 8 helix including Tyr195 (as well as the  $\alpha$ 3 helix and  $\alpha$ 2-3 hinge regions) to be the more flexible regions around the hydrophobic groove of BCL-X<sub>L</sub> (**Figure 4.1B**). Additionally, it has also been shown that under certain non-physiological conditions (eg. use of detergents such as OM, heat, or in strongly alkaline buffers) the entire  $\alpha$ 6-8 region of BCL-X<sub>L</sub> can dissociate from the protein 'core' (in a similar manner to the structural transitions which appear to be important for the physiological activation of BAK and BAX<sup>(5,6)</sup>) to allow two such monomers to come together and form a stable  $\alpha$ 6-8 domain-swapped dimer<sup>(7,8)</sup>.

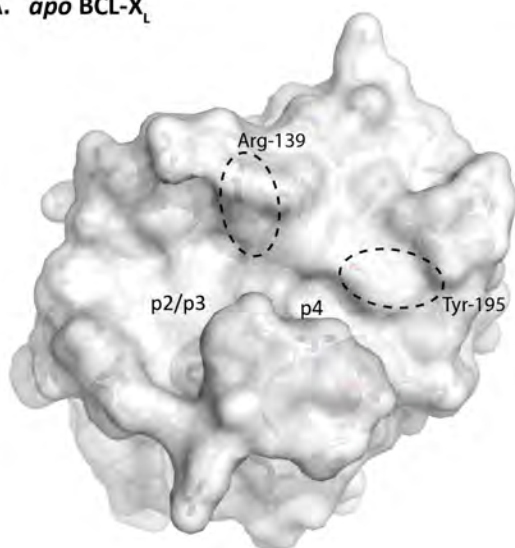
To our knowledge, the only published structures to our knowledge of small molecules that make use of this pocket are those of **ABT-263 (Navitoclax)** in complex with BCL-2 (PDB entry: 4LVT<sup>(9)</sup>) or BCL-X<sub>L</sub> (PDB entry: 4QNQ) in which the p5 pocket accommodates the trifluoromethyl sulfonyl moiety of **ABT-263** (**Figure 4.1F**). However, it was unclear whether side chain flip of Tyr195 may be favourable or unfavourable for binding of compound **1.1** or whether this interaction might be further optimised.

#### 4.1.2 Analogues probing the p5 pocket

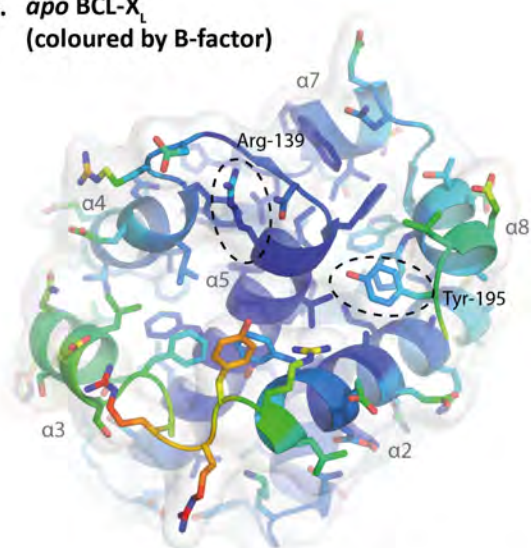
We were thus interested to initiate Structure Activity Relationship (SAR) studies around the S-benzyl group of compound **1.1** (or SO<sub>2</sub>-benzyl group of compound **1.8**) to explore the dimensions of the p5 pocket and evaluate whether additional cryptic pockets may be revealed or fruitful interactions gained.

This chapter outlines the synthesis and characterisation of a series of 15 analogues of compound **1.8** that explore substitution around the terminal benzyl aromatic ring (9 analogues), extending the linker by one methylene group (1 analogue) or replacement of the aromatic ring with aliphatic groups (6 analogues). It also describes the synthesis of a further adamantyl-substituted analogue - including development of appropriate chemistry required to access the necessary novel adamantylmethylene-substituted cysteine derivative.

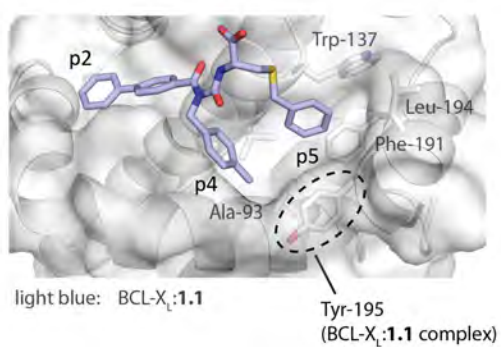
**A. apo BCL-X<sub>L</sub>**



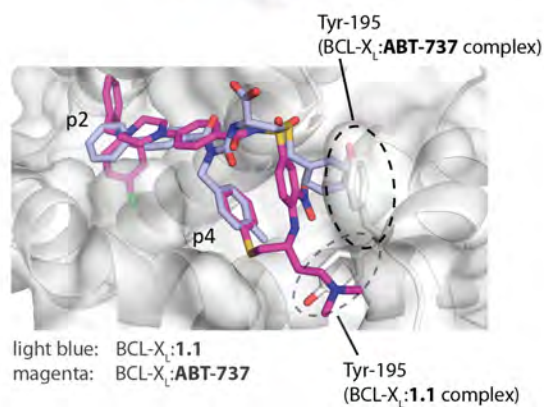
**B. apo BCL-X<sub>L</sub>  
(coloured by B-factor)**



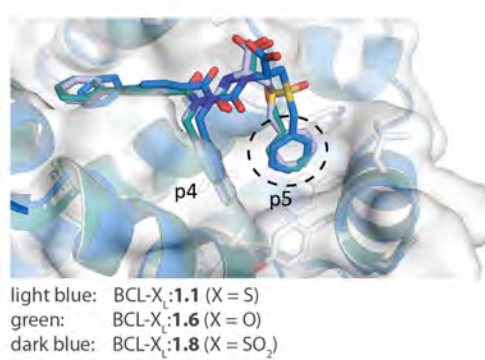
**C.**



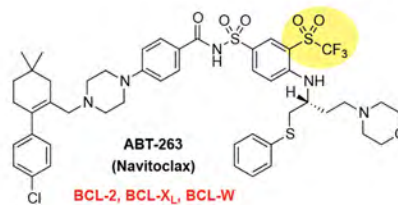
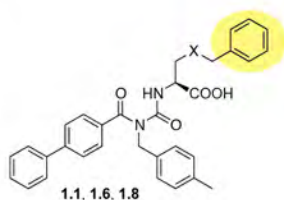
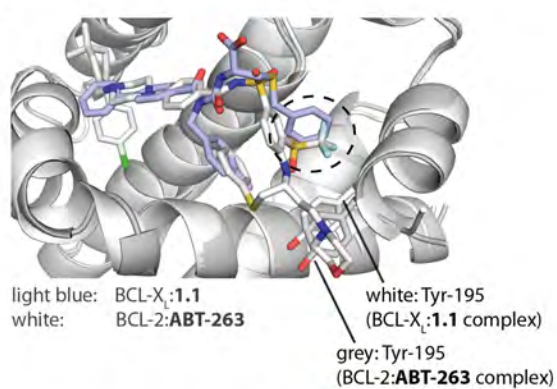
**D.**



**E.**



**F.**





#### Figure 4.1: Structural engagement of ligands in the p5 pocket of BCL-X<sub>L</sub>.

(previous page)

(A) *apo* BCL-X<sub>L</sub> (PDB: 1MAZ<sup>(1)</sup>) in surface representation showing ligand binding pockets and the positions of relevant sidechains along the hydrophobic groove and (B) coloured by B-factor (dark blue = low B-factor – red = high B-factor)

(C) BCL-X<sub>L</sub>:**1.1** complex showing displacement of Tyr195 to open p5 pocket

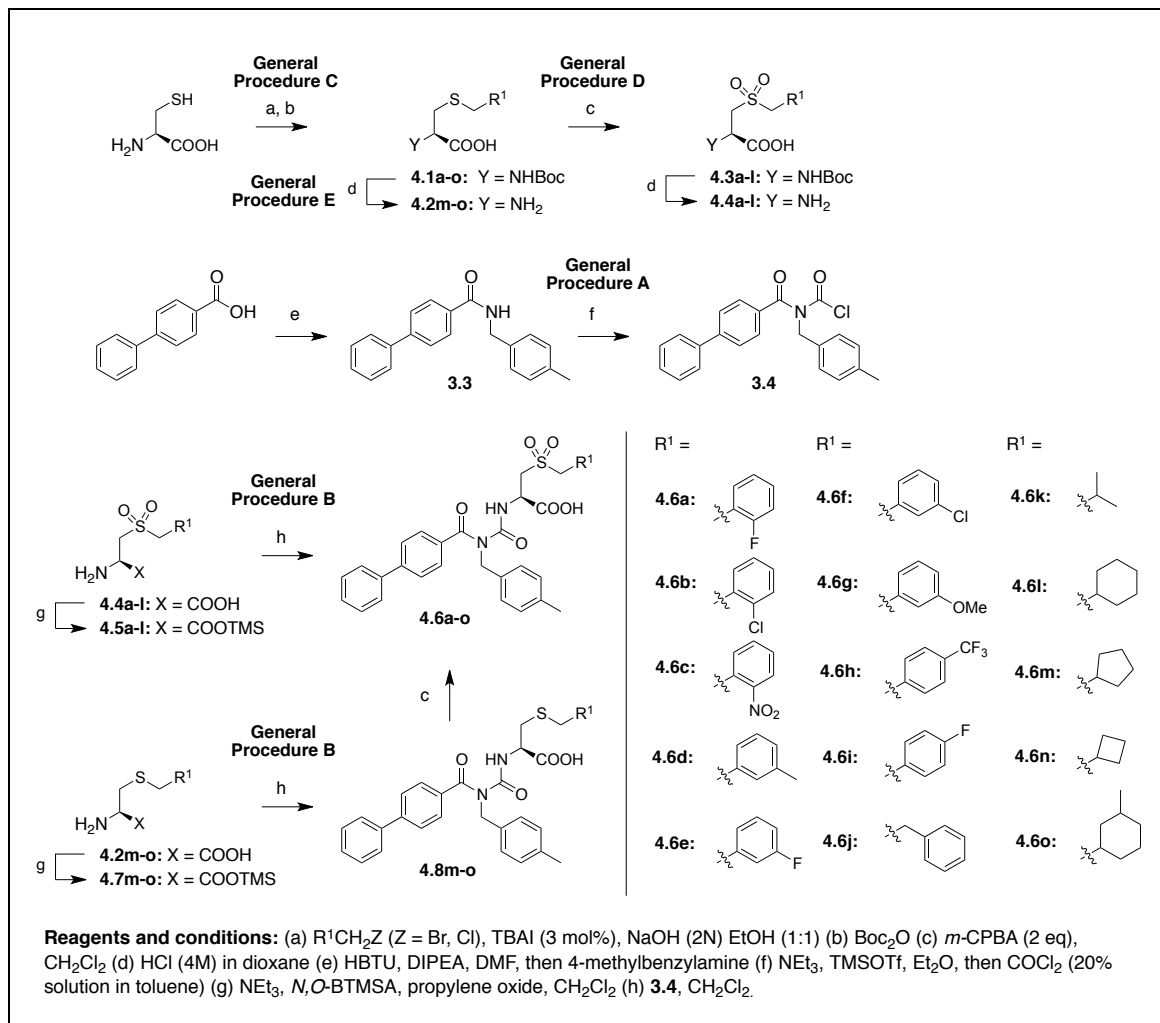
(D) Overlay of BCL-X<sub>L</sub>:**1.1** and BCL-X<sub>L</sub>:**ABT-737** (PDB entry: 2YXJ<sup>(2)</sup>) complexes.

(E) Overlay of BCL-X<sub>L</sub> complexes with compounds **1.1**, **1.6**, and **1.8** showing consistent position of the benzyl aromatic ring (highlighted) in p5 pocket.

(F) Overlay of BCL-X<sub>L</sub>:**1.1** and BCL-2:**ABT-263** (PDB entry: 4LVT<sup>(9)</sup>) complexes, showing trifluoromethyl sulfonyl moiety of **ABT-263** in p5 pocket (highlighted) and displacement of Tyr195.

## 4.2 Synthesis of p5 benzoylurea sulfonyl analogues on simple biphenyl scaffold

Using established chemistry, an initial series of 15 analogues of the sulfonyl benzoylurea compound **1.8** were generated, varying the p5 substituent (R<sup>1</sup>, **Scheme 4.1**).



**Scheme 4.1: Synthesis of sulfonyl series of p5 analogues.**

#### 4.2.1 General synthesis of p5 sulfonyl analogues (Scheme 4.1)

The required Boc-protected amino acids incorporating various R<sup>1</sup>-substituents targeting the p5 region were generated from L-cysteine in good yields according to a procedure described in the literature<sup>(10)</sup>, *via* direct alkylation of L-cysteine under basic conditions, followed by N-Boc protection. For intermediates **4.1a-o**, the thioether linkage was oxidized to the sulfone using *m*-CPBA and Boc-deprotected using HCl in dioxane. These amino acids were then subjected to benzoylurea formation by reaction with carbamoyl chloride intermediate **3.4** as described previously (**Chapter 3**). For compounds **4.1m-o**, the thioether amino acid intermediates were first deprotected and the benzoylurea formed, before subsequent oxidation to the sulfone using *m*-CPBA.

An initial series of 15 analogues were synthesised in this manner (**Figure 4.2**). These analogues explored substituents in the *ortho*-, *meta*- and *para*- positions on the p5 phenyl ring, including a range of electron withdrawing and donating groups of different relative size (compounds **4.6a-l**). Additionally, another set of analogues explored replacement of the aromatic ring with aliphatic cyclic or branched groups of various sizes (compounds **4.6k-o**), or extending the linker by one additional carbon atom (compounds **4.6j**).

Attempts were also made to synthesis an amino acid incorporating an adamantyl moiety in the p5 position, initially by direct alkylation of L-cysteine using 1-(bromomethyl)adamantane, however these initial attempts proved unsuccessful using the method adapted from Seko *et al.*<sup>(10)</sup> Further studies were required to optimise the reaction conditions in order to successfully generate this modified amino acid, which are described later in this Chapter (**Section 4.3**).

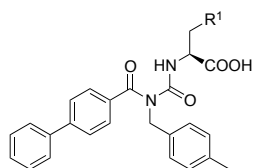
#### 4.2.2 Evaluation of BCL-X<sub>L</sub> and MCL-1 binding using AlphaScreen competition assay

All 15 analogues exploring modifications in the p5 pocket were screened for their binding towards BCL-X<sub>L</sub> and MCL-1 using the AlphaScreen competition assay described in **Chapter 1**. The resulting IC<sub>50</sub> values are summarised in **Table 4.1** and **Figure 4.2**.

##### 4.2.2.1 Effect of *ortho*-, *meta*-, *para*-substitution on phenyl ring

Addition of substituents in the *ortho*-position was found to be unfavourable, with losses in binding in the range of 2-4 fold for all substituents trialed (compounds **4.6a-c,g**, IC<sub>50</sub>(BCL-X<sub>L</sub>) ~ 4 - 8  $\mu$ M, **Table 4.1**, **Figure 4.2**). This was also the case for larger groups (whether electron withdrawing or donating) substituted in *meta*-, such as chloro or methoxy (compounds **4.6f,g**, IC<sub>50</sub>(BCL-X<sub>L</sub>) ~ 4 - 6  $\mu$ M), however smaller *meta*-substituents such as fluoro or methyl were able to be accommodated with equipotent IC<sub>50</sub> values as compared to the parent molecule with an unadorned phenyl ring (compounds **4.6d,e**, IC<sub>50</sub>(BCL-X<sub>L</sub>) = 1.6, 2.0  $\mu$ M respectively). There was a possible electronic effect due to the electron-withdrawing substituents on the aromatic ring, whereby a simple fluoro in *ortho*- or *para*- in particular, yielded a 3-4 fold loss in binding and concomitant loss in selectivity (compounds **4.6a,i**, IC<sub>50</sub>(BCL-X<sub>L</sub>) ~ 5-6  $\mu$ M, **Table 4.1**, **Figure 4.2**). Larger groups in the *para*- position were not tolerated, such as the -CF<sub>3</sub> (compound **4.6h**, IC<sub>50</sub>(BCL-X<sub>L</sub>) = 15.1  $\mu$ M), indicating that they likely clash with the protein wall. These results suggest that the p5 binding pocket does not exhibit significant plasticity to accommodate additional substitution around the terminal aromatic ring, but does harbour a very small hydrophobic pocket in an area corresponding to in the *meta*-position of the terminal aryl ring of compounds **1.1/1.8**. It was a general trend that those compounds which displayed reduced binding for BCL-X<sub>L</sub> also displayed a reduction in fold selectivity for BCL-X<sub>L</sub> relative to MCL-1, indicating that as specific interactions were lost, the remaining contribution to binding appeared to be from non-specific hydrophobic interactions.

**Table 4.1: IC<sub>50</sub> values of benzoylurea p5 sulfonyl compounds for BCL-X<sub>L</sub> and MCL-1 (determined by AlphaScreen competition assay, pre-2015 data)<sup>[a]</sup>**



Compound	IC <sub>50</sub> A.S. <sup>[b]</sup>			Fold Selectivity		BEI <sup>[c]</sup>
R <sup>1</sup>	BCL-X <sub>L</sub>	MCL-1	N =	(BCL-X <sub>L</sub> /MCL-1)		
<b>1.1</b>	4.6 ± 1.0	73.7 ± 20.3	3	16		9.9
<b>1.8</b>	1.5 ± 0.6	68.1 ± 25.4	5	44		10.2
<b>4.6a</b>	6.4 ± 0.7	89.3 ± 9.5	3	14		8.8
<b>4.6b</b>	3.5 ± 0.7	45.5 ± 10.2	2	13		9.0
<b>4.6c</b>	7.6 ± 0.7	31.5 ± 4.5	2	4		8.3
<b>4.6d</b>	1.6 ± 0.5	43.9 ± 7.5	5	27		9.9
<b>4.6e</b>	2.0 ± 0.6	43.4 ± 9.2	3	22		9.7
<b>4.6f</b>	3.6 ± 1.6	50.5 ± 3.6	2	14		9.0
<b>4.6g</b>	5.9 ± 1.3	62.4 ± 9.4	2	11		8.7
<b>4.6h</b>	15.1 ± 4.0	98.2 ± 3.6	2	6		7.5
<b>4.6i</b>	5.4 ± 0.9	49.7 ± 10.8	2	9		9.0
<b>4.6j</b>	6.5 ± 1.8	42.6 ± 6.9	3	7		8.9
<b>4.6k</b>	10.3 ± 1.3	80.6 ± 12.7	2	8		9.3
<b>4.6l</b>	1.6 ± 0.6	45.8 ± 14.4	5	29		10.1
<b>4.6m</b>	4.8 ± 0.6	86.3 ± 15.9	2	18		9.4
<b>4.6n</b>	8.3 ± 2.0	81.4 ± 13.8	2	10		9.3
<b>4.6o</b>	3.9 ± 0.7	73.9 ± 19.5	2	19		9.1

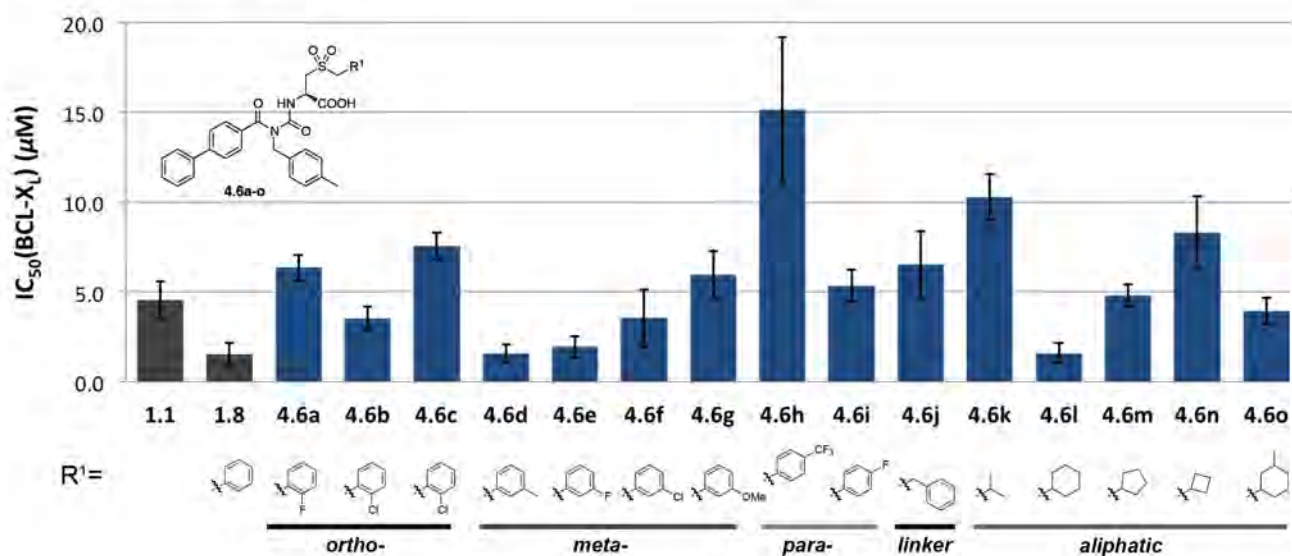
<sup>[a]</sup> Following the relocation of our Screening Group, a consistent shift in the IC<sub>50</sub> values determined using the AlphaScreen competition assay was observed.

The signifiers '**pre-2015 data**' and '**post-2015 data**' indicate respectively data acquired prior and subsequent to this relocation. For further information refer to note in **Chapter 2, Section 2.4.1.3**.

<sup>[b]</sup> IC<sub>50</sub> values are reported in  $\mu\text{M} \pm \text{S.D.}$

<sup>[c]</sup> BEI (Binding efficiency index, refer Section 1.4.1.2) =  $\text{pIC}_{50}/\text{MW}$ , where  $\text{pIC}_{50}$  is the negative base 10 logarithm of the IC<sub>50</sub> (in molar units) and MW is the compound molecular weight (in kDa).

### A. BCL-X<sub>L</sub> Affinity (AlphaScreen)



### B. Fold Selectivity BCL-X<sub>L</sub>/MCL-1

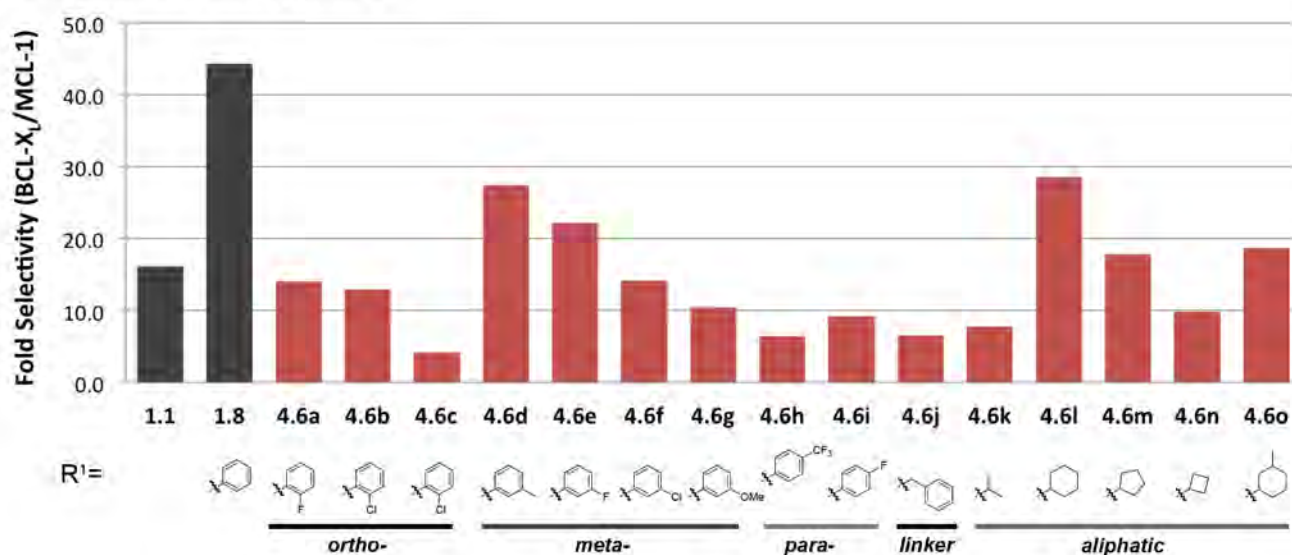


Figure 4.2: Plot of AlphaScreen data for p5 sulfonyl analogues (from Table 4.1), showing (A) IC<sub>50</sub> values for binding to BCL-X<sub>L</sub> and (B) fold selectivity for BCL-X<sub>L</sub> relative to MCL-1. IC<sub>50</sub> values are reported in μM ± S.D.

#### 4.2.2.2 Effect of aliphatic ring size/linker length

A notable result was obtained *via* replacement of the phenyl ring by the cyclohexyl moiety (compound **4.6l**,  $IC_{50}(BCL-X_L) = 1.6 \mu M$ , **Table 4.1**), which displayed equipotent binding for BCL-X<sub>L</sub> to the parent molecule (compound **1.8**,  $IC_{50}(BCL-X_L) = 1.5 \mu M$ , **Table 4.1**) as well as good retention of selectivity. This suggested that binding of the phenyl ring is driven primarily by general hydrophobic effects, rather than by specific electronic interactions such as aromatic stacking. Importantly, the cyclohexyl group also exhibits a greater three-dimensional character as compared to a planar phenyl ring. The size of this hydrophobic group appears to be important, as replacement with a smaller isopropyl substituent reduced binding by approximately 6-fold (compound **4.6k**,  $IC_{50}(BCL-X_L) = 10.3 \mu M$ , **Table 4.1**, **Figure 4.2**). It was thought that extending the linker may add to the potential degrees of freedom for the terminal aromatic ring to pack in a favourable manner, however no gains were observed by extending the linker by one carbon (compound **4.6j**,  $IC_{50}(BCL-X_L) = 6.5 \mu M$ , **Table 4.1**; approximate four-fold loss in binding).

Based on the interesting effects regarding aliphatic cyclic systems, analogues **4.6m-o** explored the effect of varying the ring size, or combining a cyclohexyl group with an additional *meta*-methyl substituent (compound **4.6o**, synthesised as a mixture of four potential diastereomers). In general, as the aliphatic ring decreased in size from 6 to 5 to 4 carbon atoms, there was a loss of ~1.5-fold in binding for each methylene removed (compounds **4.6l-n**,  $IC_{50}(BCL-X_L) = 1.6, 4.8, 8.3 \mu M$  respectively, **Table 4.1**). Even accounting for a mixture of diastereomers, no apparent improvement in binding was observed substitution of the cyclohexyl ring in the 3'-position with an additional methyl group (compound **4.6o**,  $IC_{50}(BCL-X_L) = 3.9 \mu M$ , **Table 4.1**).



### 4.2.3 Conclusions – initial p5 analogues

The results of this initial series varying the substituent in the p5 pocket of BCL-X<sub>L</sub> indicate this pocket to be in general less flexible than that of the p2 pocket of BCL-X<sub>L</sub> (as suggested by analysis of *apo* BCL-X<sub>L</sub>, **Figure 4.1B**). Adding substituents around the terminal benzyl aromatic ring of compound **1.8** did not appear to generate any new points of interaction with the protein or open any new pockets.

This work did however suggest that the size (but not the aromatic nature) of the interacting group in the p5 pocket was important for BCL-X<sub>L</sub> binding – the benzyl aromatic ring of compound **1.8** could be replaced by a cyclohexyl (compound **4.6l**) with equipotent activity. Based on calculated binding efficiency index (BEI) (**Table 4.1**), accounting for both MW and IC<sub>50</sub>, the cyclohexyl appeared optimal as compared with either 4- or 5-membered aliphatic rings (compounds **4.6m-n**).

As the cyclohexyl modification conferred some additional conformational flexibility and three-dimensionality to the molecule, whilst reducing the overall number of planar aromatic rings, we were interested to explore the effect of this same modification on the flexible THIQ scaffold (compound **1.10**) which would also engage the p2 pocket of BCL-X<sub>L</sub>. This work is described in **Chapter 6**.

Additionally, as the crystal structure of compound **1.1** in complex with BCL-X<sub>L</sub> suggested the p5 pocket might accommodate larger ring systems, we were prompted to explore incorporation of an adamantyl group in the p5 pocket. This proved to be synthetically more challenging than initially anticipated, as described in the next section.

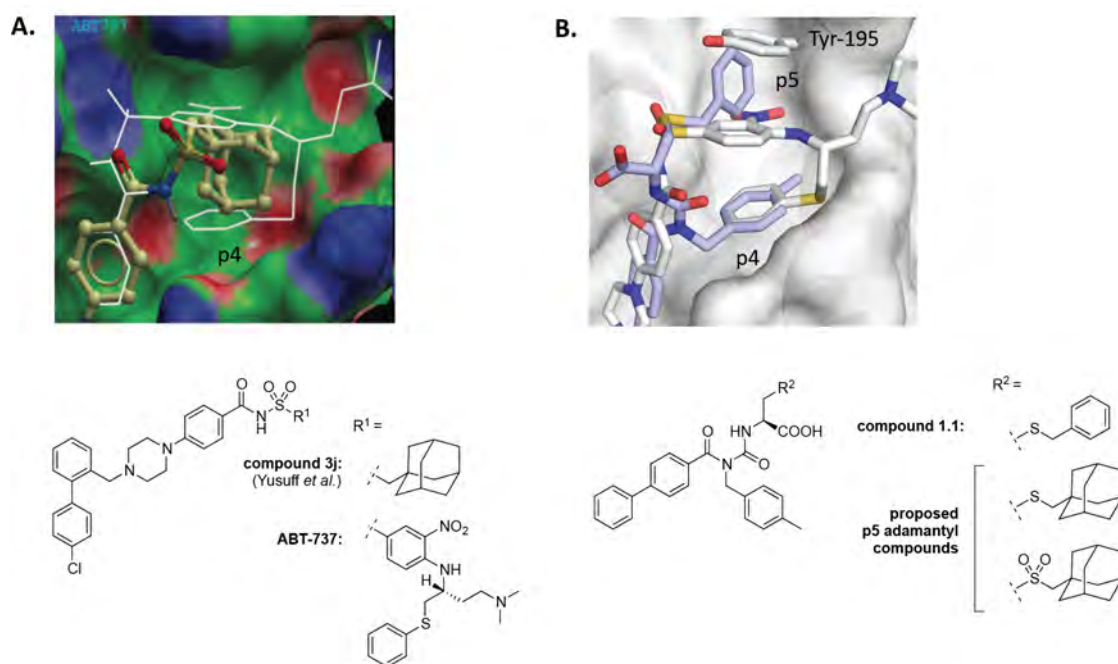
## 4.3 Synthesis of p5 adamantyl analogues

We next sought to generate two further analogues of compounds **1.1** and **1.8**, which would incorporate an adamantyl group in the p5 pocket (**Figure 4.3B**).

### 4.3.1 Introduction: the adamantyl group in drug design

Since the development during the 1940s-50s of efficient routes to access it synthetically, the adamantyl group has been utilised on many occasions in pharmaceutical development, including most famously in the (formerly) FDA-approved anti-viral drug amantadine<sup>(11)</sup>. With its stable diamond-like 3-dimensional structure and hydrophobic character, adding several logP units to a molecule, the adamantyl group is most often incorporated as a strategy to increase the lipophilicity and stability (and thus the pharmacokinetic properties) of a drug<sup>(11)</sup>. In the context of the BCL-2 family, the adamantyl group has also recently been utilised by chemists at Novartis to serve as a rigid isostere of the intramolecular pi-stacking interaction of **ABT-737** within the p4 pocket of BCL-X<sub>L</sub>/BCL-2, as confirmed by X-ray crystal structure analysis of this molecule in complex with BCL-2 (**Figure 4.3A**, compound **3j**)<sup>(12)</sup>.

By comparison, the X-ray crystal structure of compound **1.1** in complex with BCL-X<sub>L</sub> overlaid with that of **ABT-737** suggested that incorporation of an adamantyl group in the p5 pocket might instead act as an isostere of the pi-stacking interaction between the nitroaryl ring of **ABT-737** and Tyr195 of BCL-X<sub>L</sub> (**Figure 4.3B**).

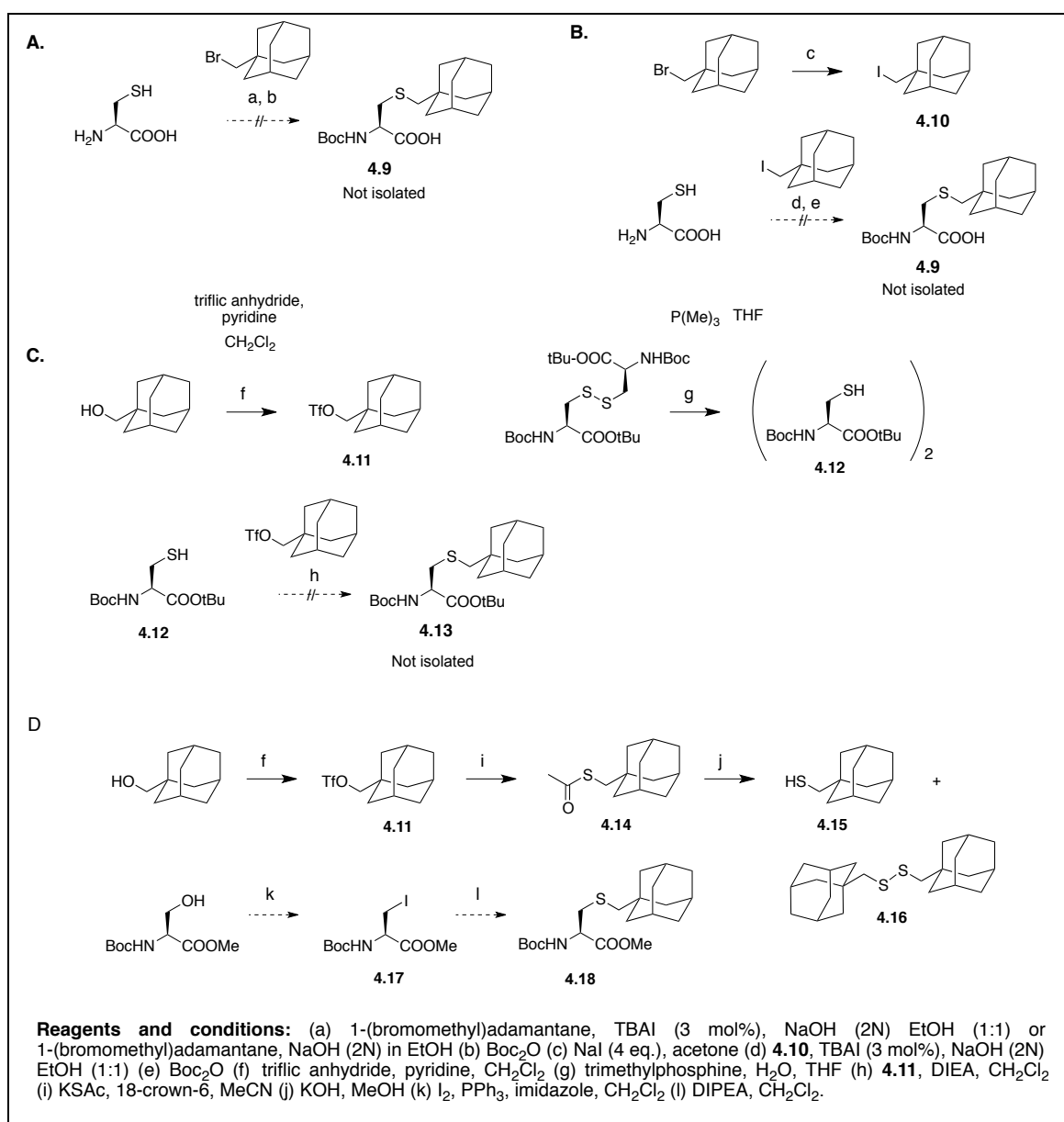


**Figure 4.3: Use of the adamantyl group as an isostere of an aromatic pi-stacking interaction in the p4 and p5 pockets of BCL-X<sub>L</sub>.**

(A) X-ray crystal structure of BCL-2 in complex with compound **3j** described by Yusuff *et al.*<sup>(12)</sup> with adamantyl substituent in p4 pocket as a mimic of the intramolecular pi-stacking aromatic rings of **ABT-737**. (Image of crystal structure reproduced from Yusuff *et al.*<sup>(12)</sup> as this structure has not been deposited in the PDB). (B) Overlay of BCL-X<sub>L</sub> in complex with compound **1.1** (light blue) and **ABT-737** (white, PDB entry 2YXJ<sup>(2)</sup>); and chemical structures of proposed adamantyl analogues based on compound **1.1** which would incorporate an adamantyl substituent into the p5 pocket of BCL-X<sub>L</sub>, as a potential isostere of the pi-stacking interaction between the nitro-phenyl aromatic ring of **ABT-737** and Tyr195 of BCL-X<sub>L</sub>.

### 4.3.2 Overcoming synthetic challenges to access adamantyl precursor

It was anticipated that the proposed adamantyl analogues (**Figure 4.3B**) would be generated from an adamantyl-substituted cysteine precursor (compound **4.9**, **Scheme 4.2** below). This modified cysteine derivative is not known in the literature and unfortunately initial attempts at its synthesis using a simple S-alkylation proved unsuccessful.



**Scheme 4.2: Proposed synthetic routes to adamantyl-substituted L-cysteine derivatives.**

#### 4.3.2.1 Standard L-cysteine alkylation conditions

Initial attempts to synthesise compound **4.9** (**Scheme 4.2**) involved S-alkylation of cysteine using 1-(bromomethyl)-adamantane as described previously (**General Procedure C, Scheme 4.1**<sup>(10)</sup>). Briefly, L-cysteine, 1-(bromomethyl)adamantane and 3 mol% TBAI in a 1:1 solution of aqueous NaOH (2N)/EtOH were stirred at room temperature for 3 days, then Boc-anhydride was added and the reaction stirred for a further 24 h at room temperature. Following this sequence, none of the desired product was observed by LCMS or NMR analysis (data not shown). The major product was N-Boc-L-cystine due to eventual oxidation of the starting material. Further optimisation of this approach was thus required.

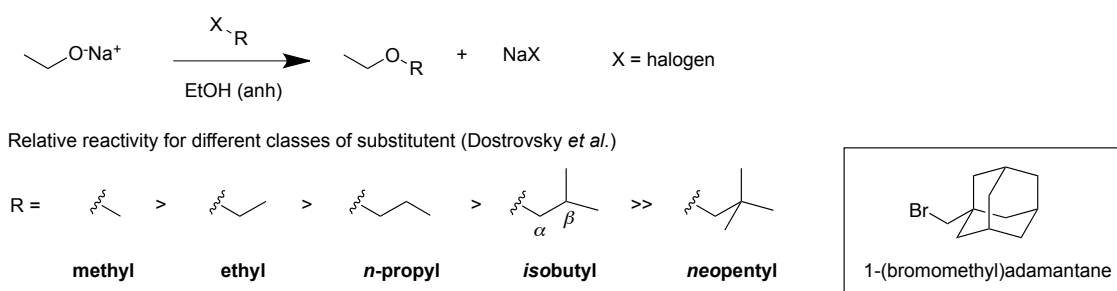
#### 4.3.2.2 'Neopentyl' type systems in nucleophilic substitution reactions

The difficulty in forming the desired product, compound **4.9**, can be primarily attributed to the nature of 1-(bromomethyl)adamantane as being similar to a 'neopentyl'-type system (**Figure 4.4** below).

In comparison to less hindered alkyl halides, *neopentyl* halides have been observed to be remarkably unreactive substrates for certain substitution reactions, in particular the  $S_N2$  (bimolecular nucleophilic substitution) reaction (**Figure 4.4**)<sup>(13)</sup>. This has primarily been attributed to steric hindrance<sup>(13, 14)</sup>; for a *neopentyl* halide to undergo the concerted  $S_N2$  reaction, the necessary backside approach of the nucleophile to the  $\alpha$ -carbon (bearing the halogen) that would be required, is significantly obstructed by the methyl groups on the  $\beta$ -carbon (**Figure 4.4**). This can dramatically decrease the rate of the reaction such that it is no longer observed in practice.

As regards the alternate  $S_N1$  (unimolecular nucleophilic substitution) reaction however, which proceeds in two discrete steps, *neopentyl* halides should still be moderately reactive under the right conditions to favour this reaction<sup>(13)</sup>. For the  $S_N1$ , the initial and rate-determining step is formation of a carbocation. This then undergoes subsequent nucleophilic attack from cysteine (thiolate) with less steric

hindrance than for the  $S_N2$ . However, for a 'neopentyl'-type system carbocation formation would be expected to be relatively slow as it produces a relatively unstable primary carbocation. An alkyl shift can also occur to form a more stable secondary carbocation, prior to nucleophilic attack. Thus, in the case of a nucleophilic substitution reaction of 1-bromomethyladamantane via the  $S_N1$  route, formation of a primary carbocation might be slow, and the occurrence of an alkyl shift to produce a more stable secondary carbocation would result in the formation of undesired homoadamantyl side-products<sup>(15)</sup>.



**Figure 4.4: Relative reactivity of various alkyl halides to nucleophilic substitution<sup>(13)</sup>.**

These general challenges associated with nucleophilic substitution on a 'neopentyl'-type system provide a basis for understanding the failure to isolate compound **4.9** on alkylation of L-cysteine with 1-bromoadamantane using the initial conditions.

The parameters considered for improving the reaction included: varying the solvent system, reaction time, reaction temperature, tuning the reactivity of the nucleofuge (**Scheme 4.2B, C**), or reversing the reactivity of the nucleophile/nucleofuge pair to reduce steric hindrance to the  $S_N2$  reaction (**Scheme 4.2D**). In general the preference was to avoid the use of a strong base, which might abstract the  $\alpha$ -proton and risk epimerization of the amino acid.

This section will describe a number of synthetic approaches that were trialed concurrently (**Scheme 4.2**).

#### 4.3.2.3 Solubility of starting material

Under the initial conditions (**Scheme 4.2A**), it was observed that 1-(bromomethyl)adamantane appeared poorly soluble. Attempts were made to repeat the same reaction in different solvent systems in which alkyl halide was more soluble, as well as extending the reaction time or gently heating. These included:

- aq. NaOH(2N)/EtOH/DMF (1:1:1), room temperature, 5d
- EtOH:THF (1:1) and  $\text{NET}_3$  (2.2 eq.), room temperature, 3d
- NaOH (2N) in EtOH for 18 h at room temperature
- NaOH (2N) in EtOH for 18 h at room temperature, followed by heating at reflux for 18 h.

In none of these cases was the desired product able to be observed by LCMS analysis (data not shown); suggesting that the poor reactivity was not primarily driven by solubility and that, at least using sodium hydroxide in ethanol, the use of elevated temperatures did not appear to facilitate the reaction.

#### 4.3.2.4 Finkelstein reaction

To test whether a better leaving group might facilitate the reaction, an attempt was made to first convert the 1-(bromomethyl)adamantane to 1-(iodomethyl)adamantane, *via* a Finkelstein reaction with NaI (4 eq.) in refluxing acetone for 18 h (**Scheme 4.2B**). The iodo-derivative was then subjected to the standard alkylation conditions described above. Once again, however no significant formation of the desired product was observed by analytical LCMS, and none of the desired product was isolated on workup (data not shown). This strategy was not pursued further - instead the use of a triflate leaving-group was evaluated next.

#### 4.3.2.5 Adamantyl triflate

The adamantyl triflate **4.11** was able to be prepared in quantitative yield from 1-(hydroxymethyl)adamantane using a procedure described in the literature<sup>(16)</sup>. To avoid O- or N- alkylation, the protected L-cysteine derivative N-Boc-L-cysteine *tert*-butyl ester (compound **4.12**) was first prepared in good yield using a modification of a procedure described in the literature<sup>(17)</sup>, *via* reduction of the commercially available N-Boc-L-cystine *tert*-butyl ester. An initial attempt to form the alkylated product compound **4.13** (**Scheme 4.2C**) using compounds **4.11** and **4.12** with diisopropylethylamine in DCM formed none of the desired product by LCMS analysis (data not shown).

#### 4.3.2.6 Reversal of reactivity

Another strategy that was evaluated concurrently was to reverse the reactivity of the nucleophile/nucleofuge (**Scheme 4.2D**) by forming the adamantyl thiol **4.15** and an iodinated amino acid derivative **4.17**. It was hoped that compound **4.17**, albeit still relatively hindered, might have improved reactivity towards the S<sub>N</sub>2 reaction as the  $\beta$ -carbon would have secondary rather than tertiary substitution, rendering it less hindered and more amenable to backside approach of the thiolate nucleophile.

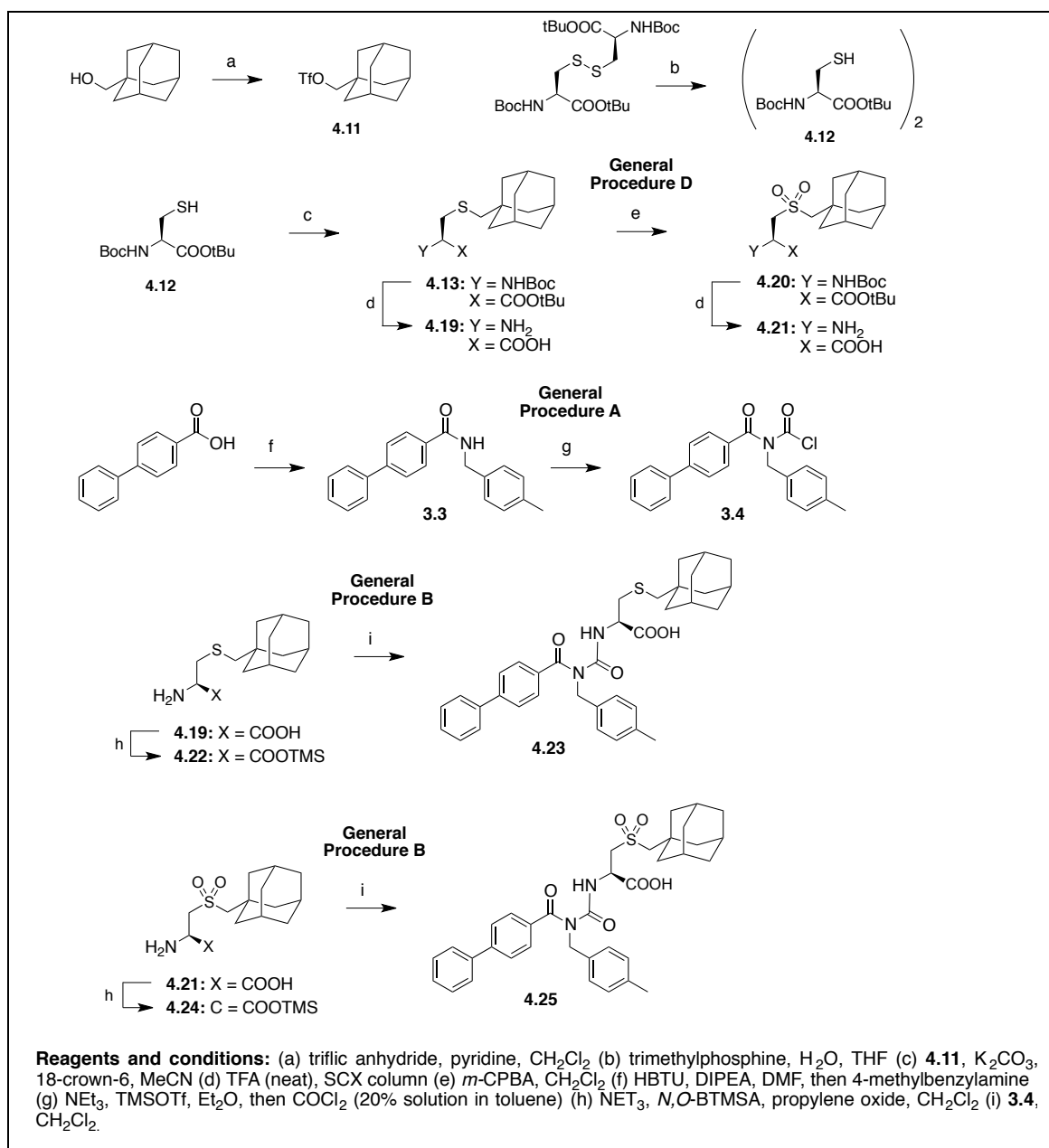
The planned reaction sequence was to form compound **4.17** by iodination of commercially available N-Boc-L-serine methyl ester according to a procedure described in the literature<sup>(18)</sup>. A sequence to form the adamantyl thioacetate compound **4.14** was also described in the literature<sup>(16)</sup> - quantitative formation of the relatively stable triflate **4.11** as described earlier would allow S-acetylation using potassium thioacetate and 18-crown-6 in acetonitrile (**Scheme 4.2D**). This proceeded in very good yield (94%), better than suggested by the reported yield for this procedure (54%)<sup>(16)</sup>. De-acetylation using potassium hydroxide in methanol as described would furnish the free 1-(Mercaptomethyl)adamantane (**4.15**)<sup>(16)</sup>. In practice however, isolation of the desired product from the reaction



mixture proved to be problematic as the thiol tended to rapidly undergo oxidation to yield mixtures contaminated with the disulfide **4.16**. The success of the above reaction conditions to allow nucleophilic substitution of the adamantyl triflate **4.11** with thioacetate to form 1-(Acetylthiomethyl)adamantane (**4.14**) suggested that similar conditions might in fact also be utilised to effect the original desired S-alkylation of L-cysteine. Thus, rather than continue the 'reversal of reactivity' strategy, this new possibility was evaluated next.

#### 4.3.2.7 Successful route to access adamantyl amino acid

Use of the reaction conditions adapted from Kitagawa *et al.*<sup>(16)</sup> enabled a successful sequence to generate the adamantyl amino acids **4.19** and **4.21** (Scheme 4.3). N-Boc-L-cysteine *tert*-butyl ester (**4.12**) (synthesised as described earlier) was reacted with adamantyl triflate **4.11** using potassium carbonate in the presence of 18-crown-6 in acetonitrile, to afford the desired protected adamantane amino acid **4.13** in excellent yield (74%). The reaction was allowed to proceed for 16 h, however TLC analysis at earlier time points suggested that the reaction was essentially complete in 2-3 h. Although this has not been explored mechanistically, the reaction conditions (polar aprotic solvent, negatively charged nucleophile) would be expected to favour the S<sub>N</sub>2 reaction. The facilitation of the reaction *via* the addition of 18-crown-6 suggests that a counter-ion effect may be at play. As the crown-ether sequesters the potassium counter-ion, the cysteine thiolate is further stabilised as a naked anion, which increases its nucleophilicity. This may be the basis for the improved rate of the S<sub>N</sub>2 reaction in this case (despite the potential steric limitations of the 'neopentyl' type system described earlier), such that it out-competes the slow oxidation of cysteine to cysteine as an undesired side-reaction.



**Scheme 4.3: Successful synthetic route to adamantyl-substituted L-cysteine derivatives **4.19** and **4.21** and benzoylurea analogues **4.23** and **4.25**.**

The amino acid **4.13** could then be directly deprotected to form **4.19**, or alternatively first oxidized to the sulfonyl derivative **4.20** using *m*-CPBA, then deprotected to form **4.21**. In each case deprotection was effected in a single step using neat TFA at room temperature for 1 h and purification by catch/release from a strong cation exchange (SCX) column to yield the final amino acids **4.19** and **4.21** as the respective freebase in moderate/very good yields (44% and 92% respectively). This represents the first reported synthesis of the modified amino acids **4.19** and **4.21**.

### 4.3.3 Synthesis of adamantyl benzoylurea analogues

Using the optimised procedure to arrive at the novel amino acids **4.19** and **4.21**, the standard benzoylurea reaction conditions were then used to furnish the desired adamantyl benzoylurea analogues **4.23** and **4.25**. These were then evaluated for BCL-X<sub>L</sub> and MCL-1 binding using the AlphaScreen Assay (**Table 4.2**).

### 4.3.4 Evaluation of BCL-X<sub>L</sub> and MCL-1 binding using AlphaScreen competition assay

Recall that following the relocation of our Screening Group, a consistent shift in the IC<sub>50</sub> values determined using the AlphaScreen competition assay was observed - this discrepancy is apparent in the binding data in **Tables 4.1** and **4.2**. The signifiers '**pre-2015 data**' and '**post-2015 data**' indicate respectively data acquired prior and subsequent to this relocation.

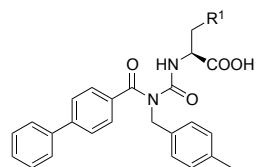
[For further information refer to note in **Chapter 2, Section 2.4.1.3.**]

All values in **Tables 4.1** and **4.2** represent the mean of at least two independent experiments run at a similar point in time. Relevant control compounds were included for comparison between sets of experiments (eg. compounds **1.1**, **1.6** – **1.9**, **4.6I**). In general, for each compound, binding values from the more recent AlphaScreen assay (**Table 4.2** – '**post-2015 data**') ranged between 6-10-fold tighter binding than from the earlier assay (**Table 4.1** – '**pre-2015 data**'). For a given compound the observed fold difference was consistent for both BCL-X<sub>L</sub> and MCL-1. Despite the difference in the absolute values, the relative affinities within a series and the rank order of compound affinities were essentially unchanged between the different AlphaScreen assay dates.

Relative to compounds **1.1** and **1.8**, replacement of the aromatic ring within the p5 pocket with an adamantyl substituent (compounds **4.23** and **4.25**) had very little effect on the overall binding of the molecules. A small (approx. 2-fold) increase in binding towards BCL-X<sub>L</sub> was observed on adamantyl incorporation

( $IC_{50}(BCL-X_L) = 0.51 \mu M$  and  $0.59 \mu M$  for compounds **1.1** and **1.8**, versus  $IC_{50}(BCL-X_L) = 0.22 \mu M$  and  $0.19 \mu M$  for **4.23** and **4.25** respectively). However, this was concomitant with a small decrease in the overall binding efficiency index of the molecules due to the added molecular weight of the adamantyl group. Compared to the earlier leads, the adamantyl compounds **4.23** and **4.25** maintained the same level of selectivity for BCL-X<sub>L</sub> over MCL-1 (**Table 4.2**).

**Table 4.2: IC<sub>50</sub> values of benzoylurea compounds 4.23 and 4.25 for BCL-X<sub>L</sub> and MCL-1 (determined by AlphaScreen competition assay, post-2015 data)<sup>[a]</sup>**



Compound		IC <sub>50</sub> A.S. <sup>[b]</sup>				Fold Selectivity	BEI <sup>[c]</sup>
R <sup>1</sup>		BCL-X <sub>L</sub>		MCL-1		N =	(BCL-X <sub>L</sub> /MCL-1)
<b>1.1</b>		0.51	±0.07	7.7	±1.6	3	15
<b>1.2</b>		13.1	±0.42	44.2	±8.5	3	3
<b>1.6</b>		1.10	± 0.05	9.9	±2.2	3	7
<b>1.7</b>		0.38	±0.07	11.8	±0.8	3	31
<b>1.8</b>		0.59	±0.11	11.6	±1.0	3	20
<b>4.6l</b>		0.46	±0.43	10.0	±2.5	3	22
<b>4.23</b>		0.22	±0.06	3.76	±0.28	3	17
<b>4.25</b>		0.19	±0.08	6.07	±0.93	3	32

<sup>[a]</sup> Following the relocation of our Screening Group, a consistent shift in the IC<sub>50</sub> values determined using the AlphaScreen competition assay was observed. The signifiers '**pre-2015 data**' and '**post-2015 data**' indicate respectively data acquired prior and subsequent to this relocation. For further information refer to note in **Chapter 2, Section 2.4.1.3**.

<sup>[b]</sup> IC<sub>50</sub> values are reported in  $\mu\text{M} \pm \text{S.D.}$

<sup>[c]</sup> BEI (Binding efficiency index, refer Section 1.4.1.2) =  $pIC_{50}/\text{MW}$ , where  $pIC_{50}$  is the negative base 10 logarithm of the IC<sub>50</sub> (in molar units) and MW is the compound molecular weight (in kDa).

## 4.4 Structural evaluation of p5 analogues using X-ray crystallography

### 4.4.1 Structure determination of the BCL-X<sub>L</sub>:**4.6I** and BCL-X<sub>L</sub>:**4.25** complexes

Relevance:

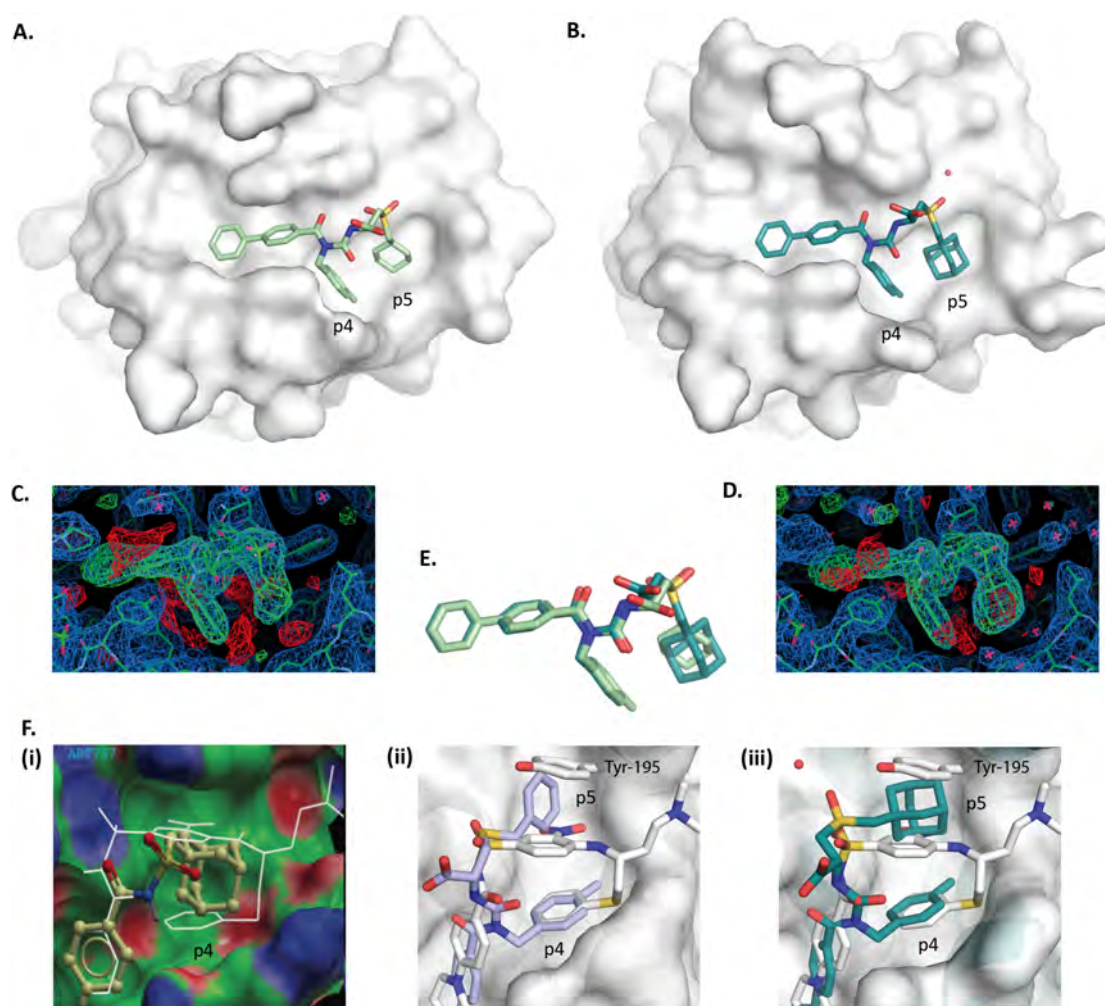
- Provide structural data on the overall binding modes and interactions in the p5 pocket of BCL-X<sub>L</sub>.

To validate the binding mode and confirm the interactions in the p5 pocket of BCL-X<sub>L</sub>, X-ray crystal structures were solved for complexes of both BCL-X<sub>L</sub>:**4.6I** (cyclohexyl analogue) and also BCL-X<sub>L</sub>:**4.25** (adamantyl analogue) to 2.25 Å and 2.15 Å resolution respectively. These two crystal structures are shown in **Figure 4.5**. Statistics for these structures are provided in **Table 4.3**. Both structures contained 12 copies of BCL-X<sub>L</sub> in the A.S.U., each of which harboured a single bound copy of the ligand. In the BCL-X<sub>L</sub>:**4.6I** complex the binding pose of every copy of compound **4.6I** was identical. In the BCL-X<sub>L</sub>:**4.25** complex, 11 of 12 copies of compound **4.25** shared the same pose (as described below), whilst the remaining copy was bound in an alternative pose that appeared to be a result of crystal packing and unlikely to reflect the bound conformation in solution (refer Section **4.6.2** for further detail).

These structures confirmed that compounds **4.6I** and **4.25** each bound to BCL-X<sub>L</sub> essentially identically to compounds **1.1** and **1.8**, and overlaid closely with one another (**Figure 4.5E**). In particular, for each of compounds **4.6I** and **4.25**, as for compound **1.8**, one oxygen atom of the sulfonyl group was engaged in a hydrogen bonding interaction with the backbone –NH of Gly138 of BCL-X<sub>L</sub>, and the other oxygen atom was hydrogen bonded to a water molecule coordinated to the backbone –NH of Trp137 of BCL-X<sub>L</sub>. Omit maps showed clear electron density for each of the appended cyclohexyl and adamantyl substituents within the p5 pocket (**Figure 4.5C,D**), albeit that for the (lower resolution) **4.6I** structure the electron density of the cyclohexyl ring was somewhat less well resolved than the remainder

of the compound, likely reflecting some conformational heterogeneity of this flexible group within the p5 pocket.

As compared to the planar phenyl ring of the S-benzyl derivative compound **1.1**, overlay of compounds **4.61** and **4.25** shows that the cyclohexyl and adamantyl groups exhibit greater three-dimensional character to fill the p5 pocket (**Figure 4.5E**). In particular, the BCL-X<sub>L</sub>:**4.25** complex reveals that as designed, the adamantyl group is able to effectively act as an isostere of the pi-stacking interaction between the nitroaryl ring of **ABT-737** and Tyr195 of BCL-X<sub>L</sub> within the p5 pocket (**Figure 4.5F(iii)**), in a similar manner to the adamantyl group of compound **3j** described by Yusuff *et al.*<sup>(12)</sup> within the p4 pocket (**Figure 4.5F(i)**).



**Figure 4.5: X-ray crystal structures of BCL-X<sub>L</sub>:4.6l and BCL-X<sub>L</sub>:4.25 complexes.**

X-ray crystal structures of (A) BCL-X<sub>L</sub>:**4.6l** (cyclohexyl) and (B) BCL-X<sub>L</sub>:**4.25** (adamantyl) complexes to 2.2 Å resolution. (C-D) Omit maps generated for BCL-X<sub>L</sub>:**4.6l** and BCL-X<sub>L</sub>:**4.25** complexes respectively, showing 2Fo-Fc contoured at 1σ (blue) and Fo-Fc contoured at ± 3σ (green/red). (E) Overlay of compounds **4.6l** and **4.25** from these structures (F) Comparison with adamantyl compound **3j** described by Yusuff *et al.*<sup>(12)</sup>, designed to mimic the intramolecular pi-stacking interaction of **ABT-737** in the p4 pocket. (i) Overlay of the X-ray crystal structures of BCL-X<sub>L</sub>:**ABT-737** and BCL-2:**3j** (image reproduced from Yusuff *et al.*<sup>(12)</sup>). (ii) Overlay of compound **1.1** (light blue) and **ABT-737** (white, PDB: 2YXJ<sup>(2)</sup>) showing Tyr195 of BCL-X<sub>L</sub> from the BCL-X<sub>L</sub>:**ABT-737** complex. (iii) Overlay of adamantyl compound **4.25** (dark green) and **ABT-737** (white, PDB entry: 2YXJ<sup>(2)</sup>), showing in comparison how adamantyl group acts here as an isostere of the pi-stacking interaction of the nitroaryl ring of **ABT-737** with Tyr195 of BCL-X<sub>L</sub> in the p5 pocket.



**Table 4.3: Crystallographic statistics for the BCL-X<sub>L</sub>:4.6l and BCL-X<sub>L</sub>:4.25 complexes.**

Structure <sup>‡</sup>	BCL-X <sub>L</sub> :4.6l	BCL-X <sub>L</sub> :4.25
Wavelength (Å)	0.9537	0.9537
Resolution range (Å)	39.87 - 2.244 (2.324 - 2.244)	46.14 - 2.147 (2.224 - 2.147)
Space group	<i>P</i> 2 <sub>1</sub>	<i>P</i> 2 <sub>1</sub>
Unit cell		
<i>a</i> , <i>b</i> , <i>c</i> (Å)	92.39, 104.65, 110.08	91.84, 103.56, 110.37
$\alpha$ , $\beta$ , $\gamma$ (°)	90 110.993 90	90 110.934 90
Total reflections	699772 (65301)	396911 (38133)
Unique reflections	93090 (8918)	104910 (10175)
Multiplicity	7.5 (7.3)	3.8 (3.7)
Completeness (%)	0.99 (0.96)	1.00 (0.97)
Mean <i>I</i> / $\sigma$ <i>I</i>	18.20 (1.78)	16.30 (1.79)
Wilson <i>B</i> factor (Å <sup>2</sup> )	49.17	41.68
<i>R</i> <sub>merge</sub>	0.06854 (1.047)	0.05474 (0.797)
<i>R</i> <sub>meas</sub>	0.07369 (1.126)	0.06397 (0.9312)
CC <sub>1/2</sub>	0.999 (0.795)	0.999 (0.702)
CC*	1 (0.941)	1 (0.908)
Reflections used in refinement	93061 (8911)	104872 (10172)
Reflections used for R-free	4653 (446)	5242 (507)
<i>R</i> <sub>work</sub>	0.1909 (0.2753)	0.2006 (0.2859)
<i>R</i> <sub>free</sub>	0.2400 (0.3364)	0.2533 (0.3453)
CC <sub>work</sub>	0.969 (0.839)	0.961 (0.816)
CC <sub>free</sub>	0.944 (0.772)	0.932 (0.707)
Number of non-hydrogen atoms	14525	14702
macromolecules	13695	13716
ligands/ions	654	676
RMS(bond lengths) (Å)	0.007	0.011
RMS(bond angles) (°)	0.98	1.43
Ramachandran favored (%)	97	96
Ramachandran allowed (%)	2.5	2.9
Ramachandran outliers (%)	0.6	0.66
Rotamer outliers (%)	2	1.4
Clashscore	18.74	12.97
Average <i>B</i> factors (Å <sup>2</sup> )	79.52	66.6
Macromolecules	79.18	66.25
ligands	92.34	80.73
solvent	58.17	51.22
Number of TLS groups	86	77

<sup>‡</sup> Statistics are outlined in Section 2.6.2.5.

## 4.5 Discussion / Conclusion

This Chapter has described the synthesis and evaluation of a small series of analogues exploring the Structure Activity Relationship (SAR) within the p5 pocket of BCL-X<sub>L</sub> (occupied by S-benzyl group of compound **1.1** and the SO<sub>2</sub>-benzyl group of **1.8**) which is opened up by a repositioning of Tyr195 of the protein. This initial series aimed to explore the flexibility and binding preferences of this relatively uncharacterised binding pocket.

These studies have confirmed that, unlike the relatively flexible p2 pocket at the other end of the canonical groove of BCL-X<sub>L</sub>, which can open up to accommodate the deep binding of ligands such as **ABT-737**<sup>(2)</sup>, the p5 pocket does not appear to exhibit such flexibility. As such, all substituents introduced around the terminal aromatic ring of compound **1.8** within the p5 pocket led to a reduction in BCL-X<sub>L</sub> binding, with the exception of relatively small substituents in the *meta*- position on the aromatic ring (*meta*-methyl or *meta*-fluoro).

Additionally, replacement of the p5 aromatic ring of compound **1.8** with aliphatic rings of varying sizes has revealed that the aromatic character of this group is not required for tight binding. Relative to smaller aliphatic rings, on this particular scaffold a cyclohexyl group appears to be optimal ring size in terms of IC<sub>50</sub> for BCL-X<sub>L</sub> and binding efficiency (improved BEI of compound **4.6I** relative to compound **1.8**, **Table 4.1**), potentially due to its greater three-dimensional character. To explore this concept further, incorporation of a larger adamantyl group in the p5 pocket appears to give a small increase in binding, but in a less atom-economical manner (small reduction in BEI) relative to the cyclohexyl moiety. Crystal structures of compounds **4.6I** and **4.25** in complex with BCL-X<sub>L</sub> have confirmed that the cyclohexyl and adamantyl substituents can be accommodated as expected within the p5 pocket and that the adamantyl group can be considered an isostere of a pi-stacking interaction.

In the process of generating the adamantyl analogues (compounds **4.23** and **4.25**), by adapting known chemistry, I have described the first reported S-alkylation of cysteine to install a 1-methyladamantyl substituent in good yield, which represents a challenging substitution on a sterically-hindered '*neopentyl*'-type system. The success of this substitution appears to be dependent on the presence of 18-crown-6 to increase the nucleophilicity of cysteine. In doing so, I have provided an example of a nucleophilic substitution which can be performed on a '*neopentyl*'-type system (despite the expectation of steric hindrance) to add to the existing literature on transformations of this nature<sup>(19)</sup> and described conditions which may be useful for others in future who wish to alkylate cysteine with other sterically hindered substituents of this type.

Based on the work described in this Chapter, the p5 cyclohexyl and adamantyl modifications were also applied to analogues based on compound **1.10**, to see whether synergistic effects might be observed on an extended scaffold which also interacts with the p2 pocket of BCL-X<sub>L</sub>. The synthesis and characterisation of these compounds are described in **Chapter 6**.

## 4.6 Experimental

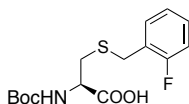
### 4.6.1 Chemical synthesis

For **General Procedures A - E**, refer to **Chapter 2, Section 2.2**.

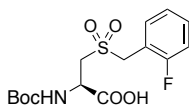
For synthesis of compounds **3.3** and **3.4**, refer to **Chapter 3, Section 3.5.1**.

#### 4.6.1.1 Synthesis of benzoylurea analogues varying the p5 substituent

##### 4.6.1.1.1 Cysteine S-alkylation, Boc-protection, thioether oxidation [Scheme 4.1(a-c)]

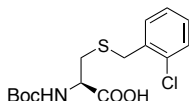


**(R)-2-((tert-butoxycarbonyl)amino)-3-((2-fluorobenzyl)thio)propanoic acid (4.1a):** **General Procedure C** was followed, using L-cysteine (200 mg, 1.65 mmol) and 2-fluorobenzyl chloride (216  $\mu$ L, 1.8 mmol) to afford the crude title compound as a pale yellow oil, which was used directly in the subsequent oxidation step without further characterisation.

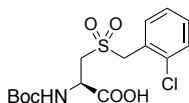


**(R)-2-((tert-butoxycarbonyl)amino)-3-((2-fluorobenzyl)sulfonyl)propanoic acid (4.3a):** **General Procedure D** was followed using compound **4.1a** (221 mg, 0.67 mmol). Purification *via* flash chromatography, eluting with a gradient of methanol/dichloromethane (0:100 to 5:95) followed by mass-directed preparative HPLC afforded the title compound as a colourless oil (211 mg, 52% over 2 steps).  $^1\text{H}$  NMR (600 MHz, MeOD)  $\delta$  7.50 (t,  $J$  = 7.1 Hz, 1H), 7.44 (dd,  $J$  = 13.6, 7.0 Hz, 1H), 7.23 (t,  $J$  = 7.5 Hz, 1H), 7.19 (t,  $J$  = 9.1 Hz, 1H), 4.68 (dd,  $J$  = 8.9, 3.2 Hz, 1H), 4.56 (d,  $J$  = 13.8 Hz, 1H), 4.50 (d,  $J$  = 13.9 Hz, 1H), 3.69 (dd,  $J$  = 14.8, 3.4 Hz, 1H), 3.59 (dd,  $J$  = 14.7, 9.0 Hz, 1H), 1.46 (s, 9H).  $^{13}\text{C}$  NMR (151 MHz, MeOD)  $\delta$  172.75, 162.93 (d,  $^1J_{\text{CF}}$  = 248.7 Hz), 157.65, 134.38 (d,  $^4J_{\text{CF}}$  = 2.8 Hz), 132.30 (d,  $^3J_{\text{CF}}$  = 8.3 Hz), 125.61 (d,  $^4J_{\text{CF}}$  = 3.3 Hz), 116.70 (d,  $^2J_{\text{CF}}$  = 22.0 Hz), 116.51 (d,  $^2J_{\text{CF}}$  = 14.9 Hz), 81.07, 54.28, 54.17 (d,  $J$  = 1.5 Hz), 50.29, 28.66. [a] MS (ES $^-$ ),  $m/z$  360.1 (M - H).

[a] One additional peak is observed in the aliphatic region due to apparent peak splitting.

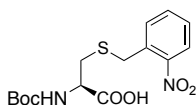


**(R)-2-((tert-butoxycarbonyl)amino)-3-((2-chlorobenzyl)thio)propanoic acid (4.1b):** **General Procedure C** was followed, using L-cysteine (200 mg, 1.65 mmol) and 2-chlorobenzyl chloride (230  $\mu$ L, 1.8 mmol) to afford the crude title compound as a white solid, which was used directly in the subsequent oxidation step without further characterisation.

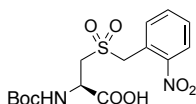


**(R)-2-((tert-butoxycarbonyl)amino)-3-((2-chlorobenzyl)sulfonyl)propanoic acid (4.3b):** **General Procedure D** was followed using compound **4.1b** (444 mg, 1.3 mmol). Purification *via* flash chromatography, eluting with a gradient of methanol/dichloromethane (0:100 to 10:90) afforded the title compound as a colourless oil (346 mg, 67% over 2 steps).  $^1\text{H}$  NMR (600 MHz,

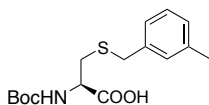
MeOD)  $\delta$  7.56 (d,  $J$  = 7.3 Hz, 1H), 7.49 (d,  $J$  = 7.9 Hz, 1H), 7.39 (td,  $J$  = 7.8 Hz, 1.2, 1H), 7.35 (t,  $J$  = 7.4 Hz, 1H), 4.72 (d,  $J$  = 13.8 Hz, 1H), 4.68 (dd,  $J$  = 7.8, 2.0 Hz, 1H), 4.64 (d,  $J$  = 13.9 Hz, 1H), 3.71 (dd,  $J$  = 14.7, 3.5 Hz, 1H), 3.63 (dd,  $J$  = 14.7, 8.8 Hz, 1H), 1.46 (s, 9H).  $^{13}\text{C}$  NMR (151 MHz, MeOD)  $\delta$  172.83, 157.62, 136.63, 134.49, 131.63, 131.01, 128.29, 127.30, 81.11, 58.03, 55.00, 50.49, 28.69. MS (ES<sup>-</sup>),  $m/z$  376.1 (M - H).



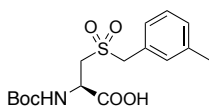
**(R)-2-((tert-butoxycarbonyl)amino)-3-((2-nitrobenzyl)thio)propanoic acid (4.1c): General Procedure C** was followed, using L-cysteine (200 mg, 1.65 mmol) and 2-nitro-benzyl bromide (392 mg, 1.8 mmol) to afford the crude title compound as a colourless oil, which was used directly in the subsequent oxidation step without further characterisation.



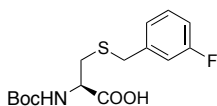
**(R)-2-((tert-butoxycarbonyl)amino)-3-((2-nitrobenzyl)sulfonyl)propanoic acid (4.3c): General Procedure D** was followed using compound **4.1c** (495 mg, 1.4 mmol). Purification *via* flash chromatography, eluting with a gradient of methanol/dichloromethane (0:100 to 5:95) afforded the title compound as a pale yellow oil (413 mg, 77% over 2 steps).  $^1\text{H}$  NMR (600 MHz, MeOD)  $\delta$  8.08 (d,  $J$  = 7.9 Hz, 1H), 7.72 (t,  $J$  = 7.4 Hz, 1H), 7.69–7.60 (m, 2H), 5.06 (d,  $J$  = 13.8 Hz, 1H), 5.00 (d,  $J$  = 13.6 Hz, 1H), 4.64 (dd,  $J$  = 8.3, 3.0 Hz, 1H), 3.72 (dd,  $J$  = 14.9, 3.5 Hz, 1H), 3.62 (dd,  $J$  = 14.8, 8.7 Hz, 1H), 1.46 (s, 9H).  $^{13}\text{C}$  NMR (151 MHz, MeOD)  $\delta$  172.61, 157.62, 151.45, 135.63, 134.45, 131.46, 126.64, 123.33, 81.20, 57.26, 55.10, 50.45, 28.68. MS (ES<sup>-</sup>),  $m/z$  387.1 (M - H).



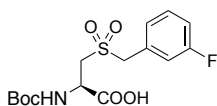
**(R)-2-((tert-butoxycarbonyl)amino)-3-((3-methylbenzyl)thio)propanoic acid (4.1d): General Procedure C** was followed, using L-cysteine (200 mg, 1.65 mmol) and 3-methylbenzyl bromide (245  $\mu\text{L}$ , 1.8 mmol) to afford the crude title compound as a pale yellow oil, which was used directly in the subsequent oxidation step without further characterisation.



**(R)-2-((tert-butoxycarbonyl)amino)-3-((3-methylbenzyl)sulfonyl)propanoic acid (4.3d): General Procedure D** was followed using compound **4.1d** (298 mg, 0.92 mmol). Purification *via* flash chromatography, eluting with a gradient of methanol/dichloromethane (0:100 to 5:95) afforded the title compound as a colourless oil (226 mg, 50% over 2 steps).  $^1\text{H}$  NMR (600 MHz, MeOD)  $\delta$  7.32–7.17 (m, 4H), 4.65 (dd,  $J$  = 8.3, 3.0 Hz, 1H), 4.39 (s, 2H), 3.61 (dd,  $J$  = 14.9, 3.3 Hz, 1H), 3.47 (dd,  $J$  = 14.7, 8.7 Hz, 1H), 2.36 (s, 3H), 1.46 (s, 9H).  $^{13}\text{C}$  NMR (151 MHz, MeOD)  $\delta$  172.76, 157.61, 139.72, 132.88, 130.59, 129.66, 129.30, 128.96, 81.13, 60.92, 53.76, 50.44, 28.71, 21.33. MS (ES<sup>-</sup>),  $m/z$  357.1 (M - H).

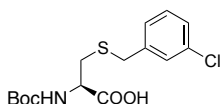


**(R)-2-((tert-butoxycarbonyl)amino)-3-((3-fluorobenzyl)thio)propanoic acid (4.1e): General Procedure C** was followed, using L-cysteine (200 mg, 1.65 mmol) and 3-fluoro-benzyl bromide (343 mg, 1.8 mmol) to afford the crude title compound as a pale yellow oil, which was used directly in the subsequent oxidation step without further characterisation.



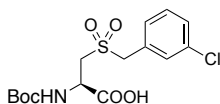
**(R)-2-((tert-butoxycarbonyl)amino)-3-((3-fluorobenzyl)sulfonyl)propanoic acid (4.3e):**

**General Procedure D** was followed using compound **4.1e** (391 mg, 1.2 mmol). Purification *via* flash chromatography, eluting with a gradient of methanol/dichloromethane (0:100 to 5:95) afforded the title compound as an opaque white solid (351 mg, 70% over 2 steps).  $^1\text{H}$  NMR (600 MHz, MeOD)  $\delta$  7.41 (dd,  $J$  = 14.0, 7.8 Hz, 1H), 7.26 (d,  $J$  = 7.5 Hz, 1H), 7.22 (d,  $J$  = 9.5 Hz, 1H), 7.14 (td,  $J$  = 8.6, 2.1 Hz, 1H), 4.66 (dd,  $J$  = 7.9, 2.7 Hz, 1H), 4.47 (s, 2H), 3.65 (dd,  $J$  = 14.9, 3.5 Hz, 1H), 3.51 (dd,  $J$  = 14.8, 8.5 Hz, 1H), 1.46 (s, 9H).  $^{13}\text{C}$  NMR (151 MHz, MeOD)  $\delta$  172.73, 164.07 (d,  $^1J_{\text{CF}}$  245.4 Hz), 157.61, 131.61 (d,  $^3J_{\text{CF}}$  = 8.3 Hz), 131.48 (d,  $^3J_{\text{CF}}$  = 8.8 Hz), 128.24 (d,  $^4J_{\text{CF}}$  = 2.8 Hz), 119.04 (d,  $^2J_{\text{CF}}$  = 22.6 Hz), 116.73 (d,  $^2J_{\text{CF}}$  = 21.5 Hz), 81.17, 60.24, 54.12, 50.45, 28.69. MS (ES $^-$ ),  $m/z$  360.1 (M - H).



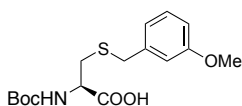
**(R)-2-((tert-butoxycarbonyl)amino)-3-((3-chlorobenzyl)thio)propanoic acid (4.1f):**

**General Procedure C** was followed, using L-cysteine (200 mg, 1.65 mmol) and 3-chlorobenzyl bromide (238  $\mu\text{L}$ , 1.8 mmol) to afford the crude title compound as a pale yellow oil, which was used directly in the subsequent oxidation step without further characterisation.



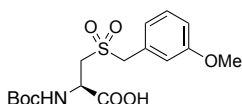
**(R)-2-((tert-butoxycarbonyl)amino)-3-((3-chlorobenzyl)sulfonyl)propanoic acid (4.3f):**

**General Procedure D** was followed using compound **4.1f** (288 mg, 0.83 mmol). Purification *via* flash chromatography, eluting with a gradient of methanol/dichloromethane (0:100 to 10:90) afforded the title compound as a colourless oil (312 mg, 85% over 2 steps).  $^1\text{H}$  NMR (600 MHz, MeOD)  $\delta$  7.49 (s, 1H), 7.43–7.35 (m, 3H), 4.66 (d,  $J$  = 5.3 Hz, 1H), 4.46 (s, 2H), 3.66 (dd,  $J$  = 14.9, 3.3 Hz, 1H), 3.51 (dd,  $J$  = 14.8, 8.5 Hz, 1H), 1.47 (s, 9H).  $^{13}\text{C}$  NMR (151 MHz, MeOD)  $\delta$  172.72, 157.63, 135.52, 132.22, 131.32, 131.20, 130.72, 130.01, 81.18, 60.09, 54.22, 50.46, 28.71. MS (ES $^-$ ),  $m/z$  376.1 (M - H).



**(R)-2-((tert-butoxycarbonyl)amino)-3-((3-methoxybenzyl)thio)propanoic acid (4.1g):**

**General Procedure C** was followed, using L-cysteine (100 mg, 0.83 mmol) and 3-methoxybenzyl chloride (128  $\mu\text{L}$ , 0.91 mmol) to afford the crude title compound as an orange oil, which was used directly in the subsequent oxidation step without further characterisation.

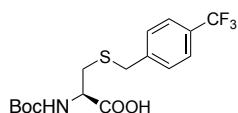


**(R)-2-((tert-butoxycarbonyl)amino)-3-((3-methoxybenzyl)sulfonyl)propanoic acid (4.3g):**

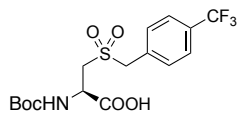
**General Procedure D** was followed using compound **4.1g** (295 mg, 0.87 mmol). Purification *via* flash chromatography, eluting with a gradient of methanol/dichloromethane (0:100 to 5:95) followed by mass-directed preparative HPLC afforded the title compound as a colourless oil (233 mg, 72% over 2 steps).  $^1\text{H}$  NMR (600 MHz, MeOD)  $\delta$  7.30 (t,  $J$  = 7.9 Hz, 1H), 7.04–6.94 (m, 3H), 4.64 (dd,  $J$  = 8.7, 3.4 Hz, 1H), 4.45–4.40 (m, 2H), 3.81 (s, 3H), 3.63 (dd,  $J$  = 14.9, 3.3 Hz, 1H), 3.48 (dd,  $J$  = 14.7, 8.8 Hz, 1H), 1.47 (s, 9H).<sup>[a][b]</sup>  $^{13}\text{C}$  NMR (151 MHz, MeOD)  $\delta$  172.79, 161.28, 157.63, 130.75, 130.44, 124.44, 117.60, 115.58, 81.08, 60.76, 55.71, 53.65, 50.36, 28.69. <sup>[a]</sup> MS (ES $^-$ ),  $m/z$  372.1 (M - H).

<sup>[a]</sup> Additional peaks are observed at  $\delta$  = 2.66 ppm ( $^1\text{H}$  NMR) and  $\delta$  = 40.33 ppm ( $^{13}\text{C}$  NMR) due to residual DMSO, utilised to solubilise the product for HPLC purification.

<sup>[b]</sup> Additional peaks are observed at  $\delta$  = 1.25, 1.24, 1.20 ppm due to a minor impurity.

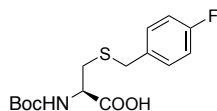


**(R)-2-((tert-butoxycarbonyl)amino)-3-((4-(trifluoromethyl)benzyl)thio)propanoic acid (4.1h):** General Procedure C was followed, using L-cysteine (85 mg, 0.7 mmol) and 4-(trifluoromethyl)benzyl bromide (185 mg, 0.77 mmol) to afford the crude title compound as a pale yellow oil, which was used directly in the subsequent oxidation step without further characterisation.

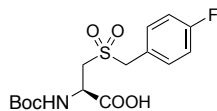


**(R)-2-((tert-butoxycarbonyl)amino)-3-((4-(trifluoromethyl)benzyl)sulfonyl)propanoic acid (4.3h):** General Procedure D was followed using compound 4.1h (175 mg, 0.46 mmol). Purification *via* flash chromatography, eluting with a gradient of methanol/dichloromethane (0:100 to 5:95) followed by mass-directed preparative HPLC afforded the title compound as a colourless solid (171 mg, 69% over 2 steps).  $^1\text{H}$  NMR (600 MHz, MeOD)  $\delta$  7.71 (d,  $J$  = 8.1 Hz, 2H), 7.65 (d,  $J$  = 7.9 Hz, 2H), 4.67 (dd,  $J$  = 8.7, 3.2 Hz, 1H), 4.57 (s, 2H), 3.68 (dd,  $J$  = 14.9, 3.5 Hz, 1H), 3.54 (dd,  $J$  = 14.9, 8.8 Hz, 1H), 1.46 (s, 9H).<sup>[a]</sup>  $^{13}\text{C}$  NMR (151 MHz, MeOD)  $\delta$  172.73, 157.66, 133.68, 133.10, 131.83 (q,  $^2J_{\text{CF}}$  = 32.4 Hz), 126.52 (q,  $^3J_{\text{CF}}$  = 3.5 Hz), 125.53 (q,  $^1J_{\text{CF}}$  = 271.4 Hz), 81.11, 60.09, 54.24, 50.37, 28.68.<sup>[a]</sup> MS (ES<sup>-</sup>),  $m/z$  410.1 (M - H).

<sup>[a]</sup> Additional peaks are observed at  $\delta$  = 2.66 ppm ( $^1\text{H}$  NMR) and  $\delta$  = 40.33 ppm ( $^{13}\text{C}$  NMR) due to residual DMSO, utilised to solubilise the product for HPLC purification.

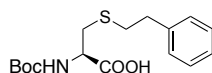


**(R)-2-((tert-butoxycarbonyl)amino)-3-((4-fluorobenzyl)thio)propanoic acid (4.1i):** General Procedure C was followed, using L-cysteine (200 mg, 1.65 mmol) and 4-fluorobenzyl bromide (226  $\mu\text{L}$ , 1.8 mmol) to afford the crude title compound as a colourless oil, which was used directly in the subsequent oxidation step without further characterisation.

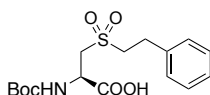


**(R)-2-((tert-butoxycarbonyl)amino)-3-((4-fluorobenzyl)sulfonyl)propanoic acid (4.3i):** General Procedure D was followed using compound 4.1i (376 mg, 1.1 mmol). Purification *via* flash chromatography, eluting with a gradient of methanol/dichloromethane (0:100 to 10:90), followed by mass-directed preparative HPLC afforded the title compound as a colourless oil (348 mg, 70% over 2 steps).  $^1\text{H}$  NMR (600 MHz, MeOD)  $\delta$  7.47 (dd,  $J$  = 7.8, 5.6 Hz, 2H), 7.14 (t,  $J$  = 8.6 Hz, 2H), 4.65 (dd,  $J$  = 8.6, 3.1 Hz, 1H), 4.44 (s, 2H), 3.63 (dd,  $J$  = 14.9, 3.3 Hz, 1H), 3.50 (dd,  $J$  = 14.9, 8.8 Hz, 1H), 1.46 (s, 9H).<sup>[a]</sup>  $^{13}\text{C}$  NMR (151 MHz, MeOD)  $\delta$  172.73, 164.56 (d,  $^1J_{\text{CF}}$  = 246.5 Hz), 157.62, 134.36 (d,  $^3J_{\text{CF}}$  = 8.3 Hz), 125.18 (d,  $^4J_{\text{CF}}$  = 3.3 Hz), 116.58 (d,  $^2J_{\text{CF}}$  = 22.0 Hz), 81.09, 59.79, 53.76, 50.33, 28.68.<sup>[a]</sup> MS (ES<sup>-</sup>),  $m/z$  360.1 (M - H).

<sup>[a]</sup> Additional peaks are observed at  $\delta$  = 1.20 ppm ( $^1\text{H}$  NMR) and  $\delta$  = 25.01 ppm ( $^{13}\text{C}$  NMR) due to a minor impurity and at  $\delta$  = 2.66 ppm ( $^1\text{H}$  NMR) and  $\delta$  = 40.33 ppm ( $^{13}\text{C}$  NMR) due to residual DMSO, utilised to solubilise the product for HPLC purification.

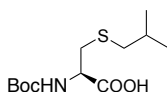


**(R)-2-((tert-butoxycarbonyl)amino)-3-(phenethylthio)propanoic acid (4.1j):** General Procedure C was followed, using L-cysteine (200 mg, 1.65 mmol) and (2-bromoethyl)benzene (248  $\mu\text{L}$ , 1.8 mmol) to afford the crude title compound as a white powder, which was used directly in the subsequent oxidation step without further characterisation.



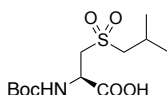
**(R)-2-((tert-butoxycarbonyl)amino)-3-(phenethylsulfonyl)propanoic acid (4.3j):**

**General Procedure D** was followed using compound **4.1j** (418 mg, 1.3 mmol). Purification *via* flash chromatography, eluting with a gradient of methanol/dichloromethane (0:100 to 10:90) afforded the title compound as a pale yellow oil (425 mg, 90% over 2 steps).  $^1\text{H}$  NMR (600 MHz, MeOD)  $\delta$  7.33–7.26 (m, 4H), 7.23 (t,  $J$  = 7.1 Hz, 1H), 4.66–4.58 (m, 1H), 3.61 (d,  $J$  = 5.3 Hz, 2H), 3.38 (dd,  $J$  = 9.4, 5.0 Hz, 2H), 3.13–3.04 (m, 2H), 1.40 (s, 9H).  $^{13}\text{C}$  NMR (151 MHz, MeOD)  $\delta$  172.71, 157.60, 139.32, 129.83, 129.59, 127.92, 81.18, 56.36, 54.82, 50.67, 28.92, 28.63. MS ( $\text{ES}^-$ ),  $m/z$  356.1 ( $\text{M} - \text{H}$ ).



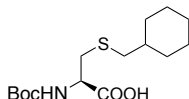
**(R)-2-((tert-butoxycarbonyl)amino)-3-(isobutylthio)propanoic acid (4.1k):**

**General Procedure C** was followed, using L-cysteine (200 mg, 1.65 mmol) and 1-bromo-2-methylpropane (197  $\mu\text{L}$ , 1.8 mmol) to afford the crude title compound as a colourless oil, which was used directly in the subsequent oxidation step without further characterisation.



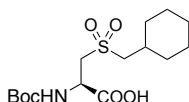
**(R)-2-((tert-butoxycarbonyl)amino)-3-(isobutylsulfonyl)propanoic acid (4.3k):**

**General Procedure D** was followed using compound **4.1k** (315 mg, 1.1 mmol). Purification *via* flash chromatography, eluting with a gradient of methanol/dichloromethane (0:100 to 10:90) afforded the title compound as a pale yellow oil (317 mg, 88% over 2 steps).  $^1\text{H}$  NMR (600 MHz, MeOD)  $\delta$  4.61 (dd,  $J$  = 7.6, 3.2 Hz, 1H), 3.62–3.52 (m, 2H), 3.07–2.99 (m, 2H), 2.31 (sept.,  $J$  = 6.7 Hz, 1H), 1.46 (s, 9H), 1.12 (d,  $J$  = 4.6 Hz, 3H), 1.10 (d,  $J$  = 4.7 Hz, 3H).  $^{13}\text{C}$  NMR (151 MHz, MeOD)  $\delta$  172.80, 157.58, 81.10, 62.25, 55.85, 50.62, 28.69, 24.68, 23.14, 22.96. MS ( $\text{ES}^-$ ),  $m/z$  308.2 ( $\text{M} - \text{H}$ ).



**(R)-2-((tert-butoxycarbonyl)amino)-3-((cyclohexylmethyl)thio)propanoic acid (4.1l):**

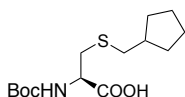
**General Procedure C** was followed, using L-cysteine (200 mg, 1.65 mmol) and (bromomethyl)cyclohexane (253  $\mu\text{L}$ , 1.8 mmol) to afford the crude title compound as a colourless oil, which was used directly in the subsequent oxidation step without further characterisation.



**(R)-2-((tert-butoxycarbonyl)amino)-3-((cyclohexylmethyl)sulfonyl)propanoic acid (4.3l):**

**General Procedure D** was followed using compound **4.1l** (314 mg, 0.99 mmol). Purification *via* flash chromatography, eluting with a gradient of methanol/dichloromethane (0:100 to 5:95) afforded the title compound as a colourless oil (307 mg, 64% over 2 steps).  $^1\text{H}$  NMR (300 MHz,  $\text{CDCl}_3$ )  $\delta$  7.07 (br s, 1H), 5.77 (d,  $J$  = 6.3 Hz, 1H), 4.68 (dd,  $J$  = 12.1, 5.1 Hz, 1H), 3.66 (d,  $J$  = 3.8 Hz, 2H), 2.95 (d,  $J$  = 6.4 Hz, 2H), 2.07 (qdd,  $J$  = 9.9, 6.5, 3.6 Hz, 1H), 1.92 (d,  $J$  = 12.7 Hz, 2H), 1.78–1.58 (m, 3H), 1.45 (s,  $J$  = 19.9, 9H), 1.39–0.97 (m, 5H).<sup>[a]</sup>  $^{13}\text{C}$  NMR (75 MHz,  $\text{CDCl}_3$ )  $\delta$  172.62, 155.76, 81.42, 77.36, 61.74, 54.81, 49.85, 33.23, 32.41, 28.40, 25.85, 25.81. MS ( $\text{ES}^-$ ),  $m/z$  348.2 ( $\text{M} - \text{H}$ ). HRMS ( $\text{ES}^+$  TOF) calculated for  $\text{C}_{15}\text{H}_{27}\text{NO}_6\text{S}$  ( $\text{M} + \text{Na}$ ): 372.1451; found 372.1452.

<sup>[a]</sup> The broad singlet observed at  $\delta$  3.66 ppm is attributed to  $-\text{COOH}$ .

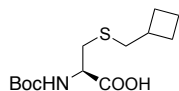


**(R)-2-((tert-butoxycarbonyl)amino)-3-((cyclopentylmethyl)thio)propanoic acid (4.1m):**

**General Procedure C** was followed, using L-cysteine (34 mg, 0.28 mmol) and

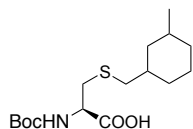


(bromomethyl)cyclopentane (39  $\mu$ L, 0.31 mmol). Purification *via* flash chromatography, eluting with a gradient of methanol/dichloromethane (0:100 to 5:95) afforded the title compound as a colourless oil, containing some minor impurities (53 mg, 62%).  $^1\text{H}$  NMR (600 MHz,  $\text{CDCl}_3$ )  $\delta$  5.37 (br s, 1H), 4.51 (br s, 1H), 3.00 (s, 2H), 2.57 (d,  $J$  = 7.3 Hz, 2H), 2.04 (hept.,  $J$  = 7.7 Hz, 1H), 1.86–1.76 (m, 2H), 1.66–1.51 (m, 4H), 1.46 (s, 9H), 1.29–1.16 (m, 2H).  $^{13}\text{C}$  NMR (151 MHz,  $\text{CDCl}_3$ )  $\delta$  174.69, 155.76, 80.80, 53.27, 39.97, 39.25, 34.51, 32.46, 32.44, 28.45, 25.34. MS (ES $^-$ ),  $m/z$  302.2 (M - H).



**(R)-2-((tert-butoxycarbonyl)amino)-3-((cyclobutylmethyl)thio)propanoic acid (4.1n):** General Procedure C was followed, using L-cysteine (121 mg, 1.0 mmol) and (bromomethyl)cyclobutane (124  $\mu$ L, 1.1 mmol, 97%). Purification *via* flash chromatography, eluting with a gradient of methanol/dichloromethane (0:100 to 5:95) afforded the title compound as a colourless oil (272 mg, 94%).  $^1\text{H}$  NMR (600 MHz,  $\text{CDCl}_3$ )  $\delta$  5.37 (d,  $J$  = 6.2 Hz, 1H), 4.52 (d,  $J$  = 4.4 Hz, 1H), 3.05–2.89 (m, 2H), 2.62 (td,  $J$  = 7.7, 1.0 Hz, 2H), 2.46 (app sept.,  $J$  = 7.6 Hz, 1H), 2.16–2.03 (m, 2H), 1.92–1.77 (m, 2H), 1.67 (pent.,  $J$  = 9.4 Hz, 2H), 1.45 (d,  $J$  = 1.2 Hz, 9H).  $^{13}\text{C}$  NMR (75 MHz,  $\text{CDCl}_3$ )  $\delta$  175.64, 155.66, 80.65, 53.35, 39.41, 35.40, 34.19, 28.43, 28.07, 28.04, 18.12.<sup>[a]</sup> MS (ES $^-$ ),  $m/z$  288.3 (M - H).

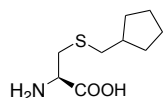
<sup>[a]</sup> An additional peak is observed at 28.12 ppm due to an impurity. One additional peak is observed in the aliphatic region due to apparent peak splitting.



**(2R)-2-((tert-butoxycarbonyl)amino)-3-(((3-methylcyclohexyl)methyl)thio)propanoic acid (4.1o):** General Procedure C was followed, using L-cysteine (27 mg, 0.23 mmol) and 1-(bromomethyl)-3-methyl cyclohexane (48 mg, 0.25 mmol). Purification *via* flash chromatography, eluting with a gradient of methanol/dichloromethane (0:100 to 5:95) afforded the title compound as a colourless oil as an inseparable mixture of diastereomers (16 mg, 22%).  $^1\text{H}$  NMR (300 MHz,  $\text{CDCl}_3$ )  $\delta$  5.37 (br s, 1H), 4.50 (br s, 1H), 2.98 (d,  $J$  = 5.1 Hz, 2H), 2.49 (dd,  $J$  = 27.1, 6.9 Hz, 2H), 1.90–0.50 (m, 22H).<sup>[a]</sup>  $^{13}\text{C}$  NMR (75 MHz,  $\text{CDCl}_3$ )  $\delta$  174.62, 155.76, 53.42, 41.60, 40.79, 38.55, 38.48, 38.32, 38.28, 38.27, 35.20, 34.91, 34.62, 33.73, 32.96, 32.72, 32.51, 31.02, 30.95, 28.47, 27.32, 26.20, 22.90, 20.82. MS (ES $^-$ ),  $m/z$  330.3 (M - H).

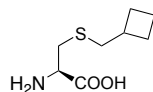
<sup>[a]</sup> The mixture of diastereomers was integrated as a single compound for the purposes of NMR analysis.

#### 4.6.1.1.2 Boc-deprotection of amino acids **4.1m-o** [Scheme 4.1 (d)]



**(R)-2-amino-3-((cyclopentylmethyl)thio)propanoic acid hydrochloride (4.2m):** General Procedure E was followed using compound **4.1m** (47 mg, 0.15 mmol), to precipitate the title compound as the HCl salt as a fine white powder (37 mg, quant.).  $^1\text{H}$  NMR (300 MHz, MeOD)  $\delta$  4.19 (dd,  $J$  = 7.2, 4.5 Hz, 1H), 3.17 (dd,  $J$  = 14.7, 4.3 Hz, 1H), 3.05 (dd,  $J$  = 14.8, 7.3 Hz, 1H), 2.63 (dd,  $J$  = 7.3, 2.5 Hz, 2H), 2.08 (app sept.,  $J$  = 7.5 Hz, 1H), 1.96–1.76 (m, 2H), 1.74–1.49 (m, 4H), 1.40–1.16 (m, 2H).  $^{13}\text{C}$  NMR (75 MHz, MeOD)  $\delta$  170.51, 53.51, 40.97, 39.48, 33.38, 33.23, 26.15, 26.10.<sup>[a]</sup> MS (ES $^+$ ),  $m/z$  204.3 (M + H).

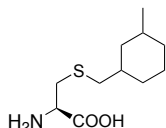
<sup>[a]</sup> One additional peak is observed in the aliphatic region due to apparent peak splitting.



**(R)-2-amino-3-((cyclobutylmethyl)thio)propanoic acid hydrochloride (4.2n):** General Procedure E was followed using compound **4.1n** (255 mg, 0.88 mmol), to precipitate the title

compound as the HCl salt as a fine white powder (147 mg, 74%).  $^1\text{H}$  NMR (600 MHz, MeOD)  $\delta$  4.19 (br s, 1H), 3.14 (dd,  $J$  = 14.7, 1.8 Hz, 1H), 3.02 (dd,  $J$  = 14.7, 7.3 Hz, 1H), 2.70 (d,  $J$  = 7.0 Hz, 2H), 2.55 (hept.,  $J$  = 7.8 Hz, 1H), 2.13 (dt,  $J$  = 10.0, 8.2 Hz, 2H), 1.98–1.81 (m, 2H), 1.76 (pent.,  $J$  = 8.9 Hz, 2H).  $^{13}\text{C}$  NMR (75 MHz, MeOD)  $\delta$  170.48, 53.51, 39.59, 36.46, 32.87, 28.83, 28.77, 18.78. MS ( $\text{ES}^+$ ),  $m/z$  190.2 ( $\text{M} + \text{H}$ ).

[a] One additional peak is observed in the aliphatic region due to apparent peak splitting.

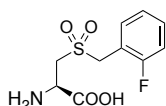


**(2R)-2-amino-3-(((3-methylcyclohexyl)methyl)thio)propanoic acid hydrochloride (4.2o):**

**General Procedure E** was followed using compound **4.1o** (11 mg, 0.034 mmol), to afford the title compound HCl salt as a mixture of inseparable diastereomers as a pale yellow powder (9 mg, quant.).  $^1\text{H}$  NMR (300 MHz, MeOD)  $\delta$  4.18 (br s, 1H), 3.14 (dd,  $J$  = 14.8, 4.0 Hz, 1H), 3.03 (dd,  $J$  = 14.8, 7.0 Hz, 1H), 2.56 (dd,  $J$  = 31.4, 7.0 Hz, 2H), 1.96–0.52 (m, 13H).<sup>[a]</sup>  $^{13}\text{C}$  NMR (75 MHz, MeOD)  $\delta$  42.58, 42.51, 40.88, 39.35, 39.33, 39.19, 38.33, 36.18, 34.75, 33.95, 33.92, 33.81, 33.67, 33.38, 33.35, 33.28, 31.74, 30.72, 28.37, 27.11, 23.16, 21.67, 21.08.

[a] The mixture of diastereomers was integrated as a single compound for the purposes of NMR analysis.

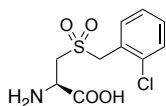
#### 4.6.1.1.3 Boc-deprotection of amino acids **4.3a-l** [Scheme 4.1(d)]



**(R)-2-amino-3-((2-fluorobenzyl)sulfonyl)propanoic acid hydrochloride (4.4a):**

**General Procedure E** was followed using compound **4.3a** (183 mg, 0.51 mmol), to precipitate the title compound as the HCl salt as a fine white powder (112 mg, 74%).  $^1\text{H}$  NMR (600 MHz, DMSO)  $\delta$  7.61 (br s, 1H), 7.55 (t,  $J$  = 7.3 Hz, 1H), 7.46 (dd,  $J$  = 12.6, 6.7 Hz, 1H), 7.32–7.21 (m, 2H), 4.77 (d,  $J$  = 14.2 Hz, 1H), 4.71 (d,  $J$  = 14.0 Hz, 1H), 3.82 (dd,  $J$  = 14.8, 2.1 Hz, 1H), 3.67 (dd,  $J$  = 9.2, 2.1 Hz, 1H), 3.32 (dd,  $J$  = 14.7, 9.1 Hz, 1H)<sup>[a]</sup> MS ( $\text{ES}^-$ ),  $m/z$  260.1 ( $\text{M} - \text{H}$ ).

[a] The broad singlet observed at  $\delta$  7.61 ppm is attributed to  $-\text{COOH}$ .

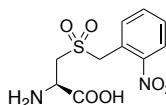


**(R)-2-amino-3-((2-chlorobenzyl)sulfonyl)propanoic acid hydrochloride (4.4b):**

**General Procedure E** was followed using compound **4.3b** (327 mg, 0.87 mmol), to afford the title compound as the HCl salt as a fine white powder (178 mg, 66%).  $^1\text{H}$  NMR (600 MHz, DMSO)  $\delta$  8.92 (br s, 1H), 7.59 (dd,  $J$  = 7.4, 1.4 Hz, 1H), 7.54 (d,  $J$  = 7.9 Hz, 1H), 7.46–7.36 (m, 2H), 4.95–4.83 (m, 2H), 4.14 (dd,  $J$  = 7.2, 4.2 Hz, 1H), 3.92 (dd,  $J$  = 15.0, 4.0 Hz, 1H), 3.65 (dd,  $J$  = 15.0, 7.3 Hz, 1H).<sup>[a]</sup>  $^{13}\text{C}$  NMR (151 MHz, DMSO)  $\delta$  167.85, 134.76, 133.58, 130.58, 129.75, 127.32, 126.11, 56.10, 52.86, 47.67.<sup>[b]</sup> MS ( $\text{ES}^-$ ),  $m/z$  276.2 ( $\text{M} - \text{H}$ ).

[a] The broad singlet observed at  $\delta$  8.92 ppm is attributed to  $-\text{COOH}$ . A small peak observed at  $\delta$  3.63 ppm is attributed to a remnant 1,4-dioxane from the reaction solvent.

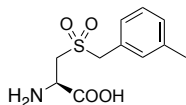
[b] A small peak observed at  $\delta$  66.35 ppm is attributed to a remnant 1,4-dioxane from the reaction solvent.



**(R)-2-amino-3-((2-nitrobenzyl)sulfonyl)propanoic acid hydrochloride (4.4c):**

**General Procedure E** was followed using compound **4.3c** (357 mg, 0.92 mmol), to precipitate the title compound as the HCl salt as a fine off-white powder (259 mg, 97%).  $^1\text{H}$  NMR (600 MHz, MeOD)  $\delta$  8.09 (d,  $J$  = 8.1 Hz, 1H), 7.81 (t,  $J$  = 7.4 Hz, 1H), 7.75 (d,  $J$  = 7.3 Hz, 1H), 7.70 (t,  $J$  = 7.7 Hz,

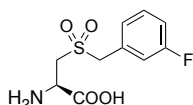
1H), 5.23 (s, 2H), 4.32–4.19 (m, 1H), 3.90 (dd,  $J = 15.0, 4.4$  Hz, 1H), 3.65 (dd,  $J = 15.0, 6.6$  Hz, 1H).  $^{13}\text{C}$  NMR (151 MHz, MeOD)  $\delta$  167.91, 149.64, 134.49, 133.70, 130.52, 125.47, 121.81, 55.20, 52.34, 47.35. MS (ES<sup>-</sup>),  $m/z$  287.1 (M - H).



**(R)-2-amino-3-((3-methylbenzyl)sulfonyl)propanoic acid hydrochloride (4.4d):**

**General Procedure E** was followed using compound **4.3d** (187 mg, 0.52 mmol), to precipitate the title compound as the HCl salt as a fine white powder, containing minor impurities (97 mg, 63%).  $^1\text{H}$  NMR (600 MHz, DMSO)  $\delta$  7.72 (br s, 1H), 7.32–7.15 (m, 4H), 4.68 (d,  $J = 13.7$  Hz, 1H), 4.57 (d,  $J = 13.7$  Hz, 1H), 3.75 (dd,  $J = 14.9, 2.9$  Hz, 1H), 3.69 (dd,  $J = 9.0, 3.1$  Hz, 1H), 3.25 (dd,  $J = 14.9, 9.0$  Hz, 1H), 2.31 (s, 3H).<sup>[a]</sup> MS (ES<sup>-</sup>),  $m/z$  256.1 (M - H).

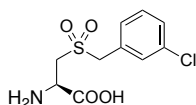
<sup>[a]</sup> The broad singlet observed at  $\delta$  7.72 ppm is attributed to  $-\text{COOH}$ .



**(R)-2-amino-3-((3-fluorobenzyl)sulfonyl)propanoic acid hydrochloride (4.4e):**

**General Procedure E** was followed using compound **4.3e** (314 mg, 0.87 mmol), to precipitate the title compound as the HCl salt as a fine off-white powder (156 mg, 60%).  $^1\text{H}$  NMR (600 MHz, DMSO)  $\delta$  8.77 (br s, 1H), 7.47 (dd,  $J = 14.5, 7.5$  Hz, 1H), 7.30 (app. d,  $J = 7.5$  Hz, 2H), 7.25 (t,  $J = 8.5$  Hz, 1H), 4.79 (d,  $J = 13.8$  Hz, 1H), 4.72 (d,  $J = 13.6$  Hz, 1H), 4.07 (dd,  $J = 7.3, 3.5$  Hz, 1H), 3.79 (dd,  $J = 15.0, 3.9$  Hz, 1H), 3.43 (dd,  $J = 15.0, 8.1$  Hz, 1H).<sup>[a]</sup>  $^{13}\text{C}$  NMR (151 MHz, MeOD)  $\delta$  167.36, 161.84 (d,  $^1J_{\text{CF}} = 243.7$  Hz), 130.73 (d,  $^3J_{\text{CF}} = 8.3$  Hz), 130.49 (d,  $^3J_{\text{CF}} = 8.3$  Hz), 127.41 (d,  $^4J_{\text{CF}} = 2.4$  Hz), 117.89 (d,  $^2J_{\text{CF}} = 22.6$  Hz), 115.49 (d,  $^2J_{\text{CF}} = 20.9$  Hz), 57.85, 51.78, 47.63. MS (ES<sup>-</sup>),  $m/z$  260.2 (M - H).

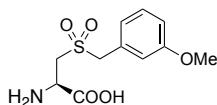
<sup>[a]</sup> The broad singlet observed at  $\delta$  8.77 ppm is attributed to  $-\text{COOH}$ .



**(R)-2-amino-3-((3-chlorobenzyl)sulfonyl)propanoic acid hydrochloride (4.4f):**

**General Procedure E** was followed using compound **4.3f** (288 mg, 0.76 mmol), to precipitate the title compound as the HCl salt as a fine off-white powder (158 mg, 66%).  $^1\text{H}$  NMR (600 MHz, DMSO)  $\delta$  8.91 (br s, 1H), 7.53 (s, 1H), 7.51–7.40 (m, 3H), 4.79 (d,  $J = 13.6$  Hz, 1H), 4.73 (d,  $J = 13.7$  Hz, 1H), 4.11 (dd,  $J = 7.1, 3.6$  Hz, 1H), 3.81 (dd,  $J = 15.2, 3.4$  Hz, 1H), 3.49 (dd,  $J = 15.0, 7.7$  Hz, 1H).<sup>[a]</sup>  $^{13}\text{C}$  NMR (151 MHz, DMSO)  $\delta$  167.60, 133.00, 130.90, 130.49, 130.38, 129.94, 128.56, 57.73, 51.88, 47.69. MS (ES<sup>-</sup>),  $m/z$  276.1 (M - H).

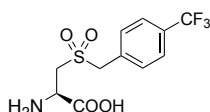
<sup>[a]</sup> The broad singlet observed at  $\delta$  8.91 ppm is attributed to  $-\text{COOH}$ .



**(R)-2-amino-3-((3-methoxybenzyl)sulfonyl)propanoic acid hydrochloride (4.4g):**

**General Procedure E** was followed using compound **4.3g** (238 mg, 0.64 mmol), to afford the title compound as the HCl salt as a pale orange powder (79 mg, 40%).  $^1\text{H}$  NMR (600 MHz, MeOD)  $\delta$  7.32 (t,  $J = 7.8$  Hz, 1H), 7.10–7.03 (m, 2H), 6.98 (d,  $J = 8.0$  Hz, 1H), 4.59 (d,  $J = 14.1$  Hz, 1H), 4.55 (d,  $J = 14.0$  Hz, 1H), 4.26 (ddd,  $J = 9.8, 2.5, 1.0$  Hz, 1H), 3.86 (ddd,  $J = 15.3, 2.6, 1.0$  Hz, 1H), 3.82 (s, 3H), 3.42 (dd,  $J = 15.0, 10.0$  Hz, 1H).  $^{13}\text{C}$  NMR (75 MHz, MeOD)  $\delta$  169.64, 161.48, 130.98, 130.21, 124.47, 117.72, 115.86, 60.59, 55.80, 52.09.<sup>[a]</sup> MS (ES<sup>-</sup>),  $m/z$  272.2 (M - H).

<sup>[a]</sup> One aliphatic peak is not observed, presumably due to overlap with the NMR solvent peak.

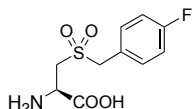


**(R)-2-amino-3-((4-(trifluoromethyl)benzyl)sulfonyl)propanoic acid hydrochloride (4.4h):**

**General Procedure E** was followed using compound **4.3h** (146 mg, 0.36 mmol), to precipitate the

title compound as the HCl salt as an off-white powder (97 mg, 78%).  $^1\text{H}$  NMR (600 MHz, DMSO)  $\delta$  8.75 (br s, 1H), 7.81 (d,  $J$  = 8.1 Hz, 2H), 7.68 (d,  $J$  = 8.1 Hz, 2H), 4.90 (d,  $J$  = 13.6 Hz, 1H), 4.86 (d,  $J$  = 13.6 Hz, 1H), 4.35 (dd,  $J$  = 6.3, 4.7 Hz, 1H), 3.86 (dd,  $J$  = 15.0, 4.2 Hz, 1H), 3.59 (dd,  $J$  = 15.0, 7.2 Hz, 1H).<sup>[a]</sup>  $^{13}\text{C}$  NMR (151 MHz, DMSO)  $\delta$  167.98, 132.69, 132.07, 129.07 (q,  $^2J_{\text{CF}}$  = 31.9 Hz), 125.41 (q,  $^3J_{\text{CF}}$  = 3.7 Hz), 124.12 (q,  $^1J_{\text{CF}}$  = 271.8 Hz), 58.1, 51.60, 47.35. MS ( $\text{ES}^-$ ),  $m/z$  310.0 ( $\text{M} - \text{H}$ ).

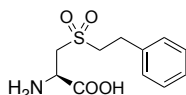
<sup>[a]</sup> The broad singlet observed at  $\delta$  8.75 ppm is attributed to  $-\text{COOH}$ .



**(R)-2-amino-3-((4-fluorobenzyl)sulfonyl)propanoic acid hydrochloride (4.4i):**

**General Procedure E** was followed using compound **4.3i** (303 mg, 0.84 mmol), to precipitate the title compound as the HCl salt as a fine white powder (165 mg, 66%).  $^1\text{H}$  NMR (600 MHz, DMSO)  $\delta$  7.60 (br s, 1H), 7.52–7.46 (m, 2H), 7.28–7.21 (m, 2H), 4.73 (d,  $J$  = 13.8 Hz, 1H), 4.63 (d,  $J$  = 13.7 Hz, 1H), 3.73 (dd,  $J$  = 15.1, 3.1 Hz, 1H), 3.66 (dd,  $J$  = 9.0, 2.9 Hz, 1H), 3.20 (dd,  $J$  = 14.9, 8.9 Hz, 1H). MS ( $\text{ES}^-$ ),  $m/z$  260.1 ( $\text{M} - \text{H}$ ).

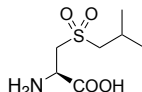
<sup>[a]</sup> The broad singlet observed at  $\delta$  7.60 ppm is attributed to  $-\text{COOH}$ .



**(R)-2-amino-3-(phenethylsulfonyl)propanoic acid hydrochloride (4.4j):**

**General Procedure E** was followed using compound **4.3j** (146 mg, 0.41 mmol), to precipitate the title compound as the HCl salt as a fine white powder (109 mg, 91%).  $^1\text{H}$  NMR (600 MHz, DMSO)  $\delta$  9.02 (br s, 1H), 7.36–7.29 (m, 4H), 7.27–7.21 (m, 1H), 4.32 (dd,  $J$  = 6.0, 4.8 Hz, 1H), 3.89 (dd,  $J$  = 15.2, 4.4 Hz, 1H), 3.68 (dd,  $J$  = 15.3, 6.9 Hz, 1H), 3.62 (td,  $J$  = 7.2, 2.9 Hz, 2H), 3.03 (dd,  $J$  = 9.7, 7.0 Hz, 2H).<sup>[a]</sup>  $^{13}\text{C}$  NMR (151 MHz, DMSO)  $\delta$  168.16, 137.94, 128.56, 128.50, 126.61, 53.87, 52.08, 47.53, 26.97. MS ( $\text{ES}^-$ ),  $m/z$  256.1 ( $\text{M} - \text{H}$ ).

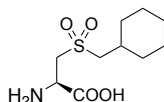
<sup>[a]</sup> The broad singlet observed at  $\delta$  9.02 ppm is attributed to  $-\text{COOH}$ .



**(R)-2-amino-3-(isobutylsulfonyl)propanoic acid hydrochloride (4.4k):**

**General Procedure E** was followed using compound **4.3k** (279 mg, 0.90 mmol), to precipitate the title compound as the HCl salt as a fine off-white powder (191 mg, 86%).  $^1\text{H}$  NMR (600 MHz, DMSO)  $\delta$  8.90 (br s, 1H), 4.34 (dd,  $J$  = 6.1, 5.1 Hz, 1H), 3.83 (dd,  $J$  = 15.2, 4.8 Hz, 1H), 3.67 (dd,  $J$  = 15.1, 6.5 Hz, 1H), 3.24 (d,  $J$  = 6.6 Hz, 2H), 2.22 (nonet,  $J$  = 6.7 Hz, 1H), 1.04 (d,  $J$  = 6.8 Hz, 6H).<sup>[a]</sup>  $^{13}\text{C}$  NMR (151 MHz, DMSO)  $\delta$  168.26, 60.06, 52.89, 47.41, 22.97, 22.35, 22.31. MS ( $\text{ES}^-$ ),  $m/z$  208.2 ( $\text{M} - \text{H}$ ).

<sup>[a]</sup> The broad singlet observed at  $\delta$  8.90 ppm is attributed to  $-\text{COOH}$ .

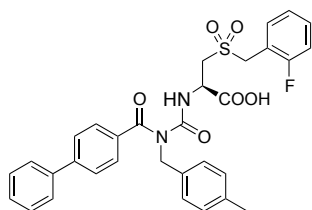


**(R)-2-amino-3-((cyclohexylmethyl)sulfonyl)propanoic acid hydrochloride (4.4l):**

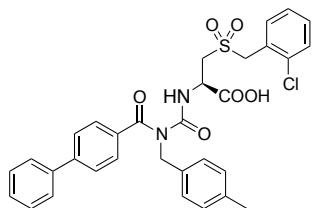
**General Procedure E** was followed using compound **4.3l** (261 mg, 0.75 mmol), to precipitate the title compound as the HCl salt as a fine off-white powder (165 mg, 77%).  $^1\text{H}$  NMR (300 MHz, MeOD)  $\delta$  4.57 (d,  $J$  = 6.6 Hz, 1H), 3.89 (d,  $J$  = 14.7 Hz, 1H), 3.60 (dd,  $J$  = 13.5, 9.0 Hz, 1H), 3.20 (d,  $J$  = 6.1 Hz, 2H), 2.09 (br s, 1H), 1.96 (d,  $J$  = 12.2 Hz, 2H), 1.72 (t,  $J$  = 16.7 Hz, 3H), 1.47–1.08 (m, 5H).  $^{13}\text{C}$  NMR (75 MHz, MeOD)  $\delta$  60.88, 53.77, 34.06, 34.02, 33.51, 26.88, 26.85.<sup>[a]</sup> MS ( $\text{ES}^-$ ),  $m/z$  248.3 ( $\text{M} - \text{H}$ ). HRMS ( $\text{ES}^+$  TOF) calculated for  $\text{C}_{10}\text{H}_{19}\text{NO}_4\text{S}$  ( $\text{M} + \text{H}$ ): 250.1108; found 250.1100.

<sup>[a]</sup> One peak is not observed due to overlap.

#### 4.6.1.1.4 Benzoylurea formation [Scheme 4.1 (f, g, h)]

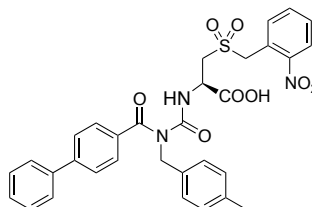


**(R)-2-(3-([1,1'-biphenyl]-4-carbonyl)-3-(4-methylbenzyl)ureido)-3-((2-fluorobenzyl)sulfonyl)propanoic acid (4.6a):** General Procedures A and B were followed using compound **3.3** (50 mg, 0.16 mmol), compound **4.4a** (70 mg, 0.24 mmol) and triethylamine (33  $\mu$ L, 0.24 mmol) to neutralise the amino acid HCl salt. Purification *via* flash chromatography, eluting with a gradient of methanol/dichloromethane (0:100 to 5:95) afforded the title compound as a pale yellow glass (81 mg, 87%).  $^1\text{H}$  NMR (600 MHz,  $\text{CDCl}_3$ )  $\delta$  9.89 (d,  $J$  = 6.9 Hz, 1H), 7.62–7.54 (m, 4H), 7.48–7.42 (m, 5H), 7.41–7.36 (m, 2H), 7.18 (td,  $J$  = 7.6, 1.1 Hz, 1H), 7.13 (ddd,  $J$  = 9.5, 8.3, 0.9 Hz, 1H), 7.03 (d,  $J$  = 7.9 Hz, 2H), 6.95 (d,  $J$  = 8.1 Hz, 2H), 5.03–4.95 (m, 3H), 4.36 (d,  $J$  = 14.1 Hz, 1H), 4.30 (d,  $J$  = 14.1 Hz, 1H), 3.74 (dd,  $J$  = 14.8, 4.3 Hz, 1H), 3.69 (dd,  $J$  = 14.8, 6.8 Hz, 1H), 2.25 (s, 3H).  $^{13}\text{C}$  NMR (151 MHz,  $\text{CDCl}_3$ )  $\delta$  175.27, 171.75, 161.28 (d,  $^1J_{\text{FC}}$  = 249.3 Hz), 155.60, 144.07, 139.90, 137.20, 134.34, 134.06, 133.09, 133.08, 131.46 (d,  $^3J_{\text{CF}}$  = 8.3 Hz), 129.46, 129.09, 128.26, 127.59, 127.29 (d,  $^3J_{\text{CF}}$  = 8.9 Hz), 126.63, 124.99 (d,  $^4J_{\text{CF}}$  = 3.3 Hz), 116.06 (d,  $^2J_{\text{CF}}$  = 21.6 Hz), 114.92 (d,  $^2J_{\text{CF}}$  = 14.5 Hz), 54.42, 52.54, 50.36, 49.68, 21.17. MS ( $\text{ES}^-$ ),  $m/z$  587.1, (M-H), 99% purity. HRMS ( $\text{ES}^+$  TOF) calculated for  $\text{C}_{32}\text{H}_{29}\text{FN}_2\text{O}_6\text{S}$  (M + H): 589.1803; found 589.1812.



**(R)-2-(3-([1,1'-biphenyl]-4-carbonyl)-3-(4-methylbenzyl)ureido)-3-((2-chlorobenzyl)sulfonyl)propanoic acid (4.6b):** General Procedures A and B were followed using compound **3.3** (50 mg, 0.16 mmol), compound **4.4b** (74 mg, 0.24 mmol) and triethylamine (33  $\mu$ L, 0.24 mmol) to neutralise the amino acid HCl salt. Purification *via* flash chromatography, eluting with a gradient of methanol/dichloromethane (0:100 to 5:95) afforded the title compound as a colourless glass (80 mg, 84%).  $^1\text{H}$  NMR (300 MHz,  $\text{CDCl}_3$ )  $\delta$  9.91 (d,  $J$  = 6.9 Hz, 1H), 7.56 (d,  $J$  = 8.1 Hz, 4H), 7.52–7.23 (m, 9H), 7.01 (d,  $J$  = 8.2 Hz, 2H), 6.95 (d,  $J$  = 8.2 Hz, 2H), 6.65 (br s, 1H), 5.07–4.90 (m, 3H), 4.54–4.35 (m, 2H), 3.88–3.68 (m, 2H), 2.22 (s, 3H).<sup>[a]</sup>  $^{13}\text{C}$  NMR (75 MHz,  $\text{CDCl}_3$ )  $\delta$  175.09, 171.99, 155.33, 143.86, 139.77, 137.02, 135.12, 134.25, 133.99, 133.21, 130.58, 130.05, 129.31, 128.94, 128.10, 127.47, 127.42, 127.17, 127.09, 126.56, 125.50, 57.94, 52.95, 50.20, 49.58, 21.01. MS ( $\text{ES}^+$ ),  $m/z$  605.9, (M+H), 98% purity. HRMS ( $\text{ES}^+$  TOF) calculated for  $\text{C}_{32}\text{H}_{29}\text{ClN}_2\text{O}_6\text{S}$  (M + H): 605.1508; found 605.1512.

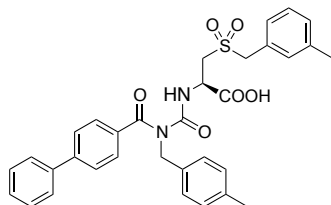
<sup>[a]</sup> The broad peak at  $\delta$  6.65 ppm is attributed to  $-\text{COOH}$ .



**(R)-2-(3-([1,1'-biphenyl]-4-carbonyl)-3-(4-methylbenzyl)ureido)-3-((2-nitrobenzyl)sulfonyl)propanoic acid (4.6c):** General Procedures A and B were followed using compound **3.3** (50 mg, 0.16 mmol), compound **4.4c** (77 mg, 0.24 mmol) and triethylamine (33  $\mu$ L, 0.24 mmol) to neutralise the amino acid HCl salt. Purification *via* flash chromatography, eluting with a gradient of methanol/dichloromethane (0:100 to 5:95) afforded the title compound as a pale yellow glass (85 mg, 87%).  $^1\text{H}$  NMR (300 MHz,  $\text{CDCl}_3$ )  $\delta$  9.87 (d,  $J$  = 6.8 Hz, 1H), 8.04 (dd,  $J$  = 7.8, 1.2 Hz, 1H), 7.56 (dd,  $J$  = 10.8, 7.2 Hz, 5H), 7.52–7.34 (m, 7H), 7.00 (d,  $J$  = 8.4 Hz, 2H), 6.96 (d,  $J$  = 8.3 Hz, 2H), 6.72 (br s, 1H), 5.07–4.92 (m, 3H), 4.80 (q,  $J$  = 13.5 Hz, 2H), 3.88 (dd,  $J$  = 15.1,

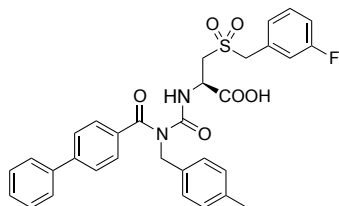
4.4 Hz, 1H), 3.80 (dd,  $J = 15.1, 6.5$  Hz, 1H), 2.19 (s, 3H).<sup>[a]</sup>  $^{13}\text{C}$  NMR (75 MHz,  $\text{CDCl}_3$ )  $\delta$  175.27, 171.80, 155.50, 149.69, 143.99, 139.85, 137.15, 134.62, 134.38, 134.05, 133.67, 130.34, 129.43, 129.06, 128.23, 127.62, 127.28, 127.22, 126.71, 125.80, 121.93, 57.17, 53.98, 50.37, 49.88, 21.10. MS ( $\text{ES}^+$ ),  $m/z$  616.7, ( $\text{M}+\text{H}$ ), 98% purity. HRMS ( $\text{ES}^+$  TOF) calculated for  $\text{C}_{32}\text{H}_{29}\text{N}_3\text{O}_8\text{S}$  ( $\text{M} + \text{H}$ ): 616.1748; found 616.1754.

<sup>[a]</sup> The broad peak at  $\delta$  6.72 ppm is attributed to  $-\text{COOH}$ .



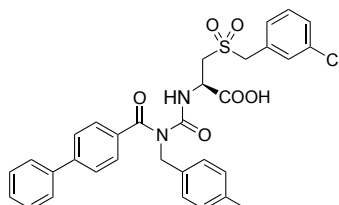
**(R)-2-(3-([1,1'-biphenyl]-4-carbonyl)-3-(4-methylbenzyl)ureido)-3-((3-methylbenzyl)sulfonyl)propanoic acid (4.6d):** General Procedures A and B were followed using compound 3.3 (50 mg, 0.16 mmol), compound 4.4d (69 mg, 0.24 mmol) and triethylamine (33  $\mu\text{L}$ , 0.24 mmol) to neutralise the amino acid HCl salt. Purification *via* flash chromatography, eluting with a gradient of methanol/dichloromethane (0:100 to 5:95) afforded the title compound as a pale orange glass (84 mg, 91%).  $^1\text{H}$  NMR (300 MHz,  $\text{CDCl}_3$ )  $\delta$  9.89 (d,  $J = 7.1$  Hz, 1H), 7.56 (d,  $J = 8.2$  Hz, 4H), 7.51–7.32 (m, 5H), 7.32–6.99 (m, 8H), 7.06 (br s, 1H), 6.95 (d,  $J = 8.1$  Hz, 2H), 5.10–4.86 (m, 3H), 4.22 (s, 2H), 3.75–3.55 (m, 2H), 2.33 (s, 3H), 2.24 (s, 3H).<sup>[a]</sup>  $^{13}\text{C}$  NMR (75 MHz,  $\text{CDCl}_3$ )  $\delta$  175.18, 172.01, 155.40, 143.89, 139.75, 138.78, 137.03, 134.27, 133.97, 131.62, 129.93, 129.35, 128.94, 128.88, 128.11, 128.01, 127.46, 127.17, 127.09, 126.96, 126.46, 61.08, 51.94, 50.21, 49.62, 21.31, 21.01. MS ( $\text{ES}^+$ ),  $m/z$  589.5, ( $\text{M}+\text{H}$ ), 99% purity. HRMS ( $\text{ES}^+$  TOF) calculated for  $\text{C}_{33}\text{H}_{32}\text{N}_2\text{O}_6\text{S}$  ( $\text{M} + \text{H}$ ): 585.2054; found 585.2059.

<sup>[a]</sup> The broad peak at  $\delta$  7.06 ppm is attributed to  $-\text{COOH}$ .



**(R)-2-(3-([1,1'-biphenyl]-4-carbonyl)-3-(4-methylbenzyl)ureido)-3-((3-fluorobenzyl)sulfonyl)propanoic acid (4.6e):** General Procedures A and B were followed using compound 3.3 (50 mg, 0.16 mmol), compound 4.4e (70 mg, 0.24 mmol) and triethylamine (33  $\mu\text{L}$ , 0.24 mmol) to neutralise the amino acid HCl salt. Purification *via* flash chromatography, eluting with a gradient of methanol/dichloromethane (0:100 to 5:95) afforded the title compound as a colourless glass (64 mg, 69%).  $^1\text{H}$  NMR (300 MHz,  $\text{CDCl}_3$ )  $\delta$  9.93 (d,  $J = 6.9$  Hz, 1H), 7.63–7.51 (m, 4H), 7.50–7.27 (m, 6H), 7.20–7.05 (m, 3H), 7.02 (d,  $J = 7.9$  Hz, 2H), 6.95 (d,  $J = 8.1$  Hz, 1H), 6.33 (s, 1H), 5.08–4.91 (m, 3H), 4.22 (s, 2H), 3.73 (dd,  $J = 15.0, 4.5$  Hz, 1H), 3.65 (dd,  $J = 15.0, 6.5$  Hz, 1H), 2.23 (s, 3H).<sup>[a]</sup>  $^{13}\text{C}$  NMR (75 MHz,  $\text{CDCl}_3$ )  $\delta$  175.40, 171.84, 164.48, 161.20, 155.50, 144.10, 139.84, 135.62 (d,  $^1J_{\text{CF}} = 245.1$  Hz), 134.36, 130.63 (d,  $^3J_{\text{CF}} = 8.3$  Hz), 129.49, 129.38 (d,  $^3J_{\text{CF}} = 8.0$  Hz), 129.08, 128.27, 127.60, 127.30, 127.26, 126.91 (d,  $^4J_{\text{CF}} = 3.1$  Hz), 126.59, 118.17 (d,  $^2J_{\text{CF}} = 22.3$  Hz), 116.34 (d,  $^2J_{\text{CF}} = 21.0$  Hz), 60.59, 52.50, 50.41, 49.81, 21.12. MS ( $\text{ES}^+$ ),  $m/z$  589.5, ( $\text{M}+\text{H}$ ), 97% purity. HRMS ( $\text{ES}^+$  TOF) calculated for  $\text{C}_{32}\text{H}_{29}\text{FN}_2\text{O}_6\text{S}$  ( $\text{M} + \text{H}$ ): 589.1803; found 589.1807.

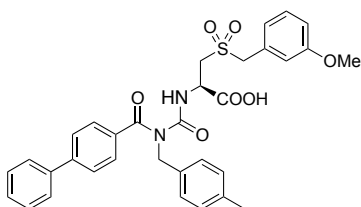
<sup>[a]</sup> The broad peak at  $\delta$  6.33 ppm is attributed to  $-\text{COOH}$ .



**(R)-2-(3-([1,1'-biphenyl]-4-carbonyl)-3-(4-methylbenzyl)ureido)-3-((3-chlorobenzyl)sulfonyl)propanoic acid (4.6f):** General Procedures A and B were followed using compound 3.3 (50 mg, 0.16 mmol), compound 4.4f (74 mg, 0.24 mmol) and triethylamine (33  $\mu\text{L}$ ,

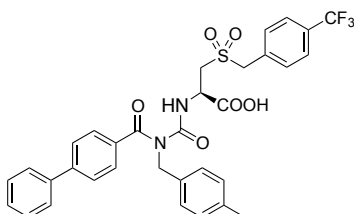
0.24 mmol) to neutralise the amino acid HCl salt. Purification *via* flash chromatography, eluting with a gradient of methanol/dichloromethane (0:100 to 5:95) afforded the title compound as a colourless glass (61 mg, 64%).  $^1\text{H}$  NMR (300 MHz,  $\text{CDCl}_3$ )  $\delta$  9.93 (d,  $J$  = 6.9 Hz, 1H), 7.62–7.52 (m, 4H), 7.49–7.21 (m, 11H), 7.02 (d,  $J$  = 8.1 Hz, 2H), 6.95 (d,  $J$  = 8.1 Hz, 2H), 6.55 (s, 1H), 5.07–4.90 (m, 3H), 4.19 (s, 2H), 3.70 (qd,  $J$  = 15.0, 5.5 Hz, 2H), 2.22 (s, 3H).<sup>[a]</sup>  $^{13}\text{C}$  NMR (75 MHz,  $\text{CDCl}_3$ )  $\delta$  175.26, 171.67, 155.36, 143.99, 139.69, 137.13, 134.74, 134.22, 133.83, 131.01, 130.17, 129.36, 129.21, 128.95, 128.15, 127.48, 127.16, 126.46, 60.35, 52.47, 50.29, 49.72, 20.99. MS ( $\text{ES}^+$ ),  $m/z$  605.7, ( $\text{M}+\text{H}$ ), 99% purity. HRMS ( $\text{ES}^+$  TOF) calculated for  $\text{C}_{32}\text{H}_{29}\text{ClN}_2\text{O}_6\text{S}$  ( $\text{M} + \text{H}$ ): 605.1508; found 605.1514.

<sup>[a]</sup> The broad peak at  $\delta$  6.55 ppm is attributed to  $-\text{COOH}$ .

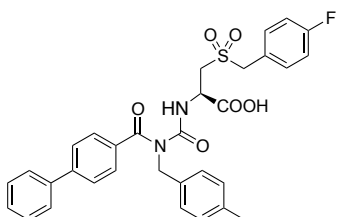


**(R)-2-(3-([1,1'-biphenyl]-4-carbonyl)-3-(4-methylbenzyl)ureido)-3-((3-methoxybenzyl)sulfonyl)propanoic acid (4.6g):** General Procedures A and B were followed using compound **3.3** (50 mg, 0.16 mmol), compound **4.4g** (73 mg, 0.24 mmol) and triethylamine (33  $\mu\text{L}$ , 0.24 mmol) to neutralise the amino acid HCl salt. Purification *via* flash chromatography, eluting with a gradient of methanol/dichloromethane (0:100 to 5:95) afforded the title compound as a yellowish colourless glass (56 mg, 59%).  $^1\text{H}$  NMR (300 MHz,  $\text{CDCl}_3$ )  $\delta$  9.89 (d,  $J$  = 6.9 Hz, 1H), 7.64–7.52 (m, 4H), 7.50–7.23 (m, 8H), 7.04 (d,  $J$  = 8.0 Hz, 2H), 6.98–6.88 (m, 4H), 5.09–4.89 (m, 3H), 4.40 (br s, 1H), 4.24 (s, 2H), 3.79 (s,  $J$  = 7.1 Hz, 3H), 3.65 (ddd,  $J$  = 21.6, 11.7, 5.9 Hz), 2.26 (s, 3H).<sup>[a]</sup>  $^{13}\text{C}$  NMR (75 MHz,  $\text{CDCl}_3$ )  $\delta$  175.17, 171.30, 159.93, 155.48, 143.96, 139.74, 137.09, 134.20, 133.90, 130.06, 129.36, 128.95, 128.49, 128.13, 127.43, 127.16, 127.11, 126.43, 123.13, 116.26, 115.02, 61.23, 55.34, 51.82, 50.20, 49.63, 21.02. MS ( $\text{ES}^+$ ),  $m/z$  601.6, ( $\text{M}+\text{H}$ ), 98% purity. HRMS ( $\text{ES}^+$  TOF) calculated for  $\text{C}_{33}\text{H}_{32}\text{N}_2\text{O}_7\text{S}$  ( $\text{M} + \text{H}$ ): 601.2003; found 601.1995.

<sup>[a]</sup> The broad peak at  $\delta$  4.40 ppm is attributed to  $-\text{COOH}$ .



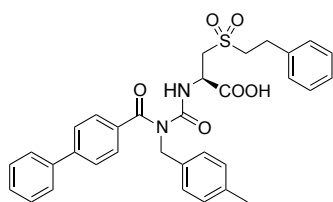
**(R)-2-(3-([1,1'-biphenyl]-4-carbonyl)-3-(4-methylbenzyl)ureido)-3-((4-(trifluoromethyl)benzyl)sulfonyl)propanoic acid (4.6h):** General Procedures A and B were followed using compound **3.3** (50 mg, 0.16 mmol), compound **4.4h** (52 mg, 0.148 mmol) and triethylamine (21  $\mu\text{L}$ , 0.148 mmol) to neutralise the amino acid HCl salt. Purification *via* flash chromatography, eluting with a gradient of methanol/dichloromethane (0:100 to 5:95) afforded the title compound as a pale orange glass (65 mg, 69%).  $^1\text{H}$  NMR (300 MHz,  $\text{CDCl}_3$ )  $\delta$  9.98 (d,  $J$  = 6.6 Hz, 1H), 7.63–7.52 (m, 6H), 7.51–7.35 (m, 7H), 7.01 (d,  $J$  = 8.0 Hz, 2H), 6.95 (d,  $J$  = 8.1 Hz, 2H), 6.41 (br s, 1H), 5.11–4.90 (m, 3H), 4.28 (s, 2H), 3.86–3.60 (m, 2H), 2.20 (s, 3H).  $^{13}\text{C}$  NMR (75 MHz,  $\text{CDCl}_3$ )  $\delta$  175.54, 171.83, 155.52, 144.23, 139.74, 137.33, 134.33, 133.86, 131.65, 131.58, 131.55, 131.06 (q,  $^3J_{\text{CF}}$  = 4.0 Hz), 129.51, 129.10, 128.33, 127.61, 127.30, 127.28, 126.59, 125.94 (q,  $^2J_{\text{CF}}$  = 30.0 Hz), 125.78, 123.97 (q,  $^1J_{\text{CF}}$  = 272.4 Hz). MS ( $\text{ES}^+$ ),  $m/z$  639.4, ( $\text{M}+\text{H}$ ), 99% purity. HRMS ( $\text{ES}^+$  TOF) calculated for  $\text{C}_{33}\text{H}_{29}\text{F}_3\text{N}_2\text{O}_6\text{S}$  ( $\text{M} + \text{H}$ ): 639.1771; found 639.1776.



**(R)-2-(3-([1,1'-biphenyl]-4-carbonyl)-3-(4-methylbenzyl)ureido)-3-((4-fluorobenzyl)sulfonyl)propanoic acid (4.6i):** General Procedures A and B were followed using compound **3.3** (50 mg, 0.16 mmol), compound **4.4i** (70 mg, 0.24 mmol) and triethylamine (33  $\mu$ L, 0.24 mmol) to neutralise the amino acid HCl salt. Purification *via* flash chromatography, eluting with a gradient of methanol/dichloromethane (0:100 to 5:95) afforded the title compound as a colourless glass (53 mg, 57%).  $^1\text{H}$  NMR (300 MHz,  $\text{CDCl}_3$ )  $\delta$  9.92 (d,  $J$  = 6.6 Hz, 1H), 7.63–7.51 (m, 4H), 7.51–7.23 (m, 8H), 7.08–6.99 (m, 4H), 6.95 (d,  $J$  = 8.1 Hz, 2H), 5.23 (br s, 1H), 5.09–4.88 (m, 1H), 4.21 (s, 1H), 3.66 (qd,  $J$  = 15.0, 5.5 Hz, 1H), 2.24 (s, 1H).<sup>[a]</sup>  $^{13}\text{C}$  NMR (75 MHz,  $\text{CDCl}_3$ )  $\delta$  175.41, 171.76, 163.42 (d,  $^1J_{\text{CF}}$  = 249.1 Hz), 155.56, 144.20, 139.83, 137.30, 134.35, 133.95, 132.98 (d,  $^3J_{\text{CF}}$  = 8.6 Hz), 129.52, 129.11, 128.31, 127.62, 127.31, 126.61, 122.98 (d,  $^4J_{\text{CF}}$  = 3.1 Hz), 116.23 (d,  $^2J_{\text{CF}}$  = 21.8 Hz), 60.31, 52.22, 50.44, 49.82, 21.15.<sup>[b]</sup> MS ( $\text{ES}^+$ ),  $m/z$  589.6, ( $\text{M}+\text{H}$ ), 99% purity. HRMS ( $\text{ES}^+$  TOF) calculated for  $\text{C}_{32}\text{H}_{29}\text{FN}_2\text{O}_6\text{S}$  ( $\text{M} + \text{H}$ ): 589.1803; found 589.1806.

<sup>[a]</sup> The broad peak at  $\delta$  5.23 ppm is attributed to  $-\text{COOH}$ .

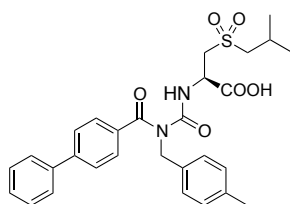
<sup>[b]</sup> One aromatic peak is not observed due to overlap.



**(R)-2-(3-([1,1'-biphenyl]-4-carbonyl)-3-(4-methylbenzyl)ureido)-3-(phenethylsulfonyl)propanoic acid (4.6j):** General Procedures A and B were followed using compound **3.3** (50 mg, 0.16 mmol), compound **4.4j** (69 mg, 0.24 mmol) and triethylamine (33  $\mu$ L, 0.24 mmol) to neutralise the amino acid HCl salt. Purification *via* flash chromatography, eluting with a gradient of methanol/dichloromethane (0:100 to 5:95) afforded the title compound as a pale yellow glass (79 mg, 86%).  $^1\text{H}$  NMR (300 MHz,  $\text{CDCl}_3$ )  $\delta$  9.93 (d,  $J$  = 6.8 Hz, 1H), 7.63–7.51 (m, 4H), 7.49–7.34 (m, 5H), 7.33–7.15 (m, 5H), 7.00 (d,  $J$  = 7.9 Hz, 2H), 6.89 (d,  $J$  = 8.0 Hz, 2H), 5.37 (br s, 1H), 5.01–4.93 (m, 3H), 3.79–3.63 (m, 2H), 3.39–3.27 (m, 2H), 3.13 (dd,  $J$  = 10.2, 6.0 Hz, 2H), 2.26 (s, 3H).<sup>[a]</sup>  $^{13}\text{C}$  NMR (75 MHz,  $\text{CDCl}_3$ )  $\delta$  175.42, 171.70, 155.47, 144.06, 139.86, 137.55, 137.18, 134.31, 134.02, 129.47, 129.10, 129.08, 128.64, 128.28, 127.51, 127.31, 127.23, 126.51, 56.30, 53.51, 50.30, 49.81, 27.97, 21.18.<sup>[b]</sup> MS ( $\text{ES}^+$ ),  $m/z$  585.5, ( $\text{M}+\text{H}$ ), 99% purity. HRMS ( $\text{ES}^+$  TOF) calculated for  $\text{C}_{33}\text{H}_{32}\text{N}_2\text{O}_6\text{S}$  ( $\text{M} + \text{H}$ ): 585.2054; found 585.2059.

<sup>[a]</sup> The broad peak at  $\delta$  5.37 ppm is attributed to  $-\text{COOH}$ .

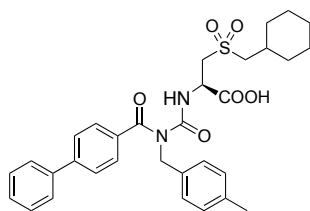
<sup>[b]</sup> One aromatic peak is not observed due to overlap.



**(R)-2-(3-([1,1'-biphenyl]-4-carbonyl)-3-(4-methylbenzyl)ureido)-3-(isobutylsulfonyl)propanoic acid (4.6k):** General Procedures A and B were followed using compound **3.3** (50 mg, 0.16 mmol), compound **4.4k** (58 mg, 0.24 mmol) and triethylamine (33  $\mu$ L, 0.24 mmol) to neutralise the amino acid HCl salt. Purification *via* flash chromatography, eluting with a gradient of methanol/dichloromethane (0:100 to 5:95) afforded the title compound as a pale orange glass (77 mg, 91%).  $^1\text{H}$  NMR (300 MHz,  $\text{CDCl}_3$ )  $\delta$  9.89 (d,  $J$  = 7.0 Hz, 1H), 7.57 (d,  $J$  = 8.4 Hz, 4H), 7.51–7.32 (m, 5H), 7.06 (d,  $J$  = 7.9 Hz, 2H), 6.95 (d,  $J$  = 8.1 Hz, 2H), 6.76 (br s, 1H), 5.09–4.87 (m, 3H), 3.85–3.59 (m, 2H), 2.95 (d,  $J$  = 6.6 Hz, 2H), 2.38 (nonet,  $J$  = 6.7 Hz, 1H), 2.29 (s, 3H), 1.09 (d,  $J$  = 6.7 Hz, 3H), 1.08 (d,  $J$  = 6.7 Hz, 3H).  $^{13}\text{C}$  NMR (75 MHz,  $\text{CDCl}_3$ )  $\delta$  175.20, 171.85, 155.33, 143.85, 139.74, 137.02, 134.30, 134.01, 129.34, 128.95, 128.11, 127.40, 127.16, 127.08, 126.49, 62.19, 54.28, 50.11, 49.62, 23.56, 22.73, 21.06. MS ( $\text{ES}^+$ ),  $m/z$  537.5, ( $\text{M}+\text{H}$ ), 99% purity. HRMS ( $\text{ES}^+$  TOF) calculated for  $\text{C}_{29}\text{H}_{32}\text{N}_2\text{O}_6\text{S}$  ( $\text{M} + \text{H}$ ): 537.2054; found 537.2057.

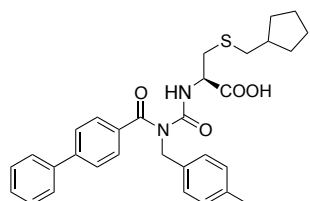
<sup>[a]</sup> The broad peak at  $\delta$  6.76 ppm is attributed to  $-\text{COOH}$ .





**(R)-2-(3-([1,1'-biphenyl]-4-carbonyl)-3-(4-methylbenzyl)ureido)-3-**

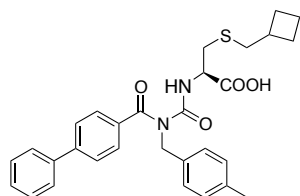
**((cyclohexylmethyl)sulfonyl)propanoic acid (4.6l):** General Procedures A and B were followed using compound **3.3** (50 mg, 0.17 mmol), compound **4.4l** (67 mg, 0.24 mmol) and triethylamine (33  $\mu$ L, 0.24 mmol) to neutralise the amino acid HCl salt. Purification *via* flash chromatography, eluting with a gradient of methanol/dichloromethane (0:100 to 5:95) afforded the title compound as a colourless glass (85 mg, 94%).  $^1\text{H}$  NMR (600 MHz,  $\text{CDCl}_3$ )  $\delta$  9.89 (d,  $J$  = 6.8 Hz, 1H), 9.76 (br s, 1H), 7.57 (d,  $J$  = 7.9 Hz, 4H), 7.48–7.36 (m, 5H), 7.06 (d,  $J$  = 7.7 Hz, 2H), 6.95 (d,  $J$  = 7.7 Hz, 2H), 5.09–4.91 (m, 3H), 3.72 (qd,  $J$  = 14.8, 5.4 Hz, 2H), 2.94 (d,  $J$  = 6.4 Hz, 2H), 2.29 (s, 3H), 2.14–2.04 (m, 1H), 1.91 (d,  $J$  = 12.1 Hz, 2H), 1.69 (dd,  $J$  = 12.6, 2.5 Hz, 2H), 1.64 (dd,  $J$  = 12.8 Hz, 1H), 1.30 (ddd,  $J$  = 25.5, 12.6, 2.6 Hz, 2H), 1.14 (ddt,  $J$  = 25.1, 12.6, 3.3 Hz, 1H), 1.06 (dd,  $J$  = 24.0, 12.1 Hz, 2H).  $^{13}\text{C}$  NMR (151 MHz,  $\text{CDCl}_3$ )  $\delta$  175.26, 172.45, 155.46, 143.96, 139.86, 137.12, 134.43, 134.14, 129.45, 129.06, 128.22, 127.52, 127.28, 127.19, 126.60, 61.28, 54.51, 50.22, 49.84, 33.23, 32.29, 25.86, 25.82, 21.20. MS ( $\text{ES}^+$ ),  $m/z$  577.9, ( $\text{M}+\text{H}$ ), 99% purity. HRMS ( $\text{ES}^+$  TOF) calculated for  $\text{C}_{32}\text{H}_{36}\text{N}_2\text{O}_6\text{S}$  ( $\text{M} + \text{H}$ ): 577.2367; found 577.2375.



**(R)-2-(3-([1,1'-biphenyl]-4-carbonyl)-3-(4-methylbenzyl)ureido)-3-**

**((cyclopentylmethyl)thio)propanoic acid (4.8m):** General Procedures A and B were followed using compound **3.3** (27 mg, 0.085 mmol), compound **4.2m** (20 mg, 0.085 mmol) and triethylamine (12  $\mu$ L, 0.085 mmol) to neutralise the amino acid HCl salt. Purification *via* flash chromatography, eluting with a gradient of methanol/dichloromethane (0:100 to 5:95) afforded the title compound as a colourless glass (25 mg, 56%).  $^1\text{H}$  NMR (300 MHz,  $\text{CDCl}_3$ )  $\delta$  9.68 (d,  $J$  = 6.9 Hz, 1H), 7.59 (d,  $J$  = 8.1 Hz, 4H), 7.52–7.31 (m, 5H), 7.08 (d,  $J$  = 8.0 Hz, 2H), 6.96 (d,  $J$  = 8.0 Hz, 2H), 6.86 (br s, 1H), 5.01 (s, 2H), 4.81 (dd,  $J$  = 11.8, 6.5 Hz, 1H), 3.13 (dd,  $J$  = 14.0, 5.1 Hz, 1H), 3.05 (dd,  $J$  = 13.9, 6.4 Hz, 1H), 2.60 (d,  $J$  = 7.4 Hz, 2H), 2.31 (s, 3H), 2.14–1.96 (m, 1H), 1.88–1.72 (m, 2H), 1.71–1.47 (m, 4H), 1.33–1.14 (m, 1H).<sup>[a]</sup>  $^{13}\text{C}$  NMR (75 MHz,  $\text{CDCl}_3$ )  $\delta$  175.21, 175.19, 155.33, 143.84, 139.96, 137.08, 134.67, 134.53, 129.42, 129.08, 128.21, 127.41, 127.30, 127.22, 126.65, 53.91, 50.13, 39.95, 39.17, 34.23, 32.46, 32.41, 25.35, 25.32, 21.21. MS ( $\text{ES}^+$ ),  $m/z$  529.2, ( $\text{M}+\text{H}$ ), 99% purity. HRMS ( $\text{ES}^+$  TOF) calculated for  $\text{C}_{32}\text{H}_{36}\text{N}_2\text{O}_6\text{S}$  ( $\text{M} + \text{H}$ ): 531.2312; found 531.2326.

<sup>[a]</sup> The broad peak at  $\delta$  6.86 ppm is attributed to  $-\text{COOH}$ .



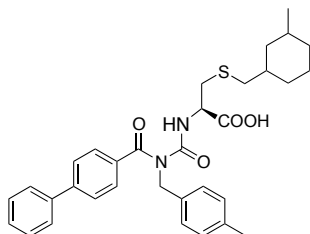
**(R)-2-(3-([1,1'-biphenyl]-4-carbonyl)-3-(4-methylbenzyl)ureido)-3-**

**((cyclobutylmethyl)thio)propanoic acid (4.8n):** General Procedures A and B were followed using compound **3.3** (63 mg, 0.20 mmol), compound **4.2n** (68 mg, 0.30 mmol) and triethylamine (83  $\mu$ L, 0.6 mmol) to neutralise the amino acid HCl salt. Purification *via* flash chromatography, eluting with a gradient of methanol/dichloromethane (0:100 to 5:95) afforded the title compound as a colourless glass (18 mg, 34%).  $^1\text{H}$  NMR (300 MHz,  $\text{CDCl}_3$ )  $\delta$  9.67 (d,  $J$  = 6.9 Hz, 1H), 7.63–7.54 (m, 4H), 7.50–7.34 (m, 5H), 7.07 (d,  $J$  = 7.8 Hz, 2H), 6.95 (d,  $J$  = 8.1 Hz, 2H), 5.00 (s, 2H), 4.78 (td,  $J$  = 6.5, 5.1 Hz, 1H), 4.54 (br s, 1H), 3.19–2.96 (m, 2H), 2.66 (d,  $J$  = 7.6 Hz, 2H), 2.49 (app sept.,  $J$  = 7.6 Hz, 1H), 2.30 (s, 3H), 2.17–2.03 (m, 2H), 1.93–1.78 (m, 2H), 1.78–1.61 (m, 2H).<sup>[a]</sup>

$^{13}\text{C}$  NMR (75 MHz,  $\text{CDCl}_3$ )  $\delta$  175.25, 174.27, 155.43, 143.89, 139.96, 137.12, 134.66, 134.51, 129.44, 129.09, 128.24, 127.42, 127.32, 127.25, 126.66, 53.89, 50.16, 39.34, 35.44, 33.69, 28.14, 28.09, 21.22, 18.16.<sup>[b]</sup> MS ( $\text{ES}^+$ ),  $m/z$  517.3, ( $\text{M}+\text{H}$ ), 98% purity. HRMS ( $\text{ES}^+$  TOF) calculated for  $\text{C}_{32}\text{H}_{36}\text{N}_2\text{O}_6\text{S}$  ( $\text{M} + \text{H}$ ): 517.2156; found 517.2163.

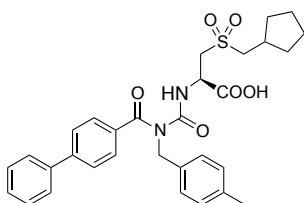
<sup>[a]</sup> The broad peak at  $\delta$  4.54 ppm is attributed to  $-\text{COOH}$ .

<sup>[b]</sup> One additional peak is observed in the aliphatic region due to apparent peak splitting.

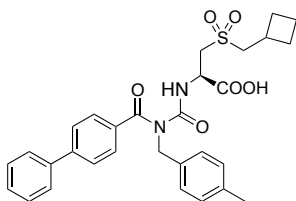


**(2R)-2-(3-([1,1'-biphenyl]-4-carbonyl)-3-(4-methylbenzyl)ureido)-3-(((3-methylcyclohexyl)methyl)thio)propanoic acid (4.8o):** General Procedures A and B were followed using compound 3.3 (27 mg, 0.085 mmol), compound 4.2o (23 mg, 0.085 mmol) and triethylamine (12  $\mu\text{L}$ , 0.085 mmol) to neutralise the amino acid HCl salt. Purification *via* flash chromatography, eluting with a gradient of methanol/dichloromethane (0:100 to 5:95) afforded the title compound as an inseparable mixture of diastereomers as a colourless glass (20 mg, 42%).  $^1\text{H}$  NMR (300 MHz,  $\text{CDCl}_3$ )  $\delta$  9.72–9.63 (m,  $J$  = 2.6 Hz, 1H), 7.62–7.55 (m, 4H), 7.52–7.34 (m, 5H), 7.07 (d,  $J$  = 7.9 Hz, 2H), 6.95 (d,  $J$  = 8.1 Hz, 2H), 5.00 (s, 2H), 4.85–4.72 (m, 1H), 3.63 (br s, 1H), 3.19–2.91 (m, 2H), 2.65–2.53 (m, 1H), 2.53–2.35 (m, 1H), 2.30 (s, 3H), 1.90–1.06 (m, 9H), 0.99–0.65 (m, 4H).<sup>[a]</sup>  $^{13}\text{C}$  NMR (75 MHz,  $\text{CDCl}_3$ )  $\delta$  175.23, 173.28, 155.50, 143.90, 139.96, 137.13, 134.66, 134.49, 129.45, 129.10, 128.25, 127.42, 127.32, 127.25, 126.66, 53.87, 50.16, 41.60, 41.54, 40.67, 38.54, 38.44, 38.18, 35.18, 34.41, 34.11, 33.75, 32.85, 32.70, 32.49, 32.43, 30.98, 30.86, 27.31, 27.29, 26.18, 22.92, 21.22, 20.82, 20.79. MS ( $\text{ES}^+$ ),  $m/z$  559.42, ( $\text{M}+\text{H}$ ), 99% purity. HRMS ( $\text{ES}^+$  TOF) calculated for  $\text{C}_{32}\text{H}_{36}\text{N}_2\text{O}_6\text{S}$  ( $\text{M} + \text{H}$ ): 559.2625; found 559.2627.

<sup>[a]</sup> The mixture of diastereomers was integrated as a single compound for the purposes of NMR analysis. The broad peak at  $\delta$  3.63 ppm is attributed to  $-\text{COOH}$ .

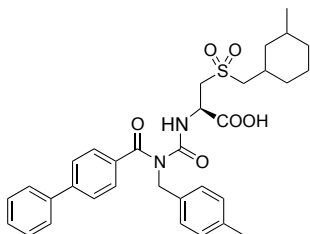


**(R)-2-(3-([1,1'-biphenyl]-4-carbonyl)-3-(4-methylbenzyl)ureido)-3-((cyclopentylmethyl)sulfonyl)propanoic acid (4.6m):** Compound 4.8m (22 mg, 0.041 mmol) was oxidised according to General Procedure D, but allowing the final step proceed for 1.5 h. Purification *via* flash chromatography, eluting with a gradient of methanol/dichloromethane (0:100 to 5:95), afforded the title compound as a colourless glass (14 mg, 60%).  $^1\text{H}$  NMR (300 MHz,  $\text{CDCl}_3$ )  $\delta$  9.86 (d,  $J$  = 3.6 Hz, 1H), 7.56 (d,  $J$  = 8.0 Hz, 4H), 7.49–7.34 (m, 5H), 7.05 (d,  $J$  = 7.9 Hz, 2H), 6.94 (d,  $J$  = 7.9 Hz, 2H), 5.14–4.85 (m, 3H), 3.74 (dd,  $J$  = 22.3, 19.9 Hz, 2H), 3.39 (br s, 1H), 3.09 (d,  $J$  = 6.8 Hz, 2H), 2.51–2.24 (m, 4H), 2.02–1.88 (m, 2H), 1.71–1.41 (m, 4H), 1.33–1.16 (m, 2H).  $^{13}\text{C}$  NMR (75 MHz,  $\text{CDCl}_3$ )  $\delta$  175.26, 172.10, 155.50, 143.96, 139.92, 137.14, 134.52, 134.23, 129.46, 129.09, 128.24, 127.54, 127.31, 127.22, 126.63, 60.32, 54.24, 50.21, 33.83, 32.88, 32.87, 24.83, 21.21. MS ( $\text{ES}^-$ ),  $m/z$  560.9, ( $\text{M}-\text{H}$ ), 98% purity. HRMS ( $\text{ES}^+$  TOF) calculated for  $\text{C}_{31}\text{H}_{34}\text{N}_2\text{O}_6\text{S}$  ( $\text{M} + \text{H}$ ): 563.2210; found 563.2215.



**(R)-2-(3-([1,1'-biphenyl]-4-carbonyl)-3-(4-methylbenzyl)ureido)-3-((cyclobutylmethyl)sulfonyl)propanoic acid (4.6n):** Compound 4.8n (12 mg, 0.023 mmol) was

oxidised according to **General Procedure D**, but allowing the final step proceed for 1.5 h. The reaction mixture was concentrated directly onto silica and purified *via* flash chromatography, eluting with a gradient of methanol/dichloromethane (0:100 to 5:95), to afford the title compound as a colourless glass (5 mg, 38%). <sup>1</sup>H NMR (600 MHz, MeOD)  $\delta$  7.64 (d,  $J$  = 7.7 Hz, 4H), 7.50 (d,  $J$  = 7.8 Hz, 2H), 7.45 (t,  $J$  = 7.2 Hz, 2H), 7.37 (t,  $J$  = 7.3 Hz, 1H), 7.09 (d,  $J$  = 7.8 Hz, 2H), 7.05 (d,  $J$  = 7.7 Hz, 2H), 5.02 (d,  $J$  = 16.3 Hz, 1H), 4.96 (d,  $J$  = 16.4 Hz, 1H), 4.77 (dd,  $J$  = 6.1, 4.0 Hz, 1H), 3.68 (dd,  $J$  = 14.7, 3.1 Hz, 1H), 3.56 (dd,  $J$  = 14.6, 7.3 Hz, 1H), 3.22 (d,  $J$  = 7.1 Hz, 2H), 2.86 (app sept.,  $J$  = 7.8 Hz, 1H), 2.29 (s, 3H), 2.21–2.12 (m, 2H), 2.02–1.81 (m, 4H).<sup>[a]</sup> MS (ES<sup>-</sup>),  $m/z$  547.1, (M-H), 96% purity. HRMS (ES<sup>+</sup> TOF) calculated for C<sub>30</sub>H<sub>32</sub>N<sub>2</sub>O<sub>6</sub>S (M + H): 549.2054; found 549.2059. <sup>[a]</sup> Peaks observed at  $\delta$  7.98, 7.94 and 7.58 ppm and at  $\delta$  1.29 ppm are due to minor 3-chlorobenzoic acid and grease impurities respectively.

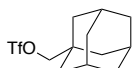


**(2R)-2-(3-([1,1'-biphenyl]-4-carbonyl)-3-(4-methylbenzyl)ureido)-3-((3-methylcyclohexyl)methyl)sulfonylpropanoic acid (4.6o):** Compound **4.8o** (10 mg, 0.018 mmol) was oxidised according to **General Procedure D**, but allowing the final step proceed for 1.5 h. Purification *via* flash chromatography, eluting with a gradient of methanol/dichloromethane (0:100 to 5:95), afforded the title compound as a colourless glass (6 mg, 52%). <sup>1</sup>H NMR (600 MHz, MeOD)  $\delta$  7.67–7.61 (m, 4H), 7.52–7.42 (m, 4H), 7.37 (t,  $J$  = 7.4 Hz, 1H), 7.08 (dd,  $J$  = 8.1, 2.6 Hz, 2H), 7.03 (t,  $J$  = 7.8 Hz, 2H), 5.04 (d,  $J$  = 16.0 Hz, 1H), 4.94 (d,  $J$  = 16.1 Hz, 1H), 4.80–4.73 (m, 1H), 3.79–3.70 (m, 1H), 3.68–3.58 (m, 1H), 3.24–2.96 (m, 2H), 2.66–0.56 (m, 16H).<sup>[a]</sup> MS (ES<sup>-</sup>),  $m/z$  589.0, (M-H), 99% purity. HRMS (ES<sup>+</sup> TOF) calculated for C<sub>33</sub>H<sub>38</sub>N<sub>2</sub>O<sub>6</sub>S (M + H): 591.2523; found 591.2529.

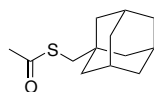
<sup>[a]</sup> The mixture of diastereomers was integrated as a single compound for the purposes of NMR analysis.

#### 4.6.1.2 Successful synthetic route to adamantyl analogue [Scheme 4.3]

##### 4.6.1.2.1 Synthesis of adamantyl amino acids

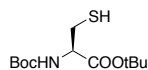


**(3r,5r,7r)-adamantan-1-ylmethyl trifluoromethanesulfonate (4.11):** Compound **4.11** was synthesised according to a procedure described in the literature<sup>(16)</sup>. Briefly, to a stirred solution of 1-adamantanemethanol (233 mg, 1.40 mmol) and pyridine (0.886 mL, 9.29 mmol) in anhydrous dichloromethane (8.0 mL) at 0°C was added dropwise over a period of 10 minutes a solution of trifluoromethane sulfonic anhydride (0.471 mL, 2.80 mmol) in anhydrous dichloromethane (8.0 mL). The reaction was allowed to proceed at for 2 h at room temperature, then diluted with dichloromethane (10 mL), washed with 1 M aqueous HCl, 5% aqueous NaHCO<sub>3</sub>, brine, then dried over anhydrous MgSO<sub>4</sub>, filtered and concentrated to yield compound **4.11** as a pale yellow oil (408 mg, 98%). The crude material was used directly in the next step without further purification. Spectral data obtained corresponded to those reported in the literature<sup>(16)</sup>.



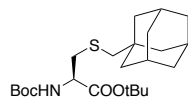
**1-(Acetylthiomethyl)adamantane (4.14):** Compound **4.14** was prepared according to a procedure described in the literature<sup>(16)</sup>. Briefly, a solution of **4.11** (0.69 g, 2.0 mmol), 18-crown-6 (1.6 g, 6.1 mmol) and potassium thioacetate (0.69 g 6.1 mmol) in acetonitrile (40 mL) was stirred at room temperature for 2 h, during which time the initially orange solution gradually changed to

yellow. The acetonitrile was evaporated and the residue was dissolved in 30 mL of ethyl ether. The ether solution was washed with 5% aq. NaCl and dried (MgSO<sub>4</sub>). The solvent was removed under reduced pressure and the crude material purified *via* flash chromatography eluting with cyclohexane (100%) to afford compound **4.14** as a pale yellow oil, which formed off-white crystals on standing (426 mg, 94%). Spectral data obtained corresponded to those reported in the literature<sup>(16)</sup>.



**(R)-tert-butyl 2-((tert-butoxycarbonyl)amino)-3-mercaptopropanoate (4.12):**

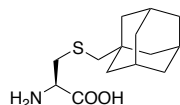
Compound **4.12** was synthesised based on a procedure described in the literature<sup>(17)</sup>, but substituting trimethylphosphine solution in THF for Tri-*n*-butylphosphine. Briefly, to a solution of L-Cystine, *N,N'*-bis[(1,1-dimethylethoxy)carbonyl]-,1,1'-bis(1,1-dimethylethyl) ester (723 mg, 1.31 mmol) in THF (6.5 mL) was added trimethylphosphine (1.1 equivalents, 1.44 mL of a 1M solution in THF). The mixture was allowed to stir at room temperature for 2 minutes and then water (158  $\mu$ L) was added. After stirring overnight, the reaction mixture was concentrated under reduced pressure. Purification of the crude oil *via* flash chromatography eluting with a gradient of EtOAc/cyclohexane (0:100 to 5:95) to afford compound **4.12** as a colourless oil, which formed colourless needles on standing (683 mg, 94%). The compound was used directly in the next step to avoid oxidation over time. Spectral data obtained corresponded to those reported in the literature<sup>(17)</sup>.



**(R)-tert-butyl 3-(((3R,5R,7R)-adamantan-1-ylmethyl)thio)-2-((tert-butoxycarbonyl)amino)propanoate (4.13):**

To a solution of **4.12** (429 mg, 1.55 mmol) in anhydrous acetonitrile (31 mL) was added **4.11** (553 mg, 1.85 mmol) followed by K<sub>2</sub>CO<sub>3</sub> (641 mg, 4.64 mmol) and 18-crown-6 (1.22 g, 6.64 mmol). The mixture was stirred at room temperature for 16 h then diluted with water (30 mL), extracted with EtOAc (3 x 20 mL), the combined organic layers were dried (MgSO<sub>4</sub>), filtered and concentrated under reduced pressure. The resulting brown-orange oil was purified *via* flash chromatography eluting with a gradient of EtOAc/cyclohexane (0:100 to 5:95) to afford compound **4.13** as a colourless oil (418 mg, 64%). <sup>1</sup>H NMR (600 MHz, CDCl<sub>3</sub>)  $\delta$  5.34 (d, *J* = 7.5 Hz, 1H), 4.42–4.33 (m, 1H), 2.99–2.84 (m, 2H), 2.36 (q, *J* = 12.4 Hz, 2H), 1.96 (br s, 3H), 1.69 (d, *J* = 12.1 Hz, 3H), 1.61 (d, *J* = 12.5 Hz, 3H), 1.53 (d, *J* = 2.3 Hz, 6H), 1.48 (s, 9H), 1.45 (s, 9H).<sup>[a]</sup> <sup>13</sup>C NMR (75 MHz, CDCl<sub>3</sub>)  $\delta$  170.29, 155.27, 82.47, 79.90, 77.36, 54.24, 48.62, 41.87, 37.01, 36.94, 34.30, 28.65, 28.51, 28.18. MS (ES<sup>+</sup>), *m/z* 426.4, (M + H). HRMS (ES<sup>+</sup> TOF) calculated for C<sub>23</sub>H<sub>39</sub>NO<sub>4</sub>S (2M + Na): 873.5092; found 873.5108.

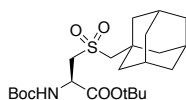
<sup>[a]</sup> The peak at 1.60 ppm (s, 2H) is an impurity, most likely water.



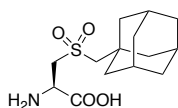
**(R)-3-(((3R,5R,7R)-adamantan-1-ylmethyl)thio)-2-aminopropanoic acid hydrochloride (4.19):**

To a stirred sample of **4.13** (356.6 mg, 0.838 mmol) under N<sub>2</sub> at room temperature was added 3 mL of a solution of HCl (4M) in 1,4-dioxane and the reaction stirred for 6 h. The reaction was concentrated under reduced pressure, the white precipitate filtered and washed with a small volume of cold diethyl ether, then dried *in vacuo* overnight to yield compound **4.19** as a fine white powder (111.8 mg, 44%). <sup>1</sup>H NMR (600 MHz, MeOD)  $\delta$  4.18 (dd, *J* = 7.3, 4.2 Hz, 2H), 3.08 (ddd, *J* = 22.0, 14.7, 5.8 Hz, 4H), 2.45 (dd, *J* = 35.1, 12.6 Hz, 4H), 1.98 (br s, 6H), 1.72 (app dd, *J* = 52.1, 11.9 Hz, 13H), 1.61 (app d, *J* = 1.6 Hz, 12H).<sup>[a]</sup> <sup>13</sup>C NMR (151 MHz, MeOD)  $\delta$  170.43, 53.74, 48.80, 42.73, 37.90, 35.31, 35.21, 29.97. MS (ES<sup>+</sup>), *m/z* 270.3s (M + H). HRMS (ES<sup>+</sup> TOF) calculated for C<sub>14</sub>H<sub>23</sub>NO<sub>2</sub>S (M + H): 270.1522; found 270.1521.

<sup>[a]</sup> An additional peak is observed at  $\delta$  4.91 ppm, most likely due to residual water in the NMR solvent.



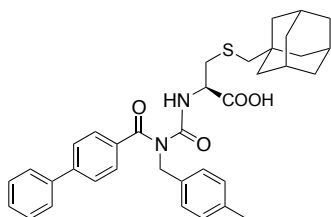
**(R)-tert-butyl 3-(((3R,5R,7R)-adamantan-1-ylmethyl)sulfonyl)-2-((tert-butoxycarbonyl)amino)propanoate (4.20):** To a stirred solution of **4.13** (203.8 mg, 0.48 mmol) in anhydrous dichloromethane (3 mL) at 0°C was added *m*-CPBA (max 77%) (214.6 mg, approx. 0.958 mmol, as a solution in 2 mL dichloromethane) dropwise over 5 minutes. The solution was allowed to stir at 0°C for 1 h, then at room temperature for 17 h. After this time, the reaction was diluted with dichloromethane (50 mL), washed with 10% aq. sodium metabisulfite (2 x 40 mL) to ensure any remaining *m*-CPBA was destroyed, then twice with 10% aq. NaHCO<sub>3</sub>, brine, dried over anhydrous MgSO<sub>4</sub> and concentrated under reduced pressure to yield compound **4.20** as colourless oil, containing minor impurities (231 mg, quant.). <sup>1</sup>H NMR (600 MHz, CDCl<sub>3</sub>) δ 5.59 (d, *J* = 5.5 Hz, 1H), 4.48 (d, *J* = 5.5 Hz, 1H), 3.66–3.50 (m, 2H), 2.84 (s, 2H), 2.00 (br s, 3H), 1.92–1.76 (m, 6H), 1.69 (dd, *J* = 24.6, 12.1 Hz, 6H), 1.53–1.39 (m, 18H). <sup>13</sup>C NMR (151 MHz, CDCl<sub>3</sub>) δ 168.34, 155.36, 83.63, 80.60, 67.50, 57.25, 50.84, 42.20, 36.55, 34.69, 28.48, 28.03, 27.07. MS (ES<sup>+</sup>), *m/z* 457.9, (*M* + *H*). HRMS (ES<sup>+</sup> TOF) calculated for C<sub>23</sub>H<sub>39</sub>NO<sub>6</sub>S (*M* + *Na*): 480.2390; found 480.2390. This compound was used directly in the next step without further purification.



**(R)-3-(((3R,5R,7R)-adamantan-1-ylmethyl)sulfonyl)-2-aminopropanoic acid (4.21):** A sample of **4.20** (215.2 mg, 0.470 mmol) was dissolved in neat TFA (2.0 mL) in a small glass vial and the reaction allowed to proceed at room temperature for 1 h, swirling every 15 minutes. The pale yellow reaction mixture was then carefully concentrated under a fine stream of N<sub>2</sub> over a 40°C heat block (caution!). The off-white residue was taken up in methanol (4 mL) then purified *via* capture/release by passing over a cation exchange column (MEGA BE-SCX, 1g, Varian), the column washed with methanol (2 x 4 mL) and the product eluted with 2M ammonia in methanol (15 mL). The eluent was concentrated under reduced pressure yielded compound **4.21** as the free amine as a fine white powder (131 mg, 92%). <sup>1</sup>H NMR (300 MHz, DMSO) δ 3.77–3.57 (m, 2H), 3.53–2.91 (m, 5H), 1.94 (s, 3H), 1.79 (d, *J* = 2.4 Hz, 6H), 1.72–1.52 (m, 6H).<sup>[a]</sup> <sup>13</sup>C NMR (75 MHz, DMSO) δ 63.64, 56.89, 48.33, 41.45, 41.27, 36.08, 33.72, 27.76. MS (ES<sup>+</sup>), *m/z* 302.2, (*M* + *H*). HRMS (ES<sup>+</sup> TOF) calculated for C<sub>14</sub>H<sub>23</sub>NO<sub>4</sub>S (*M* + *H*): 302.1421; found 302.1427.

<sup>[a]</sup> The broad overlapping peak at approximately δ 3.30 ppm (br s, 2H) is attributed to the amine -NH<sub>2</sub> protons. The small peaks at δ = 2.08 (s), 1.42 (s), 1.20 (q) ppm are due to minor impurities.

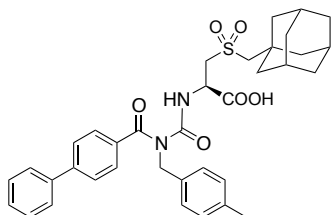
#### 4.6.1.2.2 Benzoylurea formation [Scheme 4.3 (h), (i)]



**(R)-2-(3-([1,1'-biphenyl]-4-carbonyl)-3-(4-methylbenzyl)ureido)-3-(((3R,5R,7R)-adamantan-1-ylmethyl)thio)propanoic acid (4.23):** General Procedures A and B were followed using compound **3.3** (30.1 mg, 0.100 mmol), compound **4.19** (45.9 mg, 0.150 mmol) and triethylamine (20.9 μL, 0.150 mmol) to neutralise the amino acid HCl salt. Purification *via* flash chromatography, eluting with a gradient of methanol/dichloromethane (0:100 to 5:95) afforded the title compound as a colourless glass (49.5 mg, 83%). <sup>1</sup>H NMR (300 MHz, CDCl<sub>3</sub>) δ 9.65 (d, *J* = 7.0 Hz, 1H), 7.66–7.54 (m, 4H), 7.53–7.34 (m, 5H), 7.08 (d, *J* = 7.9 Hz, 2H), 6.97 (d, *J* = 8.1 Hz, 2H), 5.12–4.88 (m, 2H), 4.79 (dd, *J* = 12.5, 5.8 Hz, 1H), 3.17–2.95 (m, 2H), 2.41 (app. q, *J* = 12.5 Hz, 2H), 2.30 (s, 3H), 1.96 (br s, 3H), 1.65 (app. q, *J* = 12.0 Hz, 6H), 1.55 (app. d, *J* = 2.4 Hz, 6H).<sup>[a]</sup> <sup>13</sup>C NMR (75 MHz, CDCl<sub>3</sub>) δ 175.27, 175.14, 155.28, 143.80, 139.95, 137.04, 134.69, 134.56, 129.41, 129.06, 128.19, 127.40, 127.29, 127.20, 126.66, 54.05, 50.09, 48.39, 41.81, 36.96, 35.96, 34.23,

28.63, 21.20. MS (ES<sup>-</sup>),  $m/z$  595.3, (M - H). HRMS (ES<sup>+</sup> TOF) calculated for C<sub>36</sub>H<sub>40</sub>N<sub>2</sub>O<sub>4</sub>S (M + H): 597.2782; found 597.2782.

[a] A minor peak observed at  $\delta$  2.18 ppm is an impurity, most likely acetone.



**(R)-2-(3-([1,1'-biphenyl]-4-carbonyl)-3-(4-methylbenzyl)ureido)-3-(((3R,5R,7R)-adamantan-1-ylmethyl)sulfonyl)propanoic acid (4.25):** General Procedures A and B were followed using compound **3.3** (30.1 mg, 0.100 mmol) and compound **4.21** (45.2 mg, 0.150 mmol). Purification *via* flash chromatography, eluting with a gradient of methanol/dichloromethane (0:100 to 5:95) afforded the title compound as a colourless glass (51 mg, 81%). <sup>1</sup>H NMR (600 MHz, CDCl<sub>3</sub>)  $\delta$  9.87 (d,  $J$  = 6.7 Hz, 1H), 7.57 (d,  $J$  = 8.1 Hz, 4H), 7.45 (t,  $J$  = 6.8 Hz, 4H), 7.38 (t,  $J$  = 7.3 Hz, 1H), 7.07 (d,  $J$  = 7.3 Hz, 2H), 6.95 (d,  $J$  = 7.0 Hz, 2H), 5.00 (s, 2H), 4.97 (dd,  $J$  = 12.1, 5.9 Hz, 1H), 3.69 (qd,  $J$  = 14.9, 5.1 Hz, 2H), 2.88 (s, 2H), 2.30 (s, 3H), 1.98 (s, 3H), 1.83 (s, 6H), 1.68 (q,  $J$  = 12.2 Hz, 6H). <sup>13</sup>C NMR (151 MHz, CDCl<sub>3</sub>)  $\delta$  175.26, 172.20, 155.51, 144.00, 139.89, 137.16, 134.43, 134.14, 129.48, 129.08, 128.25, 127.55, 127.30, 127.22, 126.62, 66.81, 56.30, 50.23, 49.83, 42.12, 36.51, 34.73, 28.48, 21.23. MS (ES<sup>+</sup>),  $m/z$  629.3, (M + H), 99% purity. HRMS (ES<sup>+</sup> TOF) calculated for C<sub>36</sub>H<sub>40</sub>N<sub>2</sub>O<sub>6</sub>S (M + H): 629.2680; found 629.2694.

## 4.6.2 Crystallisation and X-ray structure determination

### 4.6.2.1 Structure determination of the BCL-X<sub>L</sub>:**4.6I** complex

The complex of BCL-X<sub>L</sub>:**4.6I** (10 mg/mL) was prepared for crystallisation as described in **Chapter 2, Section 2.6** and crystallised under the following condition: 1.4 M ammonium sulfate, 0.1 M MES pH 6.0. Crystals were flash-cooled in cryoprotectant solution containing 1.5 M ammonium sulfate, 0.1 M MES pH 6.0 supplemented with ethylene glycol (25%). Data were collected on the MX2 beamline at the Australian Synchrotron and processed with XDS<sup>(20)</sup>. The structure was solved by molecular replacement with PHASER<sup>(21)</sup> using the structure of BCL-X<sub>L</sub> from the BCL-X<sub>L</sub>:**1.1** complex as a search model. Multiple rounds of building in COOT<sup>(22)</sup> and refinement in PHENIX<sup>(23)</sup> incorporating in the first round of refinement a simulated annealing step, resulted in the final structure. The asymmetric unit contained 12 copies of the BCL-X<sub>L</sub> monomer, arranged as six domain-swapped dimers. In each monomer a single copy of the ligand was observed to occupy the hydrophobic groove in essentially the identical conformation. Ligand geometry restraint (cif) files were generated from SMILES strings using ELBOW<sup>(24)</sup>.

### 4.6.2.2 BCL-X<sub>L</sub>:**4.25** complex

The complex of BCL-X<sub>L</sub>:**4.6I** (10 mg/mL) was prepared for crystallisation as described in **Chapter 2, Section 2.6** and crystallised under the following condition: 1.7 M ammonium sulfate, 0.1 M MES pH 6.0. Crystals were flash-cooled in cryoprotectant solution containing 1.8 M ammonium sulfate, 0.1 M MES pH 6.0 supplemented with ethylene glycol (25%). Data were collected on the MX2 beamline at the Australian Synchrotron and processed with XDS<sup>(20)</sup>. The structure was solved by molecular replacement, built and refined and ligand molecules placed as for the BCL-X<sub>L</sub>:**4.6I** complex described above. The asymmetric unit contained 12 copies of the BCL-X<sub>L</sub> monomer, arranged as six domain-swapped dimers. In 11 of the 12 copies the ligand was observed to occupy the groove in the expected conformation (as for **4.6I**), in the final copy the ligand was observed to

occupy an alternative conformation in which the adamantyl moiety did not bind into the hydrophobic groove p5 pocket, but rather bridged across to another BCL-X<sub>L</sub> monomer. This interaction mediated a crystal contact between two BCL-X<sub>L</sub> monomers and appeared to be a result of crystal packing and thus unlikely to represent the bound conformation in solution.



## 4.7 References

1. Muchmore SW, *et al.* (1996) X-ray and NMR structure of human BCL-xL, an inhibitor of programmed cell death. *Nature* 381(6580):335-341.
2. Lee EF, *et al.* (2007) Crystal structure of ABT-737 complexed with BCL-xL: implications for selectivity of antagonists of the BCL-2 family. *Cell Death and Differentiation* 14(9):1711-1713.
3. Lessene G, *et al.* (2013) Structure-guided design of a selective BCL-XL inhibitor. *Nature Chemical Biology* 9(6):390-397.
4. Ku B, *et al.* (2008) Structural and biochemical bases for the inhibition of autophagy and apoptosis by viral BCL-2 of murine  $\gamma$ -herpesvirus 68. *PLoS Pathogens* 4(2):e25.
5. Czabotar PE, *et al.* (2013) Bax crystal structures reveal how BH3 domains activate Bax and nucleate its oligomerization to induce apoptosis. *Cell* 152(3):519-531.
6. Brouwer JM, *et al.* (2014) Bak core and latch domains separate during activation, and freed core domains form symmetric homodimers. *Molecular Cell* 55(6):938-946.
7. O'Neill JW, Manion MK, Maguire B, & Hockenbery DM (2006) BCL-XL dimerization by three-dimensional domain swapping. *Journal of Molecular Biology* 356(2):367-381.
8. Rajan S, Choi M, Baek K, & Yoon HS (2015) BH3 induced conformational changes in BCL-Xl revealed by crystal structure and comparative analysis. *Proteins* 83(7):1262-1272.
9. Souers AJ, *et al.* (2013) ABT-199, a potent and selective BCL-2 inhibitor, achieves antitumor activity while sparing platelets. *Nature Medicine* 19:202-208.
10. Seko T, *et al.* (2003) Structure-activity study of l-amino acid-based N-type calcium channel blockers. *Bioorganic & Medicinal Chemistry* 11(8):1901-1913.
11. Wanka L, Iqbal K, & Schreiner PR (2013) The lipophilic bullet hits the targets: medicinal chemistry of adamantane derivatives. *Chemical Reviews* 113(5):3516-3604.

12. Yusuff N, *et al.* (2012) Lipophilic isosteres of a  $\pi$ - $\pi$  stacking interaction: new inhibitors of the BCL-2-Bak protein-protein interaction. *ACS Medicinal Chemistry Letters* 3:579-583.
13. Dostrovsky I & Hughes ED (1946) 44. Mechanism of substitution at a saturated carbon atom. Part XXVI. The role of steric hindrance. (Section A) introductory remarks, and a kinetic study of the reactions of methyl, ethyl, n-propyl, isobutyl, and neopentyl bromides with sodium ethoxide in dry ethyl alcohol. *Journal of the Chemical Society*:157-161.
14. Hughes ED (1941) Mechanism and kinetics of substitution at a saturated carbon atom. *Transactions of the Faraday Society* 37:603.
15. Olah GA, Wu AH, & Farooq O (1989) Synthetic methods and reactions. 136. Single-step one-carbon ring homologation of cyclic and polycyclic hydrocarbons via their methyl alcohols or carboxylic acids with sodium borohydride/triflic acid. *The Journal of Organic Chemistry* 54(6):1452-1453.
16. Kitagawa T, *et al.* (2006) Rigid molecular tripod with an adamantane framework and thiol legs. Synthesis and observation of an ordered monolayer on Au111. *Journal of Organic Chemistry* 71(4):1362-1369.
17. Shen F, Zhang Z-P, Li J-B, Lin Y, & Liu L (2011) Hydrazine-sensitive thiol protecting group for peptide and protein chemistry. *Organic Letters* 13(4):568-571.
18. Donohoe TJ, Winship PCM, Tatton MR, & Szeto P (2011) A short and efficient synthesis of neodysiherbaine A by using catalytic oxidative cyclization. *Angewandte Chemie International Edition* 50(33):7604-7606.
19. Dale J, *et al.* (1992) Reactivity of Neopentyl-Like Compounds in the Synthesis of Branched Polyethers. *Acta Chemica Scandinavica* 46:278-282.
20. Kabsch W (2010) Xds. *Acta Crystallographica Section D Biological Crystallography* 66(Pt 2):125-132.
21. McCoy AJ, *et al.* (2007) Phaser crystallographic software. *Journal of Applied Crystallography* 40(Pt 4):658-674.
22. Emsley P & Cowtan K (2004) Coot: model-building tools for molecular graphics. *Acta Crystallographica Section D Biological Crystallography* 60(Pt 12 Pt 1):2126-2132.

23. Adams PD, *et al.* (2010) PHENIX: a comprehensive Python-based system for macromolecular structure solution. *Acta Crystallographica Section D Biological Crystallography* 66(Pt 2):213-221.
24. Moriarty NW, Grosse-Kunstleve RW, & Adams PD (2009) electronic Ligand Builder and Optimization Workbench (eLBOW): a tool for ligand coordinate and restraint generation. *Acta Crystallographica Section D Biological Crystallography* 65(Pt 10):1074-1080.

**5 Chapter five – Structure-guided linker rescaffolding to generate novel benzoylurea amides and parallel synthesis of a library of benzoylurea amides to further explore SAR of the p5 pocket of BCL X<sub>L</sub>**

## 5.1 Introduction

**Chapter 1** introduced the benzoylurea series of BCL-X<sub>L</sub> inhibitors, including initial hit compound **1.1**, which was found to bind to BCL-X<sub>L</sub> with an IC<sub>50</sub> in the low micromolar range. The X-ray crystal structure of the BCL-X<sub>L</sub>:**1.1** complex revealed that compound **1.1** bound along the canonical hydrophobic groove. In particular, the tolyl moiety of compound **1.1** interacted directly with the p4 pocket of BCL-X<sub>L</sub> and the S-benzyl-L-cysteine moiety of compound **1.1** bridged *via* the thioether linker across into the p5 hydrophobic pocket. Interestingly, the position of the thioether linker was similar to the sulfonamide group of **ABT-737** in the published BCL-X<sub>L</sub>:**ABT-737** structure. In that structure, the acylsulfonamide sulfonyl oxygen was observed to engage in a hydrogen bond interaction with the backbone –NH of Gly138 of BCL-X<sub>L</sub> (**Figure 5.1A**). Subsequent analogues of compound **1.1** were made in which the flexible thioether linker was replaced with hydrogen-bond acceptors to try to make use of an interaction of this type. These included compound **1.8**, which incorporated a sulfonyl linker. X-ray crystal structure analysis revealed that compound **1.8** did form the designed hydrogen bond interaction with the backbone –NH of Gly138 of BCL-X<sub>L</sub> (**Figure 5.1A**), although little improvement in the measured IC<sub>50</sub> was observed.

**Chapter 3**, amongst other work, described the structure determination of a complex of BCL-X<sub>L</sub> with compound **3.1**, a further elaborated benzoylurea analogue (designed to gain additional interactions near the p2 pocket) that also incorporated a sulfonyl linker. The BCL-X<sub>L</sub>:**3.1** complex revealed that the sulfonyl linker hydrogen-bonding interaction was maintained as for compound **1.8** (**Figure 5.1C**).

**Chapter 4** outlined a series of analogues of **1.8** which began to explore the SAR of the p5 pocket, by replacing the benzyl group attached to the sulfonyl linker with a variety of other groups - including cyclohexylmethyl (compound **4.6I**) and adamantylmethylene moieties (compound **4.25**). Despite variation of the p5-interacting group, structures of BCL-X<sub>L</sub>:**4.6I** and BCL-X<sub>L</sub>:**4.25** revealed that

these compounds also still retained the hydrogen-bonding interaction of the sulfonyl linker to Gly138 of BCL-X<sub>L</sub> (**Chapter 4, Figure 4.5A,B**).

In an effort to explore such interactions further, this Chapter describes a series of benzoylurea analogues investigating replacement of the sulfonyl moiety with an amide linker (**Figure 5.1D**). The underlying rationale is described, as well as the initial synthesis of a proof-of-principle series of amide-linked benzoylurea analogues of **1.8** to evaluate different linker geometries. Next, the approach is adapted to a parallel chemistry format to enable the synthesis of two further novel series of amide-linked benzoylurea molecules exploring modifications in the p5 pocket along with biochemical and structural analyses.

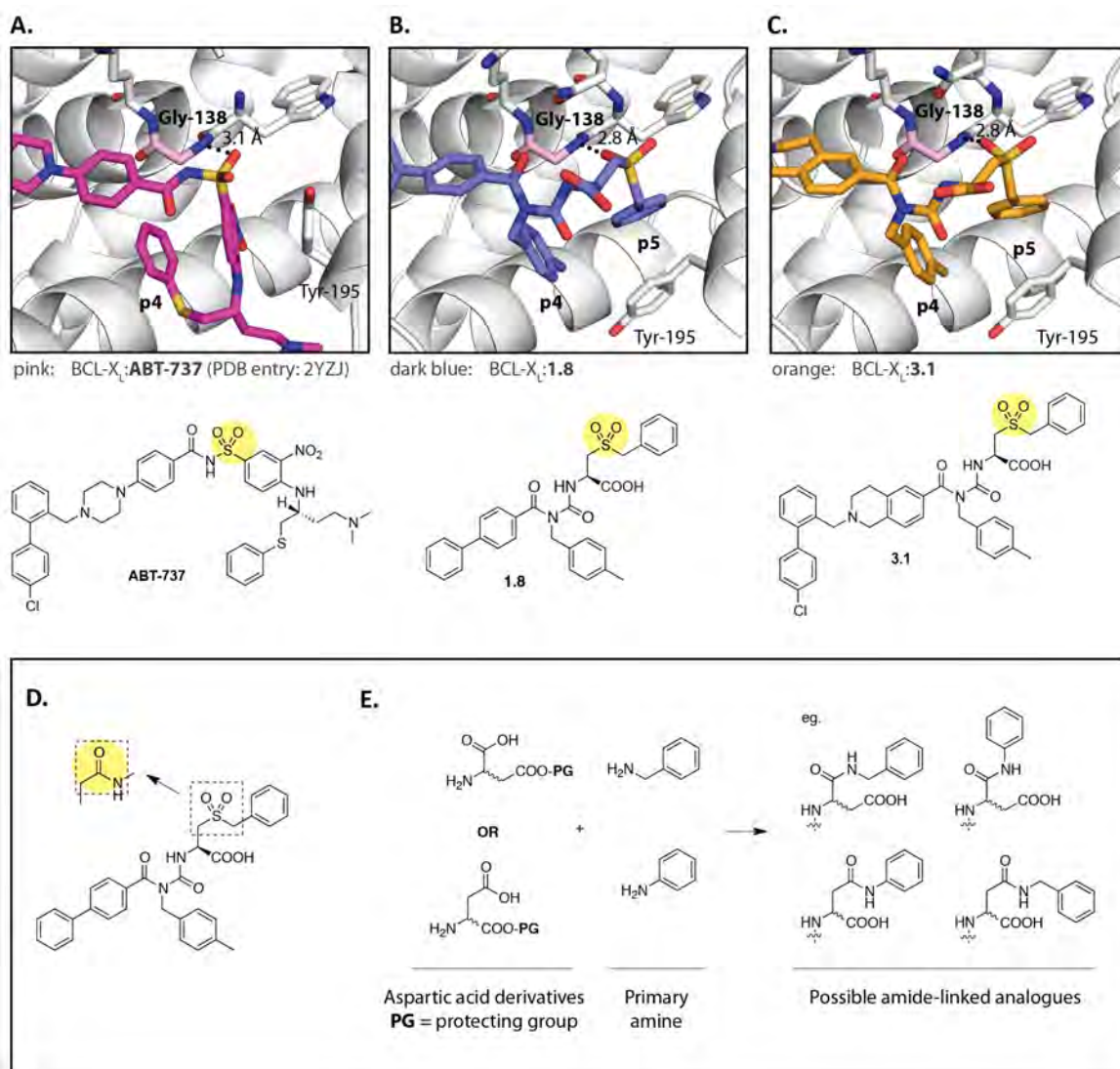
#### 5.1.1 Rationale and design of an ‘amide’ linker

Seeking to explore other linker alternatives, we hypothesized that the carbonyl of an amide moiety might provide a suitable hydrogen bond acceptor to act as a suitable isostere for the sulfonyl linker (**Figure 5.1D**). We reasoned that replacing the sulfonyl linker with an amide linker might be beneficial for a number of reasons. Firstly, an amide linker would be potentially more atom-economical as compared with comparable sulfonyl linker (one fewer atom and lower overall molecular weight). Secondly, the planarity of the amide bond would exhibit different conformational preferences and would likely reduce the overall number of degrees of freedom of the linker/p5 substituent. If the overall effect of this was to ‘lock’ the molecule into a more favourable conformation, this might ultimately prove beneficial for affinity. Thirdly, utilising an amide linkage might offer new opportunities for late-stage parallel chemistry, described further below.

We anticipated that the amide-linked benzoylurea analogues could be generated from protected aspartic acid derivatives, which could then be coupled with a primary amine such as benzyl amine or aniline to install the p5 group (**Figure 5.1E**). In comparison, the synthetic approach adopted for the benzoylurea sulfonyl series started from L-cysteine and typically installed the p5 variation

relatively early in a multi-step synthesis. We considered that if the protected aspartic acid derivative could be introduced early to form an advanced benzoylurea intermediate containing an appropriate carboxylic acid handle, the p5 substituent could be installed in the final step *via* a simple amide-coupling/deprotection sequence. This would render the amide series particularly amenable to parallel chemistry to easily vary the p5 substituent. As modern amide-coupling reagents offer the capability to form amide bonds in high yield under mild conditions, and myriad primary amine compounds are currently available from commercial suppliers, this approach appeared particularly attractive.

The main goal of this research initially was to evaluate the utility of such an amide linker – including optimising chemistry, linker length, evaluating the effect on binding and linker geometry – and then, if successful, utilising this approach to generate a new series of analogues using parallel chemistry.



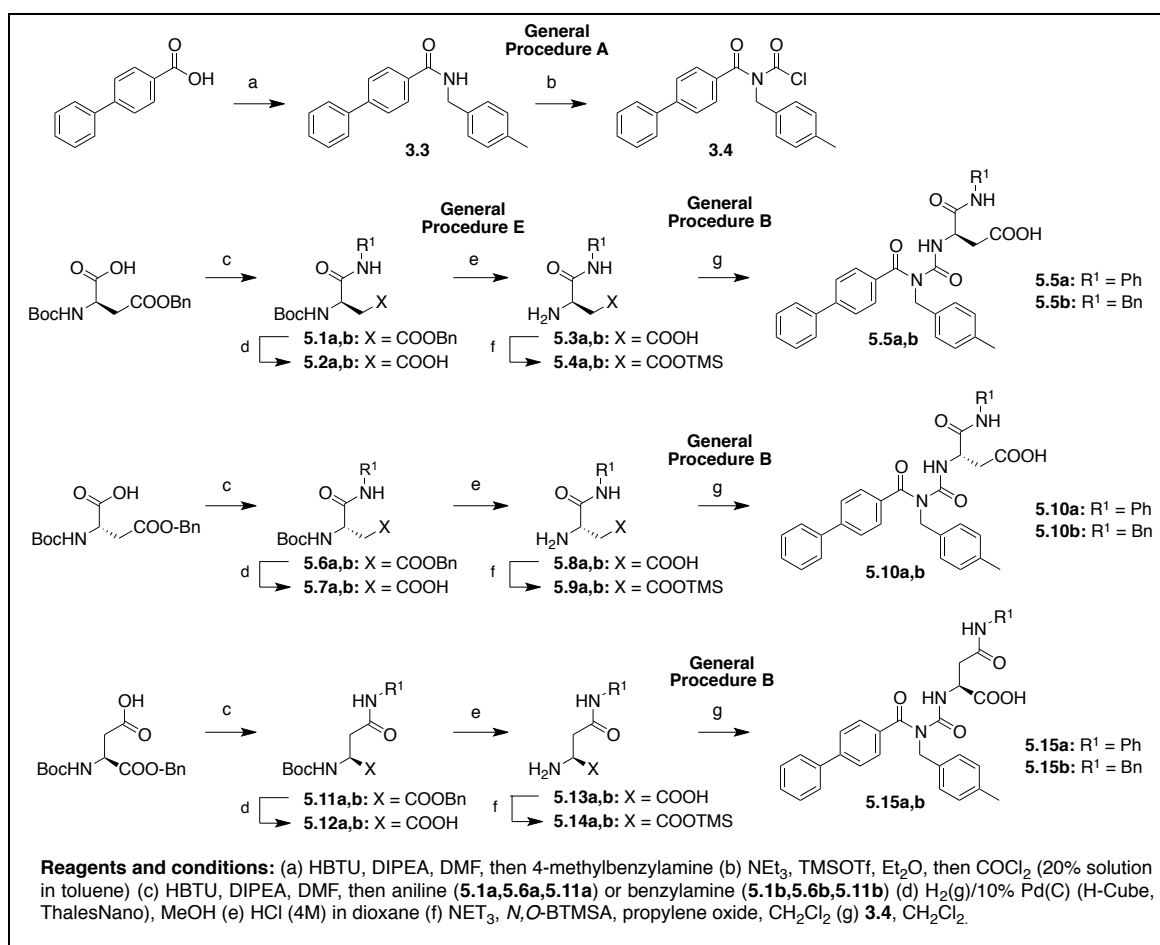
**Figure 5.1: Origins of the amide-linked series’.**

(A-C) X-ray crystal structures reveal the hydrogen-bond interaction formed between the backbone –NH of Gly138 of BCL-X<sub>L</sub> (residue highlighted in light pink) and the oxygen atom respectively of the sulfonamide moiety of **ABT-737** (PDB entry: 2YXJ<sup>(1)</sup>) and the sulfonyl moieties of each of **1.8** and **3.1**. (D-E) General concept of the amide-linked series as a potential isostere of the sulfonyl linker, based on a protected aspartic acid derivative coupled with a primary amine (such as benzyl amine or aniline).



## 5.2 Synthesis of a trial set of amide-linked analogues

A key starting point for our proposed approach was to utilise aspartic acid to introduce the chiral centre. Starting from aspartic acid (either D- or L-configuration) with one of the carboxylic acid moieties suitably protected, the remaining carboxylic acid handle could then be reacted with a primary amine, such as benzylamine or aniline, using standard amide-coupling reagents (Figure 5.1E). Subsequent removal of the protecting group would furnish the desired functionalised amino acid. Using this approach, a set of analogues could be generated of varying amide linker length, with either an  $\alpha$ - or  $\beta$ - carboxylic acid, and either stereochemistry at the chiral centre, to select the optimal linker length and geometry, as well as potentially engage the conserved Arg139 of BCL-X<sub>L</sub> with the extended carboxylic acid moiety.



**Scheme 5.1: Synthesis of trial set of amide-linked analogues.**

### 5.2.1 Synthesis of trial amide-linked analogues

An initial test series was generated based on a combinatorial approach, to explore optimal linker length and geometry for the amide linker. Starting from commercially available N-Boc-Aspartic acid (either L- or D- stereoisomers) singly protected as either the  $\alpha$ - or  $\beta$ - benzyl ester, a series of amide couplings were undertaken with either aniline or benzylamine, using HBTU in the presence of DIPEA in DMF. Hydrogenolysis of the benzyl group, followed by Boc-deprotection furnished the amino acids (**5.1a,b**, **5.6a,b**, **5.11a,b**), which were then *in situ* protected and subjected to reaction with carbamoyl chloride **3.4** to yield the final benzoylurea products (**5.5a,b**, **5.10a,b**, **5.15a,b**).

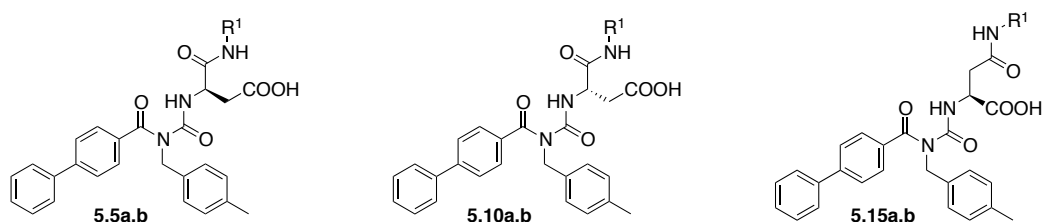
### 5.2.2 Trial amide series – evaluation of BCL-X<sub>L</sub> and MCL-1 binding using AlphaScreen competition assay

The initial series of amide-linked analogues were screened for binding to BCL-X<sub>L</sub> and MCL-1 using the AlphaScreen competition assay (described earlier). The resulting IC<sub>50</sub> values are listed in **Table 5.1**.

Relative to **1.1** or **1.8**, all of the trial amide-linked analogues bound to BCL-X<sub>L</sub> with moderately weaker binding affinities within the low micromolar range, perhaps indicating some steric strain to accommodate the amide linker. As perhaps might be anticipated, those amide analogues with the amide linker length most similar to the linker length for compounds **1.1** and **1.8** in general had the most promising binding affinities (i.e. compounds **5.5b**, **5.10b**, **5.15a**, refer **Figure 5.2**, IC<sub>50</sub>(BCL-X<sub>L</sub>) ~ 8-12  $\mu$ M), with the possible exception of compound **5.5b**, which appeared to have similar activity to compound **5.5a**. These compounds also retained similar selectivity to compound **1.8** for BCL-X<sub>L</sub> relative to MCL-1. Of the compounds with the optimal linker length, the two enantiomers, compounds **5.5b** and **5.10b**, were equipotent. This reflected a previous finding that I had made during my Honours year, that the chirality of the amino acid moiety was not a key determinant of activity - both compound **1.1** and its enantiomer were found to

have similar IC<sub>50</sub> values for BCL-X<sub>L</sub> (data not shown). The basis for this presumably lies in both the solvent-exposed position of the carboxylic acid moiety and the significant flexibility of the adjacent 'linker' to accommodate either orientation.

**Table 5.1: IC<sub>50</sub> values of initial amide-linked benzoylurea compounds for BCL-X<sub>L</sub> and MCL-1 (determined by AlphaScreen competition assay, pre-2015 data)<sup>[a]</sup>**

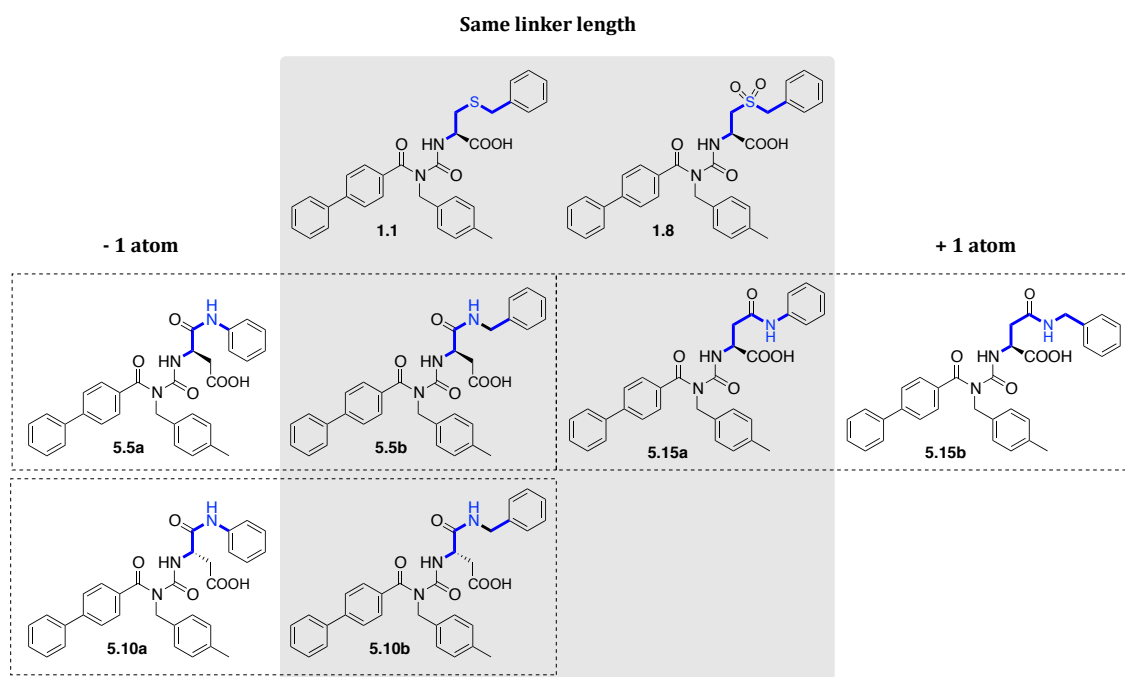


Compound		IC <sub>50</sub> A.S. <sup>[b]</sup>				Fold Selectivity	BEI <sup>[c]</sup>	
R <sup>1</sup>		BCL-X <sub>L</sub>		MCL-1		N =	(BCL-X <sub>L</sub> /MCL-1)	
1.1	-	4.6	±1.0	73.7	±20.3	3	16	9.9
1.8	-	1.5	±0.6	68.1	±25.4	5	44	10.2
5.5a	Ph	12.5	-	77	-	1	6	9.2
5.5b	Bn	11.8	±6.3	>100	-	4	> 9	9.0
5.10a	Ph	28	±5.0	95	±5	2	3	8.5
5.10b	Bn	9.4	±3.3	76	±20	4	8	9.1
5.15a	Ph	8.1	±2.0	68	±18	4	8	9.5
5.15b	Bn	12.5	±3.5	>100	-	4	> 8	8.9

<sup>[a]</sup> For further information refer to note in **Chapter 2, Section 2.4.1.3**.

<sup>[b]</sup> IC<sub>50</sub> values are reported in μM ± S.D.

<sup>[c]</sup> BEI (Binding efficiency index, refer Section 1.4.1.2) = pIC<sub>50</sub>/MW, where pIC<sub>50</sub> is the negative base 10 logarithm of the IC<sub>50</sub> (in molar units) and MW is the compound molecular weight (in kDa).



**Figure 5.2: Initial amide-linked analogues organised according to the overall linker length (highlighted in blue).**

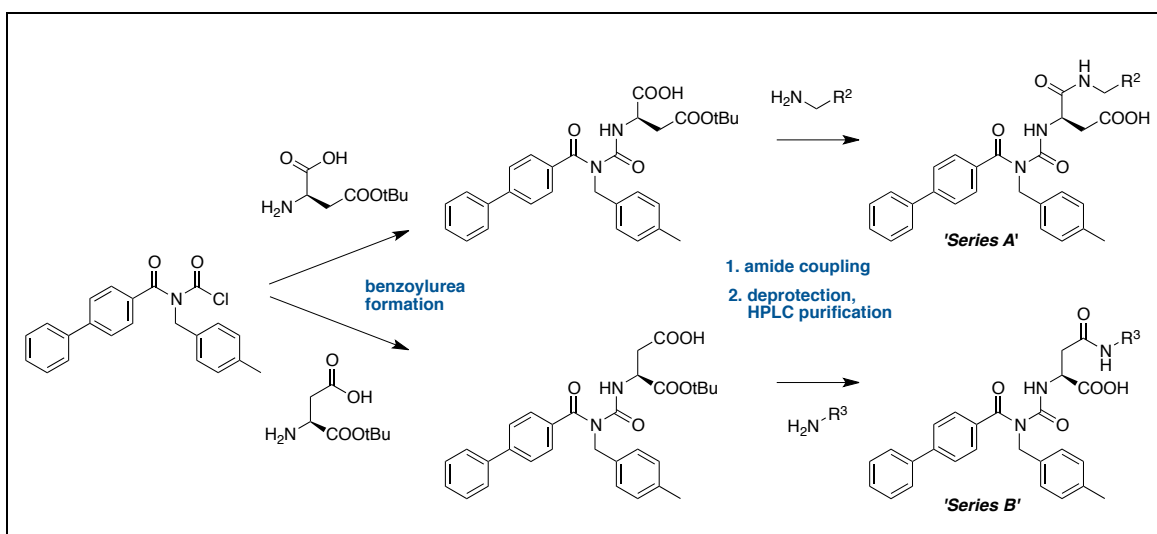
### 5.2.3 Conclusions of trial amide-linked analogues

These initial studies indicated the feasibility of incorporating an amide linker into the benzoylurea series, albeit with a small loss in binding relative to **1.8**. The optimal overall linker length was found to be similar to **1.8**. Based on this result we decided to select compounds **5.5b** and **5.15a** for further study.

### 5.3 Parallel synthesis of amide-linked analogues varying p5 substituent

Based on compounds **5.5b** and **5.15a**, the amide linking strategy was next adapted to a parallel format to enable SAR studies. The two precursors **5.5b** and **5.15a** were chosen to form the basis for two different series, Series A and B respectively (**Scheme 5.2**).

'Series A' (based on compound **5.5b**) utilised benzylamine/methylamine precursors, placing the ultimate amide carbonyl  $\alpha$  to the chiral centre and the free acid  $\beta$  to this centre (i.e. one carbon homologated). 'Series B' (based on compound **5.15a**) utilised aniline/amine precursors, placing the amide carbonyl  $\beta$  to the chiral centre and the free acid  $\alpha$  relative to this centre. These two series allowed a wide variety of substituents in the p5 pocket to be rapidly sampled, as well as the effect of amide position and free acid length to be evaluated.



**Scheme 5.2: General strategy for parallel synthesis of amide series A and B.**

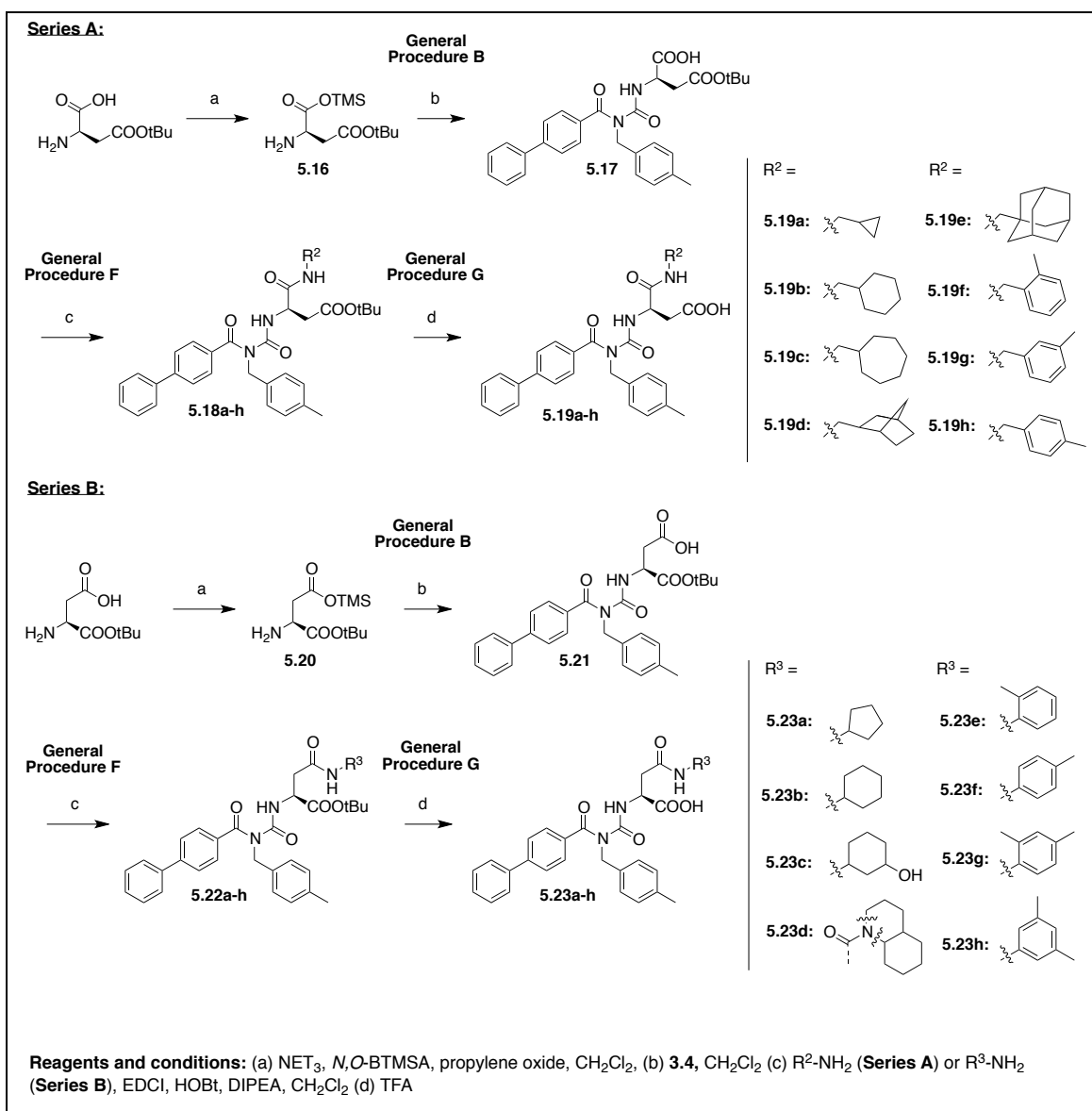
### 5.3.1 Synthetic approach for parallel chemistry

The synthetic approach for the trial series above needed several modifications to be optimally amenable for parallel synthesis (**Scheme 5.3**).

Firstly, benzoylurea formation with the protected Asp derivative was conducted in the first step, obviating the need for N-Boc protection/deprotection steps. This generated an advanced benzoylurea intermediate with a free carboxylic handle which could be reacted on a larger scale with the amide coupling reagent and aliquotted into parallel reaction vessels containing a variety of commercial primary (or secondary) amines. Secondly, the acid protecting group of choice was modified to a *tert*-butyl ester, to allow facile removal using neat TFA, which could be easily removed in a final step by heating at 40°C under a gentle stream of N<sub>2</sub>(g). Lastly, crude products were purified by mass-directed preparative HPLC to isolate sufficient quantities of purified material for analytical and functional testing.

### 5.3.2 Synthesis of amide series A and series B

Using this method eight analogues were generated in each of series A and series B exploring a range of aliphatic cyclic systems of varying size, as well as mono- and di-substituted aromatic rings (**Scheme 5.3**).



**Scheme 5.3: Parallel synthesis of amide series A and series B.**

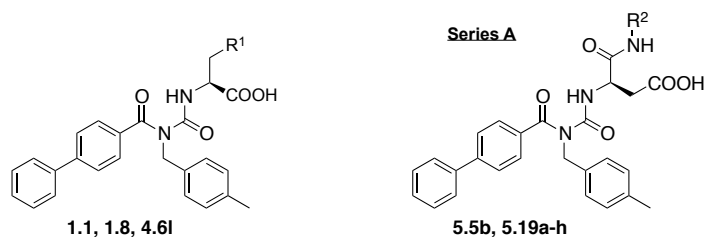
## 5.4 Evaluation of BCL-X<sub>L</sub>/MCL-1 binding and binding mode

To determine their binding to BCL-X<sub>L</sub> and MCL-1, analogues in amide series A (compounds **5.5b**, **5.19a-h**) and Series B (compounds **5.15a**, **5.23a-h**) were screened in the AlphaScreen competition assay. IC<sub>50</sub> values are listed in **Table 5.2** and **Table 5.3** (pre-2015 data, refer to **Chapter 2, Section 2.4.1.3**).

A subset of analogues from amide series A (compounds **5.5b**, **5.19b-e**) were subsequently re-screened again in this assay at a later date. IC<sub>50</sub> values for this later time point are listed in **Table 5.4** (post-2015 data, refer to **Chapter 2, Section 2.4.1.3**).



**Table 5.2: IC<sub>50</sub> values of amide series A benzoylurea compounds for BCL-X<sub>L</sub> and MCL-1 (determined by AlphaScreen competition assay, pre-2015 data)<sup>[a]</sup>**



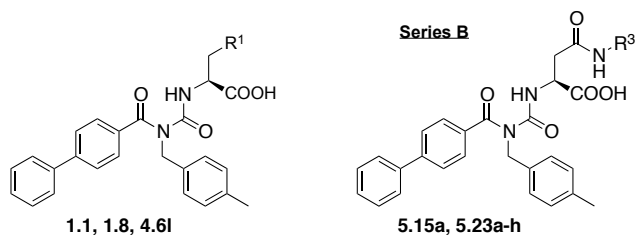
Compound		IC <sub>50</sub> A.S. <sup>[b]</sup>			Fold Selectivity	BEI <sup>[c]</sup>
	R <sup>1</sup> =	BCL-X <sub>L</sub>	MCL-1	N =	(BCL-X <sub>L</sub> /MCL-1)	
<b>1.1</b>		4.6 ±1.0	73.7 ±20.3	3	16	9.9
<b>1.8</b>		1.5 ±0.6	68.1 ±25.4	5	44	10.2
<b>4.6l</b>		1.6 ±0.6	45.8 ±14.4	5	29	10.1
<b>Series A R<sup>2</sup> =</b>						
<b>5.5b</b>		11.8 ±6.3	> 100 -	4	> 9	9.0
<b>5.19a</b>		30.3 ±4.8	> 100 -	2	> 3	8.8
<b>5.19b</b>		2.5 ±0.4	92 ±10	2	37	10.1
<b>5.19c</b>		ND -	ND -	-	-	-
<b>5.19d</b>		ND -	ND -	-	-	-
<b>5.19e</b>		1.3 ±0.1	60 ±15	2	46	9.7
<b>5.19f</b>		7.4 ±1.4	> 100 -	2	> 14	9.1
<b>5.19g</b>		6.2 ±1.0	> 100 -	2	> 16	9.2
<b>5.19h</b>		40.9 ±6.8	> 100 -	2	> 2	7.8

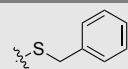
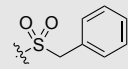
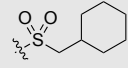
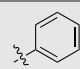
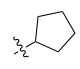
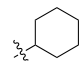
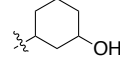
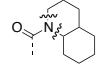
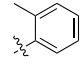
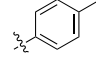
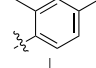
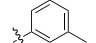
<sup>[a]</sup> For further information refer to note in **Chapter 2, Section 2.4.1.3.**

<sup>[b]</sup> IC<sub>50</sub> values are reported in  $\mu\text{M} \pm \text{S.D.}$

<sup>[c]</sup> BEI (Binding efficiency index, refer Section 1.4.1.2) =  $pIC_{50}/\text{MW}$ , where  $pIC_{50}$  is the negative base 10 logarithm of the IC<sub>50</sub> (in molar units) and MW is the compound molecular weight (in kDa).

**Table 5.3: IC<sub>50</sub> values of amide series B benzoylurea compounds for BCL-X<sub>L</sub> and MCL-1 (determined by AlphaScreen competition assay, pre-2015 data)<sup>[a]</sup>**



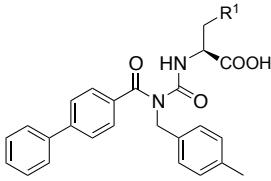
Compound		IC <sub>50</sub> A.S. <sup>[b]</sup>				Fold Selectivity	BEI <sup>[c]</sup>	
R <sup>1</sup> =		BCL-X <sub>L</sub>		MCL-1		N =	(BCL-X <sub>L</sub> /MCL-1)	
1.1		4.6	±1.0	73.7	±20.3	3	16	9.9
1.8		1.5	±0.6	68.1	±25.4	5	44	10.2
4.6l		1.6	±0.6	45.8	±14.4	5	29	10.1
<b>Series B</b> R <sup>3</sup> =								
5.15a		8.1	±2.0	68	±18	4	8	9.5
5.23a		5.8	±0.5	> 100	-	2	> 17	9.9
5.23b		4.3	±0.4	> 100	-	2	> 23	9.9
5.23c		14.8	±1.9	> 100	-	2	> 7	8.7
5.23d		5.4	±0.7	> 68	±16	2	13	9.1
5.23e		5.5	±0.3	> 100	ND	2	> 18	9.6
5.23f		23.4	±0.4	95.2	±6.4	2	4	8.4
5.23g		7.8	±0.2	88.6	±3.9	2	11	9.1
5.23h		26.1	±4.2	97.7	±4.7	2	4	8.1

<sup>[a]</sup> For further information refer to note in **Chapter 2, Section 2.4.1.3.**

<sup>[b]</sup> IC<sub>50</sub> values are reported in  $\mu\text{M} \pm \text{S.D.}$

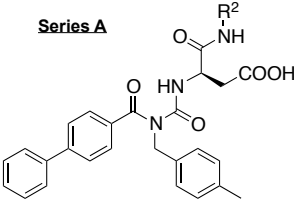
<sup>[c]</sup> BEI (Binding efficiency index, refer Section 1.4.1.2) =  $\text{pIC}_{50}/\text{MW}$ , where  $\text{pIC}_{50}$  is the negative base 10 logarithm of the IC<sub>50</sub> (in molar units) and MW is the compound molecular weight (in kDa).

**Table 5.4: IC<sub>50</sub> values of selected amide series A compounds for BCL-X<sub>L</sub> and MCL-1 (determined by AlphaScreen competition assay, post-2015 data)<sup>[a]</sup>**

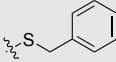
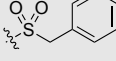
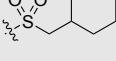

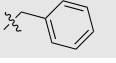
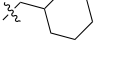
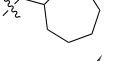

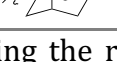


1.1, 1.8, 4.6l, 4.25

**Series A**



5.5b, 5.19b-e

Compound		IC <sub>50</sub> A.S. <sup>[b]</sup>			Fold Selectivity	BEI <sup>[c]</sup>
R <sup>1</sup> =		BCL-X <sub>L</sub>	MCL-1	N =	(BCL-X <sub>L</sub> /MCL-1)	
<b>1.1</b>		0.51 ±0.07	7.7 ±1.6	3	15	11.7
<b>1.8</b>		0.59 ±0.11	11.6 ±1.0	3	20	10.9
<b>4.6l</b>		0.46 ±0.43	10.0 ±2.5	3	22	11.0
<b>4.25</b>		0.19 ±0.08	6.07 ±0.93	3	32	10.7
<b>Series A R<sup>2</sup> =</b>						
<b>5.5b</b>		0.58 ±0.20	21.0 ±0.5	3	36	11.3
<b>5.19b</b>		0.35 ±0.17	14.5 ±3.5	3	42	11.6
<b>5.19c</b>		0.16 ±0.06	10.9 ±1.2	3	68	11.9
<b>5.19d</b>		0.096 ±0.03	14.6 ±0.6	3	153	12.4
<b>5.19e</b>		0.12 ±0.04	6.7 ±0.6	3	67	9.9

<sup>[a]</sup> Following the relocation of our Screening Group, a consistent shift in the IC<sub>50</sub> values determined using the AlphaScreen competition assay was observed. The signifiers '**pre-2015 data**' and '**post-2015 data**' indicate respectively data acquired prior and subsequent to this relocation. For further information refer to note in **Chapter 2, Section 2.4.1.3**.

<sup>[b]</sup> IC<sub>50</sub> values are reported in μM ± S.D.

<sup>[c]</sup> BEI (Binding efficiency index, refer Section 1.4.1.2) = pIC<sub>50</sub>/MW, where pIC<sub>50</sub> is the negative base 10 logarithm of the IC<sub>50</sub> (in molar units) and MW is the compound molecular weight (in kDa).

#### 5.4.1 Amide series A - evaluation of BCL-X<sub>L</sub> and MCL-1 binding using AlphaScreen competition assay

##### 5.4.1.1 Effect of ring saturation and size

For amide series A, relative to the initial compound **5.5b** ( $IC_{50}(BCL-X_L) = 11.8 \mu M$ ), replacement of the p5 phenyl ring with a cyclohexyl moiety led to a ~4-fold improvement in  $IC_{50}$  for BCL-X<sub>L</sub> (compound **5.19b**,  $IC_{50}(BCL-X_L) = 2.5 \mu M$ ) (**Table 5.2**). This reflected a similar trend observed for the sulfonyl series (**Chapter 4**), whereby an appropriately sized aliphatic ring tended to give improved binding relative to a phenyl ring in the same position. This may indicate that the more flexible cyclohexyl ring can better mitigate any steric strain induced by the planar amide linkage.

We were gratified, however, to see that the amide linker replacement could generate analogues of similar activity to the sulfonyl precursors. For example, as compared with the comparable sulfonyl cyclohexyl analogue **4.6l**, the amide cyclohexyl analogue **5.19b** had equivalent binding to BCL-X<sub>L</sub> ( $IC_{50}(BCL-X_L) = 1.6 \mu M$  and  $2.5 \mu M$  respectively), the same calculated binding efficiency ( $BEI = 10.1$  for both molecules) and selectivity for BCL-X<sub>L</sub> relative to MCL-1 that was at least equivalent if not slightly improved (29-fold and 37-fold respectively, **Table 5.2**).

The amide analogue with the smaller cyclopropyl substituent (compound **5.19a**) showed significantly lower binding to BCL-X<sub>L</sub> ( $IC_{50}(BCL-X_L) = 30.3 \mu M$ ). As observed for the sulfonyl series, relative to the cyclohexyl, the introduction of the bulkier adamantyl substituent marginally increased binding (compound **5.19e**,  $IC_{50}(BCL-X_L) = 1.3 \mu M$ ). However, as it significantly increased molecular weight, overall this led to a slight reduction in binding efficiency.

Based on the observed activity of the cyclohexyl and adamantyl analogues, the cycloheptyl amide analogue **5.19c** and the bridged bicyclo[2.2.1]heptanyl amide analogue(s) **5.19d** (as a mixture of diastereomers) were subsequently synthesised

and were thus tested in the AlphaScreen assay at a later date (**Table 5.4**). As noted in **Chapter 1**, the overall affinities of all analogues in the series appeared to be significantly higher in this later series of assays than in the earlier assays, but the general trends within a series were maintained. Relative to the equivalent cyclohexyl analogue **5.19b** ( $IC_{50}(BCL-X_L) = 0.35 \mu M$ ), this AlphaScreen data suggested that both compounds **5.19c** and **5.19d** had similar or slightly improved binding to BCL-X<sub>L</sub> ( $IC_{50}(BCL-X_L) = 0.16 \mu M$  and  $0.096 \mu M$  respectively) and a correspondingly higher binding efficiency index (**Table 5.4**).

We were particularly interested by this result for the bicyclic compound(s) **5.19d**, which represented the tightest BCL-X<sub>L</sub> binding yet observed in the series with the simple biphenyl scaffold. As this compound was synthesised and tested as an inseparable mixture of up to four stereoisomers (two sets of diastereomers), this left open the possibility that one of these individual stereoisomers might have even higher binding for BCL-X<sub>L</sub>. Chiral-HPLC indicated that at least 3 different stereoisomers were present in the mixture (data not shown) - repeat scale-up synthesis and chiral separation might enable these individual stereoisomers to be isolated for individual testing, although this has not yet been undertaken. In the meantime we sought to crystallise a complex of BCL-X<sub>L</sub>:**5.19d** in the hope that it might indicate whether a single diastereomer could be observed to preferentially bind to BCL-X<sub>L</sub> (see discussion below).

#### 5.4.1.2 Effect of substitution on phenyl ring

For amide series A, a single methyl substituent was able to be accommodated on the p5 phenyl ring in either the *ortho*- or *meta*- position without loss of binding (compounds **5.19f-g**,  $IC_{50}(BCL-X_L) = 6-7 \mu M$ , **Table 5.2**). However the very modest increase in measured binding observed for these compounds relative to the simple phenyl precursor (compound **5.5b**,  $IC_{50}(BCL-X_L) = 11.8 \mu M$ ) is on-par with the increase in binding expected for the addition of a single methyl group based on the effect of lipophilicity alone, leading to no overall improvement in the binding efficiency index.<sup>(2)</sup> As observed earlier for the sulfonyl series (**Chapter 4**), installing a methyl substituent in the *para*- position on the phenyl ring led to a

decrease in binding (compound **5.19h**,  $IC_{50}(BCL-X_L) = 40.9 \mu M$ ), due to likely steric clash with the residues lining the base of the p5 binding pocket.

#### 5.4.2 Amide series A - Structural analysis of binding interactions

To understand the binding mode for amide series A, complexes of BCL-X<sub>L</sub>:**5.19g**, BCL-X<sub>L</sub>:**5.10b** and BCL-X<sub>L</sub>:**5.19e** were crystallised and X-ray crystal structures solved for each to high resolution (1.65, 1.70 and 1.80 Å resolution respectively). Additionally, the crystal structure of the BCL-X<sub>L</sub>:**5.19d** complex was solved to a somewhat lower resolution of 2.05 Å, towards ascertaining whether one stereoisomer of the diastereomeric mixture **5.19d** (Table 5.6) might predominate in the bound state. The final structures are presented in Figures 5.3 - 5.5. The corresponding statistics for these structures are provided in Tables 5.5 - 5.7.

##### 5.4.2.1 Structure determination of the BCL-X<sub>L</sub>:**5.19g** complex

Relevance:

- Representative structure to indicate the binding mode for amide series A

The crystal structure of the BCL-X<sub>L</sub>:**5.19g** complex revealed that the amide linked analogue **5.19g** bound according to the original design (Figure 5.3A-B) – overlay with sulfonyl analogue **1.8** from the structure of the BCL-X<sub>L</sub>:**1.8** complex revealed a very similar overall binding mode (Figure 5.3C). In particular, the carbonyl oxygen of the amide linker of compound **5.19g** was overlaid closely with one of sulfonyl oxygen atoms of compound **1.8**, in a suitable position to engage in a hydrogen bond interaction with the backbone –NH of Gly138 of BCL-X<sub>L</sub> (Figure 5.3D). Additionally, the BCL-X<sub>L</sub>:**5.19g** structure shows there is a small side-pocket extending from the side of the p5 pocket that is able to accommodate the *meta*-methyl substituent of compound **5.19g** (red asterisk, Figure 5.3A, C). Given the close overlay of the phenyl ring of compounds **1.8** and **5.19g** (Figure 5.3B), this observation also indicates the likely binding mode of

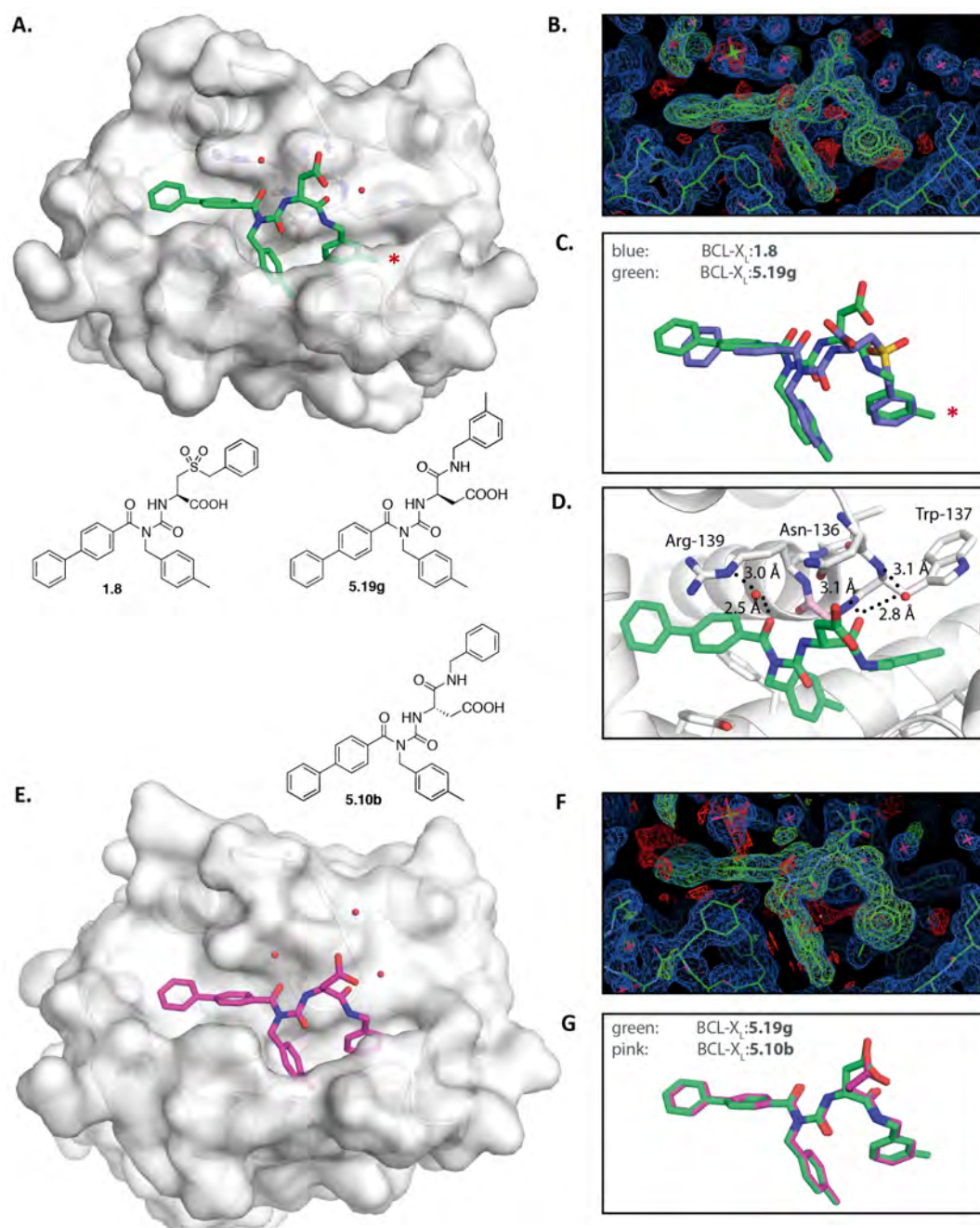
compound **4.6d**, the analogous sulfonyl linked compound containing a *meta*-methyl substituent (**Chapter 4, Table 4.1**).

#### 5.4.2.2 Structure determination of the BCL-X<sub>L</sub>:**5.10b** complex

Relevance:

- Representative structure to indicate the binding mode for amide series A

The crystal structure of the BCL-X<sub>L</sub>:**5.10b** complex reveals that compound **5.10b** binds with essentially the identical binding mode to compound **5.19g**, described earlier (**Figure 5.5E-G**). This suggests that compound **5.5b** (the enantiomer of compound **5.10b** and desmethyl equivalent of compound **5.19g**) would likely have the same pose, which provides an explanation for the equivalent binding for BCL-X<sub>L</sub> of the enantiomers **5.10b** and **5.5b** from the initial amide analogues described earlier (**Table 5.1**) – the carboxylic acid moiety of each projects directly into solvent space and there is little steric hindrance for analogues of either chirality to adopt the equivalent binding mode.



**Figure 5.3: X-ray crystal structures of BCL-X<sub>L</sub>:5.19g and BCL-X<sub>L</sub>:5.10b complexes from amide series A.**

(A) BCL-X<sub>L</sub>:5.19g complex in surface representation; (B) simulated annealing omit map; (C) BCL-X<sub>L</sub>:5.19g (green) overlaid with BCL-X<sub>L</sub>:1.8 complex (blue); and (D) compound 5.19g showing hydrogen bond from amide carbonyl oxygen to Gly138 of BCL-X<sub>L</sub> (highlighted in light pink) (E) BCL-X<sub>L</sub>:5.10b complex in surface representation; (F) simulated annealing omit map; and (G) BCL-X<sub>L</sub>:5.10b (pink) overlaid with BCL-X<sub>L</sub>:5.19g complex (green). Omit maps show 2F<sub>o</sub>-F<sub>c</sub> contoured at 1σ and F<sub>o</sub>-F<sub>c</sub> contoured at ± 3σ. The red asterisk in (A) and (C) indicates the approximate position of a small side-pocket extending from the p5 pocket.



**Table 5.5: Crystallographic statistics for the BCL-X<sub>L</sub>:5.19g and BCL-X<sub>L</sub>:5.10b complexes.**

<b>Structure <sup>Ψ</sup></b>	<b>BCL-X<sub>L</sub>:5.19g</b>	<b>BCL-X<sub>L</sub>:5.10b</b>
Wavelength (Å)	0.9537	0.9537
Resolution range (Å)	33.91 - 1.651 (1.71 - 1.651)	48.77 - 1.701 (1.762 - 1.701)
Space group	<i>P</i> 3 <sub>1</sub> 2 1	<i>P</i> 3 <sub>1</sub> 2 1
Unit cell		
<i>a</i> , <i>b</i> , <i>c</i> (Å)	97.65, 97.65, 74.03	97.53, 97.53, 73.71
α, β, γ (°)	90 90 120	90 90 120
Total reflections	509673 (32596)	487995 (43953)
Unique reflections	49102 (4791)	44728 (4403)
Multiplicity	10.4 (6.8)	10.9 (10.0)
Completeness (%)	1.00 (0.99)	1.00 (1.00)
Mean <i>I</i> / σ <i>I</i>	19.21 (2.20)	21.98 (1.98)
Wilson <i>B</i> factor (Å <sup>2</sup> )	21.35	24.24
<i>R</i> <sub>merge</sub>	0.07566 (0.7779)	0.07351 (1.246)
<i>R</i> <sub>meas</sub>	0.07958 (0.8422)	0.07717 (1.313)
CC <sub>1/2</sub>	0.999 (0.727)	0.999 (0.697)
CC*	1 (0.918)	1 (0.906)
Reflections used in refinement	49100 (4790)	44724 (4403)
Reflections used for R-free	2454 (238)	2236 (220)
<i>R</i> <sub>work</sub>	0.1754 (0.2255)	0.1715 (0.2383)
<i>R</i> <sub>free</sub>	0.1989 (0.2468)	0.1913 (0.2859)
CC <sub>work</sub>	0.959 (0.846)	0.963 (0.838)
CC <sub>free</sub>	0.948 (0.827)	0.960 (0.782)
Number of non-hydrogen atoms	2633	2743
macromolecules	2339	2409
ligands/ions	51	58
RMS(bond lengths) (Å)	0.006	0.006
RMS(bond angles) (°)	0.88	0.86
Ramachandran favored (%)	98	99
Ramachandran allowed (%)	1.8	1.4
Ramachandran outliers (%)	0	0
Rotamer outliers (%)	0.41	0.4
Clashscore	1.73	3.77
Average <i>B</i> factors (Å <sup>2</sup> )	23.62	27.87
Macromolecules	22.62	26.5
ligands	24.63	33.26
solvent	33.05	38.71

<sup>Ψ</sup> Statistics are outlined in Section 2.6.2.5.

#### 5.4.2.3 Structure determination of the BCL-X<sub>L</sub>:**5.19e** complex

Relevance:

- Reveal the binding mode of the adamantyl moiety within the p5 pocket

The crystal structure of the BCL-X<sub>L</sub>:**5.19e** complex (adamantyl analogue) (**Figure 5.4A-B**) overlays very closely with that of the *meta*-methyl phenyl analogue **5.19g** from the same series (**Figure 5.4C**). There is also a close overlay with the sulfonyl adamantyl analogue **4.25** from the crystal structure with BCL-X<sub>L</sub> described in **Chapter 4** (**Figure 5.4D**; see also **Chapter 4, Figure 4.5**). Notably the BCL-X<sub>L</sub>:**5.19e** complex is of higher resolution (1.8 Å resolution as compared to 2.2 Å resolution) such that the conformation of the adamantyl group is much more clearly resolved within the p5 pocket.

#### 5.4.2.4 Structure determination of the BCL-X<sub>L</sub>:**5.19d** complex

Relevance:

- To determine whether one of four possible stereoisomers of **5.19d** predominates in the complex, suggesting that it might bind with higher affinity to BCL-X<sub>L</sub> relative to the stereoisomers.

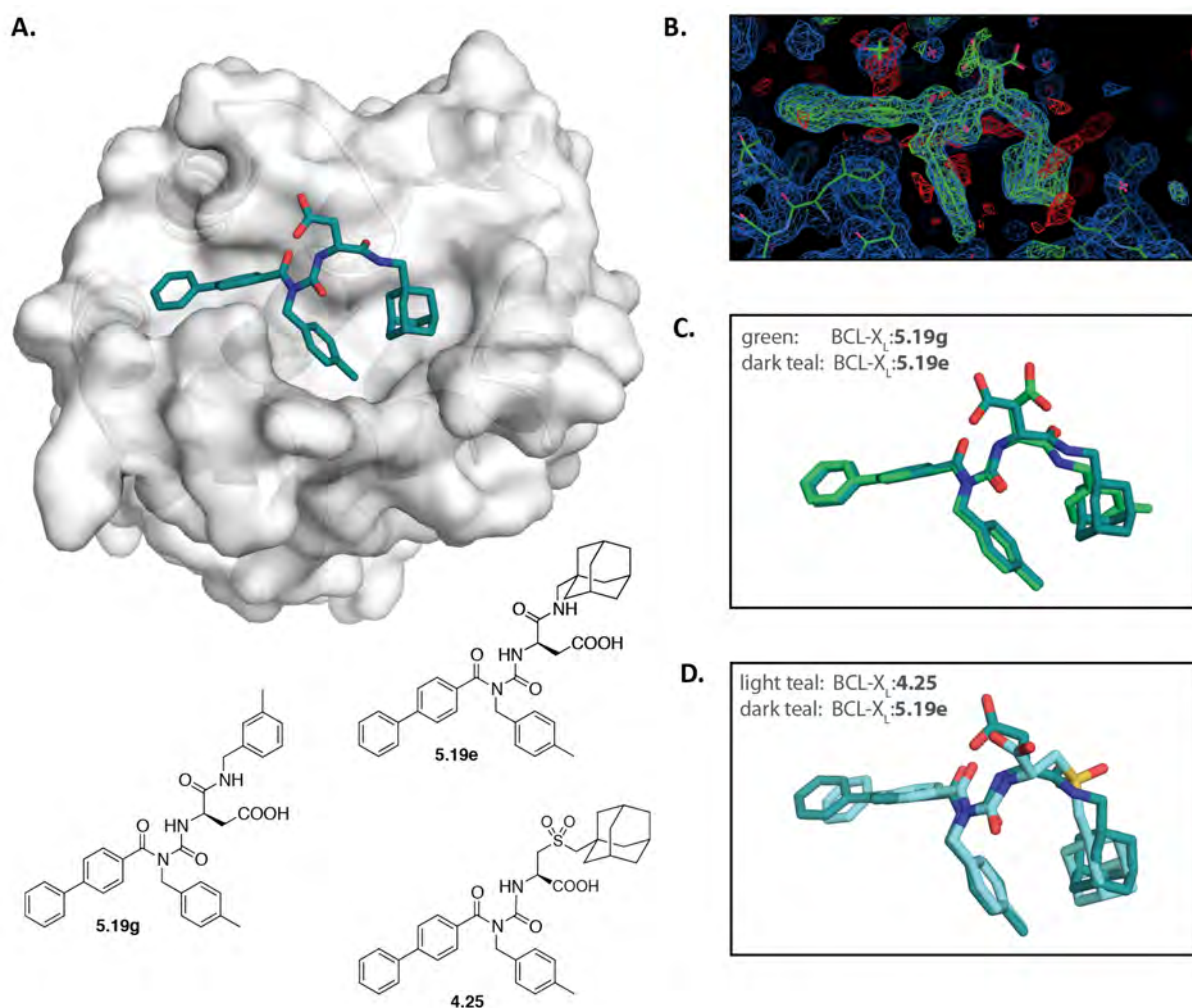
The crystal structure of the BCL-X<sub>L</sub>:**5.19d** complex (bridged bicyclic compound) was solved to a resolution of 2.05 Å. As compound **5.19d** was synthesised and tested as a mixture of four possible stereoisomers (two sets of diastereomers, as listed in **Table 5.6** and **Figure 5.5A**), by determining a crystal structure for the mixture with BCL-X<sub>L</sub> we aimed to determine whether one stereoisomers might bind with higher affinity to BCL-X<sub>L</sub> and thus predominate in the bound state. In the BCL-X<sub>L</sub>:**5.19d** structure, clear electron density corresponding to the ligand was present observed in the groove of all 12 molecules of BCL-X<sub>L</sub> in the A.S.U. (100% occupancy). Separately, each of the four possible stereoisomers was modeled into this ligand electron density (12 copies of the same ligand per A.S.U.) (**Figure 5.5A**) and the four resulting models refined. Final refinement statistics ( $R_{\text{work}}$  and  $R_{\text{free}}$ ) are provided for each in **Table 5.6**. Crystallographic statistics are

provided in **Table 5.7** for the BCL-X<sub>L</sub>:**5.19d(SRR)** model, which had the lowest  $R_{\text{free}}$  following the single round of parallel refinement.

**Table 5.6: Four diastereomers modeled into BCL-X<sub>L</sub>:5.19d structure and final refinement statistics for each.**

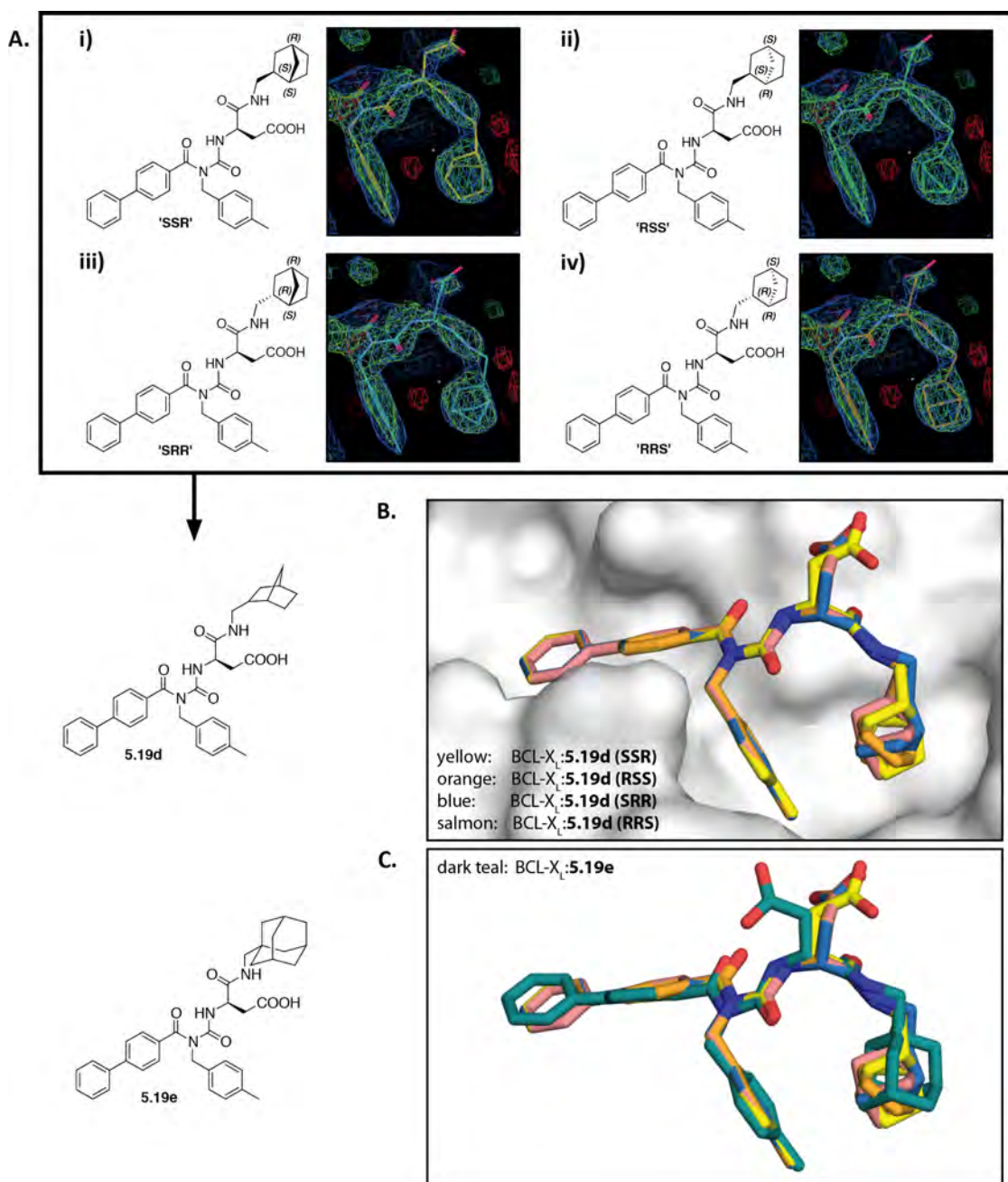
<b>5.19d</b>	<b>Compound name</b>	<b><math>R_{\text{work}}</math></b>	<b><math>R_{\text{free}}</math></b>
<b>‘SSR’</b>	( <i>R</i> )-3-(3-([1,1'-biphenyl]-4-carbonyl)-3-(4-methylbenzyl)ureido)-4-((( <b>1<i>S</i>,2<i>S</i>,4<i>R</i></b> )-bicyclo[2.2.1]heptan-2-ylmethyl)amino)-4-oxobutanoic acid	0.1844	0.2249
<b>‘RSS’</b>	( <i>R</i> )-3-(3-([1,1'-biphenyl]-4-carbonyl)-3-(4-methylbenzyl)ureido)-4-((( <b>1<i>R</i>,2<i>S</i>,4<i>S</i></b> )-bicyclo[2.2.1]heptan-2-ylmethyl)amino)-4-oxobutanoic acid	0.1842	0.2253
<b>‘SRR’</b>	( <i>R</i> )-3-(3-([1,1'-biphenyl]-4-carbonyl)-3-(4-methylbenzyl)ureido)-4-((( <b>1<i>S</i>,2<i>R</i>,4<i>R</i></b> )-bicyclo[2.2.1]heptan-2-ylmethyl)amino)-4-oxobutanoic acid	0.1836	0.2245
<b>‘RRS’</b>	( <i>R</i> )-3-(3-([1,1'-biphenyl]-4-carbonyl)-3-(4-methylbenzyl)ureido)-4-((( <b>1<i>R</i>,2<i>R</i>,4<i>S</i></b> )-bicyclo[2.2.1]heptan-2-ylmethyl)amino)-4-oxobutanoic acid	0.1837	0.2249

As indicated in **Table 5.6**, the final refinement statistics were similar for all four models and at this resolution no obvious electron density (positive or negative) was apparent following refinement to indicate whether one particular model might predominate. As is clear from the initial modeling (**Figure 5.5A**), each of the different stereoisomers appears to have sufficient flexibility to accommodate a conformation consistent with the observed electron density; the data from the crystal structure is consistent with potentially representing a crystallographic average of multiple stereoisomers having similar affinity. At this resolution, it appears that this dataset is unable to conclusively indicate either way. However, overlay of all four refined models of the different stereoisomers (**Figure 5.5B**) reveals the close packing of one face of the bridged bicyclic moiety against the p4 tolyl moiety and against the protein wall in the p5 pocket, whilst occupying a smaller overall footprint than the bulkier adamantyl group of compound **5.19e** (**Figure 5.5C**). This may contribute to the improved potency and efficiency of compound **5.19d** for BCL-X<sub>L</sub>. Whilst acquisition of another dataset at higher resolution may assist to address the outstanding question as to whether one stereoisomer is more potent, most likely it will be necessary to isolate the individual stereoisomers *via* chiral HPLC from the mixture **5.19d** and evaluate their binding individually to obtain a conclusive answer.



**Figure 5.4: Crystal structure of the BCL-X<sub>L</sub>:5.19e complex from amide series A.**

(A) BCL-X<sub>L</sub>:5.19e complex in surface representation showing predominant ligand conformation. (B) Simulated annealing omit map ( $2F_o - F_c$  contoured at  $1\sigma$ ;  $F_o - F_c$  contoured at  $\pm 3\sigma$ ) showing the two ligand conformations modeled into the final structure, with alternative positions of the carboxylic acid moiety (C) Overlay of the BCL-X<sub>L</sub>:5.19e and BCL-X<sub>L</sub>:5.19g complexes. (D) Overlay of the BCL-X<sub>L</sub>:5.19e and BCL-X<sub>L</sub>:4.25 complexes.



**Figure 5.5: Crystal structures of the BCL-X<sub>L</sub>:5.19d complex (as a mixture of stereoisomers) from amide series A.**

(A)(i-iv) Simulated annealing omit map of the BCL-X<sub>L</sub>:**5.19d** complex, focusing on the p4/p5 pockets, showing each of the four potential stereoisomers present in the **5.19d** mixture modeled into the observed electron density. For each omit map,  $2F_o - F_c$  is contoured at  $1\sigma$  and  $F_o - F_c$  is contoured at  $\pm 3\sigma$ . (B) Overlay of the refined structures of each of the four possible stereoisomers of **5.19d** – ‘SSR’ (yellow), ‘RSS’ (orange), ‘SRR’ (blue) and ‘RRS’ (salmon) – in complex with BCL-X<sub>L</sub>. (D) Overlay of the four **5.19d** structures with the BCL-X<sub>L</sub>:**5.19e** (adamantyl) complex (dark teal).

**Table 5.7: Crystallographic statistics for the BCL-X<sub>L</sub>:5.19e and BCL-X<sub>L</sub>:5.19d(SRR) complexes.**

Structure <sup>‡</sup>	BCL-X <sub>L</sub> :5.19e	BCL-X <sub>L</sub> :5.19d(SRR)
Wavelength (Å)	0.9537	0.9537
Resolution range (Å)	40.6 - 1.8 (1.864 - 1.8)	39.9 - 2.047 (2.12 - 2.047)
Space group	<i>P</i> 3 <sub>1</sub> 2 1	<i>P</i> 2 <sub>1</sub>
Unit cell		
<i>a</i> , <i>b</i> , <i>c</i> (Å)	97.42, 97.42, 73.50	92.59, 103.36, 110.61
$\alpha$ , $\beta$ , $\gamma$ (°)	90 90 120	90 110.912 90
Total reflections	395984 (25014)	692518 (62454)
Unique reflections	37540 (3602)	120033 (11303)
Multiplicity	10.5 (6.9)	5.8 (5.5)
Completeness (%)	1.00 (0.97)	0.98 (0.93)
Mean <i>I</i> / $\sigma$ <i>I</i>	28.12 (2.46)	15.72 (1.79)
Wilson <i>B</i> factor (Å <sup>2</sup> )	24.66	36.44
<i>R</i> <sub>merge</sub>	0.05785 (0.759)	0.07949 (1.074)
<i>R</i> <sub>meas</sub>	0.06082 (0.8205)	0.08743 (1.185)
CC <sub>1/2</sub>	1 (0.731)	0.999 (0.597)
CC*	1 (0.919)	1 (0.865)
Reflections used in refinement	37536 (3601)	120018 (11304)
Reflections used for R-free	1877 (180)	6003 (563)
<i>R</i> <sub>work</sub>	0.1729 (0.2490)	0.1837 (0.2878)
<i>R</i> <sub>free</sub>	0.1992 (0.2820)	0.2243 (0.3205)
CC <sub>work</sub>	0.961 (0.833)	0.964 (0.752)
CC <sub>free</sub>	0.953 (0.776)	0.958 (0.745)
Number of non-hydrogen atoms	2704	14602
macromolecules	2383	13651
ligands/ions	116	581
RMS(bond lengths) (Å)	0.006	0.008
RMS(bond angles) (°)	0.83	0.93
Ramachandran favored (%)	99	98
Ramachandran allowed (%)	1	1.4
Ramachandran outliers (%)	0	0.3
Rotamer outliers (%)	0.79	0.85
Clashscore	4.16	7.98
Average <i>B</i> factors (Å <sup>2</sup> )	26.14	50.17
Macromolecules	24.92	49.71
ligands	30.84	63.07
solvent	37.68	46.94
Number of TLS groups	NA	70

<sup>‡</sup> Statistics are outlined in Section 2.6.2.5.

### 5.4.3 Amide series B - evaluation of BCL-X<sub>L</sub> and MCL-1 binding using AlphaScreen competition assay

Binding data for the amide series B compounds (**5.15a**, **5.23a-h**), screened in the AlphaScreen competition assay, are listed in **Table 5.3** (pre-2015 data).

#### 5.4.3.1 Effect of ring saturation and size

For amide series B, relative to the initial compound **5.15a** ( $IC_{50}(BCL-X_L) = 8.1 \mu M$ ), replacement of the p5 phenyl ring with a saturated ring system of similar size, such as a cyclopentyl (compound **5.23a**,  $IC_{50}(BCL-X_L) = 5.8 \mu M$ ) or cyclohexyl moiety (compound **5.23b**,  $IC_{50}(BCL-X_L) = 4.3 \mu M$ ) gave a small increase in binding. This reflected the similar trend observed for amide series A and also the earlier sulfonyl series (**Chapter 4**). Both the cyclohexyl and cyclopentyl analogues had the same overall calculated binding efficiency index (**Table 5.3**).

Addition of a *meta*-substituted hydroxyl moiety on the p5 cyclohexyl ring (compound **5.23c**, tested as a mixture of four possible stereoisomers,  $IC_{50}(BCL-X_L) = 5.8 \mu M$ ) conferred no apparent improvement in binding relative to the parent cyclohexyl analogue **5.23b**, even accounting for potential differing activity of the different stereoisomers.

The fused bicyclic compound **5.23d** (tested as a mixture of *cis/trans* diastereomers,  $IC_{50}(BCL-X_L) = 5.4 \mu M$ ) explored whether further rigidifying the conformation of the p5 cyclohexyl ring might be beneficial for activity. However, similar to compound **5.23c**, even accounting for the potentially differing activities of the two diastereomers, compound **5.23d** showed no improvement in binding sufficient to warrant further investigation (and had a lower calculated binding efficiency index relative to the cyclohexyl analogue **5.23b**, **Table 5.3**).



#### 5.4.3.2 Effect of mono- or di-substitution on phenyl ring

For the amide series B analogues exploring substitution around the p5 phenyl ring, as for Series A, mono-substitution with a *para*-methyl substituent (compound **5.23f**,  $IC_{50}(BCL-X_L) = 23.4 \mu M$ ) was detrimental for binding, whilst a single *ortho*-methyl substituent was tolerated, leading to a small increase in binding (compound **5.23e**,  $IC_{50}(BCL-X_L) = 5.5 \mu M$ ). Both of the methyl-di-substituted analogues (**5.23g** and **5.23h**) had reduced binding to BCL-X<sub>L</sub>.

#### 5.4.4 Amide series B - Structural analysis of binding interactions

To validate the binding mode for the amide series B compounds, crystal structures were determined for two complexes, BCL-X<sub>L</sub>:**5.15a** (the parent amide series B p5 phenyl analogue) and BCL-X<sub>L</sub>:**5.23a** (p5 *meta*-methyl substituted analogue) to high-resolution (1.65 Å and 1.70 Å resolution respectively). The final structures are presented in **Figures 5.6**; corresponding statistics for the two structures are provided in **Table 5.8**.

##### 5.4.4.1 Structure determination of the BCL-X<sub>L</sub>:**5.15a** complex

Relevance:

- Representative structure to indicate the binding mode for amide series B

The crystal structure of the BCL-X<sub>L</sub>:**5.15a** complex reveals a similar binding mode of the ligand to similar structures described earlier. However, it reveals that for compound **5.15a** the alternative amide series B linker, whilst it successfully bridges across to place the terminal phenyl ring in the p5 pocket, deviates from the original design in that the amide carbonyl primarily adopts a conformation oriented away from Gly138 of BCL-X<sub>L</sub> (**Figure 5.6A-B**). Thus, unlike the sulfonyl linker of lead compound **1.8**, the amide carbonyl of compound **5.15a** does not directly interact with the backbone -NH of Gly138 (**Figure 5.6C-D**). Potentially this conformational difference might be reflected in the slightly weaker  $IC_{50}$  for



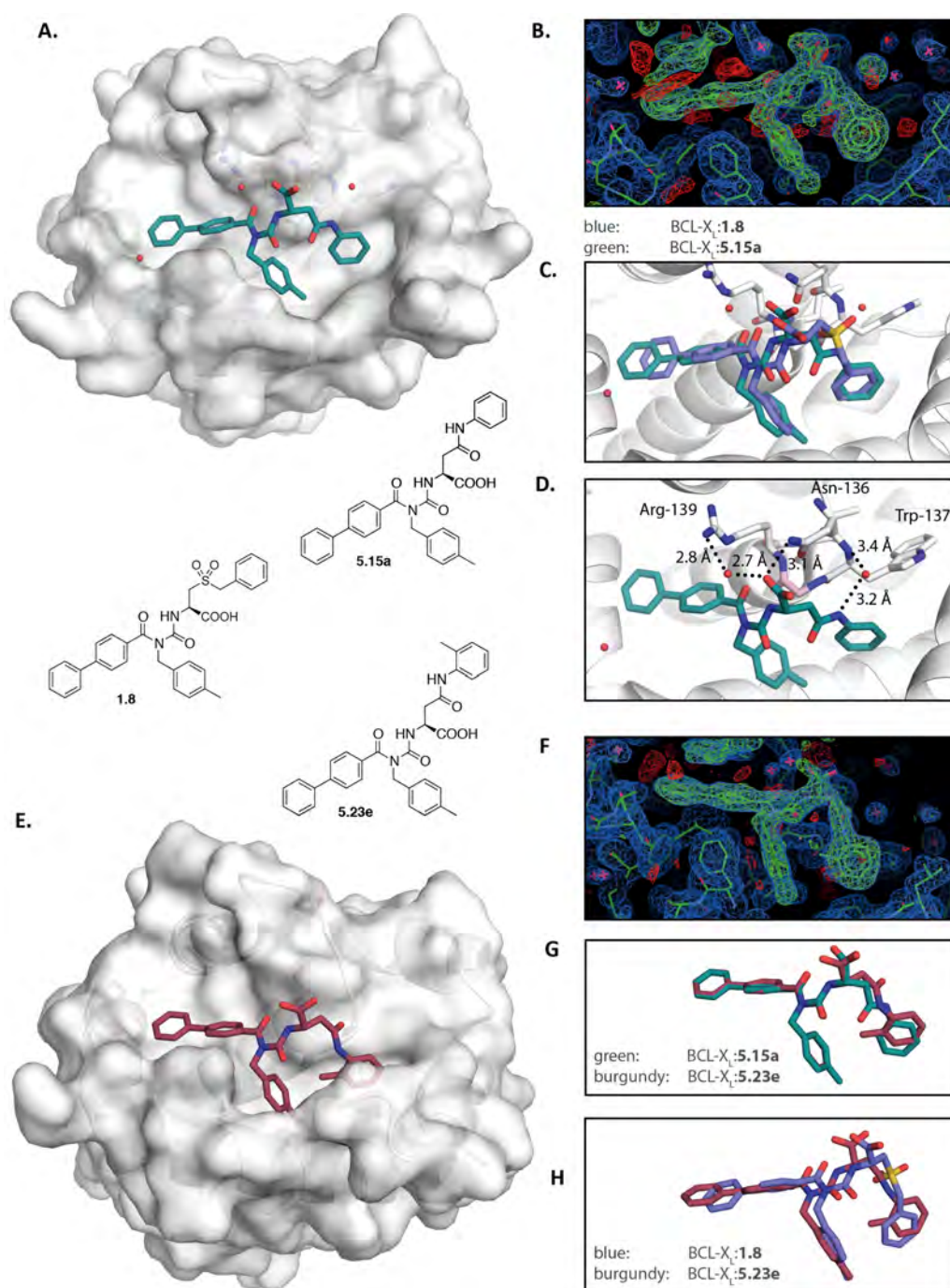
BCL-X<sub>L</sub> of the most potent amide series B analogue (cyclohexyl analogue **5.23a**, IC<sub>50</sub>(BCL-X<sub>L</sub>) = 4.3 μM, **Table 5.3**) as compared to the analogous cyclohexyl analogues from either amide series A or the sulfonyl series (respectively compound **5.19b**, IC<sub>50</sub>(BCL-X<sub>L</sub>) = 2.5 μM, and compound **1.8**, IC<sub>50</sub>(BCL-X<sub>L</sub>) = 1.6 μM, **Table 5.3**).

#### 5.4.4.2 Structure determination of the BCL-X<sub>L</sub>:**5.23e** complex

Relevance:

- Representative structure to indicate the binding mode for amide series B
- Analyse effect of *meta*-methyl substituent on phenyl ring in p5 pocket

The crystal structure of the BCL-X<sub>L</sub>:**5.23e** complex (**Figure 5.6E,F**) in comparison reveals that certain substituents can induce the Series B amide linker to adopt the designed conformation. In this structure, the *meta*-methyl substituent of compound **5.23e**, introduced onto the phenyl ring in the p5 pocket, packs closely against the neighbouring tolyl moiety of compound **5.23e** in the p4 pocket. As this would result in a steric clash between the *meta*-methyl substituent and the carbonyl of the amide linker (**Figure 5.6G**), the amide carbonyl is instead observed to occupy the designed conformation, in which it can interact with the backbone -NH of Gly138 of BCL-X<sub>L</sub> and overlays closely with the sulfonyl group of compound **1.8** (**Figure 5.6H**). This suggests that the amide series B linker can adopt the designed conformation under certain circumstances, but this will likely be context-dependent.



**Figure 5.6: Crystal structures of BCL-X<sub>L</sub>:5.15a and BCL-X<sub>L</sub>:5.23e complexes from amide series B.**

(A) BCL-X<sub>L</sub>:5.15a complex surface representation; (B) omit map; (C) BCL-X<sub>L</sub>:5.15a (green) overlaid with BCL-X<sub>L</sub>:1.8 complex (blue); and (D) compound 5.15a showing hydrogen bonding network. Gly138 of BCL-X<sub>L</sub> is highlighted in light pink. (E) BCL-X<sub>L</sub>:5.23e complex surface representation; (F) omit map; (G) BCL-X<sub>L</sub>:5.23e (burgundy) overlaid with BCL-X<sub>L</sub>:5.15a complex (green); and (G) overlaid with BCL-X<sub>L</sub>:1.8 complex (blue). Omit maps show 2F<sub>o</sub>-F<sub>c</sub> contoured at 1σ and F<sub>o</sub>-F<sub>c</sub> contoured at ± 3σ.

**Table 5.8: Crystallographic statistics for the BCL-X<sub>L</sub>:5.15a and BCL-X<sub>L</sub>:5.23e complexes.**

Structure <sup>Ψ</sup>	BCL-X <sub>L</sub> :5.15a	BCL-X <sub>L</sub> :5.23e
Wavelength (Å)	0.9537	0.9537
Resolution range (Å)	36.77 - 1.65 (1.709 - 1.65)	33.85 - 1.701 (1.762 - 1.701)
Space group	<i>P</i> 3 <sub>1</sub> 2 1	<i>P</i> 3 <sub>1</sub> 2 1
Unit cell		
<i>a</i> , <i>b</i> , <i>c</i> (Å)	97.66, 97.66, 74.40	97.61, 97.61, 73.89
α, β, γ (°)	90, 90, 120	90, 90, 120
Total reflections	519680 (33235)	489928 (44008)
Unique reflections	49332 (4833)	44767 (4346)
Multiplicity	10.5 (6.9)	10.9 (10.1)
Completeness (%)	1.00 (0.98)	1.00 (0.98)
Mean <i>I</i> / σ <i>I</i>	22.87 (2.54)	20.06 (1.92)
Wilson <i>B</i> factor (Å <sup>2</sup> )	23.85	26.72
<i>R</i> <sub>merge</sub>	0.05976 (0.7553)	0.07071 (1.284)
<i>R</i> <sub>meas</sub>	0.06282 (0.8171)	0.07424 (1.352)
CC <sub>1/2</sub>	0.999 (0.755)	0.999 (0.685)
CC*	1 (0.928)	1 (0.902)
Reflections used in refinement	49326 (4832)	44765 (4345)
Reflections used for R-free	2467 (241)	2237 (217)
<i>R</i> <sub>work</sub>	0.1741 (0.2344)	0.1818 (0.2551)
<i>R</i> <sub>free</sub>	0.2047 (0.2734)	0.2022 (0.3102)
CC <sub>work</sub>	0.960 (0.852)	0.958 (0.834)
CC <sub>free</sub>	0.945 (0.816)	0.948 (0.770)
Number of non-hydrogen atoms	2913	2683
macromolecules	2497	2381
ligands/ions	88	98
RMS(bond lengths) (Å)	0.006	0.006
RMS(bond angles) (°)	0.97	1.01
Ramachandran favored (%)	98	98
Ramachandran allowed (%)	1.7	1.7
Ramachandran outliers (%)	0	0
Rotamer outliers (%)	1.9	2
Clashscore	3	3.35
Average <i>B</i> factors (Å <sup>2</sup> )	28.48	28.62
Macromolecules	26.82	27.51
ligands	29.98	36.12
solvent	40.75	37.98

<sup>Ψ</sup> Statistics are outlined in Section 2.6.2.5.

## 5.5 Discussion/Conclusion

In this chapter the development of two novel series of benzoylurea analogues have been described, in which the 'linker group' (between the benzoylurea core and the terminal substituent in the p5 pocket) has been replaced with an amide moiety in two different ways (amide series A and B).

Binding studies and X-ray crystal structure analysis of both of these amide series have demonstrated that whilst initial analogues bind to BCL-X<sub>L</sub> with IC<sub>50</sub> values in the low micromolar range, it is the Series A amide linker variant that most closely matches the original design. That is, for Series A structural data reveals that the amide carbonyl indeed acts as an isostere of the earlier sulfonyl linker, undergoing a hydrogen bond interaction with the protein backbone –NH of Gly138 of BCL-X<sub>L</sub>.

A subsequent parallel methodology has been developed to enable synthesis of a range of simple analogues for both amide series A and B that explored further modifications in the p5 pocket. Amongst the analogues described were novel biphenyl benzoylurea analogues with which showed improved binding to BCL-X<sub>L</sub> (including an improved binding efficiency index, and selectivity for BCL-X<sub>L</sub> relative to MCL-1) relative to the most potent analogues in the earlier sulfonyl series. Most notable among these were the amide series A compounds **5.19b**, **5.19c**, and **5.19d**, which had an IC<sub>50</sub> for BCL-X<sub>L</sub> in the range 100-350 nM in the most recent series of AlphaScreen assays (**Table 5.4**).

Further studies based on the initial structural analysis described in this Chapter may lead to further improved inhibitors of BCL-X<sub>L</sub>.

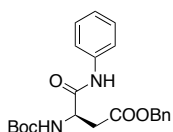
## 5.6 Experimental

For **General Procedures A, B, E - G**, refer to **Chapter 2, Section 2.2**.

For synthesis of compounds **3.3** and **3.4**, refer to **Chapter 3, Section 3.5.1**.

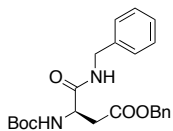
### 5.6.1 Synthesis of trial amide series

#### 5.6.1.1 Amide-coupling to protected Aspartic acids [**Scheme 5.1 (c)**]



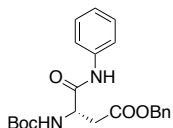
**(R)-benzyl 3-((tert-butoxycarbonyl)amino)-4-oxo-4-(phenylamino)butanoate (5.1a):**

To a stirred solution of Boc-D-Asp(OBzl)-OH (323 mg, 1.00 mmol) in DMF (2.5 mL) under N<sub>2</sub> was added HBTU (398 mg, 1.05 mmol) and DIPEA (348  $\mu$ L, 2.0 mmol) and the reaction was allowed to stir for 15 minutes at room temperature. After this time, aniline (96  $\mu$ L, 1.05 mmol) was added and the solution stirred for a further 5 h. The reaction was diluted with EtOAc (20 mL), quenched with sat. aq. NaHCO<sub>3</sub> (10 mL), the layers separated and the aqueous phase extracted with EtOAc (3 x 10 mL). The combined organic phases were washed with water, brine, dried (MgSO<sub>4</sub>) and concentrated to afford compound **5.1a** as an off-white solid (381 mg, 95%), which was used directly without further purification. <sup>1</sup>H NMR (300 MHz, CDCl<sub>3</sub>)  $\delta$  8.50 (br s, 1H), 7.48 (d, *J* = 7.7 Hz, 2H), 7.38–7.27 (m, 7H), 7.11 (t, *J* = 7.4 Hz, 1H), 5.82 (d, *J* = 6.1 Hz, 1H), 5.19 (d, *J* = 12.3 Hz, 1H), 5.13 (d, *J* = 12.2 Hz, 1H), 4.65 (br s, 1H), 3.10 (dd, *J* = 17.2, 4.3 Hz, 1H), 2.80 (dd, *J* = 17.2, 6.4 Hz, 1H), 1.48 (s, 9H). <sup>13</sup>C NMR (75 MHz, CDCl<sub>3</sub>)  $\delta$  172.06, 168.91, 137.67, 135.44, 129.14, 128.78, 128.58, 128.44, 124.64, 120.06, 81.14, 67.19, 51.48, 35.96, 28.44. MS (ES<sup>+</sup>), *m/z* 399.8 (M + H).



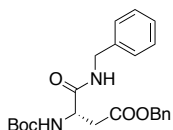
**(R)-benzyl 4-(benzylamino)-3-((tert-butoxycarbonyl)amino)-4-oxobutanoate (5.1b):**

Compound **5.1b** was prepared as for compound **5.1a**, *via* an HBTU-mediated amide coupling of Boc-D-Asp(OBzl)-OH (323 mg, 1.00 mmol) and benzylamine (115  $\mu$ L, 1.05 mmol), to afford a pale yellow glass (407 mg, 99%). This material was used directly without further purification. <sup>1</sup>H NMR (300 MHz, CDCl<sub>3</sub>)  $\delta$  7.45–7.19 (m, 10H), 6.79 (br s, 1H), 5.67 (d, *J* = 6.0 Hz, 1H), 5.21–5.04 (m, 2H), 4.63–4.30 (m, 3H), 3.10 (dd, *J* = 17.1, 4.5 Hz, 1H), 2.75 (dd, *J* = 17.2, 6.3 Hz, 1H), 1.42 (s, 9H). <sup>13</sup>C NMR (75 MHz, CDCl<sub>3</sub>)  $\delta$  171.91, 170.69, 155.65, 138.04, 135.52, 128.82, 128.77, 128.56, 128.40, 127.67, 127.62, 80.77, 67.01, 50.88, 43.69, 36.21, 28.40. MS (ES<sup>+</sup>), *m/z* 413.8 (M + H).



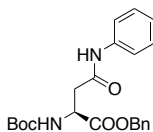
**(S)-benzyl 3-((tert-butoxycarbonyl)amino)-4-oxo-4-(phenylamino)butanoate (5.6a):**

Compound **5.6a** was prepared as for compound **5.1a**, *via* an HBTU-mediated amide coupling of Boc-L-aspartic acid  $\beta$  benzyl ester (323 mg, 1.0 mmol) and aniline (96  $\mu$ L, 1.05 mmol). An off-white solid was obtained (395 mg, 99%). This material was used directly in the next step without further purification. <sup>1</sup>H NMR (300 MHz, CDCl<sub>3</sub>)  $\delta$  8.50 (s, 1H), 7.48 (dd, *J* = 8.6, 1.0 Hz, 2H), 7.39–7.28 (m, 7H), 7.11 (t, *J* = 7.4 Hz, 1H), 5.82 (d, *J* = 4.5 Hz, 1H), 5.24–5.08 (m, 2H), 4.90–4.48 (m, 1H), 3.10 (dd, *J* = 17.2, 4.3 Hz, 1H), 2.80 (dd, *J* = 17.2, 6.5 Hz, 1H), 1.48 (s, 9H). <sup>13</sup>C NMR (75 MHz, CDCl<sub>3</sub>)  $\delta$  172.05, 168.91, 139.99, 137.66, 135.44, 129.14, 128.78, 128.58, 128.44, 124.64, 120.07, 81.12, 67.19, 51.46, 35.96, 28.44. MS (ES<sup>+</sup>), *m/z* 399.3 (M + H).



**(S)-benzyl 4-(benzylamino)-3-((tert-butoxycarbonyl)amino)-4-oxobutanoate (5.6b):**

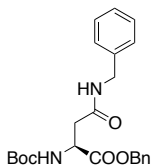
Compound **5.6b** was prepared as for compound **5.1a**, *via* an HBTU-mediated amide coupling of Boc-L-aspartic acid  $\beta$  benzyl ester (323 mg, 1.00 mmol) and benzylamine (115  $\mu$ L, 1.05 mmol). An opaque yellowish glass was obtained (408 mg, 99%). This material was used directly in the next step without further purification.  $^1\text{H}$  NMR (300 MHz,  $\text{CDCl}_3$ )  $\delta$  7.54–7.12 (m, 10H), 6.78 (s, 1H), 5.66 (d,  $J$  = 6.9 Hz, 1H), 5.28–4.94 (m, 2H), 4.68–4.21 (m, 3H), 3.10 (dd,  $J$  = 17.1, 4.5 Hz, 1H), 2.75 (dd,  $J$  = 17.1, 6.2 Hz, 1H), 1.42 (s, 9H).  $^{13}\text{C}$  NMR (75 MHz,  $\text{CDCl}_3$ )  $\delta$  171.93, 170.68, 155.74, 138.05, 135.52, 128.83, 128.78, 128.56, 128.40, 127.68, 127.62, 80.80, 67.01, 50.89, 43.70, 36.21, 28.40. MS ( $\text{ES}^+$ ),  $m/z$  413.5 ( $\text{M} + \text{H}$ ).



**(S)-benzyl 2-((tert-butoxycarbonyl)amino)-4-oxo-4-(phenylamino)butanoate (5.11a):**

Compound **5.11a** was prepared as for compound **5.1a**, *via* an HBTU-mediated amide coupling of Boc-L-aspartic acid  $\alpha$ -benzyl ester (323 mg, 1.00 mmol) and aniline (96  $\mu$ L, 1.05 mmol). An orange solid was obtained (380 mg, 95%). This material was used directly in the next step without further purification.  $^1\text{H}$  NMR (300 MHz,  $\text{CDCl}_3$ )  $\delta$  7.45 (d,  $J$  = 7.7 Hz, 3H), 7.36–7.27 (m, 7H), 7.11 (t,  $J$  = 7.4 Hz, 1H), 5.78 (d,  $J$  = 5.9 Hz, 1H), 5.23 (d,  $J$  = 12.3 Hz, 1H), 5.17 (d,  $J$  = 12.3 Hz, 1H), 4.70–4.52 (m, 1H), 3.08 (dd,  $J$  = 15.6, 4.7 Hz, 1H), 2.91 (dd,  $J$  = 16.0, 4.4 Hz, 1H), 1.42 (s, 9H).  $^{13}\text{C}$  NMR (75 MHz,  $\text{CDCl}_3$ )  $\delta$  171.35, 168.21, 155.93, 137.60, 135.48, 129.13, 128.69, 128.49, 128.37, 124.70, 120.07, 80.40, 67.66, 50.71, 39.43, 28.43.<sup>[a]</sup> MS ( $\text{ES}^+$ ),  $m/z$  399.5 ( $\text{M} + \text{H}$ ).

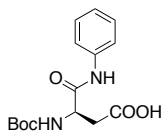
<sup>[a]</sup> One aromatic peak is not observed due to overlap.



**(S)-benzyl 4-(benzylamino)-2-((tert-butoxycarbonyl)amino)-4-oxobutanoate (5.11b):**

Compound **5.11b** was prepared as for compound **5.1a**, *via* an HBTU-mediated amide coupling of Boc-L-aspartic acid  $\alpha$ -benzyl ester (323 mg, 1.00 mmol) and benzylamine (115  $\mu$ L, 1.05 mmol). An off-white glass was obtained (410 mg, 99%). This material was used directly in the next step without further purification.  $^1\text{H}$  NMR (300 MHz,  $\text{CDCl}_3$ )  $\delta$  7.30–7.12 (m, 10H), 5.86–5.66 (m, 2H), 5.19–5.02 (m, 2H), 4.53–4.43 (m, 1H), 4.31 (d,  $J$  = 5.7 Hz, 2H), 2.85 (dd,  $J$  = 15.5, 4.3 Hz, 1H), 2.67 (dd,  $J$  = 15.7, 4.5 Hz, 1H), 1.34 (s, 9H).  $^{13}\text{C}$  NMR (75 MHz,  $\text{CDCl}_3$ )  $\delta$  171.42, 169.73, 155.85, 137.97, 135.60, 128.89, 128.68, 128.45, 128.34, 127.92, 127.77, 80.16, 67.50, 50.77, 43.78, 38.13, 28.42. MS ( $\text{ES}^+$ ),  $m/z$  413.3 ( $\text{M} + \text{H}$ ).

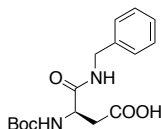
### 5.6.1.2 Hydrogenolysis of benzyl protecting group [Scheme 5.1 (d)]



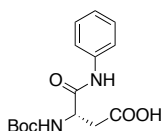
**(R)-3-((tert-butoxycarbonyl)amino)-4-oxo-4-(phenylamino)butanoic acid (5.2a):** A solution of compound **5.1a** in methanol (381 mg, 0.95 mmol, 0.05 M in methanol) was subjected to hydrogenation using an H-Cube Continuous flow Hydrogenation Reactor (Thales Nano) (10% Pd/C,

50°C, 1 bar, 1 mL/minute). TLC indicated full conversion after a single pass. Concentration *in vacuo* afforded compound **5.2a** as a colourless glass, which formed a crystalline white solid on standing (267 mg, 91%). <sup>1</sup>H NMR (300 MHz, MeOD)  $\delta$  7.54 (d, *J* = 8.0 Hz, 2H), 7.30 (t, *J* = 7.7 Hz, 2H), 7.10 (t, *J* = 7.4 Hz, 1H), 4.56 (t, *J* = 6.4 Hz, 1H), 2.85 (dd, *J* = 16.2, 6.0 Hz, 1H), 2.70 (dd, *J* = 16.4, 7.4 Hz, 1H), 1.46 (s, 9H).<sup>[a]</sup> <sup>13</sup>C NMR (151 MHz, MeOD)  $\delta$  174.22, 171.93, 157.71, 139.34, 129.74, 125.42, 121.55, 80.93, 53.28, 37.47, 28.65. MS (ES<sup>-</sup>), *m/z* 306.9 (M - H).

<sup>[a]</sup> A peak observed at  $\delta$  2.81 ppm is a minor impurity.

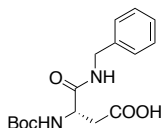


**(R)-4-(benzylamino)-3-((tert-butoxycarbonyl)amino)-4-oxobutanoic acid (5.2b):** A solution of **5.1b** in methanol (407 mg, 0.99 mmol, 0.05 M in methanol) was subjected to hydrogenation as for compound **5.2a**. Compound **5.2b** was obtained as a white glass (261 mg, 84%). <sup>1</sup>H NMR (300 MHz, MeOD)  $\delta$  7.35–7.17 (m, 5H), 4.46 (t, *J* = 6.2 Hz, 1H), 4.39 (s, 2H), 2.81 (dd, *J* = 16.5, 5.8 Hz, 1H), 2.67 (dd, *J* = 16.5, 7.3 Hz, 1H), 1.43 (s, 10H). <sup>13</sup>C NMR (151 MHz, MeOD)  $\delta$  174.12, 173.73, 157.63, 139.77, 129.45, 128.30, 128.09, 80.90, 52.76, 44.06, 37.18, 28.66. MS (ES<sup>-</sup>), *m/z* 321.1 (M - H).

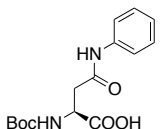


**(S)-3-((tert-butoxycarbonyl)amino)-4-oxo-4-(phenylamino)butanoic acid (5.7a):** A solution of **5.6a** in methanol (395 mg, 0.99 mmol, 0.05 M in methanol) was subjected to hydrogenation as for compound **5.2a**. Compound **5.7a** was obtained as an opaque colourless glass (258 mg, 84%). <sup>1</sup>H NMR (300 MHz, MeOD)  $\delta$  7.54 (d, *J* = 7.7 Hz, 2H), 7.30 (t, *J* = 8.0 Hz, 2H), 7.10 (tt, *J* = 7.4, 1.1 Hz, 1H), 4.57 (t, *J* = 6.1 Hz, 1H), 2.86 (dd, *J* = 16.5, 6.1 Hz, 1H), 2.71 (dd, *J* = 16.4, 7.4 Hz, 1H), 1.46 (s, 9H).<sup>[a]</sup> <sup>13</sup>C NMR (151 MHz, MeOD)  $\delta$  174.11, 171.89, 157.71, 139.34, 129.80, 129.74, 125.42, 121.55, 80.94, 53.24, 37.36, 28.65. MS (ES<sup>-</sup>), *m/z* 306.9 (M - H).

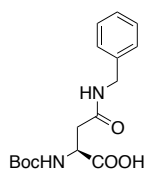
<sup>[a]</sup> A peak observed at  $\delta$  2.81 ppm is a minor impurity.



**(S)-4-(benzylamino)-3-((tert-butoxycarbonyl)amino)-4-oxobutanoic acid (5.7b):** A solution of **5.6b** in methanol (408 mg, 0.99 mmol, 0.05 M in methanol) was subjected to hydrogenation as for compound **5.2a**. Compound **5.7b** was obtained as a colourless glass (262 mg, 84%). <sup>1</sup>H NMR (300 MHz, MeOD)  $\delta$  7.50–6.97 (m, 5H), 4.46 (t, *J* = 6.1 Hz, 1H), 4.39 (s, 2H), 2.81 (dd, *J* = 16.6, 5.8 Hz, 1H), 2.67 (dd, *J* = 16.6, 7.2 Hz, 1H), 1.43 (s, 10H). <sup>13</sup>C NMR (151 MHz, MeOD)  $\delta$  174.11, 173.74, 157.65, 139.78, 129.46, 128.31, 128.09, 80.90, 52.77, 44.07, 37.17, 28.66. MS (ES<sup>-</sup>), *m/z* 320.9 (M - H).

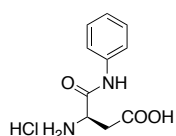


**(S)-2-((tert-butoxycarbonyl)amino)-4-oxo-4-(phenylamino)butanoic acid (5.12a):** A solution of **5.11a** in methanol (380 mg, 0.95 mmol, 0.05 M in methanol) was subjected to hydrogenation as for compound **5.2a**. Compound **5.12a** was obtained as a white glass (245 mg, 83%). <sup>1</sup>H NMR (300 MHz, MeOD)  $\delta$  7.52 (d, *J* = 7.8 Hz, 2H), 7.29 (t, *J* = 7.9 Hz, 2H), 7.08 (t, *J* = 7.4 Hz, 1H), 4.54 (t, *J* = 5.9 Hz, 1H), 2.97–2.79 (m, 2H), 1.43 (s, 9H). <sup>13</sup>C NMR (151 MHz, MeOD)  $\delta$  174.92, 170.61, 157.63, 139.55, 129.69, 125.16, 121.20, 80.68, 51.74, 39.68, 28.65. MS (ES<sup>-</sup>), *m/z* 306.9 (M - H).

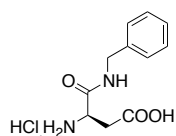


**(S)-4-(benzylamino)-2-((tert-butoxycarbonyl)amino)-4-oxobutanoic acid (5.12b):** A solution of **5.11b** in methanol (410 mg, 0.99 mmol, 0.05 M in methanol) was subjected to hydrogenation as for compound **5.2a**. Compound **5.12b** was obtained as a white glass (260 mg, 82%).  $^1\text{H}$  NMR (300 MHz, MeOD)  $\delta$  7.40–7.13 (m, 5H), 4.48 (t,  $J$  = 5.9 Hz, 1H), 4.43–4.29 (m, 2H), 2.89–2.61 (m, 2H), 1.44 (s, 9H).  $^{13}\text{C}$  NMR (151 MHz, MeOD)  $\delta$  174.89, 172.28, 157.70, 139.78, 129.51, 128.51, 128.16, 80.67, 51.97, 44.14, 38.77, 28.70. MS (ES $^-$ ),  $m/z$  321.0 (M - H).

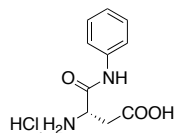
### 5.6.1.3 Boc-deprotection of amino acids [Scheme 5.1 (e)]



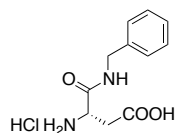
**(R)-3-amino-4-oxo-4-(phenylamino)butanoic acid hydrochloride (5.3a):** Boc-deprotection of compound **5.2a** (261 mg, 0.7 mmol) according to **General Procedure E** afforded the title compound as a brown glass (170 mg, quant.). MS (ES $^+$ ),  $m/z$  209.3 (M + H).



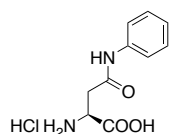
**(R)-3-amino-4-oxo-4-(phenylamino)butanoic acid hydrochloride (5.3b):** Boc-deprotection of compound **5.2b** (216 mg, 0.7 mmol) according to **General Procedure E** afforded the title compound as a yellow glass (205 mg, quant.). MS (ES $^+$ ),  $m/z$  223.2 (M + H).



**(S)-3-amino-4-oxo-4-(phenylamino)butanoic acid hydrochloride (5.8a):** Boc-deprotection of compound **5.7a** (261 mg, 0.7 mmol) according to **General Procedure E** afforded the title compound as a brown glass (167 mg, quant.). MS (ES $^+$ ),  $m/z$  209.3 (M + H).

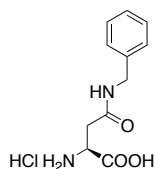


**(S)-3-amino-4-(benzylamino)-4-oxobutanoic acid hydrochloride (5.8b):** Boc-deprotection of compound **5.7b** (259 mg, 0.80 mmol) according to **General Procedure E** afforded the title compound as a yellow glass (205 mg, quant.). MS (ES $^+$ ),  $m/z$  223.2 (M + H).



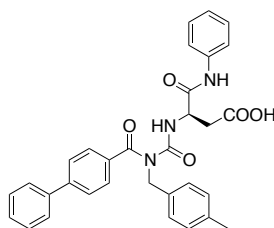
**(S)-2-amino-4-oxo-4-(phenylamino)butanoic acid hydrochloride (5.13a):** Boc-deprotection of compound **5.12a** (150 mg, 0.49 mmol) according to **General Procedure E** precipitated the title compound as a white powdery solid (110 mg, 93%). MS (ES $^+$ ),  $m/z$  209.3 (M + H).



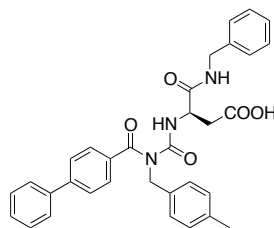


**(S)-2-amino-4-(benzylamino)-4-oxobutanoic acid hydrochloride (5.13b):** Boc-deprotection of compound **5.12b** (281 mg, 0.87 mmol) according to **General Procedure E** afforded the title compound as a yellow glass (197 mg, 87%). MS (ES<sup>+</sup>),  $m/z$  223.2 (M + H).

#### 5.6.1.4 Benzoylurea formation [Scheme 5.1 (f, g)]



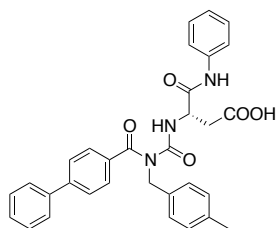
**(R)-3-(3-([1,1'-biphenyl]-4-carbonyl)-3-(4-methylbenzyl)ureido)-4-oxo-4-(phenylamino)butanoic acid (5.5a):** General Procedures A and B were followed using compound **3.3** (50 mg, 0.16 mmol), **5.3a** (58 mg, 0.24 mmol) and triethylamine (33  $\mu$ L, 0.24 mmol) to neutralise the amino acid HCl salt. Purification *via* flash chromatography, eluting with a gradient of methanol/dichloromethane (0:100 to 5:95) afforded the title compound as an opaque white glass (29 mg, 34%). <sup>1</sup>H NMR (300 MHz, CDCl<sub>3</sub>)  $\delta$  9.60 (d,  $J$  = 7.8 Hz, 1H), 8.64 (s, 1H), 7.64–7.35 (m, 10H), 7.32–7.22 (m, 3H), 7.16–6.95 (m, 5H), 5.11–4.91 (m, 3H), 3.05 (dd,  $J$  = 17.1, 4.7 Hz, 1H), 2.91 (dd,  $J$  = 17.2, 6.6 Hz, 1H), 2.29 (s, 3H), 2.07 (br s, 1H). <sup>13</sup>C NMR (151 MHz, CDCl<sub>3</sub>)  $\delta$  175.00, 173.53, 168.43, 156.13, 144.32, 139.81, 137.62, 137.39, 134.40, 133.99, 129.59, 129.12, 129.01, 128.34, 127.68, 127.38, 127.32, 126.69, 124.62, 120.17, 51.47, 50.61, 34.73, 21.23. MS (ES<sup>+</sup>),  $m/z$  536.0, (M + H), 99% purity. HRMS (ES<sup>+</sup> TOF) calculated for C<sub>32</sub>H<sub>29</sub>N<sub>3</sub>O<sub>5</sub> (M + H): 536.2180; found 536.2186.



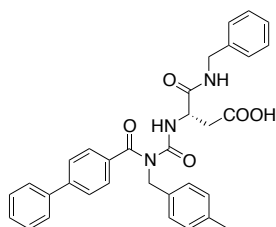
**(R)-3-(3-([1,1'-biphenyl]-4-carbonyl)-3-(4-methylbenzyl)ureido)-4-(benzylamino)-4-oxobutanoic acid (5.5b):** General Procedures A and B were followed using compound **3.3** (50 mg, 0.16 mmol), **5.3b** (61 mg, 0.24 mmol) and triethylamine (33  $\mu$ L, 0.24 mmol) to neutralise the amino acid HCl salt. Purification *via* flash chromatography, eluting with a gradient of methanol/dichloromethane (0:100 to 5:95) afforded the title compound as a colourless glass (50 mg, 58%). <sup>1</sup>H NMR (300 MHz, CDCl<sub>3</sub>)  $\delta$  9.40 (d,  $J$  = 8.1 Hz, 1H), 7.63–7.50 (m, 4H), 7.49–7.16 (m, 10H), 7.01 (d,  $J$  = 7.9 Hz, 2H), 6.97–6.85 (m, 3H), 5.04–4.90 (m, 2H), 4.85 (ddd,  $J$  = 8.1, 6.3, 4.9 Hz, 1H), 4.49–4.30 (m, 2H), 3.06 (dd,  $J$  = 17.3, 4.6 Hz, 1H), 2.82 (dd,  $J$  = 17.9, 5.8 Hz, 1H), 2.27 (s, 3H).<sup>[a]</sup> <sup>13</sup>C NMR (75 MHz, CDCl<sub>3</sub>)  $\delta$  174.85, 174.57, 170.56, 155.65, 144.17, 139.82, 137.85, 137.28, 134.42, 134.18, 129.49, 129.10, 128.81, 128.30, 127.61, 127.56, 127.31, 126.79, 126.75, 50.84, 50.32, 43.78, 35.59, 21.20.<sup>[b]</sup> MS (ES<sup>+</sup>),  $m/z$  550.2, (M + H), 98.6% purity. HRMS (ES<sup>+</sup> TOF) calculated for C<sub>33</sub>H<sub>31</sub>N<sub>3</sub>O<sub>5</sub> (M + H): 550.2336; found 550.2339.

<sup>[a]</sup> Peaks observed at  $\delta$  3.79 and 3.62 ppm are due to minor impurities.

<sup>[b]</sup> One peak in the aromatic region is not observed due to overlap.

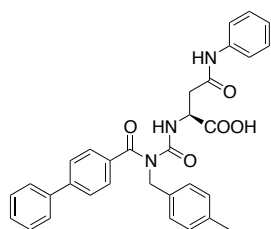


**(S)-3-(3-((1,1'-biphenyl)-4-carbonyl)-3-(4-methylbenzyl)ureido)-4-oxo-4-(phenylamino)butanoic acid (5.10a):** General Procedures A and B were followed using compound **3.3** (50 mg, 0.16 mmol), **5.8a** (58 mg, 0.24 mmol) and triethylamine (33  $\mu$ L, 0.24 mmol) to neutralise the amino acid HCl salt. Purification *via* flash chromatography, eluting with a gradient of methanol/dichloromethane (0:100 to 5:95) afforded the title compound as a colourless glass (47 mg, 56%).  $^1\text{H}$  NMR (600 MHz,  $\text{CDCl}_3$ )  $\delta$  9.56 (d,  $J$  = 7.8 Hz, 1H), 8.66 (s, 1H), 7.62–7.52 (m, 4H), 7.51–7.35 (m, 7H), 7.29–7.23 (m, 3H), 7.13–6.94 (m, 5H), 5.09–4.92 (m, 3H), 3.03 (ddd,  $J$  = 17.2, 4.6, 1.6 Hz, 1H), 2.91 (ddd,  $J$  = 17.3, 6.5, 1.5 Hz, 1H), 2.29 (s, 3H).  $^{13}\text{C}$  NMR (151 MHz,  $\text{CDCl}_3$ )  $\delta$  175.00, 174.95, 168.42, 156.11, 144.30, 139.80, 137.61, 137.37, 134.36, 133.98, 129.58, 129.10, 129.00, 128.31, 127.68, 127.37, 127.31, 126.69, 124.61, 120.20, 51.45, 50.60, 34.99, 21.22. MS ( $\text{ES}^+$ ),  $m/z$  536.0, ( $\text{M} + \text{H}$ ), 99% purity. HRMS ( $\text{ES}^+$  TOF) calculated for  $\text{C}_{32}\text{H}_{29}\text{N}_3\text{O}_5$  ( $\text{M} + \text{H}$ ): 536.218; found 536.2171.



**(S)-3-(3-((1,1'-biphenyl)-4-carbonyl)-3-(4-methylbenzyl)ureido)-4-(benzylamino)-4-oxobutanoic acid (5.10b):** General Procedures A and B were followed using compound **3.3** (50 mg, 0.16 mmol), **5.8b** (61 mg, 0.24 mmol) and triethylamine (33  $\mu$ L, 0.24 mmol) to neutralise the amino acid HCl salt. Purification *via* flash chromatography, eluting with a gradient of methanol/dichloromethane (0:100 to 5:95) afforded the title compound as a colourless glass (62 mg, 72%).  $^1\text{H}$  NMR (300 MHz,  $\text{CDCl}_3$ )  $\delta$  9.41 (d,  $J$  = 8.1 Hz, 1H), 7.62–7.51 (m, 4H), 7.50–7.16 (m, 10H), 7.01 (d,  $J$  = 7.9 Hz, 2H), 6.97–6.77 (m, 3H), 5.04–4.90 (m, 2H), 4.85 (ddd,  $J$  = 7.9, 6.2, 4.8 Hz, 1H), 4.49–4.32 (m, 2H), 3.06 (dd,  $J$  = 17.2, 4.6 Hz, 1H), 2.82 (dd,  $J$  = 17.3, 6.4 Hz, 1H), 2.27 (s, 3H).<sup>[a]</sup>  $^{13}\text{C}$  NMR (75 MHz,  $\text{CDCl}_3$ )  $\delta$  174.85, 174.56, 170.56, 155.66, 144.18, 139.82, 137.85, 137.29, 134.42, 134.18, 129.49, 129.10, 128.81, 128.30, 127.65, 127.61, 127.56, 127.31, 126.79, 126.75, 50.84, 50.32, 43.78, 35.58, 21.20. MS ( $\text{ES}^+$ ),  $m/z$  550.4, ( $\text{M} + \text{H}$ ), 99% purity. HRMS ( $\text{ES}^+$  TOF) calculated for  $\text{C}_{33}\text{H}_{31}\text{N}_3\text{O}_5$  ( $\text{M} + \text{H}$ ): 550.2336; found 550.2339.

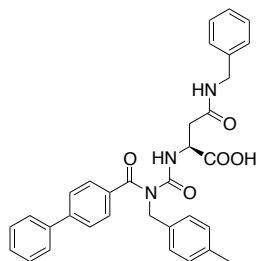
<sup>[a]</sup> Peaks observed at  $\delta$  3.79 and 3.62 ppm are due to minor impurities.



**(S)-2-(3-((1,1'-biphenyl)-4-carbonyl)-3-(4-methylbenzyl)ureido)-4-oxo-4-(phenylamino)butanoic acid (5.15a):** General Procedures A and B were followed using compound **3.3** (50 mg, 0.16 mmol), **5.13a** (58 mg, 0.24 mmol) and triethylamine (33  $\mu$ L, 0.24 mmol) to neutralise the amino acid HCl salt. Purification *via* flash chromatography, eluting with a gradient of methanol/dichloromethane (0:100 to 5:95) afforded the title compound as a colourless glass (37 mg, 44%).  $^1\text{H}$  NMR (600 MHz,  $\text{CDCl}_3$ )  $\delta$  10.01 (d,  $J$  = 4.2 Hz, 1H), 8.47 (s, 1H), 7.55 (t,  $J$  = 6.8 Hz, 4H), 7.51–7.35 (m, 7H), 7.29–7.21 (m, 2H), 7.10 (t,  $J$  = 7.2 Hz, 1H), 7.06 (d,  $J$  = 7.3 Hz, 2H), 6.97 (d,  $J$  = 7.5 Hz, 2H), 4.99 (q,  $J$  = 16.3 Hz, 2H), 4.74 (s, 1H), 2.98 (d,  $J$  = 15.8 Hz, 1H), 2.78 (dd,  $J$  = 15.1, 7.1 Hz, 1H), 2.29 (s, 3H).  $^{13}\text{C}$  NMR (151 MHz,  $\text{CDCl}_3$ )  $\delta$  175.08, 172.05, 170.03, 155.39, 144.00, 139.76, 137.36, 136.96, 134.44, 134.05, 129.59, 129.11, 129.07, 128.25, 127.41,

127.27, 126.10, 125.24, 120.52, 50.80, 50.31, 38.24, 21.20.<sup>[a]</sup> MS (ES<sup>+</sup>), *m/z* 536.2, (M + H), 99% purity. HRMS (ES<sup>+</sup> TOF) calculated for C<sub>32</sub>H<sub>29</sub>N<sub>3</sub>O<sub>5</sub> (M + H): 536.2180; found 536.2182.

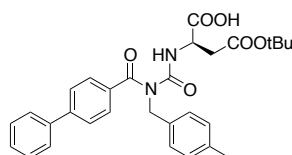
<sup>[a]</sup> One peak in the aromatic region is not observed due to overlap.



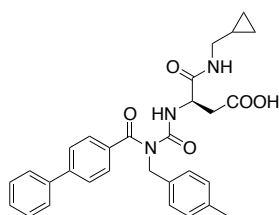
**(S)-2-(3-([1,1'-biphenyl]-4-carbonyl)-3-(4-methylbenzyl)ureido)-4-(benzylamino)-4-oxobutanoic acid (5.15b):** General Procedures A and B were followed using compound 3.3 (33 mg, 0.10 mmol), 5.13b (41 mg, 0.16 mmol) and triethylamine (22  $\mu$ L, 0.16 mmol) to neutralise the amino acid HCl salt. Purification *via* flash chromatography, eluting with a gradient of methanol/dichloromethane (0:100 to 5:95) afforded the title compound as a colourless glass (39 mg, 67%). <sup>1</sup>H NMR (600 MHz, MeOD)  $\delta$  7.65–7.61 (m, 4H), 7.53–7.18 (m, 10H), 7.07 (d, *J* = 8.2 Hz, 2H), 7.04 (d, *J* = 8.3 Hz, 2H), 4.96 (s, 2H), 4.71 (t, *J* = 5.7 Hz, 1H), 4.32 (s, 2H), 2.84–2.72 (m, 2H), 2.28 (s, 3H). <sup>13</sup>C NMR (151 MHz, CDCl<sub>3</sub>)  $\delta$  175.34, 174.20, 171.99, 157.07, 145.04, 141.17, 139.83, 138.05, 136.08, 136.05, 130.15, 130.02, 129.53, 129.10, 128.74, 128.60, 128.18, 128.13, 128.06, 127.89, 52.23, 50.60, 44.16, 38.31, 21.10. MS (ES<sup>+</sup>), *m/z* 550.0, (M + H), 99% purity. HRMS (ES<sup>+</sup> TOF) calculated for C<sub>33</sub>H<sub>31</sub>N<sub>3</sub>O<sub>5</sub> (M + H): 550.2336; found 550.2347.

## 5.6.2 Parallel Synthesis of amide series A and B

### 5.6.2.1 Parallel Synthesis of amide series A [Scheme 5.3]



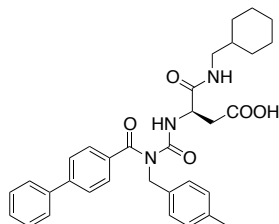
**(R)-2-(3-([1,1'-biphenyl]-4-carbonyl)-3-(4-methylbenzyl)ureido)-4-(tert-butoxy)-4-oxobutanoic acid (5.17):** General Procedures A and B were followed using compound 3.3 (300 mg, 0.95 mmol) and D-Aspartic acid beta-*tert*-butyl ester (285 mg, 1.4 mmol). Purification *via* flash chromatography, eluting with a gradient of methanol/dichloromethane (0:100 to 5:95) afforded compound 5.17 as a colourless glassy solid (327 mg, 67%). <sup>1</sup>H NMR (300 MHz, CDCl<sub>3</sub>)  $\delta$  9.72 (d, *J* = 7.8 Hz, 1H), 8.42 (br s, 1H), 7.58 (dd, *J* = 7.1, 1.5 Hz, 4H), 7.51–7.32 (m, 5H), 7.08 (d, *J* = 7.9 Hz, 2H), 6.95 (d, *J* = 8.1 Hz, 2H), 5.00 (s, 2H), 4.92 (dt, *J* = 7.9, 4.9 Hz, 1H), 3.04 (dd, *J* = 16.9, 4.8 Hz, 1H), 2.86 (dd, *J* = 16.9, 5.0 Hz, 1H), 2.31 (s, 3H), 1.47 (s, 9H). <sup>13</sup>C NMR (75 MHz, CDCl<sub>3</sub>)  $\delta$  175.78, 175.04, 169.54, 155.27, 143.74, 139.98, 137.04, 134.69, 134.63, 129.41, 129.06, 128.18, 127.31, 127.28, 127.20, 126.61, 82.48, 50.36, 50.10, 37.64, 28.09, 21.18. MS (ES<sup>+</sup>), *m/z* 517.5 (M + H), purity 99%. HRMS (ES<sup>+</sup> TOF) calculated for C<sub>30</sub>H<sub>32</sub>N<sub>2</sub>O<sub>6</sub> (M + H): 517.2333; found 517.2335.



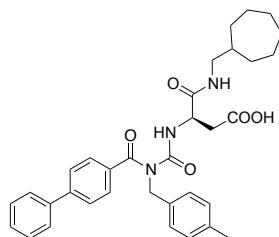
**(R)-3-(3-([1,1'-biphenyl]-4-carbonyl)-3-(4-methylbenzyl)ureido)-4-((cyclopropylmethyl)amino)-4-oxobutanoic acid (5.19a):** Using General Procedure F,

compound **5.17** (31.4 mg, 0.061 mmol) was reacted with 1-cyclopropylmethylamine (6  $\mu$ L, 0.067 mmol). Purification by passing through a short silica plug with dichloromethane, followed by purification of the crude product by mass-directed preparative HPLC, then deprotection with TFA according to **General Procedure G** (but without HPLC purification at this step), yielded compound **5.19a** as a colourless glassy solid (5.9 mg, 19%).  $^1\text{H}$  NMR (300 MHz,  $\text{CDCl}_3$ )  $\delta$  9.45 (d,  $J$  = 7.7 Hz, 1H), 7.64–7.34 (m, 9H), 7.08 (d,  $J$  = 7.8 Hz, 2H), 6.97 (d,  $J$  = 7.9 Hz, 2H), 6.82 (br s, 1H), 5.84 (br s, 1H), 5.00 (s, 2H), 4.83 (dd,  $J$  = 11.6, 6.0 Hz, 1H), 3.16–2.75 (m, 4H), 2.30 (s, 3H), 0.88 (br s, 1H), 0.46 (q,  $J$  = 5.1 Hz, 2H), 0.15 (q,  $J$  = 4.7 Hz, 2H).  $^{13}\text{C}$  NMR (75 MHz,  $\text{CDCl}_3$ )  $\delta$  175.13, 174.56, 170.89, 155.66, 144.32, 139.80, 137.39, 134.39, 134.02, 129.50, 129.13, 128.35, 127.65, 127.37, 127.31, 126.76, 50.83, 50.49, 44.87, 35.64, 21.20, 10.43, 3.50, 3.45.  $^{[a]}$  MS ( $\text{ES}^-$ ),  $m/z$  512.3 ( $\text{M} - \text{H}$ ), 98.0% purity. HRMS ( $\text{ES}^+$  TOF) calculated for  $\text{C}_{30}\text{H}_{31}\text{N}_3\text{O}_5$  ( $\text{M} + \text{H}$ ): 514.2336; found 514.2346.

$^{[a]}$  One additional peak is observed in the aliphatic region due to apparent peak splitting.

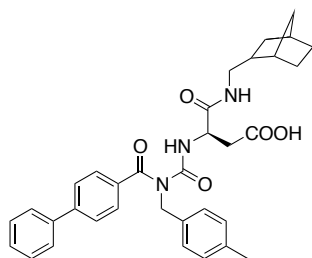


**(R)-3-(3-([1,1'-biphenyl]-4-carbonyl)-3-(4-methylbenzyl)ureido)-4-((cyclohexylmethyl)amino)-4-oxobutanoic acid (**5.19b**):** Using **General Procedure F**, compound **5.17** (31.4 mg, 0.061 mmol) was reacted with cyclohexylmethylamine (9  $\mu$ L, 0.067 mmol). Purification by passing through a short silica plug with dichloromethane, followed by purification of the crude product by mass-directed preparative HPLC, then deprotection with TFA according to **General Procedure G** (but without HPLC purification at this step), yielded compound **5.19b** as a colourless glassy solid (6.5 mg, 19%).  $^1\text{H}$  NMR (300 MHz,  $\text{CDCl}_3$ )  $\delta$  9.43 (d,  $J$  = 8.0 Hz, 1H), 7.59 (t,  $J$  = 7.7 Hz, 4H), 7.54–7.32 (m, 5H), 7.09 (d,  $J$  = 7.9 Hz, 2H), 6.96 (d,  $J$  = 8.0 Hz, 2H), 6.79 (t,  $J$  = 5.6 Hz, 1H), 5.06–4.93 (m, 2H), 4.83 (dd,  $J$  = 12.2, 6.4 Hz, 1H), 3.16–2.95 (m, 3H), 2.85 (dd,  $J$  = 17.3, 6.5 Hz, 1H), 2.31 (s, 3H), 1.66 (t,  $J$  = 13.4 Hz, 5H), 1.41 (br s, 1H), 1.29–1.01 (m, 3H), 0.86 (dd,  $J$  = 22.5, 11.2 Hz, 2H).  $^{13}\text{C}$  NMR (75 MHz,  $\text{CDCl}_3$ )  $\delta$  175.14, 174.74, 171.13, 155.69, 144.35, 139.79, 137.40, 134.33, 133.97, 129.54, 129.13, 128.36, 127.64, 127.38, 127.31, 126.72, 50.84, 50.47, 46.38, 37.70, 35.58, 30.75, 26.45, 25.87, 21.22. MS ( $\text{ES}^-$ ),  $m/z$  554.3 ( $\text{M} - \text{H}$ ), 98.0% purity. HRMS ( $\text{ES}^+$  TOF) calculated for  $\text{C}_{33}\text{H}_{37}\text{N}_3\text{O}_5$  ( $\text{M} + \text{H}$ ): 556.2806; found 556.2817.



**(R)-3-(3-([1,1'-biphenyl]-4-carbonyl)-3-(4-methylbenzyl)ureido)-4-((cycloheptylmethyl)amino)-4-oxobutanoic acid (**5.19c**):** Using **General Procedure F**, compound **5.17** (43.8 mg, 0.085 mmol) was reacted with cycloheptanemethylamine (13  $\mu$ L, 0.093 mmol). Purification by passing through a short silica plug with dichloromethane, followed by deprotection with TFA according to **General Procedure G**, then purification of the crude product by mass-directed preparative HPLC, yielded compound **5.19c** as a colourless glassy solid (7.2 mg, 15%).  $^1\text{H}$  NMR (300 MHz,  $\text{CDCl}_3$ )  $\delta$  9.35 (d,  $J$  = 7.7 Hz, 1H), 7.64–7.53 (m, 4H), 7.52–7.33 (m, 5H), 7.08 (d,  $J$  = 7.9 Hz, 2H), 6.98 (d,  $J$  = 8.0 Hz, 2H), 6.68 (t,  $J$  = 5.5 Hz, 1H), 5.08–4.89 (m, 2H), 4.78 (d,  $J$  = 4.3 Hz, 1H), 3.22–2.68 (m, 4H), 2.30 (s, 3H), 1.70–1.25 (m, 11H), 1.11 (dd,  $J$  = 18.3, 8.9 Hz, 2H).  $^{[a]}$   $^{13}\text{C}$  NMR (75 MHz,  $\text{CDCl}_3$ )  $\delta$  174.82, 170.64, 155.59, 144.16, 139.85, 137.28, 134.52, 134.24, 129.49, 129.10, 128.29, 127.62, 127.31, 126.78, 50.88, 50.30, 46.40, 39.37, 32.08, 32.06, 28.54, 26.33, 21.22.  $^{[b]}$  MS ( $\text{ES}^+$ ),  $m/z$  570.4 ( $\text{M} + \text{H}$ ), 99.0 % purity. HRMS ( $\text{ES}^+$  TOF) calculated for  $\text{C}_{34}\text{H}_{39}\text{N}_3\text{O}_5$  ( $\text{M} + \text{H}$ ): 570.2962; found 570.2972.

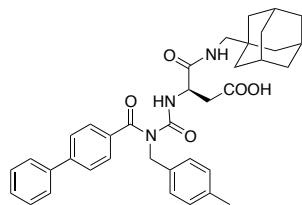
$^{[b]}$  A peak observed at  $\delta$  2.64 ppm is an impurity, most likely DMSO, utilised to solubilise the sample for HPLC purification.



**(3R)-3-(3-((1,1'-biphenyl)-4-carbonyl)-3-(4-methylbenzyl)ureido)-4-((bicyclo[2.2.1]heptan-2-ylmethyl)amino)-4-oxobutanoic acid (5.19d):** Using **General Procedure F**, compound **5.17** (43.8 mg, 0.085 mmol) was reacted with bicyclo[2.2.1]heptan-2-yl methanamine (12  $\mu$ L, 0.093 mmol). Purification by passing through a short silica plug with dichloromethane, followed by deprotection with TFA according to **General Procedure G**, then purification of the crude product by mass-directed preparative HPLC, yielded compound **5.19d** as an inseparable mixture of four diastereomers as a colourless glassy solid (9.4 mg, 20%).  $^1\text{H}$  NMR (300 MHz,  $\text{CDCl}_3$ )  $\delta$  9.35 (dd,  $J$  = 7.5, 5.5 Hz, 1H), 9.34 (d,  $J$  = 5.5 Hz, 1H), 7.63–7.54 (m, 4H), 7.52–7.33 (m, 5H), 7.08 (d,  $J$  = 7.9 Hz, 2H), 6.98 (d,  $J$  = 8.0 Hz, 2H), 6.60 (t,  $J$  = 5.3 Hz, 1H), 5.08–4.89 (m, 2H), 4.82–4.71 (m, 1H), 3.35–2.91 (m, 4H), 2.78 (dd,  $J$  = 17.2, 6.7 Hz, 1H), 2.31 (s, 3H), 2.16 (t,  $J$  = 5.0 Hz, 1H), 2.09 (d,  $J$  = 3.4 Hz, 1H), 2.00–1.83 (m, 1H), 1.73–1.57 (m, 1H), 1.57–1.19 (m, 5H), 1.16–1.00 (m, 1H), 0.68–0.54 (m, 1H).<sup>[a]</sup>  $^{13}\text{C}$  NMR (75 MHz,  $\text{CDCl}_3$ )  $\delta$  174.83, 173.76, 170.34, 155.52, 144.16, 139.88, 137.28, 134.56, 134.27, 129.48, 129.11, 128.29, 127.62, 127.32, 126.78, 126.78, 50.83, 50.29, 42.40, 42.35, 40.87, 39.91, 39.69, 39.66, 38.62, 38.56, 36.96, 35.84, 34.79, 30.02, 22.62, 21.24.<sup>[b]</sup> MS ( $\text{ES}^+$ ),  $m/z$  568.4 ( $\text{M} + \text{H}$ ), 99.0% purity. HRMS ( $\text{ES}^+$  TOF) calculated for  $\text{C}_{34}\text{H}_{37}\text{N}_3\text{O}_5$  ( $\text{M} + \text{H}$ ): 568.2806; found 568.2817.

<sup>[a]</sup> The mixture of stereoisomers was integrated as a single compound for the purposes of  $^1\text{H}$  NMR analysis. A peak observed at  $\delta$  2.62 ppm is an impurity, most likely DMSO, utilised to solubilise the sample for HPLC purification.

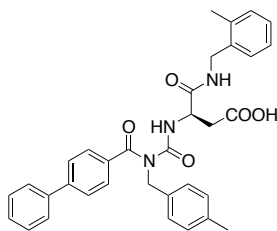
<sup>[b]</sup> A peak observed at  $\delta$  40.87 ppm is an impurity, most likely DMSO, utilised to solubilise the sample for HPLC purification.



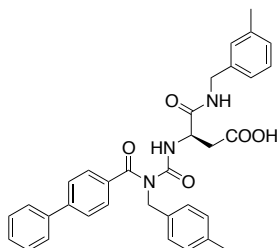
**(R)-3-(3-((1,1'-biphenyl)-4-carbonyl)-3-(4-methylbenzyl)ureido)-4-(((3R,5R,7R)-adamantan-1-ylmethyl)amino)-4-oxobutanoic acid (5.19e):** Using **General Procedure F**, compound **5.17** (20.9 mg, 0.041 mmol) was reacted with 1-adamantanemethylamine (8  $\mu$ L, 0.045 mmol). Purification by passing through a short silica plug with dichloromethane, followed by deprotection of the crude product with TFA according to **General Procedure G**, yielded compound **5.19e** as a colourless glassy solid (9.5 mg, 39%).  $^1\text{H}$  NMR (300 MHz,  $\text{CDCl}_3$ )  $\delta$  9.42 (d,  $J$  = 7.8 Hz, 1H), 7.62–7.53 (m, 4H), 7.49–7.33 (m, 5H), 7.07 (d,  $J$  = 7.9 Hz, 2H), 6.97 (d,  $J$  = 8.1 Hz, 2H), 6.72 (t,  $J$  = 6.1 Hz, 1H), 4.99 (s, 2H), 4.94 (br s, 2H), 4.82 (td,  $J$  = 7.1, 4.4 Hz, 1H), 3.07–2.74 (m, 4H), 2.30 (s, 3H), 1.94 (br s, 3H), 1.68 (d,  $J$  = 12.2 Hz, 3H), 1.58 (d,  $J$  = 11.8 Hz, 3H), 1.42 (d,  $J$  = 2.2 Hz, 6H).  $^{13}\text{C}$  NMR (75 MHz,  $\text{CDCl}_3$ )  $\delta$  174.85, 173.98, 170.82, 155.54, 144.11, 139.89, 137.23, 134.56, 134.31, 129.48, 129.10, 128.28, 127.57, 127.31, 126.75, 51.42, 50.89, 50.26, 40.17, 37.02, 35.93, 33.86, 28.34, 21.22.<sup>[b]</sup> MS ( $\text{ES}^-$ ),  $m/z$  606.3 ( $\text{M} - \text{H}$ ), 99.0% purity. HRMS ( $\text{ES}^+$  TOF) calculated for  $\text{C}_{37}\text{H}_{41}\text{N}_3\text{O}_5$  ( $\text{M} + \text{H}$ ): 608.3119; found 608.3140.

<sup>[a]</sup> A peak observed at  $\delta$  2.69 ppm is an impurity, most likely DMSO, utilised to solubilise the sample for HPLC purification. The broad peak at 4.94 ppm is attributed to  $-\text{COOH}$ .

<sup>[b]</sup> A peak observed at  $\delta$  40.38 ppm is an impurity, most likely DMSO, utilised to solubilise the sample for HPLC purification.

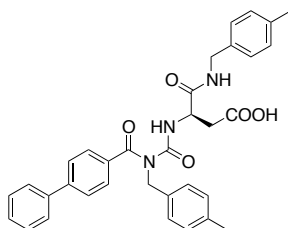


**(R)-3-(3-([1,1'-biphenyl]-4-carbonyl)-3-(4-methylbenzyl)ureido)-4-((2-methylbenzyl)amino)-4-oxobutanoic acid (5.19f):** Using **General Procedure F**, compound **5.17** (31.4 mg, 0.061 mmol) was reacted with 2-methylbenzylamine (8  $\mu$ L, 0.067 mmol). Purification by passing through a short silica plug with dichloromethane, followed by purification of the crude product by mass-directed preparative HPLC, then deprotection with TFA according to **General Procedure G** (but without HPLC purification at this step), yielded compound **5.19f** as a colourless glassy solid (5.5 mg, 16%).  $^1\text{H}$  NMR (300 MHz,  $\text{CDCl}_3$ )  $\delta$  9.51 (d,  $J$  = 7.9 Hz, 1H), 7.63–7.34 (m, 9H), 7.23–7.11 (m, 4H), 7.02 (d,  $J$  = 7.9 Hz, 2H), 6.91 (d,  $J$  = 8.1 Hz, 2H), 6.87 (t,  $J$  = 5.7 Hz, 1H), 6.08 (br s, 1H), 4.97 (s, 2H), 4.88 (dd,  $J$  = 12.4 Hz, 5.7, 1H), 4.52–4.31 (m, 2H), 3.09 (dd,  $J$  = 17.3, 4.5 Hz, 1H), 2.89 (dd,  $J$  = 17.2, 6.2 Hz, 1H), 2.28 (s, 3H), 2.25 (s, 3H).  $^{13}\text{C}$  NMR (75 MHz,  $\text{CDCl}_3$ )  $\delta$  175.18, 174.86, 170.81, 155.74, 144.31, 139.77, 137.37, 136.43, 135.00, 134.27, 133.96, 130.67, 129.53, 129.13, 128.36, 128.14, 127.96, 127.60, 127.35, 127.31, 126.66, 126.41, 50.85, 50.45, 42.23, 35.50, 21.19, 19.03. MS ( $\text{ES}^+$ ),  $m/z$  564.3 ( $\text{M} + \text{H}$ ), 98.0% purity. HRMS ( $\text{ES}^+$  TOF) calculated for  $\text{C}_{34}\text{H}_{33}\text{N}_3\text{O}_5$  ( $\text{M} + \text{H}$ ): 564.2493; found 564.2503.



**(R)-3-(3-([1,1'-biphenyl]-4-carbonyl)-3-(4-methylbenzyl)ureido)-4-((3-methylbenzyl)amino)-4-oxobutanoic acid (5.19g):** Using **General Procedure F**, compound **5.17** (31.4 mg, 0.061 mmol) was reacted with 3-methylbenzylamine (8  $\mu$ L, 0.067 mmol). Purification by passing through a short silica plug with dichloromethane, followed by purification of the crude product by mass-directed preparative HPLC, then deprotection with TFA according to **General Procedure G** (but without HPLC purification at this step), yielded compound **5.19g** as a semi-opaque colourless glassy solid (5.8 mg, 17%).  $^1\text{H}$  NMR (300 MHz,  $\text{CDCl}_3$ )  $\delta$  9.49 (d,  $J$  = 8.0 Hz, 1H), 7.64–7.34 (m, 8H), 7.26 (s, 1H), 7.20 (t,  $J$  = 7.4 Hz, 1H), 7.11–6.85 (m, 7H), 5.43 (s, 1H), 4.97 (s, 2H), 4.89 (dd,  $J$  = 11.7, 6.7 Hz, 1H), 4.51–4.25 (m, 2H), 3.08 (dd,  $J$  = 17.1, 3.9 Hz, 1H), 2.87 (dd,  $J$  = 17.1, 6.3 Hz, 1H), 2.31 (s, 3H), 2.28 (s, 3H).  $^{13}\text{C}$  NMR (75 MHz,  $\text{CDCl}_3$ )  $\delta$  175.08, 174.70, 170.89, 155.72, 144.30, 139.79, 138.56, 137.36, 134.30, 134.01, 129.51, 129.12, 128.79, 128.46, 128.39, 128.35, 127.61, 127.34, 127.31, 126.69, 124.58, 50.86, 50.43, 43.95, 35.53, 21.48, 21.19.<sup>[a]</sup> MS ( $\text{ES}^-$ ),  $m/z$  562.2 ( $\text{M} - \text{H}$ ), 98.0% purity. HRMS ( $\text{ES}^+$  TOF) calculated for  $\text{C}_{34}\text{H}_{33}\text{N}_3\text{O}_5$  ( $\text{M} + \text{H}$ ): 564.2493; found 564.2502.

<sup>[a]</sup> One aromatic peak is not observed due to overlap.



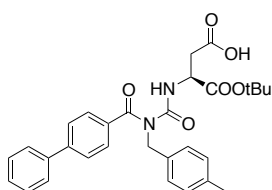
**(R)-3-(3-([1,1'-biphenyl]-4-carbonyl)-3-(4-methylbenzyl)ureido)-4-((4-methylbenzyl)amino)-4-oxobutanoic acid (5.19h):** Using **General Procedure F**, compound **5.17** (31.4 mg, 0.061 mmol) was reacted with 4-methylbenzylamine (9  $\mu$ L, 0.067 mmol). Purification by passing through a short silica plug with dichloromethane, followed by purification of the crude product by mass-directed preparative HPLC, then deprotection with TFA according to

**General Procedure G** (but without HPLC purification at this step), yielded compound **5.19h** as a colourless glassy solid (5.6 mg, 16%).  $^1\text{H}$  NMR (300 MHz,  $\text{CDCl}_3$ )  $\delta$  9.48 (d,  $J$  = 8.0 Hz, 1H), 7.61–7.53 (m, 4H), 7.50–7.35 (m, 5H), 7.15–7.05 (m, 4H), 7.02 (d,  $J$  = 7.9 Hz, 2H), 6.98–6.84 (m, 3H), 6.01 (s, 1H), 4.97 (d,  $J$  = 1.9 Hz, 2H), 4.88 (dd,  $J$  = 12.6, 6.4 Hz, 1H), 4.48–4.27 (m, 2H), 3.08 (dd,  $J$  = 17.3, 4.5 Hz, 1H), 2.88 (dd,  $J$  = 16.9, 6.5 Hz, 1H), 2.32 (s, 3H), 2.28 (s, 3H).  $^{13}\text{C}$  NMR (75 MHz,  $\text{CDCl}_3$ )  $\delta$  175.10, 174.68, 170.89, 155.73, 144.31, 139.79, 137.40, 137.36, 134.35, 134.29, 133.99, 129.56, 129.52, 129.13, 128.36, 127.62, 127.35, 127.31, 126.70, 50.86, 50.43, 43.80, 35.51, 21.23, 21.20.<sup>[b]</sup> MS ( $\text{ES}^-$ ),  $m/z$  562.2 ( $\text{M} - \text{H}$ ), 99% purity. HRMS ( $\text{ES}^+$  TOF) calculated for  $\text{C}_{34}\text{H}_{33}\text{N}_3\text{O}_5$  ( $\text{M} + \text{H}$ ): 564.2493; found 564.2501.

<sup>[a]</sup> The broad peak at  $\delta$  6.01 ppm (s, 1H) is attributed to  $-\text{COOH}$ .

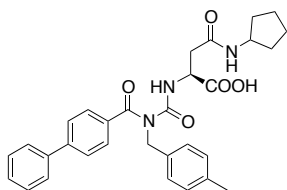
<sup>[b]</sup> One aromatic peak is not observed due to overlap.

### 5.6.2.2 Parallel Synthesis of amide series B [Scheme 5.3]



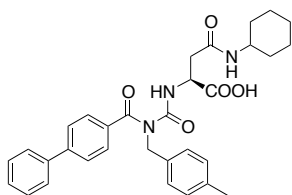
**(S)-2-(3-([1,1'-biphenyl]-4-carbonyl)-3-(4-methylbenzyl)ureido)-4-(tert-butoxy)-4-oxobutanoic acid (5.21):** General Procedures A and B were followed using compound **3.3** (300 mg, 0.95 mmol) and L-Aspartic acid  $\alpha$ -*tert*-butyl ester (268 mg, 1.418 mmol). Purification *via* flash chromatography, eluting with a gradient of methanol/dichloromethane (0:100 to 5:95) afforded the title compound as a colourless glassy solid (384 mg, 79%).  $^1\text{H}$  NMR (300 MHz,  $\text{CDCl}_3$ )  $\delta$  9.60 (d,  $J$  = 7.4 Hz, 1H), 7.60–7.52 (m, 4H), 7.49–7.33 (m, 5H), 7.06 (d,  $J$  = 7.9 Hz, 2H), 6.95 (d,  $J$  = 8.1 Hz, 2H), 4.98 (s, 2H), 4.76 (dt,  $J$  = 7.4, 5.0 Hz, 1H), 3.06 (dd,  $J$  = 17.0, 4.8 Hz, 1H), 2.93 (dd,  $J$  = 17.0, 5.2 Hz, 1H), 2.30 (s, 3H), 1.47 (s, 9H).<sup>[a]</sup>  $^{13}\text{C}$  NMR (75 MHz,  $\text{CDCl}_3$ )  $\delta$  175.54, 174.95, 169.26, 155.02, 143.73, 140.01, 137.03, 134.82, 134.72, 129.39, 129.07, 128.17, 127.39, 127.30, 127.19, 126.71, 82.95, 50.88, 50.06, 36.55, 27.98, 21.20. MS ( $\text{ES}^+$ ),  $m/z$  517.5 ( $\text{M} + \text{H}$ ), 99% purity. HRMS ( $\text{ES}^+$  TOF) calculated for  $\text{C}_{30}\text{H}_{32}\text{N}_2\text{O}_6$  ( $\text{M} + \text{H}$ ): 517.2333; found 517.2338.

<sup>[a]</sup> A small peak observed at  $\delta$  5.30 ppm is an impurity, most likely dichloromethane.



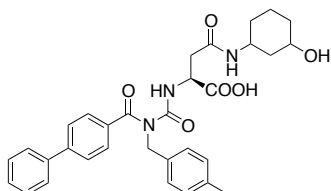
**(S)-2-(3-([1,1'-biphenyl]-4-carbonyl)-3-(4-methylbenzyl)ureido)-4-(cyclopentylamino)-4-oxobutanoic acid (5.23a):** Using General Procedure F, compound **5.21** (21 mg, 0.04 mmol) was reacted with cyclopentylamine (5  $\mu\text{L}$ , 0.05 mmol). Purification by passing through a short silica plug with dichloromethane, followed by deprotection of the crude product with TFA according to General Procedure G, yielded compound **5.23a** as a whitish opaque glassy solid (7 mg, 32%).  $^1\text{H}$  NMR (300 MHz,  $\text{CDCl}_3$ )  $\delta$  9.87 (d,  $J$  = 5.1 Hz, 1H), 7.61–7.52 (m, 4H), 7.52–7.32 (m, 5H), 7.11 (d,  $J$  = 7.9 Hz, 2H), 6.98 (d,  $J$  = 8.0 Hz, 2H), 6.75 (d,  $J$  = 7.3 Hz, 1H), 5.06–4.88 (m, 2H), 4.55 (ddd,  $J$  = 9.6, 5.0, 1.7 Hz, 1H), 4.15 (sext.,  $J$  = 6.9 Hz, 1H), 2.72 (dd,  $J$  = 15.9, 1.8 Hz, 1H), 2.45 (dd,  $J$  = 15.9, 9.9 Hz, 1H), 2.33 (s,  $J$  = 8.5 Hz, 3H), 2.03–1.87 (m, 2H), 1.74–1.50 (m, 4H), 1.45–1.28 (m, 2H).  $^{13}\text{C}$  NMR (75 MHz,  $\text{CDCl}_3$ )  $\delta$  174.92, 172.01, 171.07, 155.00, 144.11, 139.90, 137.48, 134.65, 134.32, 129.66, 129.11, 128.28, 127.43, 127.31, 126.15, 126.13, 52.22, 50.76, 50.20, 37.26, 32.87, 23.90, 23.86, 21.17.<sup>[a]</sup> MS ( $\text{ES}^-$ ),  $m/z$  526.3 ( $\text{M} - \text{H}$ ), 99.0% purity. HRMS ( $\text{ES}^+$  TOF) calculated for  $\text{C}_{31}\text{H}_{33}\text{N}_3\text{O}_5$  ( $\text{M} + \text{H}$ ): 528.2493; found 528.2504.

<sup>[a]</sup> One additional peak is observed in the aliphatic region due to apparent peak splitting.



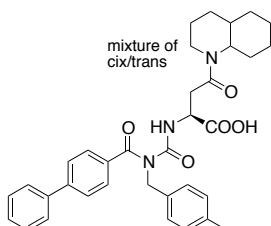
**(S)-2-(3-([1,1'-biphenyl]-4-carbonyl)-3-(4-methylbenzyl)ureido)-4-(cyclohexylamino)-4-oxobutanoic acid (5.23b):** Using **General Procedure F**, compound **5.21** (15 mg, 0.028 mmol) was reacted with cyclohexylamine (4  $\mu$ L, 0.031 mmol). Purification by passing through a short silica plug with dichloromethane, followed by deprotection of the crude product with TFA according to **General Procedure G** yielded compound **5.23b** directly as a white powdery solid containing minor impurities (7.2 mg, 47%).  $^1\text{H}$  NMR (300 MHz,  $\text{CDCl}_3$ )  $\delta$  9.83 (s, 1H), 7.70–7.31 (m, 9H), 7.09 (d,  $J$  = 7.2 Hz, 2H), 6.97 (d,  $J$  = 7.2 Hz, 2H), 6.59 (br s, 1H), 5.22–4.78 (m, 2H), 4.57 (br s, 1H), 3.70 (dd,  $J$  = 13.1, 6.4 Hz, 1H), 2.74 (d,  $J$  = 14.6 Hz, 1H), 2.55 (d,  $J$  = 8.8 Hz, 1H), 2.31 (s, 3H), 1.93–1.52 (m, 4H), 1.48–0.78 (m, 6H).<sup>[a]</sup>  $^{13}\text{C}$  NMR (75 MHz,  $\text{CDCl}_3$ )  $\delta$  174.81, 171.44, 154.95, 143.98, 139.93, 137.31, 134.73, 134.42, 129.57, 129.07, 128.93, 128.22, 127.44, 127.28, 126.26, 126.24, 50.11, 49.43, 37.53, 32.68, 32.66, 25.47, 24.86, 21.18. MS ( $\text{ES}^-$ ),  $m/z$  540.1 ( $\text{M} - \text{H}$ ), (99.0% purity). HRMS ( $\text{ES}^+$  TOF) calculated for  $\text{C}_{32}\text{H}_{35}\text{N}_3\text{O}_5$  ( $\text{M} + \text{H}$ ): 542.2649; found 542.2651.

<sup>[a]</sup> Additional peaks in the region 1.82–0.83 ppm are due to minor impurities.



**(2S)-2-(3-([1,1'-biphenyl]-4-carbonyl)-3-(4-methylbenzyl)ureido)-4-((3-hydroxycyclohexyl)amino)-4-oxobutanoic acid (5.23c):** Using **General Procedure F**, compound **5.21** (21.2 mg, 0.041 mmol) was reacted with 3-aminocyclohexan-1-ol (5  $\mu$ L, 0.045 mmol). Purification by passing through a short silica plug with dichloromethane, followed by deprotection of the crude product with TFA according to **General Procedure G**, yielded compound **5.23c** as an inseparable mixture of four diastereomers as a whitish opaque glassy solid (3.5 mg, 15%).  $^1\text{H}$  NMR (300 MHz,  $\text{CDCl}_3$ )  $\delta$  9.94–9.66 (m, 1H), 7.62–7.52 (m, 4H), 7.50–7.34 (m, 5H), 7.09 (d,  $J$  = 7.8 Hz, 2H), 6.96 (d,  $J$  = 8.0 Hz, 2H), 4.97 (s, 2H), 4.66 (s, 1H), 4.11 (d,  $J$  = 24.3 Hz, 1H), 4.00 (br s, 2H), 3.89 (d,  $J$  = 29.9 Hz, 1H), 2.31 (s, 3H), 3.01–1.10 (m, 12H).<sup>[a]</sup> MS ( $\text{ES}^+$ ),  $m/z$  558.3 ( $\text{M} + \text{H}$ ), 99.0% purity. HRMS ( $\text{ES}^+$  TOF) calculated for  $\text{C}_{32}\text{H}_{35}\text{N}_3\text{O}_6$  ( $\text{M} + \text{H}$ ): 558.2599; found 558.2610.

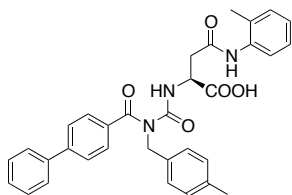
<sup>[a]</sup> The mixture of stereoisomers was integrated as a single compound for the purposes of  $^1\text{H}$  NMR analysis.



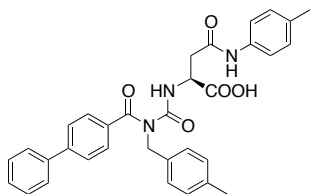
**(2S)-2-(3-([1,1'-biphenyl]-4-carbonyl)-3-(4-methylbenzyl)ureido)-4-(octahydroquinolin-1(2H)-yl)-4-oxobutanoic acid (5.23d):** Using **General Procedure F**, compound **5.21** (15 mg, 0.028 mmol) was reacted with decahydroquinoline (4.6  $\mu$ L, 0.031 mmol). Purification by passing through a short silica plug with dichloromethane, followed by deprotection of the crude product with TFA according to **General Procedure G** (but without purification *via* mass-directed preparative HPLC), yielded compound **5.23d** as an inseparable mixture of four possible cis/trans isomers directly as a colourless glassy solid (11.6 mg, 70%).  $^1\text{H}$  NMR (600 MHz,  $\text{CDCl}_3$ )  $\delta$  9.57 (ddd,  $J$  = 23.1, 22.7, 5.8 Hz, 1H), 9.36 (s, 2H), 7.58 (t,  $J$  = 7.5 Hz, 4H), 7.52–7.35 (m, 5H), 7.08 (d,  $J$  = 7.9 Hz, 2H), 6.99 (d,  $J$  = 7.9 Hz, 2H), 5.06–4.94 (m, 2H), 4.92–4.82 (m, 1H), 4.29–3.42 (m, 2H), 3.27–3.12 (m, 2H), 2.91–2.73 (m, 1H), 2.31 (s, 3H), 1.93–0.88 (m, 13H).<sup>[a]</sup> MS ( $\text{ES}^-$ ),  $m/z$  580.6 ( $\text{M} - \text{H}$ ), 98.0% purity. HRMS ( $\text{ES}^+$  TOF) calculated for  $\text{C}_{35}\text{H}_{39}\text{N}_3\text{O}_5$  ( $\text{M} + \text{H}$ ): 582.2962; found 582.2971.



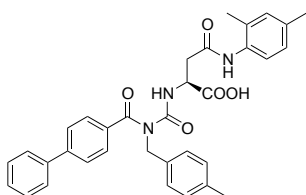
[a] The mixture of stereoisomers was integrated as a single compound for the purposes of  $^1\text{H}$  NMR analysis. The peak at  $\delta$  0.08 ppm is a minor impurity.



**(S)-2-(3-([1,1'-biphenyl]-4-carbonyl)-3-(4-methylbenzyl)ureido)-4-oxo-4-(o-tolylamino)butanoic acid (5.23e):** Using **General Procedure F**, compound **5.21** (21 mg, 0.041 mmol) was reacted with *o*-toluidine (5  $\mu\text{L}$ , 0.045 mmol). Purification by passing through a short silica plug with dichloromethane, followed by deprotection of the crude product with TFA according to **General Procedure G**, yielded compound **5.23e** as a colourless glassy solid (2.9 mg, 13%).  $^1\text{H}$  NMR (300 MHz,  $\text{CDCl}_3$ )  $\delta$  9.81 (d,  $J$  = 6.5 Hz, 1H), 7.64–7.51 (m, 5H), 7.50–7.31 (m, 5H), 7.24–6.80 (m, 7H), 5.00 (s, 2H), 4.81 (br s, 1H), 3.13 (dd,  $J$  = 15.9, 3.9 Hz, 1H), 2.99 (dd,  $J$  = 14.5, 8.2 Hz, 1H), 2.36–2.05 (m, 6H). MS ( $\text{ES}^-$ ),  $m/z$  548.3 ( $\text{M} - \text{H}$ ), 99.0% purity. HRMS ( $\text{ES}^+$  TOF) calculated for  $\text{C}_{33}\text{H}_{31}\text{N}_3\text{O}_5$  ( $\text{M} + \text{H}$ ): 550.2336; found 550.2350.

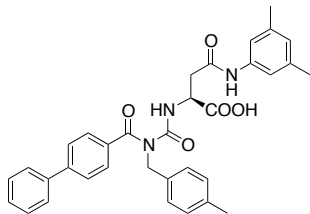


**(S)-2-(3-([1,1'-biphenyl]-4-carbonyl)-3-(4-methylbenzyl)ureido)-4-oxo-4-(p-tolylamino)butanoic acid (5.23f):** Using **General Procedure F**, compound **5.21** (21 mg, 0.041 mmol) was reacted with *p*-toluidine (5  $\mu\text{L}$ , 0.045 mmol). Purification by passing through a short silica plug with dichloromethane, followed by deprotection of the crude product with TFA according to **General Procedure G**, yielded compound **5.23f** as a whitish opaque glassy solid (7.5 mg, 33%).  $^1\text{H}$  NMR (300 MHz,  $\text{CDCl}_3$ )  $\delta$  9.82 (d,  $J$  = 5.8 Hz, 1H), 8.23 (s, 1H), 7.59–7.51 (m, 4H), 7.51–7.33 (m, 5H), 7.33–7.24 (m, 3H), 7.13–6.89 (m, 6H), 4.99 (s, 2H), 4.76 (br s, 1H), 3.01 (dd,  $J$  = 15.9, 2.4 Hz, 1H), 2.84 (dd,  $J$  = 15.9, 7.8 Hz, 1H), 2.29 (s, 6H).  $^{13}\text{C}$  NMR (75 MHz,  $\text{CDCl}_3$ )  $\delta$  174.98, 171.76, 169.94, 155.50, 144.07, 139.87, 137.36, 135.08, 134.53, 134.39, 134.22, 129.64, 129.59, 129.09, 128.26, 127.51, 127.30, 127.28, 126.32, 120.77, 50.90, 50.28, 38.34, 21.18, 21.04. MS ( $\text{ES}^-$ ),  $m/z$  548.2 ( $\text{M} - \text{H}$ ), 98.0% purity. HRMS ( $\text{ES}^+$  TOF) calculated for  $\text{C}_{33}\text{H}_{31}\text{N}_3\text{O}_5$  ( $\text{M} + \text{H}$ ): 550.2336; found 550.2346.



**(S)-2-(3-([1,1'-biphenyl]-4-carbonyl)-3-(4-methylbenzyl)ureido)-4-((2,4-dimethylphenyl)amino)-4-oxobutanoic acid (5.23g):** Using **General Procedure F**, compound **5.21** (19 mg, 0.037 mmol) was reacted with 2,4-dimethylaniline (5  $\mu\text{L}$ , 0.041 mmol). The reaction mixture was passed through a short silica plug with dichloromethane according to **General Procedure G**, then concentrated under reduced pressure. The residue was dissolved in methanol then passed through a 1g SCX column (Mega-BE SCX, Agilent) to remove unreacted aniline, eluting with methanol. Deprotection of the crude product with TFA and Prep-HPLC purification *via* according to **General Procedure G**, yielded compound **5.23g** as a colourless glassy solid (4.8 mg, 23%).  $^1\text{H}$  NMR (600 MHz,  $\text{CDCl}_3$ )  $\delta$  9.83 (d,  $J$  = 5.9 Hz, 1H), 7.65 (s, 1H), 7.59–7.54 (m, 4H), 7.49–7.43 (m, 4H), 7.40–7.35 (m, 2H), 7.07–6.94 (m, 6H), 5.03–4.95 (m, 2H), 4.77 (ddd,  $J$  = 8.8, 5.8, 3.3 Hz, 1H), 3.09 (dd,  $J$  = 15.7, 3.3 Hz, 1H), 2.93 (dd,  $J$  = 15.8, 8.1 Hz, 1H), 2.29 (s, 3H), 2.28 (s, 3H), 2.16 (s, 3H).  $^{13}\text{C}$  NMR (151 MHz,  $\text{CDCl}_3$ )  $\delta$  174.89, 171.69, 170.42, 155.49, 144.00, 139.90, 137.27, 136.51, 134.55, 134.30, 131.83, 131.46, 131.16, 129.52, 129.08, 128.24, 127.51, 127.41, 127.29, 127.27, 126.48, 124.68, 51.08, 50.20, 38.14, 21.21, 21.07, 17.88.

MS (ES<sup>-</sup>),  $m/z$  562.2 (M - H), 99.0% purity. HRMS (ES<sup>+</sup> TOF) calculated for C<sub>34</sub>H<sub>33</sub>N<sub>3</sub>O<sub>5</sub> (M + H): 564.2493; found 564.2496.



**(S)-2-(3-([1,1'-biphenyl]-4-carbonyl)-3-(4-methylbenzyl)ureido)-4-((3,5-dimethylphenyl)amino)-4-oxobutanoic acid (5.23h):** Using **General Procedure F**, compound **5.21** (21.2 mg, 0.041 mmol) was reacted with 3,5-dimethylaniline (6  $\mu$ L, 0.045 mmol). Purification by passing through a short silica plug with dichloromethane, followed by deprotection of the crude product with TFA according to **General Procedure G**, yielded compound **5.23h** as a whitish opaque glassy solid (8.5 mg, 36%). <sup>1</sup>H NMR (300 MHz, CDCl<sub>3</sub>)  $\delta$  9.87 (d,  $J$  = 5.6 Hz, 1H), 8.27 (s, 1H), 7.61–7.50 (m, 4H), 7.50–7.33 (m, 5H), 7.11–6.81 (m, 6H), 6.75 (s, 1H), 4.99 (s, 2H), 4.78–4.70 (m, 1H), 2.99 (dd,  $J$  = 16.1, 3.1 Hz, 1H), 2.81 (dd,  $J$  = 16.0, 7.8 Hz, 1H), 2.35–2.16 (m, 9H). <sup>13</sup>C NMR (75 MHz, CDCl<sub>3</sub>)  $\delta$  174.97, 171.89, 169.93, 155.52, 144.04, 139.86, 138.85, 137.34, 136.81, 134.54, 134.23, 129.59, 129.08, 128.25, 127.49, 127.29, 127.26, 127.08, 126.31, 118.41, 50.91, 50.26, 38.43, 21.44, 21.17. MS (ES<sup>-</sup>),  $m/z$  562.2 (M - H), 99.0% purity. HRMS (ES<sup>+</sup> TOF) calculated for C<sub>34</sub>H<sub>33</sub>N<sub>3</sub>O<sub>5</sub> (M + H): 564.2493; found 564.2499.

### 5.6.3 Crystallisation and X-ray structure determination

#### 5.6.3.1 Structure determination of the BCL-X<sub>L</sub>:**5.19g** complex

The complex of BCL-X<sub>L</sub>:**5.19g** (10 mg/mL) was prepared for crystallisation as described in **Chapter 2, Section 2.6** and crystallised under the following condition: 1.6 M ammonium sulfate, 0.1 M Tris pH 7.0. Crystals were flash-cooled in cryoprotectant solution containing 1.8 M ammonium sulfate, 0.1 M Tris pH 7.0 supplemented with ethylene glycol (25%). Data were collected on the MX2 beamline at the Australian Synchrotron and processed with XDS<sup>(3)</sup>. The structure was solved by molecular replacement with PHASER<sup>(4)</sup> using as a search model the BCL-X<sub>L</sub> coordinates from the previously solved BCL-X<sub>L</sub>:**5.15a** complex (described below). Multiple rounds of building in COOT<sup>(5)</sup> and refinement in PHENIX<sup>(6)</sup> incorporating in the first round of refinement a simulated annealing step, resulted in the final structure. The asymmetric unit contained two copies of the BCL-X<sub>L</sub> monomer, arranged as a domain-swapped dimer. In one monomer a single copy of the ligand was observed to occupy the hydrophobic groove; the groove of the second monomer was empty. Ligand geometry restraint (cif) files were generated from SMILES strings using ELBOW<sup>(7)</sup>.

#### 5.6.3.2 Structure determination of the BCL-X<sub>L</sub>:**5.10b** complex

The complex of BCL-X<sub>L</sub>:**10b** was crystallised as for the BCL-X<sub>L</sub>:**5.19g** complex (described above), but under the following condition: 2.0 M ammonium sulfate, 0.1 M Tris pH 7.0. Crystals were flash-cooled in cryoprotectant solution containing 2.2 M ammonium sulfate, 0.1 M Tris pH 7.0 supplemented with ethylene glycol (25%). Data collection, processing, molecular replacement, refinement and generation of ligand geometry restraints were performed as for the BCL-X<sub>L</sub>:**5.19g** complex. The asymmetric unit contained two copies of the BCL-X<sub>L</sub> monomer, arranged as a domain-swapped dimer. In one monomer a single copy of the ligand was observed to occupy the hydrophobic groove in the expected conformation. In the second monomer the ligand was observed to occupy an alternative conformation in which the benzoylurea core was in an 'open' conformation<sup>(8)</sup> and the benzyl moiety did not occupy the p5 pocket but instead bridged across to

another BCL-X<sub>L</sub> monomer. This interaction mediated a crystal contact and appeared to be a result of crystal packing and unlikely to represent the bound conformation in solution.

#### 5.6.3.3 Structure determination of the BCL-X<sub>L</sub>:**5.19e** complex

The complex of BCL-X<sub>L</sub>:**5.19e** (10 mg/mL) was crystallised, flash-cooled and data collected and processed as for the BCL-X<sub>L</sub>:**5.19g** complex (described above). The structure was solved by molecular replacement with PHASER<sup>(4)</sup> using as a search model the BCL-X<sub>L</sub> coordinates from the BCL-X<sub>L</sub>:**ABT-737** structure (PDB entry: 2YXJ)<sup>(1)</sup>. Refinement was performed as for the BCL-X<sub>L</sub>:**5.19g** complex. Ligand geometry restraint (cif) files were generated from SMILES strings using ELBOW<sup>(7)</sup>, incorporating geometry retrieved from the Cambridge Structural Database using MOGUL<sup>(9)</sup>. The asymmetric unit contained two copies of the BCL-X<sub>L</sub> monomer, arranged as a domain-swapped dimer. In one monomer a single copy of the ligand was observed to occupy the hydrophobic groove; the groove of the second monomer was empty.

#### 5.6.3.4 Structure determination of the BCL-X<sub>L</sub>:**5.19d** complex

The complex of BCL-X<sub>L</sub>:**19d** was crystallised as for the BCL-X<sub>L</sub>:**5.19g** complex (described above), but under the following condition: 1.8 M ammonium sulfate, 0.1 M MES pH 5.5. Crystals were flash-cooled in cryoprotectant solution containing 1.9 M ammonium sulfate, 0.1 M MES pH 5.5 supplemented with ethylene glycol (20%). Data collection, processing, molecular replacement, and refinement were performed as for the BCL-X<sub>L</sub>:**5.19g** complex; with the modifications that molecular replacement utilised as a search model the BCL-X<sub>L</sub> coordinates from the previously solved BCL-X<sub>L</sub>:**1.1** structure, and NCS restraints and TLS parameterisation were additionally utilised during refinement. The asymmetric unit contained 12 copies of the BCL-X<sub>L</sub> monomer, arranged as six domain-swapped dimers. Electron density corresponding with a single copy of the ligand was observed bound in the hydrophobic groove of each monomer (in an anticipated conformation). Multiple rounds of building in COOT<sup>(5)</sup> and refinement in PHENIX<sup>(6)</sup> incorporating in the

first round of refinement a simulated annealing step, and utilising NCS restraints and TLS refinement in later rounds. Explicit waters and solvent molecules located away from the ligand electron density were modeled, resulting in an advanced structure (without any ligands yet modeled). Ligand geometry restraint (cif) files were generated from SMILES strings using ELBOW<sup>(7)</sup> for each of the four possible stereoisomers described in the main text. Then, for each of the four stereoisomers, the ligand was placed into all 12 sites of observed electron density (i.e. placing a single stereoisomer at 100% occupancy) to generate four alternative models. For each of these resulting four models (BCL-X<sub>L</sub>:**5.19d(SSR)** ... **5.19d(RRS)**), a single round of refinement was run in parallel (utilising NCS restraints and TLS refinement) to generate comparative refinement statistics, which are summarised in **Table 5.6**. Although the final  $R_{\text{free}}$  value for all structures was very similar, crystallographic statistics are provided in **Table 5.7** for one of these structures, the BCL-X<sub>L</sub>:**5.19d(SRR)** structure, for which the final  $R_{\text{free}}$  value was the lowest.

#### 5.6.3.5 Structure determination of the BCL-X<sub>L</sub>:**5.15a** complex

The complex of BCL-X<sub>L</sub>:**5.15a** (10 mg/mL) was crystallised, flash-cooled and data collected and processed as for the BCL-X<sub>L</sub>:**5.19g** complex (described above). The structure was solved by molecular replacement with PHASER<sup>(4)</sup> using as a search model the BCL-X<sub>L</sub> coordinates from the BCL-X<sub>L</sub>:**1.1** structure. Refinement and generation of ligand geometry restraint (cif) files was performed as for the BCL-X<sub>L</sub>:**5.19g** complex. The asymmetric unit contained two copies of the BCL-X<sub>L</sub> monomer, arranged as a domain-swapped dimer. As for the BCL-X<sub>L</sub>:**5.10b** complex described above, one monomer harboured a single copy of the ligand in the anticipated conformation; whilst in the second monomer the ligand was in an alternative 'open' conformation that appeared to be a result of crystal packing and unlikely to reflect the bound conformation in solution.

#### 5.6.3.6 Structure determination of the BCL-X<sub>L</sub>:**5.23e** complex

The complex of BCL-X<sub>L</sub>:**5.15a** (10 mg/mL) was crystallised, crystals flash-cooled, data collected and processed, and the structure solved by molecular replacement as for the BCL-X<sub>L</sub>:**5.19g** complex (described above). Refinement and generation of ligand restraint (cif) files as for the BCL-X<sub>L</sub>:**5.19g** complex, led to the final structure. As for the BCL-X<sub>L</sub>:**5.10b** complex described above, one monomer harboured a single copy of the ligand in the anticipated conformation; whilst in the second monomer the ligand was in an alternative 'open' conformation that appeared to be a result of crystal packing and unlikely to reflect the bound conformation in solution.

## 5.7 References

1. Lee EF, *et al.* (2007) Crystal structure of ABT-737 complexed with Bcl-xL: implications for selectivity of antagonists of the Bcl-2 family. *Cell Death and Differentiation* 14(9):1711-1713.
2. Hopkins AL, Keserü GM, Leeson PD, Rees DC, & Reynolds CH (2014) The role of ligand efficiency metrics in drug discovery. *Nature Reviews. Drug Discovery* 13(2):105-121.
3. Kabsch W (2010) Xds. *Acta Crystallographica Section D Biological Crystallography* 66(Pt 2):125-132.
4. McCoy AJ, *et al.* (2007) Phaser crystallographic software. *Journal of Applied Crystallography* 40(Pt 4):658-674.
5. Emsley P & Cowtan K (2004) Coot: model-building tools for molecular graphics. *Acta Crystallographica Section D Biological Crystallography* 60(Pt 12 Pt 1):2126-2132.
6. Adams PD, *et al.* (2010) PHENIX: a comprehensive Python-based system for macromolecular structure solution. *Acta Crystallographica Section D Biological Crystallography* 66(Pt 2):213-221.
7. Moriarty NW, Grosse-Kunstleve RW, & Adams PD (2009) electronic Ligand Builder and Optimization Workbench (eLBOW): a tool for ligand coordinate and restraint generation. *Acta Crystallographica Section D Biological Crystallography* 65(Pt 10):1074-1080.
8. Lessene G, Smith BJ, Gable RW, & Baell JB (2009) Characterization of the two fundamental conformations of benzoylureas and elucidation of the factors that facilitate their conformational interchange. *Journal of Organic Chemistry* 74(17):6511-6525.
9. Bruno IJ, *et al.* (2004) Retrieval of crystallographically-derived molecular geometry information. *Journal of Chemical Information and Computer Sciences* 44(6):2133-2144.

## **6 Chapter six – Generation of p2 extended compounds and structural/biochemical evaluation**



## 6.1 Introduction

**Chapter 1** introduced the benzoylurea series of BCL-X<sub>L</sub> inhibitors, including the initial hit compound **1.1** ( $IC_{50}(BCL-X_L) = 0.51 \mu M$ , **Figure 6.1**, **Table 6.1**) and the crystal structure of the BCL-X<sub>L</sub>:**1.1** complex. Early negative SAR studies were conducted to further explore the binding of **1.1** to BCL-X<sub>L</sub>. In particular, compounds **1.2** ( $IC_{50}(BCL-X_L) = 13 \mu M$ , **Table 6.1**) and **1.5** ( $IC_{50}(BCL-X_L) = 30.8 \mu M$ , **Figure 6.1**, **Table 6.1**) highlighted the importance of interactions in the p5 and p4 pockets respectively. In the hope of gaining additional fruitful interactions in the p2 pocket of BCL-X<sub>L</sub>, structure-guided design was employed to design two 'extended' scaffolds that incorporated a chlorobiphenyl moiety similar to that of **ABT-737** (**Figure 6.1**, blue highlight). These two extended scaffolds were represented by compounds **1.9** (rigid biphenyl scaffold linked to chlorobiphenyl moiety, **Figure 6.1**, purple highlight) and **1.10** (flexible THIQ scaffold linked to chlorobiphenyl moiety, **Figure 6.1**, red highlight).

**Chapter 3**, amongst other work, described structural studies with compound **3.1** in complex with BCL-X<sub>L</sub>. These studies showed that compound **3.1** (which incorporated a sulfonyl group in the linker of compound **1.10**; refer **Figure 6.1**) gained an additional hydrogen bond interaction with the backbone -NH of Gly138 of BCL-X<sub>L</sub> whilst maintaining the deep interaction of the chlorobiphenyl in the p2 pocket similar to **ABT-737**. However despite these additional interactions, compounds **1.10** and **3.1** still had relatively modest  $IC_{50}$  values for BCL-X<sub>L</sub> ( $IC_{50}(BCL-X_L) = 0.21 \mu M$  and  $0.17 \mu M$  respectively, **Table 6.1**).

SAR studies were conducted using the simple biphenyl scaffold to explore modifications targeting the p5 pocket of BCL-X<sub>L</sub>. **Chapters 4** and **5** described respectively the synthesis and evaluation of p5 SAR analogues that utilised either a sulfonyl, or amide linker. These studies revealed that the p5 interacting group need not be aromatic; in fact, replacement of the terminal phenyl ring with a more three-dimensional cyclohexyl or adamantyl group (eg. compounds **4.6l**, **4.25**, **5.19b**, **5.19e**, **Figure 6.1**) in most cases improved affinity whilst maintaining or improving the binding efficiency index (BEI) (refer **Table 6.1**). This suggested that

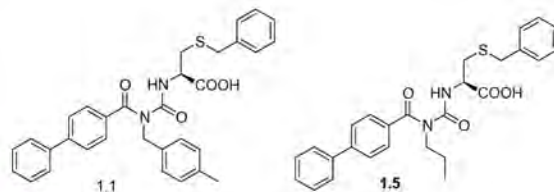
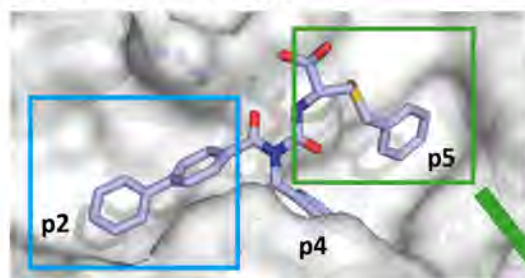
similar modifications grafted onto the p2 extended scaffold compounds might improve the affinity of the compounds for BCL-X<sub>L</sub>.

This Chapter firstly describes the synthesis of three analogues (compounds **6.1**, **6.2** and **6.3**) that explore the combined effect of incorporating a p2 extension and an optimised p5 substituent. Compounds **6.1**, **6.2** and **6.3** are based on the flexible THIQ scaffold (following from **1.10**) incorporating respectively either a cyclohexyl and adamantyl substituent on a sulfonyl linker and an adamantyl substituent on an amide linker (based on Amide Series A) (**Figure 6.1**). I describe some particular synthetic challenges encountered during the synthesis of compounds **6.2** and **6.3** and strategies employed to overcome this. Initial binding studies revealed **6.1-6.3** to be the most potent analogues for BCL-X<sub>L</sub> in the series to date (IC<sub>50</sub>(BCL-X<sub>L</sub>) ~ 30 - 45 nM, **Table 6.1**).

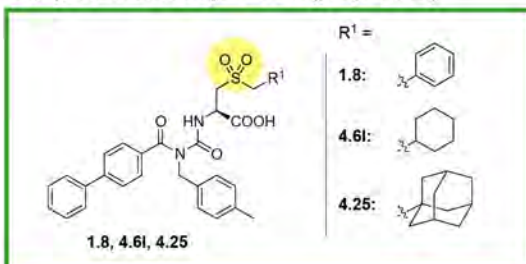
Following on from this promising binding data, this Chapter outlines early results from ongoing studies to evaluate a number of key analogues in this benzoylurea series for their selectivity, mechanism-based activity and *in vitro* cellular activity (**Figure 6.1**).

All chemical synthesis, binding and mechanistic studies described in this Chapter were performed by me, with the exception of a repeat synthesis of compound **6.2** that was performed by Amelia Vom (as explicitly noted in the relevant section(s) of the text) and the isolation of platelets that was performed by Stephane Chappaz.

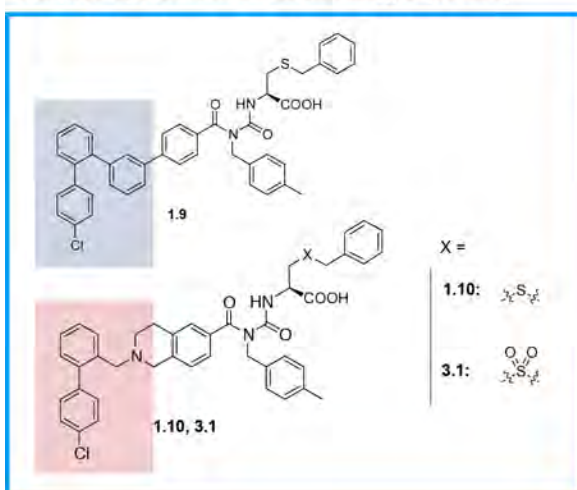
## Chapter 1: Benzoulurea series



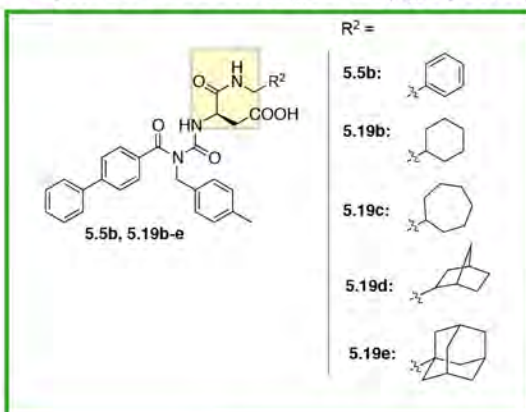
## Chapter 4: Sulfonyl Series (p5 pocket)



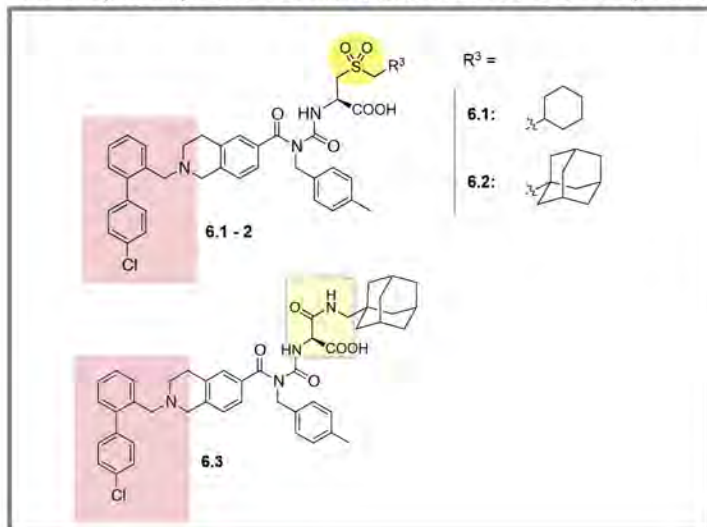
## Chapter 1,3: Extended scaffolds (p2 pocket)



## Chapter 5: Amide Series (A and B) (p5 pocket)



## This Chapter: Synthesis of THIQ extended scaffold compounds

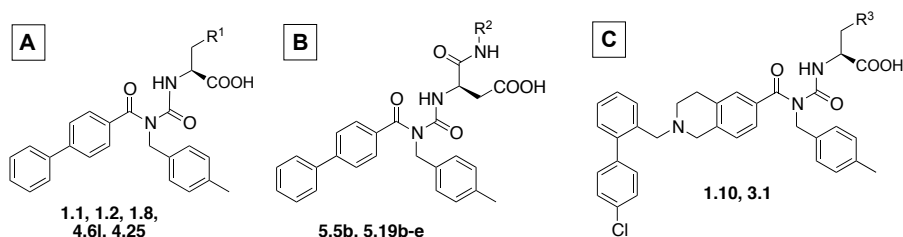


### Evaluation of:

- Selectivity (SPR Competition Assay)
- Mechanism-based activity (Cytochrome c Release Assay)
- Cellular activity (Cell killing assays)

Figure 6.1: Summary of benzoulurea series described in this Thesis.

**Table 6.1: Affinity of simple biphenyl and extended scaffold compounds for BCL-X<sub>L</sub> and MCL-1 (determined by AlphaScreen Assay, post-2015 data)<sup>[a]</sup>**



Compound		IC <sub>50</sub> A.S. <sup>[b]</sup>			Fold Selectivity		BEI <sup>[c]</sup>
R <sup>1</sup> =		BCL-X <sub>L</sub>	MCL-1	N =	(BCL-X <sub>L</sub> /MCL-1)		
<b>A</b>	<b>1.1</b>		0.51 ±0.07	7.7 ±1.6	3	15	11.7
	<b>1.2</b>		13.0 ±0.4	44 ±8.5	3	3	9.8
	<b>1.8</b>		0.59 ±0.11	11.6 ±1.0	3	20	10.9
	<b>4.6l</b>		0.46 ±0.43	10.0 ±2.5	3	22	11.0
	<b>4.25</b>		0.19 ±0.08	6.1 ±0.9	3	32	10.7
	<b>1.5</b>	-	30.8 ±9	28.2 ±9	3	0.9	9.5
R <sup>2</sup> =							
<b>B</b>	<b>5.5b</b>		0.58 ±0.20	21.0 ±0.5	3	36	11.3
	<b>5.19b</b>		0.35 ±0.17	14.5 ±3.5	3	42	11.6
	<b>5.19e</b>		0.12 ±0.04	6.7 ±0.6	3	57	11.4
R <sup>3</sup> =							
<b>C</b>	<b>1.10</b>		0.21 ±0.092	2.0 ±0.1	3	10	9.3
	<b>3.1</b>		0.17 ±0.055	5.3 ±0.4	3	31	9.0

<sup>[a]</sup> For further information refer to note in **Chapter 2, Section 2.4.1.3**.

<sup>[b]</sup> IC<sub>50</sub> values are reported in  $\mu\text{M} \pm \text{S.D.}$

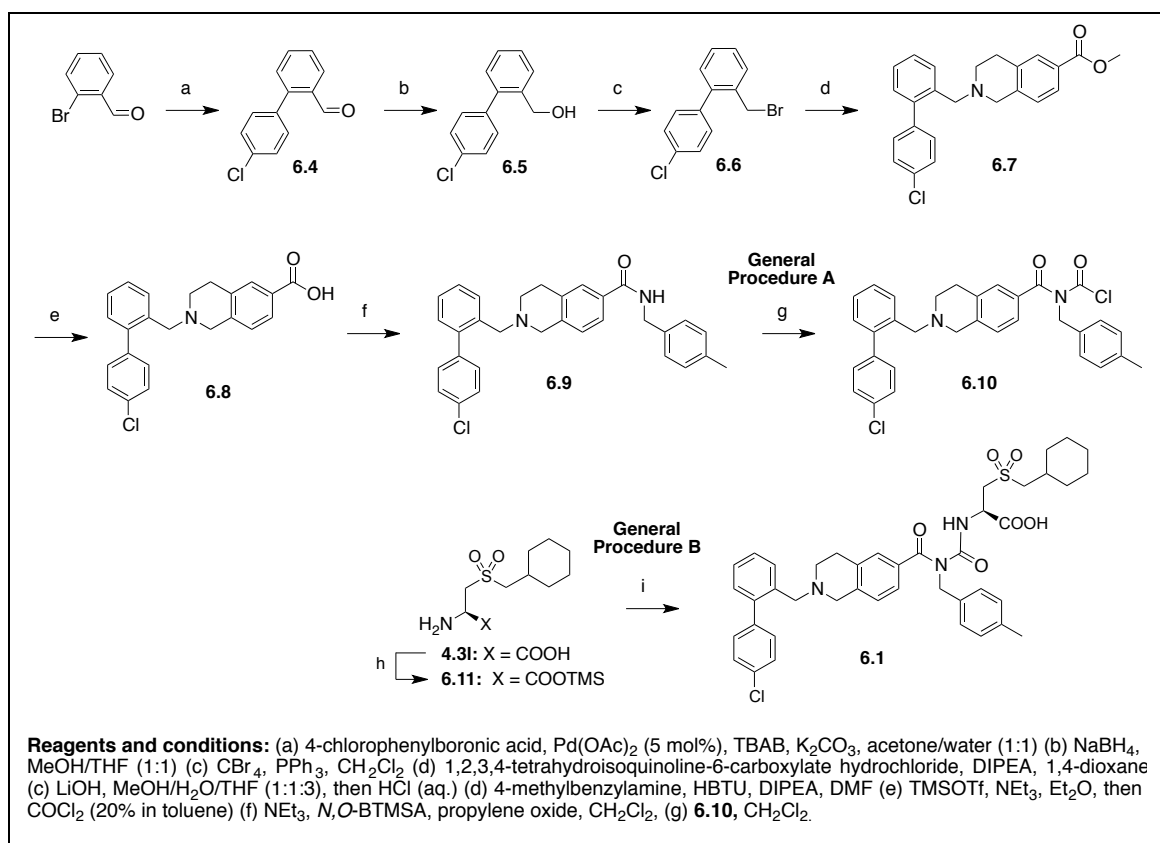
<sup>[c]</sup> BEI (Binding efficiency index, refer Section 1.4.1.2) =  $\text{pIC}_{50}/\text{MW}$ , where  $\text{pIC}_{50}$  is the negative base 10 logarithm of the IC<sub>50</sub> (in molar units) and MW is the compound molecular weight (in kDa).

## 6.2 Synthesis of cyclohexyl- and adamantyl- analogues using extended THIQ scaffold targeting the p2 pocket

As described in the Introduction, based the promising BCL-X<sub>L</sub> AlphaScreen results of benzoylurea analogues on the simple biphenyl scaffold bearing a p5 cyclohexyl substituent, (eg. analogues **4.6l** [Chapter 4] and **5.19b** [Chapter 5], Table 6.1), we next wished to explore similar modifications on the more potent extended THIQ scaffold, to generate compound **6.1**.

### 6.2.1 General synthetic approach to compound **6.1** (Scheme 6.1)

The synthetic approach to compound **6.1** was based on formation of the THIQ scaffold that would then be subjected to benzoylurea formation as described earlier (Scheme 6.1). The THIQ scaffold carboxylic acid precursor **6.8** was constructed using a five-step synthesis established in the lab previously. Starting from commercially-available 2-bromobenzaldehyde, a Suzuki–Miyaura coupling with 4-chloro-phenylboronic acid furnished the aldehyde **6.4** (81% yield), which was then reduced with sodium borohydride to the corresponding primary alcohol **6.5** (84% yield) and converted to the bromide **6.6** *via* the Appel Reaction using triphenylphosphine/carbon tetrabromide (92% yield). Next, **6.6** was utilised to N-alkylate commercially available methyl 1,2,3,4-tetrahydroisoquinoline-6-carboxylate hydrochloride to form the methyl ester **6.7** (79% yield), which was subsequently saponified using LiOH to the free carboxylic acid **6.8** (74% yield). HBTU-mediated amide coupling of compound **6.8** with 4-Methylbenzylamine formed the THIQ amide **6.9** (83% yield), which could be subjected to the standard sequence for benzoylurea formation described earlier. Activation of the amide **6.9** using triethylamine/TMSOTf followed by reaction with phosgene (20% solution in toluene) formed the carbamoyl chloride intermediate **6.10**. This was then reacted with the cyclohexyl sulfonyl amino acid **4.3l** (described in Chapter 4), which had first been protected as the TMS ester, to form compound **6.1** in (60% yield).



**Scheme 6.1: Synthesis of cyclohexyl sulfonyl analogue 6.1 on extended tetrahydroisoquinoline (THIQ) scaffold, designed to interact with p2 pocket and have modified substituent in p5 pocket.**

### 6.2.2 Synthetic challenges encountered during synthesis of compound 6.2

It was anticipated that compound **6.2** would be synthesised according to the same procedure as for compound **6.1**, but instead using the adamantyl sulfonyl amino acid **4.21** (described in **Chapter 4**).

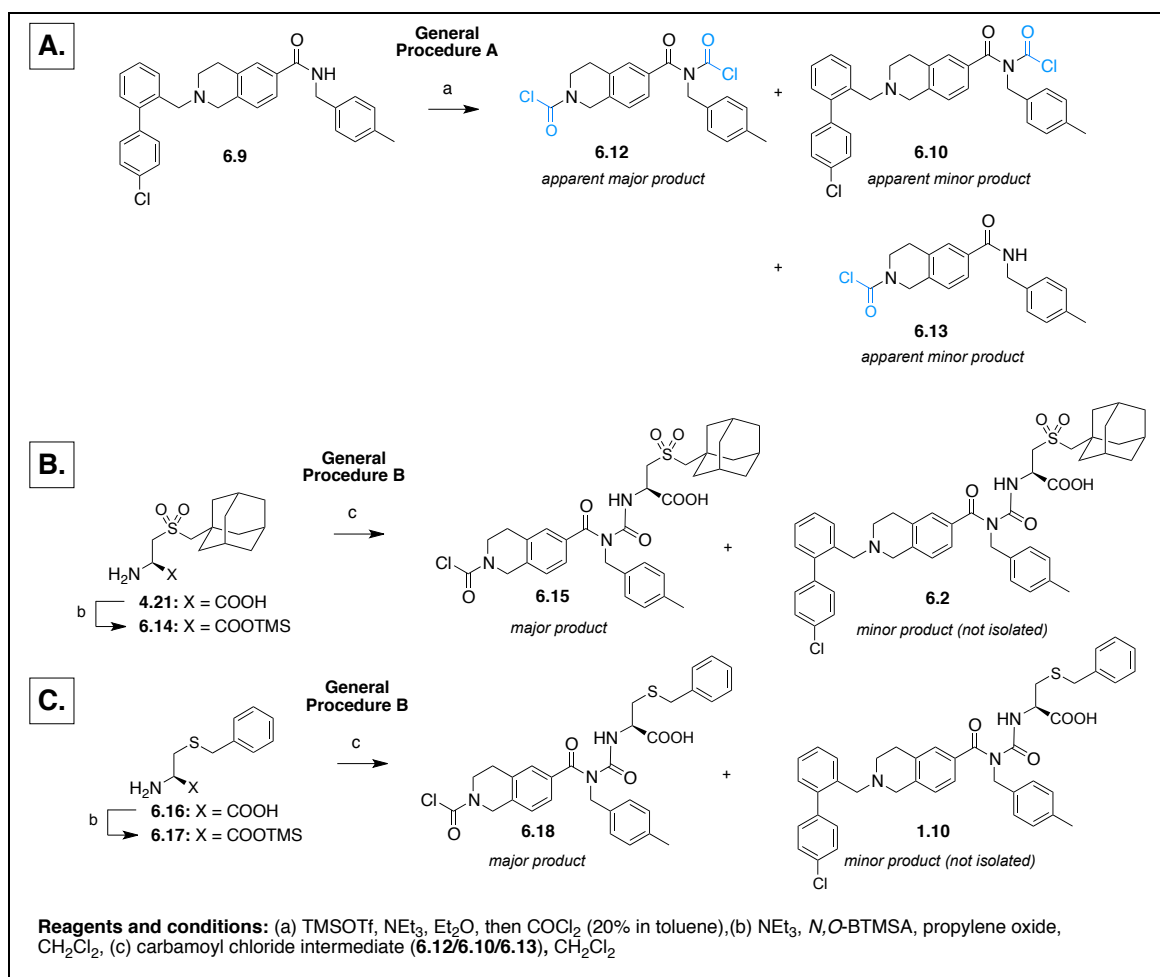
However, initial attempts at synthesising **6.2** using this method were unsuccessful and instead recovered as the major reaction product the carbamoyl chloride derivative **6.15** (**Scheme 6.2**), from which the p2 chlorobiphenyl moiety had been lost. This carbamoyl chloride was remarkably stable to both aqueous workup and purification by flash chromatography (SiO<sub>2</sub>). LCMS and <sup>1</sup>H NMR analysis of compound **6.15** are provided in **Appendix Figure A1**. Unfortunately the desired product **6.2** appeared to be formed in very low yield (based on TLC and LCMS) and was not isolated on purification (**Scheme 6.2**). Loss of the chlorobiphenyl

fragment to form **6.15** appeared to result from a side-reaction involving a debenzylation at the THIQ tertiary nitrogen, which we suspected might be phosgene-mediated.

#### *6.2.2.1 Loss of p2 chlorobiphenyl fragment due to debenzylation side-reaction*

We were surprised by this unanticipated side-reaction, given that this procedure had successfully been utilised using this same THIQ scaffold previously to yield similar benzoylurea products (including compounds **1.10**, **3.1** and **6.1**). However, some time had passed between the successful synthesis of compound **6.1** and the subsequent attempts to synthesise compound **6.2** (primarily due to synthetic challenges associated with generating the necessary adamantyl amino acid precursor **4.21**, described in **Chapter 4**) and so degradation of key reagents was a possibility. In particular, during this time the utilised stock of phosgene (approx. 20% in toluene) had been changed.

To confirm the side reaction to form **6.15** was not due to the modified amino acid precursor **4.21** (**Scheme 6.2A,B**), attempts to were made in parallel (using the same stock of carbamoyl chloride intermediate) to repeat the synthesis of **1.10** using S-benzyl-L-cysteine (**Scheme 6.2A,C**). However, this also led to formation of corresponding debenzylated product **6.18** as the major reaction product. LCMS and <sup>1</sup>H NMR analysis of compound **6.18** are provided in **Appendix Figure A2**. This suggested that the side-reaction was occurring during carbamoyl chloride formation (prior to addition of the amino acid).



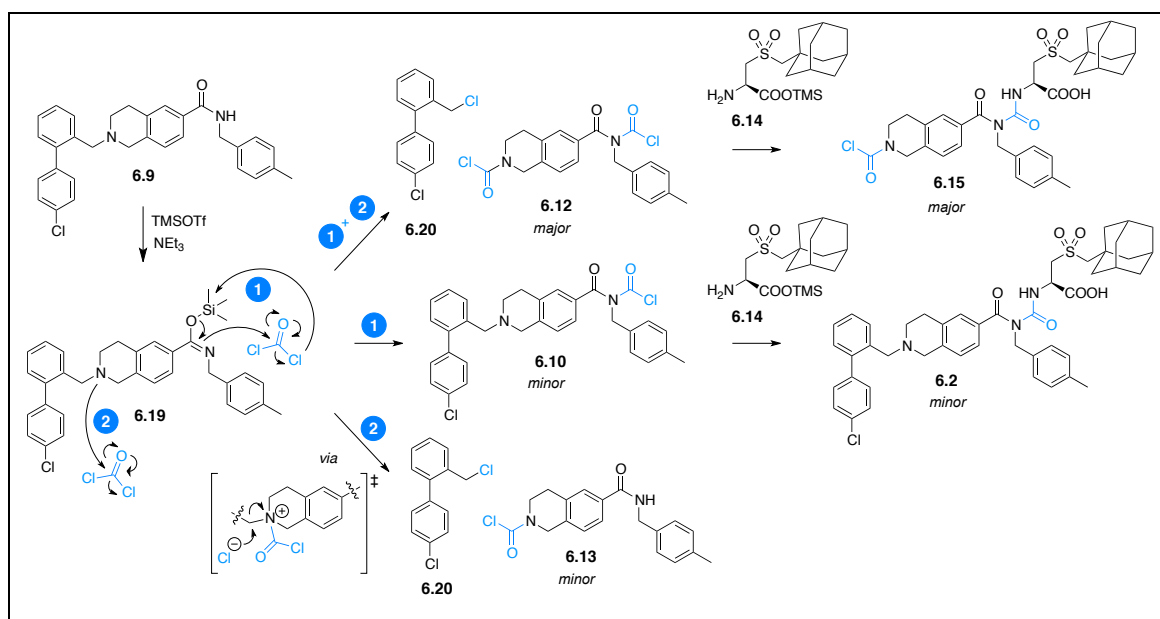
**Scheme 6.2: Unanticipated loss of p2 chlorobiphenyl fragment during synthesis of compounds **6.2** and **1.10**, to instead form debenzylated derivatives **6.15** and **6.18**.**

We hypothesised that the side-reaction might be caused by the presence of excess phosgene in the reaction relative to the activated *O*-TMS imide derivative **6.19**, to form the second carbamoyl chloride at the tertiary amine centre of the THIQ (possibly *via* a mechanism such as that described in **Scheme 6.3**). This hypothesis was supported by recent reports in the literature of the use of phosgene or triphosgene as an efficient method for debenzylation of tertiary amines (including, relevantly, *N*-benzyl THIQ derivatives)<sup>(1-3)</sup>.

In the case of the synthesis of compounds **6.2** and **1.10**, the reaction product was a difficult-to-separate mixture containing minor quantities of the desired product (compounds **6.2** or **1.10** respectively); the major product being the debenzylated carbamoyl chloride by-product (compounds **6.15** or **6.18** respectively)



(**Scheme 6.2**). Compound **6.13**, formed by debenzylation of the starting material, was also observed by LCMS as a minor side-product of the reaction (data not shown) (**Scheme 6.2**).



**Scheme 6.3: Possible mechanism of debenzyl side-reaction.**

The standard reaction for benzoylurea formation involves initial activation of the THIQ amide **6.9** to the activated O-TMS imide derivative **6.19** using triethylamine/TMSOTf. Following subsequent phosgene addition, nucleophilic attack by the imide nitrogen forms the desired carbamoyl chloride derivative **6.10**. However, in the side-reaction it appears that a second nucleophilic reaction onto phosgene can occur from the THIQ tertiary nitrogen atom, to effect the debenzylation and form the undesired intermediates **6.12** (major product) and **6.13** (minor product), as well as a chlorobiphenyl fragment (with the likely structure **6.20**). Subsequent addition of the protected amino acid **6.14** to the mixture of carbamoyl chloride derivatives, leads to formation of compounds **6.15** (major product) and **6.2** (minor product). Note that we never observed the product arising from reaction of the protected amino acid **6.14** with the THIQ carbamoyl chloride moiety (resulting from **2**); we assume that this is due to the higher reactivity of the amide carbamoyl chloride moiety (resulting from **1**). Consistent with this presumed difference in reactivity, whilst products **6.13** and **6.15** (containing the THIQ carbamoyl chloride moiety) could be isolated after aqueous workup and purification, the products **6.12** or **6.10** (containing the amide carbamoyl chloride moiety) were never observed after workup.

### 6.2.3 Modified approaches to access compound 6.2

Two alternative strategies were trialed in parallel to overcome the formation of the debenzylated carbamoyl chloride side-product **6.15** and access compound **6.2**:

- i) Control of reagent equivalents during the benzoylurea reaction to improve the yield of compound **6.2**
- ii) Development of chemistry to reinstall the chlorobiphenyl moiety onto the debenzylated carbamoyl chloride side-product **6.15**, to generate **6.2**.

Both of these methods were ultimately successful in forming compound **6.2** and will be described in turn.

#### 6.2.3.1 Control of reaction equivalents during the benzoylurea reaction

Based on our previous successful formation of compounds **1.10**, **3.1** and **6.1** in good yield (> 50% yield), we expected that under the right conditions, the first site of reaction with phosgene would be the activated O-TMS imidate (**Scheme 6.3**, ①) – as opposed to the tertiary amine of the THIQ scaffold (**Scheme 6.3**, ②). If so, the debenzylation side-reaction would be favoured by an excess of phosgene present in the reaction mixture relative to O-TMS imidate derivative **6.19** (**Scheme 6.3**). This might be the case if the concentration of phosgene added was higher than anticipated (if the stock of approx. 20% phosgene in toluene was more concentrated than expected), or if the first step forming the O-TMS imidate derivative **6.19** did not go to completion leaving un-reacted phosgene present in the reaction mixture (such as due to side-reaction of the TMSOTf or O-TMS imidate with ambient water).

Efforts were therefore made to repeat the reaction using an excess of the reagents triethylamine/TMSOTf (1.2 eq. of each relative to the amide starting material) and to limit the phosgene to sub-stoichiometric quantities (0.9 eq.). As the precise concentration of the approx. 20% phosgene in toluene was not known, these trials were largely empiric in nature. A particular confounding factor was that limiting quantities of available amide starting material necessitated that these trials be

performed on very small scale; which made dispensing accurate stoichiometric quantities of the necessary reagents incredibly challenging (eg. required volumes of moisture-sensitive reagents <10  $\mu$ L). Whilst attempts to form compound **6.2** in this way *via* direct benzoylurea formation still yielded a complex mixture of products (refer **Appendix Figure A3**, crude reaction mixture at 5 minutes) the fraction of the desired product was sufficiently improved to allow successful isolation of compound **6.2** using mass-directed preparative HPLC (albeit in a low isolated yield of 7%).

An alternative approach was also explored, utilising the carbamoyl chloride side-products **6.15** and **6.18** by finding an alternative method to reinstall the left-hand chlorobiphenyl group.

#### *6.2.3.2 Alternative approach - development of chemistry to reinstall p2 chlorobiphenyl fragment via decarbonylation/reductive amination*

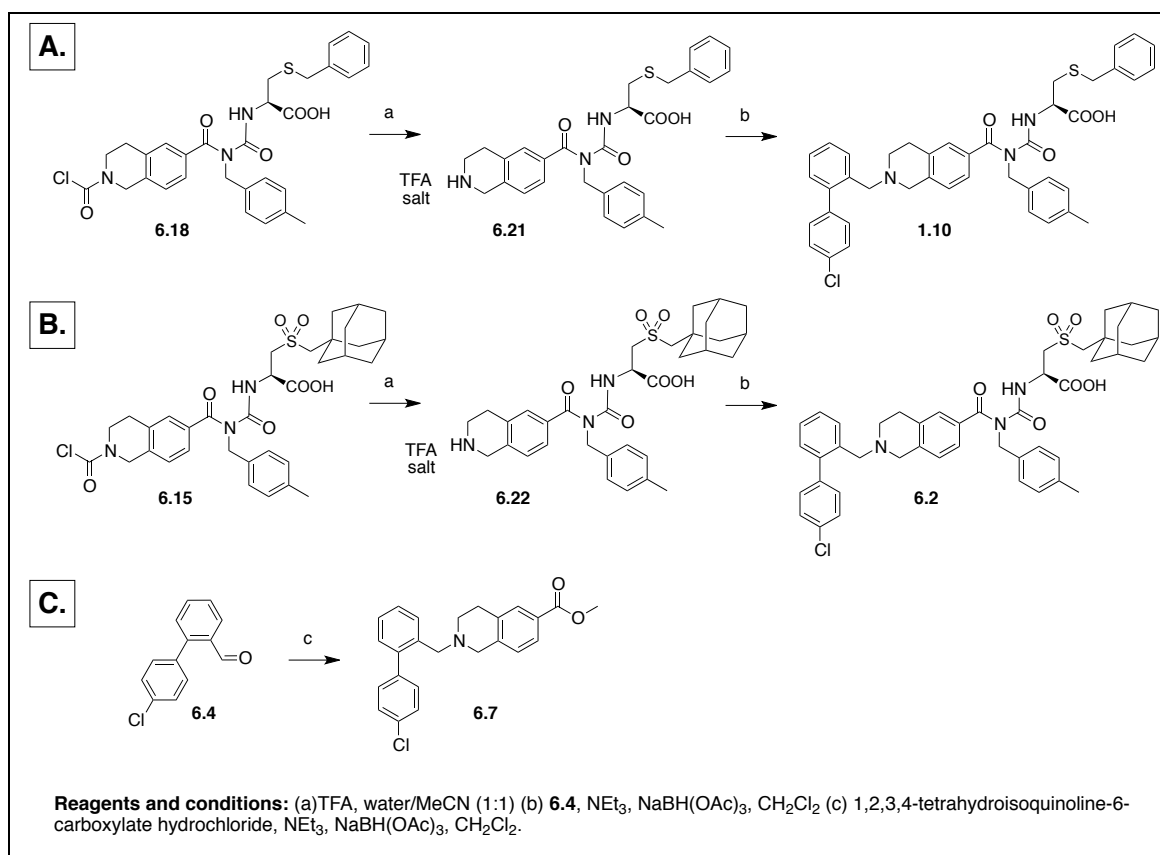
Initial trials to reinstall the p2 chlorobiphenyl fragment were conducted using compound **6.18**. Based on a procedure described in the literature<sup>(4)</sup>, it was found that gentle heating of compound **6.18** at 80°C with TFA in a (1:1) water/acetonitrile mixture for 1 h was able to successfully remove the acylchloride moiety from compound **6.18** to form the secondary amine TFA salt **6.21** with excellent conversion, monitoring disappearance of the starting peak and appearance of the product peak by LCMS (**Scheme 6.4A(a)**, refer **Appendix Figure A4**). Next, compound **6.21** was subjected to a reductive amination with compound **6.4** in the presence of sodium triacetoxyborohydride to successfully reinstall the chlorobiphenyl group. This was able to generate the desired product **1.10** in very good yield (70% isolated yield over the two-step sequence)(**Scheme 6.4A(b)**)(refer **Appendix Figure A5**).

This sequence was also utilised successfully to convert **6.15** *via* the free secondary amine TFA salt **6.22** to the desired adamantyl product **6.2** with good conversion at each step as monitored by LCMS (refer **Appendix Figures A4, A6** and data not shown) (**Scheme 6.4B(a)-(b)**). Unfortunately significant product was lost on

purification *via* flash chromatography such that compound **6.2** was isolated in relatively low yield and still contained some impurities that could not be separated (<14% isolated yield over the 2-step sequence). Subsequently, compound **6.2** was resynthesised by Amelia Vom on a larger scale *via* the initial direct route (as per **Scheme 6.1**) when additional starting material became available. LCMS and <sup>1</sup>H NMR analyses of purified **6.2** obtained using the three different syntheses are shown for direct comparison in **Appendix Figures A6-A8** – (A) direct route scale-up (Amelia Vom), (B) direct route small scale (C) alternative route *via* reductive amination.

#### 6.2.3.3 Shortened synthetic route to THIQ scaffold

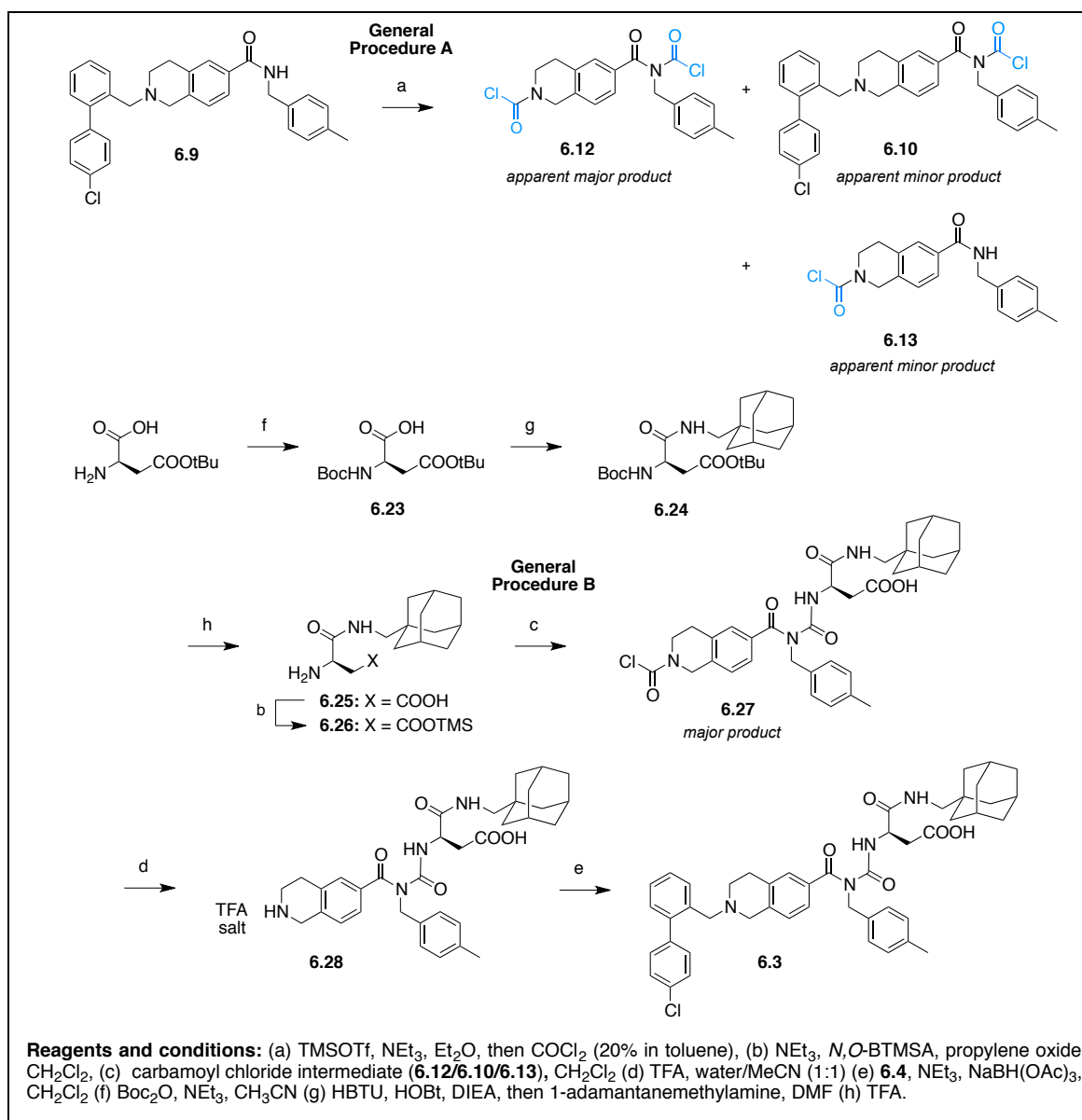
The reductive amination conditions described also enabled direct conversion of intermediate **6.4** to **6.7** in excellent yield (92% yield). This reduced the synthesis of the THIQ scaffold by two overall synthetic steps, enabling formation of intermediate **6.7** in two steps rather than four (**Scheme 6.4C**, compare **Scheme 6.1**). Comparison of the <sup>1</sup>H NMR spectra of compound **6.7** synthesised using both approaches are provided in **Appendix Figure A9**.



**Scheme 6.4: Reinstallation of p2 fragment via decarbonylation followed by reductive amination.**

#### 6.2.3.4 Synthesis of compound **6.3**

The alternative route described above was also utilised to synthesise compound **6.3**, which incorporated an amide-linked adamantyl substituent to interact with the p5 pocket of BCL-X<sub>L</sub> (similar to compound **5.19e**, described in **Chapter 5**)(**Scheme 6.5**). Briefly, N-Boc protection of D-aspartic acid beta-*t*-butyl ester formed the protected amino acid **6.23** (75% yield), which was subjected to HBTU-mediated amide coupling with 1-Adamantanemethylamine to form the protected adamantyl amino acid **6.24** (88% yield). Subsequent Boc-/*t*-butyl-deprotection using neat TFA yielded the amino acid precursor **6.25** (45% yield following purification *via* mass-directed preparative HPLC). This amino acid was then protected *in situ* as the TMS ester and subjected to the benzoylurea reaction by reacting with the carbamoyl chloride mixture **6.10/6.12/6.13** (prepared using 0.9 eq. of phosgene) (**Scheme 6.5**). Whilst a mixture of products was formed, the debenzylated benzoylurea compound **6.27** was isolated as the major product (69% yield). Compound **6.27** was then subjected to the decarbonylation/reductive amination sequence as described for compounds **1.10** and **6.2** above, to afford compound **6.3** in moderate yield after purification by mass-directed preparative HPLC (23% yield).



**Scheme 6.5: Synthesis of compound 6.3 using the alternative synthetic route.**



### 6.3 Evaluation of binding of compounds 6.1 – 6.3

Compounds **6.1**, **6.2**, and **6.3** were assayed for their binding to BCL-X<sub>L</sub> and MCL-1 using the AlphaScreen solution competition assay; IC<sub>50</sub> values for compounds **6.1-6.3** and reference compounds are provided in **Table 6.2**.

#### 6.3.1 Extended scaffold compounds 6.1 – 6.3 - evaluation of BCL-X<sub>L</sub> and MCL-1 binding using AlphaScreen competition assay

Promisingly, compounds **6.1**, **6.2** and **6.3**, which incorporated the modified cyclohexyl or adamantyl p5 substituents were all found to show ~5-fold improvement in binding to BCL-X<sub>L</sub> (IC<sub>50</sub>(BCL-X<sub>L</sub>) = 41 nM, 44 nM, 31 nM respectively, **Table 6.2**) relative to the initial THIQ extended scaffold compound **1.10** (IC<sub>50</sub>(BCL-X<sub>L</sub>) = 210 nM, **Table 6.2**). The fold selectivity for BCL-X<sub>L</sub> relative to MCL-1 was also maintained for compounds **6.1-6.3** (in the range ~40-70-fold). Compounds **6.1** and **6.3** also had improved binding efficiency indices (BEI) relative to the earlier THIQ extended scaffold compounds **1.10** or **3.1** (**Table 6.2**).

The cyclohexyl analogue **6.1** and the two adamantyl analogues **6.2** and **6.3** represent the most potent compounds in this series to date; of these three compounds, **6.1** in particular showed the highest binding efficiency index. To confirm the binding mode with BCL-X<sub>L</sub>, we decided to solve a crystal structure of the BCL-X<sub>L</sub>:**6.1** complex.

**Table 6.2: Affinity of extended scaffold compounds 6.1 – 6.3 for BCL-X<sub>L</sub> and MCL-1 (determined by AlphaScreen Assay, post-2015 data)<sup>[a]</sup>**

A		B		C		D			
1.1, 1.2, 1.8, 4.6l, 4.25		5.5b, 5.19b,e		1.10, 3.1, 6.1-2		6.3			
Compound			IC <sub>50</sub> A.S. <sup>[b]</sup>				Fold Selectivity	BEI <sup>[c]</sup>	
R <sup>1</sup> =			BCL-X <sub>L</sub>		MCL-1		N = (BCL-X <sub>L</sub> /MCL-1)		
A	1.1		0.51	±0.07	7.7	±1.6	3	15	11.7
	1.2		13.0	±0.4	44	±8.5	3	3	9.8
	1.8		0.59	±0.11	11.6	±1.0	3	20	10.9
	4.6l		0.46	±0.43	10.0	±2.5	3	22	11.0
	4.25		0.19	±0.08	6.1	±0.9	3	32	10.7
	1.5	-	30.8	±9	28.2	±9	3	0.9	9.5
R <sup>2</sup> =									
B	5.5b		0.58	±0.20	21.0	±0.5	3	36	11.3
	5.19b		0.35	±0.17	14.5	±3.5	3	42	11.6
	5.19e		0.12	±0.04	6.7	±0.6	3	57	11.4
R <sup>3</sup> =									
C	1.10		0.21	±0.092	2.0	±0.1	3	10	9.3
	3.1		0.17	±0.055	5.3	±0.4	3	31	9.0
	6.1		0.041	±0.029	1.8	±0.2	3	43	9.8
	6.2		0.044	±0.021	1.8	±1.3	3	42	9.1
D	6.3	-	0.031	±0.004	2.3	±0.1	3	73	9.5

<sup>[a]</sup> For further information refer to note in **Chapter 2, Section 2.4.1.3**.

<sup>[b]</sup> IC<sub>50</sub> values are reported in  $\mu\text{M} \pm \text{S.D.}$

<sup>[c]</sup> BEI (Binding efficiency index, refer Section 1.4.1.2) =  $pIC_{50}/\text{MW}$ , where  $pIC_{50}$  is the negative base 10 logarithm of the IC<sub>50</sub> (in molar units) and MW is the compound molecular weight (in kDa).

### 6.3.2 Crystallisation and X-ray structure determination

To validate the binding mode, a complex of BCL-X<sub>L</sub>:**6.1** was crystallised and X-ray diffraction data obtained, enabling a crystal structure of the complex to be solved to 2.19 Å resolution. The final structure of the BCL-X<sub>L</sub>:**6.1** complex is shown in **Figure 6.2** and corresponding crystallographic statistics are provided in **Table 6.3**.

#### 6.3.2.1 Structure determination of the BCL-X<sub>L</sub>:**6.1** complex

Relevance:

- Most potent analogue in series against BCL-X<sub>L</sub>.
- Understand improvement in affinity due to cyclohexyl substituent in p5 pocket.

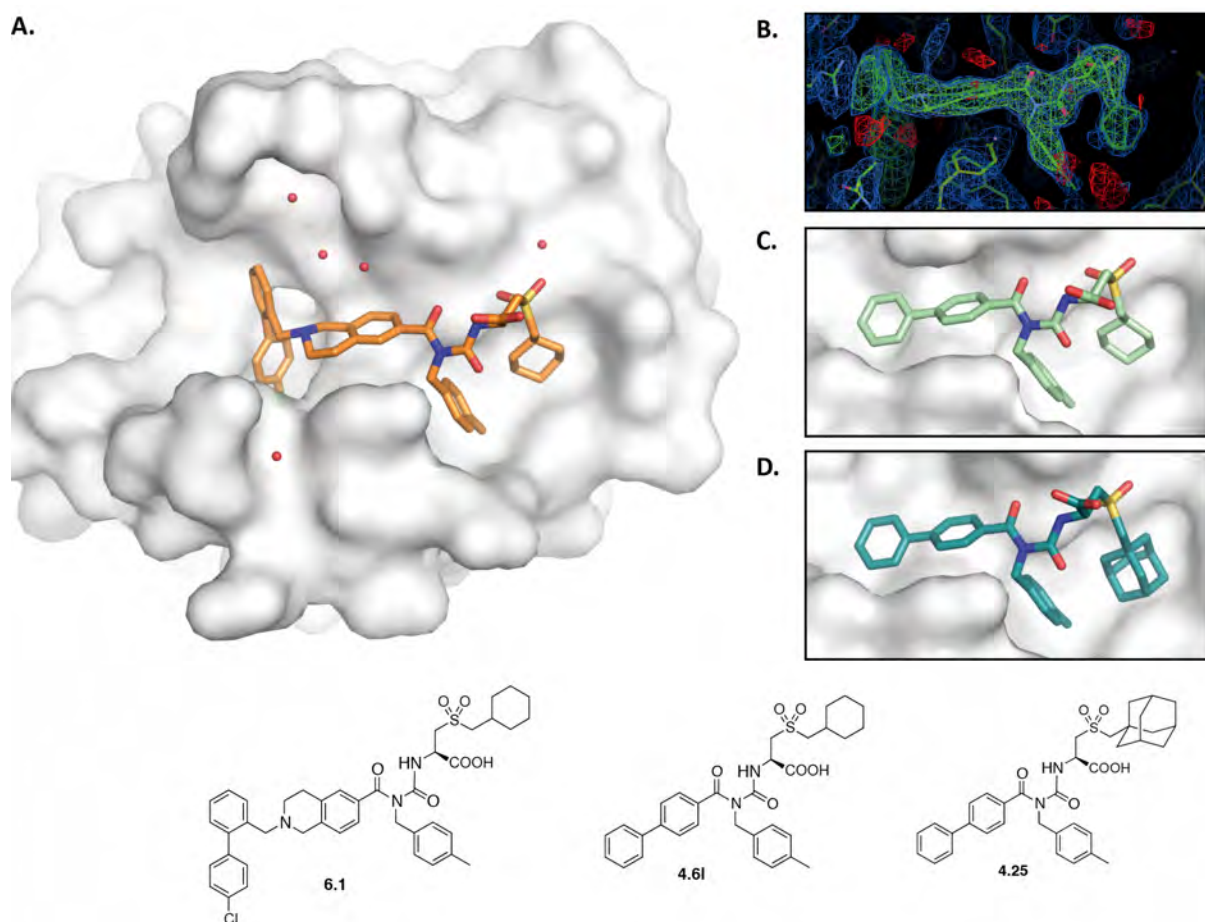
The structure of the BCL-X<sub>L</sub>:**6.1** complex shows that compound **6.1** binds along the groove of BCL-X<sub>L</sub> as intended by the design (**Figure 6.2A,B**), with the chlorobiphenyl moiety interacting with the p2 pocket, the tolyl moiety interacting with the p4 pocket and the cyclohexyl moiety occupying the p5 pocket of BCL-X<sub>L</sub>. This mirrored the binding mode of compound **3.1** described previously (refer **Chapter 3, Figure 3.3A**). In terms of chemical structure, compounds **3.1** and **6.1** differ only in the p5 substituent – for compound **3.1**, it is a phenyl ring, whilst for compound **6.1**, it is a cyclohexyl ring – but this single modification led to a > 5-fold improvement in binding to BCL-X<sub>L</sub> (IC<sub>50</sub>(BCL-X<sub>L</sub>) = 0.17 μM and 0.044 μM for compounds **3.1** and **6.1** respectively, **Table 6.2**).

The crystal structures of the BCL-X<sub>L</sub>:**3.1** and BCL-X<sub>L</sub>:**6.1** complexes show that the respective phenyl and cyclohexyl substituents occupy generally similar positions in the p5 pocket, aside from the additional ‘kink’ present in the non-planar cyclohexyl ring (modeled in the lower energy chair conformation). Hence a possible explanation for the improvement in binding affinity is the additional conformational flexibility of the cyclohexyl ring to improve shape complementarity

for the binding site. For example, if the lowest-energy bound conformation of compound **3.1** generates some partially strained bond distances/angles somewhere in the molecule, the more flexible cyclohexyl ring of compound **6.1** may better dissipate this strain than the planar phenyl ring of compound **3.1**. Alternatively, the cyclohexyl group of compound **6.1** may be better able to undergo subtle conformational changes so as to pack more closely against the p4 tolyl substituent and the protein wall within the p5 pocket.

Comparison of the BCL-X<sub>L</sub>:**6.1** complex (**Figure 6.2A**) with that of the BCL-X<sub>L</sub>:**4.6I** complex described in **Chapter 4** (simple biphenyl scaffold compound incorporating a p5 cyclohexyl substituent, **Figure 6.2C**) shows that the conformation of the cyclohexyl moiety is similar for both scaffolds. Similarly the BCL-X<sub>L</sub>:**4.25** complex, also described in **Chapter 4** (simple biphenyl scaffold compound incorporating a p5 adamantyl substituent, **Figure 6.2C**), adopts a similar binding mode and thus likely provides a good indication as to the likely bound conformation of compound **6.2** with BCL-X<sub>L</sub> (no X-ray crystal structure of this complex has been determined).

Based on the promising binding data obtained for compounds **6.1-6.3** for BCL-X<sub>L</sub>, we next sought to confirm these results and also determine the selectivity of these compounds for different prosurvival BCL-2 family proteins using a series of competitive binding assays based on surface plasmon resonance (SPR) (Biacore 3000 instrument).



**Figure 6.2: X-ray crystal structure of the BCL-X<sub>L</sub>:6.1 complex.**

(A) BCL-X<sub>L</sub>:**6.1** complex with the protein depicted in surface representation and (B) simulated annealing omit map showing ligand electron density, with  $2F_o - F_c$  contoured at  $1\sigma$  (blue) and  $F_o - F_c$  contoured at  $\pm 3\sigma$  (green/red). (C-D) For comparison, the complexes described in **Chapter 4** of BCL-X<sub>L</sub>:**4.6I** and BCL-X<sub>L</sub>:**4.25** respectively, showing similar binding mode of cyclohexyl and adamantyl moieties in p5 pocket on the simple biphenyl scaffold.

**Table 6.3: Crystallographic statistics for the BCL-X<sub>L</sub>:6.1 complex.**

<b>Structure <sup>ψ</sup></b>	<b>BCL-X<sub>L</sub>:6.1</b>
Wavelength (Å)	0.9537
Resolution range (Å)	38.12 - 2.19 (2.269 - 2.19)
Space group	<i>C</i> 2
Unit cell	
<i>a</i> , <i>b</i> , <i>c</i> (Å)	152.03, 65.93, 77.13
$\alpha$ , $\beta$ , $\gamma$ (°)	90, 98.71, 90
Total reflections	143861 (12625)
Unique reflections	38183 (3455)
Multiplicity	3.8 (3.7)
Completeness (%)	0.98 (0.90)
Mean <i>I</i> / $\sigma I$	11.66 (1.58)
Wilson <i>B</i> factor (Å <sup>2</sup> )	44.12
<i>R</i> <sub>merge</sub>	0.0738 (0.8848)
<i>R</i> <sub>meas</sub>	0.08605 (1.034)
CC <sub>1/2</sub>	0.998 (0.631)
CC*	1 (0.88)
Reflections used in refinement	38175 (3455)
Reflections used for R-free	1908 (172)
<i>R</i> <sub>work</sub>	0.2291 (0.3384)
<i>R</i> <sub>free</sub>	0.2773 (0.4069)
CC <sub>work</sub>	0.950 (0.728)
CC <sub>free</sub>	0.930 (0.572)
Number of non-hydrogen atoms	4748
macromolecules	4465
ligands/ions	216
RMS(bond lengths) (Å)	0.009
RMS(bond angles) (°)	1.17
Ramachandran favored (%)	92
Ramachandran allowed (%)	5.9
Ramachandran outliers (%)	1.7
Rotamer outliers (%)	5.6
Clashscore	7.3
Average <i>B</i> factors (Å <sup>2</sup> )	40.7
Macromolecules	40.32
ligands	50.46
solvent	34.29

<sup>ψ</sup> Statistics are outlined in Section 2.6.2.5.

### 6.3.3 Evaluation of selectivity – SPR competition assay (Biacore 3000)

To determine the relative binding for different prosurvival proteins, a subset of compounds from the benzoylurea series were next subjected to a SPR competition assay. This assay measures the ability of the compounds to displace BIM peptide from recombinant BCL-X<sub>L</sub>, BCL-W, BCL-2, MCL-1 and A1. Refer to **Chapter 2** for details on recombinant protein production and assay conditions. Compounds **1.8**, **4.6l**, **4.25**, **1.10**, **3.1**, **6.1**, **6.2** were selected as an initial sample set (**Table 6.4**).

In the assay, each test compound (as a titration series from 12.5  $\mu$ M to 0.0001  $\mu$ M) was pre-incubated with a prosurvival protein (either BCL-X<sub>L</sub>, BCL-W, BCL-2, MCL-1 or A1) and flowed over the SPR chip onto which a BIM BH3 peptide and an inactive BIM-4E peptide (negative referencing control) had been captured in different flow cells. The BIM-4E peptide is the same as the BIM BH3 peptide, but has the four conserved BH3 hydrophobic residues in the BH3 domain replaced with glutamate residues to abolish prosurvival protein binding. BH3/groove-specific binding response was calculated by subtracting the BIM-4E reference from the BIM channel (average of duplicates per experiment), followed by solvent correction as described in further detail in **Chapter 2**. Percent maximal binding response values were used to generate dose-response curves, from which IC<sub>50</sub> values were then calculated by nonlinear curve fitting of the data (average of 3 independent experiments).

Average SPR-derived IC<sub>50</sub> values for each compound and prosurvival protein are summarised in **Table 6.4** and **Figure 6.3**. Also shown in **Table 6.4** are the previously described AlphaScreen-derived IC<sub>50</sub> values for BCL-X<sub>L</sub> and MCL-1 for comparison. Note that due to access issues with the Biacore 3000 instrument, the final set of BCL-2 data for compounds **1.10**, **3.1**, **6.1** and **6.2** has not yet been determined (this work is ongoing).

As a general trend, for all compounds the SPR-derived IC<sub>50</sub> values for BCL-X<sub>L</sub> correlated closely with the IC<sub>50</sub> values previously determined by AlphaScreen Assay (**Table 6.4**). In particular, by SPR compounds **6.1** and **6.2** were again found

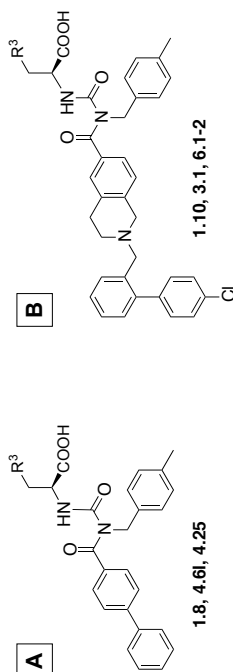
to be the most potent compounds in the series against BCL-X<sub>L</sub>, binding with SPR-derived IC<sub>50</sub> values of 36 nM and 68 nM respectively; these values compared favourably with the AlphaScreen-derived IC<sub>50</sub> values of 41 nM and 44 nM (**Table 6.4**). By SPR, all compounds had no measurable binding to MCL-1 over the concentration range tested (**Table 6.4**). This contrasted with the previous AlphaScreen data, in which these compounds showed modest but measurable binding to MCL-1 (IC<sub>50</sub> values in the range 1.8-11.6  $\mu$ M, **Table 6.4**). This discrepancy may be at least partly due to differences in the treatment of non-specific binding between the two assays. In the SPR assay, measured binding is referenced against the inactive BIM-4E peptide (such that only BH3/groove-specific binding response is calculated in the IC<sub>50</sub>), whereas referencing of this nature is not performed in the AlphaScreen Assay. Thus nonspecific binding effects of the compounds on the measured IC<sub>50</sub> value may be more pronounced in the AlphaScreen assay.

In terms of selectivity, all compounds tested by SPR showed either relatively weak or no measurable binding to MCL-1, BCL-W, and A1 (in all cases IC<sub>50</sub> values were > 4.5  $\mu$ M or unable to be measured over the concentration range tested, **Table 6.4**). Whilst BCL-2 binding is yet to be determined for compounds **1.10**, **3.1**, **6.1** and **6.2**, compounds **1.8** and **4.61** had no measurable binding to BCL-2 and compound **4.25** bound only weakly (BCL-2 IC<sub>50</sub> = 9.4  $\mu$ M, **Table 6.4**). Thus, as the affinity of the series for BCL-X<sub>L</sub> increased, the fold selectivity for BCL-X<sub>L</sub> relative to MCL-1, BCL-W, and A1 was maintained or improved (**Figure 6.3**, **Table 6.4**). In particular, the most potent compounds in the series for BCL-X<sub>L</sub>, compounds **6.1** and **6.2**, both have > 180-fold selectivity for BCL-X<sub>L</sub> relative to either MCL-1 or BCL-W and have > 125-fold and > 85-fold selectivity respectively for BCL-X<sub>L</sub> relative to A1 (BCL-2 data are yet to be determined).

Based on the promising BCL-X<sub>L</sub> binding and selectivity of compounds **6.1** and **6.2**, we next wished to evaluate whether they had measurable activity in *in-vitro* cell-based assays (cytochrome *c* release assay and cell-killing assays using cells sensitive to BCL-X<sub>L</sub> inhibition).



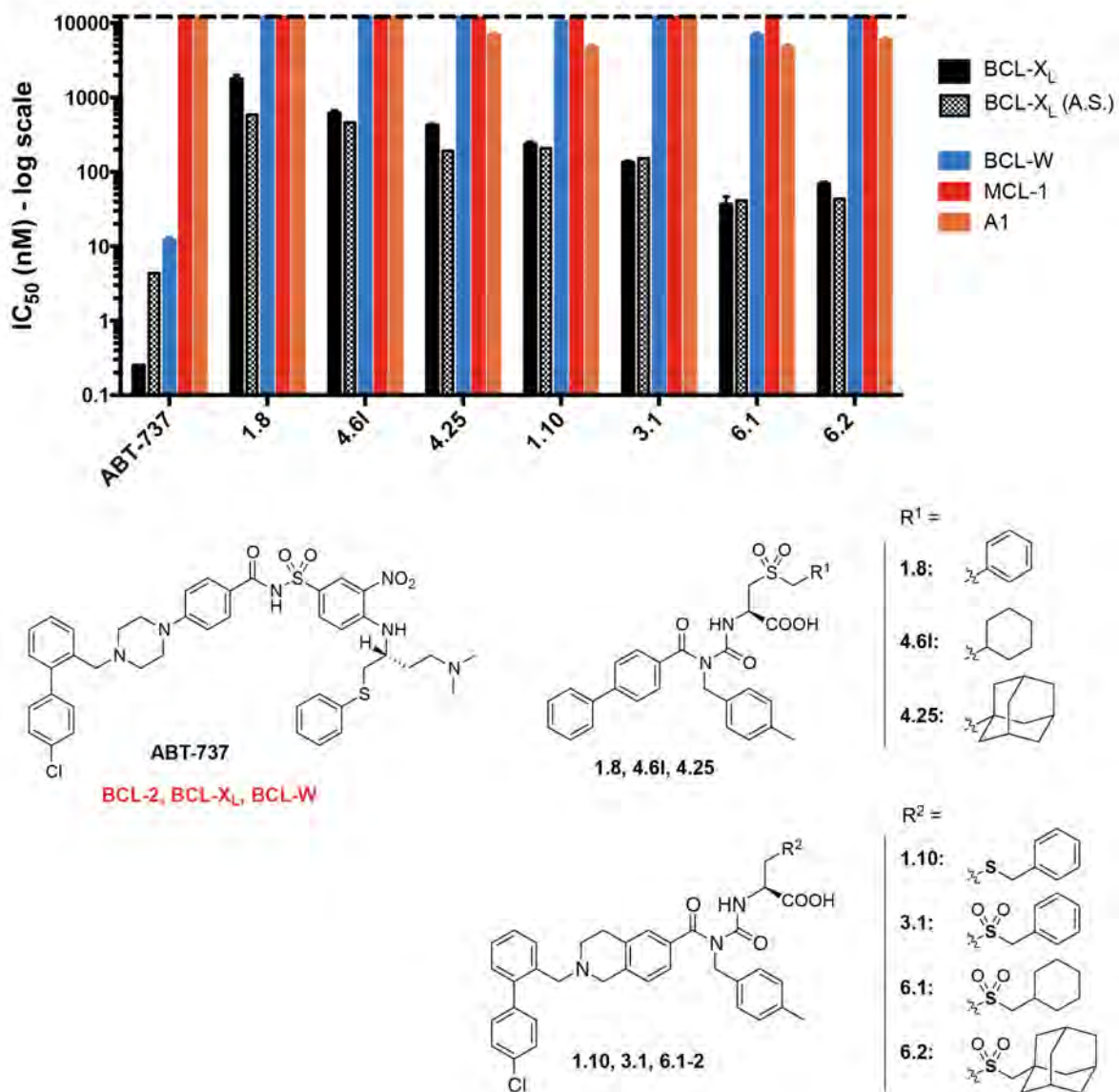
Table 6.4: Selectivity data for selected lead compounds tested against BCL-X<sub>L</sub>, BCL-2, MCL-1 and A1, determined by SPR competition assay (Biacore 3000).



Compound		IC <sub>50</sub> A.S. <sup>[a]</sup> (post-2015 data)		IC <sub>50</sub> SPR (Competition) <sup>[a]</sup>				
R <sup>3</sup> =		BCL-X <sub>L</sub>	MCL-1	BCL-X <sub>L</sub>	BCL-W	BCL-2	MCL-1	A1
<b>A</b>	<b>1.8</b>	0.59 ±0.07	11.6 ±0.6	1.8 ±0.2	>12.5 -	>12.5 -	>12.5 -	>12.5 -
	<b>4.6I</b>	0.46 ±0.25	10.0 ±1.4	0.61 ±0.06	>12.5 -	>12.5 -	>12.5 -	>12.5 -
	<b>4.25</b>	0.19 ±0.05	6.1 ±0.5	0.42 ±0.02	>12.5 -	9.4 ±0.7	>12.5 -	6.8 ±0.5
<b>B</b>	<b>1.10</b>	0.21 ±0.05	2.0 ±0.1	0.24 ±0.02	10.4 ±1.1	ND	>12.5 -	4.6 ±0.5
	<b>3.1</b>	0.17 ±0.04	5.3 ±0.3	0.13 ±0.01	>12.5 -	ND	>12.5 -	>12.5 -
	<b>6.1</b>	0.041 ±0.017	1.8 ±0.1	0.036 ±0.01	6.8 ±0.3	ND	>12.5 -	4.6 ±0.5
	<b>6.2</b>	0.044 ±0.012	1.8 ±0.7	0.068 ±0.01	>12.5 -	ND	>12.5 -	5.9 ±0.4
<b>ABT-737</b>		0.008 <sup>^</sup> ±0.002	44 <sup>^</sup> ±34	0.0003 ±0.0001	0.012 ±0.001	ND	>12.5 -	>12.5 -

<sup>[a]</sup> Unless otherwise indicated, all IC<sub>50</sub> values are reported in  $\mu\text{M}$  ( $\pm\text{S.E.M.}$ ), N = 3.

<sup>^</sup> For **ABT-737** IC<sub>50</sub> A.S. data are ( $\pm\text{S.D.}$ ), N = 2



**Figure 6.3: Plot of selectivity data (from Table 6.4) for selected lead compounds tested against BCL-X<sub>L</sub>, BCL-W, MCL-1 and A1, determined by SPR competition assay (Biacore 3000).**

Plotted are mean IC<sub>50</sub> values (± S.E.M., N = 3) for each compound against BCL-X<sub>L</sub> (solid black bars), BCL-W (blue bars), MCL-1 (red bars) and A1 (orange bars) determined by SPR. For comparison, IC<sub>50</sub> values (± S.E.M., N = 3) determined by AlphaScreen (A.S.) (post-2015 data) against BCL-X<sub>L</sub> are also shown (hashed black bars).

## 6.4 Further biochemical validation – preliminary selectivity/mechanism of action and cell-viability studies

Based on their promising IC<sub>50</sub> values for BCL-X<sub>L</sub>, we next wished to evaluate whether compounds **6.1** and **6.2** were sufficiently potent to induce cytochrome *c* release from cells sensitive to BCL-X<sub>L</sub> inhibition. To do this, we conducted a cytochrome *c* release assay for a panel of compounds using *MCL-1*<sup>-/-</sup> mouse embryonic fibroblast cells (MEFs).

This assay measures the ability of compounds to induce the release of cytochrome *c* from the intact mitochondria of digitonin-permeabilised cells (refer to **Chapter 2, Section 2.1.3**). As described earlier, wild-type MEFs will undergo BAK-mediated apoptosis (*via* the mitochondrial pathway) if both MCL-1 and BCL-X<sub>L</sub> are first neutralised. MEFs lacking MCL-1 are thus dependent solely on BCL-X<sub>L</sub> for survival. In the assay, parallel controls were also run using wild-type MEFs and *BAX*<sup>-/-</sup>/*BAK*<sup>-/-</sup> MEFs to ensure respectively that any observed activity was dependent on BCL-X<sub>L</sub> alone and also required BAX/BAK (i.e. was on-pathway; refer to discussion of ‘mechanism-based activity’ in **Chapter 1, Section 1.4.3**). In addition to compounds **6.1** and **6.2**, **ABT-737** was included as a positive control and in one of the experiments additional compounds from the same series that had weaker binding to BCL-X<sub>L</sub> were also included for reference (compounds **1.5**, **4.6I** and **4.25**, **Figure 6.4A,B**).

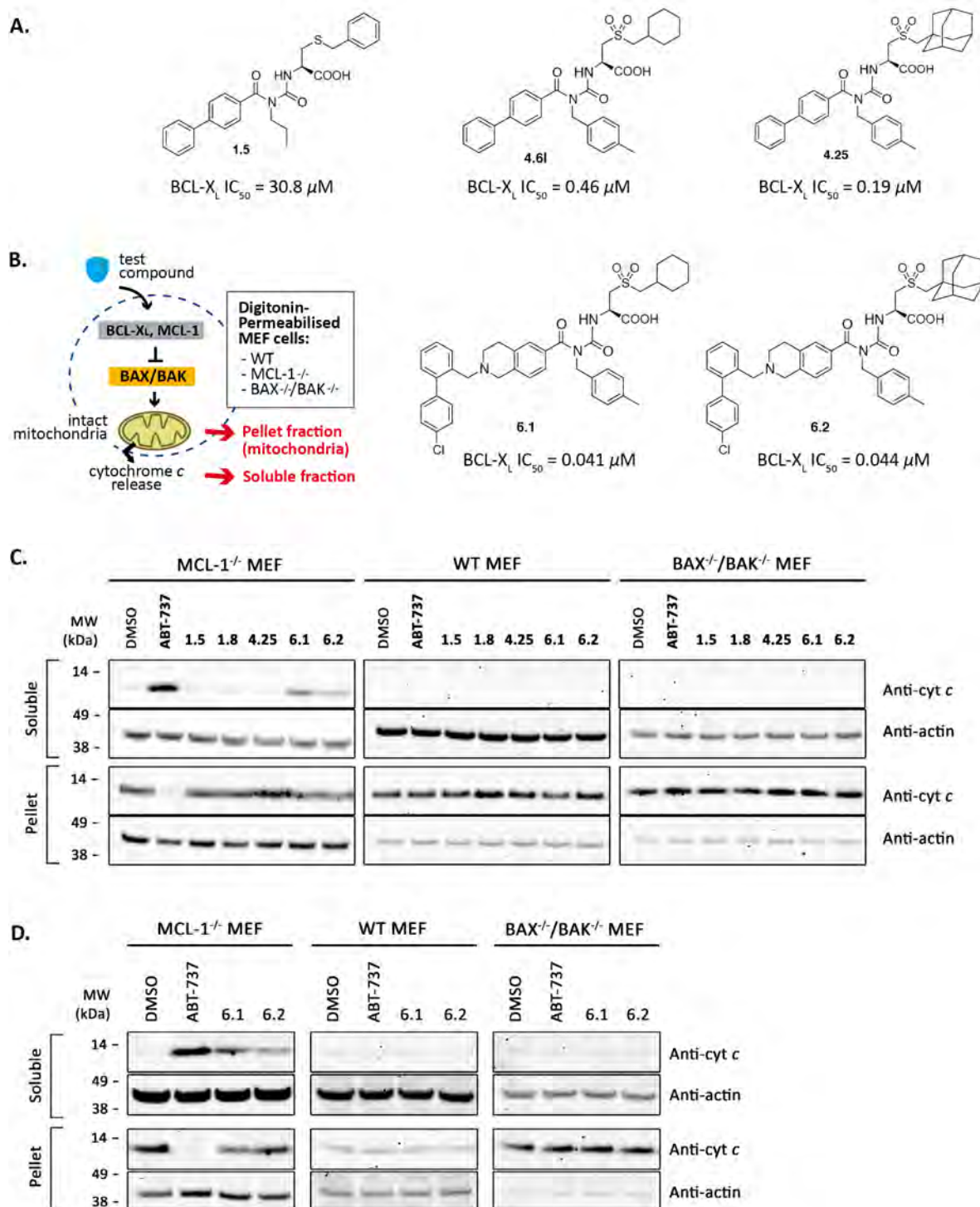
### 6.4.1 Evaluation of compounds **6.1** and **6.2** in the *in-vitro* cytochrome *c* release assay

The test compounds were evaluated in the cytochrome *c* assay by incubating for 1 h at 37°C with intact mitochondria from digitonin-permeabilised wild-type (WT), *MCL-1*<sup>-/-</sup> or *BAX*<sup>-/-</sup>/*BAK*<sup>-/-</sup> MEFs at a final concentration of 10 μM of drug. After this time, the Soluble and the Pellet (mitochondrial) fractions were isolated, analysed by SDS-PAGE and probed by Western-blot for the presence of cytochrome *c* (actin was used as a loading control) (**Figure 6.4B**). The preliminary

results of two independent experiments are shown in **Figure 6.4C-D**; further repeats will be required to confirm these results.

As shown in **Figure 6.4C-D**, as expected **ABT-737** was able to induce complete cytochrome *c* release from *MCL-1*<sup>-/-</sup> MEFs, but not from WT MEFs (which have MCL-1 present that restrains the proapoptotic activity of BAX/BAK) or *BAX*<sup>-/-</sup>/*BAK*<sup>-/-</sup> MEFs. In comparison, compounds **6.1** and **6.2** induced a partial release of cytochrome *c* in *MCL-1*<sup>-/-</sup> MEFs, but showed no release in either WT or *BAX*<sup>-/-</sup>/*BAK*<sup>-/-</sup> MEFs, suggesting that the activity is both BCL-X<sub>L</sub>- and BAX/BAK-dependent. That only a partial release was observed is consistent with the weaker IC<sub>50</sub> of compounds **6.1** and **6.2** for BCL-X<sub>L</sub> relative to **ABT-737** (refer **Table 6.4**); it appears these compounds are on the cusp of the necessary threshold to show activity in these assays. The level of cytochrome *c* release observed in both experiments appeared to be slightly higher for compound **6.1** as compared to compound **6.2**, which may reflect the slightly tighter binding of **6.1** to BCL-X<sub>L</sub> relative to **6.2** based on their SPR-derived IC<sub>50</sub> values (refer **Table 6.4**). In comparison, compounds **1.5**, **4.61** and **4.25** did not induce cytochrome *c* release in *MCL-1*<sup>-/-</sup> MEFs, consistent with their weaker binding to BCL-X<sub>L</sub> relative to compound **6.1** or **6.2** (**Figure 6.4**).

Next we conducted some preliminary cell killing assays to evaluate the activity of compounds **6.1** and **6.2** in cells reliant on BCL-X<sub>L</sub> for survival (platelets and *MCL-1*<sup>-/-</sup> MEFs).



**Figure 6.4: Preliminary results suggesting compounds 6.1 and 6.2 are able to induce a partial release of cytochrome *c* from isolated mitochondria from MCL-1<sup>-/-</sup> MEFs (which contain only BCL-X<sub>L</sub> to restrain BAK/BAX).**

(A) Chemical structures and corresponding AlphaScreen BCL-X<sub>L</sub> IC<sub>50</sub> values (post-2015 data) for compounds tested in cytochrome *c* Release Assay (B) Schematic of cytochrome *c* Release Assay. (C-D) Test compounds were

incubated at 10  $\mu$ M for 1 h at 37°C with isolated mitochondria from digitonin-permeabilised MEFs (*MCL-1*<sup>-/-</sup>, WT, or *BAX*<sup>-/-</sup>/*BAK*<sup>-/-</sup>) then fractionated and the fractionated extracts separated *via* SDS-PAGE and analysed by western blot, probing for cytochrome *c* and actin as a loading control (ECL imaging). Results from two independent cytochrome *c* release assay experiments are shown.

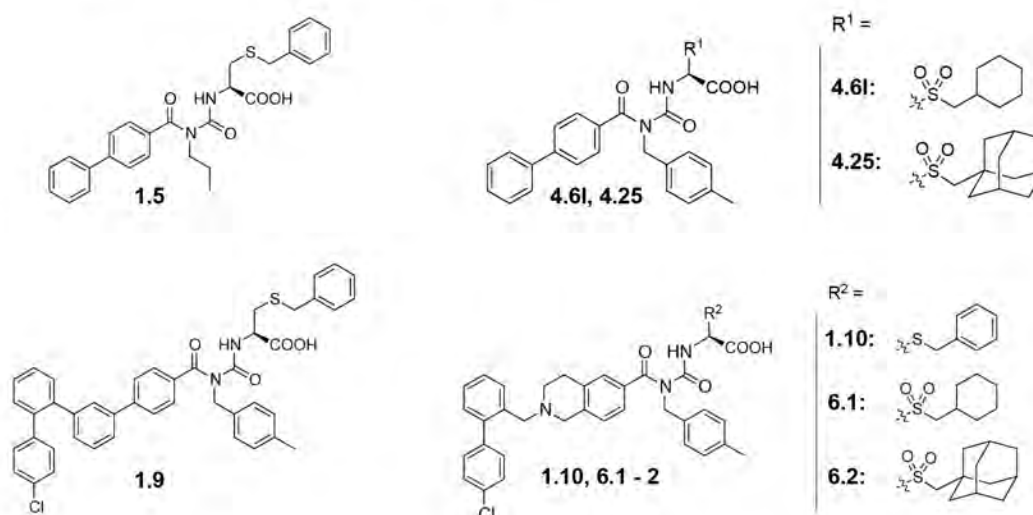
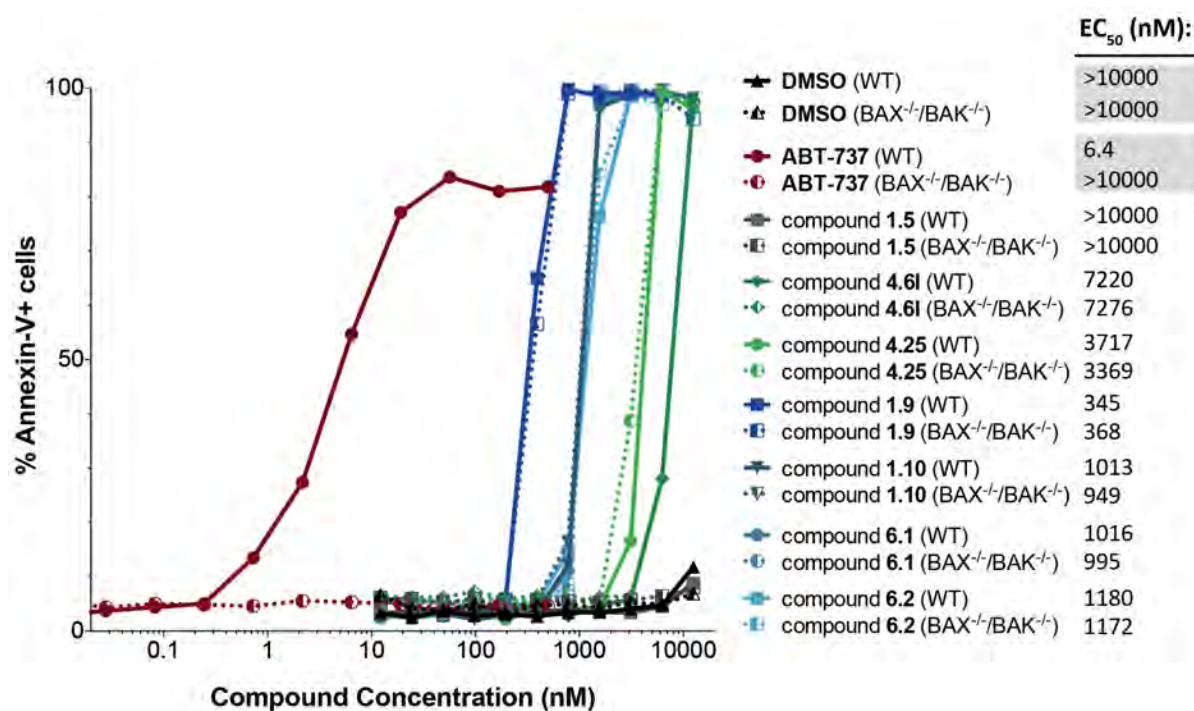
#### 6.4.2 Platelet-killing assay

Given the potent binding and relative selectivity of compounds **6.1** and **6.2** for BCL-X<sub>L</sub> in binding assays and their promising activity in initial cytochrome *c* release assays, we next wished to evaluate their activity in cells that require on BCL-X<sub>L</sub> for survival. As an initial study we decided to utilise washed murine platelets. As described in **Chapter 1**, platelets (in both mice and humans) possess a functional intrinsic apoptotic pathway and have been shown to be reliant on BCL-X<sub>L</sub> for their continued survival<sup>(5, 6)</sup>. Potent pharmacological inhibition of BCL-X<sub>L</sub> *in vivo* leads to a rapid clearance of platelets (resulting in thrombocytopenia)<sup>(7-9)</sup>. Platelets therefore constitute a good marker for on-target activity of BCL-X<sub>L</sub> inhibitors.

A panel of compounds - including **6.1** and **6.2**, earlier reference compounds from the benzoylurea series (compounds **1.5**, **4.6l**, **4.25**, **1.9** and **1.10**) and **ABT-737** as a positive control - were prepared as a titration series and incubated at 37°C for 1 h with washed platelets derived from C57 Bl/6 mice that were either wild-type (WT) or were foetal liver-derived chimeras engineered to have a hematopoietic system deficient in both BAX and BAK (*BAX*<sup>-/-</sup>/*BAK*<sup>-/-</sup>). Following incubation, the platelets were stained for CD41 (platelet maker) and Annexin-V (marker of phosphatidylserine (PS) exposure, to indicate cells undergoing apoptosis) and analysed by Flow Cytometry. The resulting dose-response curve and calculated EC<sub>50</sub> values are shown in **Figure 6.5** (single experiment).

Unfortunately, whilst the panel of compounds showed some killing activity in this assay, none of this activity appeared to be on-target - for a given compound the observed dose-response curve was essentially identical for both WT and *BAX*<sup>-/-</sup>/*BAK*<sup>-/-</sup> platelets, as were the resulting calculated EC<sub>50</sub> values (**Figure 6.5**). Analysis of FSC/SSC by flow Cytometry as a simple metric of platelet morphology did not appear to indicate PS exposure was due to platelet activation in response to drug. **ABT-737** in contrast showed potent induction of apoptosis in wild-type platelets (EC<sub>50</sub> = 6.4 nM), but showed no killing in platelets deficient in both BAX and BAK, indicating that for **ABT-737** the killing activity is mediated *via* the intrinsic apoptosis pathway. No killing was observed in the negative control containing DMSO only without drug. In general terms the off-target toxicity observed in the platelet assay with the benzoylurea compounds appears to correlate with the overall lipophilicity of the molecules, although this observation bears the important caveats that this data was from a single experiment only and that activity on isolated washed platelets is a relatively artificial measure of general cellular toxicity. It is possible that this non-specific toxicity masked any weak BCL-X<sub>L</sub>-specific activity; however the lack of on-target activity in this assay highlights that compounds that target BCL-X<sub>L</sub> with enhanced affinity and binding efficiency are likely required. To investigate the cellular activity further in another cell-type dependent on BCL-X<sub>L</sub>, we next undertook some preliminary cell viability assays using *MCL-1*<sup>-/-</sup> MEFs.





**Figure 6.5: Results from platelet killing assay using washed wild-type (WT) and BAX/BAK-deficient (BAX<sup>-/-</sup>/BAK<sup>-/-</sup>) platelets.**

Washed platelets were incubated with varying concentrations of test compounds, stained for CD41 and Annexin-V and analysed by Flow Cytometry. Platelets were identified by forward- and side-scatter and positivity for CD41. The percentage of Annexin-V positive platelets as a function of compound concentration was plotted using Prism (GraphPad) and EC<sub>50</sub> values were determined by curve-fitting using non-linear regression. Data is for a single experiment.



### 6.4.3 MEF viability assay

Compounds **6.1** and **6.2** (as well as **ABT-737** and compound **1.5** respectively as positive and negative controls) were next evaluated in a cell viability assay using either *MCL-1*<sup>-/-</sup> or wild-type MEFs. Cells were cultured for 24 h with a titration series of each compound in FMA medium supplemented with either 1% or 10% foetal calf serum (FCS). Cells were then harvested, stained using propidium iodide (PI) and analysed by Flow Cytometry. Viability plots showing the average percentage of live cells (PI negative, duplicate wells normalized to the DMSO-only control) for each titration series are shown in **Figure 6.6** and were used to determine corresponding EC<sub>50</sub> values.

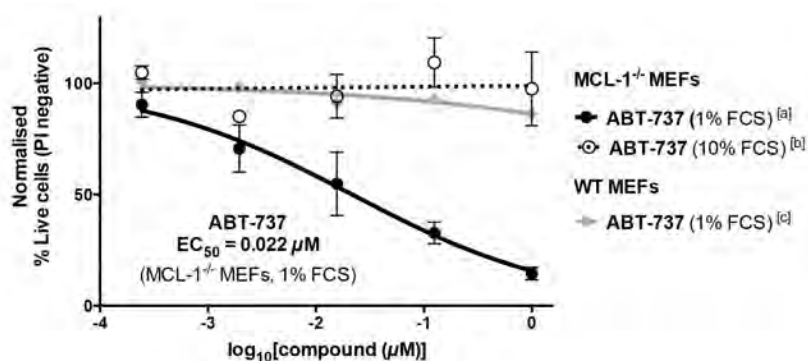
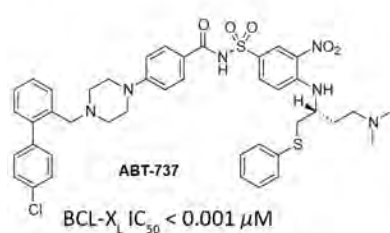
As shown in **Figure 6.6**, compounds **6.1** and **6.2** appeared able to induce killing of *MCL-1*<sup>-/-</sup> MEFs (cultured in 1% FCS) in a dose response manner, but required relatively high concentrations of compound to do so (EC<sub>50</sub> = 19.6 and 24.0  $\mu$ M respectively, **Figure 6.6C,D**), leading to a very narrow window of apparent BCL-X<sub>L</sub>-specific activity. The highest test concentration of either compound (50  $\mu$ M) also induced significant toxicity in WT MEFs (cultured in 1% FCS), presumably *via* a nonspecific mechanism. However, at the second-highest test concentration of **6.1** or **6.2** (20  $\mu$ M), little nonspecific drug-induced killing of WT MEFs was observed, whereas the viability of *MCL-1*<sup>-/-</sup> MEFs was reduced by approximately 50% (each in the presence of 1% FCS)(**Figure 6.6C,D**). However, as the effects on WT MEFs are the result of a single experiment only, further repeats would be required to confirm this apparent window of activity. In the presence of 10% FCS, the activity of either compound **6.1** or **6.2** on *MCL-1*<sup>-/-</sup> MEFs was essentially abolished over the full concentration-range tested (**Figure 6.6C,D**). This suggests that a significant level of binding to serum proteins such as bovine serum albumin (BSA) may be occurring (discussed further in **Chapter 7**).

As expected, treatment of *MCL-1*<sup>-/-</sup> MEFs with **ABT-737** in medium containing 1% FCS induced potent killing in a dose response manner (EC<sub>50</sub> = 22 nM), whilst WT MEFs under the same conditions were substantially more resistant (**Figure 6.6A**). The activity of **ABT-737** on *MCL-1*<sup>-/-</sup> MEFs was also significantly

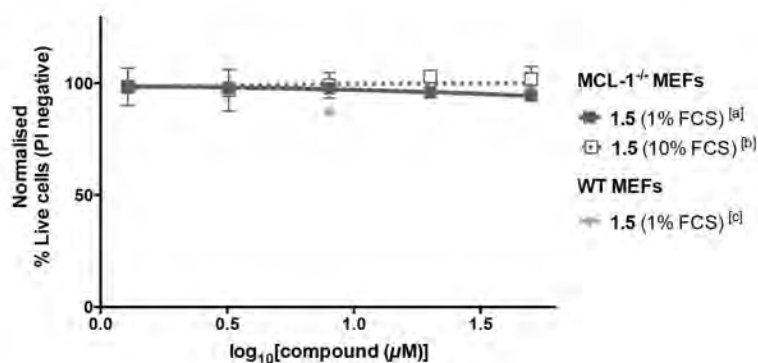
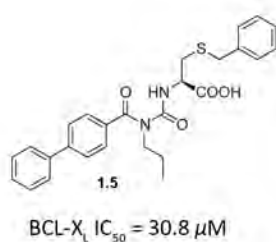
reduced in the presence of 10% FCS. Compound **1.5**, which binds very weakly to BCL-X<sub>L</sub> ( $IC_{50}(BCL-X_L) = 30.8 \mu M$ ) and represented a negative control compound from the series, showed no significant killing activity using either *MCL-1*<sup>-/-</sup> or WT MEFs (in the presence of 1% FCS) over the full concentration range tested (1.3 - 50  $\mu M$ )(**Figure 6.6B**).

These preliminary cellular viability studies using compounds **6.1** and **6.2** indicate that at best the *in vitro* cellular activity of these compounds on *MCL-1*<sup>-/-</sup> MEFs is significantly weaker (> 500-fold) than their measured  $IC_{50}$  values for BCL-X<sub>L</sub> ( $IC_{50}(BCL-X_L) \sim 0.040 \mu M$ ) - although this may be influenced by a lowered effective concentration due to binding to serum proteins, even in the presence of only 1% FCS. Further optimisation of the series to increase affinity for BCL-X<sub>L</sub> (or perhaps to decrease serum protein binding) will be necessary in order for clear on-target cellular activity to be demonstrated.

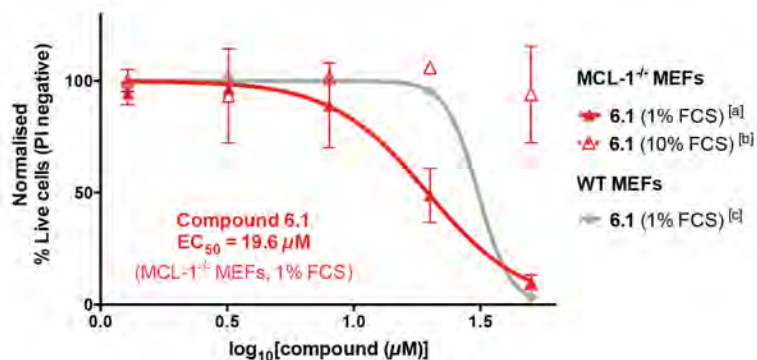
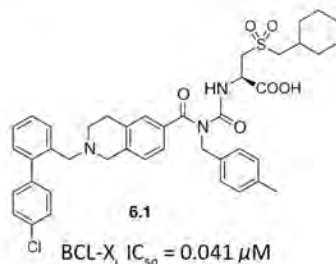
A.



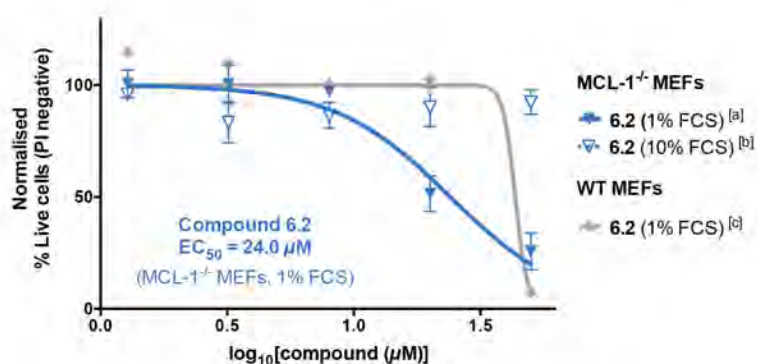
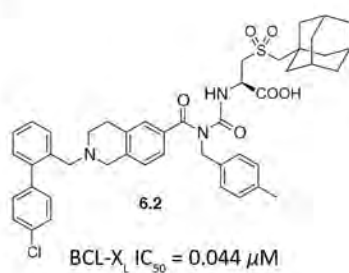
B.



C.



D.



<sup>[a]</sup> N=3, <sup>[b]</sup> N=2, <sup>[c]</sup> N=1; error bars shown are ± S.D. (for N>1)

**Figure 6.6: Results from cell viability assay using cultured *MCL-1*<sup>-/-</sup> and wild-type (WT) MEFs for (A) ABT-737 (B) compound 1.5 (C) compound 6.1 and (D) compound 6.2. (previous page)**

*MCL-1*<sup>-/-</sup> and WT MEF cells (seeded at equal concentrations into 24-well cell-culture plates) were incubated for 24 h in FMA medium supplemented with either 1% or 10% foetal calf serum (FCS) and varying concentrations of compound (1.0 - 0.00024  $\mu$ M for **ABT-737**; 50.0 - 1.3  $\mu$ M for all other compounds; final DMSO concentration 0.4%). After this time, cells were harvested, stained with propidium iodide (PI) as a marker of cell viability and analysed by Flow Cytometry. For each independent experiment, the percentage of live cells (PI negative) was determined using FlowJo (Treestar) and calculated as an average of duplicate wells normalized to 100% based on the DMSO-only control. In general, the uncorrected percentage of live cells in the DMSO-only control after incubation for 24 h in FMA medium containing either 1% or 10% FCS was approximately 78%. Cell viability curves were plotted using Prism (GraphPad) and EC<sub>50</sub> values determined by curve-fitting using non-linear regression.

## 6.5 Discussion/Conclusion

This Chapter describes the synthesis of compounds **6.1** – **6.3**, which explore the combined effect of incorporating an ‘optimised’ p5 substituent (based on work described in **Chapters 4** and **5**) onto the extended THIQ benzoylurea scaffold represented by compounds **1.10** and **3.1** which incorporates an extension designed to interact with the p2 pocket of BCL-X<sub>L</sub>. Replacement of the terminal phenyl ring of compound **3.1** (which interacts with the p5 pocket of BCL-X<sub>L</sub>) with either a cyclohexyl (compound **6.1**) or adamantyl moiety (compound **6.2**) was found to increase BCL-X<sub>L</sub> binding by approximately 4-fold ( $IC_{50}(BCL-X_L) = 0.041\ \mu M$ ,  $0.044\ \mu M$ , and  $0.17\ \mu M$  for compounds **6.1**, **6.2** and **3.1** respectively, **Table 6.2**). Similarly, compound **6.3**, which incorporated an adamantyl p5 substituent on an amide linker (but was otherwise similar to **3.1**) was found to also bind to BCL-X<sub>L</sub> with an  $IC_{50}$  in the nanomolar range ( $IC_{50}(BCL-X_L) = 0.031\ \mu M$  for compound **6.3**, **Table 6.2**). A crystal structure of the BCL-X<sub>L</sub>:**6.1** complex was solved to 2.2 Å resolution and showed that compound **6.1** indeed binds along the canonical groove of BCL-X<sub>L</sub> (interacting with the p2, p4 and p5 pockets) in a pose identical to that of compound **3.1** apart from the modified p5 substituent. The gain in affinity may possibly be due to the improved ability of the flexible cyclohexyl substituent to undergo subtle conformational changes to fill the p5 pocket. Compounds **6.1** – **6.3** thus represented the most potent compounds for BCL-X<sub>L</sub> in the benzoylurea series to date.

A particular synthetic challenge encountered during the synthesis of compounds **6.2** and **6.3** was a debenzoylation side-reaction that occurred at the tertiary amine of the THIQ scaffold during the benzoylurea formation step, resulting in loss of the p2 chlorobiphenyl substituent from the final product. I have outlined a possible mechanism for this side-reaction (mediated by excess phosgene) and also two alternative strategies that I utilised to successfully access the desired final products – (i) by careful control of reaction equivalents and (ii) by re-installing the p2 chlorobiphenyl substituent *via* reductive amination. Using this second approach I was also able to find an improved route to access the THIQ scaffold that removed two synthetic steps.

I next conducted an SPR-based solution competition assay to evaluate the selectivity profile of compounds **6.1**, **6.2** and a panel of key molecules from the benzoylurea series towards other prosurvival proteins. Although the data for BCL-2 is still yet to be determined, this SPR assay confirmed the nanomolar binding of compounds **6.1**, **6.2** to BCL-X<sub>L</sub> (SPR-IC<sub>50</sub>(BCL-X<sub>L</sub>) = 0.036 and 0.068  $\mu$ M respectively, **Table 6.4**). In addition, compounds **6.1** and **6.2** were found to both have greater than 180-fold selectivity BCL-X<sub>L</sub> relative to MCL-1 or BCL-W, and greater than 125-fold and 85-fold selectivity respectively for BCL-X<sub>L</sub> relative to A1.

In preliminary studies evaluating compounds **6.1** and **6.2** in a cytochrome *c* release assay, both compounds induced a partial release of cytochrome *c* from *MCL-1*<sup>-/-</sup> MEFs (but not from WT or *BAX*<sup>-/-</sup>/*BAK*<sup>-/-</sup> MEFs), suggesting that this observed activity is likely occurring *via* BCL-X<sub>L</sub>-inhibition and in a BAX/BAK-dependent manner. Further experimental repeats will be necessary to confirm this result. Some initial cell viability assays were also conducted using cells expected to be sensitive to BCL-X<sub>L</sub> inhibition -platelets and *MCL-1*<sup>-/-</sup> MEFs. Whilst the killing observed in studies using washed platelets appeared to be essentially all non-specific (i.e. not BAX/BAK-dependent), studies using MEF cells cultured in the presence of either compound **6.1** or **6.2** suggested a small window of BCL-X<sub>L</sub>-specific activity. *MCL-1*<sup>-/-</sup> MEFs cultured in media containing 1% FCS showed dose-dependent killing in response to either compound **6.1** or **6.2** (the EC<sub>50</sub> for either compound was approximately 20  $\mu$ M, N = 3). In comparison, WT MEFs appeared to be insensitive to compounds **6.1** or **6.2** at a concentration of 20  $\mu$ M, but showed complete killing at a concentration of 50  $\mu$ M (N = 1). Further studies would be needed to confirm these results. As highlighted from these initial studies, however, increased affinity for BCL-X<sub>L</sub> will likely be necessary for the series to demonstrate clear on-target cellular activity. Future work may additionally be directed towards improving the overall physicochemical properties of the series including improving solubility and reducing binding to serum proteins, as was necessary in the **ABT-737** series (discussed further in **Chapter 7**).

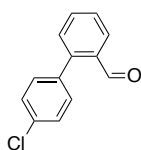
## 6.6 Experimental

### 6.6.1 Chemical synthesis

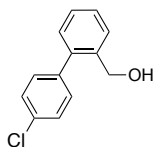
For **General Procedures A, B, G** refer to **Chapter 2, Section 2.2**.

For synthesis of compound **3.3**, refer to **Chapter 3, Section 3.5.1**.

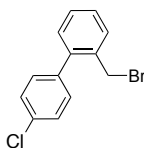
#### 6.6.1.1 Synthesis of extended scaffold compound **6.1** (**Scheme 6.1**):



**4'-chloro-[1,1'-biphenyl]-2-carbaldehyde (6.4):** 2-bromobenzaldehyde (740 mg, 4.0 mmol), 4-chloro-phenylboronic acid (751 mg, 4.8 mmol), tetra-n-butylammonium bromide (13 mg, 1 mol%) and  $K_2CO_3$  (1.658 g, 12.0 mmol) in 8 mL of a solution of acetone/water (1:1) were flushed with  $N_2$  and stirred at room temperature for 30 minutes.  $Pd(OAc)_2$  (45 mg, 5 mol%) was then added and the reaction allowed to stir for 30 minutes at 40°C. After this time, the reaction mixture was concentrated and filtered through celite, then water (20 mL) and diethyl ether (20 mL) were added and the two layers separated. The aqueous phase was extracted with diethyl ether (2 x 20 mL) and the combined organic phases were washed with water, brine, dried over  $MgSO_4$ , filtered and concentrated. Purification of the crude material *via* flash chromatography, eluting with a gradient of EtOAc/cyclohexane (0:100 to 5:95) afforded the title product as a yellow oil (703 mg, 81%). Analytical data obtained corresponded to those reported in the literature<sup>(10)</sup>.

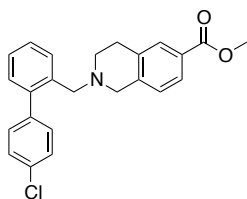


**4'-chloro-[1,1'-Biphenyl]-2-methanol (6.5):** To a mixture of compound **6.4** (835 mg, 3.9 mmol) in a solution of THF/EtOH (1:1) (7.7 mL) at room temperature was slowly added sodium borohydride (729 mg, 19 mmol). The mixture was stirred at room temperature for 30 minutes, then quenched through the addition of cold water. The reaction mixture was cooled on an ice/water bath and the pH slowly adjusted to 5-6 with HCl (5M). Diethyl ether was added to the solution and the phases separated. The aqueous layer was extracted twice with diethyl ether (2 x 30 mL). The combined organic phases were washed with brine and dried over  $MgSO_4$  and concentrated. Purification of the crude material *via* flash chromatography eluting with petroleum ether/EtOAc (100:0 to 20:80) affording the title compound as a fine white crystalline solid (713 mg, 84%). Spectral data obtained corresponded to those reported in the literature<sup>(11, 12)</sup>.



**2-(bromomethyl)-4'-chloro-1,1'-Biphenyl (6.6):** To a solution of compound **6.5** (594 mg, 2.7 mmol) in anhydrous dichloromethane (8 mL) at 0°C under  $N_2$  was added a solution of triphenylphosphine (855 mg, 3.3 mmol) in anhydrous dichloromethane (1 mL), followed by dropwise addition of a solution of carbon tetrabromide (1351 mg, 4.1 mmol) in anhydrous dichloromethane (1 mL). The reaction was allowed to warm to room temperature and proceed for 14 h, then the reaction mixture was concentrated in vacuo directly on to silica and purified *via* flash chromatography, eluting with petroleum ether/EtOAc (100:0 to 2:98) affording the title compound

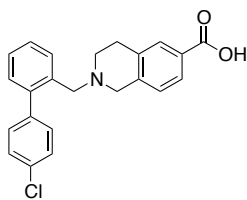
as a pale yellow oil, which formed an off-white crystalline solid on standing (703 mg, 92%). Spectral data obtained corresponded to those reported in the literature<sup>(11)</sup>.



**Methyl 2-((4'-chlorobiphenyl-2-yl)methyl)-1,2,3,4-tetrahydroisoquinoline-6-carboxylate (6.7):** To a stirred solution of methyl 1,2,3,4-tetrahydroisoquinoline-6-carboxylate hydrochloride (208 mg, 0.91 mmol) and N,N-Diisopropylethylamine (552  $\mu$ L, 3.2 mmol) in 1,4-dioxane (3.0 mL) at room temperature under a N<sub>2</sub> atmosphere, was added dropwise over 10 minutes a solution of compound **6.6** (285 mg, 1.3 mmol) in 1,4-dioxane (2.0 mL). The reaction was warmed to 40°C and stirred for 12 h at 40°C. After this time the reaction was concentrated and dried *in vacuo*, then purified directly *via* flash chromatography eluting with petroleum ether/EtOAc (98:2 to 90:10) to afford compound **6.7** as a colourless oil (282 mg, 79%). <sup>1</sup>H NMR (300 MHz, CDCl<sub>3</sub>):  $\delta$  7.80-7.76 (m, 2H), 7.65 (m, 1H), 7.43-7.38 (m, 6H), 7.29-7.26 (m, 1H), 7.03 (d,  $J$  = 7.8 Hz, 1H), 3.91 (s, 3H), 3.63 (br s, 4H), 2.92 (t,  $J$  = 5.6 Hz, 2H), 2.72 (t,  $J$  = 5.7 Hz, 2H).<sup>[a]</sup> <sup>13</sup>C NMR (75 MHz, CDCl<sub>3</sub>)  $\delta$  167.34, 141.67, 140.49, 139.93, 135.64, 134.89, 133.20, 131.04, 130.23, 130.16, 128.22, 128.14, 127.71, 127.28, 126.85, 126.76, 59.84, 55.88, 52.11, 50.31, 29.41.<sup>[a][b]</sup> MS (ES<sup>+</sup>),  $m/z$  392.1 (M + H). HRMS (ES<sup>+</sup> TOF) calculated for C<sub>24</sub>H<sub>22</sub>ClNO<sub>2</sub> (M + H): 392.1412; found 392.1428.

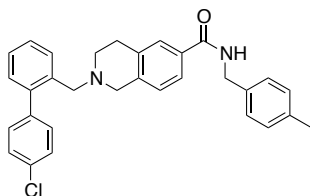
<sup>[a]</sup> The peaks at  $\delta$  1.43 ppm (<sup>1</sup>H NMR) and  $\delta$  27.07 ppm (<sup>13</sup>C NMR) are due to an impurity, most likely cyclohexane.

<sup>[b]</sup> One peak in the aromatic region is not observed due to overlap.



**2-((4'-chlorobiphenyl-2-yl)methyl)-1,2,3,4-tetrahydroisoquinoline-6-carboxylic acid (6.8):** LiOH.H<sub>2</sub>O (80 mg, 1.91 mmol) was added to a solution of compound **6.7** (188 mg, 0.48 mmol) in a mixture of methanol (0.60 mL), water (0.60 mL) and THF (1.8 mL). The reaction was stirred at room temperature for 16 hours. TLC (petroleum ether/EtOAc 90:10) indicated full conversion. The reaction mixture was concentrated in vacuo, water (10 mL) was added, then the reaction was acidified to pH ~1.0 with ~1.9 mL of 1M HCl. The resulting off-white precipitate was filtered, washed with a small volume of water and dried in a vacuum oven at 40°C overnight. This afforded compound **6.8** as the HCl salt as an off-white powdery solid (146 mg, 74%). <sup>1</sup>H NMR (600 MHz, MeOD)  $\delta$  7.83 (d,  $J$  = 8.1 Hz, 1H), 7.81 (s, 1H), 7.78-7.75 (m, 1H), 7.60-7.54 (m, 2H), 7.45 (dd,  $J$  = 8.3, 0.9 Hz, 2H), 7.43-7.40 (m, 1H), 7.35 (dd,  $J$  = 8.2, 0.8 Hz, 2H), 7.12 (d,  $J$  = 8.1 Hz, 1H), 4.46 (s, 2H), 4.16 (s, 2H), 3.36 (t,  $J$  = 5.6 Hz, 2H), 3.08 (t,  $J$  = 6.3 Hz, 2H). <sup>13</sup>C NMR (75 MHz, MeOD)  $\delta$  167.62, 142.80, 138.23, 133.80, 132.44, 131.11, 130.85, 130.79, 130.53, 129.74, 129.67, 128.61, 128.56, 127.71, 127.46, 126.82, 55.62, 52.40, 49.17, 24.58.<sup>[a]</sup> MS (ES<sup>+</sup>),  $m/z$  378.2 (M + H). HRMS (ES<sup>+</sup> TOF) calculated for C<sub>23</sub>H<sub>20</sub>ClNO<sub>2</sub> (M + H): 378.1255; found 378.1254.

<sup>[a]</sup> One peak in the aromatic region is not observed due to overlap.

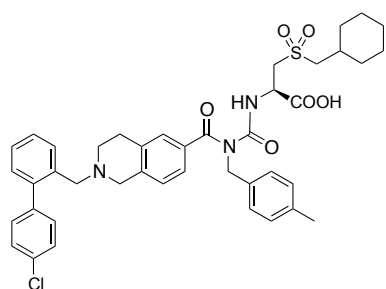


**2-((4'-chlorobiphenyl-2-yl)methyl)-N-(4-methylbenzyl)-1,2,3,4-tetrahydro-isoquinoline-6-carboxamide (6.9):** The procedure used to prepare compound **3.3** was followed using compound **6.8** (99 mg, 0.26 mmol), DIPEA (183  $\mu$ L, 1.05 mmol) and 4-methylbenzylamine (67  $\mu$ L, 0.52 mmol). The reaction mixture was poured onto ice-water whereupon an orange solid precipitated.



This compound was taken up in EtOAc and the two phases separated. The aqueous phase was further extracted twice with EtOAc, then the pooled organic phases were washed with brine, dried over  $\text{MgSO}_4$  and concentrated. The resulting crude brown oil was purified *via* flash chromatography eluting with petroleum ether/EtOAc (100:0 to 0:100) affording compound **6.9** as a white solid (105 mg, 83%).  $^1\text{H}$  NMR (300 MHz,  $\text{CDCl}_3$ )  $\delta$  7.53-7.45 (m, 1H), 7.43 (s, 1H), 7.39 (dd,  $J$  = 7.8, 1.5 Hz, 1H), 7.31-7.19 (m, 6H), 7.19-7.10 (m, 3H), 7.06 (d,  $J$  = 7.9 Hz, 2H), 6.89 (d,  $J$  = 8.0 Hz, 1H), 6.28 (t,  $J$  = 5.3 Hz, 1H), 4.48 (d,  $J$  = 5.6 Hz, 2H), 3.46 (d,  $J$  = 4.4 Hz, 4H), 2.75 (t,  $J$  = 5.7 Hz, 2H), 2.56 (t,  $J$  = 5.8 Hz, 2H), 2.24 (s, 3H).<sup>[a]</sup>  $^{13}\text{C}$  NMR (75 MHz,  $\text{CDCl}_3$ )  $\delta$  167.35, 141.64, 139.91, 138.91, 137.42, 135.64, 135.37, 135.09, 133.15, 132.36, 131.02, 130.22, 130.20, 129.55, 128.18, 128.07, 127.67, 127.57, 127.25, 126.85, 124.12, 59.82, 55.69, 50.28, 43.99, 29.43, 21.22. MS ( $\text{ES}^+$ ),  $m/z$  481.0 ( $\text{M} + \text{H}$ ). HRMS ( $\text{ES}^+$  TOF) calculated for  $\text{C}_{31}\text{H}_{29}\text{ClN}_2\text{O}$  ( $\text{M} + \text{H}$ ): 481.2041; found 481.2021.

<sup>[a]</sup> A broad singlet observed at  $\delta$  1.69 ppm is an impurity, most likely water.

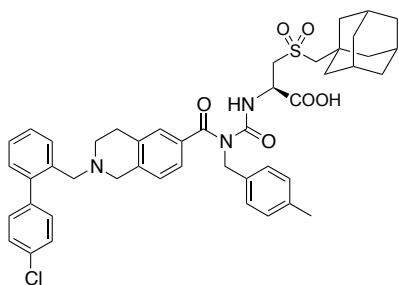


**(R)-2-(3-(2-((4'-chloro-[1,1'-biphenyl]-2-yl)methyl)-1,2,3,4-tetrahydroisoquinoline-6-carbonyl)-3-(4-methylbenzyl)ureido)-3-((cyclohexylmethyl)sulfonyl)propanoic acid (6.1):**

**General Procedure A** was followed using compound **6.9** (47 mg, 0.10 mmol), triethylamine (15  $\mu\text{L}$ , 0.11 mmol) and TMSOTf (19  $\mu\text{L}$ , 0.11 mmol), with the modification that after addition of TMSOTf, the reaction was allowed to proceed at room temperature for 1.5 h. Phosgene (194  $\mu\text{L}$ , 2 mL per mmol of amide starting material, 20% w/v in toluene, **CAUTION!**) added to the yellow-brown solution at  $0^\circ\text{C}$  and the reaction allowed to warm to room temperature and stir for 1.5 h. Concentration *in vacuo* (using an in-line solvent trap) over a room temperature water bath afforded the yellow carbamoyl chloride residue, which was used in the subsequent benzoylurea formation step without further purification. **General Procedure B** was followed using the amino acid HCl salt **4.31** (41 mg, 0.15 mmol), with the modifications that anhydrous dichloromethane as the reaction solvent and triethylamine (20  $\mu\text{L}$ , 0.15 mmol) was first added to neutralise the amino acid. The reaction containing the *in situ* protected amino acid was cooled to  $0^\circ\text{C}$ , then the carbamoyl chloride (resuspended in anhydrous dichloromethane (1 mL)) was added dropwise at  $0^\circ\text{C}$ . The reaction was then allowed to warm to room temperature and proceed for 1.5 h. After this time, water (10 mL) was added, the reaction was extracted three times with dichloromethane and the combined organic layers washed with water, brine, dried over  $\text{MgSO}_4$ , filtered and concentrated. Purification *via* flash chromatography, eluting with a gradient of methanol/dichloromethane (0:100 to 5:95) afforded the title compound as a colourless glass (44 mg, 60%).  $^1\text{H}$  NMR (300 MHz,  $\text{MeOD}$ )  $\delta$  7.72-7.65 (m, 1H), 7.53-7.28 (m, 7H), 7.21 (dd,  $J$  = 8.0, 1.7 Hz, 1H), 7.12 (d,  $J$  = 1.2 Hz, 1H), 7.09-7.01 (m, 4H), 6.99 (d,  $J$  = 8.1 Hz, 1H), 4.99-4.77 (m, 2H), 4.67 (dd,  $J$  = 7.6, 4.0 Hz, 1H), 4.10 (s, 2H), 3.85 (s, 2H), 3.62 (dd,  $J$  = 14.9, 4.0 Hz, 1H), 3.47 (dd,  $J$  = 14.8, 7.6 Hz, 1H), 3.08-2.92 (m, 4H), 2.85 (t,  $J$  = 5.5 Hz, 2H), 2.28 (s,  $J$  = 6.5 Hz, 3H), 2.08-1.93 (m, 1H), 1.88 (d,  $J$  = 12.5 Hz, 2H), 1.66 (dd,  $J$  = 18.4, 8.7 Hz, 3H), 1.40-0.99 (m, 5H).<sup>[a]</sup>  $^{13}\text{C}$  NMR (75 MHz,  $\text{MeOD}$ )  $\delta$  174.91, 173.66, 156.92, 143.72, 140.52, 138.01, 136.33, 136.10, 134.96, 134.76, 133.99, 132.28, 131.99, 131.94, 131.75, 130.12, 129.96, 129.70, 129.47, 128.39, 128.23, 127.86, 126.10, 60.95, 58.72, 56.52, 55.05, 52.17, 50.83, 50.50, 34.16, 34.14, 33.44, 27.71, 26.95, 26.89, 21.13.<sup>[b]</sup> MS ( $\text{ES}^+$ ),  $m/z$  756.9, ( $\text{M} + \text{H}$ ), 98.0% purity. HRMS ( $\text{ES}^+$  TOF) calculated for  $\text{C}_{42}\text{H}_{46}\text{ClN}_3\text{O}_6\text{S}$  ( $\text{M} + \text{H}$ ): 756.2869; found 756.2881.

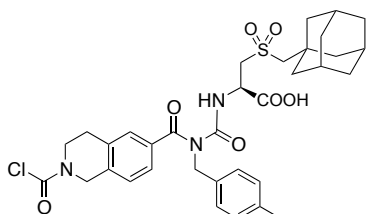
<sup>[a]</sup> The peak at  $\delta$  4.89 (m, 2H,  $\text{CH}_2$ ) overlaps with a peak at  $\delta$  4.85 from residual water in the NMR solvent.

### 6.6.1.2 Direct synthesis of extended scaffold compound **6.2**:



**(R)-3-(((3R,5R,7R)-adamantan-1-ylmethyl)sulfonyl)-2-(3-(2-((4'-chloro-[1,1'-biphenyl]-2-yl)methyl)-1,2,3,4-tetrahydroisoquinoline-6-carbonyl)-3-(4-methylbenzyl)ureido)propanoic acid (**6.2**):** This synthesis utilised a modified procedure based on **General procedure A**. To a stirred solution of the amide **6.9** (42 mg, 0.087 mmol) in anhydrous Et<sub>2</sub>O (0.3 mL) in an oven-dried Schlenk tube under N<sub>2</sub> was added triethylamine (15  $\mu$ L, 0.10 mmol, 1.2 eq.), followed by TMSOTf (19  $\mu$ L, 0.10 mmol, 1.2 eq.) and the reaction was stirred under N<sub>2</sub> at room temperature for 15 minutes. All taps of the Schlenk tube were then sealed and the reaction was allowed to proceed for 16 h at room temperature. After this time, the reaction was cooled to -5°C (dry ice/acetonitrile bath) and phosgene (48  $\mu$ L, **0.55 mL per mmol of amide starting material** (approx. 0.95 eq.), 20% w/v in toluene, **CAUTION!**) was added dropwise at -5°C. The reaction was then stirred at -5-0°C for 1.5 h, briefly allowed to room temperature and the reaction was concentrated *in vacuo* (using an in-line solvent trap) over a room temperature water bath to afford the carbamoyl chloride residue. **General Procedure B** was then followed using the amino acid **4.21** (39 mg, 0.13 mmol), propylene oxide (0.17 mL) and bistrimethylsilylacetamide (48  $\mu$ L, 0.19 mmol) using anhydrous dichloromethane as the reaction solvent and the following modified workup. Following dropwise addition of the carbamoyl chloride intermediate(s) at 0°C, the reaction was warmed to room temperature and stirred for 30 minutes. LCMS analysis of the reaction mixture indicated a complex mixture of products, including the desired product **6.2**. The reaction mixture was diluted with dichloromethane and poured onto water (10 mL), extracted three times with dichloromethane, the combined organic layers washed with water, brine, dried over MgSO<sub>4</sub>, filtered and concentrated. Purification of the crude material by mass-directed preparative HPLC afforded compound **6.2** as an opaque off-white glass (5.2 mg, 7%). <sup>1</sup>H NMR (600 MHz, MeOD)  $\delta$  7.68 (d, *J* = 7.1 Hz, 1H), 7.51–7.34 (m, 7H), 7.25 (d, *J* = 7.7 Hz, 1H), 7.16 (s, 1H), 7.09 (s, 4H), 7.03 (d, *J* = 8.1 Hz, 1H), 4.97 (d, *J* = 16.0 Hz, 1H), 4.69 (br s, 1H), 4.05 (s, 2H), 3.84 (s, 2H), 3.62 (d, *J* = 13.2 Hz, 1H), 3.46 (dd, *J* = 14.3, 6.4 Hz, 1H), 3.03–2.93 (m, 4H), 2.87 (br s, 2H), 2.30 (s, 3H), 1.97 (br s, 3H), 1.85 (s, 6H), 1.76 (d, *J* = 12.2 Hz, 3H), 1.71 (d, *J* = 12.0 Hz, 3H). MS (ES<sup>+</sup>), *m/z* 808.2, (*M* + *H*), 97.0% purity. HRMS (ES<sup>+</sup> TOF) calculated for C<sub>46</sub>H<sub>50</sub>ClN<sub>3</sub>O<sub>6</sub>S (*M* + *H*): 808.3182; found 808.3186.

### 6.6.1.3 Alternative synthesis of extended scaffold compound **6.2** via reductive amination approach (**Schemes 6.2B, 6.4B**):

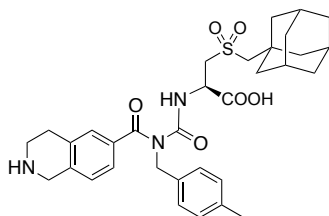


**(R)-3-(((3R,5R,7R)-adamantan-1-ylmethyl)sulfonyl)-2-(3-(2-(chlorocarbonyl)-1,2,3,4-tetrahydroisoquinoline-6-carbonyl)-3-(4-methylbenzyl)ureido)propanoic acid (**6.15**):** **General procedure A** was followed using compound **6.9** (37 mg, 0.078 mmol) with the following modifications: following addition of a reduced volume of phosgene (78  $\mu$ L, **1 mL per mmol of amide starting material**, 20% w/v in toluene, **CAUTION!**) at 0°C, the reaction was stirred at 0°C for 1 h, then allowed to room temperature and stirred for 30 minutes. **General Procedure B** was followed using compound **4.21** (35 mg, 0.12 mmol), propylene oxide (0.16 mL) and

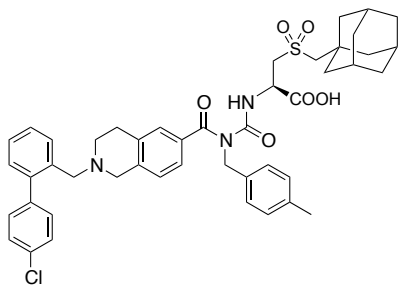
bistrimethylsilylacetamide (43  $\mu$ L, 0.18 mmol) and the carbamoyl chloride intermediate(s) (**6.12/6.10/6.13**) with a modified workup. Following dropwise addition of the carbamoyl chloride intermediate(s) at 0°C, the reaction was warmed to room temperature and stirred for 30 minutes. After this time, the reaction was diluted with dichloromethane and poured onto water (10 mL). The reaction mixture was extracted three times with dichloromethane. The combined organic layers were washed with water, brine, dried over  $\text{MgSO}_4$ , filtered and concentrated. Analysis of the crude material by ESI-MS indicated that the major product was the carbamoyl chloride derivative with the structure **6.15**. Purification of this crude material *via* flash chromatography, eluting with a gradient of methanol/dichloromethane (0:100 to 5:95) afforded the major product **6.15** as a pale yellow glass (35.9 mg, 69%).  $^1\text{H}$  NMR (300 MHz,  $\text{CDCl}_3$ )  $\delta$  9.69 (d,  $J$  = 6.6 Hz, 1H), 7.25–7.02 (m, 5H), 6.92 (d,  $J$  = 7.8 Hz, 2H), 5.03–4.87 (m, 3H), 4.79 (d,  $J$  = 26.7 Hz, 2H), 3.85 (dt,  $J$  = 25.3, 5.8 Hz, 2H), 3.74–3.59 (m, 2H), 2.92–2.77 (m, 4H), 2.30 (s, 3H), 1.98 (br s, 3H), 1.82 (d,  $J$  = 2.3 Hz, 6H), 1.76–1.58 (m, 6H).<sup>[a]</sup>  $^{13}\text{C}$  NMR (75 MHz,  $\text{CDCl}_3$ )  $\delta$  174.70, 171.76, 155.32, 148.89, 137.23, 135.15, 134.79, 134.48, 134.41, 129.48, 127.44, 127.32, 126.58, 126.53, 126.45, 125.06, 66.90, 56.20, 50.08, 49.75, 47.97, 46.25, 44.04, 42.13, 36.50, 34.72, 28.47, 21.21.<sup>[b]</sup> MS ( $\text{ES}^+$ ),  $m/z$  670.2, ( $\text{M} + \text{H}$ ). HRMS ( $\text{ES}^+$  TOF) calculated for  $\text{C}_{34}\text{H}_{40}\text{ClN}_3\text{O}_7\text{S}$  ( $\text{M} + \text{Na}$ ): 692.2168; found 692.2165.

<sup>[a]</sup> An additional peak at  $\delta$  5.30 ppm is due to an impurity, most likely dichloromethane.

<sup>[b]</sup> Two additional peaks are observed in the aliphatic region due to apparent peak splitting.



**(R)-3-(((3R,5R,7R)-adamantan-1-ylmethyl)sulfonyl)-2-(3-(4-methylbenzyl)-3-(1,2,3,4-tetrahydroisoquinoline-6-carbonyl)ureido)propanoic acid (TFA salt) (**6.22**):** This synthesis was based on a procedure described in the literature<sup>(4)</sup>. To a solution of compound **6.15** (23 mg, 0.033 mmol) in 3 mL of a solution of water/acetonitrile (1:1) under  $\text{N}_2$  was added TFA (6  $\mu$ L, 0.08 mmol) and the colourless solution stirred at 80°C for 1 h. After this time, analytical LCMS indicated complete conversion of starting material into product. The reaction mixture was concentrated under reduced pressure, the colourless residue taken up in toluene and concentrated (2 x) to remove excess TFA, then suspended in 10 mL of a solution of water/acetonitrile (1:1) and freeze-dried to afford compound **6.22** (TFA salt) as a fluffy white solid (20 mg). MS ( $\text{ES}^+$ ),  $m/z$  608.3, ( $\text{M} + \text{H}$ ). This material was used directly in the next step without further characterisation.

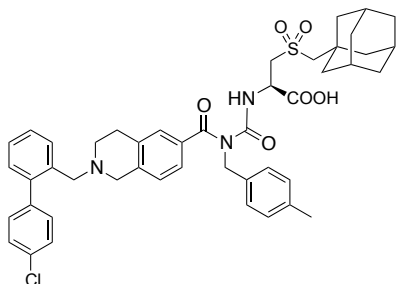


**(R)-3-(((3R,5R,7R)-adamantan-1-ylmethyl)sulfonyl)-2-(3-(2-((4'-chloro-[1,1'-biphenyl]-2-yl)methyl)-1,2,3,4-tetrahydroisoquinoline-6-carbonyl)-3-(4-methylbenzyl)ureido)propanoic acid (**6.2**):** To a stirred solution of compound **6.22** (20 mg, approx. 0.03 mmol) in 1.0 mL of anhydrous dichloromethane under  $\text{N}_2$  at room temperature was added triethylamine (10  $\mu$ L, 0.07 mmol) followed by compound **6.4** (9 mg, 0.04 mmol). After 30 minutes, sodium triacetoxyborohydride (16 mg, 0.07 mmol) was added and the reaction stirred at room temperature for 20 h. The reaction mixture was diluted with dichloromethane (20 mL) poured over water (20 mL), the two layers separated and the aqueous phase extracted further with dichloromethane (2 x 10 mL). The combined organic phases were washed with brine, dried over  $\text{MgSO}_4$ , filtered and concentrated. Purification of this crude material *via* flash chromatography, eluting with a gradient of methanol/dichloromethane (0:100 to 10:90) afforded compound **6.2** as an opaque off-white glass containing some impurities which were not able to be separated (3.8 mg, <14%).  $^1\text{H}$  NMR (600 MHz,  $\text{MeOD}$ )  $\delta$  7.72 (dd,  $J$  = 5.3, 3.5 Hz, 1H),

7.62–7.34 (m, 8H), 7.25 (d,  $J = 7.4$  Hz, 1H), 7.18–7.01 (m, 5H), 5.02–4.84 (m, 2H), 4.73 (br s, 1H), 4.25 (br s, 1H), 3.98 (s, 1H), 3.69 (d,  $J = 17.1$  Hz, 1H), 3.53 (br s, 1H), 3.17–3.05 (m, 2H), 2.97 (s, 2H), 2.91 (t,  $J = 6.4$  Hz, 1H), 2.30 (s, 3H), 1.97 (br s, 3H), 1.85 (s, 6H), 1.77 (d,  $J = 11.8$  Hz, 3H), 1.70 (d,  $J = 11.6$  Hz, 3H). MS (ES<sup>+</sup>),  $m/z$  808.2, (M + H), 70% purity.<sup>[a]</sup> HRMS (ES<sup>+</sup> TOF) calculated for C<sub>46</sub>H<sub>50</sub>ClN<sub>3</sub>O<sub>6</sub>S (M + H): 808.3182; found 808.3166.

<sup>[a]</sup> This material was not utilised for binding studies or biological evaluation.

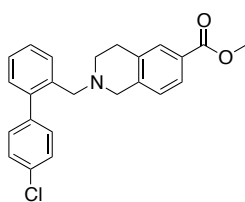
#### 6.6.1.4 Reference analytical data for compound 6.2 via direct scale-up resynthesis (synthesised by Amelia Vom):



**(R)-3-(((3R,5R,7R)-adamantan-1-ylmethyl)sulfonyl)-2-(3-(2-((4'-chloro-[1,1'-biphenyl]-2-yl)methyl)-1,2,3,4-tetrahydroisoquinoline-6-carbonyl)-3-(4-methylbenzyl)ureido)propanoic acid (6.2):** opaque white glassy solid. <sup>1</sup>H NMR (600 MHz, CDCl<sub>3</sub>)  $\delta$  9.10 (br s, 1H), 7.85 (d,  $J = 7.3$  Hz, 1H), 7.44 (t,  $J = 7.5$  Hz, 1H), 7.41 (t,  $J = 7.5$  Hz, 1H), 7.38 (dd,  $J = 8.2, 1.5$  Hz, 2H), 7.27 (d,  $J = 8.9$  Hz, 2H), 7.23 (dd,  $J = 8.2, 1.4$  Hz, 2H), 7.06–6.88 (m, 6H), 6.84 (d,  $J = 7.8$  Hz, 1H), 4.73 (dd,  $J = 52.1, 15.4$  Hz, 2H), 4.64 (dd,  $J = 10.3, 5.5$  Hz, 1H), 4.30 (d,  $J = 11.5$  Hz, 1H), 4.10 (d,  $J = 11.9$  Hz, 1H), 3.85–3.64 (m, 3H), 3.60 (dd,  $J = 14.1, 5.4$  Hz, 1H), 3.06–2.74 (m, 6H), 2.27 (s, 3H), 1.95 (br s, 3H), 1.79 (br s, 6H), 1.71–1.60 (m, 6H). <sup>13</sup>C NMR (151 MHz, CDCl<sub>3</sub>)  $\delta$  173.72, 172.91, 154.80, 142.22, 139.09, 136.84, 135.10, 134.93, 133.92, 132.75, 131.58, 130.96, 130.54, 129.33, 128.99, 128.91, 127.08, 126.93, 126.84, 124.60, 66.66, 57.14, 57.03, 53.14, 51.41, 49.66, 49.33, 42.12, 36.60, 34.52, 28.52, 26.63, 21.23.<sup>[a]</sup> MS (ES<sup>+</sup>),  $m/z$  808.3, (M + H), 96% purity. HRMS (ES<sup>+</sup> TOF) calculated for C<sub>46</sub>H<sub>50</sub>ClN<sub>3</sub>O<sub>6</sub>S (M + H): 808.3182; found 808.3198.

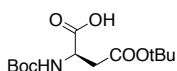
<sup>[a]</sup> Three peaks in the aromatic region are not observed due to overlap.

#### 6.6.1.5 Alternative synthesis of 6.7 via reductive amination:

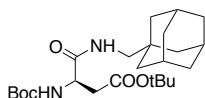


**Methyl 2-((4'-chlorobiphenyl-2-yl)methyl)-1,2,3,4-tetrahydroisoquinoline-6-carboxylate (6.7):** To a stirred solution of methyl 1,2,3,4-tetrahydroisoquinoline-6-carboxylate hydrochloride (20 mg, 0.088 mmol) and triethylamine (25  $\mu$ L, 0.176 mmol) in anhydrous dichloromethane (2.0 mL) at room temperature under a N<sub>2</sub> atmosphere, was added compound 6.4 (19 mg, 0.088 mmol). After 30 minutes, sodium triacetoxyborohydride (37 mg, 0.176 mmol) was added and the reaction stirred at room temperature for 18 h. The reaction mixture was poured over aq. sat. NaHCO<sub>3</sub>, the two phases separated and the aqueous phase extracted with dichloromethane. The combined organic extracts were dried over MgSO<sub>4</sub>, filtered and concentrated under reduced pressure. Purification of the crude oil *via* flash chromatography eluting with petroleum ether/EtOAc (0 to 85:15) to afford compound 6.7 as a colourless oil (32 mg, 92%). <sup>1</sup>H NMR (600 MHz, CDCl<sub>3</sub>)  $\delta$  7.80–7.73 (m, 2H), 7.60 (d,  $J = 7.5$  Hz, 1H), 7.40–7.30 (m, 5H), 7.28–7.23 (m, 2H), 7.01 (d,  $J = 7.9$  Hz, 1H), 3.89 (s,  $J = 1.2$  Hz, 3H), 3.61 (s, 4H), 2.89 (t,  $J = 5.5$  Hz, 2H), 2.70 (t,  $J = 5.5$  Hz, 2H). <sup>13</sup>C NMR (151 MHz, CDCl<sub>3</sub>)  $\delta$  167.27, 141.70, 140.00, 139.82, 135.09, 134.64, 133.25, 131.02, 130.33, 130.25, 130.14, 128.26, 128.23, 127.79, 127.42, 126.91, 126.78, 59.43, 55.58, 52.13, 50.13, 29.08. MS (ES<sup>+</sup>),  $m/z$  392.2 (M + H).

### 6.6.1.6 Synthesis of extended scaffold compound **6.3** via reductive amination approach (**Scheme 6.5**):

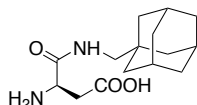


**(R)-4-((tert-butoxy)-2-((tert-butoxycarbonyl)amino)-4-oxobutanoic acid (6.23):** To a stirred solution of D-Aspartic acid beta-*t*-butyl ester monohydrate (207 mg, 1.0 mmol) in anhydrous acetonitrile (5 mL) under N<sub>2</sub> at 0°C were added di-*tert*-butyl dicarbonate (253  $\mu$ L, 1.1 mmol) followed by triethylamine (139  $\mu$ L, 1.0 mmol). The reaction was allowed to warm to room temperature and proceed for 3 h, diluted with EtOAc (30 mL) then poured over 10% aq. citric acid solution (20 mL). The two phases were separated and the aqueous phase extracted further with EtOAc (2 x 30 mL). The combined organic phases were washed with water, brine, dried over MgSO<sub>4</sub>, filtered and concentrated. Purification of the crude oil *via* flash chromatography, eluting with a gradient of methanol/dichloromethane (0:100 to 5:95) afforded the title compound as a colourless oil (218 mg, 75%). <sup>1</sup>H NMR (600 MHz, CDCl<sub>3</sub>)  $\delta$  5.53 (d, *J* = 7.3 Hz, 1H), 4.56 (s, 1H), 2.92 (d, *J* = 16.0 Hz, 1H), 2.74 (dd, *J* = 16.9, 3.2 Hz, 1H), 1.45 (s, 18H). MS (ES<sup>-</sup>), *m/z* 288.5, (M - H). HRMS (ES<sup>+</sup> TOF) calculated for C<sub>13</sub>H<sub>23</sub>NO<sub>6</sub> (M + H): 312.1418; found 312.1422.



**(R)-tert-butyl 4-(((3R,5R,7R)-adamantan-1-ylmethyl)amino)-3-((tert-butoxycarbonyl)amino)-4-oxobutanoate (6.24):** To a stirred solution of **6.23** (93 mg, 0.3 mmol) in anhydrous DMF (5 mL) were added HBTU (146 mg, 0.4 mmol) and HOBt (52 mg, 0.4 mmol) followed by DIEA (140  $\mu$ L, 0.8 mmol) and the reaction was stirred under N<sub>2</sub> at room temperature for 15 minutes. Then 1-Adamantanemethylamine (85  $\mu$ L, 0.5 mmol) was added to this mixture and the reaction was allowed to proceed at room temperature for 18 h. After this time, the reaction was diluted with EtOAc (20 mL) and poured over a 10% aq. solution of sodium bicarbonate (30 mL). The layers were separated and the aq. layer was further extracted with EtOAc (2 x 20 mL), then the combined organic layers were dried over MgSO<sub>4</sub>, filtered and concentrated under reduced pressure. The resulting oil was purified *via* flash chromatography eluting with a gradient of EtOAc/cyclohexane (5:95–10:90) to afford the title compound a yellowish oil (123.5 mg, 88%). <sup>1</sup>H NMR (600 MHz, CDCl<sub>3</sub>)  $\delta$  6.60 (s, 1H), 5.75 (d, *J* = 6.3 Hz, 1H), 4.41 (s, 1H), 2.91 (qd, *J* = 13.3, 6.3 Hz, 2H), 2.71 (ddd, *J* = 23.7, 16.9, 5.7 Hz, 2H), 1.93 (s, 3H), 1.63 (dd, *J* = 49.5, 11.9 Hz, 6H), 1.49–1.39 (m, 24H).<sup>[a]</sup> HRMS (ES<sup>+</sup> TOF) calculated for C<sub>24</sub>H<sub>40</sub>N<sub>2</sub>O<sub>5</sub> (M + H): 437.3010; found 437.2997.

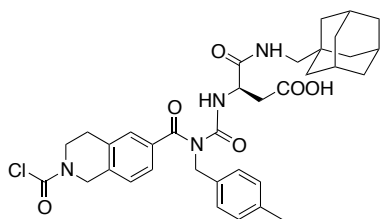
<sup>[a]</sup> Additional peaks observed at  $\delta$  4.10 (q), 2.02 (s), 1.24 (t) ppm and the peak at  $\delta$  1.38 ppm are due to impurities, most likely EtOAc and cyclohexane respectively.



**(R)-4-(((3R,5R,7R)-adamantan-1-ylmethyl)amino)-3-amino-4-oxobutanoic acid (6.25):** Compound **6.24** (126 mg, 0.3 mmol) was deprotected using TFA (200  $\mu$ L) according to **General Procedure G**. Purification of the resulting crude yellow oil *via* mass-directed preparative HPLC yielded the title compound as a colourless glassy solid (40 mg, 45%). <sup>1</sup>H NMR (300 MHz, MeOD)  $\delta$  4.19 (dd, *J* = 7.6, 5.5 Hz, 1H), 3.17–2.73 (m, 4H), 1.96 (s, 3H), 1.72 (q, *J* = 12.0 Hz, 6H), 1.58–1.43 (m, 6H).<sup>[a]</sup> <sup>13</sup>C NMR (75 MHz, MeOD)  $\delta$  173.1, 169.45, 52.33, 51.19, 41.18, 40.44, 37.95, 36.63, 35.18, 29.73.<sup>[b]</sup> MS (ES<sup>+</sup>), *m/z* 281.1, (M + H), 99% purity. HRMS (ES<sup>+</sup> TOF) calculated for C<sub>15</sub>H<sub>24</sub>N<sub>2</sub>O<sub>3</sub> (M + H): 281.1860; found 281.1859.

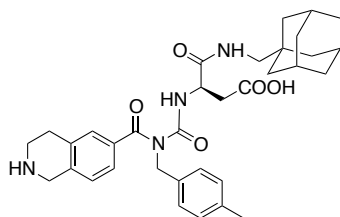
<sup>[a]</sup> Additional peaks observed at  $\delta$  4.91 ppm (br s) and 2.66 ppm (s) are impurities, most likely H<sub>2</sub>O and DMSO respectively.

<sup>[b]</sup> The peak at  $\delta$  40.44 ppm is an impurity, most likely DMSO, which was utilised to solubilise the crude material for HPLC purification.

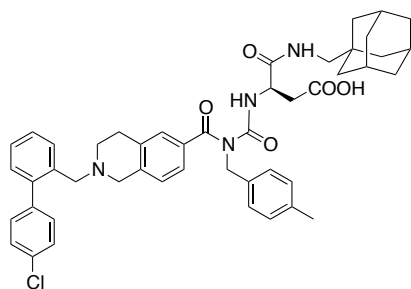


**(R)-4-(((3R,5R,7R)-adamantan-1-ylmethyl)amino)-3-(3-(2-(chlorocarbonyl)-1,2,3,4-tetrahydroisoquinoline-6-carbonyl)-3-(4-methylbenzyl)ureido)-4-oxobutanoic acid (6.27):** General procedure A was followed using compound **6.9** (37 mg, 0.078 mmol) with the following modifications: following addition of a reduced volume of phosgene (78  $\mu$ L, **1 mL per mmol of amide starting material**, 20% w/v in toluene, **CAUTION!**) at 0°C, the reaction was stirred at 0°C for 1 h, then allowed to room temperature and stirred for 30 minutes. General Procedure B was followed using compound **6.25** (29.8 mg, 0.106 mmol), propylene oxide (0.16 mL) and bistrimethylsilylacetamide (39  $\mu$ L, 0.16 mmol) and the carbamoyl chloride intermediate(s) (**6.12/6.10/6.13**) with a modified workup. Following dropwise addition of the carbamoyl chloride intermediate(s) at 0°C, the reaction was warmed to room temperature and stirred for 30 minutes. After this time, the reaction was diluted with dichloromethane and poured onto water (10 mL). The reaction mixture was extracted three times with dichloromethane. The combined organic layers were washed with water, brine, dried over  $\text{MgSO}_4$ , filtered and concentrated. Analysis of the crude material by ESI-MS indicated that the major product was the carbamoyl chloride derivative with the structure **6.27**. Purification of this crude material *via* flash chromatography, eluting with a gradient of methanol/dichloromethane (0:100 to 5:95) afforded the major product **6.27** as a pale yellow glass (35.9 mg, 69%).  $^1\text{H}$  NMR (300 MHz,  $\text{CDCl}_3$ )  $\delta$  9.37 (d,  $J$  = 7.9 Hz, 1H), 7.29–6.87 (m, 8H), 6.69 (t,  $J$  = 6.2 Hz, 1H), 5.02–4.54 (m, 5H), 3.85 (dt,  $J$  = 25.6, 5.9 Hz, 2H), 3.08–2.68 (m, 6H), 2.30 (s, 3H), 1.93 (s, 3H), 1.62 (dd,  $J$  = 32.0, 12.0 Hz, 6H), 1.41 (d,  $J$  = 1.9 Hz, 6H).<sup>[a]</sup> MS ( $\text{ES}^+$ ),  $m/z$  649.3, ( $M + \text{H}$ ). HRMS ( $\text{ES}^+$  TOF) calculated for  $\text{C}_{35}\text{H}_{41}\text{ClN}_4\text{O}_6$  ( $M + \text{H}$ ): 649.2787; found 649.2794.

<sup>[a]</sup> One extra proton in the region  $\delta$  7.29–6.87 ppm is attributed to  $\text{CDCl}_3$ .



**(R)-4-(((3R,5R,7R)-adamantan-1-ylmethyl)amino)-3-(3-(4-methylbenzyl)-3-(1,2,3,4-tetrahydroisoquinoline-6-carbonyl)ureido)-4-oxobutanoic acid (TFA salt) (6.28):** This synthesis was based on a procedure described in the literature<sup>(4)</sup>. To a solution of compound **6.27** (27 mg, 0.04 mmol) in 3 mL of a solution of water/acetonitrile (1:1) under  $\text{N}_2$  was added TFA (8  $\mu$ L, 0.1 mmol) and the colourless solution stirred at 80°C for 1 h. After this time, analytical LCMS indicated complete conversion of starting material into product. The reaction mixture was concentrated under reduced pressure, the colourless residue taken up in toluene and concentrated (2 x) to remove excess TFA, then suspended in 10 mL of a solution of water/acetonitrile (1:1) and freeze-dried to afford compound **6.28** (TFA salt) as a fluffy white solid (23 mg). MS ( $\text{ES}^+$ ),  $m/z$  587.3, ( $M + \text{H}$ ). This material was used directly in the next step without further characterisation.



**(R)-4-(((3R,5R,7R)-adamantan-1-ylmethyl)amino)-3-(3-(2-((4'-chloro-[1,1'-biphenyl]-2-yl)methyl)-1,2,3,4-tetrahydroisoquinoline-6-carbonyl)-3-(4-methylbenzyl)ureido)-4-oxobutanoic acid (6.3):**

To a stirred solution of compound **6.28** (23 mg, approx. 0.03 mmol) in 1.0 mL of anhydrous dichloromethane under N<sub>2</sub> at room temperature was added triethylamine (11  $\mu$ L, 0.08 mmol) followed by compound **6.4** (11 mg, 0.05 mmol). After 30 minutes, sodium triacetoxyborohydride (19 mg, 0.09 mmol) was added and the reaction stirred at room temperature for 20 h. The reaction mixture was diluted with dichloromethane (20 mL) poured over water (20 mL), the two layers separated and the aqueous phase extracted further with dichloromethane (2 x 10 mL). The combined organic phases were washed with brine, dried over MgSO<sub>4</sub>, filtered and concentrated. The crude material was purified by mass-directed preparative HPLC. A colourless glass was obtained (7.3 mg, 23% over two steps). <sup>1</sup>H NMR (600 MHz, CDCl<sub>3</sub>)  $\delta$  7.60 (d, *J* = 6.8 Hz, 1H), 7.42–7.22 (m, 8H), 7.13 (d, *J* = 8.5 Hz, 2H), 7.05 (dd, *J* = 15.2, 7.8 Hz, 4H), 6.92 (d, *J* = 7.6 Hz, 1H), 6.57 (br s, 1H), 5.00–4.78 (m, 2H), 4.70 (br s, 1H), 3.75 (s, 2H), 3.58 (q, *J* = 15.1 Hz, 2H), 3.06 (s, 1H), 2.92–2.49 (m, 8H), 2.29 (s, 3H), 1.91 (s, 3H), 1.66 (d, *J* = 11.9 Hz, 3H), 1.56 (d, *J* = 11.7 Hz, 3H), 1.36 (s, 6H).<sup>[a]</sup> MS (ES<sup>+</sup>), *m/z* 787.1, (M + H), 98% purity. HRMS (ES<sup>+</sup> TOF) calculated for C<sub>47</sub>H<sub>51</sub>ClN<sub>4</sub>O<sub>5</sub> (M + H): 787.3621; found 787.3641.

<sup>[a]</sup> The peak at  $\delta$  3.06 ppm (br s) is attributed to –COOH.

## 6.6.2 Crystallisation and X-ray structure determination

### 6.6.2.1 Structure determination of the BCL-X<sub>L</sub>:**6.1** complex

The complex of BCL-X<sub>L</sub>:**6.1** (10 mg/mL) was prepared for crystallisation as described in **Chapter 2, Section 2.6** and crystallised under the following condition: 1.3 M ammonium sulfate, 0.1 M Tris pH 7.0. Crystals were flash-cooled in cryoprotectant solution containing 1.4 M ammonium sulfate, 0.1 M Tris pH 7.0 supplemented with ethylene glycol (25%). Data were collected on the MX2 beamline at the Australian Synchrotron and processed with XDS <sup>(13)</sup>. The structure was solved by molecular replacement with PHASER <sup>(14)</sup> using as a search model the BCL-X<sub>L</sub> coordinates from the BCL-X<sub>L</sub>:**1.10** complex. Multiple rounds of building in COOT <sup>(15)</sup> and refinement in PHENIX <sup>(16)</sup> incorporating in the first round of refinement a simulated annealing step, resulted in the final structure. The asymmetric unit contained four copies of the BCL-X<sub>L</sub> monomer, arranged as two domain-swapped dimers. In each monomer a single copy of the ligand was observed to occupy the hydrophobic groove in the anticipated conformation. Ligand geometry restraint (cif) files were generated from SMILES strings using ELBOW <sup>(17)</sup>.



## 6.7 References

1. Lemoucheux L, Rouden J, Ibazizene M, Sobrio F, & Lasne M-C (2003) Debenzylation of tertiary amines using phosgene or triphosgene: an efficient and rapid procedure for the preparation of carbamoyl chlorides and unsymmetrical ureas. Application in carbon-11 chemistry. *The Journal of Organic Chemistry* 68(19):7289-7297.
2. Jorand-Lebrun C, Valognes D, & Halazy S (1998) Use of triphosgene for direct preparation of carbamoyl chlorides from tertiary benzylamines. *Synthetic Communications* 28(7):1189-1195.
3. Banwell MG, Coster MJ, Harvey MJ, & Moraes J (2003) Selective Cleavage of N-Benzyl-Protected Secondary Amines by Triphosgene. *The Journal of Organic Chemistry* 68(2):613-616.
4. Baraldi PG, *et al.* (2012) Water-soluble pyrazolo[4,3-e][1,2,4]triazolo[1,5-c]pyrimidines as human A3 adenosine receptor antagonists. *Journal of Medicinal Chemistry* 55(11):5380-5390.
5. Mason KD, *et al.* (2007) Programmed anuclear cell death delimits platelet life span. *Cell* 128(6):1173-1186.
6. Zhang H, *et al.* (2007) BCL-2 family proteins are essential for platelet survival. *Cell Death and Differentiation* 14(5):943-951.
7. Tse C, *et al.* (2008) ABT-263: a potent and orally bioavailable BCL-2 family inhibitor. *Cancer Research* 68(9):3421-3428.
8. Wilson WH, *et al.* (2010) Navitoclax, a targeted high-affinity inhibitor of BCL-2, in lymphoid malignancies: a phase 1 dose-escalation study of safety, pharmacokinetics, pharmacodynamics, and antitumour activity. *The Lancet Oncology* 11(12):1149-1159.
9. Roberts AW, *et al.* (2012) Substantial susceptibility of chronic lymphocytic leukemia to BCL2 inhibition: results of a phase I study of navitoclax in patients with relapsed or refractory disease. *Journal of Clinical Oncology* 30(5):488-496.
10. Ye F, *et al.* (2011) Expeditious synthesis of phenanthrenes via CuBr<sub>2</sub>-catalyzed coupling of terminal alkynes and N-tosylhydrazones derived from O-formyl biphenyls. *Org. Lett.* 13(19):5020-5023.

11. Baell JB, *et al.* (2008) WO2008061208A2.
12. Hwang SJ, Kim HJ, & Chang S (2009) Highly efficient and versatile synthesis of polyarylfuorenes via Pd-catalyzed C–H bond activation. *Organic Letters* 11(20):4588-4591.
13. Kabsch W (2010) Xds. *Acta Crystallographica Section D Biological Crystallography* 66(Pt 2):125-132.
14. McCoy AJ, *et al.* (2007) Phaser crystallographic software. *Journal of Applied Crystallography* 40(Pt 4):658-674.
15. Emsley P & Cowtan K (2004) Coot: model-building tools for molecular graphics. *Acta Crystallographica Section D Biological Crystallography* 60(Pt 12 Pt 1):2126-2132.
16. Adams PD, *et al.* (2010) PHENIX: a comprehensive Python-based system for macromolecular structure solution. *Acta Crystallographica Section D Biological Crystallography* 66(Pt 2):213-221.
17. Moriarty NW, Grosse-Kunstleve RW, & Adams PD (2009) electronic Ligand Builder and Optimization Workbench (eLBOW): a tool for ligand coordinate and restraint generation. *Acta Crystallographica Section D Biological Crystallography* 65(Pt 10):1074-1080.

## **7 Chapter seven – Conclusions**

## 7.1 Conclusions and future directions

This study has described the structure-guided lead development of a novel series of benzoylurea inhibitors of the prosurvival protein BCL-X<sub>L</sub> (**Figure 7.1**). This series originated from a rational design strategy using a benzoylurea scaffold as a potential  $\alpha$ -helical topographical mimetic (**Figure 7.1A**). Screening of a small library of benzoylurea (~ 130 compounds) led to discovery of the initial hit, compound **1.1**, which bound to BCL-X<sub>L</sub> with an IC<sub>50</sub> in the low-sub micromolar range. Guided by the crystal structure of **1.1** in complex with BCL-X<sub>L</sub> (**Figure 7.1B**) and known inhibitors such as **ABT-737**, this Thesis has outlined the synthesis and evaluation of analogues of **1.1** aimed at improving affinity for BCL-X<sub>L</sub>. In particular, analogues of **1.1** are described that explore modifying the thioether 'linker' and targeting additional interactions in the p2 and p4/p5 pockets of BCL-X<sub>L</sub> (**Figure 7.1B**). This has led to discovery of compounds **6.1** and **6.2**, which have improved binding to BCL-X<sub>L</sub> (IC<sub>50</sub> values in the nanomolar range), exhibit significant selectivity for this protein and show early signs of weak but measurable BCL-X<sub>L</sub>-dependent activity in *in vitro* cellular assays.

**Chapter 1** introduced 'BH3 mimetics' as a relatively recent class of targeted therapeutics that antagonise prosurvival BCL-2 family proteins (such as BCL-2 or BCL-X<sub>L</sub>) and offer significant promise in particular for cancer therapy. The origins of the benzoylurea series and discovery of compound **1.1** were described, including structural characterisation of the BCL-X<sub>L</sub>:**1.1** complex, analogues exploring negative SAR of **1.1** and analogues incorporating hydrogen-bonding moieties into the thioether 'linker'. One such linker modification was the introduction of a sulfonyl 'linker' (compound **1.8**, **Figure 6.1**); in a crystal structure solved of a BCL-X<sub>L</sub>:**1.1** complex, one oxygen atom of the sulfonyl moiety was shown to form a hydrogen bond interaction with the backbone -NH of Gly138 of BCL-X<sub>L</sub>, which provided a starting point for subsequent work described in **Chapter 4** and **Chapter 5**. Also introduced in **Chapter 1** was a structure-guided rescaffolding effort that led to compounds **1.9** and **1.10**, which incorporate a chlorobiphenyl extension designed to interact in the vicinity of the p2 pocket of BCL-X<sub>L</sub> (**Figure 6.1**). Compound **1.9** represents a more rigid scaffold, based on a

fused bis-biphenyl core, whilst compound **1.10** is more flexible, based on a tetrahydroisoquinoline (THIQ) core and provided the starting point for analogues described in **Chapter 6**.

**Chapter 3** described some initial structural studies with some of these early lead molecules, as well as two novel series attempting to form an additional pi-stacking interaction with Tyr195 of BCL-X<sub>L</sub>. Firstly, I described novel crystal structures of two complexes, BCL-X<sub>L</sub>:**1.9** and BCL-X<sub>L</sub>:**3.1**. Compound **3.1** is a derivative of **1.10** that incorporates a 'sulfonyl' linker, similar to compound **1.8** (**Figure 6.1**). These two structures confirmed the deep binding interaction of each compound in the vicinity of the p2 pocket of BCL-X<sub>L</sub> and provided structural detail to guide new modifications. In particular, the structure of the BCL-X<sub>L</sub>:**3.1** complex paved the way for subsequent derivatives of compound **3.1** described in **Chapter 6**. Comparison of the BCL-X<sub>L</sub>:**1.9** complex to another published series of inhibitors of BCL-X<sub>L</sub> sharing the same binding mode<sup>(1)</sup>, highlighted sites of potential modification that might improve the selectivity of these compounds for BCL-X<sub>L</sub> in future.

**Chapter 3** next described two approaches to modify compound **1.1** by replacing the S-benzyl-cysteine moiety with groups attempting to form an additional pi-stacking interaction with the side-chain of Tyr195 of BCL-X<sub>L</sub>; similar to the pi-stacking interaction made by the nitroaryl and S-phenyl rings of **ABT-737** in the published structure of the BCL-X<sub>L</sub>:**ABT-737** complex<sup>(2)</sup>. The first approach involved a series of benzoylurea arylsulfonamides (compounds **3.2a-c**, **Figure 3.2C**). I described the crystal structure in complex with BCL-X<sub>L</sub> of a proof-of-principle molecule, compound **3.2c** (synthesised by Amelia Vom), in which both the S-benzyl-L-cysteine and tolyl moieties of **1.1** (which occupy the p5 and p4 pockets of BCL-X<sub>L</sub>) were replaced *in toto* by the nitroaryl/S-phenyl fragment from **ABT-737** (**Figure 3.2C**). This structure confirmed that a nitroaryl ring incorporated adjacent to the benzoylurea core could indeed form the desired pi-stacking interaction with Tyr195 of BCL-X<sub>L</sub> (**Figure 3.5**). I next described attempts to synthesise compounds **3.2a** and **3.2b**, which retained the tolyl moiety of compound **1.1** and replaced only the S-benzyl-L-cysteine moiety with either a benzenesulfonamide or 3-nitrobenzenesulfonamide group respectively

(**Figure 7.1C**, **Figure 3.2C**). However, these two compounds appeared to be unstable and they were not able to be isolated successfully. It was necessary to try an alternative strategy towards targeting this pi-stacking interaction with Tyr195 of BCL-X<sub>L</sub>.

The second approach I describe in **Chapter 3** explored whether modifying the S-benzyl-cysteine substituent of **1.1** by reducing the length of the central 'linker' and/or incorporating an alternative terminal aryl group might achieve the desired pi-stacking interaction. A small set of seven analogues were synthesised and tested (compounds **3.7 - 3.16**, **Figure 7.1C**, **Figure 3.2D**) however none exhibited improved binding to BCL-X<sub>L</sub> relative to compound **1.1**. I described a crystal structure solved in complex with BCL-X<sub>L</sub> of one of these seven compounds, compound **3.10c**, which had affinity most similar to compound **1.1**. This structure confirmed that the desired pi-stacking interaction was not achieved, but showed a unique alternative binding mode adopted by the benzothiophene-containing amino acid moiety of compound **3.10c** in the p5 pocket of BCL-X<sub>L</sub> (**Figure 3.6**), which may be useful for future design efforts targeting the p5 pocket. Achieving the appropriate geometry for the terminal aryl group to interact with Tyr195 of BCL-X<sub>L</sub> is likely a key obstacle to this approach - detailed conformational modeling/molecular docking of proposed analogues may assist to achieve this in the future.

The crystal structures of compounds **1.1**, **1.8**, **1.9**, **1.10** and **3.1** in complex with BCL-X<sub>L</sub> all revealed that the terminal benzyl group of each molecule occupied a similar binding mode in a pocket we have termed p5 (**Figure 7.1B**, **Figure 3.3**, **Figure 4.1C**). The p5 pocket is formed *via* a side-chain flip of Tyr195 of BCL-X<sub>L</sub> and is little-explored to date in the scientific literature. We wondered whether the p5 pocket might be an additional targetable pocket of BCL-X<sub>L</sub> for drug-design efforts (**Figure 4.1**). **Chapter 4** described a set of inhibitors based on compound **1.8** (incorporating a sulfonyl linker) that explore some initial SAR within the p5 pocket. I described the synthesis and binding studies of 16 novel benzoylurea sulfonyl analogues (compounds **4.6a-o**, **4.25**), canvassing mono-substitution at different positions around the benzyl phenyl ring, extending the carbon linker,

or replacing the phenyl ring with a variety of aliphatic groups (**Figure 7.1D**, **Table 4.1**). Combined, this series revealed some key characteristics of the p5 pocket of BCL-X<sub>L</sub>. Firstly, it was shown to be relatively rigid, in contrast to the unexpected flexibility previously observed for the p2 pocket<sup>(2, 3)</sup>). Secondly, the p5 pocket was found to favour hydrophobic substituents (aliphatic rather than aromatic) of a defined size with a certain element of three-dimensionality. I illustrated this by presenting the crystal structures solved with BCL-X<sub>L</sub> of two of the most potent analogues in the sulfonyl series, compounds **4.61** and **4.25** (which respectively incorporate cyclohexyl and adamantyl substituents in the p5 pocket, **Figure 4.5**). These structures highlighted the three-dimensional character of the cyclohexyl and adamantyl groups within the p5 pocket and I suggested how the adamantyl group might be considered effectively to be an isostere of a pi-stacking interaction in this pocket. The work in this Chapter provided the basis for subsequent work described in **Chapter 6** using the extended THIQ scaffold (based on compounds **1.10** and **3.1**).

As part of the synthetic work described in **Chapter 4** to generate the adamantyl compound **4.25**, I described optimisation efforts necessary to enable S-alkylation of cysteine with the necessary adamantylmethylene substituent. I explained how the low reactivity of *neopentyl*-type systems to nucleophilic substitution hampered this step in the synthesis and described strategies that were explored to overcome this. The successful route I described to the adamantyl amino acid intermediate **4.13** represented the first reported synthesis of this particular cysteine derivative (**Scheme 4.3**). This synthetic method may also be of broader utility in the generation of other modified cysteine derivatives that incorporate hindered *neopentyl*-type substituents, for example for use in the synthesis of peptide inhibitors bearing non-natural amino acids.

**Chapter 5** outlined a series of benzoylurea analogues investigating incorporation of an amide linker as a potential isostere of the sulfonyl moiety of compound **1.8** (**Figure 7.1D**). We reasoned that similar to the sulfonyl oxygen, the amide carbonyl oxygen placed correctly might also mediate a hydrogen bond interaction with Gly138 of BCL-X<sub>L</sub>, whilst overall the amide linker might be more

atom-economical, exhibit useful conformational differences to the sulfonyl linker and also be amenable to late-stage parallel chemistry. I described an initial trial series of six analogues that were synthesised to validate this general concept (compounds **5.5a,b**, **5.10a,b**, **5.15a,b**; **Scheme 5.1**). These analogues, derived from L- or D-aspartic acid, varied the stereochemistry at the chiral center and overall length of the amide linker. Based on this, I selected compounds **5.5b** and **5.15a** as having the optimal linker. I then adapted this approach to a parallel format and compounds **5.5b** and **5.15a** provided respective starting points for the synthesis of two further amide-linked series that varied the p5 substituent (Series A, 8 examples, compounds **5.19a-h**; and Series B, 8 examples, compounds **5.23a-h**)(**Figure 7.1E**, **Scheme 5.3**). For each series I showed binding data to BCL-X<sub>L</sub> and MCL-1 and solved crystal structures for representative examples to validate the binding mode of the amide linker. Based on this data I showed that the Series A amide linker represented the better isostere of the sulfonyl moiety. The SAR study of the p5 pocket of BCL-X<sub>L</sub> using these amide analogues confirmed the general trends observed for the sulfonyl series, including the apparent preference in this pocket for cyclic aliphatic substituents with significant three-dimensional character. The work in this Chapter led to analogues with improved binding to BCL-X<sub>L</sub> and selectivity for BCL-X<sub>L</sub> relative to MCL-1 – including compounds **5.19b** (cyclohexyl analogue), **5.19c** (cycloheptyl analogue), **5.19d** (bridged bicyclo[2.2.1]heptanyl analogue) and **5.19e** (adamantyl analogue) (**Figure 7.1D**). In particular, compounds **5.19c** and **5.19d** represent the most potent compounds to date on the simple biphenyl scaffold ( $IC_{50}(BCL-X_L) = 0.096 \mu M$  and  $0.12 \mu M$ ,  $BEI = 11.9$  and  $12.4$  respectively; as compared to compound **1.8**,  $IC_{50}(BCL-X_L) = 0.59 \mu M$  and  $BEI = 10.9$ ; **Table 5.4**). Based on AlphaScreen Assay, compounds **5.19c** and **5.19d** also show improved selectivity (68- and 153-fold selectivity respectively for BCL-X<sub>L</sub> relative to MCL-1, as compared to only 20-fold for compound **1.8**; **Table 5.4**).

The promising results in **Chapter 5** suggest avenues to further improve the overall affinity of the series in future. Firstly, as compound **5.19d** was synthesised and tested as a mixture of 4 diastereomers, one of these individual stereoisomers may bind to BCL-X<sub>L</sub> with higher affinity than the mixture. In **Chapter 5** I described a



crystal structure solved of the BCL-X<sub>L</sub>:**5.19d** complex, but this was not of sufficient resolution to definitively identify whether one stereoisomer predominated in the bound state (**Figure 5.5**). Resynthesis of compound **5.19d** on a larger scale and resolution of the individual stereoisomers *via* chiral preparative HPLC for separate binding evaluation will address this outstanding question. Secondly, most of the promising amide-linked modifications described in **Chapter 5** to target the p5 pocket of BCL-X<sub>L</sub> (eg. compounds **5.19b-d**) have not yet been evaluated on either of the extended scaffolds that interact with the p2 pocket of the protein (eg. compounds **1.9** and **1.10**). Synergistic effects might be observed by combining these modifications, extending from initial work described in **Chapter 6**.

In **Chapter 6**, I outlined the synthesis, selectivity studies and initial mechanism-of-action/cellular studies of three THIQ extended-scaffold analogues, compounds **6.1**, **6.2** and **6.3**. These analogues explored the combined effect of incorporating an optimised substituent targeting the p5 pocket with the flexible THIQ scaffold (based on compound **1.10**) that interacts with the p2 pocket of BCL-X<sub>L</sub> (**Figure 7.1F,G**, **Figure 6.1**). Compounds **6.1** and **6.2** incorporate a cyclohexyl and adamantyl substituent respectively on a sulfonyl linker (drawing on work described in **Chapter 4**), whilst compound **6.3** incorporates an adamantyl substituent on the amide Series A linker (drawing on work described in **Chapter 5**). I described a side reaction (debenzylation) encountered during the benzoylurea formation step using the THIQ scaffold and outlined two strategies that were utilised to overcome this to reach the desired products compounds **6.1** - **6.3**. One strategy utilised a reductive amination sequence and I show that this method also provides an improved route to furnish the THIQ scaffold precursor (removing two synthetic steps). Initial binding studies by AlphaScreen assay revealed **6.1**, **6.2**, and **6.3** to be the most potent analogues for BCL-X<sub>L</sub> in the benzoylurea series to date, with measured IC<sub>50</sub> values for BCL-X<sub>L</sub> of 41 nM, 44 nM and 31 nM respectively (**Figure 7.1G**, **Table 6.1**).

Next, in **Chapter 6** I described SPR binding studies using compounds **6.1** and **6.2** that confirmed their nanomolar binding to BCL-X<sub>L</sub> using an orthogonal technique (**Figure 7.1G**) and I also used this assay to evaluate the selectivity profile of these

compounds. In SPR studies conducted to date, compounds **6.1** and **6.2** showed significant selectivity for BCL-X<sub>L</sub> as compared to other prosurvival BCL-2 family proteins tested (>180-fold selectivity for BCL-X<sub>L</sub> relative to BCL-W or MCL-1 and >80-fold selectivity for BCL-X<sub>L</sub> relative to A1; **Figure 7.1G**, **Table 6.4**). Experiments using BCL-2 are still ongoing. I also presented a crystal structure solved of the most potent analogue, compound **6.1**, in complex with BCL-X<sub>L</sub>, showing its interaction along the canonical hydrophobic groove of the protein (**Figure 7.1G**).

Finally, in **Chapter 6** I also provided results from some preliminary mechanism-of-action studies using compounds **6.1** and **6.2**. I showed that in an *in vitro* cytochrome *c* release assay, compounds **6.1** and **6.2** (at 10  $\mu$ M) were found to induce partial release of cytochrome *c* from the intact mitochondria of *MCL-1*<sup>-/-</sup> MEFs, but not wild-type or *BAX*<sup>-/-</sup>/*BAK*<sup>-/-</sup> MEFs (N = 2). This suggests, at least in a subset of the cell population, the level of BCL-X<sub>L</sub> inhibition is sufficient to trigger BAX/BAK-mediated MOMP and subsequent cytochrome *c* release and that this both requires BAX or BAK and is prevented by the presence of MCL-1. In cell viability assays, compounds **6.1** and **6.2** reduced the viability of *MCL-1*<sup>-/-</sup> MEFs cultured in the presence of 1% FCS in a dose-dependent manner (EC<sub>50</sub> of approximately 20  $\mu$ M for either compound, N = 3). In contrast, wild-type MEFs cultured under the same conditions were insensitive to the presence of either compound up to a concentration of 20  $\mu$ M (N = 1). Whilst preliminary, this data warrants further investigation, but also highlighted some non-specific effects. Firstly, at the highest test concentration (50  $\mu$ M) using wild-type MEFs, significant nonspecific toxicity was observed such that the window of selective activity was small. Secondly, both compounds showed no activity on *MCL-1*<sup>-/-</sup> MEFs when cultured in the presence of 10% FCS. These challenges are discussed in further detail below. Combined, the initial cell-viability assay and cytochrome *c* assay results described in **Chapter 6** provide early evidence that compounds **6.1** and **6.2** exhibit weak, but detectable, on-target BCL-X<sub>L</sub>-dependent cellular activity. Further experimental repeats will be required to confirm this. The results also highlight that further optimisation of this series

will be required – to further improve affinity for BCL-X<sub>L</sub> and also to reduce serum binding and mitigate off-target toxicity.

Whilst promising preliminary data, the results from the cellular assays described in **Chapter 6** highlight some general challenges experienced by many groups in the development of effective BCL-2 protein family inhibitors. It has been observed that in general to demonstrate clear mechanism-based activity in a cellular context, BH3 mimetic molecules must have very high affinity (subnanomolar binding affinity, to out-compete potent endogenous ligands such as BIM) and selectivity for the target protein (relative both to other BCL-2 family proteins as well as unrelated cellular proteins)<sup>(4)</sup>. Arkin and Wells have also noted that cell-based activity for BCL-2 family inhibitors in general is 100- to 1000-fold weaker than binding affinity, attributable to factors such as permeability, protein kinetics, or cellular context<sup>(5)</sup>. Relevantly, compounds **6.1** and **6.2** showed a 500-fold difference between cellular activity ( $EC_{50} \sim 20 \mu\text{M}$  using *MCL-1*<sup>-/-</sup> MEFs, 1% FCS) and  $IC_{50}$  for BCL-X<sub>L</sub> ( $IC_{50}(\text{BCL-X}_L) \sim 0.040 \mu\text{M}$ ). One particular off-target binding interaction of relevance is the general propensity of lipophilic acids to interact with serum albumin. Domain III of human serum albumin (HSA) - the most abundant protein in human serum - harbours a fatty acid binding site which can bind many drug-like molecules with high affinity (in particular small anionic aromatic compounds)<sup>(6, 7)</sup>. During the development of **ABT-737**, to mitigate the significantly decreased activity of the series in the presence of human serum attributed to HSA-III binding, a structure-guided approach was utilised to introduce basic moieties in suitable positions not to interfere with BCL-2 family binding but which reduced affinity to HSA-III<sup>(6, 8, 9)</sup>. As described in **Chapter 6**, the complete loss of cellular activity of compounds **6.1** and **6.2** in the presence of 10% foetal calf serum (and significantly diminished activity of **ABT-737** under the same conditions) is likely due to this effect. Similar optimisation to reduce serum binding of this series may be important in the future. This will also need to be carefully balanced with the overall physicochemical properties of the series. The large difference between cellular activity and  $IC_{50}$  observed for compounds **6.1** and **6.2** may at least in part be attributable to physicochemical properties, in particular

the zwitterionic character of the THIQ scaffold that may limit cellular permeability. Similarly, nonspecific toxicity observed at high concentrations may arise from poor physicochemical properties, in particular low solubility, as well as a certain level of promiscuous binding. Appending suitable basic/polar groups or incorporating heterocycles is one possible approach to improve serum binding and solubility, whilst further avenues also exist to improve target affinity and selectivity as outlined below.

The work described in this Thesis has demonstrated how relatively simple changes such as the cyclohexyl modification leading to compound **6.1** can give rise to significant improvements in overall binding affinity. The X-ray crystal structure of the BCL-X<sub>L</sub>:**6.1** complex (**Figure 7.1G**) highlights some key successes of the original benzoylurea scaffold design. Whilst all analogues in the series based on compound **1.1** bind along the groove in the reverse orientation from the original *de novo* design (**Figure 7.1A**)<sup>(10)</sup>, the benzoylurea core provides both structural preorganization essential to the overall binding mode as well as providing the basis for the modular synthesis of the series. The pseudo 6-membered ring formed by the benzoylurea core<sup>(11)</sup> in the BCL-X<sub>L</sub>:**6.1** complex (**Figure 7.1G**) successfully pre-organises compound **6.1** within the hydrophobic groove and positions the THIQ moiety towards the p2 pocket, the tolyl moiety into the p4 pocket (as a close topographical mimetic of h4 residue side chain of a BH3 domain, compare **Figure 7.1A**) and the cyclohexyl moiety into the p5 pocket. Extending from this work, a number of avenues still remain unexplored to potentially further improve the affinity of the benzoylurea series for BCL-X<sub>L</sub> in the future. In particular, derivatives of compounds **6.1** and **6.2** might be generated based on the work described in **Chapter 5**, to incorporate some of the optimised amide-linked p5 substituents. This may further improve in the overall affinity/selectivity of the series and reduce off-target binding. Potential also exists to explore further conformational preorganization of the series, in particular to 'lock' flexible regions such as the thioether/sulfonyl linker that might possibly suffer an entropic penalty upon binding. If the resulting geometry is appropriate, a conformational lock may increase affinity by improving the Gibbs free energy of binding. This might be

approached by incorporation of cyclic fragments in the p4/p5 pocket, or perhaps exploring other conformationally-restricted linker alternatives.

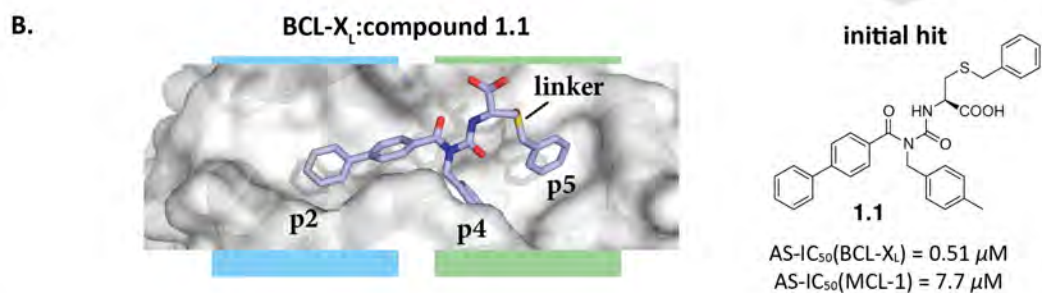
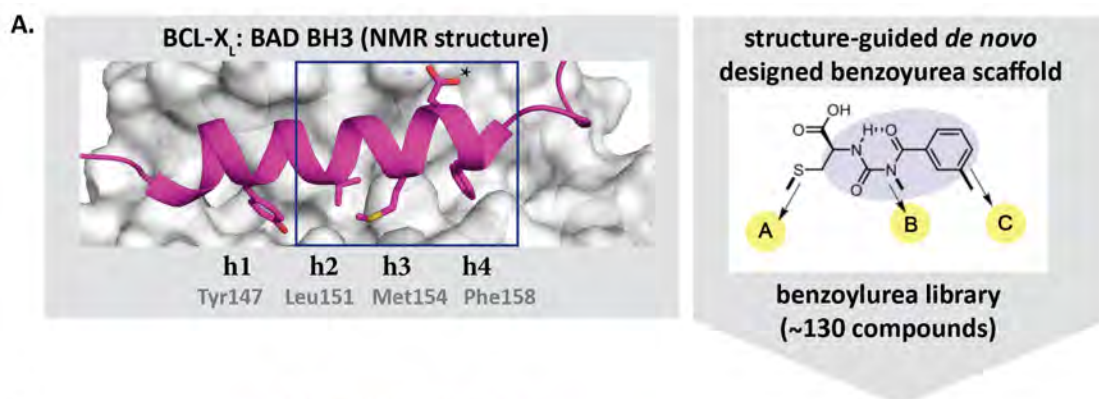
BCL-X<sub>L</sub> constitutes a compelling oncology target for the development of new therapeutics (both as a single agent or for combination therapy). Copy-number alterations leading to elevated BCL-X<sub>L</sub> levels are seen in a wide variety of cancers<sup>(12)</sup> and in a variety of tumour cell lines across the NCI-ACDS panel the level of BCL-X<sub>L</sub> expression was shown to correlate with resistance to diverse chemotherapeutic agents<sup>(13)</sup>. In terms of combination therapy, BCL-X<sub>L</sub>-selective inhibitors have recently been shown to have significant potential to enhance the efficacy of docetaxel in solid tumors <sup>(14)</sup>. In the infectious disease context, the use of BCL-X<sub>L</sub> inhibitors is also being explored in host-directed approaches targeting BCL-X<sub>L</sub> to reduce the disease burden of intracellular pathogens such as legionella<sup>(15)</sup>.

In addition to their potential development as therapeutics, novel series' of highly potent and selective small molecule inhibitors of BCL-2 family proteins are providing new opportunities as chemical probes. One particular avenue is for use in 'BH3-profiling'. BH3-profiling is a peptide-based technique that has been used for a variety of tumor cell types to determine the *in vitro* cellular dependence on individual prosurvival BCL-2 family proteins, based on the response of mitochondria to perturbation by BH3-peptides <sup>(16)</sup>. This offers potential for use in personalised medicine to assist in predicting response to chemotherapy, including combination therapy, which may assist in determining optimal therapeutic strategy<sup>(17-19)</sup>. Use of cell-penetrating small molecule chemical probes for 'chemical BH3-profiling' may enable simpler assessment of cellular response using simple cell viability assays<sup>(14)</sup>.

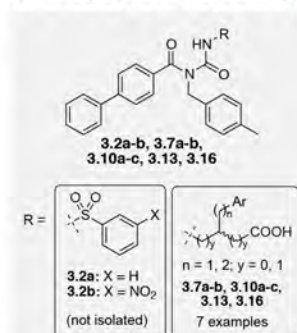
As described in **Chapter 1 (Section 1.4.3)**, four criteria have been proposed to characterise a 'true' BH3-mimetic <sup>(20)</sup>: i) Tight binding (nM - sub nM range) to one or more prosurvival BCL-2 family proteins; ii) BAX/BAK-dependent biological activity; iii) Cytotoxicity correlated with expression levels of targeted prosurvival proteins and the compound selectivity profile; and iv) *In vivo* observation of biomarkers indicative of *on-target* side-effects. Based on the work I have described

in **Chapter 6**, compounds **6.1** and **6.2** satisfy the first of these criteria and preliminary evidence has been provided in support of criteria two and three. Originating from a structure-guided *de novo* designed scaffold and optimised using a structure-guided approach, this work has shown the benzoylurea series to be a novel contribution to the growing literature of validated BH3-mimetics and exemplifies the utility of SBDD in the development of new therapeutics.

Combined, this study adds to our knowledge of the molecular determinants required for targeting individual BCL-2 family proteins using small molecule inhibitors. With the recent FDA approval of Venetoclax (**ABT-199**), the first BH3-mimetic to reach the market, which selectivity targets BCL-2, new chemical entities targeting this protein are of particular commercial interest. Whilst the binding of compounds **6.1** and **6.2** to BCL-2 *via* SPR is yet to be determined, these proof-of-principle studies have shown that the benzoylurea scaffold can generate potent inhibitors of BCL-X<sub>L</sub>. In future it may be also possible to further tune the affinity of the benzoylurea series to selectivity target BCL-2. In addition, the suite of novel benzoylurea compounds described in this thesis form part of a growing benzoylurea library that can be screened against diverse targets relevant to human disease, in particular other helix/groove protein-protein interactions.

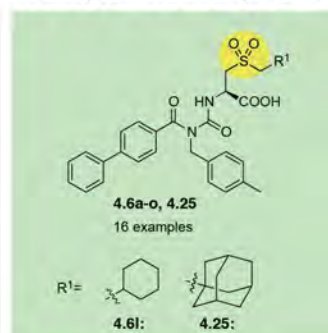


**C. Chapter 3: Pi-stacking**



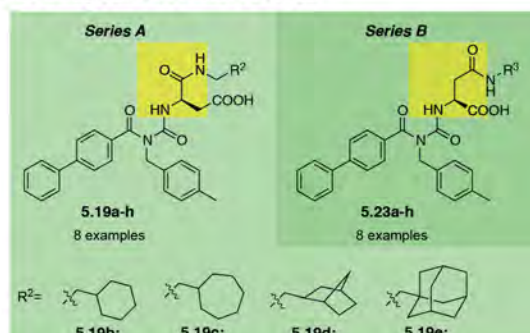
AS-IC<sub>50</sub>(BCL-X<sub>L</sub>) (μM) = 0.46 0.19  
AS-IC<sub>50</sub>(MCL-1) (μM) = 10.0 6.1

**D. Chapter 4: Sulfonyl series**

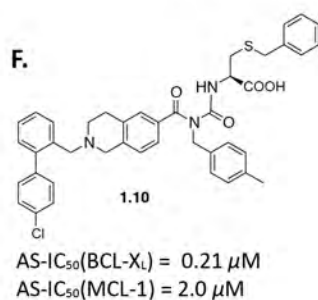


AS-IC<sub>50</sub>(BCL-X<sub>L</sub>) (μM) = 0.46 0.19  
AS-IC<sub>50</sub>(MCL-1) (μM) = 10.0 6.1

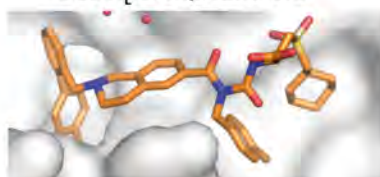
**E. Chapter 5: Amide series**



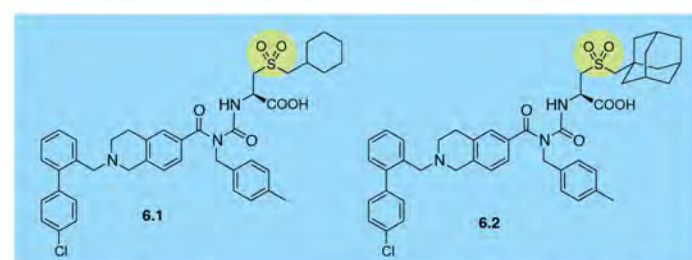
AS-IC<sub>50</sub>(BCL-X<sub>L</sub>) (μM) = 0.35 0.16 0.096 0.12  
AS-IC<sub>50</sub>(MCL-1) (μM) = 14.5 10.9 14.6 6.7



**BCL-X<sub>L</sub>: compound 6.1**



**G. Chapter 6: THIQ extended scaffold compounds**



AS-IC<sub>50</sub>(BCL-X<sub>L</sub>) = 0.041 μM  
AS-IC<sub>50</sub>(MCL-1) = 1.8 μM

SPR-IC<sub>50</sub>(BCL-X<sub>L</sub>) = 0.036 μM  
SPR-IC<sub>50</sub>(BCL-W) = 6.8 μM  
SPR-IC<sub>50</sub>(MCL-1) > 12.5 μM  
SPR-IC<sub>50</sub>(A1) = 4.6 μM

AS-IC<sub>50</sub>(BCL-X<sub>L</sub>) = 0.044 μM  
AS-IC<sub>50</sub>(MCL-1) = 1.8 μM

SPR-IC<sub>50</sub>(BCL-X<sub>L</sub>) = 0.068 μM  
SPR-IC<sub>50</sub>(BCL-W) > 12.5 μM  
SPR-IC<sub>50</sub>(MCL-1) > 12.5 μM  
SPR-IC<sub>50</sub>(A1) = 5.9 μM

**Figure 7.1: Summary of benzoylurea series progression described in this Thesis (previous page).**

(A.) Using the published NMR structure of BCL-X<sub>L</sub>:BAD BH3 complex (PDB entry: 1G5J)<sup>(21)</sup> and computer modeling to find novel scaffolds as potential  $\alpha$ -helical topographical mimetics to target the p2 – p4 pockets of BCL-X<sub>L</sub>, a benzoylurea scaffold was selected, which could be modified in a modular fashion in positions A – C (refer to **Figure 1.4**). A small library of benzoylurea molecules were generated and screened for binding to BCL-X<sub>L</sub>. (B.) Compound **1.1** was identified as an initial hit based on its promising binding to BCL-X<sub>L</sub> and selectivity relative to MCL-1. The crystal structure of compound **1.1** in complex with BCL-X<sub>L</sub> (solved by Peter Czabotar) is depicted, highlighting the p2, p4 and p5 hydrophobic pockets and the thioether ‘linker’ of **1.1** (discussed in the text). (C-E.) Depicted are representative chemical structures and IC<sub>50</sub> values of relevant compounds from **Chapters 3 - 5** discussed in the main text. (F.) Structure-guided design led to compound **1.10**, which utilised a THIQ scaffold to gain additional interaction in the vicinity of the p2 pocket of BCL-X<sub>L</sub> (refer **Chapter 1, Section 1.8.3** for further detail). (G.) Compounds **6.1** and **6.2**, described in **Chapter 6**, were designed to incorporate modifications targeting the p5 pocket (based on **Chapter 4**) onto the THIQ extended scaffold of compound **1.10**. Also depicted are binding IC<sub>50</sub> values for compounds **6.1** and **6.2** to BCL-X<sub>L</sub>, BCL-W, MCL-1 and A1 as well as the crystal structure of the BCL-X<sub>L</sub>:**6.1** complex described in **Chapter 6**. In all cases ‘AS’ refers to IC<sub>50</sub> values determined by AlphaScreen Assay (post-2015 data) and ‘SPR’ refers to IC<sub>50</sub> values determined by SPR competition assay (Biacore 3000).



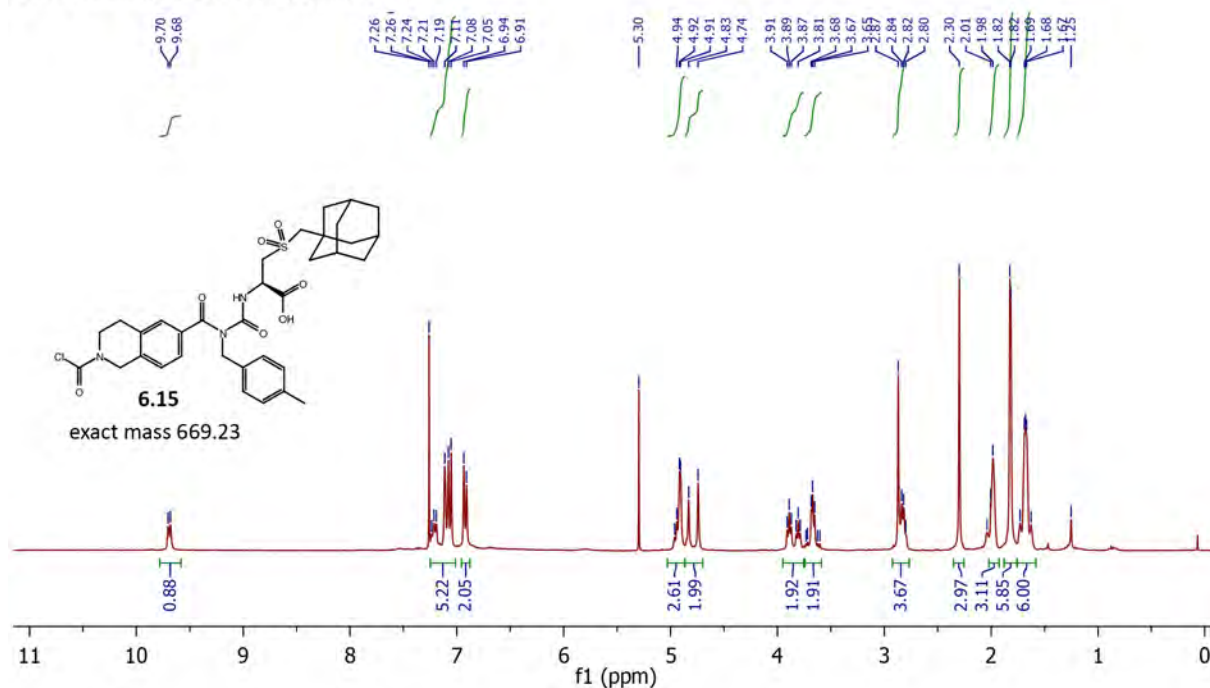
## 7.2 References

1. Zhou H, *et al.* (2012) Design of BCL-2 and BCL-xL inhibitors with subnanomolar binding affinities based upon a new scaffold. *Journal of Medicinal Chemistry* 55(10):4664-4682.
2. Lee EF, *et al.* (2007) Crystal structure of ABT-737 complexed with BCL-xL: implications for selectivity of antagonists of the BCL-2 family. *Cell Death and Differentiation* 14(9):1711-1713.
3. Bruncko M, *et al.* (2007) Studies leading to potent, dual inhibitors of BCL-2 and BCL-xL. *Journal of Medicinal Chemistry* 50(4):641-662.
4. Bruncko M, *et al.* (2015) Structure-guided design of a series of MCL-1 inhibitors with high affinity and selectivity. *Journal of Medicinal Chemistry* 58(5):2180-2194.
5. Arkin MR, Tang Y, & Wells JA (2014) Small-molecule inhibitors of protein-protein interactions: progressing toward the reality. *Chemistry & Biology*.
6. Mao H, *et al.* (2001) Rational design of diflunisal analogues with reduced affinity for human serum albumin. *Journal of the American Chemical Society* 123(43):10429-10435.
7. Alam MA, Awal MA, Subhan N, & Mostofa M (2009) In-vitro relationship between protein-binding and free drug concentrations of a water-soluble selective beta-adrenoreceptor antagonist (atenolol) and its interaction with arsenic. *Journal of Health, Population, and Nutrition* 27(1):20-30.
8. Petros AM, *et al.* (2006) Discovery of a potent inhibitor of the antiapoptotic protein BCL-xL from NMR and parallel synthesis. *Journal of Medicinal Chemistry* 49(2):656-663.
9. Oltersdorf T, *et al.* (2005) An inhibitor of BCL-2 family proteins induces regression of solid tumours. *Nature* 435(7042):677-681.
10. Brady RM, *et al.* (2014) De-novo designed library of benzoylureas as inhibitors of BCL-XL: synthesis, structural and biochemical characterization. *Journal of Medicinal Chemistry* 57(4):1323-1343.
11. Lessene G, Smith BJ, Gable RW, & Baell JB (2009) Characterization of the two fundamental conformations of benzoylureas and elucidation of the

- factors that facilitate their conformational interchange. *Journal of Organic Chemistry* 74(17):6511-6525.
12. Beroukhim R, *et al.* (2010) The landscape of somatic copy-number alteration across human cancers. *Nature* 463(7283):899-905.
  13. Amundson SA, *et al.* (2000) An informatics approach identifying markers of chemosensitivity in human cancer cell lines. *Cancer Research*:6101-6110.
  14. Levenson JD, *et al.* (2015) Exploiting selective BCL-2 family inhibitors to dissect cell survival dependencies and define improved strategies for cancer therapy. *Science Translational Medicine* 7(279):279ra240.
  15. Speir M, *et al.* (2016) Eliminating Legionella by inhibiting BCL-XL to induce macrophage apoptosis. *Nature Microbiology* 1:15034.
  16. Del Gaizo Moore V & Letai A (2013) BH3 profiling – Measuring integrated function of the mitochondrial apoptotic pathway to predict cell fate decisions. *Cancer Letters* 332(2):202-205.
  17. Chonghaile TN, *et al.* (2011) Pretreatment mitochondrial priming correlates with clinical response to cytotoxic chemotherapy. *Science* 334(6059):1129-1133.
  18. Vo T-T, *et al.* (2012) Relative mitochondrial priming of myeloblasts and normal HSCs determines chemotherapeutic success in AML. *Cell* 151(2):344-355.
  19. Deng J, *et al.* (2007) BH3 profiling identifies three distinct classes of apoptotic blocks to predict response to ABT-737 and conventional chemotherapeutic agents. *Cancer Cell* 12(2):171-185.
  20. Lessene G, Czabotar PE, & Colman PM (2008) BCL-2 family antagonists for cancer therapy. *Nature Reviews. Drug Discovery* 7(12):989-1000.
  21. Petros AM, *et al.* (2000) Rationale for BCL-xL/Bad peptide complex formation from structure, mutagenesis, and biophysical studies. *Protein Science* 9(12):2528-2534.

## **8 Appendices**

### A. $^1\text{H}$ -NMR data for compound 6.15



### B. LCMS data for compound 6.15

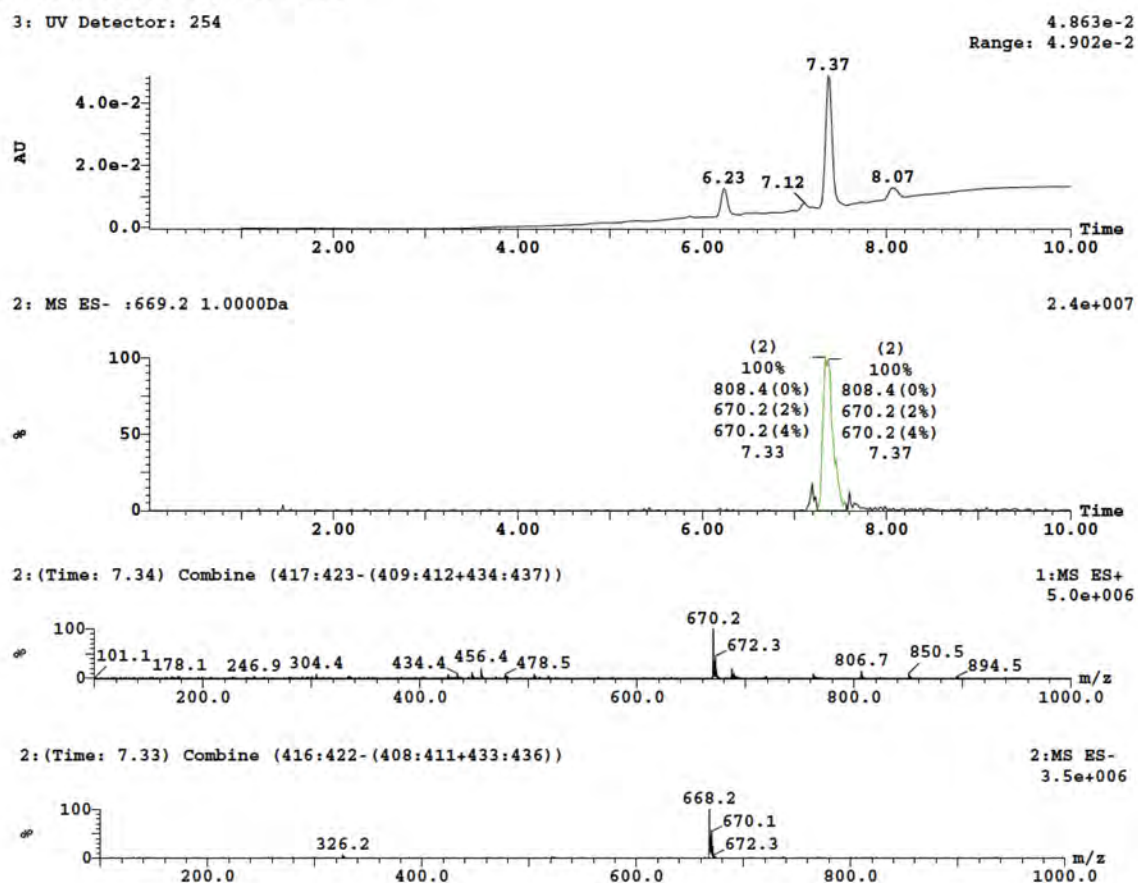
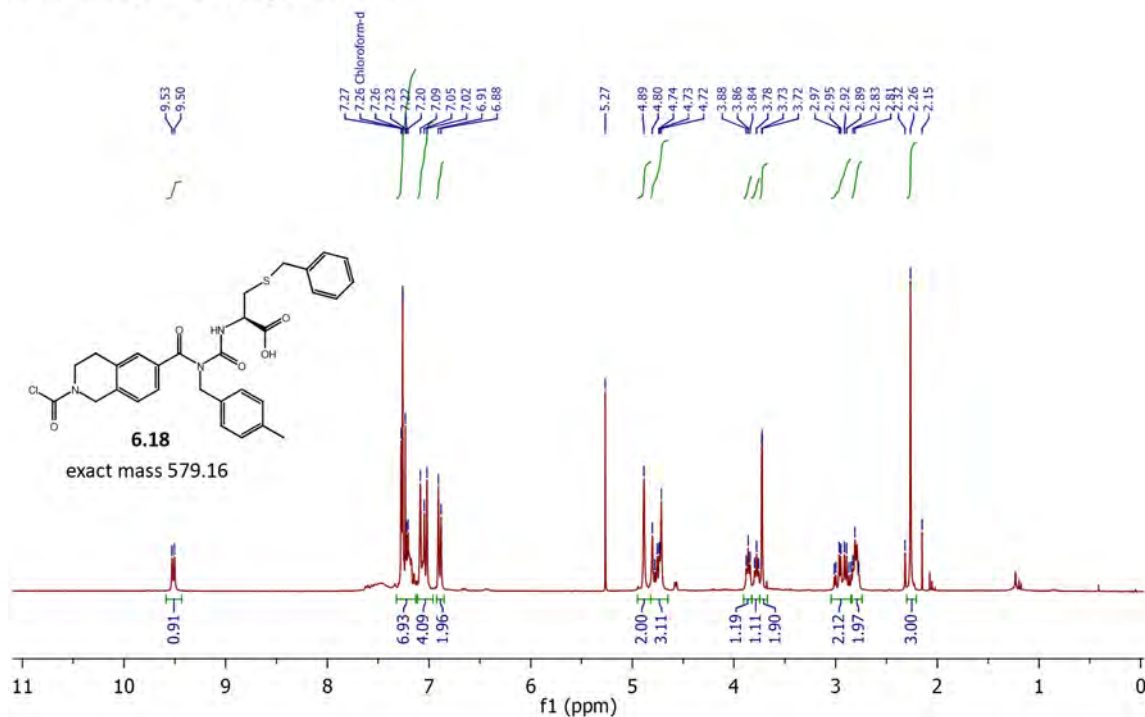


Figure A1:  $^1\text{H}$  NMR and LCMS data for compound 6.15.

A.  $^1\text{H}$ -NMR data for compound 6.18



B. LCMS data for compound 6.18

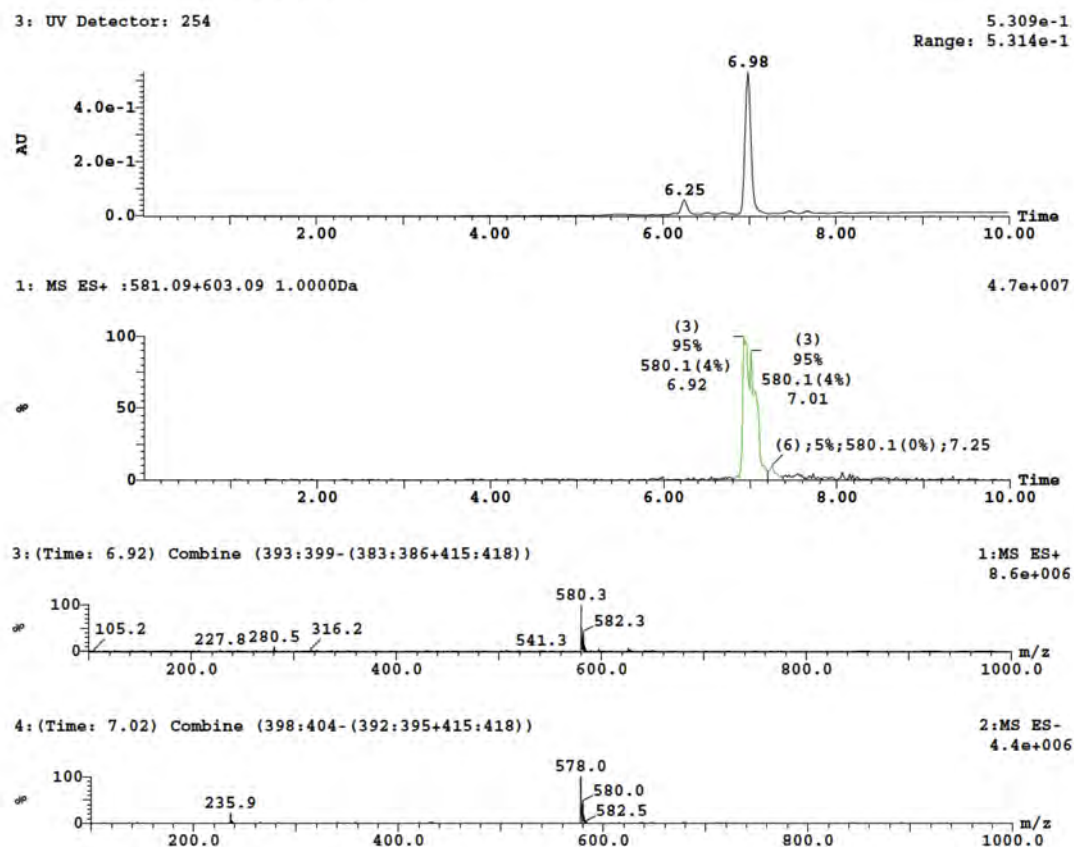


Figure A2:  $^1\text{H}$  NMR and LCMS data for compound 6.18.

Sample LCMS Analysis of direct benzoylurea reaction to form compound 6.2  
(crude reaction mixture after 5 minutes)

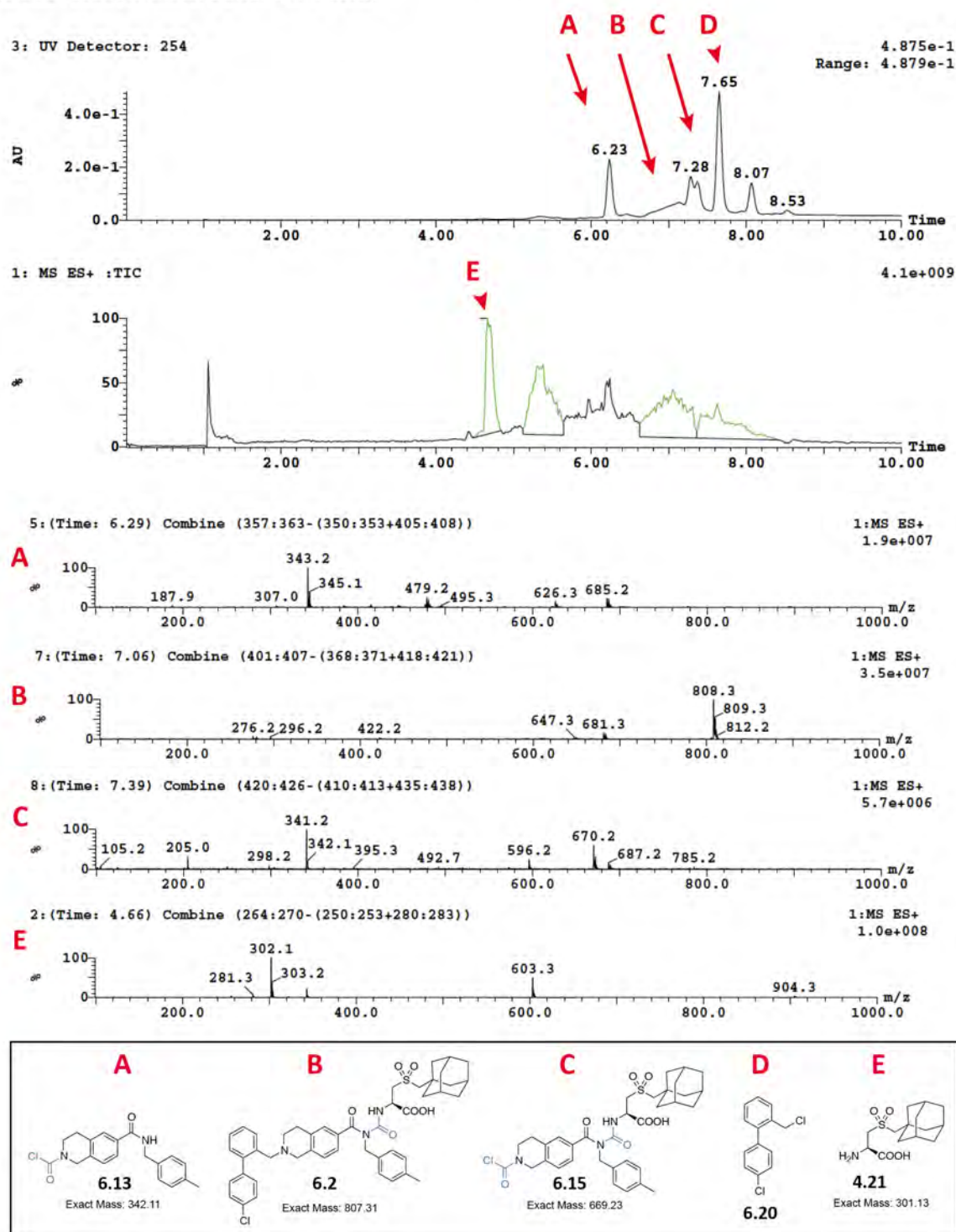
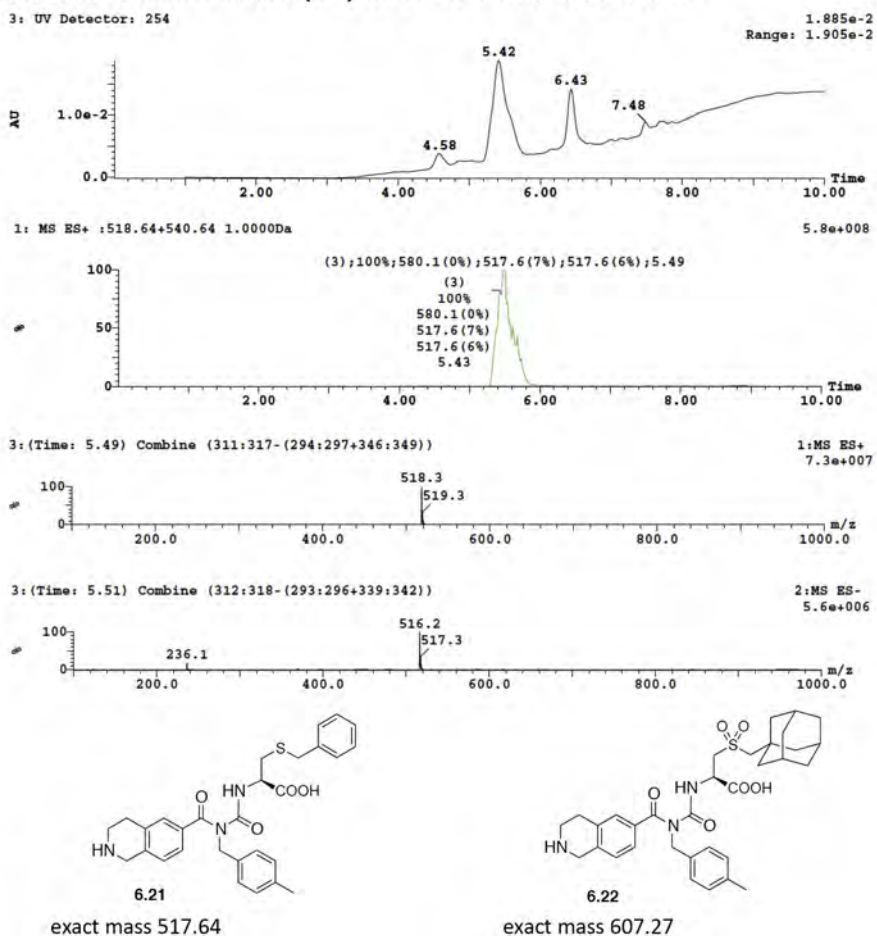


Figure A3: Sample LCMS Analysis of direct benzoylurea reaction to form compound 6.2 (reaction mixture at 5 minutes), showing formation of species A-E and the assigned chemical structures of these species (black box).



### A. LCMS of reaction mixture (1 h) for conversion of 6.18 to 6.21



### B. LCMS of reaction mixture (1 h) for conversion of 6.15 to 6.22

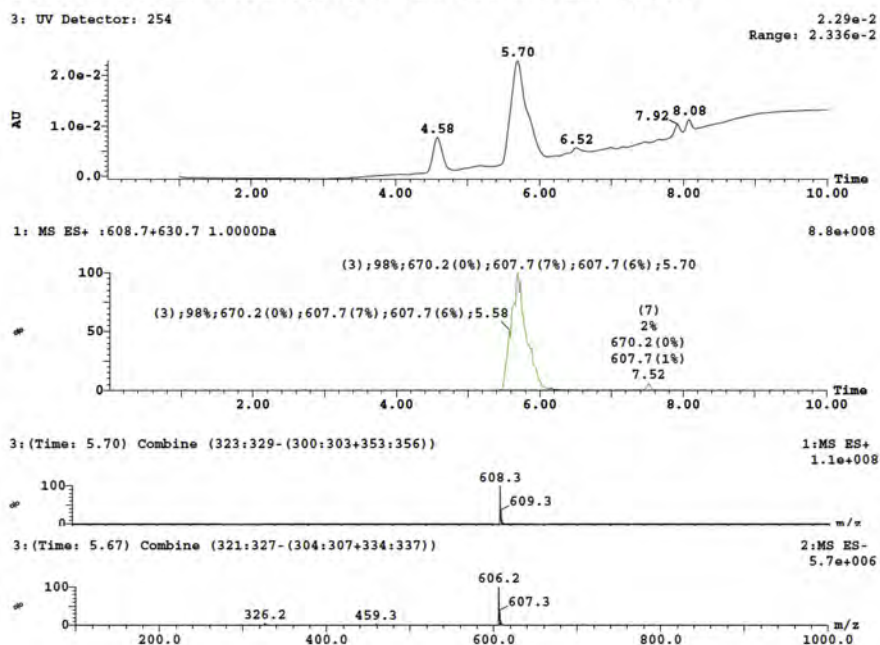
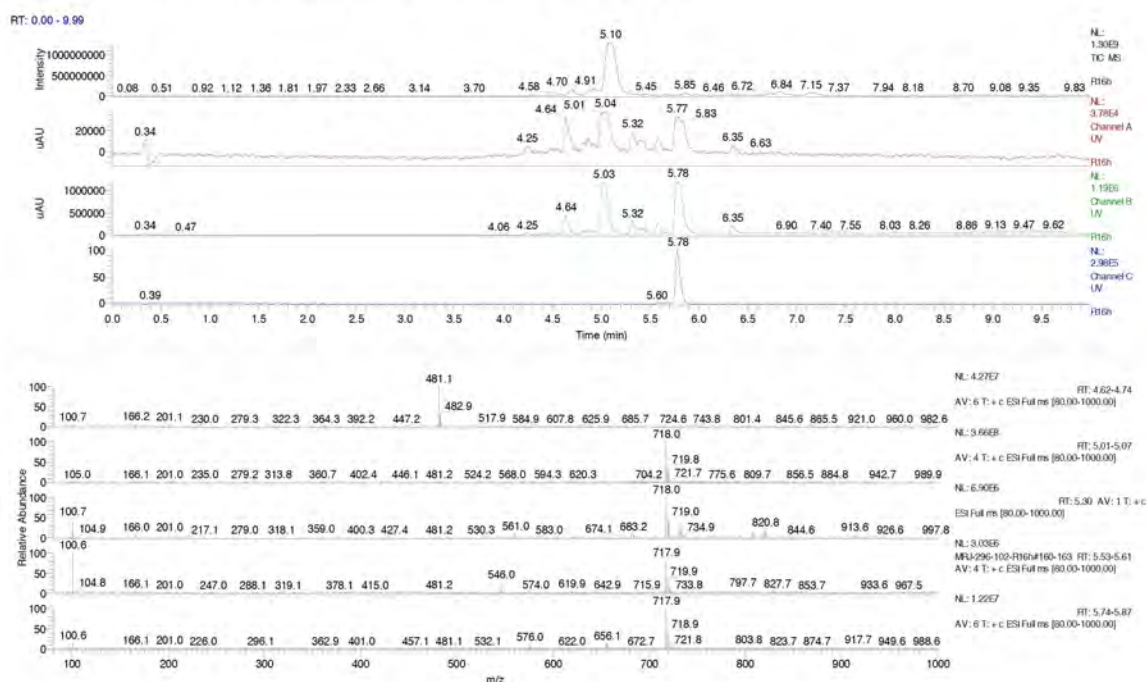


Figure A4: (A) LCMS of reaction mixture (at 1 h) for conversion of compound 6.18 to 6.21. (B) LCMS of reaction mixture (at 1 h) for conversion of compound 6.15 to 6.22.

### A. LCMS of reaction mixture (16 h) for conversion of 6.21 to 1.10



### B. $^1\text{H}$ NMR spectrum (MeOD) of 1.10

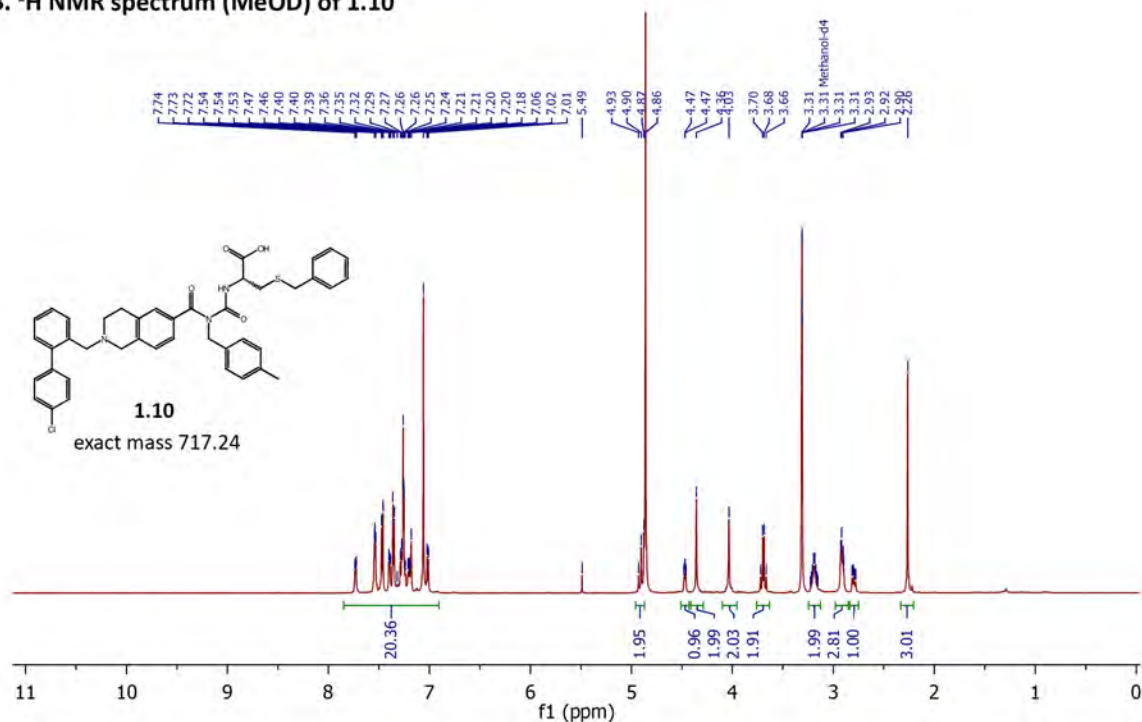
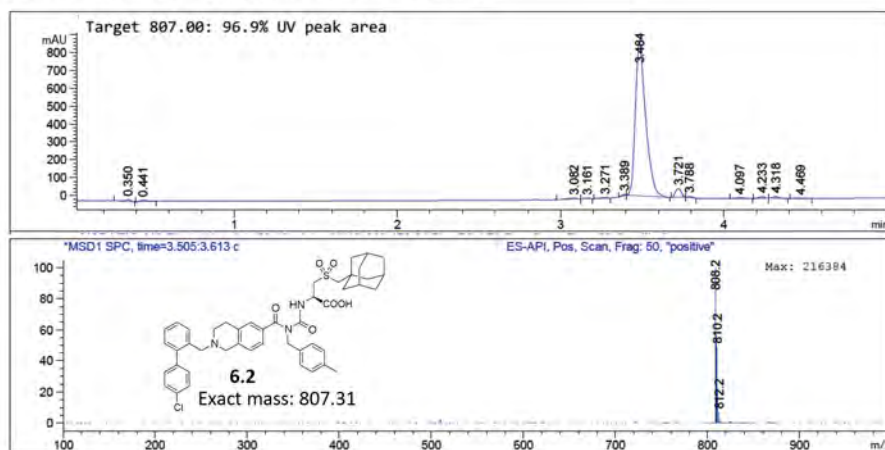


Figure A5: (A) LCMS Analysis of reaction mixture (16 h) for conversion of compound 6.21 to 1.10, showing peak for product formation. (B)  $^1\text{H}$  NMR spectrum (MeOD) of purified compound 1.10.

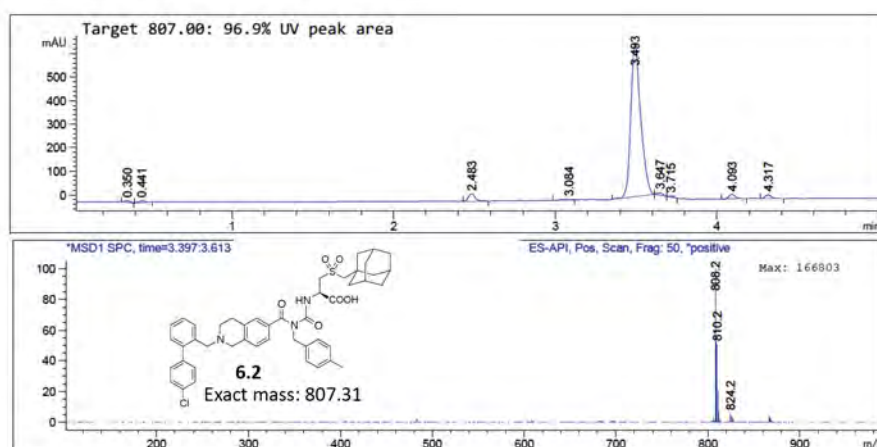


## LCMS Analysis of compound 6.2

### A. Direct route, scale-up resynthesis (Amelia Vom)



### B. Direct route, small scale



### C. Alternative route - chlorobiphenyl fragment reinstalled *via* reductive amination

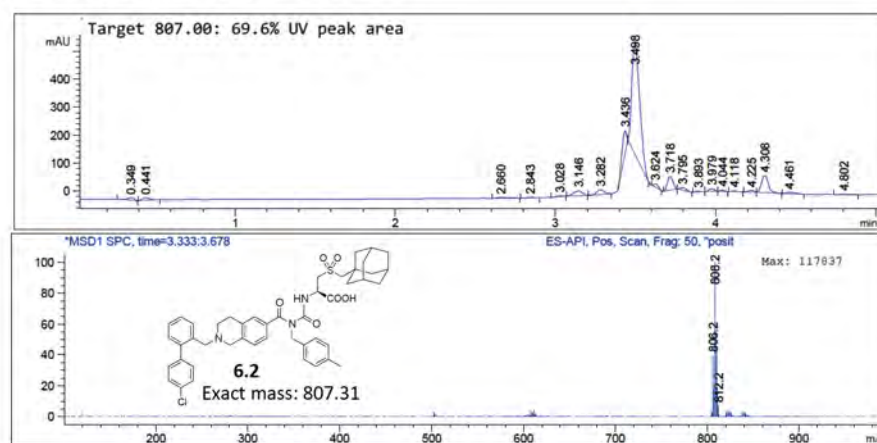
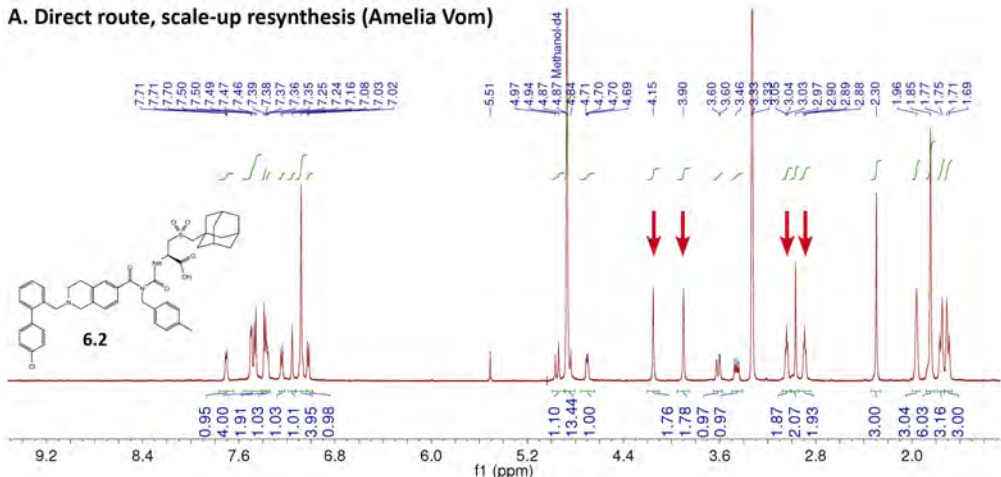


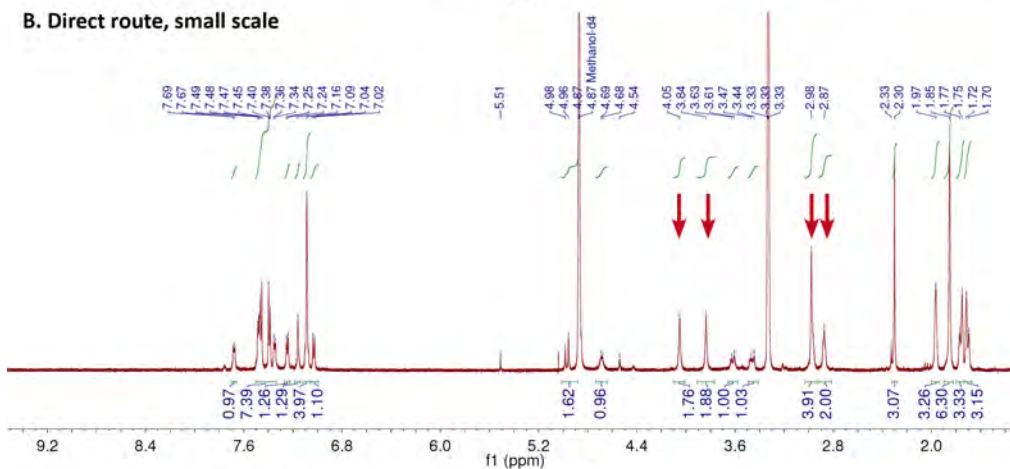
Figure A6: LCMS Analysis of compound 6.2 synthesised using the direct route (A, B) or alternative route *via* reductive amination (C), showing the same retention time (~3.49 minutes) and molecular ion ( $m/z$  808.2) in the ES<sup>+</sup> spectrum. Samples (A) and (B) are 97% pure by UV absorbance ( $A_{280}$ ), whilst (C) contains an additional peak at 3.44 minutes due to an impurity (~70% pure).

<sup>1</sup>H NMR of compound 6.2 (MeOD)

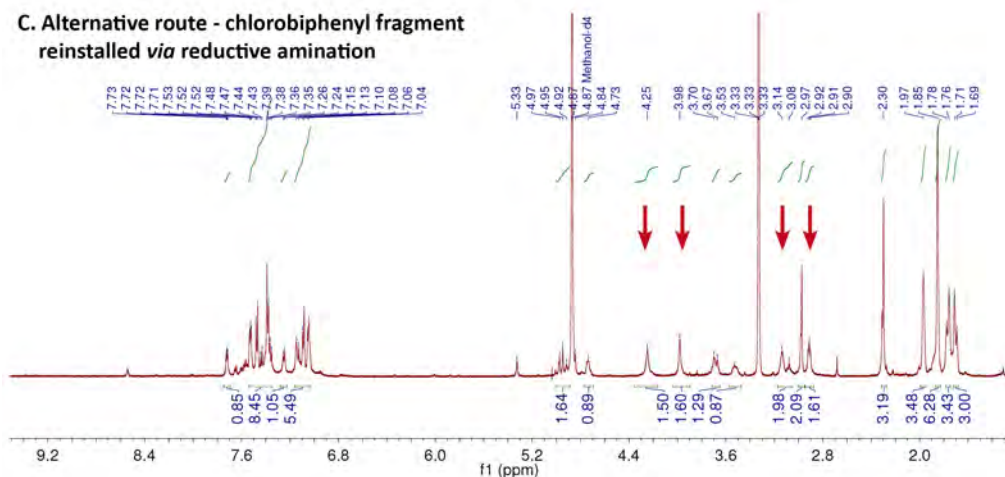
A. Direct route, scale-up resynthesis (Amelia Vom)



B. Direct route, small scale

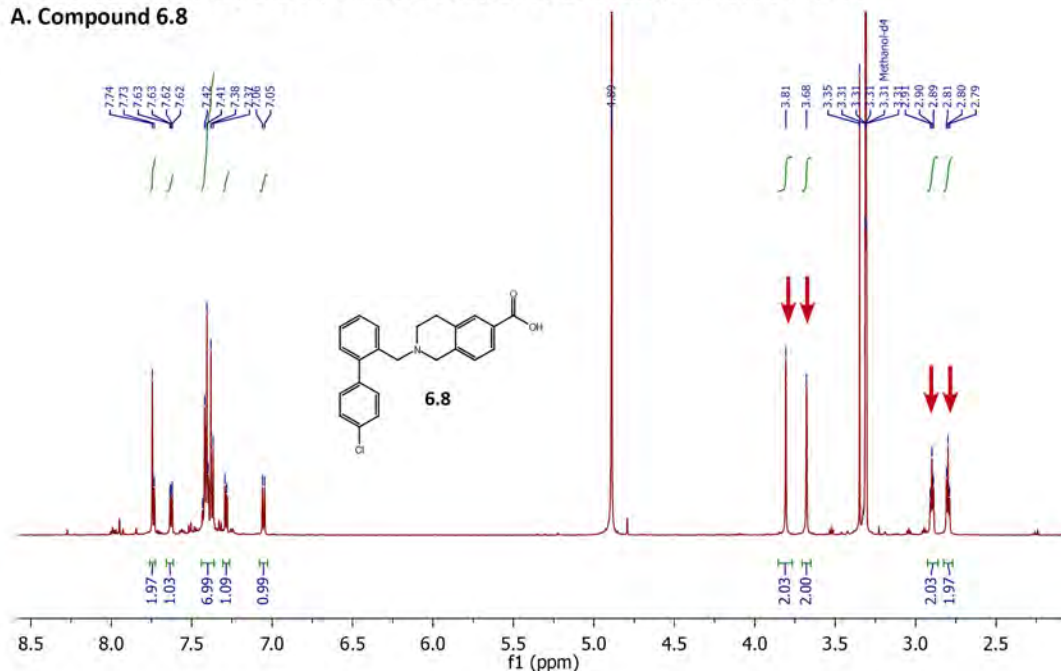


C. Alternative route - chlorobiphenyl fragment reinstalled *via* reductive amination



**Figure A7:** <sup>1</sup>H NMR spectra of compound 6.2 synthesised using the direct route (A, B) and alternative route *via* reductive amination (C). Some variation is observed in the chemical shifts of the four methylene protons adjacent to the THIQ tertiary amine (red arrows), which appears to be attributable to the protonation state of the tertiary amine. Refer to discussion for similar effects observed for compound 6.8 (Figure A8). Additional peaks are present in sample (C) due to an inseparable impurity.

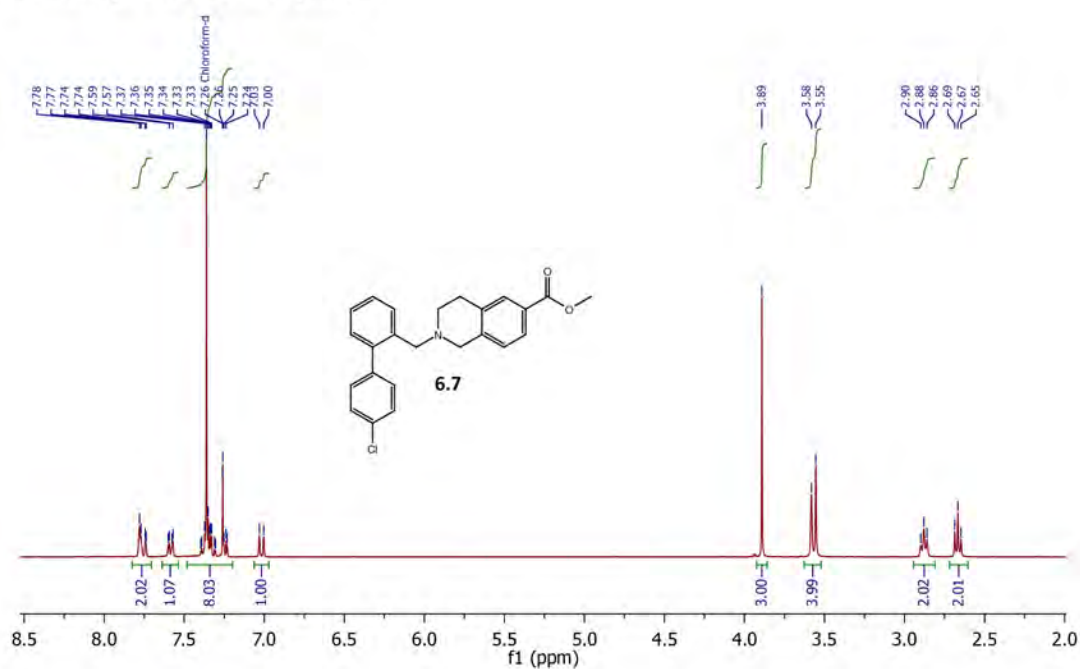
### A. Compound 6.8

[illegible]

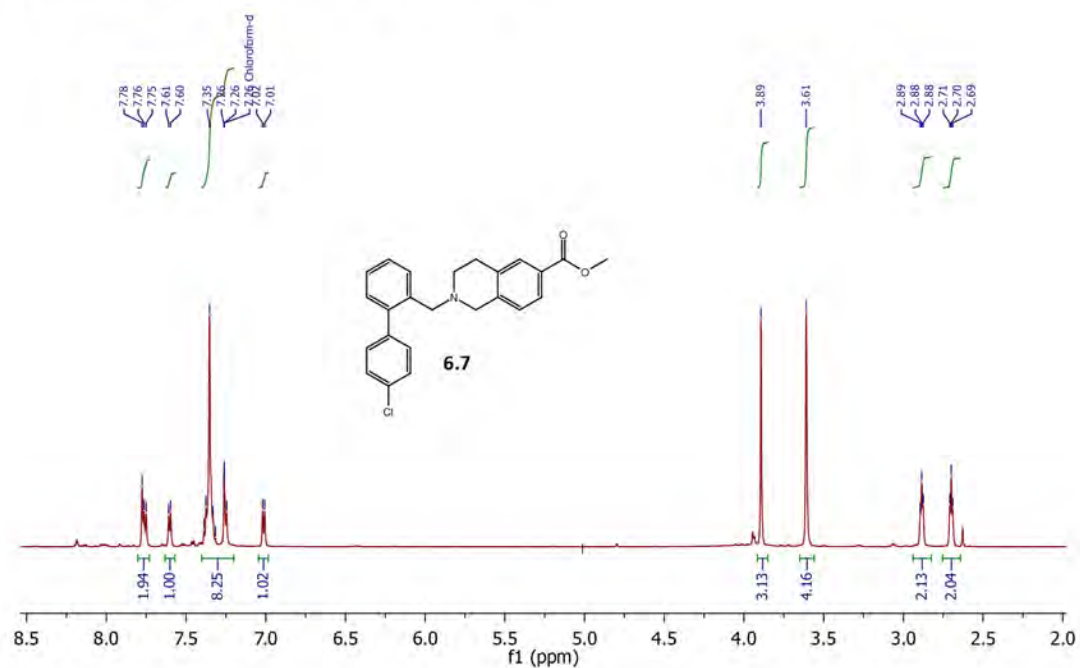
A8

**<sup>1</sup>H NMR of compound 6.7 (CDCl<sub>3</sub>)**

**A. Initial synthesis *via* N-alkylation**



**B. Alternative synthesis *via* reductive amination**



**Figure A9: <sup>1</sup>H NMR spectra of compound 6.7 synthesised using two different methods, either (A) *via* N-alkylation with compound 6.6, or (B) *via* reductive amination with compound 6.4. Note that the two spectra were obtained using different instruments (300 MHz and 600 MHz respectively).**

Minerva Access is the Institutional Repository of The University of Melbourne

**Author/s:**

Roy, Michael James

**Title:**

Towards novel BH3-mimetics: structure-guided development of small molecule inhibitors targeting prosurvival BCL-2 family proteins

**Date:**

2016

**Persistent Link:**

<http://hdl.handle.net/11343/129237>

**File Description:**

Towards novel BH3-mimetics: structure-guided development of small molecule inhibitors targeting prosurvival BCL-2 family proteins

**Terms and Conditions:**

Terms and Conditions: Copyright in works deposited in Minerva Access is retained by the copyright owner. The work may not be altered without permission from the copyright owner. Readers may only download, print and save electronic copies of whole works for their own personal non-commercial use. Any use that exceeds these limits requires permission from the copyright owner. Attribution is essential when quoting or paraphrasing from these works.